

molecules

Feature Papers in Food Chemistry

Edited by
Mirella Nardini

Printed Edition of the Special Issue Published in *Molecules*

Feature Papers in Food Chemistry

Feature Papers in Food Chemistry

Editor

Mirella Nardini

MDPI • Basel • Beijing • Wuhan • Barcelona • Belgrade • Manchester • Tokyo • Cluj • Tianjin



Editor

Mirella Nardini
CREA Research Centre for
Food and Nutrition
Council for Agricultural
Research and Economics (CREA)
Rome
Italy

Editorial Office

MDPI
St. Alban-Anlage 66
4052 Basel, Switzerland

This is a reprint of articles from the Special Issue published online in the open access journal *Molecules* (ISSN 1420-3049) (available at: www.mdpi.com/journal/molecules/special_issues/Food_FP).

For citation purposes, cite each article independently as indicated on the article page online and as indicated below:

LastName, A.A.; LastName, B.B.; LastName, C.C. Article Title. <i>Journal Name</i> Year , <i>Volume Number</i> , Page Range.
--

ISBN 978-3-0365-6333-6 (Hbk)

ISBN 978-3-0365-6332-9 (PDF)

© 2023 by the authors. Articles in this book are Open Access and distributed under the Creative Commons Attribution (CC BY) license, which allows users to download, copy and build upon published articles, as long as the author and publisher are properly credited, which ensures maximum dissemination and a wider impact of our publications.

The book as a whole is distributed by MDPI under the terms and conditions of the Creative Commons license CC BY-NC-ND.

Contents

About the Editor	vii
Mirella Nardini Feature Papers in Food Chemistry Reprinted from: <i>Molecules</i> 2022 , <i>27</i> , 8638, doi:10.3390/molecules27248638	1
Maria Chiara Fontanella, Lucrezia Lamastra and Gian Maria Beone Determination of Glyphosate in White and Brown Rice with HPLC-ICP-MS/MS Reprinted from: <i>Molecules</i> 2022 , <i>27</i> , 8049, doi:10.3390/molecules27228049	7
Georgios A. Koulis, Aristeidis S. Tsagkaris, Panagiota A. Katsianou, Panagiotis-Loukas P. Gialouris, Ioannis Martakos and Fotis Stergiou et al. Thorough Investigation of the Phenolic Profile of Reputable Greek Honey Varieties: Varietal Discrimination and Floral Markers Identification Using Liquid Chromatography–High-Resolution Mass Spectrometry Reprinted from: <i>Molecules</i> 2022 , <i>27</i> , 4444, doi:10.3390/molecules27144444	21
Yibo Li, Lingxiao Zhao, Lingshang Lin, Enpeng Li, Qinghe Cao and Cunxu Wei Relationships between X-ray Diffraction Peaks, Molecular Components, and Heat Properties of C-Type Starches from Different Sweet Potato Varieties Reprinted from: <i>Molecules</i> 2022 , <i>27</i> , 3385, doi:10.3390/molecules27113385	39
Antonietta Cerulli, Milena Masullo, Cosimo Pizza and Sonia Piacente Metabolite Profiling of “Green” Extracts of <i>Cynara cardunculus</i> subsp. <i>scolymus</i> , Cultivar “Carciofo di Paestum” PGI by ¹ H NMR and HRMS-Based Metabolomics Reprinted from: <i>Molecules</i> 2022 , <i>27</i> , 3328, doi:10.3390/molecules27103328	53
Koji Nagao, Nao Inoue, Keisuke Tsuge, Akira Oikawa, Tomoko Kayashima and Teruyoshi Yanagita Dried and Fermented Powders of Edible Algae (<i>Neopyropia yezoensis</i>) Attenuate Hepatic Steatosis in Obese Mice Reprinted from: <i>Molecules</i> 2022 , <i>27</i> , 2640, doi:10.3390/molecules27092640	69
Yibo Li, Lingxiao Zhao, Laiquan Shi, Lingshang Lin, Qinghe Cao and Cunxu Wei Sizes, Components, Crystalline Structure, and Thermal Properties of Starches from Sweet Potato Varieties Originating from Different Countries Reprinted from: <i>Molecules</i> 2022 , <i>27</i> , 1905, doi:10.3390/molecules27061905	83
Manol Ognyanov, Petko Denev, Desislava Teneva, Yordan Georgiev, Sabina Taneva and Iskra Totseva et al. Influence of Gamma Irradiation on Different Phytochemical Constituents of Dried Rose Hip (<i>Rosa canina</i> L.) Fruits Reprinted from: <i>Molecules</i> 2022 , <i>27</i> , 1765, doi:10.3390/molecules27061765	101
Qiannan Li, Jieying Zhang, Guiju Zhang and Baocai Xu L-Lysine-Based Gelators for the Formation of Oleogels in Four Vegetable Oils Reprinted from: <i>Molecules</i> 2022 , <i>27</i> , 1369, doi:10.3390/molecules27041369	121
Muchtaridi Muchtaridi, Rina Fajri Nuwarda, Emmy Hainida Khairul Ikram, Aisyah Saad Abdul Rahim, Amirah Mohd Gazzali and Habibah A. Wahab Neuraminidase Inhibitor of <i>Garcinia atroviridis</i> L. Fruits and Leaves Using Partial Purification and Molecular Characterization Reprinted from: <i>Molecules</i> 2022 , <i>27</i> , 949, doi:10.3390/molecules27030949	133

José M. Malga, Marcos Trigo, Beatriz Martínez and Santiago P. Aubourg Preservative Effect on Canned Mackerel (<i>Scomber colias</i>) Lipids by Addition of Octopus (<i>Octopus vulgaris</i>) Cooking Liquor in the Packaging Medium Reprinted from: <i>Molecules</i> 2022 , 27, 739, doi:10.3390/molecules27030739	149
Yuan He, Leilei Zhu, Jialun Chen, Xin Tang, Mingluo Pan and Weiwei Yuan et al. Efficacy of Probiotic Compounds in Relieving Constipation and Their Colonization in Gut Microbiota Reprinted from: <i>Molecules</i> 2022 , 27, 666, doi:10.3390/molecules27030666	163
Zhongqi He, Sunghyun Nam, Hailin Zhang and Ocen Modesto Olanya Chemical Composition and Thermogravimetric Behaviors of Glanded and Glandless Cottonseed Kernels Reprinted from: <i>Molecules</i> 2022 , 27, 316, doi:10.3390/molecules27010316	181
Tatijana Markoska, Davor Daniloski, Todor Vasiljevic and Thom Huppertz Structural Changes of β -Casein Induced by Temperature and pH Analysed by Nuclear Magnetic Resonance, Fourier-Transform Infrared Spectroscopy, and Chemometrics Reprinted from: <i>Molecules</i> 2021 , 26, 7650, doi:10.3390/molecules26247650	199
Laiquan Shi, Yibo Li, Lingshang Lin, Xiaofeng Bian and Cunxu Wei Effects of Variety and Growing Location on Physicochemical Properties of Starch from Sweet Potato Root Tuber Reprinted from: <i>Molecules</i> 2021 , 26, 7137, doi:10.3390/molecules26237137	209

About the Editor

Mirella Nardini

Dr. Nardini is a biologist with a Ph.D. in Biochemistry. She is employed as senior technologist at the National Institute of Nutrition (INN), National Institute for Food and Nutrition Research (INRAN), and currently is affiliated with the Council for Agricultural Research and Economics (CREA). She has been responsible for many research projects, charged in Codex Alimentarius in the group: "Oils and Fats". She performs teaching activities, and is a reviewer for many international scientific journals. From 2000 to 2001, Dr. Nardini was a research scholar at the University of Davis (CA, USA). The results of her studies have been published in many international scientific journals. Her field of interest focuses on the nutritional quality of food and the role of food in the modulation and prevention of oxidative stress and related pathologies, particularly cardiovascular diseases. She has gained extensive experience in antioxidants and polyphenol compounds, through many studies concerning the identification, characterization, biological activity, bioavailability, and metabolism of phenolic compounds.

Editorial

Feature Papers in Food Chemistry

Mirella Nardini 

CREA, Research Centre for Food and Nutrition, Via Ardeatina 546, 00178 Rome, Italy; mirella.nardini@crea.gov.it

The Special Issue, entitled “Feature Papers in Food Chemistry”, is a collection of important high-quality papers (original research articles or comprehensive review papers) published in open access format. This Special Issue discusses new knowledge and new cutting-edge developments in the food chemistry field through selected works, in the hope of making a great contribution to the community through the dissemination of excellent research findings as well as by sharing innovative ideas in the field.

To be more specific, this Special Issue collects manuscripts on food composition with special emphasis on chemical characterization, the content of bioactive compounds, contaminants, and analytical aspects. The role of variety, cultivation, growing conditions, and technological processes on the nutritional quality of foods was also considered. Research studies dealing with the biological activity and healthy effects of food components were also presented.

The first research article of this Special Issue by Shi et al. [1] described the effect of different varieties and growing locations pertaining to the physicochemical properties of starch obtained from sweet potato root tuber. Three sweet potato varieties were studied: purple-, yellow-, and white-fleshed root tubers, planted in four growing locations. The starches isolated from root tubers were analyzed for size, crystalline structure, ordered degree, lamellar thickness, swelling power, water solubility and pasting, thermal and digestion properties, iodine absorption, and amylose content. Starches exhibited significantly different swelling powers, water solubility, pasting viscosities, thermal properties, amylose contents, iodine absorptions, and granule sizes. The ordered degree and lamellar thickness of starches were affected by different varieties and growing locations of sweet potatoes. Statistical analyses showed that starch physicochemical properties were significantly affected by different varieties and growing locations, as well as their interaction. Therefore, in consideration of starch applications, an appropriate variety for planting sweet potatoes in a specific growing location should be chosen.

The study of Markovska et al. [2] investigated the structural changes in β -casein as a function of temperature and pH, by means of nuclear magnetic resonance (NMR), as well as Fourier-transform infrared spectroscopy in conjunction with chemometric analysis. Both temperature (4 and 20 °C) and pH (3.9 and 7.0) strongly affected the secondary structure of the β -casein molecule, particularly the regions involving random coils and α -helix. The changes in secondary structure components were linked to the decreased hydrophobic interactions at lower temperatures and increasing pH levels. The results obtained may help to establish the structural behavior of β -casein during β -casein production, as well as process milk and milk-derived products. The combination of analytical methods used in this study can be further expanded to other proteins and assist in understanding protein behaviors during food processing.

Another study by He Z. [3] et al. comparatively evaluated the chemical composition and thermogravimetric behaviors of two types of cottonseed kernels: glanded and glandless cottonseed kernels. Chemical analysis and Fourier transform infrared (FTIR) spectroscopy showed that the two types of kernels had similar chemical components and mineral contents, but the former was slightly higher in protein, starch, and phosphorus content. The thermal behaviors and stability of the two types of cottonseed kernels were also

Citation: Nardini, M. Feature Papers in Food Chemistry. *Molecules* **2022**, *27*, 8638. <https://doi.org/10.3390/molecules27248638>

Received: 21 November 2022

Accepted: 5 December 2022

Published: 7 December 2022

Publisher's Note: MDPI stays neutral with regard to jurisdictional claims in published maps and institutional affiliations.



Copyright: © 2022 by the author. Licensee MDPI, Basel, Switzerland. This article is an open access article distributed under the terms and conditions of the Creative Commons Attribution (CC BY) license (<https://creativecommons.org/licenses/by/4.0/>).

investigated. The common glanded cottonseeds exhibited a high content of gossypol, a toxic compound. Glandless cottonseeds, in contrast, showed a trace gossypol level so that it can be used for animal feeds and human foods. The findings of this study enhance the potential application of glanded and glandless cottonseed kernels for food application.

The research article by He Y. [4] et al. investigated the efficacy of probiotics on constipation relief and their capacity to colonize the intestinal tract in mice. The probiotic compounds tested, including *Lactobacillus acidophilus*, *Lacticaseibacillus rhamnosus*, *Limosilactobacillus reuteri*, *Lactiplantibacillus plantarum*, and *Bifidobacterium animalis*, showed relief of constipation when administered to mice with loperamide-induced constipation. The effects of probiotics on constipation were associated with various aspects, including the gastrointestinal transit rate, the number and weight of stools, serum and gastrointestinal regulatory hormones, and serum cytokines. Moreover, some of the probiotic compounds were found to colonize the intestinal tract. This study yields a new perspective for the clinical use of probiotics to relieve constipation symptoms by combining strains with different mechanisms of action.

In the article of Malga et al. [5], the preservative properties of waste liquor obtained from octopus (*Octopus vulgaris*) cooking were investigated. Three different volumes of such liquor were included in the packaging medium employed for Atlantic Mackerel (*Scomber colias*) canning and were compared to control canned fish. The effects of octopus cooking liquor packaging on lipid hydrolysis, lipid oxidation, fatty acid profiles, and fatty acids ratios in canned mackerel were determined. The presence of the high and medium concentrations of octopus cooking liquor led to significantly lower levels of lipid oxidation and an average increase in the polyene index and monounsaturated fatty acid content with respect to control canned fish. This study constitutes a novel strategy to enhance the quality of commercial canned fish, thus enabling environmental sustainability and circular economy.

The study of Muchtaridi et al. [6] describes a new potential neuraminidase inhibitor from *Garcinia atroviridis* L. fruits and leaves. Neuraminidase is an enzyme preventing virion aggregation within the host cell and promoting cell-to-cell spread by cleaving glycosidic linkages to sialic acid, thus facilitating virus movement. The development of anti-influenza drugs that inhibit neuraminidase activity has emerged as a promising approach in the treatment of influenza. A bioassay-guided fractionation method was applied to isolate and identify the bioactive inhibitory compounds garcinia acid and naringenin from *Garcinia atroviridis* L. fruits and leaves, respectively. Garcinia acid demonstrated the highest inhibitory activity when compared to naringenin. Based on molecular docking results, garcinia acid was found to form strong ionic interaction with arginine triad residues of the viral neuraminidase, suggesting that garcinia acid has the potential to act as a neuraminidase inhibitor.

The article of Li Q. et al. [7] focused on the synthesis of four L-lysine-based gelators and their use to spur the formation of oleo-gels in four kinds of vegetable oils (corn germ oil, soybean oil, olive oil, and linseed oil). Gelation ability is not only affected by the structure of the gelators, but also by the composition of oils. The minimum gel concentration increased with the increase in the acyl-carbon chain length of the gelators. The strongest gelation ability was displayed in the olive oil for the same gelator. Rheological properties showed that the mechanical strength and thermal stability of the oleo-gels varied with the carbon-chain length of gelators and the type of vegetable oil.

In the study of Ognyanov et al. [8], the effects of gamma irradiation on dried rose hip (*Rosa canina* L.) phytochemicals were studied by employing several analytical techniques (GC-FID, HPLC-UV, HPSEC-RID, IR-FT, and SEM). The changes in macronutrients and micronutrients (e.g., carbohydrates, lipids, organic acids, and phenolics) were examined. The irradiation treatment increased the glucose content and released cellobiose, thus revealing cellulose destruction, and resulting in higher pectin yield. The exposure to the highest dose did not change the content of total carotenoids, β -carotene, ascorbic acid, and saturated and unsaturated fatty acids, while it affected tocopherols levels. A slight effect on conjugated dienes content was also measured with the highest dose. Gamma

irradiation had a negligible effect on phenolic constituents (chlorogenic acid, quercetin, rutin, catechin, and epicatechin) and did not significantly affect antioxidant activity. From the results obtained, the authors concluded that the exposition of dried rose hip to gamma irradiation is safe and can be successfully applied for the microbial decontamination of fruits without affecting their nutritional value and biological activity.

The research article of Li Y. et al. [9] investigated the sizes, components, crystalline structures, and thermal properties of starches from 44 sweet potato varieties originating from 15 different countries, planted in the same growing conditions, to reveal the similarities and differences in their physicochemical properties. The granule size, iodine absorption, amylose content, X-ray diffraction patterns, and thermal properties of starches were studied, revealing significant differences among all sweet potato varieties. The thermograms of starches exhibited one-, two-, or three-peak curves, leading to a significantly different gelatinization temperature range. The significantly different starch properties divided the 44 sweet potato varieties into different groups due to their different genotype backgrounds. The research offers references for the utilization of sweet potato germplasm.

The study of Nagao et al. [10] investigated the effects of dried and fermented powders of edible algae (*Neopyropia Yezoensis*) on hepatic steatosis in obese mice. Edible algae *Neopyropia Yezoensis* was used as “Nori”, its dried product, in Japanese cuisine. In this study, Nori powder and Koji-fermented nori powder were used to supplement the diet of male *db/db* mice for 4 weeks. Eicosapentaenoic acid was found in the serum and liver of mice fed with nori or fermented nori diets in a dose-dependent manner. Both nori and fermented nori reduced hepatic triglyceride accumulation and hepatic injury with similar mechanisms. Although the eicosapentaenoic content of fermented Nori powder was one-third of that of nori powder, metabolomic analysis revealed that bioactive betaine analogs, such as stachydrine, betaine, and carnitine, were detected only in with fermented nori powder. In conclusion, the lipid components of nori, mainly eicosapentaenoic acid, are readily absorbable by the body to exert lipid-lowering effects. Moreover, the fermentation of nori produced anti-inflammatory and lipid-lowering betaine analogs, which, together with lipid components, can exert hepatic steatosis-alleviating effects.

The article by Cerulli et al. [11] provided a comprehensive analysis of green extracts of *Cynara cardunculus* subsp. *scolymus*, with cultivar “Carciofo di Paestum” PGI heads. Ethanol/water extracts, infusions, and decoctions were analyzed by LC-ESI/QExactive/MS/MS and NMR analysis. A total of 17 compounds corresponding to caffeoylquinic acid derivatives, phenolics, flavonoids, and terpenoids were identified. Principal component analysis (PCA) showed significant differences among the extraction methods. Moreover, 5-caffeoylquinic acid (known as chlorogenic acid) and 1,5-dicaffeoylquinic acid (known as cynarin) quantization, phenolic content, antioxidant activity, and the α -glucosidase inhibitory activity of “Carciofo di Paestum” extracts were evaluated.

The second research article by Li Y. et al. [12] described the relationships between the X-ray diffraction peaks, molecular components, and heat properties of C-type starches from seven different sweet potato varieties. C-type starches contains both A- and B-type crystallinities. C-type starches with different proportions of A- and B-type crystallinities have different intensities and crystallinities of X-ray diffraction peaks. The relative crystallinities of diffraction peaks and total crystallinities showed some differences among some sweet potato varieties. These parameters were affected by amylose content, amylopectin structure, crystallinity type, and granule size. The thermograms of seven starches exhibited significant differences in peak shapes, widths, and gelatinization temperatures. The score plot of principle component analysis showed that the molecular components and heat properties parameters could differentiate the C-type starches and agreed with their characteristics of X-ray diffraction peaks. The starch properties, especially crystalline structure, affect the utilizations of starches. This study provides some information for the utilizations of C-type starches through their X-ray diffraction patterns.

In the research of Koulis et al. [13], the phenolic profile of Greek honey varieties was investigated using liquid chromatography–high-resolution mass spectrometry, and

botanical origin markers were identified by metabolomic approaches. Three blossom honey markers were identified, namely galangin, pinocembrin, and chrysin, while gallic acid level was found to be significantly higher in oak honey. Twelve additional bioactive compounds were identified and semi-quantified, achieving comprehensive honey metabolomic characterization. Moreover, it was possible to discriminate thyme from blossom honey and develop discriminatory models with high predictive value.

The research article by Fontanella et al. [14] described a simplified method for the determination of herbicide glyphosate in white and brown rice by means of liquid chromatography coupled with inductively coupled mass triple quadrupole. This molecule, authorized for a wide variety of crop and non-crop uses, is an active substance in plant protection products. The debate on using glyphosate in Europe is still very active concerning the risk for human health. In 2015, the International Agency for Research on Cancer and the European Food Safety Agency put forward two conflicting views on the carcinogenic hazard of glyphosate to humans. In 2013, the European Commission established 0.1 mg/Kg as maximum residual level for rice, as the lower limit of analytical determination. Several methods are available for the determination of this molecule and its metabolites in different kinds of matrices, such as apples, cereals, soybean, as well as surface water and wastewater. The method proposed by Fontanella et al. is characterized by rapidity and simplicity in comparison with other existing procedures which are laborious and include several purification steps. In this study, the quantification of glyphosate was validated in terms of LOD, LOQ, accuracy, precision, linearity, and matrix effect. The matrix effect, which is a well-known critical problem in pesticide residue analysis, could be avoided by using a matrix-matched calibration line to avoid artefact results. The described procedure can be considered useful for the determination of glyphosate in different types of rice and designed and adapted for other cereals.

Funding: This research received no external funding.

Institutional Review Board Statement: Not applicable.

Informed Consent Statement: Not applicable.

Data Availability Statement: Not applicable.

Acknowledgments: All the authors who kindly contributed to this Special Issue are gratefully acknowledged.

Conflicts of Interest: The authors declare no conflict of interest.

Sample Availability: Samples of the compounds are not available from the authors.

References

1. Shi, L.; Li, Y.; Bian, X.; Wei, C. Effects of variety and growing location on physicochemical properties of starch from sweet potato root tuber. *Molecules* **2021**, *26*, 7137. [CrossRef] [PubMed]
2. Markovska, T.; Daniloski, D.; Vasiljevic, T.; Huppertz, T. Structural changes of β -casein induced by temperature and pH analysed by nuclear magnetic resonance, Fourier-transform infrared spectroscopy, and chemometrics. *Molecules* **2021**, *26*, 7650. [CrossRef] [PubMed]
3. He, Z.; Nam, S.; Zhang, H.; Olanya, O.M. Chemical composition and thermogravimetric behaviors of glanded and glandless cottonseed kernels. *Molecules* **2022**, *27*, 316. [CrossRef] [PubMed]
4. He, Y.; Zhu, L.; Chen, J.; Tang, X.; Pan, M.; Yuan, W.; Wang, H. Efficacy of probiotic compounds in relieving constipation and their colonization in gut microbiota. *Molecules* **2022**, *27*, 666. [CrossRef] [PubMed]
5. Malga, J.M.; Trigo, M.; Martinez, B.; Aubourg, S.P. Preservative effect on canned mackerel (*Scorpaenidae*) lipids by addition of Octopus (*Octopus vulgaris*) cooking liquor in the packaging medium. *Molecules* **2022**, *27*, 739. [CrossRef] [PubMed]
6. Muchtaridi, M.; Nuwarda, R.F.; Ikram, E.H.K.; Rahim, A.S.A.; Gazzali, A.M.; Wahab, H.A. Neuraminidase inhibitor of *Garcinia atroviridis* L. fruits and leaves using partial purification and molecular characterization. *Molecules* **2022**, *27*, 949. [CrossRef] [PubMed]
7. Li, Q.; Zhang, J.; Zhang, G.; Xu, B. L-Lysine-based gelators for the formation of oleogels in four vegetable oils. *Molecules* **2022**, *27*, 1369. [CrossRef] [PubMed]
8. Ognyanov, M.; Denev, P.; Teneva, D.; Georgiev, Y.; Taneva, S.; Totseva, I.; Kamenova-Nacheva, M.; Nikolova, Y.; Momchilova, S. Influence of gamma irradiation on different phytochemical constituents of dried rose hip (*Rosa canina* L.) fruits. *Molecules* **2022**, *27*, 1765. [CrossRef] [PubMed]

9. Li, Y.; Zhao, L.; Shi, L.; Lin, L.; Cao, Q.; Wei, C. Sizes, components, crystalline structure, and thermal properties of starches from sweet potato varieties originating from different countries. *Molecules* **2022**, *27*, 1905. [CrossRef] [PubMed]
10. Nagao, K.; Inoue, N.; Tsuge, K.; Oikawa, A.; Kayashima, T.; Yanagita, T. Dried and fermented powders of edible algae (*Neopyropia Yezoensis*) attenuate hepatic steatosis in obese mice. *Molecules* **2022**, *27*, 2640. [CrossRef] [PubMed]
11. Cerulli, A.; Masullo, M.; Pizza, C.; Piacente, S. Metabolite profiling of “green” extracts of *Cynara cardunculus* subsp. *scolymus*, cultivar “Carciofo di Paestum” PGI by ¹H NMR and HRMS-based metabolomics. *Molecules* **2022**, *27*, 3328. [CrossRef] [PubMed]
12. Li, Y.; Zhao, L.; Lin, L.; Li, E.; Cao, Q.; Wei, C. Relationships between X-ray diffraction peaks, molecular components, and heat properties of C-type starches from different sweet potato varieties. *Molecules* **2022**, *27*, 3385. [CrossRef] [PubMed]
13. Koulis, G.A.; Tsagkaris, A.S.; Katsianou, P.A.; Gialouris, P.-L.P.; Martakos, I.; Stergiou, F.; Fiore, A.; Panagopoulou, E.I.; Karabournioti, S.; Baessmann, C.; et al. Through investigation of the phenolic profile of reputable Greek honey varieties: Varietal discrimination and floral markers identification using liquid chromatography-high-resolution mass spectrometry. *Molecules* **2022**, *27*, 4444. [CrossRef] [PubMed]
14. Fontanella, M.C.; Lamastra, L.; Beone, G.M. Determination of glyphosate in white and brown rice with HPLC-ICP-MS/MS. *Molecules* **2022**, *27*, 8049. [CrossRef] [PubMed]

Article

Determination of Glyphosate in White and Brown Rice with HPLC-ICP-MS/MS

Maria Chiara Fontanella *, Lucrezia Lamastra and Gian Maria Beone 

Department for Sustainable Food Process, Università Cattolica del Sacro Cuore, Via Emilia Parmense 84, 29122 Piacenza, Italy

* Correspondence: mariachiara.fontanella@unicatt.it; Tel.: +39-05-23-59-9216

Abstract: Background: In 2017, the European Commission renewed the approval of glyphosate (GLY) but only for five years. GLY remains one of the most controversial and studied molecules. Method: A simplified method was tested for the determination of GLY in white rice (WR) and brown rice (BR), after extraction only with a methanol solution, by liquid chromatography coupled with inductively coupled mass triple quadrupole (HPLC-ICP-MS/MS) with a PRP-X100 anionic column. After performing a test on groundwater, the quantification of GLY in WR and BR was validated in terms of the LOD, LOQ, accuracy, precision, linearity, and the matrix effect. Results: The LOD was 0.0027 mg kg⁻¹ for WR and 0.0136 mg kg⁻¹ for BR. The LOQ was 0.0092 mg kg⁻¹ for WR and 0.0456 mg kg⁻¹ for BR. The mean recoveries were within 76–105% at three fortification levels. The relative standard deviation for the analysis (five replicates for three spike levels) was < 11% for both matrices. A linear response was confirmed in all cases in the entire concentration range ($R^2_{WR} = 1.000$ and $R^2_{BR} = 0.9818$). Conclusion: The proposed method could be considered useful for the determination of GLY in different types of rice and designed and adapted for other cereals. The matrix effect, quantified in BR matrix extraction, could be avoided by using a matrix-matched calibration line.

Keywords: glyphosate; HPLC-ICP-MS/MS; white and brown rice; LOD; LOQ; matrix effect

Citation: Fontanella, M.C.; Lamastra, L.; Beone, G.M. Determination of Glyphosate in White and Brown Rice with HPLC-ICP-MS/MS. *Molecules* **2022**, *27*, 8049. <https://doi.org/10.3390/molecules27228049>

Academic Editor: Mirella Nardini

Received: 13 September 2022

Accepted: 11 November 2022

Published: 19 November 2022

Publisher's Note: MDPI stays neutral with regard to jurisdictional claims in published maps and institutional affiliations.



Copyright: © 2022 by the authors. Licensee MDPI, Basel, Switzerland. This article is an open access article distributed under the terms and conditions of the Creative Commons Attribution (CC BY) license (<https://creativecommons.org/licenses/by/4.0/>).

1. Introduction

Glyphosate (GLY) was approved in 2002 for the first time at the EU level for ten years under a directive replaced in 2011 by Regulation 1107/2009 [1], but it had been on the market in most countries under national legislation since the 1970s [2].

Glyphosate is the ISO common name for N-phosphono methyl glycine (the IUPAC name). It is a small molecule with three functional groups that make it highly polar, stable, and soluble in water. Moreover, it is easily absorbed by the main components of the soil, such as clays, iron oxides, and humic substances. Combined with GLY, aminomethylphosphonic acid (AMPA) is considered an indicator of the application of the GLY molecule, because it is a product of its degradation and has similar chemical characteristics to its precursor. This molecule is an active substance in plant protection products, and their products are authorized for a wide variety of crop and non-crop uses, for example, on railways, hard surfaces, etc. Its application occurs either pre-sowing, preharvest, or postharvest, due to its unparalleled action on annual and perennial weeds [3].

The debate on using GLY in Europe is still very active in terms of human health. In 2015, the International Agency for Research on Cancer (IARC) and the European Food Safety Agency (EFSA) put forward two conflicting views on the carcinogenic hazard of GLY to humans. In 2016, it blocked a 15-year renewal proposal for the use of this molecule. In 2017, the European Chemical Agency (ECHA) classified GLY as non-carcinogenic. In the same year, on 12 December 2017, the European Commission renewed the approval of GLY but only for five years. It will be up for assessment again in 2022 [2,4]. Before considering

the decisions concerning the danger of this molecule, environments such as streams and groundwater are being impacted by the application of GLY, and European legislation established maximum residue limits, $0.1 \mu\text{g L}^{-1}$, in water for human consumption with the Directive 1998/83/EC [5]. In the USA, the maximum contaminant level of GLY is $700 \mu\text{g L}^{-1}$ [6].

Water is an essential element in the grain food chain (irrigation, food processing, food intake, etc.) and is a source of contamination with herbicides. Myers et al. (2016) [7] demonstrated that glyphosate-based herbicides had contaminated drinking water and agricultural systems. In 2013, the European Commission uploaded maximum residue levels (MRLs) for GLY in several crops according to European regulation EU No. 293/2013 [8]. The new European MRLs for rice are 0.1mg kg^{-1} , as the lower limit of analytical determination. On some cereals, such as rice, where minimal processing is desired, and consumption of the outer coat is recommended for associated health benefits [9], further studies should also be conducted for GLY in grains at different cleaning stages.

Several methods are available for the determination of this molecule and its metabolites in different kinds of matrices, such as apples [10], cereals [11], soybean [12,13], and surface and wastewater [14,15]. GLY and its metabolite have been determined by different analytical techniques, including GC [10,13,16,17], LC [13,15,16,18–20], hydrophilic interaction chromatography [21], capillary electrophoresis [22,23], Flow-Injection-MS/MS [24,25], GC-MS/MS, and LC-MS/MS [10,13,16,26–32], but the chemical characteristics, such as solubility and polarity, have been an obstacle with these techniques. Derivatization and purification of the molecules are methods for detection and chromatographic separation of the compounds in the matrices, but these actions are time-consuming and costly. The numerous sample preparation steps have increased interest in developing new methods to reduce the number of actions, from sample collection to analysis, and to reduce the cost.

Different authors have described GLY determination combined with AMPA and/or other phosphorus herbicides with HPLC–single quadrupole ICP-MS [14,33–36]. From 2019, in the literature, the number of articles showing applications of triple quadrupole with inductively coupled plasma and HPLC are few, and they show applications on aqueous samples. Lajin and Goessler (2019) [37] developed an HPLC-ICP-MS/MS speciation analysis method to determine this pesticide in tap, ground, and river water. Subsequently, Tiago et al. (2020) [38] also observed the exudation process of GLY molecules in water from hydroponic systems. In the same year, Pimenta et al. [39] compared two detection systems coupled to HPLC in quantifying GLY and AMPA in natural water samples from artesian wells, dams, water springs, and cisterns.

Applying ICP-MS/MS with HPLC improves the selectivity and the detection limits compared to the single quadrupole ICP-MS, due to its elimination of polyatomic interferences on m/z 31. The technology is based on two quadrupoles and a reaction cell; the first quadrupole could be used as a filter to select a specific m/z , and after the reaction with a specific gas, the second quadrupole could be applied as a selector. Even if the detection of phosphorous is highly compromised by its high ionization potential, the reaction cell can chemically resolve $^{31}\text{P}^+$ from polyatomic ions by its oxidation to $^{31}\text{P}^{16}\text{O}^+$ after preferential reaction with oxygen gas supplied to the cell by shifting analytes to new product ion mass [40].

Our attention is focused on the development and validation of ionic determination based on liquid chromatography with the inductively coupled plasma tandem mass of molecules of GLY in different types of rice (white and brown rice), based on rapidity and simplicity.

2. Results and Discussion

In order to develop the HPLC-ICP-MS/MS for the detection of GLY and AMPA, the first experiments were realized to select the optimal reaction gas flux, instrument parameters, appropriate mobile phase concentration, and column characteristics in the analysis of ultrapure water with standard addition. In order to study how it is possible to

quantify GLY in more complex solutions and an eventual matrix effect, the method was applied in groundwater spiked with GLY and AMPA (Figure 1).

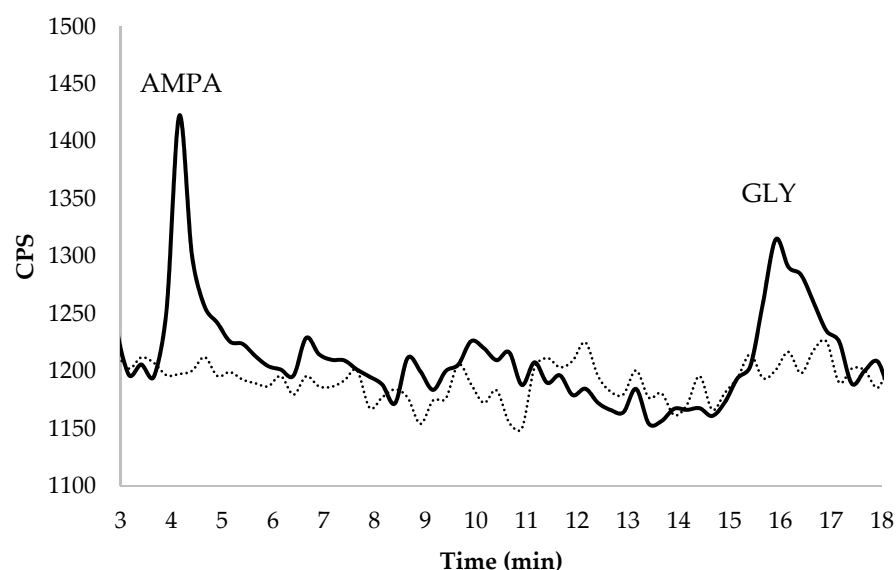


Figure 1. Chromatographic separation in spiked groundwater at $2.7 \mu\text{g GLY L}^{-1}$ and $1.8 \mu\text{g AMPA L}^{-1}$ of the target analytes ($RT_{\text{AMPA}} = 4.15 \text{ min}$; $RT_{\text{GLY}} = 16.5 \text{ min}$). The dashed line represents the chromatogram of unspiked water.

The LOQ, determined as the lowest fortification level for GLY ($1.8 \mu\text{g L}^{-1}$, with a mean recovery equal to 99% and an RSD equal to 2%), was $0.29 \mu\text{g GLY L}^{-1}$ in groundwater. Tiago et al. (2020) [38] published an LOQ value of $1.09 \mu\text{g GLY L}^{-1}$ in water samples. Lajin and Goessler (2019) [37] and Pimenta et al. (2020) [39] found $1.05 \mu\text{g GLY L}^{-1}$ and $8.2 \mu\text{g GLY L}^{-1}$, as detection limits in their respective method. These cited authors used the same type of analytical instrument, HPLC-ICP-MS/MS. One of the most important results in our early stage of method development was that our limit of quantification in groundwater was lower than the maximum residue limit, $0.1 \mu\text{g L}^{-1}$, established in the Directive 1998/83/EC [5] in water for human consumption.

Before applying this analytical method to rice, the matrix effect was studied to compare and understand when the quantification of our molecules in groundwater differed from the quantification of the same content in the mobile phase with this analytical technique. We noticed a matrix effect of 92% by comparing the calibration curve realized with the standard addition in groundwater to the same calibration curve constituted in the mobile phase, proving that there was a matrix suppression effect. The study of the matrix effect is a crucial point when starting to study more complex matrices. The same configuration was applied to discriminate compounds in a more complex matrix, such as a cereal. The composition of the mobile phase remained the same. Only the concentration of malonic acid was diluted to ensure that the GLY peak was as far away from the phosphate peak as possible. Of course, the tests on the groundwater were useful to find satisfactory parameters for both instrumental and chromatographic areas to start with an adequate background. An important parameter, which allowed improvement of the quantification, was the application of an anionic exchange chromatographic column with Poly (styrene-divinylbenzene) with a tri-methyl ammonium exchanger-like support material, the option to use up to 60° at a pH between 1 and 7.9, and a hardware inner diameter equal to 2.1 mm. The same type of chromatographic column with a greater inner diameter (4.6 mm) did not adequately quantify $0.05 \text{ mg GLY kg}^{-1}$ in WR, with a low recovery ($54\% \pm 11\%$).

The extraction solution was based on an aqueous composition. We changed the acid component, introducing different percentages of formic acid, because the retention time (RT) of GLY was not stable during the time of analysis with the application of only ultrapure

water. Unfortunately, the formic acid strongly altered the repeatability conditions of the analysis from one sample to another, especially the background line of the chromatogram. The choice of methanol was suggested in numerous articles that aimed to analyze GLY in food matrices. The European Reference Laboratory (EURL, EU Reference Laboratory) developed a generic method named the Quick Polar Pesticides Methods (QuPPE) [41] based on the extraction of polar pesticides from a sample with acidified methanol and liquid chromatography coupled to tandem mass spectrometry (LC-MS/MS). This was used to determine polar pesticides in different foods [42]. Some authors applied an aqueous extraction with methanol, such as Nagatomi et al. (2013) [27] on beer, barley tea (liquid), malt, and corn, or with acidified methanol, such as Herrera Lopez et al. (2019) [32] on grapes, orange, lettuce, oat, and soya beans. Those publications performed GLY determination by LC-MS/MS (Q-TRAP hybrid triple quadrupole) and LC-ESI-QTRAP-MS, respectively.

The validation parameters were the accuracy, precision, LOQ, LOD, and the matrix effect. An external calibration solution was employed to quantify the GLY.

The trueness in terms of the recovery percentage was calculated for the GLY at three fortification levels, 0.01, 0.03, and 0.05 mg kg⁻¹ from WR and 0.05, 0.14, and 0.27 mg kg⁻¹ from BR. The average recoveries ranged from 76 to 105%, with RSDr <15% for all spiking levels studied and for white and brown rice. The trueness and precision were within the specifications, because the obtained percentages were between 70 and 120%, and the RSD values were less than 20%, as recommended by the main legislations [43]. Table 1 shows the recoveries, standard deviation, and relative standard deviation for both types of rice. Figures 2 and 3 show the chromatogram of the enriched samples at the spiked level of 0.01 mg GLY kg⁻¹ in the WR (Caravaggio variety) and 0.1 mg GLY kg⁻¹ in the BR (Barone variety).

Table 1. Average recoveries (%), standard deviation (SD), and coefficient of variation (CV%) at different spiked levels of the extracted solution from white and brown rice. † Three replicates for each level. ‡ Five replicated samples at each fortification level.

Matrix	Spiked Levels (mg kg ⁻¹)	Recovery (%) †	Standard Deviation (SD)	Coefficient of Variation (CV%) ‡
White rice	0.01	76	8	11
	0.03	90	6	6
	0.05	105	3	3
Brown rice	0.05	94	8.3	8.8
	0.14	99	1.3	1.4
	0.27	97	2.6	2.7

2.1. Linearity and Matrix Effect

The linearity was evaluated for GLY in the extraction solution (aqueous solution with 30% of methanol) and in the extraction solution after application of the extraction solution on different rice matrices. The range concentration of the calibration curves applied to study the linearity in the WR solution, with standard additions, ranged from 0.003 to 0.055 mg GLY kg⁻¹ (Figure 4).

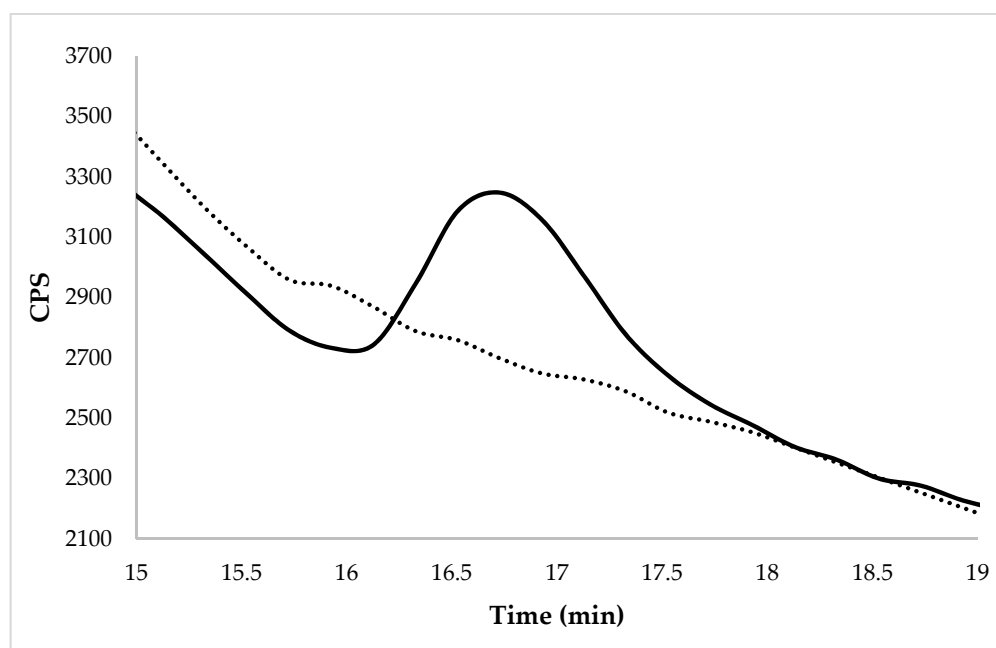


Figure 2. Chromatogram of WR (Caravaggio variety) at the spiked level of 0.01 mg kg^{-1} by HPLC-ICP-MS/MS. The dotted line represents the same un-enriched sample.

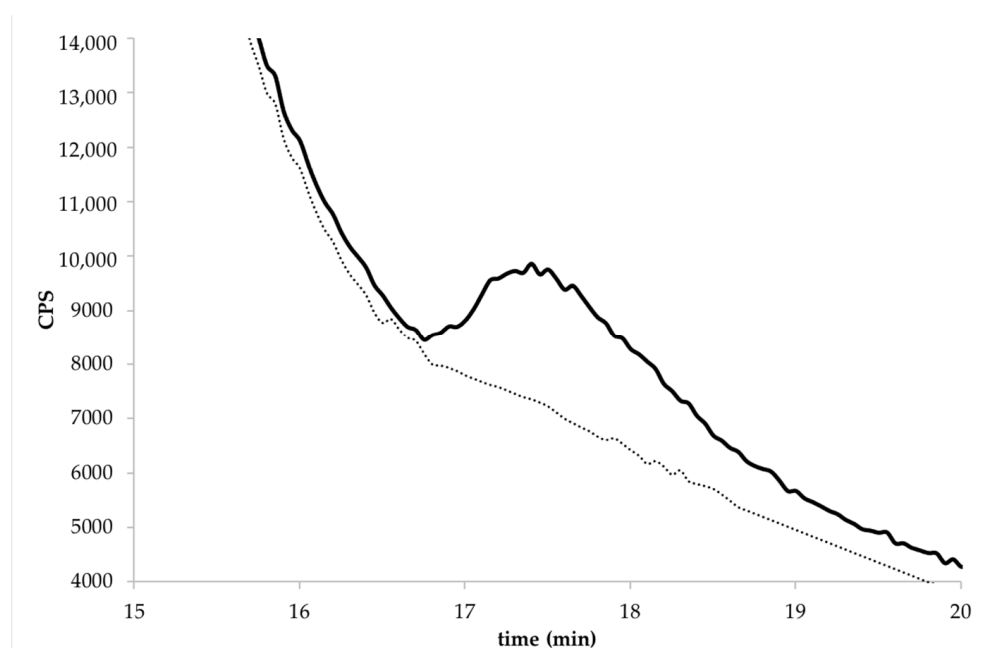


Figure 3. Chromatogram of BR (Barone variety) at the spiked level of 0.1 mg kg^{-1} by HPLC-ICP-MS/MS. The dotted line represents the same un-enriched sample.

The range concentration of the calibration curves applied to study the linearity in the BR solution, with standard additions, ranged from 0.11 to $0.55 \text{ mg GLY kg}^{-1}$ (Figure 5).

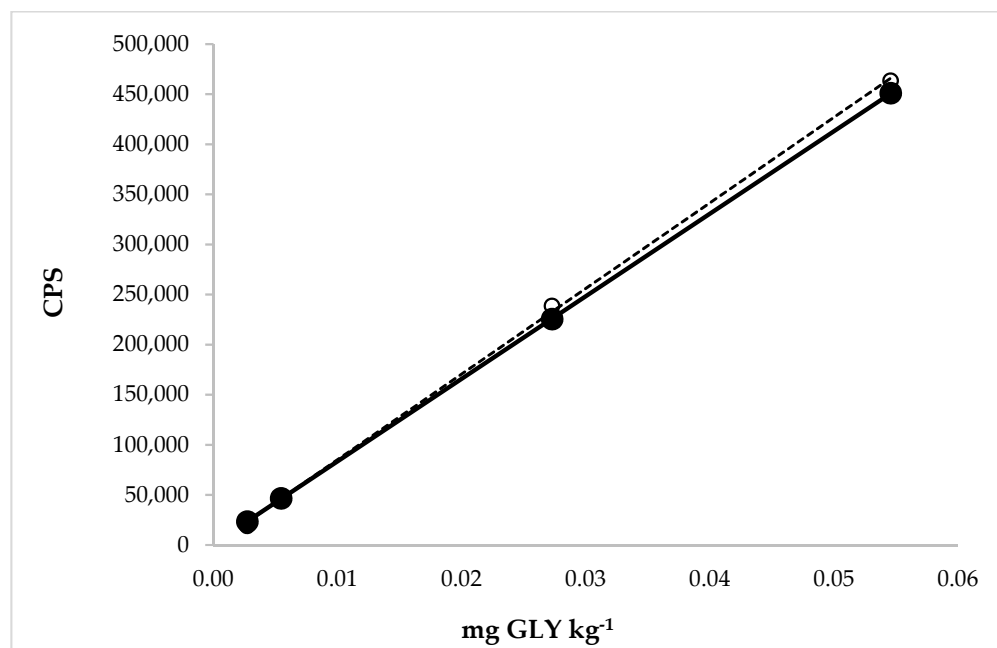


Figure 4. Comparison between the calibration curves of GLY in the extraction solution (dotted line) with linear equation $y = 8.543 \times 10^6x - 244.4$ and regression fit 0.999 and in the extraction solution with the matrix (white rice, solid line) with linear equation $y = 8.240 \times 10^6x + 1100$ and regression fit 1.000.

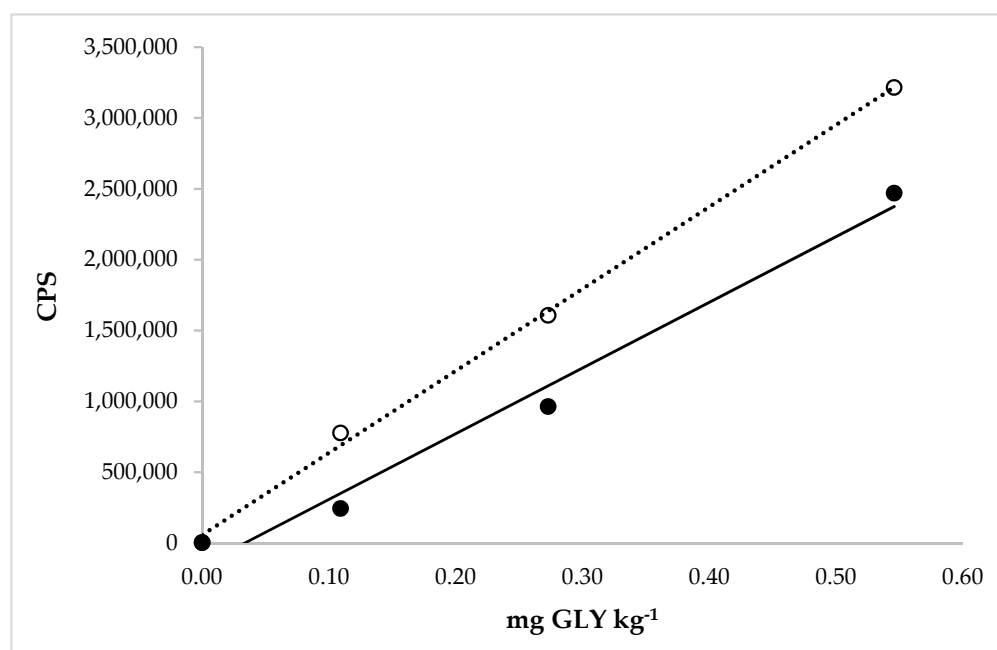


Figure 5. Comparison between the calibration curves of GLY in the extraction solution (dotted line) with linear equation $y = 5.789 \times 10^6x + 57,500$ and regression fit 0.998 and in the extraction solution with the matrix (brown rice, solid line) with linear equation $y = 4.636 \times 10^6x - 155,600$ and regression fit 0.982.

Good correlation coefficients were obtained for both types of calibration curves. The calibration curves demonstrated that the detector response was linear in the concentration range for both types of rice.

Moreover, in Figures 4 and 5, it was possible to observe and calculate the matrix effect in the WR and BR extraction solution on the GLY determination. The matrix effect depends

on the instrument used for the analysis, the type of matrix, the properties of the molecules, and the analyte concentration. Consequently, the matrix effect can vary for each analyte and matrix, which was exactly what we observed. The ratios between the slopes obtained from the analytical curve in the matrix and only in the extraction solution were expressed in percentages. The corresponding values were 96% and 80% for GLY quantification in WR and BR, respectively. The first value revealed a nonsignificant matrix effect in determining this molecule in the white rice extraction solution by HPLC-ICP-MS/MS. A significant matrix effect was recorded when the BR became the extraction object, showing a matrix suppression on its analyte. This value was very near to the MEs calculated in rice by Botero-Coy et al. (2013) [26] and Santilio et al. (2019) [31]. In particular, in this case, using a matrix-matched calibration line was necessary to obtain more accurate results and avoid the underestimation of the concentration of GLY in rice. Table 2 shows that the GLY in cereals was quantified with LC tandem MS in most articles, with the tendency to eliminate the derivatization for the application of internal standards marked isotopically and the use of a calibration line built into the matrix solution.

Table 2. Literature on the glyphosate determination in cereals, with details of the matrix effect.

Articles	Matrix	Instrument	Derivatization	Isotopic Internal Standard	Clean up	ME
Botero-Coy et al., (2013) [26]	rice	LC-MS/MS	/	ILIS-isotope labeled GLY	/	70–80%
Botero-Coy et al., (2013) [26]	maize	LC-MS/MS	/	ILIS-isotope labeled GLY	OASIS HLB	75%
Nagatomi et al., (2013) [27]	corn	LC-MS/MS	/	/	OASIS MCX + INERT SEK	only mention
Mol and van Dam 2014 [25]	wheat flour	FI-MS/MS ^c	/	yes	/	20 < ME < 40
Chamkasem and Harmon, (2016) [28]	corn	LC-MS/MS	/	yes	OASIS HLB	101%
Liao et al. (2018) [29]	rice, wheat, maize	LC-MS/MS	FMOC-Cl ^a	yes	SPE-C18 cartridge (60 mg)	/
Zoller et al., 2018 [30]	wheat, white flour	LC-MS/MS	/	yes	SPE cartridge	no indication of disturbing matrix effects
Gotti et al., 2019 [23]	wheat	CE-UV	FMOC-Cl ^a	Taurine ^b	SPE C18 cartridge SAX cartridge	no significant differences were found
Herrera López et al. (2019) [32]	oat	LC-MS/MS	/	ILIS-isotope labeled GLY	/	34%
Santilio et al., (2019) [31]	rice	LC-MS/MS	/	yes	/	77%
Santilio et al., (2019) [31]	maize	LC-MS/MS	/	yes	/	104%
Ciasca et al., 2020 [24]	wheat	FI-MS/MS ^c	/	yes	OASIS HLB	no effect
This study	white rice	HPLC-ICP-MS/MS	/	⁸⁹ Y	/	96%
This study	brown rice	HPLC-ICP-MS/MS	/	⁸⁹ Y	/	80%

^a 9-fluorenylmethylchloroformate. ^b internal standard for CE-UV. ^c flow injection tandem mass spectrometry.

2.2. LOD and LOQ

In the procedure for GLY extraction in WR, the LOD was 0.0027 mg kg⁻¹, and the LOQ was 0.0092 mg kg⁻¹ (the lowest fortification level, which achieved acceptable accuracy). In the procedure for GLY extraction in BR, the LOD was 0.0136 mg kg⁻¹, and the LOQ was 0.0456 mg kg⁻¹. These values obtained in our study were lower than 0.1 mg kg⁻¹, the lower limit of analytical determination, established in EU No. 293/2013 [8].

There are several published methods to detect GLY in cereals and several analytical techniques (Table 3). Our values, validated for WR analysis, were similar to those obtained by Santillo et al. (2019) [31] and Nagatomi et al. (2013) [27] in rice and maize and the last one in corn achieved by LC-MS/MS. While our limits found in the BR procedure were similar to those reported by Chamkasem and Harmon (2016) [28] in corn with LC-MS/MS application, they were lower than the other LODs mentioned by Mol and van Dam (2014) [25] in wheat flour by Flow injection-MS/MS, by Herrera López et al. (2019) [32] in oat by LC-MS/MS, and by Gotti et al. (2019) [23] in wheat by CE-UV.

Table 3. Literature on the glyphosate determination in cereals, with details on the LOD and LOQ.

Articles	Matrix	Instrument	Fortification Level of Matrix	LOD	LOQ
Botero-Coy et al., (2013) [26]	rice	LC-MS/MS	0.1 mg GLY kg ⁻¹	0.008 mg GLY kg ⁻¹	0.03 mg GLY kg ⁻¹
Botero-Coy et al., (2013) [26]	maize	LC-MS/MS	0.1 mg GLY kg ⁻¹	0.007 mg GLY kg ⁻¹	0.02 mg GLY kg ⁻¹
Nagatomi et al., (2013) [27]	corn-malt	LC-MS/MS	0.010 mg GLY kg ⁻¹		0.010 mg GLY kg ⁻¹
Mol and van Dam (2014) [25]	wheat flour	FI-MS/MS *	0.2 mg GLY kg ⁻¹		0.1 mg GLY kg ⁻¹
Chamkasem and Harmon, (2016) [28]	corn	LC-MS/MS	0.1 mg GLY kg ⁻¹	0.015 mg GLY kg ⁻¹	0.045 mg GLY kg ⁻¹
Liao et al. (2018) [29]	rice, wheat, maize	LC-MS/MS	0.005 mg GLY kg ⁻¹	0.0017 mg GLY kg ⁻¹	0.005 mg GLY kg ⁻¹
Zoller et al., 2018 [30]	wheat, white flour	LC-MS/MS	0.001 mg GLY kg ⁻¹	0.0003 mg GLY kg ⁻¹	0.001 mg GLY kg ⁻¹
Gotti et al., 2019 [23]	wheat	CE-UV			0.1 mg GLY kg ⁻¹
Herrera López et al. (2019) [32]	oat	LC-MS/MS	0.1 mg GLY kg ⁻¹		0.1 mg GLY kg ⁻¹
Santillo et al., (2019) [31]	rice	LC-MS/MS	0.01 mg GLY kg ⁻¹	0.002 mg GLY kg ⁻¹	0.01 mg GLY kg ⁻¹
Santillo et al., (2019) [31]	maize	LC-MS/MS	0.01 mg GLY kg ⁻¹	0.004 mg GLY kg ⁻¹	0.01 mg GLY kg ⁻¹
Ciasca et al., 2020 [24]	wheat	FI-MS/MS *			2.0 mg GLY kg ⁻¹
This study	white rice	HPLC-ICP-MS/MS		0.0027 mg GLY kg ⁻¹	0.0092 mg GLY kg ⁻¹
This study	brown rice	HPLC-ICP-MS/MS		0.0136 mg GLY kg ⁻¹	0.0456 mg GLY kg ⁻¹

* flow injection tandem mass spectrometry.

3. Material and Methods

3.1. Chemical and Reagents

Glyphosate, aminomethylphosphonic acid, and malonic acid were purchased from Merck (Darmstadt, Germany). Ammonia solution (30%) and methanol were purchased from Carlo Erba (Milan, Italy). Standard solutions of phosphorous (10,000 mg L⁻¹) were obtained from Inorganic Ventures (Lakewood, NJ, USA).

HPLC-grade water was obtained from an ultrapure water purification system (18.2 MΩ cm, ELGA PURELAB flex, Veolia Water Solutions and Technologies, Ontario, Canada).

3.2. Chromatographic and Mass Spectrometry Conditions

Separation was performed on a Hamilton PRP-X100 column (250 × 2.1 mm, 5 μm particle size), which was installed in an Agilent 1260 Bio-inert LC system, consisting of a G5654A Bio-inert pump and G5668A Bio Multisampler (Agilent Technologies, Santa Clara, CA, USA). The column was maintained at a controlled temperature for all analysis. The outlet of the LC column was connected directly to the ICP-MS nebulizer. The operating conditions for the LC are shown in Table 4. For the determination of GLY as P with ICP-MS/MS (8900, Agilent Technologies), O₂ was used as a reaction gas in the octopole reaction cell. The Q1 was set to transmit m/z 31, and the Q2 was selected to monitor m/z 47, so that the product ion ³¹P¹⁶O⁺ could be detected free of any interferences.

Table 4. The operating conditions of the anion exchange chromatography combined with inductively coupled mass spectrometry triple quadrupole (ICP-MS/MS).

HPLC Parameters	
HPLC	Agilent 1260 Bio-inert LC system
Column:	Hamilton, PRP-X100, 250 × 2.1 mm, 5 μm particle size
Column temperature:	50 °C
Mobile phase:	2 mM malonic acid (C ₃ H ₄ O ₄) at pH 5.3
Injection volume:	60 μL
Flow rate:	0.6 mL min ⁻¹
Acquisition time:	25 min
ICP-QQQ-MS	
Scan mode	MS/MS
RF applied power (W)	1550
Sampling depth (mm)	8.0
Lens type	s-lens
Octopole bias (V)	-5.0
Octopole RF (V)	180
KED (V)	0
Cell reaction gas	O ₂
Cell gas flow rate (%)	25
Cell entrance (V)	-50
Cell exit (V)	-70
Deflect (V)	6.0
Plate bias (V)	-60
Monitored mass (Q1)	31–60
Monitored mass (Q2)	47

3.3. Sample Preparations

Rice grain samples, divided between white rice samples (WR) and brown rice (BR), were ground with a blender. Then, 2.0 g of pulverized rice grains were extracted using 20 mL of ultrapure water with 30% of methanol in centrifuge tubes. The centrifuge tubes with samples were subjected to mechanical agitation for 60 min and ultrasounds for 15 min. Then, the samples were centrifuged at 2044 × g for 10 min. The supernatant was recovered, filtered through an 0.2 μm nylon filter, and inserted into HPLC vials.

3.4. Method Validation

The quantification of GLY in different types of rice was validated in terms of the linearity, trueness, precision, LOD, LOQ, linearity, and the matrix effect.

3.5. Accuracy and Precision

The trueness of the method was calculated as the percentage recovery of the GLY from the fortified WR spiked at 0.01, 0.03, and 0.05 mg kg⁻¹, expressed as GLY, and from the fortified BR samples spiked at 0.05, 0.14, 0.27, mg kg⁻¹, with the addition of appropriate volumes of the working standard solution.

Three replicates were prepared and analyzed for each level, according to the methods described.

The precision in the case of repeatability [relative standard deviation repeatability (RSDr)] was determined by analyzing five replicated samples at each fortification level, for both white and brown rice) on the same day.

3.6. LOD and LOQ

In order to determine the LOD for each analyte, 10 independent sample blanks fortified at 0.01 for WR and 0.05 mg kg⁻¹ for BR were injected, and it was expressed as the analyte concentration corresponding to three times the standard deviation.

The LOQ was determined as the lowest fortification level for glyphosate, for which there was acceptable accuracy in terms of trueness (mean recoveries in the range of 70–120%) and precision (RSDr < 20%).

3.7. Calibration Curve and Linearity

Calibration curves were made by plotting the mean peak area of 31P → 47 versus concentration, expressed as the molecule concentration. The linearity was evaluated by calculating the coefficient of determination (R²), intercept, and slope of the regression line at 0.5, 1, 5, and 10 µg GLY L⁻¹ in the WR extraction solution and 20, 50, and 100 µg GLY L⁻¹ in the BR extraction solution.

Each calibration solution was prepared by dilution of the GLY stock solution.

3.8. Matrix Effects

The response of the target analyte may be enhanced or suppressed compared to the solvent-based standards. To assess the matrix effect, we developed calibration curves in extraction solutions from two types of rice free of GLY. These effects were estimated by comparing an analyte's ICP-MS/MS response at any given concentration of the spiked post-extraction sample to a spiked concentration in the solvent (standard solutions). We calculated the matrix effect, as in Chamkasem et al. (2016) [28], applying this expression:

$$\text{ME} = (\text{slope of the calibration curve of the analyte in the sample matrix} / \text{slope of the calibration curve of the analyte in the solvent matrix}) \times 100.$$

A value of 100% means that no matrix effect was present. If the value was less than 100%, it means that there was matrix suppression, but if the value was more than 100%, it means that there was matrix enhancement.

4. Conclusions

There are several methods for GLY analysis in different types of cereals; most of these procedures are laborious and include various purification steps. Derivatization is not always applied, and the development of new methods to reduce the pretreatment steps in the analysis of polar molecules is of interest to the scientific community. The present study's method is faster than the other options, as it does not require pre-cleanup or derivatization, while it is good enough to detect and quantify GLY. These results were possible by using a metal-free liquid chromatography system, with the absence of iron and steel in the solvent delivery lines, and using an anionic column designated to separate the different chemical species containing phosphorus with 2.1 mm of diameter. ICP-MS/MS is a robust detector with a reaction cell that chemically resolves ³¹P⁺ quantification from polyatomic ions with oxygen gas. The matrix effect is well known as one of the critical problems for pesticide residue analysis, and the quantification procedures, performed using the calibration curves constructed in matrices as a reference and taking into account the response of the corresponding matrix, are a reliable way to avoid artefact results.

Author Contributions: Conceptualization, M.C.F. and G.M.B.; methodology, M.C.F. and L.L.; validation, M.C.F. and G.M.B.; formal analysis, M.C.F.; investigation, M.C.F.; resources, G.M.B. and L.L.; data curation, M.C.F.; writing—original draft preparation, M.C.F.; writing—review and editing,

M.C.F. and G.M.B.; visualization, L.L.; supervision, G.M.B.; project administration, G.M.B.; funding acquisition, G.M.B. and L.L. All authors have read and agreed to the published version of the manuscript.

Funding: This research received no external funding.

Conflicts of Interest: The authors declare no conflict of interest.

Sample Availability: Samples of the compounds are available from the authors.

References




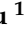




- European Commission. Regulation (EC) No. 1107/2009 of the European Parliament and of the Council of 21 October 2009 Concerning the Placing of Plant Protection Products on the Market and Repealing Council Directives 79/117/EEC and 91/414/EEC. *Off. J. Eur. Union* **2009**, *52*, L 309.
- Kudsk, P.; Mathiassen, S.K. Pesticide Regulation in the European Union and the Glyphosate Controversy. *Weed Sci.* **2020**, *68*, 214–222. [CrossRef]
- Bresnahan, G.A.; Manthey, F.A.; Howatt, K.A.; Chakraborty, M. Glyphosate Applied Preharvest Induces Shikimic Acid Accumulation in Hard Red Spring Wheat (*Triticum aestivum*). *J. Agric. Food Chem.* **2003**, *51*, 4004–4007. [CrossRef] [PubMed]
- European Commission. Commission Implementing Regulation (EU) 2017/2324 of 12 December 2017 Renewing the Approval of the Active Substance Glyphosate in Accordance with Regulation (EC) No. 1107/2009 of the European Parliament and of the Council Concerning the Placing of Plant Protection Products on the Market, and Amending the Annex to Commission Implementing Regulation (EU) No. 540/2011. *Off. J. Eur. Union* **2017**, *60*, L 333.
- Council of the European Union. Council Directive 98/83/EC of 3 November 1998 on the Quality of Water Intended for Human Consumption. *Off. J. Eur. Union* **1998**, *41*, L 330.
- EPA. *National Primary Drinking Water Regulations*; EPA: Washington, DC, USA, 2020.
- Myers, J.P.; Antoniou, M.N.; Blumberg, B.; Carroll, L.; Colborn, T.; Everett, L.G.; Hansen, M.; Landrigan, P.J.; Lanphear, B.P.; Mesnage, R.; et al. Concerns Over use of Glyphosate-Based Herbicides and Risks Associated with Exposures: A Consensus Statement. *Environ. Health* **2016**, *15*, 19. [CrossRef] [PubMed]
- European Commission. Commission Regulation (EU) No. 293/2013 of 20 March 2013 Amending Annexes II and III to Regulation (EC) No. 396/2005 of the European Parliament and of the Council as Regards Maximum Residue Levels for Emamectin Benzoate, Etofenprox, Etoxazole, Flutriafol, Glyphosate, Phosmet, Pyraclostrobin, Spinosad and Spirotetramat in Or on Certain Products Text with EEA Relevance. *Off. J. Eur. Union* **2013**, *56*, L 96.
- Awika, J.M.; Rose, D.J.; Simsek, S. Complementary Effects of Cereal and Pulse Polyphenols and Dietary Fiber on Chronic Inflammation and Gut Health. *Food Funct.* **2018**, *9*, 1389–1409. [CrossRef]
- Qian, K.; Tang, T.; Shi, T.; Li, P.; Li, J.; Cao, Y. Solid-Phase Extraction and Residue Determination of Glyphosate in Apple by Ion-Pairing Reverse-Phase Liquid Chromatography with Pre-Column Derivatization. *J. Sep. Sci.* **2009**, *32*, 2394–2400. [CrossRef]
- Krueve, A.; Auling, R.; Herodes, K.; Leito, I. Study of Liquid Chromatography/Electrospray Ionization Mass Spectrometry Matrix Effect on the Example of Glyphosate Analysis from Cereals. *Rapid Commun. Mass Spectrom.* **2011**, *25*, 3252–3258. [CrossRef]
- Martins-Júnior, H.A.; Lebre, D.T.; Wang, A.Y.; Pires, M.A.F.; Bustillos, O.V. An Alternative and Fast Method for Determination of Glyphosate and Aminomethylphosphonic Acid (AMPA) Residues in Soybean using Liquid Chromatography Coupled with Tandem Mass Spectrometry. *Rapid Commun. Mass Spectrom.* **2009**, *23*, 1029–1034. [CrossRef] [PubMed]
- Ehling, S.; Reddy, T.M. Analysis of Glyphosate and Aminomethylphosphonic Acid in Nutritional Ingredients and Milk by Derivatization with Fluorenylmethoxycarbonyl Chloride and Liquid Chromatography–Mass Spectrometry. *J. Agric. Food Chem.* **2015**, *63*, 10562–10568. [CrossRef] [PubMed]
- Popp, M.; Hann, S.; Mentler, A.; Fuerhacker, M.; Stinger, G.; Koellensperger, G. Determination of Glyphosate and AMPA in Surface and Waste Water using High-Performance Ion Chromatography Coupled to Inductively Coupled Plasma Dynamic Reaction Cell Mass Spectrometry (HPIC–ICP–DRC–MS). *Anal. Bioanal. Chem.* **2008**, *391*, 695–699. [CrossRef]
- Ibáñez, M.; Pozo, Ó.J.; Sancho, J.V.; López, F.J.; Hernández, F. Re-Evaluation of Glyphosate Determination in Water by Liquid Chromatography Coupled to Electrospray Tandem Mass Spectrometry. *J. Chromatogr. A* **2006**, *1134*, 51–55. [CrossRef] [PubMed]
- Steinborn, A.; Alder, L.; Michalski, B.; Zomer, P.; Bendig, P.; Martinez, S.A.; Mol, H.G.J.; Class, T.J.; Costa Pinheiro, N. Determination of Glyphosate Levels in Breast Milk Samples from Germany by LC-MS/MS and GC-MS/MS. *J. Agric. Food Chem.* **2016**, *64*, 1414–1421. [CrossRef] [PubMed]
- Motojyuku, M.; Saito, T.; Akieda, K.; Otsuka, H.; Yamamoto, I.; Inokuchi, S. Determination of Glyphosate, Glyphosate Metabolites, and Glufosinate in Human Serum by Gas Chromatography–mass Spectrometry. *J. Chromatogr. B Anal. Technol. Biomed. Life Sci.* **2008**, *875*, 509–514. [CrossRef] [PubMed]
- Ridlen, J.S.; Klopff, G.J.; Nieman, T.A. Determination of Glyphosate and Related Compounds using HPLC with Tris(2,2'-Bipyridyl)Ruthenium(II) Electrogenerated Chemiluminescence Detection. *Anal. Chim. Acta* **1997**, *341*, 195–204. [CrossRef]
- Hanke, L.; Singer, H.; Hollender, J. Ultratrace-Level Determination of Glyphosate, Aminomethylphosphonic Acid and Glufosinate in Natural Waters by Solid-Phase Extraction Followed by Liquid Chromatography-Tandem Mass Spectrometry: Performance Tuning of Derivatization, Enrichment and Detection. *Anal. Bioanal. Chem.* **2008**, *391*, 2265–2276. [CrossRef]

20. Jensen, P.K.; Wujcik, C.E.; McGuire, M.K.; McGuire, M.A. Validation of Reliable and Selective Methods for Direct Determination of Glyphosate and Aminomethylphosphonic Acid in Milk and Urine using LC-MS/MS. *J. Environ. Sci. Health Part B Pestic. Food Contam. Agric. Wastes* **2016**, *51*, 254–259. [CrossRef]
21. Coutinho, C.F.B.; Coutinho, L.F.M.; Mazo, L.H.; Nixdorf, S.L.; Camara, C.A.P.; Lanças, F.M. Direct Determination of Glyphosate using Hydrophilic Interaction Chromatography with Coulometric Detection at Copper Microelectrode. *Anal. Chim. Acta* **2007**, *592*, 30–35. [CrossRef]
22. Pinto, E.; Soares, A.G.; Ferreira, I.M.P.L.V.O. Quantitative Analysis of Glyphosate, Glufosinate and AMPA in Irrigation Water by in Situ Derivatization–dispersive Liquid–liquid Microextraction Combined with UPLC-MS/MS. *Anal. Methods* **2018**, *10*, 554–561. [CrossRef]
23. Gotti, R.; Fiori, J.; Bosi, S.; Dinelli, G. Field-Amplified Sample Injection and Sweeping Micellar Electrokinetic Chromatography in Analysis of Glyphosate and Aminomethylphosphonic Acid in Wheat. *J. Chromatogr. A* **2019**, *1601*, 357–364. [CrossRef] [PubMed]
24. Ciasca, B.; Pecorelli, I.; Lepore, L.; Paoloni, A.; Catucci, L.; Pascale, M.; Lattanzio, V.M.T. Rapid and Reliable Detection of Glyphosate in Pome Fruits, Berries, Pulses and Cereals by Flow Injection–Mass Spectrometry. *Food Chem.* **2020**, *310*, 125813. [CrossRef] [PubMed]
25. Mol, J.G.J.; van Dam, R.C.J. Rapid Detection of Pesticides Not Amenable to Multi-Residue Methods by Flow Injection-Tandem Mass Spectrometry. *Anal. Bioanal. Chem.* **2014**, *406*, 6817–6825. [CrossRef] [PubMed]
26. Botero-Coy, A.M.; Ibáñez, M.; Sancho, J.V.; Hernández, F. Improvements in the Analytical Methodology for the Residue Determination of the Herbicide Glyphosate in Soils by Liquid Chromatography Coupled to Mass Spectrometry. *J. Chromatogr. A* **2013**, *1292*, 132–141. [CrossRef]
27. Nagatomi, Y.; Yoshioka, T.; Yanagisawa, M.; Uyama, A.; Mochizuki, N. Simultaneous LC-MS/MS Analysis of Glyphosate, Glufosinate, and their Metabolic Products in Beer, Barley Tea, and their Ingredients. *Biosci. Biotechnol. Biochem.* **2013**, *77*, 2218–2221. [CrossRef] [PubMed]
28. Chamkasem, N.; Harmon, T. Direct Determination of Glyphosate, Glufosinate, and AMPA in Soybean and Corn by Liquid Chromatography/Tandem Mass Spectrometry. *Anal. Bioanal. Chem.* **2016**, *408*, 4995–5004. [CrossRef]
29. Liao, Y.; Berthion, J.; Colet, I.; Merlo, M.; Nougadère, A.; Hu, R. Validation and Application of Analytical Method for Glyphosate and Glufosinate in Foods by Liquid Chromatography-Tandem Mass Spectrometry. *J. Chromatogr. A* **2018**, *1549*, 31–38. [CrossRef]
30. Zoller, O.; Rhyn, P.; Rupp, H.; Zarn, J.A.; Geiser, C. Glyphosate Residues in Swiss Market Foods: Monitoring and Risk Evaluation. *Food Addit. Contam. Part B Surveill.* **2017**, *11*, 83–91. [CrossRef]
31. Santilio, A.; Pompili, C.; Giambenedetti, A. Determination of Glyphosate Residue in Maize and Rice using a Fast and Easy Method Involving Liquid Chromatography-Mass Spectrometry (LC/MS/MS). *J. Environ. Sci. Health Part B Pestic. Food Contam. Agric. Wastes* **2019**, *54*, 205–210. [CrossRef]
32. Herrera López, S.; Scholten, J.; Kiedrowska, B.; de Kok, A. Method Validation and Application of a Selective Multiresidue Analysis of Highly Polar Pesticides in Food Matrices using Hydrophilic Interaction Liquid Chromatography and Mass Spectrometry. *J. Chromatogr. A* **2019**, *1594*, 93–104. [CrossRef] [PubMed]
33. Guo, Z.; Cai, Q.; Yang, Z. Ion Chromatography/Inductively Coupled Plasma Mass Spectrometry for Simultaneous Determination of Glyphosate, Glufosinate, Fosamine and Ethephon at Nanogram Levels in Water. *Rapid Commun. Mass Spectrom.* **2007**, *21*, 1606–1612. [CrossRef] [PubMed]
34. Guo, Z.; Cai, Q.; Yang, Z. Determination of Glyphosate and Phosphate in Water by Ion Chromatography—Inductively Coupled Plasma Mass Spectrometry Detection. *J. Chromatogr. A* **2005**, *1100*, 160–167. [CrossRef]
35. Sadi, B.B.M.; Vonderheide, A.P.; Caruso, J.A. Analysis of Phosphorus Herbicides by Ion-Pairing Reversed-Phase Liquid Chromatography Coupled to Inductively Coupled Plasma Mass Spectrometry with Octapole Reaction Cell. *J. Chromatogr. A* **2004**, *1050*, 95–101. [CrossRef]
36. Kazui, Y.; Seto, Y.; Inoue, H. Phosphorus-Specific Determination of Glyphosate, Glufosinate, and their Hydrolysis Products in Biological Samples by Liquid Chromatography–inductively Coupled Plasma–mass Spectrometry. *Forensic Toxicol.* **2014**, *32*, 317–322. [CrossRef]
37. Lajin, B.; Goessler, W. Direct Speciation Analysis of Organophosphorus Environmental Pollutants in Water by HPLC-ICPMS/MS. *Talanta* **2019**, *196*, 357–361. [CrossRef]
38. Tiago, J.P.F.; Sicupira, L.C.; Barros, R.E.; de Pinho, G.P.; Silvério, F.O. Simultaneous and Direct Determination of Glyphosate and AMPA in Water Samples from the Hydroponic Cultivation of Eucalyptus Seedlings using HPLC-ICP-MS/MS. *J. Environ. Sci. Health Part B Pestic. Food Contam. Agric. Wastes* **2020**, *55*, 558–565. [CrossRef]
39. Pimenta, E.; da Silva, F.; Barbosa, É.; Cacique, A.; Cassimiro, D.; de Pinho, G.; Silvério, F. Quantification of Glyphosate and AMPA by HPLC-ICP-MS/MS and HPLC-DAD: A Comparative Study. *J. Braz. Chem. Soc.* **2020**, *31*, 298–304. [CrossRef]
40. Fernández, S.D.; Sugishama, N.; Encinar, J.R.; Sanz-Medel, A. Triple Quad ICPMS (ICPQQQ) as a New Tool for Absolute Quantitative Proteomics and Phosphoproteomics. *Anal. Chem.* **2012**, *84*, 5851–5857. [CrossRef]
41. Anastassiades, M.; Kolberg, D.I.; Benkenstein, A.; Eichhorn, E.; Zechmann, S.; Mack, D.; Wildgrube, C.; Sigalov, I.; Dörk, D.; Barth, A. *Quick Method for the Analysis of Numerous Highly Polar Pesticides in Foods of Plant Origin Via LC-MS/MS Involving Simultaneous Extraction with Methanol (QuPPE-Method)*; EU Reference Laboratory for Pesticides Requiring Single Residue Methods (EURL-SRM); CVUA: Stuttgart, Germany, 2015.

42. Adams, S.; Guest, J.; Dickinson, M.; Fussell, R.J.; Beck, J.; Schoutsen, F. Development and Validation of Ion Chromatography–Tandem Mass Spectrometry-Based Method for the Multiresidue Determination of Polar Ionic Pesticides in Food. *J. Agric. Food Chem.* **2017**, *65*, 7294–7304. [CrossRef]
43. Thompson, M.; Ellison, S.L.R.; Wood, R. Harmonized Guidelines for Single-Laboratory Validation of Methods of Analysis (IUPAC Technical Report). *Pure Appl. Chem.* **2002**, *74*, 835–855. [CrossRef]

Article

Thorough Investigation of the Phenolic Profile of Reputable Greek Honey Varieties: Varietal Discrimination and Floral Markers Identification Using Liquid Chromatography–High-Resolution Mass Spectrometry

Georgios A. Koulis ^{1,2}, Aristeidis S. Tsagkaris ³, Panagiota A. Katsianou ¹, Panagiotis-Loukas P. Gialouris ^{1,2}, Ioannis Martakos ^{1,2}, Fotis Stergiou ^{1,4}, Alberto Fiore ⁴, Eleni I. Panagopoulou ¹, Sofia Karabournioti ⁵, Carsten Baessmann ⁶, Noud van der Borg ⁶, Marilena E. Dasenaki ^{2,*}, Charalampos Proestos ² and Nikolaos S. Thomaidis ^{1,*}

Citation: Koulis, G.A.; Tsagkaris, A.S.; Katsianou, P.A.; Gialouris, P.-L.P.; Martakos, I.; Stergiou, F.; Fiore, A.; Panagopoulou, E.I.; Karabournioti, S.; Baessmann, C.; et al. Thorough Investigation of the Phenolic Profile of Reputable Greek Honey Varieties: Varietal Discrimination and Floral Markers Identification Using Liquid Chromatography–High-Resolution Mass Spectrometry. *Molecules* **2022**, *27*, 4444. <https://doi.org/10.3390/molecules27144444>

Academic Editor: Mirella Nardini

Received: 8 June 2022

Accepted: 5 July 2022

Published: 11 July 2022

Publisher's Note: MDPI stays neutral with regard to jurisdictional claims in published maps and institutional affiliations.



Copyright: © 2022 by the authors. Licensee MDPI, Basel, Switzerland. This article is an open access article distributed under the terms and conditions of the Creative Commons Attribution (CC BY) license (<https://creativecommons.org/licenses/by/4.0/>).

- ¹ Analytical Chemistry Laboratory, Chemistry Department, National and Kapodistrian University of Athens, Panepistimiopolis Zographou, 15771 Athens, Greece; georgekoulis@chem.uoa.gr (G.A.K.); katsianp@chem.uoa.gr (P.A.K.); pgialour@chem.uoa.gr (P.-L.P.G.); johnmrtk@chem.uoa.gr (I.M.); fotis.stergiou@outlook.com (F.S.); elenapanag@chem.uoa.gr (E.I.P.)
- ² Food Chemistry Laboratory, Department of Chemistry, National and Kapodistrian University of Athens, Panepistimiopolis Zographou, 15771 Athens, Greece; harpro@chem.uoa.gr
- ³ Department of Food Analysis and Nutrition, Faculty of Food and Biochemical Technology, University of Chemistry and Technology Prague, Technická 5, 16628 Prague, Czech Republic; tsagkara@vscht.cz
- ⁴ Division of Engineering and Food Science, School of Applied Science, Abertay University, Bell Street, Dundee DD1 1HG, UK; a.fiore@abertay.ac.uk
- ⁵ Attiki Honey SA, Kryoneri Attikis, 14568 Athens, Greece; skar@attiki-pittas.gr
- ⁶ Bruker Daltonik GmbH, Fahrenheitstraße 4, 28359 Bremen, Germany; carsten.baessmann@bruker.com (C.B.); noud.van_der_borg@bruker.com (N.v.d.B.)
- * Correspondence: mdasenaki@chem.uoa.gr (M.E.D.); ntho@chem.uoa.gr (N.S.T.); Tel.: +30-210-727-4326 (M.E.D.); +30-210-727-4430 (N.S.T.)

Abstract: Honey is a highly consumed commodity due to its potential health benefits upon certain consumption, resulting in a high market price. This fact indicates the need to protect honey from fraudulent acts by delivering comprehensive analytical methodologies. In this study, targeted, suspect and non-targeted metabolomic workflows were applied to identify botanical origin markers of Greek honey. Blossom honey samples ($n = 62$) and the unifloral fir ($n = 10$), oak ($n = 24$), pine ($n = 39$) and thyme ($n = 34$) honeys were analyzed using an ultra-high-performance liquid chromatography hybrid quadrupole time-of-flight mass spectrometry (UHPLC-q-TOF-MS) system. Several potential authenticity markers were revealed from the application of different metabolomic workflows. In detail, based on quantitative targeted analysis, three blossom honey markers were found, namely, galangin, pinocembrin and chrysin, while gallic acid concentration was found to be significantly higher in oak honey. Using suspect screening workflow, 12 additional bioactive compounds were identified and semi-quantified, achieving comprehensive metabolomic honey characterization. Lastly, by combining non-targeted screening with advanced chemometrics, it was possible to discriminate thyme from blossom honey and develop binary discriminatory models with high predictive power. In conclusion, a holistic approach to assessing the botanical origin of Greek honey is presented, highlighting the complementarity of the three applied metabolomic approaches.

Keywords: honey; phenolic compounds; metabolomics; Greek honey; chemometrics; botanical origin; authenticity; discrimination; high-resolution mass spectrometry

1. Introduction

Honey is a natural sweetener widely consumed worldwide due to its potential health-promoting benefits, such as immune-modulatory, anti-proliferative and anti-inflammatory

effects [1], upon certain dietary consumption. However, considering the great nutritional value of honey in combination with its high price and significant market share, it is a commodity highly susceptible to fraudulent practices. Botanical or geographical origin mislabeling, the addition of low-cost syrups and dilution of honey with water are among the most common fraudulent acts [2]. Thus, it is necessary to develop analytical methods to assure honey quality and protect consumers and market sustainability.

A plethora of analytical techniques has been used to assess honey authenticity. As we comprehensively discussed in our recent publication [3], chromatographic and spectroscopic techniques, alongside conventional methods measuring physicochemical properties, such as electrical conductivity or acidity, are commonly applied in the field. Although spectroscopic methods usually provide non-destructive analysis and conventional methods are widely available due to their low-cost, combining chromatography with mass spectrometry (MS) permits the detection of various analyte classes, e.g., pesticide residues (to check bio-production) [4], sugars (to evaluate quality characteristics towards established regulation, Directive 2001/110/EC) [5] or phenolic compounds (to estimate geographical, botanical or entomological origin) [6,7]. Importantly, phenolic compounds determination in honey authenticity studies can have a binary character, in detail, both as characteristic markers as well as to evaluate the nutritional value of honey due to their bioactivity [8]. Thus, phenolic compound fingerprinting can be used as a tool to investigate both the origin and potential bioactivity of reputable honey types, such as honey produced in Greece.

Greek honey is generally considered of high quality due to its organoleptic characteristics [9], biological activity [10] and the biodiversity of the Greek countryside, which includes many endemic plant species [11]. In addition, Greece plays a decisive role in EU honey production and exportation. Indicatively, Greece exported 856 tons of honey to third countries outside the EU from January 2020 to August 2020, a 79% increase compared to its total exports during the corresponding period in 2019. Moreover, Greece had the most hives per beekeeper (147 hives per beekeeper, while the EU average is 21), indicating honey production's impact on the national economy and agriculture (https://ec.europa.eu/info/sites/default/files/food-farming-fisheries/animals_and_animal_products/documents/market-presentation-honey_spring2020_en.pdf, last accessed 11 May 2022).

Considering the discussed facts, we analyzed a total of 169 honey samples with different botanical origins, namely blossom ($n = 62$) and the unifloral fir ($n = 10$), oak ($n = 24$), pine ($n = 39$) and thyme ($n = 34$) honeys to reveal botanical origin markers of Greek honey through their phenolic compound content. To achieve that, our recently developed ultra-high-performance liquid chromatography hybrid quadrupole time-of-flight mass spectrometry (UHPLC-q-TOF-MS) method [12] was verified, and the analyte target list was updated, including a total of 24 target phenolic compounds. Besides targeted metabolomics, suspect and non-targeted workflows were also utilized. A more comprehensive estimation of the phenolic compound concentration of Greek unifloral honey was accomplished through suspect screening and semi-quantification, while non-target screening provided a diagnostic tool for honey authenticity assessment. All in all, the present study documents the phenolic profile of Greek honey and showcases metabolomic approaches to identify its botanical origin.

2. Results and Discussion

2.1. Target Screening

The developed target list was used to screen and quantify the content of phenolic compounds in all the tested honey samples (Table 1). Whisker's plots were prepared using the acquired concentrations for all the analytes in every honey matrix to depict the monitored distribution through its quartiles (Figure 1 and Figures S1–S4 in the Supplementary Materials). Importantly, analysis of variance (ANOVA) revealed statistically significant differences ($\alpha = 0.05$) among varieties for the acquired concentrations of all the target analytes, except eriodictyol, luteolin, quercetin, genistein, rosmarinic acid, vanillin

and vanillic acid. Actually, 15 out of 17 analytes showed significant differences with a p -Value <0.001 , whilst p -coumaric acid was <0.01 and vanillic acid <0.05 ($\alpha = 0.05$, in all cases). Following ANOVA, a Tukey's multiple comparison test was performed, revealing four potential botanical origin markers, namely galangin, pinocembrin and chrysin for blossom honey and gallic acid for oak honey (Figure 1). In terms of the blossom honey, a p -Value <0.001 was attained in the case of galangin (Figure 1a), pinocembrin (Figure 1c) and chrysin (Figure 1d) against the 4 other botanical origins, while the other groups showed non-significant differences among them. The same pattern was monitored for gallic acid in the case of oak honey (Figure 1b). Galangin, pinocembrin and chrysin have been previously reported in high concentrations in blossom honey (also known as polyfloral honey, blossom honey is a mixture of nectar collected by various plants) and were proposed as discrimination markers of Serbian honey [13]. It is important to mention that these three flavones originate from propolis in the case of European honeys [13]. In addition, all three analytes were identified among the main phenolic compounds in heather blossom honey from Portugal [14] and citrus blossom honey from Spain [15], all Mediterranean countries with similar climatological conditions to Greece. In the case of gallic acid in oak honey, our results are in line with previous studies identifying gallic acid among the main compounds of Turkish oak honey [16]. Actually, oak honey has demonstrated bioactivity inhibiting different enzymes, namely urease and xanthine oxidase [17] as well as hyaluronidase [18]. In fact, in these cases, gallic acid is considered responsible for enzyme inhibition due to its high concentration in oak honey. All in all, it was revealed that by using the developed target list, it was feasible to acquire an indication of which analytes are statistically different per botanical origin, indicating their potential as botanical markers. Of course, to verify this argument, it would be necessary to analyze more samples collected during different years.

Table 1. Targeted screening results expressed as median concentration (mg kg^{-1}) of phenolic compounds in the 5 different honey matrices.

Compound	LOD	Blossom, $n = 62$	Fir, $n = 10$	Oak, $n = 24$	Pine, $n = 39$	Thyme, $n = 34$
2,5 dihydroxybenzoic acid	0.070	0.21	0.71	0.82	0.92	0.11
3,4 dihydroxybenzoic acid	0.083	1.0	3.4	10	4.7	0.50
4 hydroxybenzoic acid	0.098	1.5	1.3	1.0	1.8	0.35
apigenin	0.082	0.15	0.10	0.12	0.11	0.17
caffeic acid	0.065	0.77	0.21	0.38	0.49	0.080
chrysin	0.032	3.6	0.35	0.72	0.65	0.061
cinnamic acid	0.043	0.26	0.17	0.24	0.13	0.022
eriodictyol	0.048	0.098	<LOD	0.10	0.28	0.10
ferulic acid	0.030	0.58	0.21	0.27	0.37	0.045
galangin	0.070	1.2	0.15	0.27	0.21	0.12
gallic acid	0.067	0.092	0.37	1.8	0.37	<LOD
genistein	0.081	0.089	<LOD	0.098	0.10	0.11
luteolin	0.079	0.14	0.34	0.15	0.16	0.14
naringenin	0.050	1.4	0.25	0.59	0.60	0.073
p -coumaric acid	0.16	0.60	0.59	0.72	0.94	0.27
pinobanksin	0.055	1.4	0.25	0.57	0.59	0.069
pinocembrin	0.076	2.1	0.15	0.40	0.44	<LOD
quercetin	0.067	0.15	0.49	0.20	0.18	0.15

Table 1. Cont.

Compound	LOD	Blossom, <i>n</i> = 62	Fir, <i>n</i> = 10	Oak, <i>n</i> = 24	Pine, <i>n</i> = 39	Thyme, <i>n</i> = 34
rosmarinic acid	0.084	<LOD	0.14	<LOD	<LOD	0.12
salicylic acid	0.33	0.76	0.81	1.6	1.3	0.34
syringic acid	0.081	<LOD	<LOD	0.25	0.36	<LOD
taxifolin	0.084	0.18	0.32	0.20	0.41	0.23
vanillic acid	0.12	0.12	0.15	<LOD	0.12	<LOD
vanillin	0.037	0.50	0.16	0.27	0.59	0.098

LOD: limit of detection.

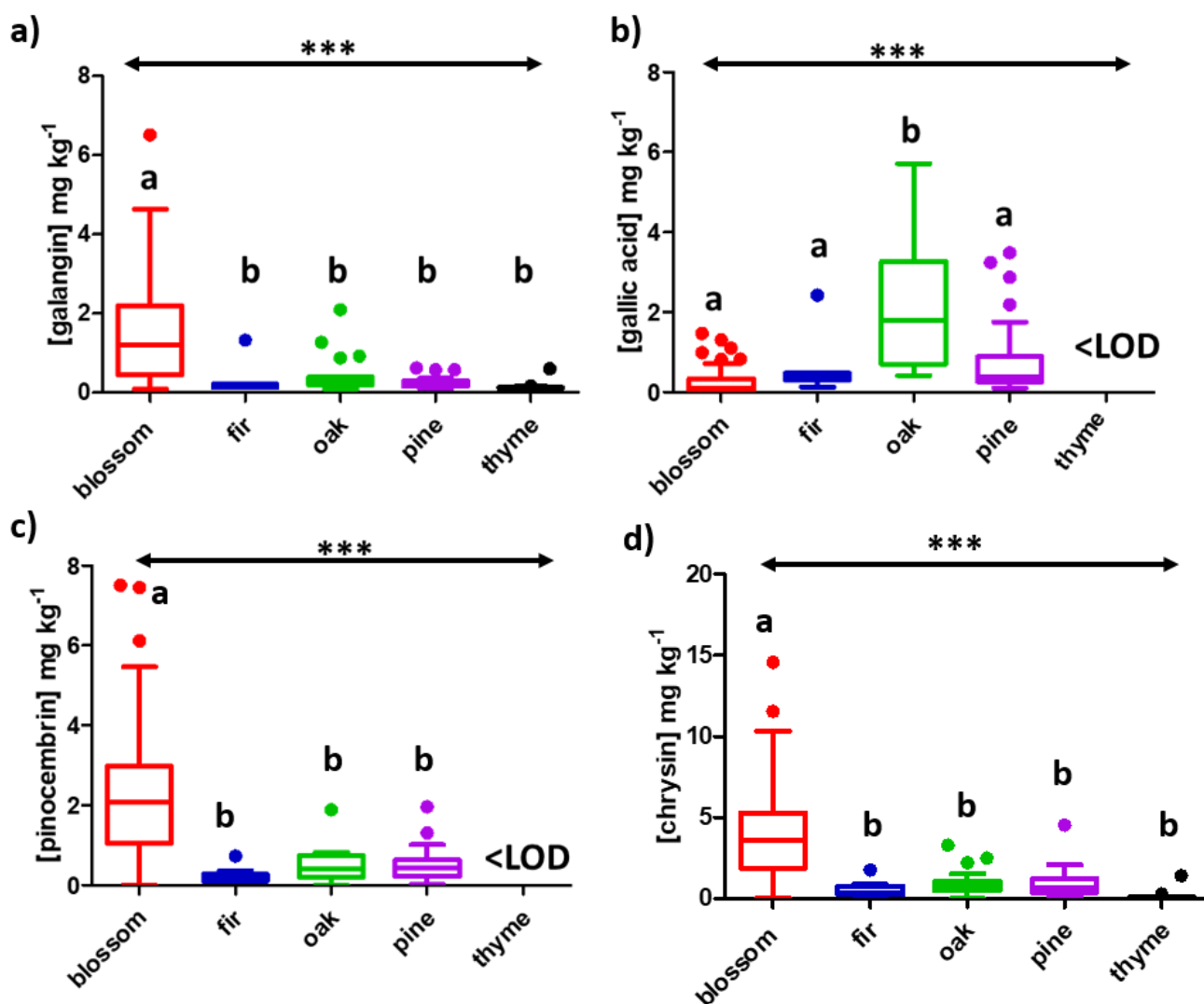


Figure 1. Whisker's plot for (a) galangin, (b) gallic acid, (c) pinocembrin and (d) chrysin performed at the 95% confidence level; ***, *p*-Value < 0.001. Tukey's multiple comparison test was also performed, and different letters indicate significant differences among the groups.

2.2. Suspect Screening

Through suspect screening, 12 phenolic compounds, namely 2-trans,4-trans-abscisic acid, 2-cis,4-trans-abscisic acid, acacetin, dehydrovomifoliol, homogentisic acid, isokaempferide, isorhamnetin, lumichrome, methyl syringate, phenyllactic acid, sakuranetin and tectochrysin,

were identified and semi-quantified in Greek honey varieties. Table S1 summarizes the occurrence of all identified analytes in the analyzed honey varieties.

All identified compounds showed high mass accuracy, below 2 mDa, isotoping fitting below 50 mSigma and retention time (tR) tolerance below 0.2 min. Especially for isokaempferide and tectochrysin, which were not included in our previous suspect screening workflow [12], their identification was accomplished by comparing experimental MS/MS fragments with MS/MS spectra found in the mass spectral library MassBank of North America. Additionally, differences between the experimental and predicted tR were considered. The detailed identification data for isokaempferide is presented below (Figure 2), while for tectochrysin, it can be found in Figure S5 of the Supplementary Materials.

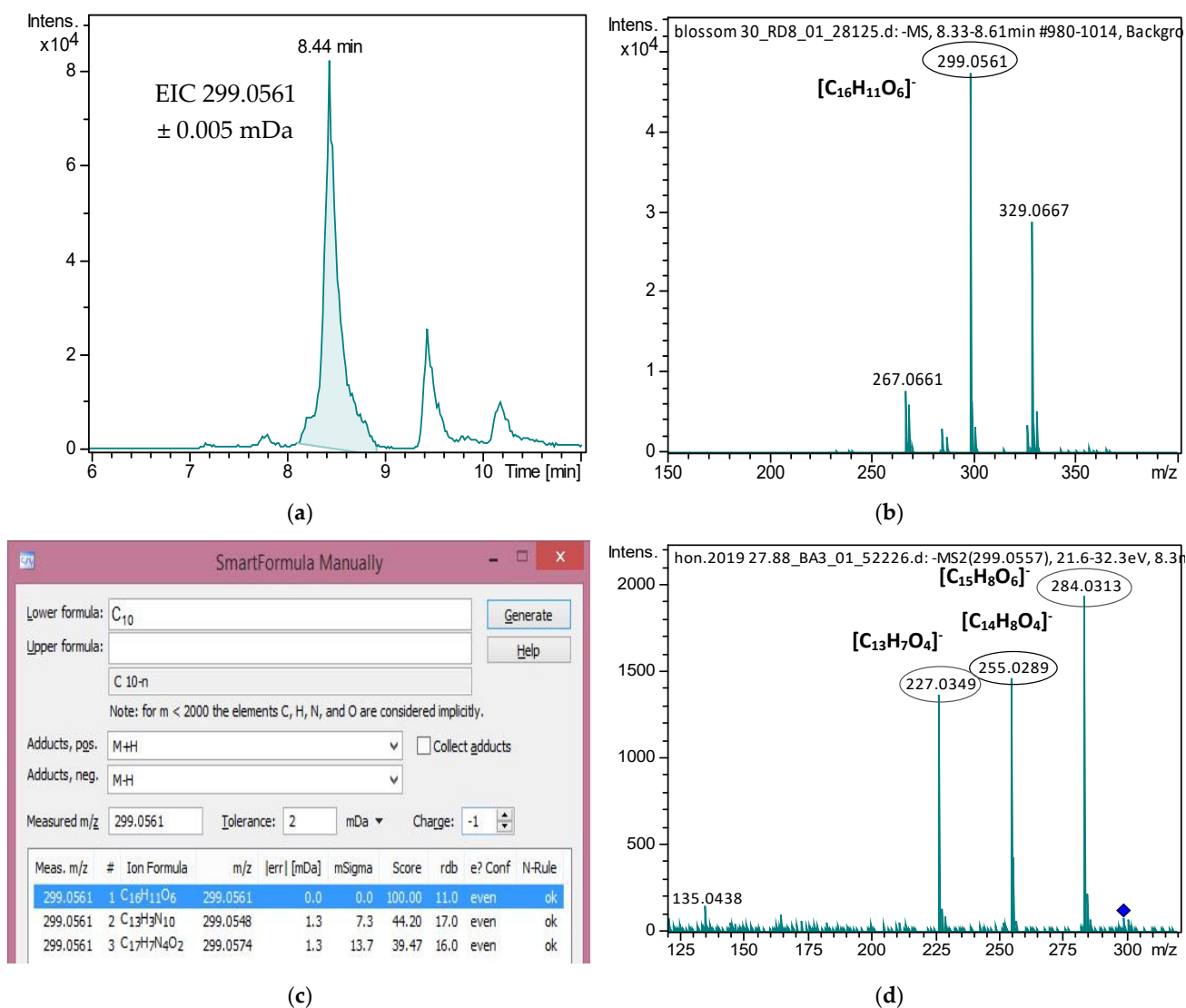


Figure 2. Cont.

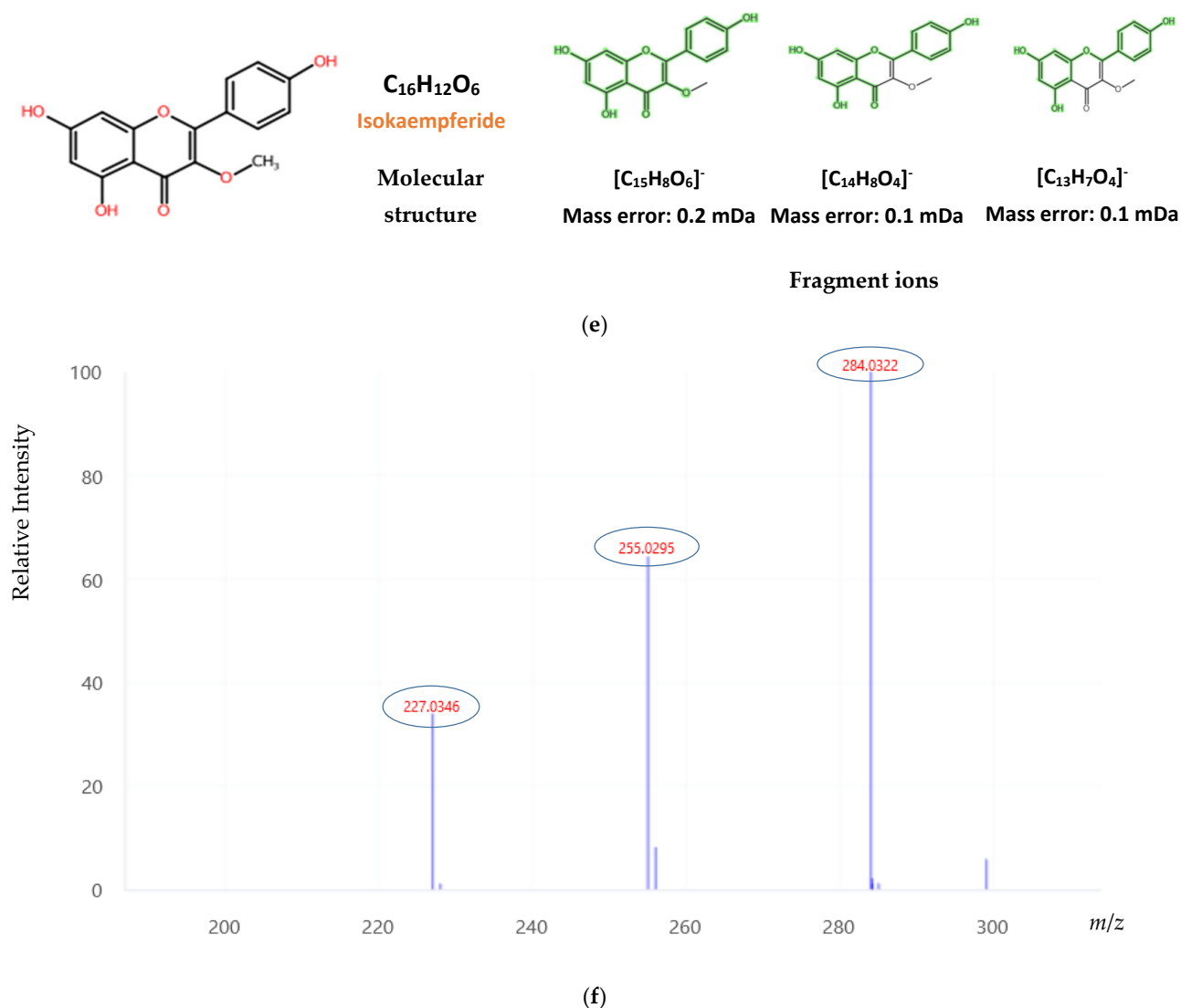


Figure 2. Identification data for the mass feature m/z 299.0561_8.44 min (Isokaempferide). (a) EIC of m/z 299.0561 in a blossom Honey; (b) Background subtracted MS Spectra from 8.3 to 8.6 min; (c) Molecular Formula Annotation of m/z 299.0561; (d) DDA MS/MS Spectra of 299.0561; (e) Structures of precursor and fragment ions (green part of the structure) of Isokaempferide; (f) Vaniya/Fiehn Natural Products Library Record VF-NPL-QTOF008090 (Isokaempferide).

All compounds were semi-quantified using an in-house semi-quantification protocol described in the Section 3. “Materials and Methods”. Specifically, 2-trans,4-trans abscisic acid was semi-quantified with its isomer, 2-cis,4-trans-abscisic acid. For the semi-quantification of homogentisic acid, 3,4-dihydroxybenzoic acid was selected. At the same time, apigenin was the most suitable compound to semi-quantify both isokaempferide and isorhamnetin, while lumichrome and methyl syringate were semi-quantified using eriodictyol. Finally, for phenyllactic acid and tectochrysin semi-quantification, p-coumaric acid and chrysin were selected, respectively. Especially for acetin, 2-cis,4-trans-abscisic acid and sakuranetin, analytical standards were purchased to verify their identification and reduce uncertainty in determining their concentration. All results are presented in Table 2.

Table 2. Semi-quantification of the analytes identified through suspect screening in the 5 different honey matrices.

Analytes	Honey Matrix									
	Blossom		Fir		Oak		Pine		Thyme	
	Mean (mg/Kg)	SD	Mean (mg/Kg)	SD	Mean (mg/Kg)	SD	Mean (mg/Kg)	SD	Mean (mg/Kg)	SD
Acacetin	0.092	0.13	ND	-	0.053	0.032	0.062	0.043	ND	-
2-trans,4-trans-abscisic acid	0.21	0.37	0.31	0.58	0.92	1.4	0.17	0.19	0.12	0.052
2-cis,4-trans-abscisic acid	0.37	0.58	0.46	0.88	1.4	1.8	0.33	0.40	0.19	0.12
Sakuranetin	0.024	0.030	0.010	0.010	0.022	0.011	ND	-	ND	-
Homogentisic acid	0.41	1.0	0.051	0.12	0.93	2.1	0.41	1.7	0.30	0.79
Dehydrovomifoliol	1.1	2.2	0.72	1.1	1.8	2.2	1.7	1.9	1.04	1.2
Isokaempferide	0.040	0.061	ND	-	0.023	0.021	0.023	0.030	ND	-
Isorhamnetin	0.071	0.12	0.10	0.13	0.11	0.084	0.074	0.14	0.033	0.043
Lumichrome	0.33	1.1	ND	-	0.11	0.15	0.29	0.55	0.15	0.36
Methyl Syringate	0.78	1.5	0.33	0.53	0.65	1.1	0.32	0.49	1.4	1.9
Phenyllactic acid	1.8	2.7	0.96	1.0	4.7	4.1	2.8	3.0	1.4	1.2
Tectochrysin	0.049	0.091	ND	-	0.030	0.030	0.024	0.043	ND	-

SD: standard deviation, ND: not detected.

According to the results presented in Table 2, the concentrations of some analytes varied significantly in the different floral varieties. Oak honey was richer in abscisic acid isomers compared to the other varieties. Abscisic acid has been characterized as a main phenolic compound of honeydew honeys [19]. In our study, the greatest amount of 2-cis,4-trans-abscisic acid was found in oak honey, followed by fir honey, with a mean concentration of 1.4 and 0.46 mg/Kg, respectively. These results agree with other studies reporting similar concentration levels for these varieties [20]. Greek thyme honey was richer in methyl syringate than blossom, oak, fir and pine honeys, with methyl syringate being a phenolic compound related to the scavenging activity of superoxides [21]. Methyl syringate was reported in thyme honeys previously [22]. Oak honey was also rich in phenyllactic acid and homogentisic acid, compounds that were previously used for honey authentication [23].

All the other suspect compounds were determined in low concentration levels and did not show any potential for discrimination among varieties. Sakuranetin was not identified in pine and fir honeys, while its average content was also low in oak, blossom and thyme honeys. These results are in accordance with previously published studies, with honeydew honeys from New Zealand containing 0.02 mg/Kg and different nectar honeys between 0.0060 and 0.062 mg/Kg [24,25]. Acacetin was not identified in thyme and fir samples; however, it was present in the other three varieties. An average concentration of 0.053 mg/Kg was detected in Greek oak honeys, comparable to Turkish honeys previously studied (0.04 mg/Kg).

Dehydrovomifoliol has also been formerly identified in honey. It has been proposed as a potential marker of heather honey, especially Polish honey [12]. Oak honey was the richest in our results, reaching 1.8 mg/Kg as an average concentration. Another detected suspect compound was isorhamnetin, with an average concentration ranging from 0.033 mg/Kg in thyme samples to 0.11 mg/Kg in oak variety, which was comparable to previous studies [26]. Regarding lumichrome, the highest average concentration was found in blossom honeys; nevertheless, this concentration of 0.33 mg/Kg is significantly lower than the corresponding concentrations reported in Croatian and Italian honey samples [27]. Finally,

tectochrysin was identified as a minor constituent in Greek honeys. Tectochrysin has been reported previously in Spanish floral honeys from Galicia with an average concentration of 0.31 mg/Kg, significantly higher than the one calculated in Greek honeys [28].

2.3. Non-Target Screening

Applying non-targeted screening workflow in honey samples resulted in a bucket table containing 3631 features. Worthwhile to note is that samples collected only during 2016 were processed by the non-targeted screening workflow. Multivariate statistical analysis revealed important features that can be used as authenticity markers to discriminate Greek honey varieties. Score plots, as well as the goodness of fit (R^2), the goodness of prediction (Q^2) and model accuracy of each PLS-DA model, can be found in the Supplementary Materials, along with the five most significant variables of each model and their box plots (Figures S6–S26).

Initially, a PLS-DA model was constructed, attempting to differentiate all 5 honey varieties. Figure S6 shows the final PLS-DA model developed, and the ellipses are drawn at 95% probability level. The score plot shows a distinct separation between blossom and thyme honeys. On the other hand, all samples belonging to the honeydew class (fir, oak and pine) were not well-separated and were distributed between the blossom and thyme groups (Figure S6). This model did not prove to be accurate, although it showed a predictive ability of 0.59 using the first four components. Many factors that increase the variance in the sample set may have influenced model accuracy, such as the different regions from where the samples were collected, the various climatic conditions prevailing in different collecting periods, and the diverse flora occurring in each area [29]. A better separation could have been achieved by using physicochemical parameters and/or melissopalynological analysis as a preliminary step to remove samples that do not comply with specific parameters defined by the legislation (Directive 2001/10/EC). The top five important features with the highest VIP scores were those with monoisotopic masses of 284.0684, 284.1048, 242.1517, 166.0996 and 508.1157 (Figure S7). Their box plots are found in the Supplementary Materials (Figure S8).

Subsequently, identification of the VIPs was undertaken. Indicatively, the following process was applied for the mass feature with m/z 284.1048 in $tR = 9.75$ min: First, the molecular formula $C_{17}H_{16}O_4$ was assigned by Smart Formula manually 3D with a 100% score, as it showed a mass error of 0.22 mDa and an isotopic fitting of 27 mSigma. Then, the Compound Crawler tool was used to search public libraries such as ChEBI, Pubchem and ChemSpider. ChEBI library was preferred compared to the others as it incorporates chemical entities of biological interest. However, no candidates were recovered in the ChEBI library, so Pubchem and Chemspider were used, resulting in 17 possible candidates. The candidates were then processed with the in silico fragmentation tool MetFrag using the MS/MS spectra that have been assigned in this feature during data treatment. Metafrag showed the highest score for the candidate phenethyl caffeate, a phenethyl alcohol ester of caffeic acid, which constitutes a bioactive component of honeybee hive propolis, providing many beneficial properties [30]. Its main fragments were explained, namely m/z 170.0353, 135.0451 and 161.0245, and the molecular features $[C_9H_7O_4]^-$ corresponding to the ion formula of caffeic acid, $[C_8H_7O_2]^-$, corresponding to the main fragment of caffeic acid (target list, Table S7) and $[C_9H_5O_3]^-$ were assigned. As the last step, mass spectral libraries such as MassBank Europe, MassBank of North America and METLIN were searched to find an MS/MS spectrum of a reference standard to reach a higher confidence level in the identification, but it was not available in this case.

Following the procedure mentioned above, the compound acacetin was assigned in the mass feature of 284.0684 and confirmed by a reference standard. In addition, acacetin was also identified through the suspect screening procedure, and it showed a higher average concentration in blossom honey, in line also with non-target screening findings. Moreover, the mass feature with m/z 508.1157 corresponds to the $[2M - H]^-$ ion of chrysin, an important compound already detected and quantified through the targeted screening.

Finally, the mass features with m/z 242.1517 and 166.0996, which show a higher intensity in thyme honey, are in-source fragments of the m/z 301.1656, as proposed by metaboscape (Figure S27). The molecular formula $C_{15}H_{26}O_6$ was assigned to the mass feature m/z 301.1656. A total of 2232 candidates were found in PubChem based on the given molecular formula, and further information (such as intense and clean MS/MS fragments) was needed to proceed to higher identification confidence. Therefore, this mass is tentatively identified at identification confidence level 4, according to the categorization proposed previously [12]. All annotations of important features of all PLS-DA models are presented in Table 3.

A new model was created after removing the samples belonging to the honeydew class in order to investigate the discrimination between blossom and thyme varieties. Thyme, one of the most widespread and important Greek unifloral honeys, is usually degraded by adding, without declaration, other nectar honeys or blossom honey and mislabeled as thyme honey [31]. Thus, it is of paramount importance to create a model to certify its authenticity. A highly accurate model leading to $R^2 = 0.99587$ and $Q^2 = 0.81258$ was achieved using the first five components (Figure S9). The first five variables in descending order were 508.1157, 544.1364, 284.0684, 286.0841 and 314.0790, which shows a higher concentration level in blossom honeys (Figure S10). Their box plots can be found in the Supplementary Materials (Figure S11). The monoisotopic masses 508.1157 and 284.0684 were common with the previous model, and they correspond to $[2M - H]^-$ of chrysin and acacetin, respectively. The mass features with m/z 544.1364 and 314.0790 were annotated as $[2M - H]^-$ of pinobanksin and pinobanksin 3-O-acetate, respectively. Both of the MS/MS spectra of these features contain the fragments with m/z 271.0612, 253.0495, 197.0597 and 225.0546, corresponding to the pseudomolecular ion of pinobanksin and its main fragments (Table S7). Pinobanksin constitutes a significant phenolic compound found in different honey matrices and provides many beneficial properties to human health [12]. As revealed in the targeted screening results, pinobanksin showed a much higher average concentration in blossom honeys and can be considered a potential biomarker for this variety. Finally, for the mass feature with m/z 286.0841, the molecular formula $C_{16}H_{14}O_5$ was assigned; however, this led to many possible candidates, making its unequivocal identification very difficult.

Since it was not feasible to attain sample discrimination using all five different honey classes, in the next step, we worked with binary discriminatory models to reveal significant compounds found in these varieties. Thus, two classes were formed in each model. The first one included the samples from a selected variety, while the second contained the rest of the samples. So, five models were developed. PLS-DA score plots, cross-validation details, important features, and their box plots are presented in the Supplementary Materials (Figure S12–S26). The most satisfactory results in terms of accuracy and predictive ability were obtained in the separation models of thyme and blossom categories with $Q^2 = 0.82468$ and $Q^2 = 0.74198$, respectively. On the other hand, fir, pine and oak models showed lower predictive ability ranging from 0.58 to 0.64. Honeydew honeys are often more difficult to differentiate as their composition depends mainly on the beekeeping plants that exist in the forests of each region. Therefore, honeydew honey may contain a high portion of nectar, and its composition must be checked so that it complies with the EU legislation (Directive 2001/10/EC).

In the discrimination model of blossom honeys, two important markers were identified by comparing their MS/MS spectra with those obtained by *in silico* fragmentation. The first marker was phenethyl caffeate, a compound that has already been mentioned before as a significant feature of Greek blossom honey [30]. The second marker, prenyl caffeate, is also a caffeic acid derivative, and it has been reported in Serbian polyfloral [13] samples and Algerian honeys [29]. Other markers could not be identified as many possible structures were retrieved for their assigned molecular formula. Regarding the thyme discrimination model, eudesmic acid was recognized by comparing experimental MS/MS data with those in the MoNA spectral library, while 3-methylgalangin with *in silico* MS/MS data produced by Metfrag. Eudesmic acid is cited as an important compound for Manuka honey, while 8-

methylgalangin has been reported for Chilean honeys [32,33]. The oak model revealed three important markers. As previously mentioned, gallic acid is a marker for oak honey samples and was identified with a reference standard. Scopoletin has formerly been reported in cotton honey [34], and its identity was confirmed by comparison with the MoNA library. Finally, taxifolin proved to be an important compound for Greek pine honeys, confirmed by target screening results.

Table 3. Identification of Important markers proposed by PLS-DA models.

PLS-DA Model	Variable (<i>m/z</i> , Monoisotopic Mass)	VIP Value	Rt (min)	Molecular Formula	$\Delta m/z$ [mDa]	mSigma	Name
All varieties	284.0685	4.52	10.14	C ₁₆ H ₁₂ O ₅	0.159	5.6	Acacetin
	284.1048	4.29	9.75	C ₁₇ H ₁₆ O ₄	−0.222	6.9	Phenethyl caffeate
	242.1517	4.21	4.72	C ₁₃ H ₂₂ O ₄	−0.437	21.0	Unknown 1
	166.0996	4.15	4.72	C ₁₀ H ₁₄ O ₂	0.021	3.6	Unknown 2
	508.1157	4.13	9.68	C ₃₀ H ₂₀ O ₈	−0.567	35.8	[2M − H] [−] of Chrysin
Blossom vs. Thyme	508.1157	5.50	9.68	C ₃₀ H ₂₀ O ₈	−0.567	35.8	[2M − H] [−] of Chrysin
	544.1364	5.35	7.25	C ₃₀ H ₂₄ O ₁₀	1.912	38.8	[2M − H] [−] of Pinobanksin
	284.0685	5.06	10.14	C ₁₆ H ₁₂ O ₅	0.159	5.6	Acacetin
	286.0841	4.65	6.97	C ₁₆ H ₁₄ O ₅	−0.125	11.2	unknown 1
	314.0790	4.57	9.01	C ₁₇ H ₁₄ O ₆	1.010	4.6	Pinobanksin 3-O-acetate
Blossom	237.0999	3.34	4.07	C ₉ H ₁₇ O ₇	0.495	32.3	Unknown 1
	284.1048	3.20	9.75	C ₁₇ H ₁₆ O ₄	−0.222	6.9	Phenethyl caffeate
	248.1047	2.57	9.45	C ₁₄ H ₁₆ O ₄	−0.257	15.2	Prenyl caffeate
	364.1522	2.56	4.89	C ₁₉ H ₂₄ O ₇	0.612	17.9	Unknown 2
	378.1673	2.49	5.05	C ₂₀ H ₂₆ O ₇	−0.032	36.6	Unknown 3
Thyme	212.0686	3.50	3.55	C ₁₀ H ₁₂ O ₅	0.215	7.8	Eudesmic acid
	282.1094	3.43	5.59	C ₁₄ H ₁₈ O ₆	0.845	10.5	Unknown 1
	242.0579	3.21	5.72	C ₁₄ H ₁₀ O ₄	−0.217	6.1	Unknown 2
	284.0684	3.05	9.92	C ₁₃ H ₂₂ O ₄	0.074	7.7	3-methylgalangin
	242.1517	3.04	4.72	C ₁₆ H ₁₂ O ₅	−0.437	12.9	Unknown 3
Fir	130.0631	4.03	1.34	C ₆ H ₁₀ O ₃	−1.607	34.2	unknown 1
	124.0164	3.28	1.68	C ₆ H ₄ O ₃	0.961	11.2	unknown 2
	160.1090	2.92	5.61	C ₈ H ₁₆ O ₃	−0.755	14.9	unknown 3
	62.9962	2.88	4.09	-	-	-	unknown 4
	120.0416	2.87	2.55	C ₄ H ₈ O ₄	−1.835	32.2	unknown 5
Oak	222.0891	4.73	4.34	C ₁₂ H ₁₄ O ₄	1.808	13.7	unknown 1
	192.0424	4.47	4.95	C ₁₀ H ₈ O ₄	1.486	7.7	scopoletin
	278.1278	4.43	4.43	C ₁₉ H ₁₈ O ₂	1.619	17.8	unknown 2
	170.0215	4.26	1.27	C ₇ H ₆ O ₅	−0.002	12.7	gallic acid
	292.0211	4.25	3.47	C ₂₀ H ₄ O ₃	−1.151	31.0	unknown 3
Pine	378.1673	2.74	5.05	C ₂₀ H ₂₆ O ₇	−0.032	36.6	unknown 1
	516.1989	2.63	4.20	C ₂₇ H ₃₂ O ₁₀	1.281	46.0	unknown 2
	264.0786	2.53	7.08	C ₁₇ H ₁₂ O ₃	0.066	4.8	Unknown 3
	350.1364	2.43	4.25	C ₁₈ H ₂₂ O ₇	−0.275	4.8	Unknown 4
	304.0582	2.39	4.88	C ₁₅ H ₁₂ O ₇	−0.037	23.6	Taxifolin

3. Materials and Methods

3.1. Chemicals

All chemicals, solvents and reagents used were of high analytical purity. Ammonium acetate, sodium sulfate anhydrous and EtAc (purity 99.0% or greater) were purchased from Sigma-Aldrich, while ACN and LC-MS grade methanol (MeOH) were provided by Merck.

A Milli-Q Millipore system purification system (Direct-Q UV, Millipore, Bedford, MA, USA) was used to prepare the aqueous solutions. Additionally, 2,5 dihydroxybenzoic acid (purity $\geq 99.0\%$), 3,4 dihydroxybenzoic acid (purity $\geq 97.0\%$), 4 hydroxybenzoic acid (purity $\geq 99\%$), apigenin (purity $\geq 99\%$), caffeic acid (purity $\geq 98.0\%$), chrysin (purity $\geq 99.0\%$), cinnamic acid (purity $\geq 99\%$), eriodictyol (purity $\geq 98.0\%$), ferulic acid (purity $\geq 99\%$), galangin (purity $\geq 99.0\%$), gallic acid (purity $\geq 99.0\%$), genistein (purity $\geq 99.0\%$), luteolin (purity $\geq 97.0\%$), naringenin (purity $\geq 99.0\%$), p-coumaric acid (purity $\geq 98.0\%$), pinobanksin (purity $\geq 99.0\%$), pinocembrin (purity $\geq 99.0\%$), quercetin (purity $\geq 95\%$), rosmarinic acid (purity $\geq 99.0\%$), salicylic acid (purity $\geq 99.0\%$), syringic acid (purity $\geq 98\%$), taxifolin (purity $\geq 85\%$), vanillic acid (purity $\geq 97\%$), vanillin (purity $\geq 99\%$), acacetin (purity $\geq 97\%$), sakuranetin (purity $\geq 98\%$) and 2-cis,4-trans-abscisic acid (purity $\geq 98\%$) were purchased by Sigma-Aldrich (St. Louis, MO, USA). Finally, regenerated cellulose syringe filters (R.C. filters, pore size $0.2\ \mu\text{m}$, diameter 15mm) were acquired from Phenomenex (Torrance, CA, USA).

3.2. Standard Preparation

A $1000\ \text{mg L}^{-1}$ in MeOH stock solution was prepared for each target compound. Then, the standards were stored at $-20\ ^\circ\text{C}$ in amber glass bottles to avoid photodegradation. Two mixture working solutions at two different concentrations, 25 and $50\ \text{mg L}^{-1}$, were also prepared and stored in the refrigerator. Dilution of the stock solution with mobile phase, MeOH: H_2O (50:50), yielded working solutions at 0.25 , 0.50 , 1.0 , 2.0 , and $5.0\ \text{mg L}^{-1}$. Calibration curves were obtained by plotting the peak areas of the standards against their concentration. Similar calibration curves were constructed in a blank honey matrix (matrix-matched calibration curve) to assess important method performance characteristics, namely, linearity, precision and matrix effects as well as analyte quantification. The matrix-matched standards were prepared by spiking the compounds in a blank honey extract prior to injection.

3.3. Honey Samples and Sample Preparation

One hundred and sixty-nine ($n = 169$) Greek honey samples from blossom ($n = 62$), fir ($n = 10$), oak ($n = 24$), pine ($n = 39$) and thyme ($n = 34$) varieties were collected by ATTIKI Honey SA from different regions of Greece (see supplementary material for further details, Table S2). Importantly, the samples were collected and analyzed during two consecutive years (2016 and 2017) to enhance the variability of the tested parameters. The samples were stored in amber glass containers at $4\ ^\circ\text{C}$. Before analysis, the samples were mixed vigorously for 3 minutes to be homogenized and in case of crystallization, samples were put in a water bath at $40\ ^\circ\text{C}$ till they were liquified. Sample preparation was based on a previously published study of our group [12]. Briefly, $1\ \text{g}$ of honey sample was weighted in a $15\ \text{mL}$ centrifuge tube and diluted with $5\ \text{mL}$ of acidified water ($\text{pH} < 2$) containing 2% sodium chloride. After vortexing for $1\ \text{min}$, the samples were extracted three times with $5\ \text{mL}$ EtAc. The samples were centrifuged between each extraction step to better separate the two phases. The combined extracts were collected in a glass tube and dried with anhydrous sodium sulfate. Afterwards, the extracts were evaporated under a gentle nitrogen stream to dryness and then reconstituted to $0.2\ \text{mL}$ with a final proportion of MeOH: H_2O (50:50). Before being injected into the HPLC system, all samples were filtered using cellulose syringe filters (R.C. filters, pore size $0.2\ \mu\text{m}$, diameter 15mm). In addition, to assess potential drifts and evaluate the reproduction of the analysis, a quality control (QC) sample was prepared by mixing $20\ \mu\text{L}$ of each honey sample extract to attain analytical information from all different botanical and geographical origins. Finally, ultrapure water was used to prepare a procedural blank, subjecting the whole sample preparation protocol to subtract possible contamination during data processing.

3.4. Method Verification

To monitor the analytical performance of the method, all the necessary quality performance characteristics were investigated, namely trueness, repeatability, intermediate precision, selectivity, linearity, limits of detection (LODs) and limit of quantification (LOQs). Considering that the current study is based on an in-house validated method [12], on this occasion, method verification was performed and seven additional analytes were included in the target list, namely, chrysin, galangin, genistein, naringenin, pinobanksin, pinocembrin and rosmarinic acid, resulting in a target list of 24 analytes. All the investigated performance characteristics were calculated as described in our previous paper [12], and detailed verification results can be found in the (Supplementary Material Tables S3–S5).

3.5. UPLC-QToF-MS Analysis

A UHPLC system (Dionex UltiMate 3000 RSLC, Thermo Fisher Scientific) coupled with a Q-ToF MS (Maxis Impact, Bruker Daltonics) was utilized. The chromatographic separation was performed on an Acclaim RSLC C18 column (2.1×100 mm, $2.2 \mu\text{m}$) from Thermo Fischer Scientific (Waltham, MA, USA), equipped with an Acquity UPLC BEH C18 VanGuard Pre-Column from Waters (Milford, MA, USA) at 30°C . The mobile phase mixtures comprised (A) Milli-Q H_2O : MeOH (90:10) and (B) MeOH, both A and B containing 5 mM ammonium acetate. The LC gradient elution and flow rate program is described in Table S6 of the Supplementary Materials. The injection volume was set to $5 \mu\text{L}$. The QToF-MS system was equipped with an ESI source, operating in negative ionization mode. The operation parameters for ESI were set as follows: capillary voltage, 3500 V; endplate offset, 500 V; nebulizer gas pressure 2 bar (N_2); drying gas, 8 L min^{-1} and dry temperature, 200°C .

The QTOF-MS system was operating in broadband collision-induced dissociation (bbCID) acquisition mode and recorded spectra over the m/z range 50–1000 with a scan rate of 2 Hz. The Bruker bbCID mode is a data-independent acquisition mode (DIA) that provides MS and MS/MS spectra at the same time, working at two different collision energies; at low collision energy (4 eV), MS spectra are acquired, while at high collision energy (25 eV), MS/MS spectra are collected. In addition, honey samples from each botanical and geographical origin, as well as the pool QC sample, were also analyzed using a data-dependent acquisition mode (DDA), AutoMS. In AutoMS, the five most abundant ions per MS scan are selected and fragmented, providing precise and compound-specific MS/MS spectra. Thus, this mode is most suitable for the structure elucidation of unknowns.

A QTOF-MS external calibration was performed before analysis with a 10 mM sodium formate solution in a mixture of water/isopropanol (50:50). The exact theoretical masses of calibration ions with formulas $\text{HCOO}(\text{NaCOOH})_{1-14}$ in the range of 50–1000 Da were used for calibration. Internal calibration was also performed using a calibrant injection at the beginning of each run in a dedicated calibration segment (0.1–0.25 min).

3.6. Targeted, Suspect and Non-Targeted Screening Workflows

An accurate-mass target screening database was compiled and used to identify and quantify 24 phenolic compounds in all honey samples (see Supplementary Materials, Table S7). Briefly, the identification criteria were as follows: retention time tolerance lower than ± 0.2 min, mass accuracy of the precursor and qualifier ions less than 5 mDa, isotopic fit less or equal than 50 mSigma (Bruker mSigma is a measure of the goodness of fit between the measured and the theoretical isotopic pattern) and the existence of at least two qualifier ions. The target screening was performed using the software TASQ 1.4 and DataAnalysis 4.4 (Bruker Daltonics, Bremen, Germany) along with other tools included in this software, such as Bruker Compass Isotope Pattern and SmartFormula Manually. Instead of external standard calibration curves for analyte quantification, matrix-matched calibration curves were used to compensate for ion suppression or enhancement in the ionization source. To identify statistically significant differences among the five botanical groups based on the attained concentration of each target analyte, ANOVA followed by Tukey's multiple

comparison test was performed at a significance level, $\alpha = 0.05$ using GraphPad prism 5.0 software (San Diego, CA, USA). Additionally, to visualize the variance of the attained concentration for each target analyte, Whisker's plots are provided, developed in GraphPad prism 5.0 software.

The suspect screening workflow is thoroughly described in a previously published work [12]. Firstly, eight compounds contained in the suspect list from our previous work were bought and incorporated into the target list. Then, the suspect list was enlarged by adding eight more compounds, namely, isokaempferide, caffeic acid isoprenyl ester, (–)-epigallocatechin gallate, 4-hydroxyphenylacetic acid, arbutin, baicalein, astragalin and kynurenic acid that have been mentioned to exist in honey. Information about formulas, monoisotopic masses and pseudomolecular ions, possible fragment and adduct ions as well as the predicted retention times [35] for these specific compounds are meticulously presented in Supplementary Materials (Table S8, [12,22,36–41]). Furthermore, the experimental retention times for the compounds that have been previously identified have also been added to the suspect list and used to increase identification confidence. Then, the final list, containing 60 compounds, was used to screen the honey samples to gain a deeper knowledge of phenolic compounds in Greek varieties. Mass accuracy threshold of 5 mDa, isotopic fit below or equal to 50 mSigma, ion intensity more than 1000 and peak area threshold of more than 2000 were utilized for creating the extracted ion chromatogram. For this purpose, the program TASQ 1.4 (Bruker Daltonics, Bremen, Germany) was used.

The identification workflow was followed for all compounds found in the suspect list. Briefly, MS spectra were meticulously examined for the existence of possible in-source fragments and/or adducts, and a formula for the precursor ion was proposed from Smart Formula manually. Then, MS/MS spectra were compared to those that exist in mass spectral libraries such as Fiehn Lab MassBank of North America (<https://mona.fiehnlab.ucdavis.edu/>, last accessed 8 June 2022) and METLIN [42] or by in silico fragmentation tools such as MetFrag [43]. Furthermore, experimental retention times were compared with theoretical to distinguish potential isomers and eliminate false positive results [12].

The identified suspect compounds were then semi-quantified in order to estimate their concentration levels in Greek honey samples. A popular way to perform semi-quantification is to use similar structural compounds found in the target list; however, this is not the most suitable method as important parameters such as logD and RT are not considered [44]. A more accurate way is to search for structurally similar compounds based on the number of similar functional groups, as well as the distance between functional groups. The online tool, ChemMine (<https://chemminetools.ucr.edu/>, last accessed 8 June 2022) was used for this goal. The Smile of each suspect compound was imported, and the comparison with compounds found in the PubChem database ensued, using a similarity cutoff of 0.9. The analytes with the highest structural similarity were recorded and the target compound with the higher similarity score was selected for semi-quantification. The similarity score is calculated as the Tanimoto similarity of substructure-based fingerprints [44].

Non-target screening workflow was performed using Bruker Metaboscape 3.0, an integrated software capable of implementing the entire procedure from peak peaking to multivariate analysis. The workflow contains automatic calibration using a calibrant (sodium formate solution) injection at the start of each run, as well as non-linear retention time alignment using T-ReX 3D, which connects isotopes, adducts and fragments of each feature together. The parameters used for bucket table formation were as follows: intensity threshold higher than 2000 counts, minimum peak length of 8 spectra, a mass range of 50–1000 m/z , Rt range of 0.5–12 min, an extracted ion chromatograms (EIC) correlation of 0.8 (only features above this threshold can be treated as adducts or fragments), primary ion $[M - H]^-$, seed ion $[M + Cl]^-$ and common Ion $[M - H - H_2O]^-$. Background features were discarded by subtracting procedural blank runs. Furthermore, if a feature is not found in at least 25% of the samples of a group is also removed [45].

Multivariate statistical analysis was performed to spot new markers that can differentiate the samples according to their botanical origin. The bucket table produced by

Metaboscape, after blank buckets removal, was exported as a csv file. Then, multivariate statistical analysis was performed by importing this file into the online platform Metaboanalyst 5.0, a dedicated platform for metabolomics applications. Firstly, the group labels were added to all samples, and missing values were replaced by 1/5 of min positive values of their corresponding variables. Data filtering was not used, and the bucket table was normalized by sum to reduce systematic variation among samples. In addition, data were transformed using the logarithm function and scaled using the auto-scaling algorithm, which mean-centered the data and divided the standard deviation of each variable. Finally, Partial Least Squares Discriminant Analysis (PLS-DA) was used to discriminate the different varieties and obtain the most influential variables that can be used as markers. Thus, the features with the 5 higher VIP scores of the PLS-DA model were kept and further examined to be identified. Ten-fold cross-validation (CV) was performed where the whole dataset was divided into 10 parts, 9 parts were used for training the model, and 1 part was kept as a test set. This procedure happens 10 times, and the total error is the mean of the errors produced after each test. As a model performance measure, the Q^2 was used, which is the model's predictive ability.

Complementary to the previous model, 5 PLS-DA two-class models were created, each one referring to the discrimination of a class compared to the rest of the samples. These models were built to find important variety-specific biomarkers that discriminate each variety. The workflow was similar to that described above and included one more step. Before obtaining the csv file used for building each model and importing it in Metaboanalyst 5.0, a t-test significance test was implemented in Metaboscape 3.0 to keep only statistically significant variables with $p < 0.05$. Thus, a file containing the intensities of all samples for the selected buckets was acquired, and the multivariate statistical analysis ensued.

The identification of the above-mentioned important features was based on the interpretation of MS and MS/MS data, with Metaboscape software providing all the necessary tools. Firstly, the target list containing information about standard compounds was imported into Metaboscape as an analyte list, helping to identify some buckets based on specific criteria such as mass accuracy, isotopic fitting, tR tolerance and existence of fragments ions. Another vital tool was Smart Formula manually 3D, with which molecular Formulas were assigned to possible markers in terms of mass accuracy and isotoping fitting. After molecular formula assignment, potential compounds were retrieved using Compound Crawler by public libraries such as PubChem and ChemSpider. Finally, a comparison between experimental MS/MS data with *in silico* fragmentation produced by Metrfag ensued. Spectral libraries such as Mass Bank Europe, Massbank of North America and Metlin were used to reach a higher level of confidence in the identification.

4. Conclusions

The application of the various HRMS metabolomic approaches provided successful discrimination of Greek honey from five different botanical sources. Targeted, suspect and non-targeted workflows were utilized, providing fruitful information on the Greek honey polyphenolic compound profile. In terms of targeted analysis, it was proven that potential botanical origin markers could be attained even by using univariate analysis, *i.e.*, ANOVA. Nevertheless, analytical standards are used to quantify the targeted analytes, increasing the method cost. Suspect screening can be used complementary to targeted analysis to acquire a detailed characterization of the honey metabolomic profile. Semi-quantification is also possible by using a few analytical standards based on the structural similarity of the analytes. In contrast to the previous two cases, the non-targeted analysis did not require any analytical standards, and further enhanced sample clustering based on advanced chemometrics. Overall, the present study provides a wealth of knowledge on the metabolomic composition of Greek honey, and the proposed markers may be used to make national honey production more secure.

Supplementary Materials: Detailed experimental results information can be downloaded at: <https://www.mdpi.com/article/10.3390/molecules27144444/s1>.

Author Contributions: Conceptualization, N.S.T., C.P. and M.E.D.; Data curation, G.A.K., A.S.T., P.A.K., P.-L.P.G., I.M., F.S., C.B., N.v.d.B.; formal analysis, G.A.K., A.S.T., P.-L.P.G., P.A.K., C.B. and N.v.d.B.; investigation, P.A.K., F.S. and E.I.P.; Methodology, P.A.K., G.A.K., A.S.T., P.-L.P.G., I.M., F.S.; Project administration, N.S.T.; resources, S.K., C.P., N.S.T.; Supervision, N.S.T., M.E.D., C.P. and A.F.; validation, P.A.K., F.S. and E.I.P.; visualization, G.A.K., A.S.T., P.A.K., P.-L.P.G.; Writing—original draft, G.A.K., A.S.T., P.-L.P.G.; Writing—review and editing, M.E.D., C.P. and N.S.T. All authors have read and agreed to the published version of the manuscript.

Funding: The authors acknowledge support of this work by the project “FoodOmicsGR – National Research Infrastructure for the Comprehensive Characterization of Foods” (MIS 5029057), which is implemented under the Action “Reinforcement of the Research and Innovation Infrastructure”, funded by the Operational Programme “Competitiveness, Entrepreneurship and Innovation” (NSRF 2014–2020) and co-financed by Greece and the European Union (European Regional Development Fund).

Institutional Review Board Statement: Not applicable.

Informed Consent Statement: Not applicable.

Data Availability Statement: Data are available upon request.

Conflicts of Interest: The authors declare no conflict of interest.

Sample Availability: Not available.

References

1. Afrin, S.; Haneefa, S.M.; Fernandez-Cabezudo, M.J.; Giampieri, F.; Al-Ramadi, B.K.; Battino, M. Therapeutic and preventive properties of honey and its bioactive compounds in cancer: An evidence-based review. *Nutr. Res. Rev.* **2020**, *33*, 50–76. [CrossRef] [PubMed]
2. Raptopoulou, K.G.; Pasiadis, I.N.; Proestos, C. Recent Advances in Analytical Techniques for the Determination of Authenticity and Adulteration of Honey and its Products. *Recent Adv. Anal. Tech.* **2020**, *4*, 125–145.
3. Tsagkaris, A.S.; Koulis, G.A.; Danezis, G.P.; Martakos, I.; Dasenaki, M.; Georgiou, C.A.; Thomaidis, N.S. Honey authenticity: Analytical techniques, state of the art and challenges. *RSC Adv.* **2021**, *11*, 11273–11294. [CrossRef]
4. Oymen, B.; Aşır, S.; Türkmen, D.; Denizli, A. Determination of multi-pesticide residues in honey with a modified QuEChERS procedure followed by LC-MS/MS and GC-MS/MS. *J. Apic. Res.* **2021**, 1–13. [CrossRef]
5. Soyseven, M.; Sezgin, B.; Arli, G. A novel, rapid and robust HPLC-ELSD method for simultaneous determination of fructose, glucose and sucrose in various food samples: Method development and validation. *J. Food Compos. Anal.* **2022**, *107*, 104400. [CrossRef]
6. Vazquez, L.; Armada, D.; Celeiro, M.; Dagnac, T.; Llompert, M. Evaluating the Presence and Contents of Phytochemicals in Honey Samples: Phenolic Compounds as Indicators to Identify Their Botanical Origin. *Foods* **2021**, *10*, 2616. [CrossRef]
7. Wang, X.; Li, Y.; Chen, L.; Zhou, J. Analytical Strategies for LC-MS-Based Untargeted and Targeted Metabolomics Approaches Reveal the Entomological Origins of Honey. *J. Agric. Food Chem.* **2022**, *70*, 1358–1366. [CrossRef] [PubMed]
8. Habib, H.M.; Kheadr, E.; Ibrahim, W.H. Inhibitory effects of honey from arid land on some enzymes and protein damage. *Food Chem.* **2021**, *364*, 130415. [CrossRef] [PubMed]
9. Xagoraris, M.; Skouria, A.; Revelou, P.-K.; Alissandrakis, E.; Tarantilis, P.A.; Pappas, C.S. Response Surface Methodology to Optimize the Isolation of Dominant Volatile Compounds from Monofloral Greek Thyme Honey Using SPME-GC-MS. *Molecules* **2021**, *26*, 3612. [CrossRef]
10. Tsavea, E.; Vardaka, F.-P.; Savvidaki, E.; Kellil, A.; Kanelis, D.; Bucekova, M.; Grigorakis, S.; Godocikova, J.; Gotsiou, P.; Dimou, M.; et al. Physicochemical Characterization and Biological Properties of Pine Honey Produced across Greece. *Foods* **2022**, *11*, 943. [CrossRef]
11. Graikou, K.; Andreou, A.; Chinou, I. Chemical profile of Greek Arbutus unedo honey: Biological properties. *J. Apic. Res.* **2022**, *61*, 100–106. [CrossRef]
12. Koulis, G.A.; Tsagkaris, A.S.; Aalizadeh, R.; Dasenaki, M.E.; Panagopoulou, E.I.; Drivelos, S.; Halagarda, M.; Georgiou, C.A.; Proestos, C.; Thomaidis, N.S. Honey Phenolic Compound Profiling and Authenticity Assessment Using HRMS Targeted and Untargeted Metabolomics. *Molecules* **2021**, *26*, 2769. [CrossRef] [PubMed]
13. Gašić, U.; Kečkeš, S.; Dabić, D.; Trifković, J.; Milojković-Opsenica, D.; Natić, M.; Tešić, Z. Phenolic profile and antioxidant activity of Serbian polyfloral honeys. *Food Chem.* **2014**, *145*, 599–607. [CrossRef] [PubMed]
14. Cheung, Y.; Meenu, M.; Yu, X.; Xu, B. Phenolic acids and flavonoids profiles of commercial honey from different floral sources and geographic sources. *Int. J. Food Prop.* **2019**, *22*, 290–308. [CrossRef]

15. Escriche, I.; Kadar, M.; Juan-Borrás, M.; Domenech, E. Using flavonoids, phenolic compounds and headspace volatile profile for botanical authentication of lemon and orange honeys. *Food Res. Int.* **2011**, *44*, 1504–1513. [CrossRef]
16. Can, Z.; Yildiz, O.; Sahin, H.; Akyuz Turumtay, E.; Silici, S.; Kolayli, S. An investigation of Turkish honeys: Their physico-chemical properties, antioxidant capacities and phenolic profiles. *Food Chem.* **2015**, *180*, 133–141. [CrossRef]
17. Sahin, H. Honey as an apitherapeutic product: Its inhibitory effect on urease and xanthine oxidase. *J. Enzyme Inhib. Med. Chem.* **2016**, *31*, 490–494. [CrossRef]
18. Kolayli, S.; Sahin, H.; Can, Z.; Yildiz, O.; Sahin, K. Honey shows potent inhibitory activity against the bovine testes hyaluronidase. *J. Enzyme Inhib. Med. Chem.* **2016**, *31*, 599–602. [CrossRef]
19. Recklies, K.; Peukert, C.; Kölling-Speer, I.; Speer, K. Differentiation of Honeydew Honeys from Blossom Honeys and According to Their Botanical Origin by Electrical Conductivity and Phenolic and Sugar Spectra. *J. Agric. Food Chem.* **2021**, *69*, 1329–1347. [CrossRef]
20. Bertoneclj, J.; Polak, T.; Kropf, U.; Korošec, M.; Golob, T. LC-DAD-ESI/MS analysis of flavonoids and abscisic acid with chemometric approach for the classification of Slovenian honey. *Food Chem.* **2011**, *127*, 296–302. [CrossRef]
21. Kato, Y.; Fujinaka, R.; Ishisaka, A.; Nitta, Y.; Kitamoto, N.; Takimoto, Y. Plausible authentication of manuka honey and related products by measuring leptosperin with methyl syringate. *J. Agric. Food Chem.* **2014**, *62*, 6400–6407. [CrossRef] [PubMed]
22. Mannina, L.; Sobolev, A.P.; Di Lorenzo, A.; Vista, S.; Tenore, G.C.; Daglia, M. Chemical Composition of Different Botanical Origin Honeys Produced by Sicilian Black Honeybees (*Apis mellifera* ssp. *sicula*). *J. Agric. Food Chem.* **2015**, *63*, 5864–5874. [CrossRef] [PubMed]
23. Burns, D.T.; Dillon, A.; Warren, J.; Walker, M.J. A Critical Review of the Factors Available for the Identification and Determination of Mānuka Honey. *Food Anal. Methods* **2018**, *11*, 1561–1567. [CrossRef]
24. Jonathan Chessum, K.; Chen, T.; Hamid, N.; Kam, R. A comprehensive chemical analysis of New Zealand honeydew honey. *Food Res. Int.* **2022**, 111436. [CrossRef]
25. Stompor, M. A Review on Sources and Pharmacological Aspects of Sakuranetin. *Nutrients* **2020**, *12*, 513. [CrossRef] [PubMed]
26. Ciucure, C.T.; Geană, E. Phenolic compounds profile and biochemical properties of honeys in relationship to the honey floral sources. *Phytochem. Anal.* **2019**, *30*, 481–492. [CrossRef] [PubMed]
27. Tuberoso, C.I.G.; Jerković, I.; Bifulco, E.; Marijanovic, Z.; Congiu, F.; Bubalo, D. Riboflavin and lumichrome in Dalmatian sage honey and other unifloral honeys determined by LC–DAD technique. *Food Chem.* **2012**, *135*, 1985–1990. [CrossRef]
28. Escuredo, O.; Silva, L.R.; Valentão, P.; Seijo, M.C.; Andrade, P.B. Assessing *Rubus* honey value: Pollen and phenolic compounds content and antibacterial capacity. *Food Chem.* **2012**, *130*, 671–678. [CrossRef]
29. Ouchemoukh, S.; Amessis-Ouchemoukh, N.; Gómez-Romero, M.; Aboud, F.; Giuseppe, A.; Fernández-Gutiérrez, A.; Segura-Carretero, A. Characterisation of phenolic compounds in Algerian honeys by RP-HPLC coupled to electrospray time-of-flight mass spectrometry. *LWT-Food Sci. Technol.* **2017**, *85*, 460–469. [CrossRef]
30. Tolba, M.F.; Azab, S.S.; Khalifa, A.E.; Abdel-Rahman, S.Z.; Abdel-Naim, A.B. Caffeic acid phenethyl ester, a promising component of propolis with a plethora of biological activities: A review on its anti-inflammatory, neuroprotective, hepatoprotective, and cardioprotective effects. *IUBMB Life* **2013**, *65*, 699–709. [CrossRef]
31. Soares, S.; Amaral, J.S.; Oliveira, M.B.P.P.; Mafra, I. A comprehensive review on the main honey authentication issues: Production and origin. *Compr. Rev. Food Sci. Food Saf.* **2017**, *16*, 1072–1100. [CrossRef] [PubMed]
32. Gašić, U.M.; Milojković-Opsenica, D.M.; Tešić, Ž.L. Polyphenols as possible markers of botanical origin of honey. *J. AOAC Int.* **2017**, *100*, 852–861. [CrossRef] [PubMed]
33. Bridi, R.; Montenegro, G. The value of Chilean honey: Floral origin related to their antioxidant and antibacterial activities. *Honey Anal.* **2017**, 63–78.
34. Kaškonienė, V.; Venskutonis, P.R. Floral Markers in Honey of Various Botanical and Geographic Origins: A Review. *Compr. Rev. Food Sci. Food Saf.* **2010**, *9*, 620–634. [CrossRef] [PubMed]
35. Aalizadeh, R.; Nika, M.C.; Thomaidis, N.S. Development and application of retention time prediction models in the suspect and non-target screening of emerging contaminants. *J. Hazard. Mater.* **2019**, *363*, 277–285. [CrossRef] [PubMed]
36. Seraglio, S.K.T.; Schulz, M.; Brugnerotto, P.; Silva, B.; Gonzaga, L.V.; Fett, R.; Costa, A.C.O. Quality, composition and health-protective properties of citrus honey: A review. *Food Res. Int.* **2021**, *143*, 110268. [CrossRef]
37. de Melo, F.H.C.; Menezes, F.N.D.D.; de Sousa, J.M.B.; dos Santos Lima, M.; da Silva Campelo Borges, G.; de Souza, E.L.; Magnani, M. Prebiotic activity of monofloral honeys produced by stingless bees in the semi-arid region of Brazilian Northeastern toward *Lactobacillus acidophilus* LA-05 and *Bifidobacterium lactis* BB-12. *Food Res. Int.* **2020**, *128*, 108809. [CrossRef]
38. Jerković, I.; Marijanović, Z.; Tuberoso, C.I.G.; Bubalo, D.; Kezić, N. Molecular diversity of volatile compounds in rare willow (*Salix* spp.) honeydew honey: Identification of chemical biomarkers. *Mol. Divers.* **2010**, *14*, 237–248. [CrossRef]
39. Floris, I.; Pusceddu, M.; Satta, A. The Sardinian Bitter Honey: From Ancient Healing Use to Recent Findings. *Antioxidants* **2021**, *10*, 506. [CrossRef]
40. Campillo, N.; Viñas, P.; Férez-Melgarejo, G.; Hernández-Córdoba, M. Dispersive liquid-liquid microextraction for the determination of flavonoid aglycone compounds in honey using liquid chromatography with diode array detection and time-of-flight mass spectrometry. *Talanta* **2015**, *131*, 185–191. [CrossRef]
41. Gośliński, M.; Nowak, D.; Szwengiel, A. Multidimensional Comparative Analysis of Bioactive Phenolic Compounds of Honeys of Various Origin. *Antioxidants* **2021**, *10*, 530. [CrossRef] [PubMed]

42. Smith, C.A.; O'Maille, G.; Want, E.J.; Qin, C.; Trauger, S.A.; Brandon, T.R.; Custodio, D.E.; Abagyan, R.; Siuzdak, G. METLIN: A metabolite mass spectral database. *Ther. Drug Monit.* **2005**, *27*, 747–751. [CrossRef] [PubMed]
43. Wolf, S.; Schmidt, S.; Müller-Hannemann, M.; Neumann, S. In silico fragmentation for computer assisted identification of metabolite mass spectra. *BMC Bioinform.* **2010**, *11*, 1–12. [CrossRef] [PubMed]
44. Malm, L.; Palm, E.; Souihi, A.; Plassmann, M.; Liigand, J.; Krueve, A. Guide to Semi-Quantitative Non-Targeted Screening Using LC/ESI/HRMS. *Molecules* **2021**, *26*, 3524. [CrossRef] [PubMed]
45. Olmo-García, L.; Wendt, K.; Kessler, N.; Bajoub, A.; Fernández-Gutiérrez, A.; Baessmann, C.; Carrasco-Pancorbo, A. Exploring the Capability of LC-MS and GC-MS Multi-Class Methods to Discriminate Virgin Olive Oils from Different Geographical Indications and to Identify Potential Origin Markers. *Eur. J. Lipid Sci. Technol.* **2019**, *121*, 1800336. [CrossRef]

Article

Relationships between X-ray Diffraction Peaks, Molecular Components, and Heat Properties of C-Type Starches from Different Sweet Potato Varieties

Yibo Li ^{1,2,†}, Lingxiao Zhao ^{3,†}, Lingshang Lin ^{1,2}, Enpeng Li ^{1,2}, Qinghe Cao ^{3,*}  and Cunxu Wei ^{1,2,*} 

¹ Key Laboratory of Crop Genetics and Physiology of Jiangsu Province/Joint International Research Laboratory of Agriculture & Agri-Product Safety of the Ministry of Education, Yangzhou University, Yangzhou 225009, China; dx120180133@yzu.edu.cn (Y.L.); 007520@yzu.edu.cn (L.L.); lep@yzu.edu.cn (E.L.)

² Co-Innovation Center for Modern Production Technology of Grain Crops of Jiangsu Province/Jiangsu Key Laboratory of Crop Genomics and Molecular Breeding, Yangzhou University, Yangzhou 225009, China

³ Xuzhou Institute of Agricultural Sciences in Jiangsu Xuhuai District, Xuzhou 221131, China; zhaolxiao2019@163.com

* Correspondence: cqhe75@yahoo.com (Q.C.); cxwei@yzu.edu.cn (C.W.)

† These authors contributed equally to this work.

Abstract: C-type starches with different proportions of A- and B-type crystallinities have different intensities and crystallinities of X-ray diffraction peaks. In this study, the intensities and crystallinities of X-ray diffraction peaks, molecular components and heat properties of C-type starches were investigated in seven sweet potato varieties, and their relationships were analyzed. The intensity and crystallinity of a diffraction peak at 5.6° were significantly positively correlated to the DP6-12 branch-chains of amylopectin and significantly negatively correlated to the true amylose content (TAC) determined by concanavalin A precipitation, gelatinization temperature, gelatinization enthalpy, water solubility at 95 °C, and pasting temperature. The intensity of diffraction peaks at 15° and 23° were significantly positively correlated to the gelatinization temperature and pasting temperature and significantly negatively correlated to the pasting peak viscosity. The significantly positive relationships were detected between the crystallinity of a diffraction peak at 15° and the DP13-24 branch-chains of amylopectin, gelatinization conclusion temperature and water solubility, between the crystallinity of diffraction peak at 17–18° and the TAC, gelatinization onset temperature, water solubility and pasting temperature, between the crystallinity of a diffraction peak at 23° and the gelatinization conclusion temperature and pasting peak time, and between the total crystallinity and the TAC, gelatinization conclusion temperature, water solubility and pasting temperature. The score plot of principle component analysis showed that the molecular components and heat property parameters could differentiate the C-type starches and agreed with their characteristics of X-ray diffraction peaks. This study provides some references for the utilizations of C-type starches.

Keywords: sweet potato; C-type starch; molecular component; heat properties; principal component analysis

Citation: Li, Y.; Zhao, L.; Lin, L.; Li, E.; Cao, Q.; Wei, C. Relationships between X-ray Diffraction Peaks, Molecular Components, and Heat Properties of C-Type Starches from Different Sweet Potato Varieties. *Molecules* **2022**, *27*, 3385. <https://doi.org/10.3390/molecules27113385>

Academic Editor: Mirella Nardini

Received: 24 April 2022

Accepted: 23 May 2022

Published: 24 May 2022

Publisher's Note: MDPI stays neutral with regard to jurisdictional claims in published maps and institutional affiliations.



Copyright: © 2022 by the authors. Licensee MDPI, Basel, Switzerland. This article is an open access article distributed under the terms and conditions of the Creative Commons Attribution (CC BY) license (<https://creativecommons.org/licenses/by/4.0/>).

1. Introduction

Starches are semi-crystalline granules and have A- and B-type crystallinities [1,2]. The A- and B-type crystallinities have different properties. For example, the B-type crystallinity has higher resistance to hydrolysis and exhibits lower gelatinization temperature than the A-type crystallinity [3]. Native starches from botanical resources are usually divided into A-, B- and C-type according to their containing crystallinity types. The A- and B-type starches have only A- and B-type crystallinity, respectively, and the C-type starch contains both A- and B-type crystallinities [1,2]. Normal cereal crops have A-type starches, some tuberous and high-amylose crops have B-type starches, and some legume and rhizome

crops have C-type starches [1,2]. The A- and B-type starches have been widely studied and utilized [4,5]. However, the C-type starches are less studied than the A- and B-type starches.

The C-type starches are more complex than A- and B-type starches, and can be further classified into C_A -, C_C - and C_B -types according to the ratio of A- and B-type crystallinities from high to low [1,2]. In fact, the distributions of A- and B-type crystallinities in C-type starches are also different due to their different botanical resources [2]. The A- and B-type crystallinities are located in the outer and inner regions of C-type starch granules from pea, respectively [6], but they are distributed in the inner and outer regions of C-type starch granules from high-amylose rice with inhibition of starch branching enzymes, respectively [7]. For the C-type starch with eccentric hilum from lotus rhizome, the periphery and distal region of hilum have A- and B-type crystallinities, respectively, and the center of granule has a mixture of A- and B-type crystallinities [8]. The C-type starch from root tuber of *Apios fortunei* has A- and B-type starch granules, meaning that the A- and B-type crystallinities are distributed in the different granules [9]. The different distribution patterns of A- and B-type crystallinities even further increase the complexity of C-type starches.

The root tuber of sweet potato (*Ipomoea batatas*) has high starch content (about 15–30% wet weight and 50–80% dry weight) [10,11], and is an important starch resource. The C-type starches from root tubers have been widely reported in sweet potato varieties. Significantly different X-ray diffraction (XRD) patterns and different scanning calorimetric (DSC) thermograms are detected in C-type starches from sweet potato varieties, and reflect different proportions of A- and B-type crystallinities [10,12–18]. The growing soil with high temperature increases the accumulation of A-type crystallinity in root tuber [13]. The C-type starches from sweet potato varieties grown in the same condition have significantly different XRD patterns and DSC thermograms, indicating that the genotypes play a major role in determining the accumulation of A- and B-type crystallinities [10,14,17]. Guo et al. [14] fitted the DSC curve of sweet potato starch with wide gelatinization temperature range (ΔT) into three peaks, and concluded that sweet potato root tuber has B-, C- and A-type starches, corresponding to the fitted peak with low, middle, and high gelatinization temperature, respectively. The starch properties, especially crystalline structure, affect the utilizations of starches [2,11]. However, it is no way to separate the A-, B- and C-type starches from sweet potato root tubers in practical production. Though it is easy to evaluate the proportion of A- and B-type crystallinities in starches using XRD patterns [1,19], it is unclear whether there are significant relationships between X-ray diffraction peaks and physicochemical properties of C-type starches.

In this study, C-type starches were isolated from seven sweet potato varieties, the XRD patterns, molecular components, and heat properties were investigated, and their relationships were analyzed. The objective of this study was to provide some information for the utilizations of C-type starches through investing their XRD patterns.

2. Results and Discussion

2.1. X-ray Diffraction Peaks of C-Type Starches

The starches from seven sweet potato varieties all exhibited C-type XRD patterns with diffraction peaks at 5.6° , 15° , 17° and 23° 2θ (Figure 1). The peaks at 5.6° and 23° are characteristic peaks of B- and A-type crystallinities, respectively [1,19]. In this study, the relative intensities of XRD patterns were normalized to the equal intensity (1000 counts) from the lowest point at 2θ about 4.3° to the highest point at 2θ 17 – 18° , resulting in that the intensities of diffraction peaks between different starches were at the same relative scale and therefore directly comparable. Though the seven starches all exhibited C-type XRD patterns, significant differences in the intensities of diffraction peaks were detected (Figure 1, Table 1). The intensity of diffraction peak decreased at 5.6° (from 146 to 38) and increased at 23° (from 592 to 727) from SY192 to SY6, SY148, SY175, SY4, SY19 and Kokei 14. In addition, the peak at 18° , a characteristic peak of A-type crystallinity [1,2], appeared as a shoulder peak in SY148 and its intensity increased from SY175 to SY4, SY19 and Kokei 14. The intensity variations of diffraction peaks indicated that the proportion of

B-type crystallinity decreased and that of A-type crystallinity increased in C-type starch from SY192 to SY6, SY148, SY175, SY4, SY19 and Kokei 14. The C-type starches are usually divided into C_A -, C_C - and C_B -type according to the ratio of A- to B-type crystallinity in C-type starch from high to low. The C_B -type starch has diffraction peaks at 22° and 24° , and the C_A -type starch has a diffraction peak at 18° [2]. The XRD patterns and peak intensities showed that the starch changed from C_C -type to C_A -type from SY192 to SY6, SY148, SY175, SY4, SY19 and Kokei 14 (Figure 1, Table 1).

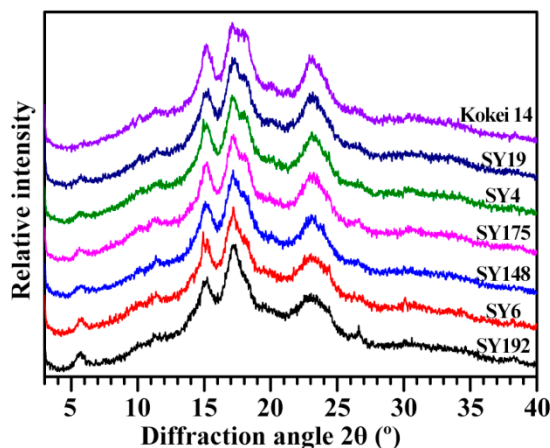


Figure 1. XRD patterns of C-type starches from different sweet potato varieties.

Table 1. Relative intensities and crystallinities of diffraction peaks in XRD patterns of C-type starches.

Accession ID	RI of Diffraction Peak (Counts)			RC of Diffraction Peak (%)				
	RI _{5,6°}	RI _{15°}	RI _{23°}	RC _{5,6°}	RC _{15°}	RC _{17–18°}	RC _{23°}	RC _{Total}
SY192	146 ± 9 a	716 ± 6 d	592 ± 2 f	1.23 ± 0.18 a	3.50 ± 0.10 d	9.70 ± 0.14 de	8.35 ± 0.28 b	22.84 ± 0.31 cd
SY6	115 ± 7 b	761 ± 1 bc	617 ± 4 e	0.74 ± 0.08 b	3.63 ± 0.12 cd	9.27 ± 0.01 e	8.15 ± 0.22 b	21.96 ± 0.46 d
SY148	80 ± 1 c	751 ± 2 c	639 ± 2 d	0.56 ± 0.08 bc	3.94 ± 0.06 bc	11.17 ± 0.01 bc	8.35 ± 0.40 b	24.23 ± 0.65 bc
SY175	79 ± 2 c	778 ± 3 bc	676 ± 5 c	0.46 ± 0.04 bc	3.71 ± 0.21 cd	10.21 ± 0.25 d	9.77 ± 0.08 a	24.21 ± 0.41 bc
SY4	69 ± 2 c	788 ± 12 b	706 ± 8 b	0.34 ± 0.05 cd	4.40 ± 0.01 a	10.88 ± 0.08 c	9.02 ± 0.28 ab	24.84 ± 0.28 ab
SY19	67 ± 4 c	751 ± 15 c	708 ± 3 b	0.33 ± 0.10 cd	4.16 ± 0.10 ab	11.50 ± 0.33 ab	9.69 ± 0.20 a	25.93 ± 0.45 a
Kokei 14	38 ± 3 d	826 ± 6 a	727 ± 5 a	0.09 ± 0.01 d	4.20 ± 0.12 ab	11.92 ± 0.13 a	9.10 ± 0.41 ab	25.49 ± 0.34 ab
Sig.	0.558	0.906	0.547	0.516	0.713	0.830	0.275	0.723

RI: relative intensity; RC: relative crystallinity. The RIs of XRD patterns are normalized to the equal intensity (1000 counts) from the lowest point at 2θ about 4.3° to the highest point at 2θ about $17\text{--}18^\circ$. Sig.: the significance of normal distribution of the 7 samples by the Shapiro–Wilk test. Data are means \pm standard deviations ($n = 2$). The values with different letters in the same column are significantly different ($p < 0.05$).

Sweet potatoes have C_A -, C_B - and C_C -type starches in different colored root tubers [10,13–18]. The types of C-type starches have no relationships with the color of root tuber, and are determined by the genotypes of sweet potato varieties [10,14,16,17]. Genkina et al. [13] concluded that the soil temperature affects the crystalline type of sweet potato starch with C_A -type starch at soil temperature above 33°C and C_B -type starch at soil temperature below 15°C . In fact, the temperature, the moisture and starch content in starch storage tissue and the branch-chain length of amylopectin all influence the crystal conformation during starch synthesis. The low temperature, high moisture, low starch content, and amylopectin long branch-chains tend to form B-type crystallinity, and the high temperature, low moisture, high starch content, and amylopectin short branch-chains tend to form A-type crystallinity [20]. The C-type starch from sweet potato grown at low soil temperature has higher ratio of B-type crystallinity and lower contents of starch and amylopectin long branch-chains than at high soil temperature [21], indicating that the temperature, moisture and starch content play more important roles in the formation of crystalline structure in sweet potato than the amylopectin structure. The relative crystallinities (RCs) of diffraction peaks and total RCs showed some differences among some sweet

potato varieties (Table 1). The RC at 5.6°, 15°, 17–18° and 23° varied from 0.09% (Kokei 14) to 1.23% (SY192), from 3.50% (SY192) to 4.40% (SY4), from 9.27% (SY6) to 11.92% (Kokei 14) and from 8.15% (SY6) to 9.77% (SY175), respectively, and the RC at all crystalline diffraction peaks (RC_{Total}) ranged from 21.96% (SY6) to 25.93% (SY19) among seven starches. The RC is affected by amylose content, amylopectin structure, crystallinity type, and granule size [1,12,22–24].

2.2. Molecular Components of C-Type Starches

The starch–iodine absorption spectrum was detected (data not shown). The data of optical density (OD) at 620 nm (OD620) and 550 nm (OD550) were obtained from the spectrum, and their ratio (OD620/550) reflects the relative proportion of long chains in starch [25]. The OD620/550 ranged from 1.146 (SY175) to 1.220 (SY4) among seven starches (Table 2), indicating that they had different amylose and amylopectin contents. The ratio of amylose and amylopectin is the most important structure parameter, determining the physicochemical properties and applications of starch [25,26]. The apparent amylose content (AAC) determined by iodine colorimetry usually overestimates the amylose content of starch due to the fact that the branch-chains of amylopectin can also bind the iodine. For concanavalin A (Con A) precipitation method, starch is completely dissolved into amylose and amylopectin. The Con A specifically binds and precipitates the amylopectin. The quality percentage of amylose to both amylose and amylopectin is usually defined as true amylose content (TAC) due to the fact that the amylose content is not influenced by the purity and moisture of starch and non-starch components (lipid and protein) [25]. Among seven starches, AAC and TAC ranged from 20.2% (SY6) to 29.2% (SY175) and from 14.7% (SY192) to 19.7% (Kokei 14), respectively, and the TAC was significantly lower than the AAC (Table 2).

Table 2. Molecular components of C-type starches from different sweet potato varieties.

Accession ID	OD620/550	AAC (%)	TAC (%)	Components of Isoamylase-Debranched Starch			
				AM (%)	AP-L (%)	AP-S (%)	AP-S/L
SY192	1.208 ± 0.011 a	21.8 ± 0.2 c	14.7 ± 0.3 d	20.7 ± 0.1 a	21.5 ± 0.2 c	57.8 ± 0.3 ab	2.69 ± 0.04 a
SY6	1.203 ± 0.018 ab	20.2 ± 0.3 c	15.2 ± 0.7 d	19.3 ± 1.0 ab	23.8 ± 0.7 ab	56.9 ± 0.3 abc	2.39 ± 0.06 b
SY148	1.186 ± 0.001 abc	28.5 ± 0.2 a	17.2 ± 0.5 bc	19.9 ± 0.6 ab	23.9 ± 0.1 ab	56.3 ± 0.5 bcd	2.36 ± 0.01 b
SY175	1.146 ± 0.015 d	29.2 ± 1.3 a	17.7 ± 0.7 bc	19.8 ± 0.2 ab	25.1 ± 0.1 a	55.1 ± 0.3 d	2.19 ± 0.02 b
SY4	1.220 ± 0.018 a	21.5 ± 1.0 c	16.2 ± 0.1 cd	19.5 ± 0.3 ab	22.2 ± 0.1 bc	58.3 ± 0.3 a	2.62 ± 0.01 a
SY19	1.160 ± 0.012 cd	25.7 ± 0.8 b	18.2 ± 0.4 ab	18.7 ± 0.4 b	25.3 ± 0.9 a	56.0 ± 0.5 cd	2.21 ± 0.10 b
Kokei 14	1.169 ± 0.019 bcd	28.3 ± 0.2 a	19.7 ± 0.4 a	19.7 ± 0.3 ab	24.2 ± 1.1 ab	56.2 ± 0.9 bcd	2.33 ± 0.14 b
Sig.	0.787	0.156	0.925	0.871	0.440	0.810	0.331

OD620/550: absorption ratio of OD620 to OD550; AAC: apparent amylose content evaluated by the OD620 of starch–iodine absorption; TAC: true amylose content determined by the concanavalin A precipitation method; AM: amylose; AP-L: long branch-chains of amylopectin; AP-S: short branch-chains of amylopectin; AP-S/L: content ratio of short to long branch-chains of amylopectin. Sig.: the significance of normal distribution of the 7 samples by Shapiro–Wilk test. Data are means ± standard deviations ($n = 3$ for OD620/550 and AAC and = 2 for the others). The values with different letters in the same column are significantly different ($p < 0.05$).

The molecular weight distribution of isoamylase-debranched starch is presented in Figure 2A. The peak of low, middle and high molecular weight presents the amylopectin short branch-chains (AP-S), amylopectin long branch-chains (AP-L), and amylose molecules (AM), respectively [24,25]. Their area percentages reflect the starch components, and the area ratio of low to middle molecular weight peak (AP-S/L) is positively correlated to the branching degree of amylopectin [24,25]. The seven sweet potato varieties had different starch components with AM from 18.7% (SY19) to 20.7% (SY192), AP-L from 21.5% (SY192) to 25.3% (SY19), AP-S from 55.1% (SY175) to 58.3% (SY4), and AP-S/L from 2.19 (SY175) to 2.69 (SY192) (Table 2). The chain length distribution of amylopectin was further analyzed (Figure 2B,C). Usually, amylopectin branch-chains are divided into A chains (DP6–12), B1 chains (DP13–24), B2 chains (DP25–36), and B3+ chains (DP > 36) [27]. The seven sweet potato starches exhibited different amylopectin chain length distributions with A chains

from 20.2% (SY148) to 25.1% (SY192), B1 chains from 44.0% (SY192) to 49.0% (SY4), B2 chains from 12.7% (SY148) to 13.9% (SY192), B3+ chains from 15.6% (SY4) to 18.8% (SY175), and average branch-chain length (ACL) from 22.9 (SY4) to 24.6 DP (SY175) (Table 3).

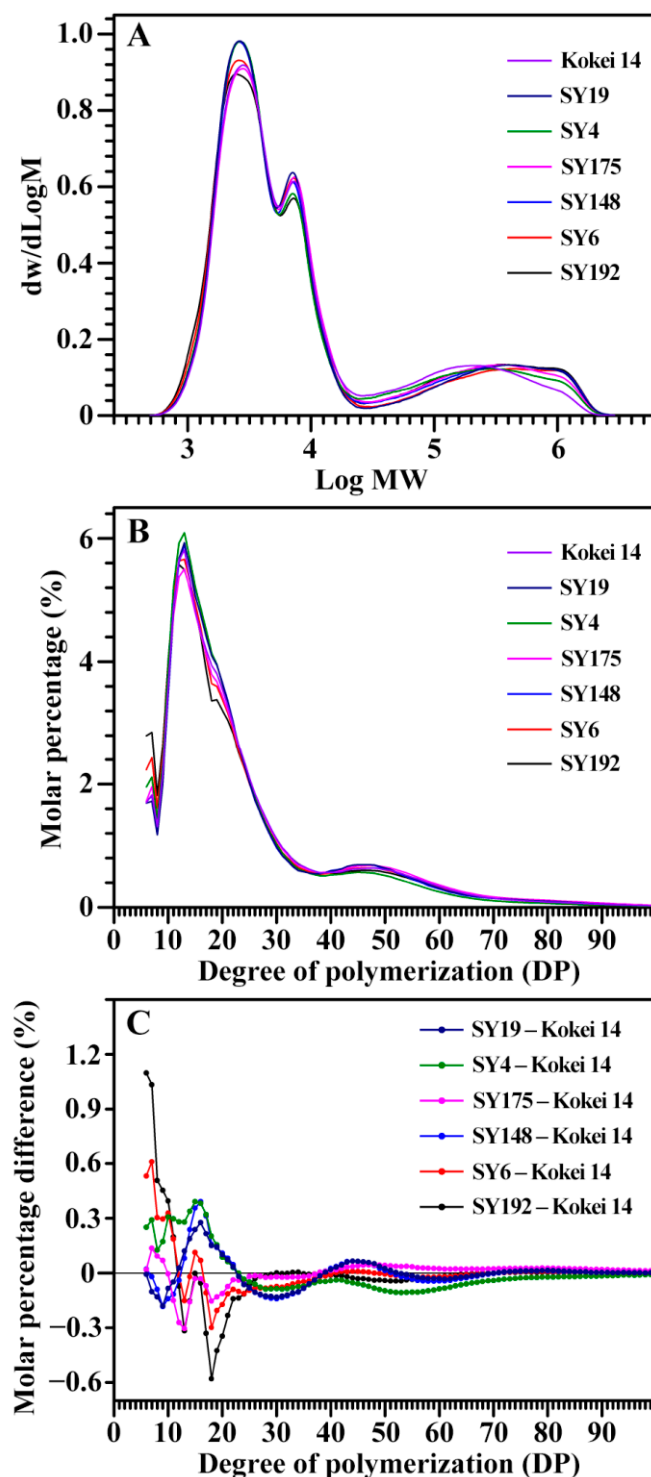


Figure 2. Gel permeation chromatography profiles of isoamylase-debranched starches (A) and fluorophore-assisted capillary electrophoresis profiles of isoamylase-debranched amylopectins (B,C) from different sweet potato varieties.

Table 3. Chain length distributions of isoamylase-debranched amylopectins from C-type starches of different sweet potato varieties.

Accession ID	DP6-12 (%)	DP13-24 (%)	DP25-36 (%)	DP > 36 (%)	ACL (DP)
SY192	25.1 ± 0.5 a	44.0 ± 0.6 e	13.9 ± 0.1 a	17.0 ± 0.1 ab	23.5 ± 0.1 ab
SY6	23.5 ± 0.2 b	45.7 ± 0.4 d	13.0 ± 0.2 b	17.7 ± 0.4 ab	23.7 ± 0.1 ab
SY148	20.2 ± 0.5 d	48.9 ± 0.3 a	12.7 ± 0.1 b	18.1 ± 0.7 ab	24.1 ± 0.4 ab
SY175	21.1 ± 0.1 cd	46.2 ± 0.3 cd	13.8 ± 0.1 a	18.8 ± 0.4 a	24.6 ± 0.2 a
SY4	22.4 ± 0.7 bc	49.0 ± 0.6 a	13.0 ± 0.1 b	15.6 ± 1.4 b	22.9 ± 0.7 b
SY19	20.3 ± 0.4 d	48.4 ± 0.4 ab	12.8 ± 0.1 b	18.4 ± 0.7 a	24.3 ± 0.3 a
Kokei 14	21.4 ± 0.3 cd	47.4 ± 0.1 bc	13.8 ± 0.3 a	17.5 ± 0.2 ab	24.0 ± 0.1 ab
Sig.	0.438	0.467	0.066	0.583	0.924

ACL: average chain length of amylopectin. Sig.: the significance of normal distribution of the 7 samples by Shapiro–Wilk test. Data are means ± standard deviations ($n = 2$). The values with different letters in the same column are significantly different ($p < 0.05$).

In order to reveal the relationships between X-ray diffraction peaks and molecular components of C-type starches, the Pearson correlation coefficients between the intensities/crystallinities of X-ray diffraction peaks and the molecular components were evaluated (Table 4). The TAC was significantly positively correlated to the intensity of diffraction peak at 23° and the crystallinity of diffraction peak at $17\text{--}18^\circ$ and significantly negatively correlated to the intensity and crystallinity of diffraction peak at 5.6° . The DP6-12 of amylopectin was significantly positively correlated to the intensity and crystallinity of diffraction peak at 5.6° . The DP13-24 of amylopectin was significantly positively correlated to the crystallinity of diffraction peak at 15° and significantly negatively correlated to the intensity of diffraction peak at 5.6° (Table 4). The DP6-12 of amylopectin is positively correlated to the ratio of B-type crystallinity in C-type starch from sweet potato grown at different soil temperatures [21], which is in line with the present study. For A- or B-type starches, the intensities and crystallinities of crystalline diffraction peaks are significantly negatively correlated to the amylose content and positively to the amylopectin short branch-chains [1,23,24]. However, Dhital et al. [12] separated maize A-type starch and potato B-type starch into different-sized fractions and found that the amylose content is significantly positively correlated to the RC of starch. The present results exhibited that C-type starches were more complex than A- and B-type starches in starch molecular components, especially for C-type starches with different proportions of A- and B-type crystallinities.

Table 4. Pearson correlation coefficients between intensities/crystallinities of X-ray diffraction peaks and molecular components of C-type starches.

	RI _{5.6°}	RI _{15°}	RI _{23°}	RC _{5.6°}	RC _{15°}	RC _{17-18°}	RC _{23°}	RC _{Total}
OD620/550	0.486	−0.270	−0.431	0.466	−0.006	−0.393	−0.735	−0.490
AAC	−0.613	0.370	0.436	−0.521	0.175	0.614	0.524	0.574
TAC	−0.903 **	0.703	0.822 *	−0.856 *	0.571	0.855 *	0.651	0.824 *
AM	0.530	−0.306	−0.578	0.635	−0.533	−0.346	−0.448	−0.447
AP-L	−0.566	0.329	0.471	−0.601	0.144	0.376	0.615	0.440
AP-S	0.409	−0.232	−0.272	0.400	0.123	−0.263	−0.548	−0.301
AP-S/L	0.544	−0.324	−0.432	0.573	−0.091	−0.350	−0.596	−0.404
DP6-12	0.792 *	−0.397	−0.643	0.764 *	−0.547	−0.734	−0.570	−0.731
DP13-24	−0.764 *	0.424	0.676	−0.752	0.864 *	0.746	0.311	0.711
DP25-36	0.161	0.161	−0.068	0.209	−0.385	−0.179	0.160	−0.128
DP > 36	−0.094	−0.116	−0.044	−0.087	−0.384	0.042	0.335	0.067
ACL	−0.265	0.040	0.139	−0.241	−0.240	0.211	0.491	0.250

The abbreviations are listed in Tables 1–3. The * and ** indicate the significance at $p < 0.05$ and $p < 0.01$ level, respectively ($n = 7$).

2.3. Heat Properties of C-Type Starches

The gelatinization properties of starch are analyzed with DSC. The DSC thermograms of seven starches exhibited significant differences in peak shapes, widths, and gelatinization

temperatures (Figure 3, Table 5). Similar DSC thermograms are also reported in sweet potato starches from different varieties [15,28–30]. For example, Osundahunsi et al. [30] and Duan et al. [28] reported one- and two-peak thermograms of sweet potato starches, respectively, and Kim et al. [15] found a large variation in gelatinization temperature range (ΔT) from 13.0 to 36.7 °C among eight sweet potato starches. Genkina et al. [13] fitted the two-peak DSC curve of sweet potato starch into two gelatinization peaks with the low gelatinization temperature peak for B-type crystallinity and the high gelatinization temperature peak for A-type crystallinity. Guo et al. [14] fitted the DSC curve of sweet potato starch into three gelatinization peaks, and the peaks with low, middle and high gelatinization temperature correspond to the gelatinization of B-, C- and A-type starch, respectively, meaning that sweet potato root tuber contains A-, B- and C-type starches. In the present study, the gelatinization temperature and enthalpy (ΔH) exhibited significant differences. The Kokei 14 starch had the highest gelatinization temperature including onset (T_o), peak (T_p) and conclusion (T_c) temperature and the narrowest ΔT , and the SY192 starch had the lowest gelatinization temperature and ΔH among starches (Table 5). The sweet potato starches containing different proportions of A-, B- and C-type starches have different DSC thermograms [14]. The significantly different DSC thermograms of seven sweet potato starches might be due to their different proportions of A-, B- and C-type starches, and this agreed with their XRD patterns.

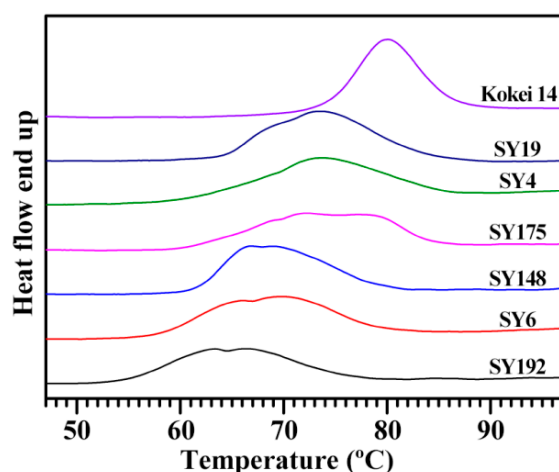


Figure 3. DSC thermograms of C-type starches from different sweet potato varieties.

Table 5. Thermal property parameters, swelling powers and water solubilities of C-type starches from different sweet potato varieties.

Accession ID	Thermal Property Parameters					SP (g/g)	WS (%)
	T_o (°C)	T_p (°C)	T_c (°C)	ΔT (°C)	ΔH (J/g)		
SY192	54.4 ± 0.2 f	65.8 ± 0.7 e	76.6 ± 1.2 d	22.2 ± 1.0 b	12.6 ± 0.3 c	26.2 ± 0.5 a	10.4 ± 0.8 b
SY6	57.9 ± 0.1 e	69.9 ± 0.1 d	79.9 ± 0.1 c	22.0 ± 0.1 b	14.9 ± 0.3 b	27.1 ± 0.3 a	10.7 ± 0.6 b
SY148	61.0 ± 0.4 c	66.8 ± 0.1 e	79.7 ± 0.1 c	18.7 ± 0.3 c	14.7 ± 0.3 b	27.6 ± 0.4 a	11.0 ± 0.2 ab
SY175	60.3 ± 0.1 d	72.5 ± 0.4 c	84.7 ± 0.6 b	24.4 ± 0.6 a	14.7 ± 0.2 b	24.5 ± 0.4 b	10.7 ± 0.1 b
SY4	60.3 ± 0.1 d	74.0 ± 0.3 b	85.8 ± 0.8 ab	25.5 ± 0.9 a	14.4 ± 0.3 b	26.4 ± 0.4 a	11.8 ± 0.4 ab
SY19	64.0 ± 0.1 b	73.6 ± 0.1 b	84.8 ± 0.4 b	20.8 ± 0.4 b	16.8 ± 0.5 a	26.4 ± 0.9 a	12.3 ± 0.6 a
Kokei 14	73.8 ± 0.1 a	80.0 ± 0.1 a	86.9 ± 0.1 a	13.1 ± 0.1 d	16.2 ± 0.1 a	24.0 ± 0.3 b	12.4 ± 0.8 a
Sig.	0.232	0.728	0.311	0.424	0.528	0.328	0.192

T_o : gelatinization onset temperature; T_p : gelatinization peak temperature; T_c : gelatinization conclusion temperature; ΔT : gelatinization temperature range ($T_c - T_o$); ΔH : gelatinization enthalpy; SP: swelling power; WS: water solubility. The SP and WS were determined at 95 °C. Sig.: the significance of normal distribution of the 7 samples by Shapiro–Wilk test. Data are means ± standard deviations ($n = 2$ for thermal property parameters and $n = 3$ for SP and WS). The values with different letters in the same column are significantly different ($p < 0.05$).

The swelling power (SP) and water solubility (WS) at 95 °C ranged from 24.0 (Kokei 14) to 27.6 g/g (SY148) and from 10.4% (SY192) to 12.4% (Kokei 14), respectively, among seven sweet potato starches (Table 5). Collado et al. [31] reported that the SP and WS vary from 24.5 to 32.7 g/g and from 12.1% to 24.1%, respectively, among 44 sweet potato starches. The pasting properties of starches were analyzed using a rapid visco analyzer (RVA) (Figure 4). The RVA profiles and pasting property parameters including pasting viscosity and temperature and peak time exhibited significant differences among seven sweet potato starches (Figure 4, Table 6). Kokei 14 starch had significantly lower peak (PV) (3265 mPa·s), hot (HV) (1789 mPa·s) and final viscosity (FV) (2341 mPa·s) and higher pasting temperature (P_{Temp}) (81.4 °C) than the other starches, SY6 starch had the highest HV (3220 mPa·s) and FV (3993 mPa·s), and the SY148 starch had the highest PV (5152 mPa·s). The breakdown viscosity (BV) was the lowest for SY4 (1173 mPa·s) and the highest for SY148 (2503 mPa·s), and the setback viscosity (SV) was the lowest for SY148 (500 mPa·s) and the highest for SY6 (773 mPa·s). The peak time (P_{Time}) was the lowest for SY192 (4.18 min). The PV and HV are the maximum and lowest viscosity of the heating starch paste, respectively, and they reflect the ability of binding water and granule swelling of starch [32]. The FV reflects the stability of cooled starch paste [33]. The BV (PV–HV) and SV (FV–HV) reflect the paste resistance to heat and shear and the paste retrogradation to cool, respectively, and the P_{Time} reflects the rate of starch swelling during heating [34]. The P_{Temp} is the critical temperature. Before the P_{Temp} , starch granules in an excess of water continue to swell with increasing heat temperature, and mainly amylose but also some amylopectin leach out of the granules; after reaching the P_{Temp} , starch granules begin to lose their granular shapes, and both the increased surface interactions between the swelling granules and the leached-out starch components will lead to a rise in viscosity [35]. The above RVA parameters are influenced by granule morphology and size, amylose content, crystalline structure, and starch purity [32–34]. Guo et al. [14] reported that the pasting properties of sweet potato starches have no relationship with the color of root tuber, and are determined by the genotypes of sweet potato varieties.

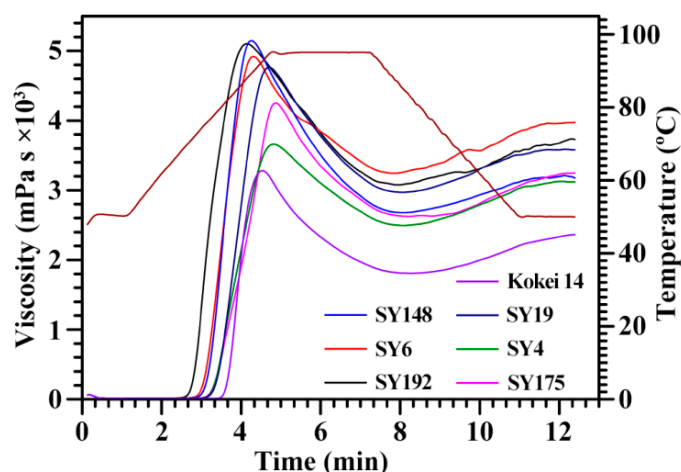


Figure 4. RVA profiles of C-type starches from different sweet potato varieties.

The Pearson correlations between intensities/crystallinities of X-ray diffraction peaks and heat property parameters of C-type starches were analyzed (Table 7). The gelatinization temperature and ΔH were significantly negatively correlated to the intensity and crystallinity of diffraction peak at 5.6°. The gelatinization temperature was significantly positively correlated to the intensity of diffraction peaks at 15° and 23°. In addition, the gelatinization conclusion temperature (T_c) was positively correlated to the crystallinity of diffraction peaks at 15° and 23°. The present results agreed with the previous report that B-type crystallinity has lower gelatinization temperature than A-type crystallinity [3,9]. The SP had no significant relationships with the intensity and crystallinity of crystalline

diffraction peaks, but the WS was significantly positively correlated to the intensity of the diffraction peak at 23° and the crystallinity of diffraction peaks at 15° and 17–18°. For RVA parameters, the intensity of diffraction peak at 5.6° was significantly positively correlated to the HV and FV but significantly negatively correlated to the P_{Temp}. The intensity of the diffraction peak at 15° was significantly negatively correlated to the PV, HV and FV, but significantly positively correlated to the P_{Temp}. The intensity of diffraction peak at 23° was significantly negatively correlated to the PV and significantly positively correlated to the P_{Time} and P_{Temp}. The total crystallinity was positively correlated to the P_{Temp}, and the crystallinity of diffraction peak at 17–18° was negatively correlated to the FV and SV and positively correlated to the P_{Temp} (Table 7). For rice A-type starches, the RC is positively correlated to the To and negatively to the SP [23]. For high-amylose maize B-type starch, the RC is negatively correlated to the Tp, Tc and ΔT and positively to the ΔH, SP and WS [24]. Among different-sized fractions of starch, the total crystallinity is significantly positively correlated to the PV, HV and FV and significantly negatively correlated to the P_{Temp} and Tc for maize A-type starch, and significantly positively correlated to the ΔH and significantly negatively correlated to the Tp, Tc, HV and FV for potato B-type starch [12]. The present results show that the complex relationships between X-ray diffraction peaks and heat properties might be due to the different proportions of A- and B-type crystallinities in C-type starches.

Table 6. Pasting property parameters of C-type starches from different sweet potato varieties.

Accession ID	PV (mPa·s)	HV (mPa·s)	BV (mPa·s)	FV (mPa·s)	SV (mPa·s)	P _{Time} (min)	P _{Temp} (°C)
SY192	5140 ± 19 a	3062 ± 16 b	2078 ± 4 b	3722 ± 48 b	660 ± 65 b	4.18 ± 0.08 e	70.4 ± 0.5 d
SY6	4944 ± 51 b	3220 ± 59 a	1724 ± 9 d	3993 ± 42 a	773 ± 34 a	4.31 ± 0.08 d	73.6 ± 0.5 c
SY148	5152 ± 36 a	2648 ± 26 c	2503 ± 14 a	3148 ± 44 de	500 ± 35 d	4.27 ± 0.01 de	74.2 ± 0.1 c
SY175	4257 ± 52 c	2579 ± 35 c	1678 ± 29 d	3215 ± 27 d	636 ± 9 bc	4.82 ± 0.04 a	76.6 ± 0.1 b
SY4	3651 ± 31 d	2478 ± 13 d	1173 ± 18 f	3100 ± 36 e	622 ± 23 bc	4.82 ± 0.04 a	76.5 ± 0.1 b
SY19	4877 ± 58 b	3011 ± 42 b	1867 ± 32 c	3622 ± 37 c	611 ± 31 bc	4.67 ± 0.01 b	77.1 ± 0.5 b
Kokei 14	3265 ± 50 e	1789 ± 16 e	1476 ± 36 e	2341 ± 20 f	552 ± 6 cd	4.56 ± 0.04 c	81.4 ± 0.1 a
Sig.	0.139	0.439	0.980	0.658	0.816	0.293	0.857

PV: peak viscosity; HV: hot viscosity; BV: breakdown viscosity (PV–HV); FV: final viscosity; SV: setback viscosity (FV–HV); P_{Time}: peak time; P_{Temp}: pasting temperature. Sig.: the significance of normal distribution of the 7 samples by Shapiro–Wilk test. Data are means ± standard deviations (*n* = 3). The values with different letters in the same column are significantly different (*p* < 0.05).

Table 7. Pearson correlation coefficients between intensities/crystallinities of X-ray diffraction peaks and heat properties of C-type starches.

	RI _{5.6°}	RI _{15°}	RI _{23°}	RC _{5.6°}	RC _{15°}	RC _{17–18°}	RC _{23°}	RC _{Total}
To	−0.879 **	0.819 *	0.804 *	−0.844 *	0.631	0.827 *	0.419	0.718
Tp	−0.834 *	0.900 **	0.902 **	−0.860 *	0.682	0.635	0.597	0.670
Tc	−0.904 **	0.845 *	0.974 **	−0.934 **	0.784 *	0.672	0.766 *	0.782 *
ΔT	0.458	−0.424	−0.280	0.378	−0.201	−0.599	0.097	−0.333
ΔH	−0.793 *	0.560	0.760 *	−0.832 *	0.596	0.679	0.543	0.682
SP	0.457	−0.641	−0.534	0.433	−0.122	−0.305	−0.609	−0.390
WS	−0.825 *	0.608	0.883 **	−0.816 *	0.879 **	0.870 *	0.490	0.862 *
PV	0.716	−0.918 **	−0.779 *	0.721	−0.651	−0.500	−0.433	−0.517
HV	0.779 *	−0.854 *	−0.698	0.708	−0.584	−0.705	−0.329	−0.598
BV	0.397	−0.672	−0.601	0.486	−0.501	−0.095	−0.400	−0.246
FV	0.789 *	−0.803 *	−0.691	0.703	−0.601	−0.759 *	−0.330	−0.643
SV	0.596	−0.263	−0.433	0.456	−0.506	−0.822 *	−0.226	−0.690
P _{Time}	−0.650	0.579	0.799 *	−0.702	0.608	0.377	0.857 *	0.628
P _{Temp}	−0.950 **	0.907 **	0.933 **	−0.953 **	0.721	0.770 *	0.625	0.766 *

The abbreviations are listed in Tables 1, 5 and 6. The * and ** indicate the significance at *p* < 0.05 and *p* < 0.01 level, respectively (*n* = 7).

2.4. Principal Component Analysis of Molecular Components and Heat Properties of C-Type Starches

The molecular components (Tables 2 and 3) and heat properties (Tables 5 and 6) of seven sweet potato starches were subjected to principal component analysis (PCA) (Figures 5 and 6). The first, second and third principal components could explain 47.8%, 21.8% and 13.6%, respectively, of the overall variation. The loading plot of PCA can exhibit the relationships among starch property parameters, and the score plot can show the similarities and differences among starches from different varieties [35]. In the present study, only the TAC was significantly positively correlated to the T_o , T_p , T_c , ΔH and P_{Temp} (Figure 5). Cai et al. [23] reported that the AP-S is significantly correlated negatively to the T_o , T_p , T_c and WS and positively to the SP, and the AM is significantly positively correlated to the T_o , T_p , T_c , ΔH and WS and significantly negatively correlated to the SP in rice A-type starches with different amylose contents. Lin et al. [24] reported that the T_o , T_p , T_c and ΔT are positively correlated to the AAC, AM and AP-L and negatively correlated to the AP-S, and the ΔH , SP and WS are correlated negatively to the AAC, AM and AP-L and positively to the AP-S in high-amylose maize B-type starch. In C-type starch from sweet potato, the DP6-12 of amylopectin is negatively correlated to the gelatinization temperature and pasting temperature, and positively correlated to the SV [21], which agrees with the present study. Among different-sized fractions of starch, the AM is significantly positively correlated to the PV, HV and FV and significantly negatively correlated to the P_{Temp} and T_c for maize A-type starch, and positively to the PV and ΔH and negatively to the T_p , T_c , HV and FV for potato B-type starch [12]. It is more complex for C-type starch to reveal the relationships between molecular components and heat properties, especially for sweet potato starch with a mixture of A-, B- and C-type starches. For P_{Temp} , it was significantly positively correlated to gelatinization temperatures including T_o , T_p and T_c (Figure 5). Similar results have been reported in C-type starches from sweet potato [34] and A-type starches from endosperms of dicotyledon plants [36]. The score plot of PCA based on the molecular components and heat properties could differentiate the types of C-type starches (Figure 6), and agreed with their XRD patterns (Figure 1, Table 1). For example, Kokei 14 and SY192 were located at the far right and left of the score plot in principal component 1, respectively, indicating that they had significantly different properties and agreed with their X-ray diffraction peak characteristics.

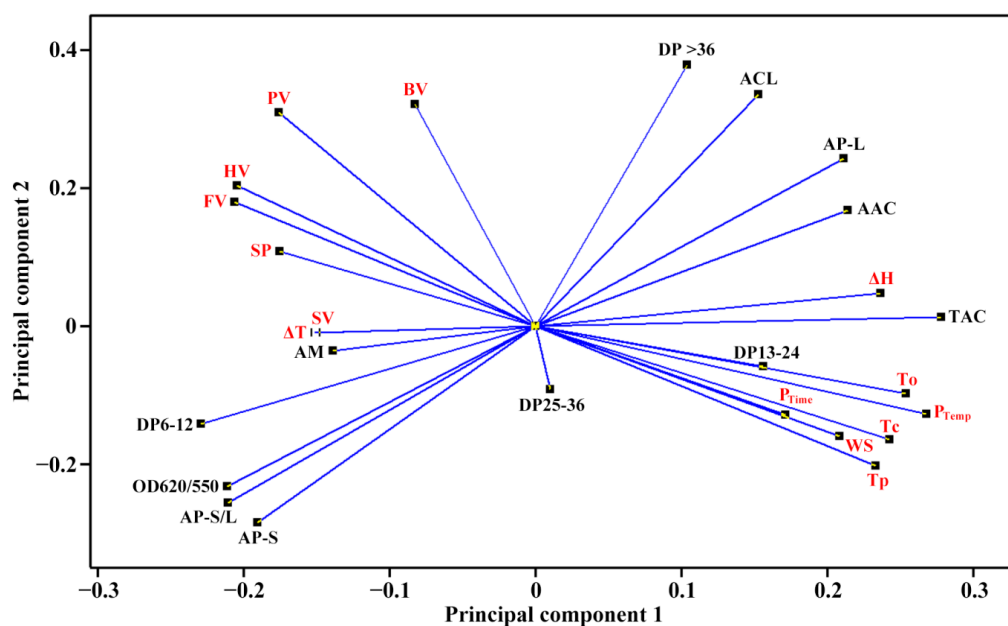


Figure 5. Loading plot of PCA based on the molecular components and heat properties of C-type starches. The abbreviations are listed in Tables 2, 3, 5 and 6. The molecular components are in black, and the heat properties are in red.

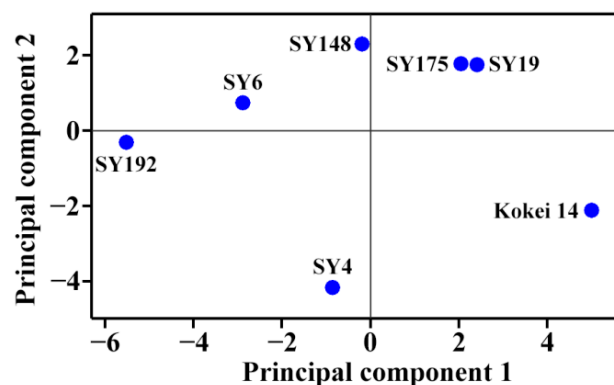


Figure 6. Score plot of PCA based on the molecular components and heat properties of C-type starches.

3. Materials and Methods

3.1. Plant Materials

The 7 sweet potato varieties (SY4, SY6, SY19, SY148, SY175, SY192 and Kokei 14) were selected as plant materials due to the fact that their starches exhibited different C-type XRD patterns according to our previous study [37]. These germplasm resources are conserved in Xuzhou Sweetpotato Research Center, China. The SY4, SY6, SY19, SY148, SY175 and SY192 are origin accession IDs in China National Sweetpotato Genebank. The variety SY19 and SY192 originate from China, the variety SY148 and Kokei 14 originate from Japan, the variety SY4 and SY6 originate from the United States, and the variety SY175 originates from Peru. These sweet potato varieties were all planted simultaneously in the farm of Xuzhou Sweetpotato Research Center (32°27' N, 117°29' E), Jiangsu Province, China on 28 April, and harvested on 26 October 2020.

3.2. Isolation of Starch

Starches were isolated from fresh root tubers after harvest following the method of Guo et al. [10] with some modifications. Briefly, the pieces of root tubers in H₂O were smashed and homogenized in a home blender. The starch-water slurry was filtered through 150, 75 and 50 µm sieves successively, and centrifuged (3000× g, 5 min) in a centrifuge (5430R, Eppendorf, Hamburg, Germany). The dirty surface layer above precipitated starch was removed off. The starch was washed successively with H₂O (5 times) and anhydrous ethanol (3 times), and dried at 40 °C. The starch was filtered through 50 µm sieve, and stored at 4 °C.

3.3. Measurement of Starch–Iodine Absorption and Amylose Content

The starch–iodine absorption spectrum was analyzed following the procedures of Man et al. [22]. Briefly, starch was dissolved in dimethyl sulfoxide containing 10% 6.0 M urea (95 °C, 1 h). The dissolved amylose and amylopectin were colorized with iodine solution (0.2% I₂ and 2% KI) in 50 mL volumetric flask containing 1 mL starch sample, 1 mL iodine solution, and 48 mL H₂O. The sample was scanned using a spectrophotometer (BioMate 3S, Thermo Scientific, Chino, CA, USA). The absorbance data at 550 and 620 nm were obtained from the starch–iodine spectrum. The OD₆₂₀ was used to measure the apparent amylose content (AAC). In order to avoid the effects of amylopectin and lipid on amylose content, the ratio of amylose to both amylose and amylopectin (usually defined as TAC) was determined with the concanavalin A precipitation method using an amylose/amylopectin assay kit (K-AMYL, Megazyme, Bray, Ireland).

3.4. Molecular Weight Distribution Analysis of Starch

The isoamylase-debranched starch was analyzed with a gel permeation chromatography (GPC) system (PL-GPC220, Agilent Technologies UK Limited, Shropshire, UK) following the procedures of Lin et al. [38] exactly. Briefly, the starch deproteinized by

protease was dissolved in dimethyl sulphoxide (DMSO) solution, and then centrifuged ($4000 \times g$, 10 min). The supernatant was precipitated with anhydrous ethanol. The precipitated starch was dissolved and debranched with isoamylase (E-ISAMY, Megazyme, Bray, Ireland). The sample was freeze-dried. The dry starch powder was dissolved in DMSO and analyzed with GPC system with three columns of PL110-6100, 6300 and 6525 and a differential refractive index detector.

3.5. Chain Length Distribution Analysis of Amylopectin

The above isoamylase-debranched starch was labeled with the fluorophore APTS (8-amino-1,3,6-pyrenetrisulfonic acid) following the method of Lin et al. [27]. The sample was analyzed with a fluorophore-assisted capillary electrophoresis (FACE) system (PA800, Beckman-Coulter, Fullerton, CA, USA) following the procedures of Lin et al. [27].

3.6. Crystalline Structure Analysis of Starch

The dry starch powder was treated to absorb some moisture in a sealed container with a saturated NaCl solution for maintaining a 75% relative humidity at 25 °C for 10 d. The sample was detected using an X-ray diffractometer (D8, Bruker, Karlsruhe, Germany) at 40 kV, 40 mA, and 0.02° step size from 3° to 40° 2 θ . The relative crystallinity (RC) was evaluated using the area percentage of crystalline peaks and total diffraction peaks between 4° to 30° 2 θ following the method of Wei et al. [7].

3.7. Thermal Property Analysis of Starch

Five mg starch and 15 μ L water were mixed and sealed in an aluminum pan. The sample was equilibrated at 4 °C overnight and 25 °C for 2 h before analysis, and detected using a differential scanning calorimeter (DSC200-F3, NETZSCH, Selb, Germany). The heating rate was 10 °C/min from 25 to 130 °C.

3.8. Measurement of Swelling Power and Water Solubility of Starch

The 2% (v/v) starch-water slurry was incubated in a ThermoMixer (1000 rpm, 95 °C, 30 min). The sample was centrifuged ($5000 \times g$, 10 min) after cooling at 25 °C for 10 min. The carbohydrates in the supernatant were quantified with an anthrone-H₂SO₄ method to measure the water solubility (WS), and the precipitation was weighed to measure the swelling power (SP) following the method of Guo et al. [10].

3.9. Pasting Property Analysis of Starch

Starch (2.5 g) and water (25 mL) slurry was analyzed using a rapid visco analyzer (3D, Newport Scientific, Warriewood, Australia). The programmed heating process included at 50 °C for 1 min, from 50 to 95 °C for 3.75 min (heating rate of 12 °C/min), at 95 °C for 2.5 min, from 95 to 50 °C for 3.75 min (cooling rate of 12 °C/min), and at 50 °C for 1.4 min. The pasting parameters including PV, HV, BV, FV, SV, P_{Time} and P_{Temp} were automatically calculated by the instrument software.

3.10. Principal Component Analysis (PCA)

The starch property parameters with significance of normal distribution over 0.05 were used for PCA with Minitab V.16.0 software (IBM Company, Chicago, IL, USA).

3.11. Statistical Analysis

The statistical differences, normal distribution, and Pearson correlation of data were evaluated with SPSS 16.0. Only the data with significance of normal distribution over 0.05 were used for Pearson correlation analysis.

4. Conclusions

The intensity of diffraction peak at 5.6° was significantly positively correlated to the DP6-12, HV and FV and significantly negatively correlated to the TAC, DP13-24, To, Tp,

Tc, ΔH , WS and P_{Temp} . The intensity of diffraction peak at 15° was significantly positively correlated to the To, Tp, Tc and P_{Temp} and significantly negatively correlated to the PV, HV and FV. The intensity of the diffraction peak at 23° was significantly positively correlated to the TAC, To, Tp, Tc, ΔH , WS, P_{Time} and P_{Temp} and significantly negatively correlated to the PV. The crystallinity of diffraction peak at 5.6° was significantly positively correlated to the DP6-12 and significantly negatively correlated to the TAC, To, Tp, Tc, ΔH , WS and P_{Temp} . The crystallinity of diffraction peak at 15° was significantly positively correlated to the DP13-24, Tc and WS. The crystallinity of diffraction peak at $17\text{--}18^\circ$ was significantly positively correlated to the TAC, To, WS and P_{Temp} and significantly negatively correlated to the FV and SV. The crystallinity of the diffraction peak at 23° was significantly positively correlated to the Tc and P_{Time} . The total crystallinity was significantly positively correlated to the TAC, Tc, WS and P_{Temp} . The score plot of PCA based on molecular components and heat properties could differentiate the type of C-type starches.

Author Contributions: C.W. and Q.C. conceived the study and designed the experiments; Y.L., L.Z., L.L. and E.L. performed the experiments; Y.L. and L.Z. wrote the original draft manuscript; and C.W. reviewed and edited the manuscript. All authors discussed the contents of the manuscript and approved the submission. All authors have read and agreed to the published version of the manuscript.

Funding: This study was financially supported by grants from the National Key Research and Development Program of China (2018YFD1000705, 2018YFD1000700), Accurate Identification of Sweetpotato Excellent Germplasm Resources (19211139), and Priority Academic Program Development of Jiangsu Higher Education Institutions.

Institutional Review Board Statement: Not applicable.

Informed Consent Statement: Not applicable.

Data Availability Statement: The data are available upon request from the corresponding author.

Conflicts of Interest: The authors declare no conflict of interest.

Sample Availability: Samples of some starches are available from the corresponding author upon reasonable request.


References

- Guo, Z.; Jia, X.; Zhao, B.; Zeng, S.; Xiao, J.; Zheng, B. C-type starches and their derivatives: Structure and function. *Ann. N. Y. Acad. Sci.* **2017**, *1398*, 47–61. [CrossRef] [PubMed]
- He, W.; Wei, C. Progress in C-type starches from different plant sources. *Food Hydrocoll.* **2017**, *73*, 162–175. [CrossRef]
- Ouyang, Q.; Wang, X.; Xiao, Y.; Luo, F.; Lin, Q.; Ding, Y. Structural changes of A-, B- and C-type starches of corn, potato and pea as influenced by sonication temperature and their relationships with digestibility. *Food Chem.* **2021**, *358*, 129858. [CrossRef] [PubMed]
- Barreto, F.F.V.; Bello-Perez, L.A. Chemical, structural, technological properties and applications of Andean tuber starches: A review. *Food Rev. Int.* **2021**. [CrossRef]
- Dereje, B. Composition, morphology and physicochemical properties of starches derived from indigenous Ethiopian tuber crops: A review. *Int. J. Biol. Macromol.* **2021**, *187*, 911–921. [CrossRef]
- Bul on, A.; G erard, C.; Riekkel, C.; Vuong, R.; Chanzy, H. Details of the crystalline ultrastructure of C-starch granules revealed by synchrotron microfocuss mapping. *Macromolecules* **1998**, *31*, 6605–6610. [CrossRef]
- Wei, C.; Qin, F.; Zhou, W.; Yu, H.; Xu, B.; Chen, C.; Zhu, L.; Wang, Y.; Gu, M.; Liu, Q. Granule structure and distribution of allomorphs in C-type high-amylose rice starch granule modified by antisense RNA inhibition of starch branching enzyme. *J. Agric. Food Chem.* **2010**, *58*, 11946–11954. [CrossRef]
- Cai, C.; Cai, J.; Man, J.; Yang, Y.; Wang, Z.; Wei, C. Allomorph distribution and granule structure of lotus rhizome C-type starch during gelatinization. *Food Chem.* **2014**, *142*, 408–415. [CrossRef]
- Fan, X.; Zhao, L.; Zhang, L.; Xu, B.; Wei, C. A new allomorph distribution of C-type starch from root tuber of *Apios fortunei*. *Food Hydrocoll.* **2017**, *66*, 334–342. [CrossRef]
- Guo, K.; Liu, T.; Xu, A.; Zhang, L.; Bian, X.; Wei, C. Structural and functional properties of starches from root tubers of white, yellow, and purple sweet potatoes. *Food Hydrocoll.* **2019**, *89*, 829–836. [CrossRef]
- Zhu, F.; Wang, S. Physicochemical properties, molecular structure, and uses of sweetpotato starch. *Trends Food Sci. Technol.* **2014**, *36*, 68–78. [CrossRef]
- Dhital, S.; Shrestha, A.K.; Hasjim, J.; Gidley, M.J. Physicochemical and structural properties of maize and potato starches as a function of granule size. *J. Agric. Food Chem.* **2011**, *59*, 10151–10161. [CrossRef] [PubMed]

13. Genkina, N.K.; Wasserman, L.A.; Noda, T.; Tester, R.F.; Yuryev, V.P. Effects of annealing on the polymorphic structure of starches from sweet potatoes (Ayamurasaki and Sunnyred cultivars) grown at various soil temperatures. *Carbohydr. Res.* **2004**, *339*, 1093–1098. [CrossRef] [PubMed]
14. Guo, K.; Zhang, L.; Bian, X.; Cao, Q.; Wei, C. A-, B- and C-type starch granules coexist in root tuber of sweet potato. *Food Hydrocoll.* **2020**, *98*, 105279. [CrossRef]
15. Kim, J.; Ren, C.; Shin, M. Physicochemical properties of starch isolated from eight different varieties of Korean sweet potatoes. *Starch-Stärke* **2013**, *65*, 923–930. [CrossRef]
16. Wang, H.; Yang, Q.; Ferdinand, U.; Gong, X.; Qu, Y.; Gao, W.; Ivanistau, A.; Feng, B.; Liu, M. Isolation and characterization of starch from light yellow, orange, and purple sweet potatoes. *Int. J. Biol. Macromol.* **2020**, *160*, 660–668. [CrossRef]
17. Zhang, L.; Zhao, L.; Bian, X.; Guo, K.; Zhou, L.; Wei, C. Characterization and comparative study of starches from seven purple sweet potatoes. *Food Hydrocoll.* **2018**, *80*, 168–176. [CrossRef]
18. Zhu, F.; Xie, Q. Rheological and thermal properties in relation to molecular structure of New Zealand sweetpotato starch. *Food Hydrocoll.* **2018**, *83*, 165–172. [CrossRef]
19. Frost, K.; Kaminski, D.; Kriwan, G.; Lascaris, E.; Shanks, R. Crystallinity and structure of starch using wide angle X-ray scattering. *Carbohydr. Polym.* **2009**, *78*, 543–548. [CrossRef]
20. Pérez, S.; Baldwin, P.M.; Gallant, D.J. Structural features of starch granules I. In *Starch: Chemistry and Technology*, 3rd ed.; BeMiller, J., Whistler, R., Eds.; Elsevier Inc.: New York, NY, USA, 2009; pp. 149–192.
21. Noda, T.; Kobayashi, T.; Suda, I. Effect of soil temperature on starch properties of sweet potatoes. *Carbohydr. Polym.* **2001**, *44*, 239–246. [CrossRef]
22. Man, J.; Lin, L.; Wang, Z.; Wang, Y.; Liu, Q.; Wei, C. Different structures of heterogeneous starch granules from high-amylose rice. *J. Agric. Food Chem.* **2014**, *62*, 11254–11263. [CrossRef] [PubMed]
23. Cai, J.; Man, J.; Huang, J.; Liu, Q.; Wei, W.; Wei, C. Relationship between structure and functional properties of normal rice starches with different amylose contents. *Carbohydr. Polym.* **2015**, *125*, 35–44. [CrossRef] [PubMed]
24. Lin, L.; Guo, D.; Zhao, L.; Zhang, X.; Wang, J.; Zhang, F.; Wei, C. Comparative structure of starches from high-amylose maize inbred lines and their hybrids. *Food Hydrocoll.* **2016**, *52*, 19–28. [CrossRef]
25. Lin, L.; Zhang, Q.; Zhang, L.; Wei, C. Evaluation of the molecular structural parameters of normal rice starch and their relationships with its thermal and digestion properties. *Molecules* **2017**, *22*, 1526. [CrossRef]
26. Huang, L.; Sreenivasulu, N.; Liu, Q. Waxy editing: Old meets new. *Trends Plant Sci.* **2020**, *25*, 963–966. [CrossRef]
27. Lin, L.; Cai, C.; Gilbert, R.G.; Li, E.; Wang, J.; Wei, C. Relationships between amylopectin molecular structures and functional properties of different-sized fractions of normal and high-amylose maize starches. *Food Hydrocoll.* **2016**, *52*, 359–368. [CrossRef]
28. Duan, W.; Zhang, H.; Xie, B.; Wang, B.; Zhang, L. Impacts of nitrogen fertilization rate on the root yield, starch yield and starch physicochemical properties of the sweet potato cultivar Jishu 25. *PLoS ONE* **2019**, *14*, e0221351. [CrossRef]
29. Lee, B.H.; Lee, Y.T. Physicochemical and structural properties of different colored sweet potato starches. *Starch* **2017**, *69*, 1600001. [CrossRef]
30. Osundahunsi, O.F.; Fagbemi, T.N.; Kesselman, E.; Shimoni, E. Comparison of the physicochemical properties and pasting characteristics of flour and starch from red and white sweet potato cultivars. *J. Agric. Food Chem.* **2003**, *51*, 2232–2236. [CrossRef]
31. Collado, L.S.; Mabesa, R.C.; Corke, H. Genetic variation in the physical properties of sweet potato starch. *J. Agric. Food Chem.* **1999**, *47*, 4195–5201. [CrossRef]
32. Shar, T.; Sheng, Z.H.; Ali, U.; Fiaz, S.; Wei, X.J.; Xie, L.H.; Jiao, C.A.; Ali, F.; Shao, G.N.; Hu, S.K.; et al. Mapping quantitative trait loci associated with starch paste viscosity attributes by using double haploid populations of rice (*Oryza sativa* L.). *J. Int. Agric.* **2020**, *19*, 1691–1703. [CrossRef]
33. Singh, N.; Kaur, L.; Ezekiel, R.; Guraya, H.S. Microstructural, cooking and textural characteristics of potato (*Solanum tuberosum* L) tubers in relation to physicochemical and functional properties of their flours. *J. Sci. Food Agric.* **2005**, *85*, 1275–1284. [CrossRef]
34. Abegunde, O.K.; Mu, T.H.; Chen, J.W.; Deng, F.M. Physicochemical characterization of sweet potato starches popularly used in Chinese starch industry. *Food Hydrocoll.* **2013**, *33*, 169–177. [CrossRef]
35. Hellemans, T.; Abera, G.; De Leyn, I.; Van der Meeren, P.; Dewettinck, K.; Eeckhout, M.; De Meulenaer, B.; Van Bockstaele, F. Composition, granular structure, and pasting properties of native starch extracted from *Plectranthus edulis* (Oromo dinich) tubers. *J. Food Sci.* **2017**, *82*, 2794–2804. [CrossRef] [PubMed]
36. Ren, Y.; Guo, K.; Zhang, B.; Wei, C. Comparison of physicochemical properties of very small granule starches from endosperms of dicotyledon plants. *Int. J. Biol. Macromol.* **2020**, *154*, 818–825. [CrossRef] [PubMed]
37. Li, Y.; Zhao, L.; Shi, L.; Lin, L.; Cao, Q.; Wei, C. Sizes, components, crystalline structure, and thermal properties of starches from sweet potato varieties originating from different countries. *Molecules* **2022**, *27*, 1905. [CrossRef]
38. Lin, L.; Zhao, S.; Li, E.; Guo, D.; Wei, C. Structural properties of starch from single kernel of high-amylose maize. *Food Hydrocoll.* **2022**, *124*, 107349. [CrossRef]

Article

Metabolite Profiling of “Green” Extracts of *Cynara cardunculus* subsp. *scolymus*, Cultivar “Carciofo di Paestum” PGI by ¹H NMR and HRMS-Based Metabolomics

Antonietta Cerulli, Milena Masullo, Cosimo Pizza and Sonia Piacente * 

Dipartimento di Farmacia, Università degli Studi di Salerno, Via Giovanni Paolo II n. 132, 84084 Fisciano, SA, Italy; acerulli@unisa.it (A.C.); mmasullo@unisa.it (M.M.); pizza@unisa.it (C.P.)

* Correspondence: piacente@unisa.it; Tel.: +39-089969763

Abstract: Globe artichoke (*Cynara cardunculus* L. var. *scolymus* L.), is a perennial plant widely cultivated in the Mediterranean area, known for its edible part named capitula or heads. Its functional properties are related to its high levels of polyphenolic compounds and inulin. “Carciofo di Paestum”, an Italian traditional cultivar, is a labeled PGI (Protected Geographical Indication) product of the Campania region, representing an important economic resource. So far, a few chemical investigations were performed on this cultivar, mainly focused on the analysis of methanol extracts. Due to the increasing use of food supplements, in this study, a comprehensive analysis of green extracts of “Carciofo di Paestum” PGI heads was performed. EtOH, EtOH: H₂O (80:20, 70:30, 60:40) extracts, as well as infusions and decoctions prepared according to Pharmacopeia XII were analyzed by LC-ESI/QExactive/MS/MS. A total of 17 compounds corresponding to caffeoylquinic acid derivatives, phenolics, flavonoids, and terpenoids were identified. The extracts were further submitted to NMR analysis to highlight the occurrence of primary metabolites. Both LCMS and NMR data were analyzed by Principal Component Analysis (PCA), showing significant differences among the extraction methods. Moreover, 5-caffeoylquinic acid and 1,5-dicaffeoylquinic acid were quantified in the extracts by LC-ESI/QTrap/MS/MS using the Multiple Reaction Monitoring (MRM) method. Furthermore, the phenolic content, antioxidant activity, and α-glucosidase inhibitory activity of *C. cardunculus* var. *scolymus* “Carciofo di Paestum” extracts were evaluated.

Keywords: *Cynara cardunculus* subsp. *scolymus* “Carciofo di Paestum” PGI; green extracts; ¹H NMR and HRMS-based metabolomics; multivariate data analysis

Citation: Cerulli, A.; Masullo, M.; Pizza, C.; Piacente, S. Metabolite Profiling of “Green” Extracts of *Cynara cardunculus* subsp. *scolymus*, Cultivar “Carciofo di Paestum” PGI by ¹H NMR and HRMS-Based Metabolomics. *Molecules* **2022**, *27*, 3328. <https://doi.org/10.3390/molecules27103328>

Academic Editor: Mirella Nardini

Received: 27 April 2022

Accepted: 19 May 2022

Published: 22 May 2022

Publisher’s Note: MDPI stays neutral with regard to jurisdictional claims in published maps and institutional affiliations.



Copyright: © 2022 by the authors. Licensee MDPI, Basel, Switzerland. This article is an open access article distributed under the terms and conditions of the Creative Commons Attribution (CC BY) license (<https://creativecommons.org/licenses/by/4.0/>).

1. Introduction

Globe artichoke (*Cynara cardunculus* L. var. *scolymus* L.), belonging to the family Asteraceae, is a perennial plant widely cultivated in the Mediterranean area. The edible parts of the plant are the large immature inflorescences, named capitula or heads, with edible fleshy leaves. Specifically, *C. cardunculus* L. shows three botanical varieties including the well-known globe artichoke variety (var. *scolymus* (L.)), cultivated or leafy cardoon (var. *altilis* DC.) and their wild perennial progenitor (var. *sylvestris* (Lamk)) [1]. The globe artichoke is widely investigated for its chemical profile and valued for its nutraceutical and medicinal properties [2–7]. Globe artichokes contain a very little amount of fats and high levels of minerals (potassium, sodium, phosphorus), vitamin C, fiber, inulin and polyphenols, hydroxycinnamates, and flavones [8,9]. The functional properties of the artichoke are related to its high levels of polyphenolic compounds and inulin [10–12]. In artichoke flower heads, the most abundant phenolic substances are caffeoylquinic acid derivatives, especially chlorogenic acid, cynarin, and flavonoids, mainly apigenin and luteolin, both present as glucosides and rutosides [3]. The antioxidant capacity of the artichoke has been associated to its high phenolic content [2,13–15]. Phenolic profiles of different *C. cardunculus* genotypes show significant differences, but apigenin and caffeoylquinic acid

derivatives were generally the main compounds in all the samples. Genotype influence has also been observed in relation to antioxidant activity [16–18]. Investigations performed on infusion, decoction, and hydroalcoholic extracts of artichoke leaves revealed different concentrations of phenolic compounds and differences in antioxidant activity [13,19,20]

The edible portion of the artichoke is also a rich source of inulin (19–32% on a dry matter basis), a carbohydrate reserve with a high value in human nutrition due to its prebiotic properties. Inulin resists digestion in the small intestine due to the β -(2→1) fructosyl-fructose linkages but can be fermented by colonic microflora, stimulating the proliferation of commensal bacteria such as *Bifidobacteria* spp. and *Lactobacillus* spp [3,21,22]. For these reasons, artichokes are a valuable source of prebiotic dietary fibers but also of low-calorie carbohydrates with the potential to be used in the production of fat-reduced foods. The positive effects consist in blood glucose attenuation, in the control of cholesterol and serum lipids levels, and in mineral bioavailability [21].

In Italy, the globe artichoke represents one of the most important horticultural crops, with a production of about 384,000 tons in 2021 [23]. Italy is also the richest source of artichoke germplasm, with numerous commercial and local varieties adapted to different environments, which can differ in chemical composition, especially of the polyphenolic fraction, hence exhibiting different nutraceutical and pharmacological properties [14]. “Carciofo di Paestum”, an Italian traditional late clone cultivar, which produces purple heads with light green coloration from March to May [8], is a labeled PGI (Protected Geographical Indication) product of the Campania region, representing an important economic resource.

Previous investigations aimed at assessing and quantifying polyphenols and hydroxycinnamic acids in the globe artichoke “Carciofo di Paestum” were performed mainly on methanol extracts by HPLC-DAD-ESI/MSⁿ [24,25]. A metabolomics approach to characterize CH₂Cl₂/MeOH/H₂O extracts of “Carciofo di Paestum” heads was performed also by NMR analysis [26]. Moreover, “Carciofo di Paestum” by-products were investigated by UHPLC-UV-HRMS [21].

The term “nutraceuticals” derives from “nutrition” and “pharmaceuticals” and is used for nutrition products that are also used as medicine [27]. Nutraceuticals refer to compounds aimed at supplementing the normal diet, containing substances alone or in combination with vitamins and minerals, or herbal products. Thus, they are referred to as “dietary supplements,” or “food supplements” [27–29].

Their use has been steadily increasing all over the world for the last decades, in the form of capsules, liquids, pills, and tablets in measured doses. They are very attractive because of their relatively low prices, non-prescription status, huge promotion, and the perception that natural products are safe [29]. Food supplements are generally extracted with atoxic solvents, such as ethanol and water. Ethanol is the most common bio-solvent, completely biodegradable, and obtained by the fermentation of sugar-rich materials such as sugar beet and cereals; therefore, green solvents such as water and aqueous ethanol solutions are among the preferred ones for extraction processes [30]. Moreover, it is very common to drink the infusion (teas) made with artichoke leaves for liver and digestive issues [13]. In recent years, with an increasing interest in the development of green and environmentally friendly extraction methods, new technologies and methods of extraction have been used [31].

These considerations prompted us to investigate the chemical composition of ethanol: water and water extracts of the globe artichoke “Carciofo di Paestum” since only methanol extracts have thus far been analyzed. The extraction procedures can greatly affect the fingerprints of the extracts. To the best of our knowledge, this is the first comprehensive investigation of green extracts of “Carciofo di Paestum” by a combination of LC-MS and NMR analysis. Metabolomic analysis generates huge datasets that make the application of chemometric methods necessary. Multivariate data analysis (MVDA) was used to identify the metabolite variation among green extracts.

2. Results and Discussion

2.1. LC-ESI/QExactive/MS/MS Analysis of MeOH Extract of “Carciofo di Paestum” PGI

“Carciofo di Paestum” PGI heads were extracted with MeOH to compare this extract with those obtained by green extractions. To identify the specialized metabolites occurring in the MeOH extract of the artichoke, an analytical approach based on LC-MS was carried out [32].

Hyphenated techniques are playing increasingly important roles in support of phytochemical investigations, and in particular, high liquid chromatography (HPLC) coupled to mass spectrometry (MS) is considered a powerful tool [33]. In this case, high-performance liquid chromatography coupled with electrospray ionization and hybrid Quadrupole-Orbitrap mass spectrometry (LC-ESI/QExactive/MS/MS) was used.

According to their accurate mass, characteristic fragmentation pattern, retention time, and literature data, 17 compounds (Figure 1), corresponding to caffeoylquinic acids (**1**, **2**), dicaffeoylquinic acids (**3**, **9**, **12**), phenolic compounds (**4**, **14**), flavonoid derivatives (**5–8**, **10**, **11**, **13**, **16**), and terpenoids (**15**, **17**), could be identified. In particular, on the basis of characteristic product ions at m/z 191 and 179, compounds **1** and **2** were identified as 5- and 3-caffeoylquinic acids, respectively [34]. The identity of 5-caffeoylquinic acid (chlorogenic acid) was confirmed by comparison with a standard compound. Dicaffeoylquinic acids were identified by their fragmentations at m/z 353, 335, and 191 [35,36]. Moreover, 1,5-dicaffeoylquinic acid (**9**) was confirmed by comparison with the reference compound. Regarding flavonoid derivatives, information on sugar moieties and aglycone was derived by characteristic fragmentation patterns. In particular, compounds **5–7** showed a characteristic fragment at m/z 285 corresponding to luteolin, whereas compounds **8**, **10**, and **11** displayed a typical product ion at m/z 269 corresponding to apigenin (Figure 1 and Table S1).

2.2. Isolation and Identification of Specialized Metabolites

To unambiguously identify specialized metabolites in artichoke extracts, isolation of compounds from MeOH extract by HPLC-UV was carried out. In this way, 17 compounds were isolated and characterized by NMR analysis. The isolated compounds were identified as: 5-caffeoylquinic acid (**1**), 3-caffeoylquinic acid (**2**), 1,3-dicaffeoylquinic acid (**3**), 5-feruloylquinic acid (**4**), luteolin-7-*O*-rutinoside (**5**), luteolin-7-*O*- β -D-glucopyranoside (**6**), luteolin-7-*O*- β -D-glucuronide (**7**), apigenin-7-*O*-rutinoside (**8**), 1,5-dicaffeoylquinic acid (**9**), apigenin-7-*O*- β -D-glucopyranoside (**10**), apigenin-7-*O*- β -D-glucuronide (**11**), 4,5-dicaffeoylquinic acid (**12**), luteolin (**13**), salviaflaside (**14**), cynarasaponin J (**15**), apigenin (**16**), and cynarasaponin A (**17**) (Figure 1).

2.3. Metabolite Fingerprint of “Carciofo di Paestum” PGI Green Extracts by LC-ESI/QExactive/MS/MS

To evaluate the possibility to use heads of *C. cardunculus* subsp. *scolymus* as a food supplement in the nutraceutical field but also in cosmetic formulations, simple and fast extraction methods based on the use of cheap and relatively non-toxic solvents were carried out [37]. EtOH was selected as a “green” solvent considering that it is a good solvent for polyphenol extraction and safe for human consumption. Therefore, the heads of “Carciofo di Paestum” PGI were extracted by maceration with EtOH and with different mixtures of EtOH:H₂O (80:20, 70:30, 60:40); moreover, based on Pharmacopeia XII, the artichoke was submitted to infusion and decoction. All the obtained extracts were analyzed by LC-ESI/QExactive/MS/MS.



Figure 1. Specialized metabolites isolated from MeOH extract of *C. cardunculus* subsp. *scolymus*: cultivar “Carciofo di Paestum” PGI.

Among all the extracts, hydroalcoholic, infusion, and decoction extracts were the most interesting, showing higher peaks for flavonoids and quinic acid derivatives than MeOH extract; moreover, with respect to the latter, the “green” extracts allowed a better extraction of cynarasaponin J (15) and A (17) (Figure 2).

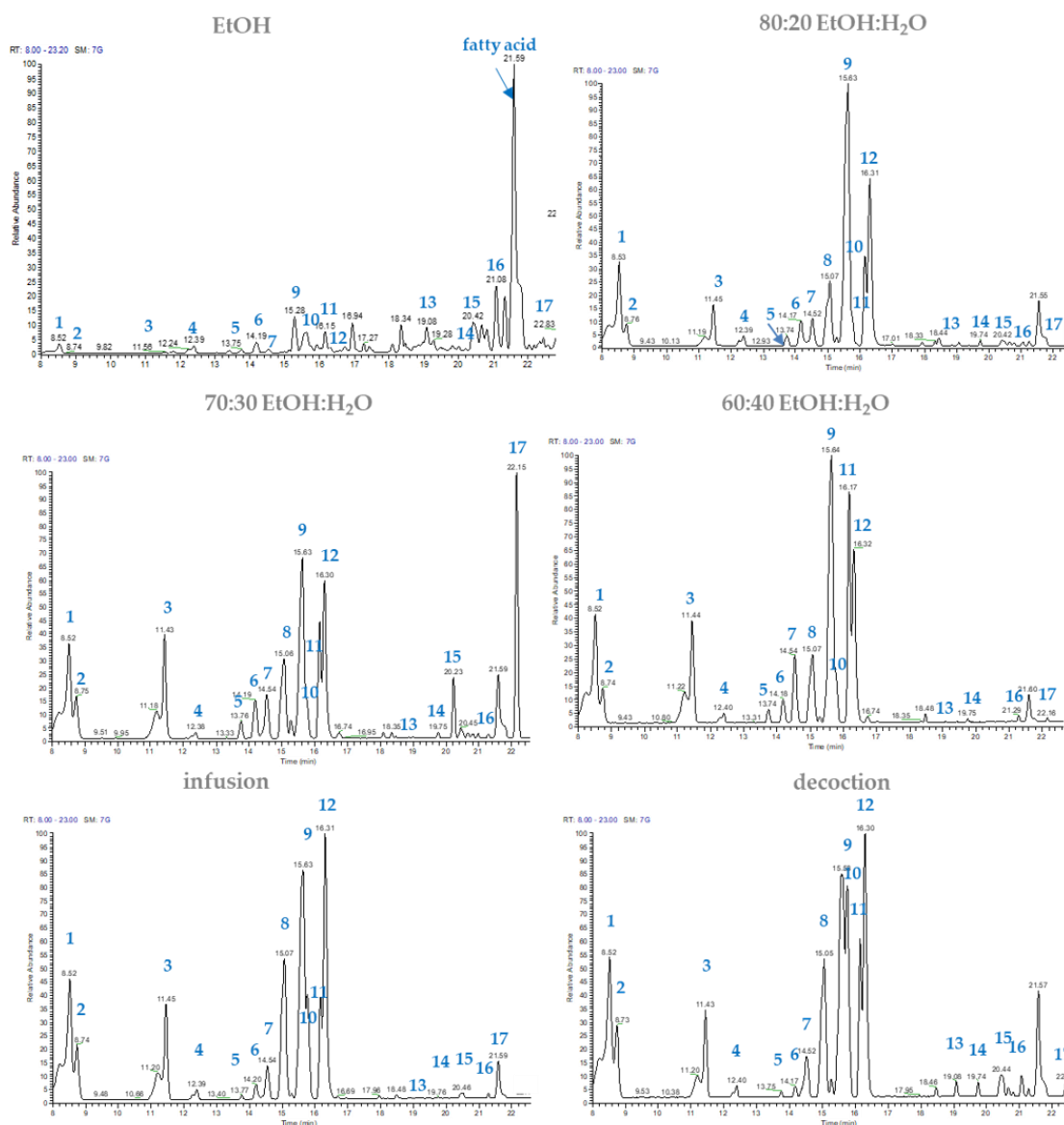


Figure 2. LC-ESI/QExactive/MS profile of different extracts of heads of “Carciofo di Paestum” PGI.

2.4. Targeted Multivariate Statistical Analysis of Secondary Metabolites

To identify similarities in the chemical profile among different samples, the metabolite profiles of different “green” extracts of the artichoke in triplicate were analyzed by multivariate statistical analysis. The raw data were first filtered using MZ mine 2.0 software and then processed using SIMCA-P+ software.

The result of the validation test further emphasized the significance and predictability of the model when the targeted approach was applied; in particular, PC1 contributed to 67.9% of the variance, followed by PC2, which contributed to 18.1%.

The Principal Component Analysis (PCA) highlighted significant differences among the extraction methods. Methanol extracts and the “eco-friendly” extracts were located on the opposite side of the plot, confirming the different selectivity of the employed methods. In the PCA score plot, three clusters could be considered, the first in the left region with EtOH and MeOH extracts, the second cluster in the upper right with hydroalcoholic extracts, and the third cluster in the lower region including infusion and decoction (Figure 3A). The PCA loading plot highlighted that hydroalcoholic extracts were richer than other extracts in flavonoid glycoside derivatives. Meanwhile, infusion and decoction were more abundant in 5-caffeoylquinic acid (5-CQA) and 1,5-dicaffeoylquinic acid (1,5-diCQA) (Figure 3B,C).

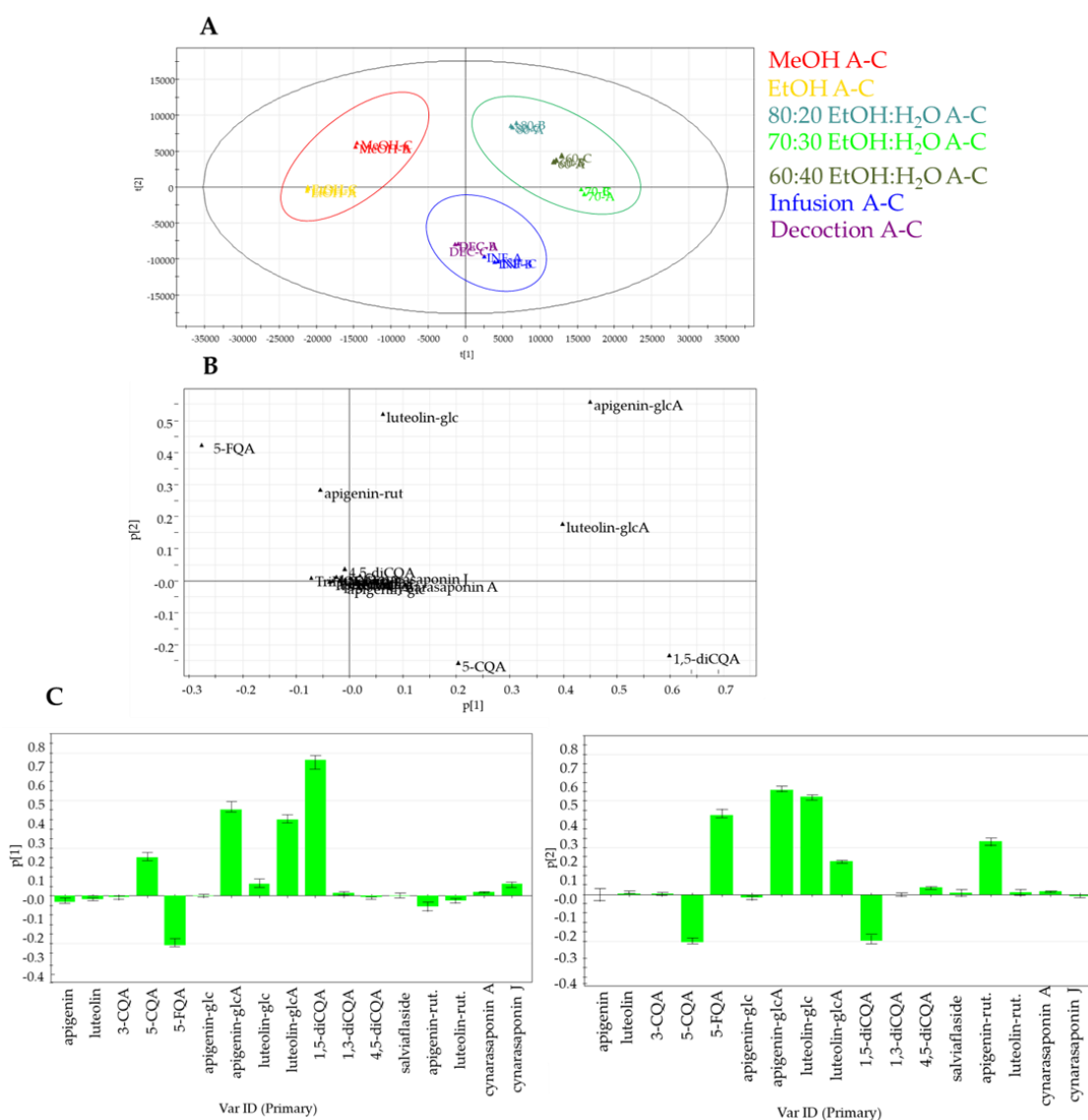


Figure 3. Principal component analysis of specialized metabolites in artichoke extracts obtained by LC-MS targeted analysis: (A) PCA score scatter plot; (B) PCA loading plot; (C) PCA loading column plots. CQA, caffeoylquinic acid; FQA, feruloylquinic acid; diCQA, dicaffeoylquinic acid; rut, rutinoside; glc, glucoside; glcA, glucuronide.

2.5. Quantitative Analysis of 5-Caffeoylquinic Acid (1) and 1,5-Dicaffeoylquinic Acid (9)

The two compounds 5-caffeoylquinic acid (chlorogenic acid) (1) and 1,5-dicaffeoylquinic acid (9) are reported as the main quinic acid derivatives occurring in *C. cardunculus* subsp. *scolymus* [21]. Thus, these two compounds were quantified in the different extracts of *C. cardunculus* subsp. *scolymus* heads by LC-ESI/QTrap/MS/MS analysis. Multiple Reaction Monitoring (MRM), a very accurate and sensitive tandem mass spectrometric technique, was used [38].

Based on the transitions selected for MRM experiments, the amount (mg/g of extract) of each compound in “green” and MeOH extracts was determined.

The compound 5-caffeoylquinic acid (1) occurred in a concentration range of 0.49–5.05 mg/g extract, showing the highest concentration in the infusion and decoction, according to PCA loading plot results; moreover, the abovementioned preparations were also the richest ones of 1,5-dicaffeoylquinic acid (9), although this compound was also very abundant in the other green preparations (Tables 1 and S2).

Table 1. Quantitative results of compounds 1 and 9 (mg/g extract \pm SD) in extracts of *C. cardunculus* subsp. *scolymus* heads.

Compound	MeOH	EtOH	EtOH:H ₂ O 80:20	EtOH:H ₂ O 70:30	EtOH:H ₂ O 60:40	Infusion	Decoction
5-caffeoylquinic acid (1)	0.49 \pm 0.05	2.15 \pm 0.30	1.71 \pm 0.12	1.36 \pm 0.20	0.90 \pm 0.04	5.05 \pm 0.71	2.90 \pm 0.13
1,5-dicaffeoylquinic acid (9)	26.15 \pm 3.88	27.85 \pm 0.41	58.05 \pm 0.92	30.45 \pm 0.50	36.60 \pm 1.27	87.65 \pm 6.29	65.50 \pm 4.50

2.6. Metabolite Fingerprint of Primary Metabolites of *C. cardunculus* subsp. *scolymus* “Green” Extracts by Multivariate Data Analysis based on ¹H NMR

Food supplements are known to contain one or more dietary compounds such as vitamins, minerals, amino acids, carbohydrates, and other substances with a nutritional or physiological effect. As previously described, inulin represents a carbohydrate reserve with a high value in human nutrition, typically occurring in artichokes. To obtain complete information not only about the occurrence of specialized metabolites but also of primary metabolites, as inulin in the different extracts of “Carciofo di Paestum” PGI, a multivariate approach based on ¹H NMR analysis has been carried out.

In the first step, to assign a key signal for each primary metabolite, ¹H NMR of all extracts, in triplicate, were acquired; in this way, 12 primary metabolites including free amino acids, fatty acids, γ -aminobutyric acid, as well as sugars were identified. In detail, the following amino acids were assigned: isoleucine (0.94, t, J = 7.0 Hz), leucine (1.07, d, J = 7.0 Hz), alanine (1.47, d, J = 7.2 Hz), lysine (1.87, d, J = 8.0 Hz), glutamate (2.07, m), aspartic acid (2.75, dd, J = 16.0, 3.0 Hz), and phenylalanine (7.32, m); the key signals at 1.27 (s) and 2.27 (t, J = 7.2 Hz) were attributed to fatty acids and γ -aminobutyric acid (GABA), respectively. Moreover, in the carbohydrate region, ¹NMR spectra displayed characteristic signals assigned to β -fructofuranoside (4.19, d, J = 2.3 Hz) and β -glucopyranoside (4.47, d, J = 8.0 Hz), as well as inulin (5.40, d, J = 5.0 Hz) (Figures S1–S8 and Table S3).

In the second step, to investigate the impact of the different solvents on the extraction of primary metabolites, PCA analysis was carried out. PCA was performed by measuring the selected peak area for each identified metabolite in the ¹H-NMR dataset and by using these areas (variables) as rows of a matrix, while the different extracts of *C. cardunculus* subsp. *scolymus* (observations) were the columns of the matrix. The resulting model, obtained after scaling data by Pareto scaling, showed good fitness and the absence of outliers. PC1 contributed to 86.3% of the variance followed by PC2, which contributed to 7.7%. Thus, the first two PCs exhibited a total variance of 94.0%.

A PCA score plot (Figure 4A) highlighted evident differences between EtOH and MeOH extracts with hydroalcoholic extracts and infusion and decoction. In detail, the PCA loading plot (Figure 4B,C) displayed how carbohydrates are characteristic of infusion and decoction, while fatty acids are typical of EtOH extract, in agreement with the polarity of the solvent used for extractions.

2.7. Evaluation of Phenolic Content and Antioxidant Activity of “Carciofo di Paestum” PGI Extracts

ROS production has been demonstrated to contribute to the development of some diseases including cancer and cardiovascular diseases [39]. Polyphenols can react directly with ROS, preventing their concentrations from reaching harmful intracellular levels. To evaluate the radical scavenging activity by spectrophotometric assay, the preliminary phenolic content was tested by the Folin–Ciocalteu method [40]. The results of the total phenolic content determination indicated a high phenolic content for EtOH:H₂O extracts. Mixtures EtOH:H₂O 80:20, 70:30, and 60:40 showed GAE (milligrams of gallic acid equivalents for gram of extract) values corresponding to 565.14, 512.30, and 562.17, respectively. The high phenolic content shown by the EtOH:H₂O extracts could be attributed to the synergistic effect of the two solvents in the extraction of phenolic compounds; in detail, water could

have an important role in the swelling of plant material, whereas ethanol is responsible for disrupting the binding between the solutes and plant matrix (Figure 5 and Table S4).

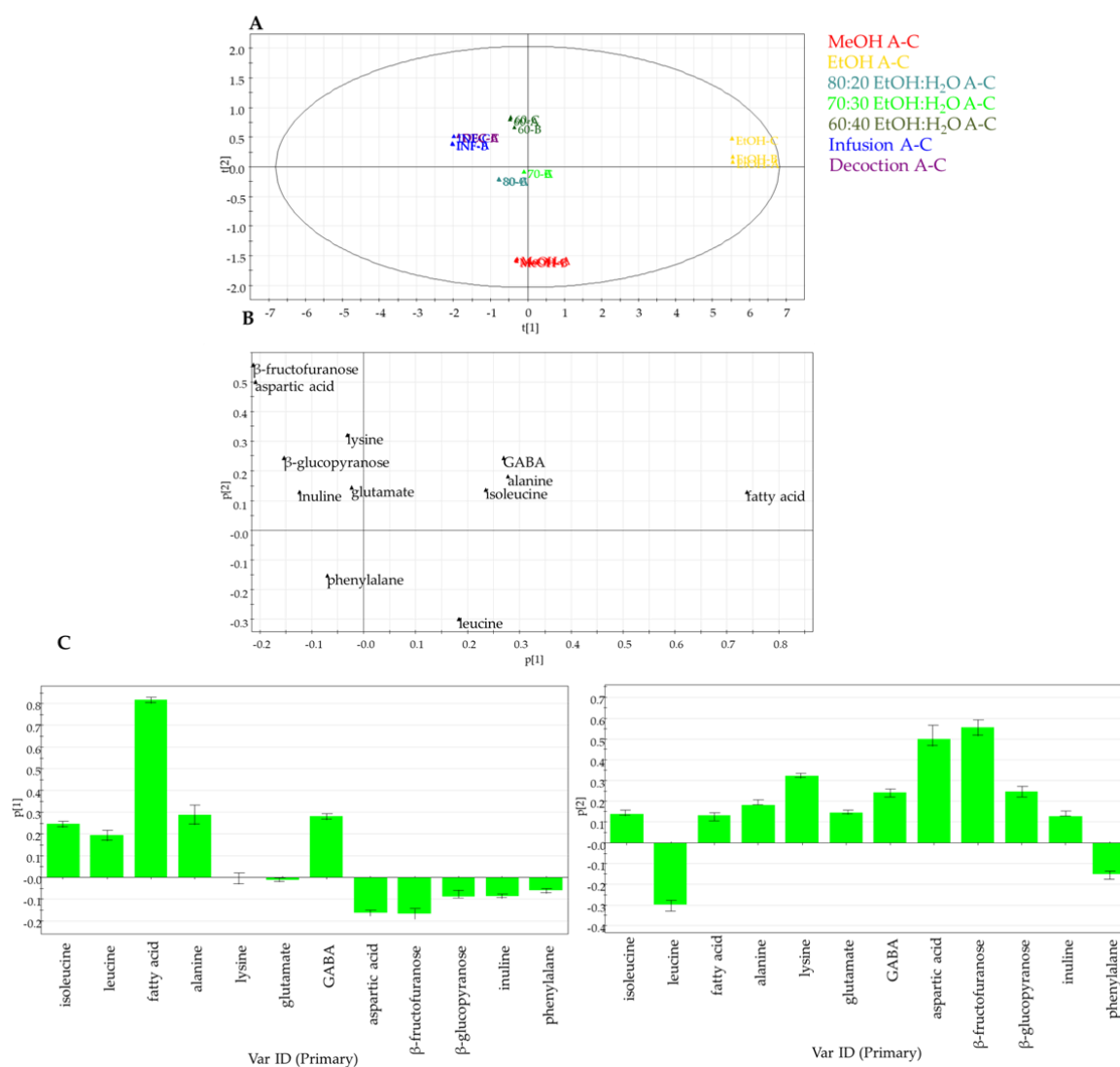


Figure 4. Principal component analysis of primary metabolites in artichoke extracts obtained by NMR targeted analysis: (A) PCA score scatter plot; (B) PCA loading plot; (C) PCA loading column plots.

Successively, the antioxidant activity of “Carciofo di Paestum” PGI extracts was tested by TEAC and DPPH assays. The TEAC assay highlighted a concentration-dependent free-radical scavenging activity for hydroalcoholic extracts as well as infusion and decoction. In detail, hydroalcoholic extracts displayed a radical scavenging activity (1.73–1.78 mM) comparable to quercetin (2.30 mM), used as a reference compound. The DPPH assay displayed how hydroalcoholic extracts exerted a promising antioxidant activity; in particular, EtOH:H₂O 80:20 showed the strongest activity ($EC_{50} = 80.51 \mu\text{g}/\text{mL}$), followed by the other hydroalcoholic extracts and by infusion and decoction. The weakest antioxidant activities were shown by MeOH and EtOH extracts, confirming the results obtained by the TEAC assay (Figure 5 and Table S4).

The ABTS and DPPH values of different artichoke extracts against their corresponding total phenolic content (TPC) values were correlated using Pearson’s method (Table S5). Thaipong et al. reported that Pearson’s correlation coefficient was significantly negative if $-0.61 \leq r \leq -0.97$ and significantly positive if $0.61 \leq r \leq 0.97$ [41]. In particular, there was a positive and significant correlation between TEAC and TPC. About the DPPH assay, the increase in TPC may be related to the increase in antioxidant activities, indicated by

lower IC_{50} DPPH. Therefore, TPC was significantly negatively correlated with IC_{50} DPPH (Table S5).

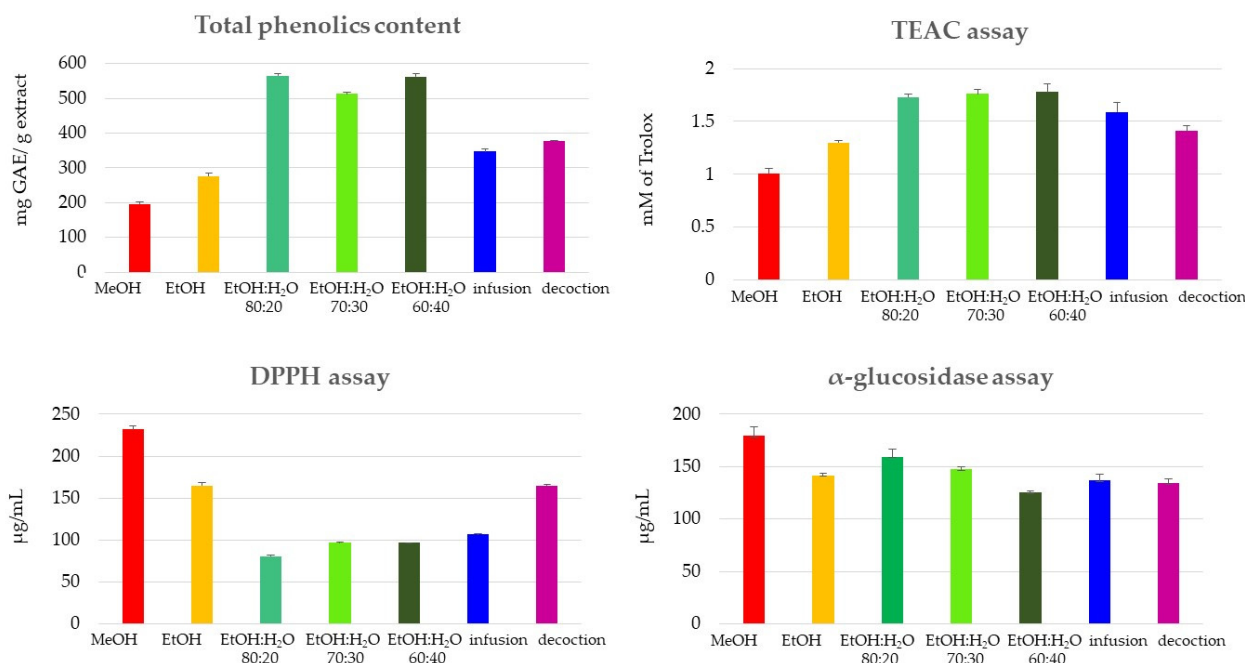


Figure 5. Phenolic content, TEAC, DPPH, and α -glucosidase assays of MeOH and green extracts of *C. cardunculus* subsp. *scolymus*, cultivar “Carciofo di Paestum” PGI.

2.8. α -Glucosidase Inhibitory Activities of “Carciofo di Paestum” PGI Extracts

The inhibitory effects of the “Carciofo di Paestum” PGI extracts against α -glucosidase were evaluated in comparison with those exerted by the antidiabetic compound acarbose. The enzyme α -Glucosidase is the key catalyzing enzyme involved in the process of carbohydrate digestion and glucose release. Inhibition of α -glucosidase is a very effective way of delaying glucose absorption and lowering the postprandial blood glucose level, which can potentially suppress the progression of diabetes mellitus [42].

Extracts and positive control (acarbose) were evaluated in the concentration range of 200–500 μ g/mL. All tested extracts, except the MeOH extract, showed moderate activity with IC_{50} values ranging from 125.3 to 159.3 μ g/mL, comparable to acarbose (Figure 5 and Table S6). In detail, EtOH:H₂O 80:20 (IC_{50} : 125.3) was more active than acarbose (IC_{50} : 132.5), while the other hydroalcoholic extracts and the EtOH extract displayed an activity comparable to acarbose.

3. Materials and Methods

3.1. Chemicals

The solvent for extractions, LC-MS and NMR analysis, Folin-Ciocalteu phenol reagent, 2,2-Diphenyl-1-picrylhydrazyl (DPPH \bullet), vitamin C, 2,2'-azino-bis(3-ethylbenzothiazoline-6-sulphonic acid) (ABTS), potassium persulfate (K₂S₂O₈), phosphate-buffered saline (PBS) solution, Trolox, α -glucosidase enzyme (from *Saccharomyces cerevisiae*), and 4-nitrophenyl α -D-glucopyranoside (PNPG), were purchased from Sigma Aldrich (Milano, Italy).

3.2. Plant Material and Sample Preparation

The heads of *C. cardunculus* subsp. *scolymus*. cv. “Carciofo di Paestum” were collected at commercial maturity, at Paestum, Salerno, Italy in March 2017. A voucher specimen has been deposited in this department.

3.3. Sample Extraction

After harvest, the heads of *C. cardunculus* subsp. *scolymus*, cultivar “Carciofo di Paestum” were transported to the laboratory and crushed into little parts; immediately after, the heads were stored in the freezer at a temperature of $-20\text{ }^{\circ}\text{C}$. After 10 days, they were submitted to lyophilization. At this point, a ratio of 2.0 g/200 mL solvent (*w/v*) of dried heads was used for each extraction, using as solvents MeOH, EtOH, EtOH: H₂O (8:2), EtOH: H₂O (7:3), EtOH: H₂O (6:4), for 3 days, 3 times. After filtration and evaporation of the solvent to dryness in vacuo, dried extracts were obtained. In this way, four different “green” extracts, together with a MeOH extract, were obtained.

Based on Pharmacopeia XII, infusion and decoction were prepared.

The infusion was carried out by adding boiled distilled water to the plant with a specified solid–solvent ratio (1:10 *w/v*), leaving it in touch the solvent and the plant for 10 min under moderate stirring. After this time, stirring was stopped, and the solvent was filtrated to obtain the infusion that was submitted to the analysis.

For decoction, the plant was boiled in an open-type extractor in a specified solid–solvent ratio (1:20 *w/v*) for 2 h, using moderate stirring. Both beakers were covered by aluminum and protected with plastic parafilm both to permit the conservation of a stable temperature and to prevent solvent evaporation and light reaction; then the solvents were filtered under reduced pressure.

3.4. LC-ESI/QExactive/MS/MS Analysis

The extracts of *C. cardunculus* subsp. *scolymus* heads were analyzed using liquid chromatography coupled with electrospray ionization and a high-resolution mass spectrometer (QExactive: hybrid Quadrupole-Orbitrap Mass Spectrometer, ThermoFischer, Waltham, MA, USA), operating in negative ion mode.

LC-MS analysis was carried out on a Kinetex C18 2.6 mm (100 mm \times 2.1 mm) column (Phenomenex, Aschaffenburg, Germany), using a flow rate of 0.2 mL/min. A binary solvent system was used (eluent A: water with 0.1% formic acid (99.9:0.1, *v/v*), eluent B: acetonitrile with 0.1% formic acid (99.9:0.1, *v/v*)). The HPLC gradient started at 5% B. After 10 min, % B was at 20%, after 20 min, it was at 60%, in 2 min % B arrived at 95%, holding at this percentage for 5 min, before returning to the starting percentage. The autosampler was set to inject 4 μL of each extract (1.0 mg/mL MeOH). The auxiliary gas was set at 10 (arbitrary units), and the sheath gas was set at 50 (arbitrary units).

3.5. Isolation of Specialized Metabolites

MeOH extract of *C. cardunculus* subsp. *scolymus* was analyzed by a RP-HPLC-UV system setting wavelength at 254 nm. The elution gradient was obtained using water with 0.1% formic acid as eluent A (99.9:0.1, *v/v*), and acetonitrile with 0.1% formic acid (99.9:0.1, *v/v*), as B at a flow rate of 2.0 mL/min. A Phenomenex Sinergy Hydro Prep MS C18 column (250 mm \times 10 mm, 10 micron) was used. The HPLC gradient started at 10% B and remained at 10% for 5 min; after 12 min, % B was at 20%, after 13 min, it was set at 26%, after 10 min, % B was at 38%, after 10 min, it was at 90%, and finally after 2 min at 100%; it was held at 100 % for 10 min before returning to the starting percentage. Compounds **1** (5.8 mg, $t_R = 22.0$ min), **2** (1.7 mg, $t_R = 24.09$ min), **3** (4.2 mg, $t_R = 29.27$ min), **4** (2.3 mg, $t_R = 31.03$ min), **5** (2.9 mg, $t_R = 31.30$ min), **6** (3.1 mg, $t_R = 32.87$ min), **7** (3.8 mg, $t_R = 33.52$ min), **8** (2.1 mg, $t_R = 35.70$ min), **9** (5.8 mg, $t_R = 37.29$ min), **10** (3.3 mg, $t_R = 39.49$ min), **11** (4.2 mg, $t_R = 41.95$ min), **12** (4.5 mg, $t_R = 44.52$ min), **13** (2.3 mg, $t_R = 45.39$ min), **14** (2.4 mg, $t_R = 47.10$ min), **15** (3.6 mg, $t_R = 48.5$ min), **16** (2.5 mg, $t_R = 49.8$ min), and **17** (4.6 mg, $t_R = 50.6$ min) were obtained.

3.6. Multivariate Data Analysis of Specialized Metabolites

Xcalibur 2.2 from Thermo Fisher Scientific was used to check the exact mass of each secondary metabolite identified by LC-MS analysis (negative ion mode). MZMine 2.10

was used for LC-MS data processing (<http://mzmine.sourceforge.net> (accessed on 10 March 2022)).

MZMine software was used to filter the noise and detect and align the peaks observed in LC-MS profiles (noise level 1.0×10^4 ; all data points below this intensity level were ignored) after exporting the processed data in tabular format (.csv file). Each sample was analyzed in triplicate.

For targeted analysis of specialized metabolites, the peak area obtained from LC/MS analysis was considered. Pareto scaling was applied before multivariate data analysis; in detail, the matrix was constituted of 17 variables, corresponding to the peak area of *m/z* values of specific specialized metabolites of *C. cardunculus* subsp. *scolymus*, and 7 observations, represented by different extracts.

3.7. Quantitative Analysis of 5-Caffeoylquinic Acid (1) and 1,5-dicaffeoylquinic Acid (9)

Quantitative analyses were performed on a LC-ESI/QTrap/MS system working in Multiple Reaction Monitoring (MRM) mode. HPLC separation was conducted by Kinetex Omega μ m RP C18 column (100 mm \times 2.1 mm i.d) at a flow rate of 0.3 μ L/min.

Linear gradient elution was carried out by using H₂O with 0.1% formic acid as eluent A (99.9:0.1, *v/v*), and acetonitrile with 0.1% formic acid (99.9:0.1, *v/v*), as eluent B. The HPLC gradient started at 5% B; after 2.1 min, % B was at 15%, changing from 15% B to 35% B in 4.3 min, from 35% B to 80% B in 2.1 min, and returning to the starting percentage in 2.1 min. The instrument operated in the negative ion mode for internal standard (resveratrol, 1 μ g/mL for each solution) and external standards 5-caffeoylquinic acid (1) and 1,5-dicaffeoylquinic acid (9) specific values of declustering potential, focusing potential, entrance potential, collision energy, and collision cell exit potential were used (Table S2). *C. cardunculus* subsp. *scolymus* extracts were diluted by using methanol, and 5 μ L (1.0 mg/mL) were injected in triplicate; solutions of different ES concentrations (0.5, 1.0, 5.0, 10, 20, 30, 50, and 70 μ g/mL) were used. Linear regression analysis was performed using the Analyst 1.6.2 Software provided by the manufacturer (AB Sciex, Milan, Italy).

Linearity was evaluated by correlation values of calibration curves. The limit of quantification (LOQ; equivalent to sensitivity) was evaluated by injecting a series of increasingly diluted standard solutions until the signal-to-noise ratio was reduced to 10. The limit of detection (LOD) was estimated by injecting a series of increasingly diluted standard solutions until the signal-to-noise ratio was reduced to 3 [43] (Table S2).

3.8. NMR Analysis and Data Processing

NMR analyses were carried out on a Bruker Ascend-600 spectrometer (Bruker BioSpin GmbH, Rheinstetten, Germany) equipped with a Bruker 5 mm. Methanol-*d*₄ (99.95%, Sigma-Aldrich) was used as solvent for each extract. The NMR data were processed using TopSpin 3.2 software. For HSQC, a spectral width of 12 ppm and 165 ppm in the proton and carbon dimensions, respectively, were used with 1 K data points, 64 scans, 256 t1 increments, and a recycle delay of 2 s. HMBC was obtained with a spectral width of 12 ppm and 230 ppm in the proton and carbon dimensions, respectively, 4 K data points, 120 scans, 256 t1 increments, and a recycle delay of 2 s.

For the targeted multivariate analysis, all samples were acquired in methanol-*d*₄ (99.95%, Sigma-Aldrich). The peak of TPS (3-(Trimethylsilyl)-propionic-2,2,3,3-*d*₄ acid sodium salt at 0.9% (*w/w*) in D₂O 99.9 atom%) at 0 ppm was used as the chemical shift external reference. All samples were run at 300 K, using the zgesgp pulse sequence; the relaxation delay was 4.0 s, and the acquisition time was 5.45 s, with 128 number scans and data collected into 64 k data points. Each free induction decay (FID) was zero-filled to 128 k data points. Before Fourier transformation, an exponential window function with a line broadening factor of 0.3 Hz was applied. After the acquisition, the spectra were analyzed by MestreNova 10 software. In particular, the spectra were manually phased and the baseline corrected. Spectra were referenced using the TSP, obtaining good peak alignment. Bucketing was performed within the 0.5–8.2 ppm region (spectral buckets of

0.004 ppm), excluding the signals of the residual non-deuterated methanol and deuterated methanol. The obtained dataset was normalized by range area (0.5–8.2 ppm) normalization. Finally, the spectra were converted to an ASCII format. Each sample was analyzed in triplicate [37].

Pareto scaling was applied before multivariate data analysis; in detail, the matrix was constituted of 12 variables, corresponding to key chemical shift of primary metabolites of *C. scolymus*, and 7 observations, represented by different extracts.

3.9. Total Phenolic Content, DPPH, and TEAC Assays

Folin–Ciocalteu, DPPH, and TEAC assays for each extract have been performed as previously reported with slight modification [44].

The total phenolic content of the extracts was determined by Folin–Ciocalteu assay; gallic acid was used as a reference compound (calibration equation: $y = 0.0038x + 0.145$, $R^2 = 0.998$). All the experiments were performed in triplicate, and results were expressed as the means of gallic acid equivalents (GAEmg/g dried extract) (Table S4).

Radical scavenging activity was determined by spectrophotometric assays of DPPH and TEAC. In particular, in the TEAC assay, the antioxidant activities of analyzed extracts (range = 0.25–1.00 mg/mL) were expressed as TEAC values in comparison with the TEAC activity of quercetin; TEAC values are expressed as concentration (mM) of a standard Trolox solution exerting the same antioxidant activity of a 1 mg/mL solution of the tested extract (calibration equation for Trolox: $y = 31.683x + 52.436$, $R^2 = 1.00$) (Table S4).

For DPPH, the percentage of DPPH• radical scavenging activity (%) was plotted against the extract concentration ($\mu\text{g/mL}$) to determine the IC_{50} . In brief, stock solutions (1 mg/mL) of all the obtained extracts were used in the range of 50–200 $\mu\text{g/mL}$, and an aliquot (5.0 μL) of the methanol solution containing different amounts of each extract was added to 195 μL of daily prepared DPPH• solution. Absorbance at 517 nm was measured on a UV-visible spectrophotometer (Multiskans skyhigh, Thermo Fisher Scientific, Milan, Italy) 10 min after starting the reaction.

All the experiments were performed in triplicate. Range = 50–200 $\mu\text{g/mL}$ was tested for each extract, and vitamin C was used as positive control and analyzed by linear regression [45] (Table S4).

3.10. α -Glucosidase Inhibition Assay

All α -Glucosidase inhibitory activity was evaluated as previously reported in Masullo 2022 [36,42]. In detail, 0.1 M phosphate buffer at pH 7.0 (150 μL) was added to each well; after 10 μL of samples (dissolved in MeOH at concentrations of 200, 300, 500 μM) were added, the reaction was started by the addition of 15 μL of the α -glucosidase enzyme (2 U/mL) in each well, and the plate was incubated for 5 min at 37 °C; after 5 min, 75 μL of the substrate (2.5 mM) 4-nitrophenyl α -D-glucopyranoside were added, and the plate was submitted to incubation for 10 min at 37 °C. The absorbance was measured at 405 nm before (T_0') and after the incubation with the enzyme (T_{10}'). Acarbose was used as positive control, and negative control absorbance (phosphate buffer in place of the sample) was also evaluated. Inhibition of the enzyme was calculated, and the results were expressed as IC_{50} values. All experiments were carried out in triplicate.

IC_{50} values were calculated through non-linear regression using Graphpad Prism 5 Software and expressed as means of the standard deviation (SD) of three independent experiments. The results were considered statistically significant with values of $p < 0.05$.

3.11. Statistics and Data Analysis

Values were expressed as the average values \pm standard deviation (SD) of at least triplicate experiments. The correlation coefficients among means were determined using Pearson's method (Table S5) [41].

4. Conclusions

Considering the increasing interest in the production of artichoke-based food supplements, this work was aimed at defining the chemical profile of the green extracts of “Carciofo di Paestum” PGI. For the first time, a comprehensive investigation of green extracts was performed by LC-MS and NMR analysis to highlight the occurrence of both specialized and primary metabolites, respectively. Moreover, the use of statistical analysis to process the obtained data provided easy and clear visualization of the best extraction method. The globe artichoke is a source of caffeoylquinic acids, responsible for its healthy properties.

Among the occurring caffeoylquinic acids, 5-caffeoylquinic acid known as chlorogenic acid represents one of the most available acids among phenolic acid compounds [46]. In addition, 5-caffeoylquinic acid and 1,5-dicaffeoylquinic acid known as cynarin play several important and therapeutic roles such as antioxidant activity, antibacterial, anticancer, hepatoprotective, cardioprotective, anti-inflammatory, antipyretic, neuroprotective, antiviral, anti-microbial, anti-hypertensive, free radicals scavenging, and central nervous system stimulating [46,47]. Literature data showed how 5-caffeoylquinic acid is able to modulate lipid and glucose metabolisms in metabolic-related disorders [46]. Recent reports have highlighted the role of 1,5-dicaffeoylquinic acid in the treatment of Alzheimer’s disease [47]. Considering the interesting activity reported for these molecules, this work highlights how 5-caffeoylquinic acid (5-CQA) and 1,5-dicaffeoylquinic acid (1,5-diCQA), occur in the highest amount in infusion and decoction. Noteworthy, the mixtures ethanol:water exerted a better ability to extract flavonoid glycosides.

The radical scavenging activity of the extracts is predominantly ascribed to phenolic compounds. According to the results obtained by LC-MS multivariate data analysis, the ethanol–water extracts showed the best total phenolic content as well as the best radical scavenging activity measured by DPPH assay.

A comprehensive chemical profile of the extracts is necessary to highlight the occurrence of primary metabolites such as amino acids and carbohydrates. This approach allowed us to identify the occurrence in *C. cardunculus* subsp. *scolymus* of inulin which represents one of the molecules responsible for artichoke health benefits. Preparations as infusions and decoctions contain a higher amount of inulin than methanol and ethanol extracts.

In conclusion, this work highlights the differences in the chemical profile of extracts obtained with different solvents and is aimed at providing clear and punctual knowledge on the chemical composition of Carciofo di Paestum PGI for its potential use as a food supplement.

Supplementary Materials: The following supporting information can be downloaded at: <https://www.mdpi.com/article/10.3390/molecules27103328/s1>, Table S1. Compounds identified in *C. scolymus* MeOH extract by LC-ESI/QExactive/MS/MS (negative ion mode); Table S2. LC-MS/MS conditions for quantitation of compounds **1** and **9** by negative ion MRM mode; Figures S1–S7. ¹H NMR Spectra (600 MHz, CD₃OD) of extracts; Figure S8. ¹H NMR Spectrum with annotations of identified primary metabolites detected in *C. scolymus* heads EtOH H₂O (80:20) extract; Table S3. Characteristic ¹H NMR peaks of primary metabolites identified in *C. scolymus* extracts. Table S4. Phenolic content and antioxidant activity of green extracts of “Carciofo di Paestum” PGI extracts.; Table S5. Correlation between TPC evaluated by Folin–Ciocalteu and antioxidant activity evaluated by the ABTS, and DPPH methods. The correlation coefficients among means were determined using Pearson’s method; Table S6. α -glucosidase inhibitory activity of “Carciofo di Paestum” PGI extracts.

Author Contributions: Conceptualization, M.M., C.P. and S.P.; methodology, A.C. and M.M.; formal analysis, A.C. and M.M.; investigation, A.C.; resources, S.P.; data curation, A.C. and M.M.; writing-original draft preparation, A.C. and M.M.; writing-review and editing, C.P. and S.P.; supervision, S.P.; project administration, S.P.; funding acquisition, S.P. All authors have read and agreed to the published version of the manuscript.

Funding: This research received no external funding.

Institutional Review Board Statement: Not applicable.

Informed Consent Statement: Not applicable.

Data Availability Statement: The data presented in this study are available in supplementary materials.

Acknowledgments: The authors thank TerraOrti, Eboli (SA), Italy, for providing globe artichokes *Cynara cardunculus* subsp. *scolymus* “Carciofo di Paestum” PGI as a kind gift.

Conflicts of Interest: The authors declare no conflict of interest.

Sample Availability: Samples of the compounds 1–17 are available from the authors.

References

- Zayed, A.; Serag, A.; Farag, M.A. *Cynara cardunculus* L.: Outgoing and potential trends of phytochemical, industrial, nutritive and medicinal merits. *J. Funct. Foods* **2020**, *69*, 103937. [CrossRef]
- Lattanzio, V.; Kroon, P.A.; Linsalata, V.; Cardinali, A. Globe artichoke: A functional food and source of nutraceutical ingredients. *J. Funct. Foods* **2009**, *1*, 131–144. [CrossRef]
- Gostin, A.I.; Waisundara, V.Y. Edible flowers as functional food: A review on artichoke (*Cynara cardunculus* L.). *Trends Food. Sci. Technol.* **2019**, *86*, 381–391. [CrossRef]
- Grabowska, A.; Caruso, G.; Mehrafarin, A.; Kalisz, A.; Gruszecki, R.; Kunicki, E.; SÄ™kara, A. Application of modern agronomic and biotechnological strategies to valorise worldwide globe artichoke (*Cynara cardunculus* L.) potential—An analytical overview. *Ital. J. Agron.* **2018**, *13*, 279–289. [CrossRef]
- Blanco, E.; Sabetta, W.; Danzi, D.; Negro, D.; Passeri, V.; Lisi, A.; Paolucci, F.; Sonnante, G. Isolation and Characterization of the Flavonol Regulator CcMYB12 from the Globe Artichoke [*Cynara cardunculus* var. *scolymus* (L.) Fiori]. *Front. Plant Sci.* **2018**, *9*, 941. [CrossRef] [PubMed]
- Abu-Reidah, I.M.; Arraez-Roman, D.; Segura-Carretero, A.; Fernandez-Gutierrez, A. Extensive characterisation of bioactive phenolic constituents from globe artichoke (*Cynara scolymus* L.) by HPLC-DAD-ESI-QTOF-MS. *Food Chem.* **2013**, *141*, 2269–2277. [CrossRef]
- Salekzamani, S.; Ebrahimi-Mameghani, M.; Rezazadeh, K. The antioxidant activity of artichoke (*Cynara scolymus*): A systematic review and meta-analysis of animal studies. *Phytother. Res.* **2019**, *33*, 55–71. [CrossRef]
- Pandino, G.; Lombardo, S.; Mauromicale, G. Mineral profile in globe artichoke as affected by genotype, head part and environment. *J. Sci. Food Agric.* **2011**, *91*, 302–308. [CrossRef]
- Rocchetti, G.; Lucini, L.; Corrado, G.; Colla, G.; Cardarelli, M.; Pascale, S.; Roupheal, Y. Phytochemical Profile, Mineral Content, and Bioactive Compounds in Leaves of Seed-Propagated Artichoke Hybrid Cultivars. *Molecules* **2020**, *25*, 3795. [CrossRef]
- Demir, T.; Agaoglu, S. Antioxidant, Antimicrobial and Metmyoglobin Reducing Activity of Artichoke (*Cynara scolymus*) Powder Extract-Added Minced Meat during Frozen Storage. *Molecules* **2021**, *26*, 5494. [CrossRef]
- Turkiewicz, I.P.; Wojdylo, A.; Tkacz, K.; Nowicka, P.; Hernandez, F. Antidiabetic, Anticholinesterase and Antioxidant Activity vs. Terpenoids and Phenolic Compounds in Selected New Cultivars and Hybrids of Artichoke *Cynara scolymus* L. *Molecules* **2019**, *24*, 1222. [CrossRef] [PubMed]
- Xia, N.; Pautz, A.; Wollscheid, U.; Reifenberg, G.; Forstermann, U.; Li, H. Artichoke, cynarin and cyanidin downregulate the expression of inducible nitric oxide synthase in human coronary smooth muscle cells. *Molecules* **2014**, *19*, 3654–3668. [CrossRef] [PubMed]
- Pistón, M.; Machado, I.; Branco, C.S.; Cesio, V.; Heinzen, H.; Ribeiro, D.; Fernandes, E.; Chisté, R.C.; Freitas, M. Infusion, decoction and hydroalcoholic extracts of leaves from artichoke (*Cynara cardunculus* L. subsp. *cardunculus*) are effective scavengers of physiologically relevant ROS and RNS. *Food Res. Int.* **2014**, *64*, 150–156. [CrossRef] [PubMed]
- Fратиanni, F.; Tucci, M.; Palma, M.D.; Pepe, R.; Nazzaro, F. Polyphenolic composition in different parts of some cultivars of globe artichoke (*Cynara cardunculus* L. var. *scolymus* (L.) Fiori). *Food Chem.* **2007**, *104*, 1282–1286. [CrossRef]
- Pérez-García, F.; Adzet, T.; Cañigüeral, S. Activity of artichoke leaf extract on reactive oxygen species in human leukocytes. *Free Radic. Res.* **2000**, *33*, 661–665. [CrossRef]
- Dias, M.I.; Barros, L.; Barreira, J.C.M.; Alves, M.J.; Barracosa, P.; Ferreira, I.C.F.R. Phenolic profile and bioactivity of cardoon (*Cynara cardunculus* L.) inflorescence parts: Selecting the best genotype for food applications. *Food Chem.* **2018**, *268*, 196–202. [CrossRef]
- Luca, S.V.; Kulinowski, L.; Ciobanu, C.; Zengin, G.; Czerwińska, M.E.; Granica, S.; Xiao, J.; Skalicka-Woźniak, K.; Trifan, A. Phytochemical and multi-biological characterization of two *Cynara scolymus* L. varieties: A glance into their potential large scale cultivation and valorization as bio-functional ingredients. *Ind. Crops Prod.* **2022**, *178*, 114623. [CrossRef]
- Nouraei, S.; Rahimmalek, M.; Saeidi, G. Variation in polyphenolic composition, antioxidants and physiological characteristics of globe artichoke (*Cynara cardunculus* var. *scolymus* Hayek L.) as affected by drought stress. *Sci. Hortic.* **2018**, *233*, 378–385. [CrossRef]

19. Kuczmanna, A.; Gal, P.; Varinska, L.; Tremel, J.; Kovac, I.; Novotny, M.; Vasilenko, T.; Dall'Acqua, S.; Nagy, M.; Mucaji, P. *Agrimonia eupatoria* L. and *Cynara cardunculus* L. Water Infusions: Phenolic Profile and Comparison of Antioxidant Activities. *Molecules* **2015**, *20*, 20538–20550. [CrossRef]
20. Kollia, E.; Markaki, P.; Zoumpoulakis, P.; Proestos, C. Comparison of Different Extraction Methods for the Determination of the Antioxidant and Antifungal Activity of *Cynara scolymus* and *C. cardunculus* Extracts and Infusions. *Nat. Prod. Commun.* **2017**, *12*, 423–426. [CrossRef]
21. Pagano, I.; Piccinelli, A.L.; Celano, R.; Campone, L.; Gazzero, P.; De Falco, E.; Rastrelli, L. Chemical profile and cellular antioxidant activity of artichoke by-products. *Food Funct.* **2016**, *7*, 4841–4850. [CrossRef] [PubMed]
22. Ito, H.; Takemura, N.; Sonoyama, K.; Kawagishi, H.; Topping, D.L.; Conlon, M.A.; Morita, T. Degree of polymerization of inulin-type fructans differentially affects number of lactic acid bacteria, intestinal immune functions, and immunoglobulin A secretion in the rat cecum. *J. Agric. Food Chem.* **2011**, *59*, 5771–5778. [CrossRef] [PubMed]
23. Istat. Available online: <https://www.istat.it/> (accessed on 22 April 2022).
24. Pandino, G.; Courts, F.L.; Lombardo, S.; Mauromicale, G.; Williamson, G. Caffeoylquinic acids and flavonoids in the immature inflorescence of globe artichoke, wild cardoon, and cultivated cardoon. *J. Agric. Food Chem.* **2010**, *58*, 1026–1031. [CrossRef] [PubMed]
25. Lombardo, S.; Pandino, G.; Mauromicale, G.; Knödler, M.; Carle, R.; Schieber, A. Influence of genotype, harvest time and plant part on polyphenolic composition of globe artichoke [*Cynara cardunculus* L. var. *scolymus* (L.) Fiori]. *Food Chem.* **2010**, *119*, 1175–1181. [CrossRef]
26. de Falco, B.; Incerti, G.; Pepe, R.; Amato, M.; Lanzotti, V. Metabolomic Fingerprinting of Romaneschi Globe Artichokes by NMR Spectroscopy and Multivariate Data Analysis. *Phytochem. Anal.* **2016**, *27*, 304–314. [CrossRef]
27. Siddiqui, R.A.; Moghadasian, M.H. Nutraceuticals and Nutrition Supplements: Challenges and Opportunities. *Nutrients* **2020**, *12*, 1593. [CrossRef]
28. Carrizzo, A.; Moltedo, O.; Damato, A.; Martinello, K.; Di Pietro, P.; Oliveti, M.; Acernese, F.; Giugliano, G.; Izzo, R.; Sommella, E.; et al. New Nutraceutical Combination Reduces Blood Pressure and Improves Exercise Capacity in Hypertensive Patients Via a Nitric Oxide-Dependent Mechanism. *J. Am. Heart Assoc.* **2020**, *9*, e014923. [CrossRef]
29. Chaloupkova, P.; Petryl, M.; Verner, V.; Kokoska, L. Dietary supplements versus functional foods: Consumers' attitudes to their consumption. *Br. Food J.* **2020**, *122*, 3853–3868. [CrossRef]
30. Cerulli, A.; Masullo, M.; Piacente, S. Metabolite Profiling of *Helichrysum italicum* Derived Food Supplements by ¹H-NMR-Based Metabolomics. *Molecules* **2021**, *26*, 6619. [CrossRef]
31. Orbenes, G.; Rodriguez-Seoane, P.; Torres, M.D.; Chamy, R.; Zuniga, M.E.; Dominguez, H. Valorization of Artichoke Industrial By-Products Using Green Extraction Technologies: Formulation of Hydrogels in Combination with Paulownia Extracts. *Molecules* **2021**, *26*, 4386. [CrossRef]
32. Masullo, M.; Mari, A.; Cerulli, A.; Bottone, A.; Kontek, B.; Olas, B.; Pizza, C.; Piacente, S. Quali-quantitative analysis of the phenolic fraction of the flowers of *Corylus avellana*, source of the Italian PGI product "Nocciola di Giffoni": Isolation of antioxidant diarylheptanoids. *Phytochemistry* **2016**, *130*, 273–281. [CrossRef] [PubMed]
33. Masullo, M.; Cerulli, A.; Montoro, P.; Pizza, C.; Piacente, S. In depth LC-ESIMS(n)-guided phytochemical analysis of *Ziziphus jujuba* Mill. leaves. *Phytochemistry* **2019**, *159*, 148–158. [CrossRef] [PubMed]
34. Materska, M.; Olszówka, K.; Chilczuk, B.; Stochmal, A.; Pecio, L.; Pacholczyk-Sienicka, B.; Piacente, S.; Pizza, C.; Masullo, M. Polyphenolic profiles in lettuce (*Lactuca sativa* L.) after CaCl₂ treatment and cold storage. *Eur. Food Res. Technol.* **2019**, *245*, 733–744. [CrossRef]
35. Mari, A.; Napolitano, A.; Masullo, M.; Pizza, C.; Piacente, S. Identification and quantitative determination of the polar constituents in *Helichrysum italicum* flowers and derived food supplements. *J. Pharm. Biomed. Anal.* **2014**, *96*, 249–255. [CrossRef] [PubMed]
36. Kilinc, H.; Masullo, M.; D'Urso, G.; Karayildirim, T.; Alankus, O.; Piacente, S. Phytochemical investigation of *Scabiosa sicula* guided by a preliminary HPLC-ESIMS(n) profiling. *Phytochemistry* **2020**, *174*, 112350. [CrossRef] [PubMed]
37. Cerulli, A.; Masullo, M.; Montoro, P.; Hosek, J.; Pizza, C.; Piacente, S. Metabolite profiling of "green" extracts of *Corylus avellana* leaves by ¹H NMR spectroscopy and multivariate statistical analysis. *J. Pharm. Biomed. Anal.* **2018**, *160*, 168–178. [CrossRef] [PubMed]
38. Cerulli, A.; Napolitano, A.; Hosek, J.; Masullo, M.; Pizza, C.; Piacente, S. Antioxidant and in vitro preliminary anti-inflammatory activity of *Castanea sativa* (Italian cultivar "marrone di roccadaspide" PGI) burs, leaves and chestnuts extracts and their metabolite profiles by LC-ESI/LTQOrbitrap/MS/MS. *Antioxidants* **2021**, *10*, 278. [CrossRef]
39. Balestrieri, C.; Felice, F.; Piacente, S.; Pizza, C.; Montoro, P.; Oleszek, W.; Visciano, V.; Balestrieri, M.L. Relative effects of phenolic constituents from *Yucca schidigera* Roez. bark on Kaposi's sarcoma cell proliferation, migration, and PAF synthesis. *Biochem. Pharmacol.* **2006**, *71*, 1479–1487. [CrossRef]
40. Santos, C.C.D.; Masullo, M.; Cerulli, A.; Mari, A.; Estevam, C.D.; Pizza, C.; Piacente, S. Isolation of antioxidant phenolics from *Schinopsis brasiliensis* based on a preliminary LC-MS profiling. *Phytochemistry* **2017**, *140*, 45–51. [CrossRef]
41. Thaipong, K.; Boonprakob, U.; Crosby, K.; Cisneros-Zevallos, L.; Hawkins Byrne, D. Comparison of ABTS, DPPH, FRAP, and ORAC assays for estimating antioxidant activity from guava fruit extracts. *J. Food Compos. Anal.* **2006**, *19*, 669–675. [CrossRef]
42. Masullo, M.; Lauro, G.; Cerulli, A.; Bifulco, G.; Piacente, S. *Corylus avellana*: A Source of Diarylheptanoids With alpha-Glucosidase Inhibitory Activity Evaluated by in vitro and in silico Studies. *Front. Plant Sci.* **2022**, *13*, 805660. [CrossRef] [PubMed]

43. Cerulli, A.; Napolitano, A.; Masullo, M.; Hosek, J.; Pizza, C.; Piacente, S. Chestnut shells (Italian cultivar “Marrone di Roccadaspide” PGI): Antioxidant activity and chemical investigation with in depth LC-HRMS/MSn rationalization of tannins. *Food Res. Int.* **2020**, *129*, 108787. [CrossRef] [PubMed]
44. Masullo, M.; Cerulli, A.; Pizza, C.; Piacente, S. *Pouteria lucuma* Pulp and Skin: In Depth Chemical Profile and Evaluation of Antioxidant Activity. *Molecules* **2021**, *26*, 5236. [CrossRef] [PubMed]
45. Masullo, M.; Cerulli, A.; Mari, A.; de Souza Santos, C.C.; Pizza, C.; Piacente, S. LC-MS profiling highlights hazelnut (Nocciola di Giffoni PGI) shells as a byproduct rich in antioxidant phenolics. *Food Res. Int.* **2017**, *101*, 180–187. [CrossRef]
46. Naveed, M.; Hejazi, V.; Abbas, M.; Kamboh, A.A.; Khan, G.J.; Shumzaid, M.; Ahmad, F.; Babazadeh, D.; Xia, F.F.; Modarresi-Ghazani, F.; et al. Chlorogenic acid (CGA): A pharmacological review and call for further research. *Biomed. Pharmacother.* **2018**, *97*, 67–74. [CrossRef]
47. Magana, A.A.; Kamimura, N.; Soumyanath, A.; Stevens, J.F.; Maier, C.S. Caffeoylquinic acids: Chemistry, biosynthesis, occurrence, analytical challenges, and bioactivity. *Plant J.* **2021**, *107*, 1299–1319. [CrossRef]

Article

Dried and Fermented Powders of Edible Algae (*Neopyropia yezoensis*) Attenuate Hepatic Steatosis in Obese Mice

Koji Nagao ^{1,2,*}, Nao Inoue ¹ , Keisuke Tsuge ³, Akira Oikawa ⁴, Tomoko Kayashima ⁵ and Teruyoshi Yanagita ¹

¹ Department of Biological Resource Science, Saga University, 1 Honjo-machi, Saga 840-8502, Japan; d5589@cc.saga-u.ac.jp (N.I.); yanagitt@cc.saga-u.ac.jp (T.Y.)

² The United Graduate School of Agricultural Sciences, Kagoshima University, Kagoshima 890-0065, Japan
³ Saga Regional Industry Support Center, Saga 849-0932, Japan; tsuge@saga-itc.jp

⁴ Graduate School of Agriculture, Kyoto University, Uji 611-0011, Japan; oikawa.akira.7j@kyoto-u.ac.jp

⁵ Faculty of Education, Saga University, 1 Honjo-machi, Saga 840-8502, Japan; kaya@cc.saga-u.ac.jp

* Correspondence: knagao@cc.saga-u.ac.jp; Tel.: +81-952-28-8781

Abstract: Edible algae *Neopyropia yezoensis* is used as “Nori”, its dried sheet product, in Japanese cuisine. Its lipid components reportedly improve hepatic steatosis in obese *db/db* mice. In this study, we prepared “Nori powder (NP)” and “fermented Nori powder (FNP)” to utilize the functional lipids contained in “Nori” and examined their nutraceutical effects in vivo. Male *db/db* mice were fed a basal AIN-76 diet, a 10% NP-supplemented diet, or a 10% FNP-supplemented diet for 4 weeks. We detected eicosapentaenoic acid (EPA) present in both NP and FNP in the serum and liver of *db/db* mice in a dose-dependent manner. The NP diet reduced hepatic triglyceride accumulation (by 58%) in *db/db* mice by modulating gene expression, which resulted in the inhibition of lipogenic enzyme activity. Additionally, NP intake significantly suppressed the expression of inflammatory genes in the liver and hepatic injury marker levels in the sera (by 26%) of *db/db* mice. The FNP diet also led to a marked reduction in hepatic triglyceride accumulation (by 50%) and hepatic injury (by 28%) in *db/db* mice, and the mechanism of these alleviative actions was similar to that of the NP diet. Although the EPA content of FNP was one-third that of NP, metabolomic analysis revealed that bioactive betaine analogs, such as stachydrine, betaine, and carnitine, were detected only in FNP. In conclusion, we suggest that (1) mechanical processing of “Nori” makes its lipid components readily absorbable by the body to exert their lipid-lowering effects, and (2) fermentation of “Nori” produces anti-inflammatory molecules and lipid-lowering molecules, which together with the lipid components, can exert hepatic steatosis-alleviating effects.

Citation: Nagao, K.; Inoue, N.; Tsuge, K.; Oikawa, A.; Kayashima, T.; Yanagita, T. Dried and Fermented Powders of Edible Algae (*Neopyropia yezoensis*) Attenuate Hepatic Steatosis in Obese Mice. *Molecules* **2022**, *27*, 2640. <https://doi.org/10.3390/molecules27092640>

Academic Editor: Mirella Nardini

Received: 31 March 2022

Accepted: 19 April 2022

Published: 20 April 2022

Publisher’s Note: MDPI stays neutral with regard to jurisdictional claims in published maps and institutional affiliations.



Copyright: © 2022 by the authors. Licensee MDPI, Basel, Switzerland. This article is an open access article distributed under the terms and conditions of the Creative Commons Attribution (CC BY) license (<https://creativecommons.org/licenses/by/4.0/>).

Keywords: *Neopyropia yezoensis*; Koji fermentation; hepatic steatosis; obese *db/db* mouse; eicosapentaenoic acid; stachydrine; betaine; carnitine

1. Introduction

Obesity is the central pathology of the metabolic syndrome, a cluster of metabolic abnormalities that contributes to increased cardiovascular morbidity and mortality in developed countries [1,2]. Non-alcoholic fatty liver disease (NAFLD) is a spectrum of conditions ranging from hepatic steatosis to steatohepatitis, advanced fibrosis, and cirrhosis. The presence of metabolic syndrome is associated with potentially progressive severe liver disease [3,4]. Liver-related morbidity and mortality due to NAFLD are mostly observed in patients with advanced fibrosis and cirrhosis. Therefore, the effective use of dietary factors to alleviate hepatic steatosis, the early NAFLD pathogenesis, and preventing its worsening can solve a serious public health problem. *db/db* mice, which have leptin receptor gene mutations, share many features with human metabolic syndrome [5–7]. These mice are well-suited for evaluating how dietary components affect the development of obesity-induced hepatic steatosis [8].

The nutritional value and bioactive components of algae have been reported to be useful for improving health, and therefore the laver industry is expected to develop it as a source of edible seaweed and useful compounds [9]. The edible seaweed *Neopyropia yezoensis*, formerly known as *Porphyra yezoensis* or *Pyropia yezoensis*, is dried into sheets as “Nori” and used to wrap sushi and rice balls in Japanese cuisine. These edible red algae, recognized as one of the most delicious seaweeds and are stably obtained, are used not only in Japan but also worldwide. Nori is rich in nutrients and its lipid components include eicosapentaenoic acid (EPA) bound to glycolipids and phospholipids [10–12]. We previously reported that complex lipids extracted from Nori improved hepatic steatosis in obese *db/db* mice [12]. However, since the membrane lipid components of seaweed are surrounded by the cell wall, it is assumed that humans cannot utilize the lipid components of Nori if they eat it as is.

Therefore, we prepared “Nori powder (NP)” by mechanical processing and aimed to make the functional lipids in Nori bioavailable by cell wall fragmentation. Additionally, since a previous report indicated that Koji fermentation of Nori releases EPA and the degrades cell wall polysaccharides [13], we also prepared “fermented Nori powder (FNP)” as a biochemically processed product. In this study, incorporation of EPA from these dried powders, NP and FNP, and their nutraceutical effects were evaluated in vivo using obese *db/db* mice.

2. Results

2.1. Preparation and Characterization of Nori Powder and Fermented Nori Powder

We used scanning electron microscopy (SEM) to confirm the physical and biochemical breakdown of Nori (Figure 1A). The NP prepared by mechanical processing retained its cell wall structure, suggesting that digestive enzymes can act on the cross-section in vivo. However, the prepared FNP, biochemically processed by Koji fermentation, had a less distinct cell wall structure and a smaller size due to the *Aspergillus oryzae* growth and digestion. Interestingly, upon measuring the EPA content by GC-MS, we found that it was 19.7 mg/g and 5.87 mg/g in the NP and FNP, respectively (Figure 1B, Supplementary Table S1).

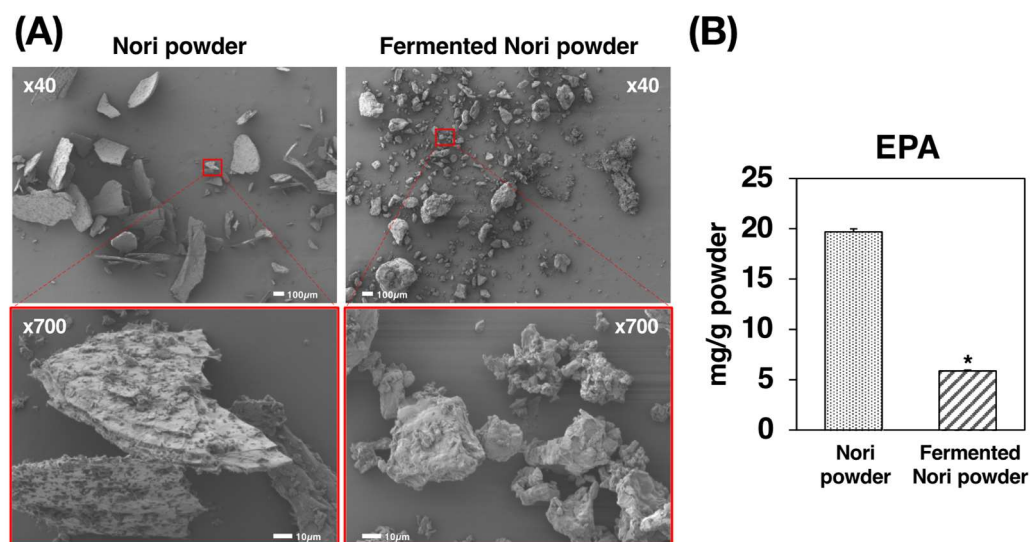


Figure 1. (A) Scanning electron micrographs and EPA contents of NP and FNP. (B) Values are expressed as the mean \pm standard error ($n = 3$). Asterisk shows significant difference ($p < 0.05$) between the two powders. NP: Nori powder, FNP: fermented Nori powder, EPA: eicosapentaenoic acid.

2.2. Effects of Experimental Diets on Growth Parameters

To assess the impact of the sample powder ingestion, we set up three test groups. We divided the *db/db* mice into three groups that were fed one of three diets: (1) a basal semisynthetic AIN-76 diet (Co group, $n = 5$); (2) a semisynthetic AIN-76 diet supplemented

with 10% NP at the expense of sucrose (Np group, $n = 6$); or (3) a semisynthetic AIN-76 diet supplemented with 10% FNP at the expense of sucrose (Fp group, $n = 6$). After 4 weeks of feeding the mice with the experimental diets, we found that the three groups did not differ in initial body weight, final body weight, weight gain, food intake, and abdominal white adipose tissue (WAT) weights. No differences in feed preference or side effects, such as diarrhea, were observed. However, the Np and the Fp groups displayed significantly reduced liver weights as compared with the Co group, as shown in Table 1.

Table 1. Effect of experimental diet on growth parameters in *db/db* mice.

	Co	Np	Fp
Initial body weight (g)	34.8 ± 0.4	34.9 ± 0.4	34.9 ± 0.3
Final body weight (g)	42.0 ± 1.0	40.6 ± 1.4	40.4 ± 1.1
Body weight gain (g)	7.16 ± 0.64	5.77 ± 1.13	5.55 ± 0.81
Food intake (g)	142 ± 3	141 ± 1	141 ± 4
Liver weight (g/100 g body weight)	6.87 ± 0.32 ^a	4.87 ± 0.13 ^b	5.15 ± 0.37 ^b
White adipose tissue weight (g/100 g body weight)			
Total	8.00 ± 0.36	8.20 ± 0.19	8.06 ± 0.34
Epididymal	4.60 ± 0.10	4.61 ± 0.13	4.87 ± 0.25
Perirenal	3.39 ± 0.29	3.59 ± 0.18	3.19 ± 0.12

^{ab} Different superscript letters show significant differences at $p < 0.05$. Co group: mice fed a basal diet ($n = 5$), Np group: mice fed a 10% NP-supplemented diet ($n = 6$), Fp group: mice fed a 10% FNP-supplemented diet ($n = 6$).

2.3. Incorporation of EPA in the Serum and Liver of *db/db* Mice

After a 4-week feeding period, the EPA in the serum and liver was 1.48 mg/dL and 0.0515 mg/g liver, respectively, in the Co group (without dietary EPA). However, in the Np group, EPA in the serum and liver was 24.3 mg/dL and 0.681 mg/g liver, respectively, while in the Fp group, it was 8.78 mg/dL and 0.276 mg/g liver, respectively. These results indicate that both physical and biochemical breakdown of Nori makes its lipid components readily absorbable by the body, with the EPA being detected in each mice group reflecting the relative EPA content of the diets (Figure 2, Supplementary Tables S1–S3).

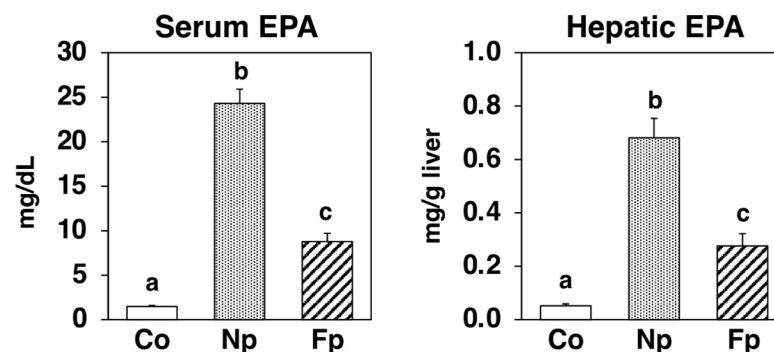


Figure 2. EPA levels in the sera and livers of *db/db* mice fed a basal diet (Co group), 10% NP-supplemented diet (Np group), or 10% FNP-supplemented diet (Fp group) for 4 weeks. Values are expressed as the mean ± standard error ($n = 5–6$). ^{abc} Different letters denote significant differences ($p < 0.05$) among the three groups. EPA: eicosapentaenoic acid.

2.4. Effects of Experimental Diets on Liver Histology and Triglyceride Levels

We observed macrovesicular hepatocytes and hepatic triglyceride accumulation in obese *db/db* mice in the Co group (Figure 3). However, these were markedly alleviated in both the Np and Fp groups as compared with the Co group.

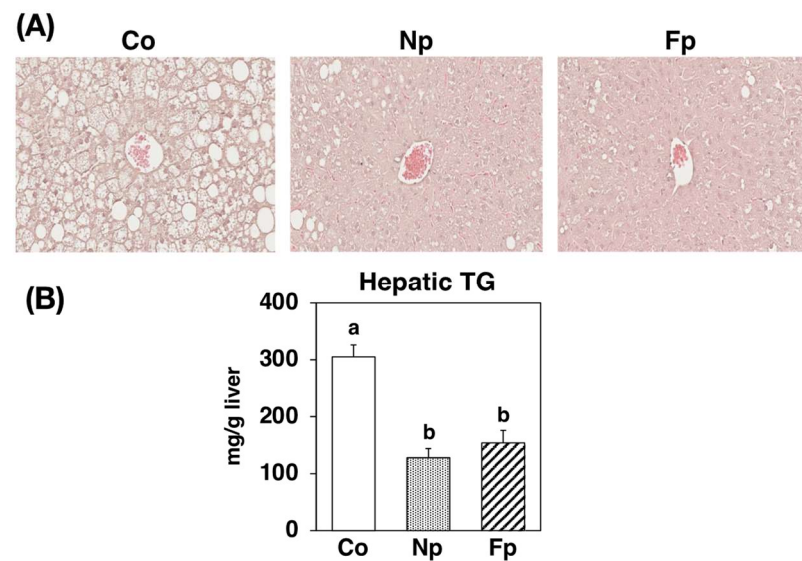


Figure 3. Liver histology and triglyceride levels in *db/db* mice fed a basal diet (Co group), 10% NP-supplemented diet (Np group), or 10% FNP-supplemented diet (Fp group) for 4 weeks. (A) Hematoxylin and eosin staining of liver sections from mice representative of each experimental group. (B) Values are expressed as the mean \pm standard error ($n = 5-6$). ^{ab} Different letters denote significant differences ($p < 0.05$) among the 3 groups. TG: triglyceride.

2.5. Effects of Experimental Diets on Hepatic Expression of Genes Related to Lipid Metabolism

To elucidate the hepatic steatosis alleviating effects of the experimental diets, we analyzed the hepatic expression of genes related to lipid metabolism using real-time PCR (Figure 4). Concomitant with decreased triglyceride levels, the hepatic mRNA expression of lipogenic enzymes like acetyl-CoA carboxylase-1 (ACC1) and fatty acid synthase (FAS) was significantly suppressed in both the Np and Fp groups as compared with that of the Co group. In contrast, among groups, there was no significant difference in the mRNA levels of carnitine palmitoyltransferase-1a (CPT1a), a key enzyme of mitochondrial fatty acid β -oxidation, and acyl-CoA oxidase-1 (ACO1), a key enzyme of peroxisomal fatty acid β -oxidation.

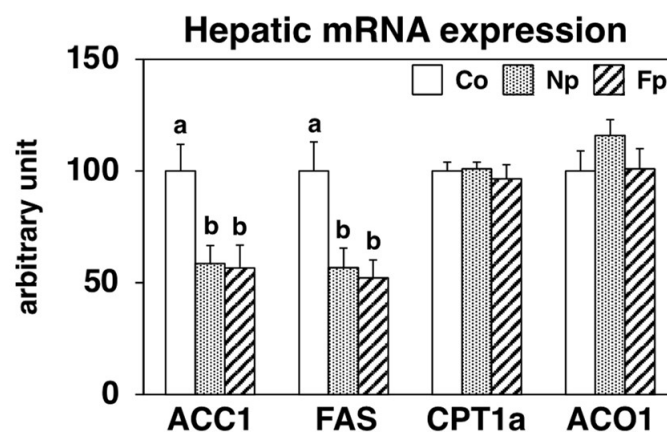


Figure 4. mRNA expression levels of genes related to lipid metabolism in the liver of *db/db* mice fed a basal diet (Co group), 10% NP-supplemented diet (Np group), or 10% FNP-supplemented diet (Fp group) for 4 weeks. Values are expressed as the mean \pm standard error ($n = 5-6$). ^{ab} Different letters denote significant differences ($p < 0.05$) among the three groups. ACC1: acetyl-CoA carboxylase-1, FAS: fatty acid synthase, CPT1a: carnitine palmitoyltransferase-1a, ACO1: acyl-CoA oxidase-1.

2.6. Effects of Experimental Diets on Activities of Enzymes Related to Lipid Metabolism in the Liver

To further examine the effects of the powders on the liver, we measured the activities of key enzymes related to lipid metabolism (Figure 5). In the Np and the Fp groups, the activities of FAS (a key enzyme for the de novo synthesis of fatty acids) significantly decreased as compared with that of the Co group. Additionally, the activities of both malic enzyme and glucose-6-phosphate dehydrogenase (G6PDH), which supplies nicotinamide adenine dinucleotide phosphate required for FAS activity, significantly decreased in the Np and the Fp groups as compared with the Co group. There was no significant difference in the activity of CPT, a key enzyme in mitochondrial fatty acid β -oxidation, among groups.

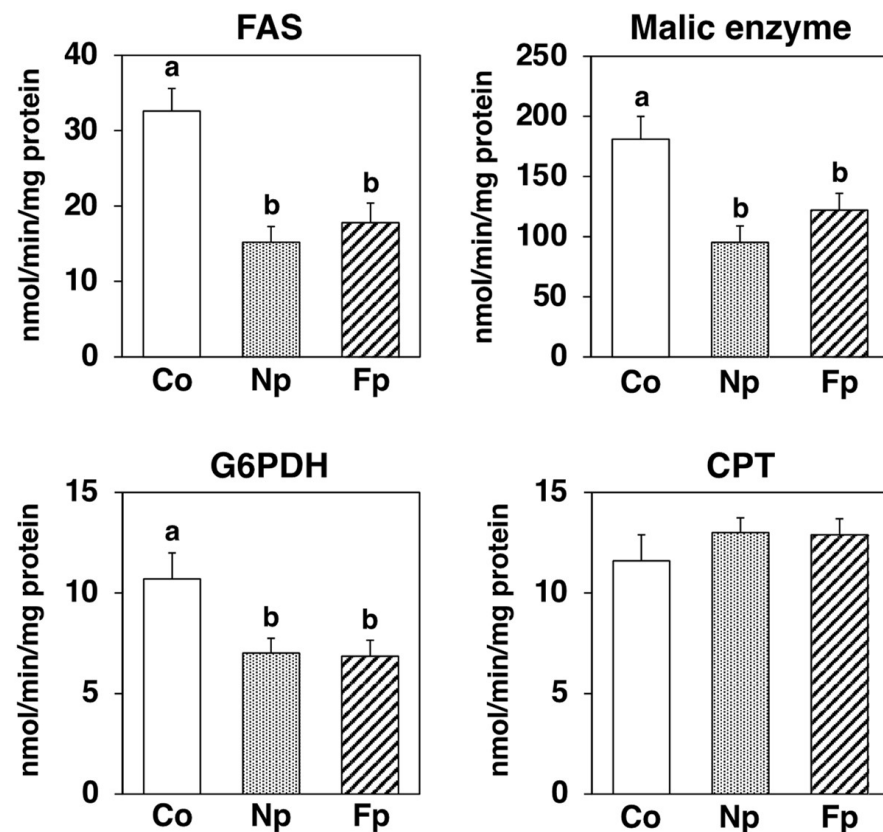


Figure 5. Activities of hepatic enzymes related to lipid metabolism in *db/db* mice fed a basal diet (Co group), 10% NP-supplemented diet (Np group), or 10% FNP-supplemented diet (Fp group) for 4 weeks. Values are expressed as the mean \pm standard error ($n = 5-6$). ^{ab} Different letters denote significant differences ($p < 0.05$) among the three groups. FAS: fatty acid synthase, G6PDH: glucose-6-phosphate dehydrogenase, CPT: carnitine palmitoyltransferase.

2.7. Effects of Experimental Diets on Hepatic Inflammatory and Injury Marker Levels

To gain an insight into the effect of the powders on the liver, we also examined the hepatic mRNA expression of genes related to inflammatory and hepatic injury marker levels in the serum (Figure 6). Compared with the Co group, the mRNA expression of monocyte chemoattractant protein-1 (MCP-1) and tumor necrosis factor α (TNF α), which exacerbate chronic inflammation and injury in the liver, was markedly decreased in both the Np and Fp groups. Moreover, the activity of the hepatic injury marker alanine aminotransferase (ALT) in the serum was significantly lower in both the Np and Fp groups than in the Co group.

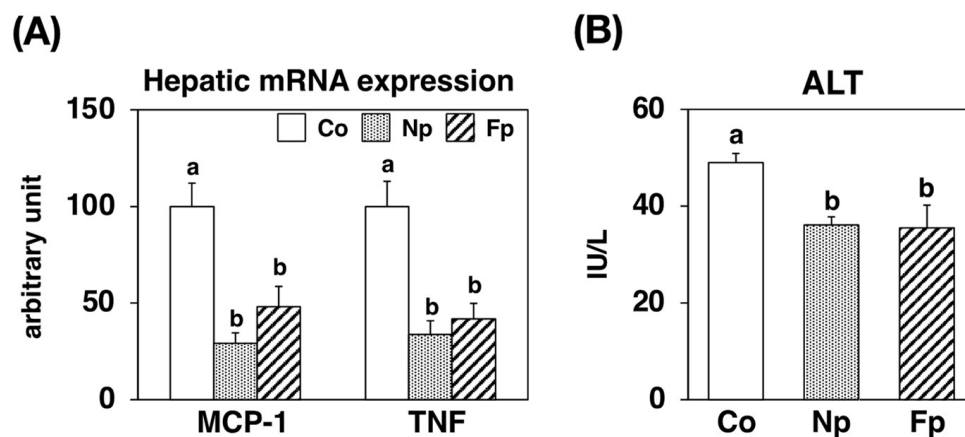


Figure 6. mRNA expression levels of genes related to inflammation in the liver and the hepatic injury marker levels in *db/db* mice fed a basal diet (Co group), 10% NP-supplemented diet (Np group), or 10% FNP-supplemented diet (Fp group) for 4 weeks. Values are expressed as the mean \pm standard error ($n = 5-6$). ^{ab} Different letters denote significant differences ($p < 0.05$) among the three groups. MCP-1: monocyte chemoattractant protein-1, TNF: tumor necrosis factor, ALT: alanine aminotransferase.

2.8. Contribution of EPA Incorporation into the Liver on the Alleviation of Hepatic Injury

To further investigate the ameliorating effects of each powder on liver damage, we analyzed how hepatic EPA incorporation reduced hepatic injury markers using a single regression analysis between the Co and Np groups and between the Co and Fp groups (Figure 7). Liver EPA levels exhibited a significant negative correlation with hepatic injury markers in the sera of *db/db* mice (ALT vs. EPA, $r = 0.829$, $p < 0.05$) between the Co and Np groups. However, there was no statistically significant correlation between hepatic EPA incorporation and ALT reduction ($r = 0.592$) between the Co and Fp groups. These results suggest that there are additional factors to EPA incorporation, by which the FNP diet effectively attenuates hepatic injury in *db/db* mice.

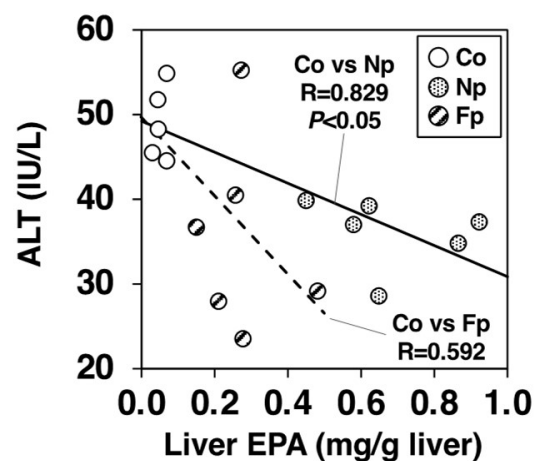


Figure 7. Correlations between hepatic injury marker levels (ALT activities) in the sera vs EPA levels in the livers of *db/db* mice. The mice were fed a basal diet (Co group), 10% NP-supplemented diet (Np group), or 10% FNP-supplemented diet (Fp group) for 4 weeks. Individual values are shown ($n = 17$). EPA: eicosapentaenoic acid, ALT: alanine aminotransferase.

2.9. Metabolomic Changes in Nori Powder before and after Koji Fermentation

We performed metabolomic analyses on NP and the FNP to examine differences in metabolites before and after Koji fermentation. We identified and quantified 93 metabolites in the cationic mode of CE-TOF MS analysis, of which 32 and 61 were decreased and increased, respectively, by Koji fermentation (Figure 8A). Ninety-six metabolites were

identified and quantified in the anionic mode of CE-TOF MS analysis, of which 33 and 63 were decreased and increased, respectively, by Koji fermentation (Figure 8B). Of the 189 metabolites, we lost 4 and newly detected 64 after Koji fermentation. As shown in the biplots and loading plots of the principal component analysis (PCA), Koji fermentation promoted the synthesis of three betaine structural analogues: stachydrine, betaine, and carnitine (Figure 8C, labeled variables were detected only in FNP). The results showed that 1.76 mg/g (9.80 $\mu\text{mol/g}$), 0.908 mg/g (7.75 $\mu\text{mol/g}$) and 0.184 mg/g (1.14 $\mu\text{mol/g}$) of stachydrine, betaine and carnitine, respectively, were markedly synthesized through Koji fermentation (Figure 9).

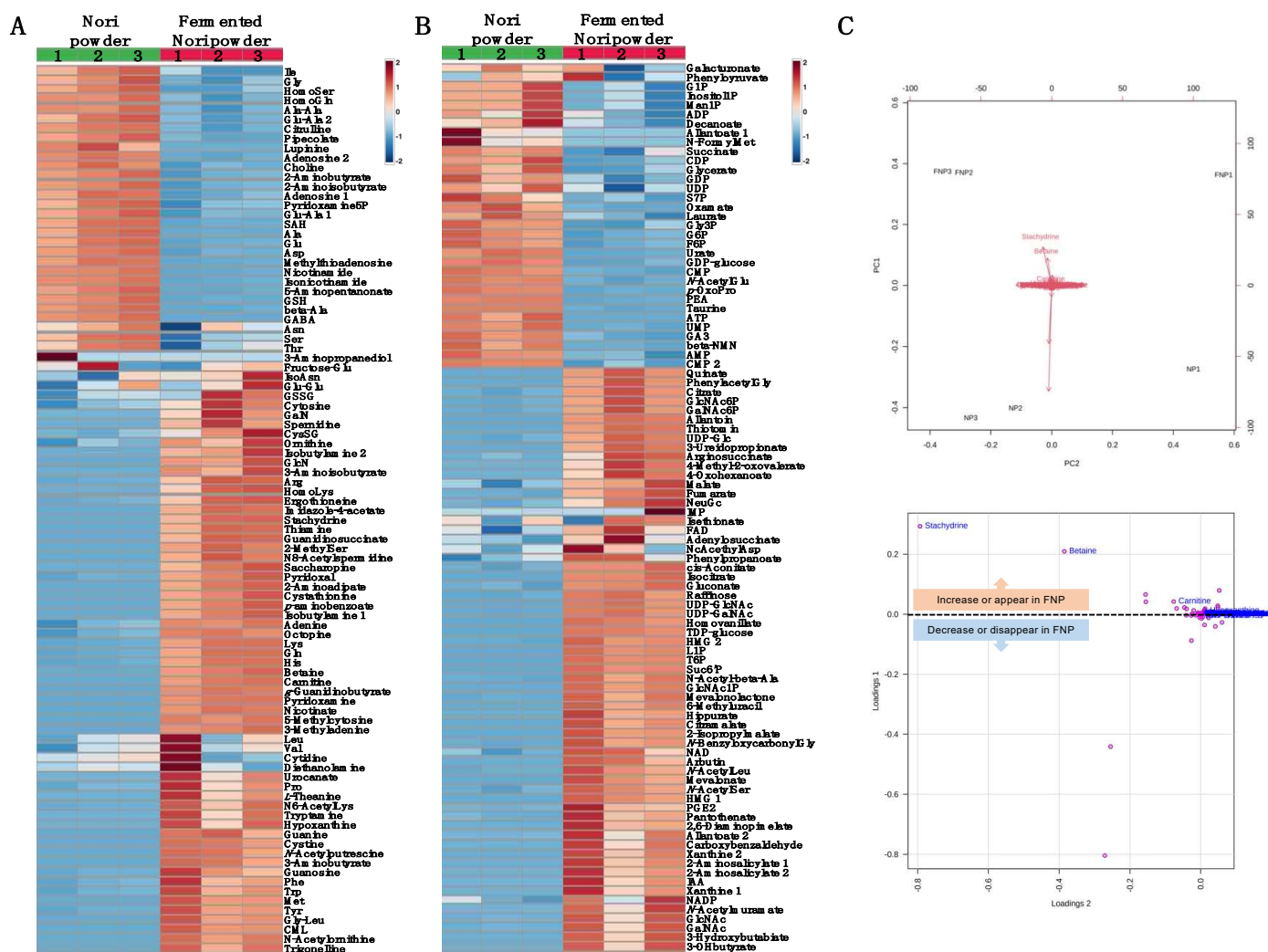


Figure 8. Heat map analysis and principal component analysis of the 189 metabolites significantly modified by Koji fermentation. (**A**: Cationic mode, **B**: Anionic mode) The normalized values were transformed into a z-score and shown as a color scale. The high and low metabolite levels were represented as reddish and blueish scales, respectively. (**C**) Principal components analysis: biplot (upper figure) and loading plot (lower figure) from metabolites of powders before and after Koji fermentation. Labeled variables were detected only in FNP. NP: Nori powder, FNP: fermented Nori powder.

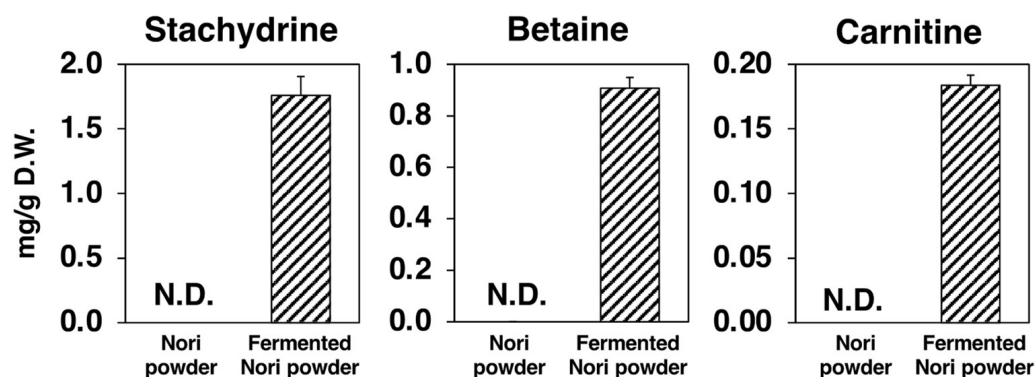


Figure 9. Amounts of representative metabolites of each group. Values are expressed as the mean \pm standard error ($n = 3$). N.D.: not detected.

3. Discussion

EPA (C20:5, ω 3) is one of the most reliable functional fatty acids which reportedly prevent cardiovascular diseases [14]. Its ethyl ester agents (Epadel, Vasepia) are used as treatments for hyperlipidemia [14,15]. The dried sheet product of *Neopyropia yezoensis*, Nori, has a characteristic fatty acid composition, consisting mostly of EPA (>50% of total fatty acids) and palmitic acid (C16:0, ~30% of total fatty acids). However, the EPA in Nori is not a component of storage lipids like free fatty acids or triglycerides but of the cell membrane structural lipids like glycolipids and phospholipids [10–12]. Although it has been reported that the intestinal bacteria of some Japanese people have enzymes to digest seaweed [16], we hypothesized that the Nori in powder form could increase the bioavailability of EPA in Nori by cell wall fragmentation (Figure 1A). After 4 weeks of feeding the NP-supplemented diet, significant amounts of EPA were detected in the sera and livers of *db/db* mice, suggesting that the mechanical processing of Nori promotes the *in vivo* uptake of its lipid components (Figure 2). In addition, we also performed Koji fermentation for the biochemical processing of Nori. Koji fermentation using *Aspergillus oryzae* is essential for the production of many traditional Japanese foods, like miso, soy sauce, and sake [17–19]. Consistent with previous studies indicating that Koji fermentation of Nori degraded cell wall polysaccharides and liberated EPA [13], the structure of Nori was indeed found broken down by fermentation (Figure 1A), and more EPA was detected in the sera and livers of the Fp group than in the Co group (Figure 2). However, the reason that the EPA content per dry weight of FNP was one-third that of NP is not yet known (Figure 1B). However, it was also shown that the EPA content of the powders was reflected in the amounts of EPA incorporated into the body (Figure 2).

In this study, in addition to confirming the uptake of EPA from the prepared powders, we also studied the effects of ingesting these powders on NAFLD development in obese *db/db* mice. After 4 weeks of feeding, the Np group showed no change in WAT weight, but the liver weight and liver triglyceride levels were significantly reduced compared with those in the Co group (Table 1, Figure 3). To investigate the mechanism of the hepatic lipid-lowering effect, we first examined its effect on the expression of genes related to lipid metabolism in the liver, and we found the NP diet significantly decreased the mRNA levels of ACC1 and FAS (Figure 4). The transcription factor sterol regulatory element binding protein (SREBP)-1 regulates the gene expression of these lipogenic enzymes, and interestingly ω 3 polyunsaturated fatty acids (PUFAs) exert their lipid-lowering effects by inhibitory SREBP-1 signaling [20]. Furthermore, consistent with the inhibitory effect on lipid synthesis at the gene expression level, the activities of lipogenic enzymes (FAS, G6PDH and Malic Enzyme) in the liver were significantly reduced in the Np group as compared with the Co group (Figure 5). However, whether EPA was the sole lipid synthesis inhibitory component incorporated from NP in this experiment needs further exploration. Although EPA has been reported to act as a ligand for peroxisome proliferator-activated receptor- α , a transcription factor that regulates the expression of lipolytic genes [20], in this study, the

mRNA levels of CPT1a and ACO1 (Figure 4) and CPT enzyme activity (Figure 5) were not altered by the NP diet. Since previous studies have suggested that *db/db* mice are not suitable for evaluating the lipolysis-enhancing effects of functional dietary components [12], whether the EPA from NP can affect lipolysis needs to be re-evaluated in other animal models. In addition, ω 3 PUFAs reportedly not only inhibited lipid accumulation in cells (which is the “first hit” of the “two-hit” hypothesis of NAFLD development) but also the inflammatory stress injury to hepatocytes, which is the “second hit” [12,20]. Therefore, we examined how NP affected the expression of inflammatory factors in the livers of *db/db* mice and found that the mRNA levels of MCP-1 and TNF α were significantly lower in the Np group than in the Co group (Figure 6A). The levels of liver damage markers in the serum were also significantly lower in the Np group than in the Co group (Figure 6B). These results suggest that ingestion of NP prepared by the mechanical processing of Nori effectively inhibits the progression of NAFLD.

The Fp group, which consumed the Koji-fermented FNP diet for 4 weeks, showed marked improvement in liver enlargement, hepatic steatosis, and hepatic injury in *db/db* mice as compared with the Co group (Table 1, Figures 3–6). The mechanism of alleviative actions of the FNP diet was similar to that of the NP diet, but the EPA (the main bioactive component) content in FNP was only one-third that in NP (Figure 1B). A single regression analysis of the contribution of hepatic EPA incorporation to the ameliorative effect on hepatic injury also suggested that there were additional factors to EPA incorporation, by which the FNP diet effectively attenuated hepatic injury in *db/db* mice (Figure 8). In other words, we hypothesized that functional molecules that improve NAFLD may be produced during Koji fermentation of Nori. In fact, Koji fermentation reportedly produces a variety of bioactive substances in grains [21–24].

Metabolomic analysis of NP and FNP using CE-TOF MS and PCA of metabolite changes revealed that three betaine analogs (stachydrine, betaine, and carnitine) were predominantly produced by Koji fermentation of Nori (Figure 8). Betaine is a general term for compounds with a positive charge and a negative charge in non-adjacent positions within the same molecule, with no dissociable hydrogen bonded to the positively charged atoms and no charge on the molecule as a whole. Stachydrine, known as proline betaine and (2S)-1,1-dimethylpyrrolidinium-2-carboxylate, one of the main components of the medicinal plant *Leonurus heterophyllus*, has demonstrated various bioactivities for treating several diseases, including NAFLD [25]. Stachydrine, in particular, exhibits anti-inflammatory properties by inhibiting the nuclear factor- κ B signaling pathway and is expected to be used therapeutically against cardiovascular diseases [25–27]. Betaine, known as glycine betaine and trimethylammonioacetate, was named after its discovery in sugar beet (*Beta vulgaris subsp. vulgaris*) and has also been reported to have preventive and therapeutic effects on liver diseases [28–30]. The improvement in liver diseases by betaine is attributed to a variety of molecular mechanisms, including inhibiting the inflammatory response and fatty acid synthesis [29,30]. Carnitine, also known as lysine betaine and γ -trimethyl- β -oxybutyrobetain, is synthesized from lysine and methionine mainly in the liver of animals, including humans, and may have a therapeutic role in liver diseases, like NAFLD [31,32]. Many studies have suggested that L-carnitine treatment reduces the fat accumulation in the liver by increasing fatty acid β -oxidation [31,32]. As these betaines are present in a considerable amount in FNP, we believe that their bioactivity may contribute to the therapeutic effect of the FNP diet on hepatic steatosis and liver injury in *db/db* mice.

The main limitation of this study is that we fed the mice with high doses of both NP and FNP and focused on the uptake of EPA into the body over a short feeding period. Further studies wherein model animals are fed a low-volume supplemented diet for a longer feeding period could provide more insights into the robustness of the test and its practicality for the human diet. Additional studies are necessary to analyze the inhibitory effect of the ingestion of both the powders on NAFLD progression, in conjunction with more detailed histological evaluation (Oil Red O, CD45, or F4/80 staining, etc.), using animal models of NAFLD that develop steatohepatitis and advancing fibrosis [8].

In conclusion, we suggested that (1) mechanical processing of Nori makes its lipid components readily absorbable by the body to exert their lipid-lowering effects, and (2) fermentation of Nori produces anti-inflammatory and lipid-lowering molecules, which, together with functional lipid components, also exert their hepatic steatosis-alleviating effects.

4. Materials and Methods

4.1. Preparation and Characterization of Nori Powder and Fermented Nori Powder

Nori sheets, a hot-air-dried form of the seaweed *Neopyropia yezoensis*, were supplied by JA Saga (Saga, Japan). NP was prepared using a hammer crusher (Sansho Industry Co., Ltd., Osaka, Japan) and FNP was prepared by Koji fermentation of Nori using *Aspergillus oryzae* (Maruhide Shoyu Co., Ltd., Saga, Japan) [33]. The sample powders were characterized using SEM and gas chromatography-mass spectrometry (GC-MS). Lipids from the powders were extracted as described by Bligh and Dyer [34]. The powders were coated with OsO₄ using an osmium coater (HPC-1S, Vacuum Devices Co. Ltd., Mito, Ibaraki, Japan), and images were obtained using a JSM-7500F scanning electron microscope (JEOL Ltd., Tokyo, Japan). GC-MS conditions were as follows: equipment, GC2010 + QP2010 (Shimadzu Corp., Tokyo, Japan); column, SP2380 (L 100 m × I.D. 0.25 mm × d 0.2 μm, Sigma-Aldrich Co., Tokyo, Japan); carrier gas flow rate, 20 cm/s (helium); column temperature, 140 °C for 5 min, 140–205 °C at 1.5 °C/min, 205–240 °C at 10 °C/min, 240 °C for 8 min; injection, 1 μL; split ratio 20:1 at 250 °C; ion source, electron ionization. Samples and standards were treated with 0.5 M potassium hydroxide-methanol solution (100 °C for 9 min) followed by 10% BF₃-methanol solution (100 °C for 7 min) to derivatize into fatty acid methyl esters prior to GC-MS.

4.2. Animals

All experiments were conducted under with the guidelines provided by the Ethical Committee for Experimental Animal Care at Saga University (Certificate Number: 28-058-1). Six-week-old male *db/db* mice were purchased from Japan SLC (Shizuoka, Japan). The mice were housed individually in plastic cages in a temperature-controlled room (24 °C) under a 12-h light/dark cycle. Basal semisynthetic diets were prepared according to the recommendations of the American Institute of Nutrition (AIN-76TM) [35] and they contained (in weight %): casein, 20; cornstarch, 15; cellulose, 5; vitamin mixture (AIN-76TM), 1; mineral mixture (AIN-76TM), 3.5; DL-methionine, 0.3; choline bitartrate, 0.2; corn oil, 7; and sucrose, 48. The *db/db* mice were divided into three groups that were fed one of three diets: a basal semisynthetic AIN-76 diet (Co group, *n* = 5), a semisynthetic AIN-76 diet supplemented with 10% Nori powder at the expense of sucrose (Np group, *n* = 6), or a semisynthetic AIN-76 diet supplemented with 10% fermented Nori powder at the expense of sucrose (Fp group, *n* = 6). The mice were fed the diets ad libitum using Rodent CAFE (KBT Oriental, Saga, Japan) for four weeks. At the end of the feeding period, the mice were sacrificed by exsanguination from the heart under isoflurane anesthesia after a 9-h starvation period. WAT and liver were excised immediately, and the serum was separated from the blood.

4.3. Physiological and Histochemical Evaluation of Serum and Livers

Lipids from serum was extracted by the method of Bligh and Dyer [34] and from liver was extracted using the method described by Folch et al. [36]. Measurement of fatty acid contents in the serum and liver were carried out using GC-MS. Hematoxylin and eosin staining was carried out to microscopically evaluate the degree of hepatic steatosis and hepatic triglyceride concentrations were quantified using the method of Fletcher et al. [37] Alanine aminotransferase (ALT) activity in the serum was analyzed using a Transaminase CII-test Wako kit (Wako Pure Chemical Industries, Ltd., Osaka, Japan).

4.4. Assays of Hepatic Enzyme Activity

Liver cytosol and mitochondrial fractions were prepared by homogenization and centrifugation. The protein concentration of each fraction was analyzed by the method of Lowry [38]. The enzyme activity of FAS [39] and G6PDH [40] in cytosol fraction were measured by the method of Kelly. Malic enzyme in cytosol fraction and CPT in mitochondrial fraction were assayed by the method of Ochoa [41] and Markwell et al. [42], respectively.

4.5. Analysis of mRNA Expression in the Liver

Total RNA was extracted from 100 mg of liver using the RNeasy Lipid Tissue Mini Kit (Qiagen, Tokyo, Japan). TaqMan Universal PCR Master Mix (Applied Biosystems, Tokyo, Japan) and Assay-on-Demand, Gene Expression Products (Mn01304289_m1 for ACC1, Mn00662319_m1 for FAS, Mn00550438_m1 for CPT1a, Mn00443579_m1 for ACO1, Mn00441242_m1 for MCP1, Mn00443258_m1 for TNF α , and Mm04277571_s1 for 18S rRNA, all from Applied Biosystems, Tokyo, Japan) were used for quantitative RT-PCR analysis of ACC1, FAS, CPT1a, ACO1, MCP1, TNF α , and 18S RNA expression in the liver. Amplifications were carried out using an ABI Prism 7000 RT-PCR sequence detection system (Applied Biosystems, Tokyo, Japan).

4.6. Capillary Electrophoresis Mass Spectrometry

NP and FNP (10mg each) were suspended in five hundred microliters of methanol containing 8 μ M of internal standards (methionine sulfone for cation and camphor 10-sulfonic acid for anion analyses), 500 μ L of chloroform and 200 μ L of Milli-Q water, and centrifuged (20,400 \times g, 3 min, 4 $^{\circ}$ C). The upper layer of each solution was transferred to a 1.5-mL test tube, evaporated for 30 min with a centrifugal concentrator and then separated into two layers. The upper layer was centrifugally filtered through a PALL Nanosep 3-kD cutoff filter at 9100 \times g at 4 $^{\circ}$ C. The filtrate was dried with the centrifugal concentrator. The residue was dissolved in 20 μ L of Milli-Q water containing 200 μ M of internal standards (3-aminopyrrolidine for cation and trimesic acid for anion analyses). The CE-MS system and its conditions were as described by Oikawa et al. [43]. All CE-TOFMS experiments were performed using an Agilent G7100A CE Instrument (Agilent Technologies, Sacramento, CA, USA), an Agilent G6224A TOF LC/MS system, an Agilent 1200 Infinity series G1311C Quad Pump VL, and the G1603A Agilent CE-MS adapter and G1607A Agilent CE-ESI-MS sprayer kit. The G1601BA 3D-CE ChemStation software for CE and G3335-64002 MH Workstation were used. Separations were carried out using a fused silica capillary (50 μ m i.d. \times 100 cm total length) filled with 1 M formic acid for cation analyses or with 20 mM ammonium formate (pH 10.0) for anion analyses as the electrolyte. The sample solutions were injected at 50 mbar for 15 s (15 nL). Prior to each run, the capillary was flushed with the electrolyte for 5 min. The applied voltage was set at 30 kV. The capillary temperature was maintained at 20 $^{\circ}$ C, and the sample tray was cooled to below 4 $^{\circ}$ C. Fifty percent (*v/v*) methanol/water containing 0.5 μ M reserpine was delivered as the sheath liquid at 10 μ L/min. ESI-TOF MS was conducted in the positive ion mode for cation analyses or in the negative ion mode for anion analyses, and the capillary voltage was set at 4 kV. The flow rate of the heated dry nitrogen gas (heater temperature, 300 $^{\circ}$ C) was maintained at 10 psig. In TOF MS, the fragmentor, skimmer and Oct RFV voltages were set at 110 V, 50 V and 160 V for cation analyses or at 120 V, 60 V and 220 V for anion analyses, respectively. Each acquired spectrum was automatically recalibrated using the reference masses of reference standards. The methanol dimer ion ($[2M + H]^+$, $m/z = 65.0597$) and reserpine ($[M + H]^+$, $m/z = 609.2806$) for cation analyses or the formic acid dimer ion ($[2M - H]^-$, $m/z = 91.0037$) and reserpine ($[M - H]^-$, $m/z = 607.2661$) for anion analyses provided the lock mass for exact mass measurements. Exact mass data were acquired at a rate of 1.5 cycles/s in the range of 50–1000 m/z . Metabolites were identified and quantified as described by Oikawa et al. [43]

4.7. Statistical Analysis

All data values were expressed as the mean \pm standard error. To assess differences among the three groups, data were analyzed by one-way ANOVA, and all differences were analyzed by the Fisher's LSD post hoc test using the KaleidaGraph software version 4.5 (Synergy Software, Reading, PA, USA). Student's *t*-test was used to determine the statistical significance of the differences between the data from Nori powder and fermented Nori powder. Pearson's correlation coefficient was calculated and linear regression analysis was also carried out using the StatPlus:mac Pro v. 8.0.1.0 (AnalystSoft Inc., Walnut, CA, USA). Differences were considered significant at $p < 0.05$. Principal component analysis (PCA) and heatmap clustering of altered metabolic profiling analysis were performed using MetaboAnalyst 5.0 (<https://www.metaboanalyst.ca/>, last accessed on 28 March 2022).

Supplementary Materials: The following supporting information can be downloaded at: <https://www.mdpi.com/article/10.3390/molecules27092640/s1>, Table S1: Fatty acid contents of Nori powder and Fermented Nori powder; Table S2: Fatty acid contents of serum lipids in *db/db* mice; Table S3: Fatty acid contents of hepatic lipids in *db/db* mice.

Author Contributions: Conceptualization, K.N., N.I., K.T., A.O., T.K. and T.Y.; methodology, K.N., N.I., K.T., A.O. and T.K.; software, K.N., N.I., K.T., A.O. and T.K.; validation, K.N., N.I., K.T., A.O. and T.K.; formal analysis, K.N., N.I., K.T., A.O. and T.K.; investigation, K.N., N.I., K.T., A.O. and T.K.; resources, K.N., N.I. and K.T.; data curation, K.N., N.I., K.T., A.O. and T.K.; writing—original draft preparation, K.N. and N.I.; writing—review and editing, K.N., N.I., K.T., A.O., T.K. and T.Y.; visualization, K.N. and N.I.; supervision, K.N., A.O. and T.Y.; project administration, K.N. and K.T.; funding acquisition, K.N. All authors have read and agreed to the published version of the manuscript.

Funding: Part of this research was funded by JSPS KAKENHI, grant number 19K11693 from the Japan Society for the Promotion of Science (JSPS).

Institutional Review Board Statement: All aspects of the experiment were conducted according to the guidelines provided by the ethical committee for experimental animal care of Saga University (certificate number: 28-058-1).

Informed Consent Statement: Not applicable.

Data Availability Statement: The datasets used and/or analyzed during the current study are available from the corresponding author.

Acknowledgments: The author acknowledges the laboratory members of Nutrition Biochemistry in Saga University.

Conflicts of Interest: The authors declare no conflict of interest.

Sample Availability: Samples of the compounds are not available from the authors.

References



- Jahangir, E.; De Schutter, A.; Lavie, C.J. The relationship between obesity and coronary artery disease. *Transl. Res.* **2014**, *164*, 336–344. [CrossRef] [PubMed]
- Bastien, M.; Poirier, P.; Lemieux, I.; Després, J.P. Overview of epidemiology and contribution of obesity to cardiovascular disease. *Prog. Cardiovasc. Dis.* **2014**, *56*, 369–381. [CrossRef] [PubMed]
- Harrison, S.A.; Diehl, A.M. Fat and the liver—A molecular overview. *Semin. Gastrointest. Dis.* **2002**, *13*, 3–16. [PubMed]
- Youssef, W.; McCullough, A.J. Diabetes mellitus, obesity, and hepatic steatosis. *Semin. Gastrointest. Dis.* **2002**, *13*, 17–30. [PubMed]
- Hummel, K.P.; Dickie, M.M.; Coleman, D.L. Diabetes, a new mutation in the mouse. *Science* **1966**, *153*, 1127–1128. [CrossRef]
- Chen, H.; Charlat, O.; Tartaglia, L.A.; Woolf, E.A.; Weng, X.; Ellis, S.J.; Lakey, N.D.; Culpepper, J.; More, K.J.; Breitbart, R.E.; et al. Evidence that the diabetes gene encodes the leptin receptor: Identification of a mutation in the leptin receptor gene in *db/db* mice. *Cell* **1996**, *84*, 491–495. [CrossRef]
- Lee, G.H.; Proenca, R.; Montez, J.M.; Carroll, K.M.; Darvishzadah, J.G.; Lee, G.I.; Freidman, J.M. Abnormal splicing of the leptin receptor in diabetic mice. *Nature* **1996**, *379*, 632–635. [CrossRef]
- Anstee, Q.M.; Goldin, R.D. Mouse models in non-alcoholic fatty liver disease and steatohepatitis research. *Int. J. Exp. Paht.* **2006**, *87*, 1–16. [CrossRef]

9. Cho, T.J.; Rhee, M.S. Health functionality and quality control of laver (*Porphyra, Pyropia*): Current issues and future perspectives as an edible seaweed. *Mar. Drugs* **2019**, *18*, 14. [CrossRef]
10. Araki, S.; Sakurai, T.; Omata, T.; Kawaguchi, A.; Murata, N. Lipid and fatty acid composition in the red alga, *Porphyra yezoensis*. *Jpn. J. Phycol.* **1986**, *34*, 94–100.
11. Araki, S.; Sakurai, T.; Omata, T.; Kawaguchi, A.; Murata, N. Positional distribution of fatty acids in glycerolipids of the marine red alga, *Porphyra yezoensis*. *Plant Cell Physiol.* **1987**, *28*, 761–766. [CrossRef]
12. Yanagita, T.; Tsuge, K.; Koga, M.; Inoue, N.; Nagao, K. Eicosapentaenoic acid-containing polar lipids from seaweed *Susabinori* T (*Pyropia yezoensis*) alleviate hepatic steatosis in obese *db/db* mice. *Arch. Biochem. Biophys.* **2020**, *691*, 108486. [CrossRef] [PubMed]
13. Hama, Y.; Yamagata, E.; Takahama, N.; Yoshimura, Y.; Yanagida, R.; Mitsutake, S. Liberation of eicosapentaenoic acid and degradation of the major cell wall polysaccharide porphyran by fermentation of nori, the dried thalli of *Pyropia yezoensis*, with *koji*. *J. Appl. Phycol.* **2021**, *33*, 4105–4111. [CrossRef]
14. Watanabe, Y.; Tatsuno, I. Prevention of Cardiovascular Events with Omega-3 Polyunsaturated Fatty Acids and the Mechanism Involved. *J. Atheroscler. Thromb.* **2020**, *27*, 183–198. [CrossRef] [PubMed]
15. Curfman, G.; Shehada, E. Icosapent ethyl: Scientific and legal controversies. *Open Heart* **2021**, *8*, e001616. [CrossRef] [PubMed]
16. Hehemann, J.H.; Correc, G.; Barbeyron, T.; Helbert, W.; Czjzek, M.; Michel, G. Transfer of carbohydrate-active enzymes from marine bacteria to Japanese gut microbiota. *Nature* **2010**, *464*, 908–912. [CrossRef]
17. Kusumoto, K.I.; Yamagata, Y.; Tazawa, R.; Kitagawa, M.; Kato, T.; Isobe, K.; Kashiwagi, Y. Japanese Traditional Miso and Koji Making. *J. Fungi* **2021**, *7*, 579. [CrossRef]
18. Ito, K.; Matsuyama, A. Koji Molds for Japanese Soy Sauce Brewing: Characteristics and Key Enzymes. *J. Fungi* **2021**, *7*, 658. [CrossRef]
19. Akaike, M.; Miyagawa, H.; Kimura, Y.; Terasaki, M.; Kusaba, Y.; Kitagaki, H.; Nishida, H. Chemical and Bacterial Components in Sake and Sake Production Process. *Curr. Microbiol.* **2020**, *77*, 632–637. [CrossRef]
20. Nagao, K.; Yanagita, T. Bioactive lipids in metabolic syndrome. *Prog. Lipid Res.* **2008**, *47*, 127–146. [CrossRef]
21. Takahashi, H.; Chi, H.Y.; Mohri, S.; Kamakari, K.; Nakata, K.; Ichijo, N.; Nakata, R.; Inoue, H.; Goto, T.; Kawada, T. Rice Koji Extract Enhances Lipid Metabolism through Proliferator-Activated Receptor Alpha (PPAR α) Activation in Mouse Liver. *J. Agric. Food Chem.* **2016**, *64*, 8848–8856. [CrossRef] [PubMed]
22. Son, H.K.; Shin, H.W.; Jang, E.S.; Moon, B.S.; Lee, C.H.; Lee, J.J. Comparison of Antiobesity Effects Between Gochujangs Produced Using Different Koji Products and Tabasco Hot Sauce in Rats Fed a High-Fat Diet. *J. Med. Food* **2018**, *21*, 233–243. [CrossRef] [PubMed]
23. Maeda, K.; Ogino, Y.; Nakamura, A.; Nakata, K.; Kitagawa, M.; Ito, S. Identification of Rice Koji Extract Components that Increase beta-Glucocerebrosidase Levels in Human Epidermal Keratinocytes. *Foods* **2018**, *7*, 94. [CrossRef] [PubMed]
24. Lee, H.; Lee, S.; Kyung, S.; Ryu, J.; Kang, S.; Park, M.; Lee, C. Metabolite Profiling and Anti-Aging Activity of Rice Koji Fermented with *Aspergillus oryzae* and *Aspergillus cristatus*: A Comparative Study. *Metabolites* **2021**, *11*, 524. [CrossRef]
25. Cheng, F.; Zhou, Y.; Wang, M.; Guo, C.; Cao, Z.; Zhang, R.; Peng, C. A review of pharmacological and pharmacokinetic properties of stachydrine. *Pharmacol. Res.* **2020**, *155*, 104755. [CrossRef]
26. Meng, J.; Zhou, C.; Zhang, W.; Wang, W.; He, B.; Hu, B.; Jiang, G.; Wang, Y.; Hong, J.; Li, S.; et al. Stachydrine prevents LPS-induced bone loss by inhibiting osteoclastogenesis via NF-kappaB and Akt signalling. *J. Cell Mol. Med.* **2019**, *23*, 6730–6743. [CrossRef]
27. Shao, Z.; Lu, J.; Zhang, C.; Zeng, G.; Chen, B.; Liang, H.; Wu, A.; Zhang, X.; Wang, X. Stachydrine ameliorates the progression of intervertebral disc degeneration via the PI3K/Akt/NF-kappaB signaling pathway: In vitro and in vivo studies. *Food Funct.* **2020**, *11*, 10864–10875. [CrossRef]
28. Day, C.R.; Kempson, S.A. Betaine chemistry, roles, and potential use in liver disease. *Biochim. Biophys. Acta* **2016**, *1860*, 1098–1106. [CrossRef]
29. Wang, C.; Ma, C.; Gong, L.; Dai, S.; Li, Y. Preventive and therapeutic role of betaine in liver disease: A review on molecular mechanisms. *Eur. J. Pharmacol.* **2021**, *912*, 174604. [CrossRef]
30. Arumugam, M.K.; Paal, M.C.; Donohue, T.M., Jr.; Ganesan, M.; Osna, N.A.; Kharbanda, K.K. Beneficial Effects of Betaine: A Comprehensive Review. *Biology* **2021**, *10*, 456. [CrossRef]
31. Savic, D.; Hodson, L.; Neubauer, S.; Pavlides, M. The Importance of the Fatty Acid Transporter L-Carnitine in Non-Alcoholic Fatty Liver Disease (NAFLD). *Nutrients* **2020**, *12*, 2178. [CrossRef] [PubMed]
32. Li, N.; Zhao, H. Role of Carnitine in Non-alcoholic Fatty Liver Disease and Other Related Diseases: An Update. *Front. Med.* **2021**, *8*, 689042. [CrossRef] [PubMed]
33. Uchida, M.; Hideshima, N.; Araki, T. Development of koji by culturing *Aspergillus oryzae* on nori (*Pyropia yezoensis*). *J. Biosci. Bioeng.* **2019**, *127*, 183–189. [CrossRef] [PubMed]
34. Bligh, E.G.; Dyer, W.J. A rapid method extraction and purification. *Can. J. Biochem. Physiol.* **1959**, *37*, 911–917. [CrossRef]
35. American Institute of Nutrition. Report of the American Institute of Nutrition ad hoc committee on standards for nutritional studies. *J. Nutr.* **1977**, *107*, 1340–1348. [CrossRef] [PubMed]
36. Folch, J.; Lees, M.; Sloane-Stanley, G.H. A simple method for the isolation and purification of total lipids from animal tissues. *J. Biol. Chem.* **1957**, *226*, 497–509. [CrossRef]
37. Fletcher, M.J. A colorimetric method for estimating serum triglycerides. *Clin. Chim. Acta* **1968**, *22*, 393–397. [CrossRef]

38. Lowry, O.H.; Rosebrough, N.J.; Farr, A.L.; Randall, R.J. Protein measurement with the Folin phenol reagent. *J. Biol. Chem.* **1951**, *193*, 265–275. [CrossRef]
39. Kelley, D.S.; Nelson, G.J.; Hunt, J.E. Effect of prior nutritional status on the activity of lipogenic enzymes in primary monolayer cultures of rat hepatocytes. *Biochem. J.* **1986**, *235*, 87–90. [CrossRef]
40. Kelley, D.S.; Kletzien, R.F. Ethanol modulation of the hormonal and nutritional regulation of glucose 6-phosphate dehydrogenase activity in primary cultures of rat hepatocytes. *Biochem. J.* **1984**, *217*, 543–549. [CrossRef]
41. Ochoa, S. Malic enzyme. In *Methods in Enzymology*; Colowick, S.P., Kaplan, N.O., Eds.; Academic Press: New York, NY, USA, 1955; Volume 1, pp. 739–753.
42. Markwell, M.A.; McGroarty, E.J.; Bieber, L.L.; Tolbert, N.E. The subcellular distribution of carnitine acyltransferases in mammalian liver and kidney. A new peroxisomal enzyme. *J. Biol. Chem.* **1973**, *248*, 3426–3432. [CrossRef]
43. Oikawa, A.; Matsuda, F.; Kikuyama, M.; Mimura, T.; Saito, K. Metabolomics of a single vacuole reveals metabolic dynamism in an alga *Chara australis*. *Plant Physiol.* **2011**, *157*, 544–551. [CrossRef] [PubMed]

Article

Sizes, Components, Crystalline Structure, and Thermal Properties of Starches from Sweet Potato Varieties Originating from Different Countries

Yibo Li ^{1,2,†}, Lingxiao Zhao ^{3,†}, Laiquan Shi ^{1,2}, Lingshang Lin ^{1,2}, Qinghe Cao ^{3,*}  and Cunxu Wei ^{1,2,*} 

¹ Key Laboratory of Crop Genetics and Physiology of Jiangsu Province/Joint International Research Laboratory of Agriculture & Agri-Product Safety of the Ministry of Education, Yangzhou University, Yangzhou 225009, China; dx120180133@yzu.edu.cn (Y.L.); mz120201523@yzu.edu.cn (L.S.); 007520@yzu.edu.cn (L.L.)

² Co-Innovation Center for Modern Production Technology of Grain Crops of Jiangsu Province/Jiangsu Key Laboratory of Crop Genomics and Molecular Breeding, Yangzhou University, Yangzhou 225009, China

³ Xuzhou Institute of Agricultural Sciences in Jiangsu Xuhuai District, Xuzhou 221131, China; zhaolxiao2019@163.com

* Correspondence: cqhe75@yahoo.com (Q.C.); cxwei@yzu.edu.cn (C.W.)

† These authors contributed equally to this work.

Abstract: Sweet potato is a root tuber crop and an important starch source. There are hundreds of sweet potato varieties planted widely in the world. Starches from varieties with different genotype types and originating from different countries have not been compared for their physicochemical properties. In the research, starches from 44 sweet potato varieties originating from 15 countries but planted in the same growing conditions were investigated for their physicochemical properties to reveal the similarities and differences in varieties. The results showed that the 44 starches had granule size (D[4,3]) from 8.01 to 15.30 μm . Starches had different iodine absorption properties with OD680 from 0.259 to 0.382 and OD620/550 from 1.142 to 1.237. The 44 starches had apparent amylose content from 19.2% to 29.2% and true amylose content from 14.2% to 20.2%. The starches exhibited A-, C_A-, C_C-, or C_B-type X-ray diffraction patterns. The thermograms of 44 starches exhibited one-, two-, or three-peak curves, leading to a significantly different gelatinization temperature range from 13.1 to 29.2 °C. The significantly different starch properties divide the 44 sweet potato varieties into different groups due to their different genotype backgrounds. The research offers references for the utilization of sweet potato germplasm.

Keywords: sweet potato; germplasm; starch; crystalline structure; thermal properties

Citation: Li, Y.; Zhao, L.; Shi, L.; Lin, L.; Cao, Q.; Wei, C. Sizes, Components, Crystalline Structure, and Thermal Properties of Starches from Sweet Potato Varieties Originating from Different Countries. *Molecules* **2022**, *27*, 1905. <https://doi.org/10.3390/molecules27061905>

Academic Editor: Mirella Nardini

Received: 2 March 2022

Accepted: 14 March 2022

Published: 15 March 2022

Publisher's Note: MDPI stays neutral with regard to jurisdictional claims in published maps and institutional affiliations.



Copyright: © 2022 by the authors. Licensee MDPI, Basel, Switzerland. This article is an open access article distributed under the terms and conditions of the Creative Commons Attribution (CC BY) license (<https://creativecommons.org/licenses/by/4.0/>).

1. Introduction

Sweet potato (*Ipomoea batatas*), an important root tuber crop, provides food and energy for people, especially in Asia and Africa [1]. Sweet potato contains 15–30% and 46–68% starch in its wet and dry root tuber, respectively, among different varieties, and has become the first choice for producing starch due to its short growth cycle, strong environment adaptability, low planting cost, and high yield in the world, especially in developing countries [2,3]. Starch isolated from the sweet potato root tuber has been used to produce noodles and vermicelli. In addition, it is also a good thickening agent in cooking foods and an important raw material in producing syrup, film, lactic acid, ethanol, and other chemicals [4,5]. The applications of starch are influenced by its physicochemical properties including size, components, crystalline structure, and thermal properties [3,6–9].

Sweet potato is planted widely in the world, and has hundreds of varieties or lines due to artificial selection, natural hybrids, and mutations [1,4]. The root tuber of sweet potato has different colored skin and flesh, but starch properties have no significant correlation with skin and flesh color, and are determined by the genotypes of varieties [2,10,11].

Starches from different sweet potato varieties have been studied for their structures, functional properties, and applications [10,12–14]. For example, Collado et al. [12] investigated the genetic variation in physical properties of sweet potato starches from 44 genotypes adapted to Philippine conditions, and found that wide variation and distinctly different pasting properties exist among genotypes. Zhu and Xie [14] studied the swelling power, water solubility, rheological properties, gelatinization, and retrogradation of starches from seven New Zealand sweet potatoes, and concluded that the starch properties from different varieties exhibit significant diversity due to their different internal unit chain parameters of amylopectin. Kim et al. [13] compared the physicochemical properties of starches from eight Korean sweet potato varieties including purple-, orange-, and white/cream-fleshed tubers. The starches exhibit polygonal and semi-oval shapes with different granule sizes among different varieties, and have A- and C_B-type X-ray diffraction patterns. The pasting properties, amylose contents and water binding capacities of starches are closely related to the chain length distribution of amylopectin, and have no relationship with tuber color. Similar results are also reported in starches from eight Chinese sweet potato varieties with light yellow-, orange-, and purple-fleshed tubers. The molecular structure of amylose and amylopectin exhibits differences among different varieties, and is the main influencing factor in determining starch physicochemical properties [10]. Though the above references have reported the differences in starches from different varieties, the varieties originate from the same country or region in the same report. At present, no research reports the starch properties of sweet potato varieties originating from different countries. The growing environment and field management significantly influence the development and properties of starch in plant resources [15–18]. In addition, the measuring and analysis methods of starch properties also affect the property parameters. Therefore, it is necessary to study the characteristics of starches from sweet potato varieties originating from different countries but planted in the same growing conditions.

In this research, 44 sweet potato varieties originating from 15 countries were planted in the same conditions, and their starches were isolated and investigated for granule size, iodine absorption, amylose content, crystalline structure, and thermal properties. The hierarchical cluster analysis was carried out to reveal the differences in sweet potato varieties based on the starch property parameters. The objective of this study was to evaluate the germplasm resources of sweet potato starch. This research offers some references for the utilization of sweet potato germplasm.

2. Results and Discussion

2.1. Granule Morphology and Size Distribution of Starch

The granule morphology and size are important properties of starch, affecting functional properties and applications of starch [9]. The morphologies of isolated starches were observed under normal and polarized light (Figure 1). Starch granules had round, polygonal, oval, and semi-oval shapes, and contained small and large granules with typical “Maltese crosses” having the hila in the center of the granules. No significant differences in starch morphology were observed among all sweet potato varieties. Similar morphology has also been reported in sweet potato starch [19,20]. However, the granule size distributions exhibited significant differences among some sweet potato starches (Table 1). The surface- ($D[3,2]$) and volume-weighted mean diameter ($D[4,3]$) are usually used to indicate the size of starch, and ranged from 3.866 to 7.681 μm and from 8.013 to 15.296 μm among 44 sweet potato starches, respectively. The starch size in this study agreed with the previous report of sweet potato starch [2,19,20]. The starch size is influenced by plant source, variety genotype, plant physiology, and growing environment [9,21,22].

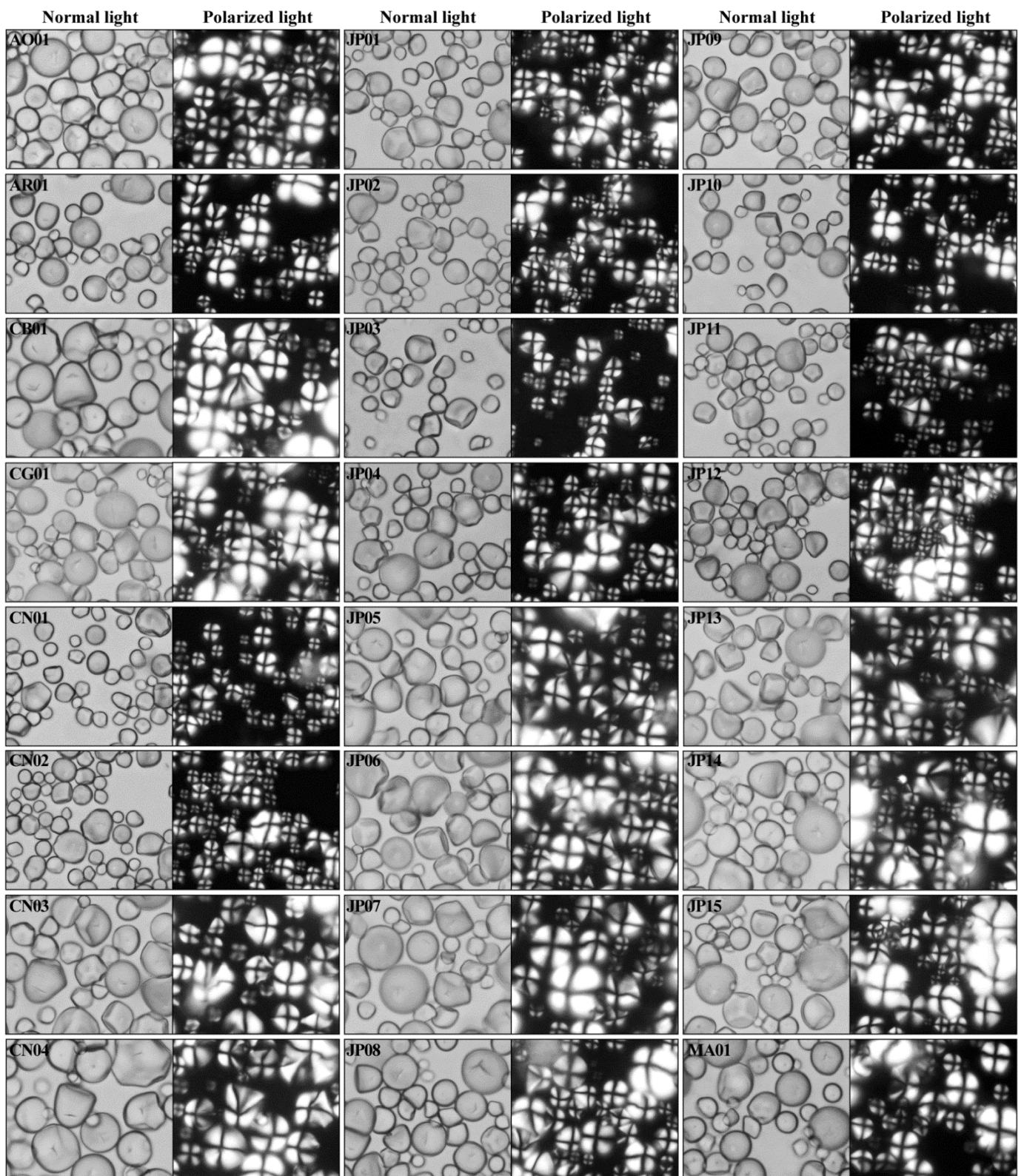


Figure 1. Cont.

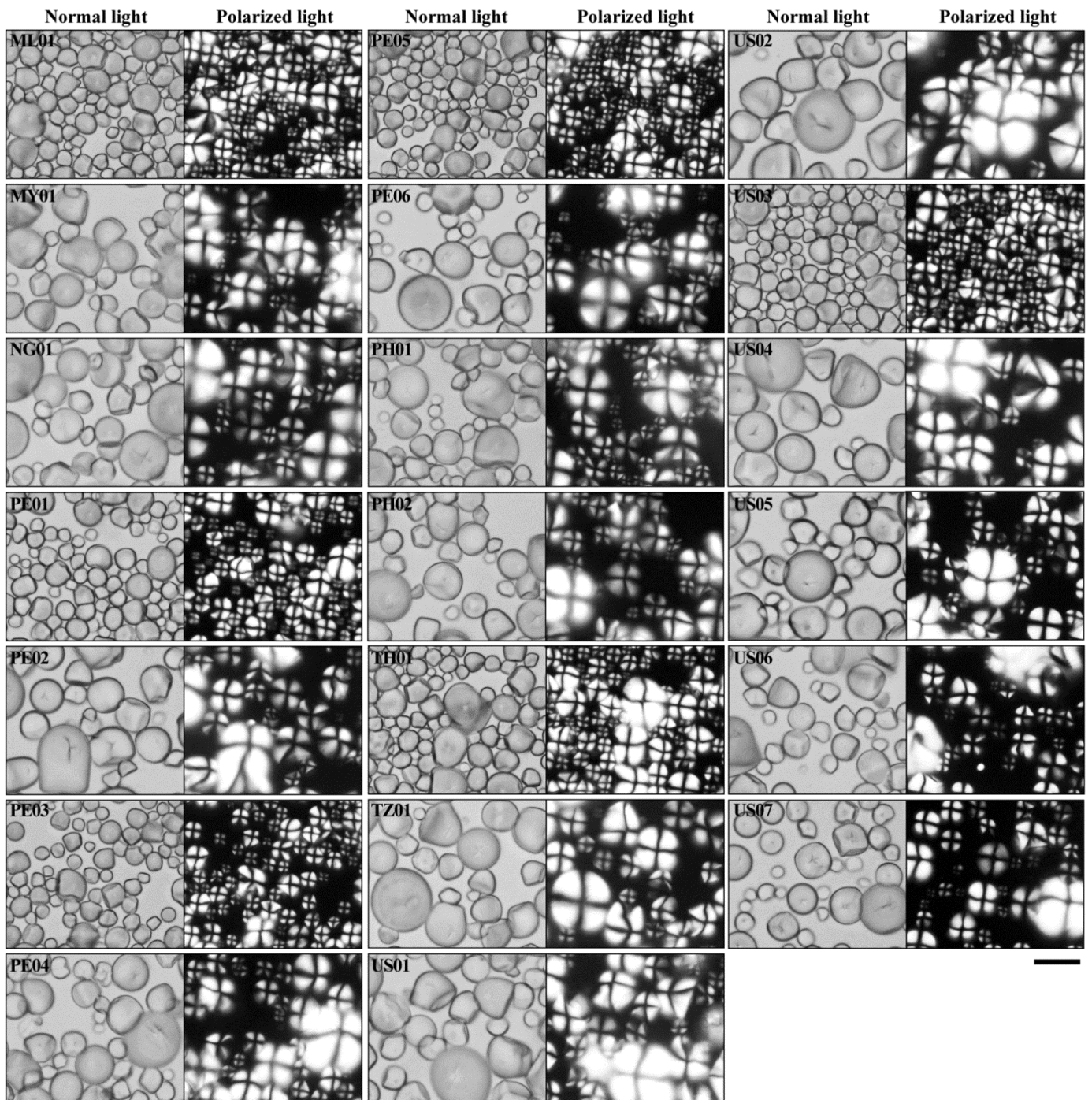


Figure 1. Morphologies of starch granules under normal light and polarized light. Scale bar = 20 μ m.

Table 1. Granule size distribution of starches from 44 sweet potato varieties.

Accession ID	d(0.2) (μm)	d(0.5) (μm)	d(0.8) (μm)	D[3,2] (μm)	D[4,3] (μm)
AO01	7.573 ± 0.002 mn	12.817 ± 0.005 tu	19.452 ± 0.005 γ	6.226 ± 0.002 s	13.464 ± 0.004 x
AR01	7.480 ± 0.002 lm	10.881 ± 0.003 l	14.967 ± 0.007 l	5.986 ± 0.002 o	11.023 ± 0.005 l
CB01	7.166 ± 0.002 j	10.331 ± 0.003 i	14.071 ± 0.003 h	5.689 ± 0.002 ij	10.383 ± 0.003 h
CG01	6.466 ± 0.001 f	10.084 ± 0.001 h	14.492 ± 0.002 i	5.335 ± 0.001 f	10.333 ± 0.001 gh
CN01	7.586 ± 0.020 mn	10.911 ± 0.036 l	14.808 ± 0.052 k	5.732 ± 0.010 l	10.941 ± 0.036 k
CN02	7.355 ± 0.003 k	11.003 ± 0.004 m	15.402 ± 0.007 m	5.675 ± 0.003 i	11.161 ± 0.005 m
CN03	6.762 ± 0.004 h	11.099 ± 0.006 n	16.654 ± 0.006 r	5.920 ± 0.001 m	11.648 ± 0.005 o
CN04	11.111 ± 0.002 z	14.669 ± 0.001 β	18.705 ± 0.000 z	7.612 ± 0.001 ζ	14.456 ± 0.001 γ
JP01	7.159 ± 0.001 j	11.018 ± 0.004 m	15.878 ± 0.010 o	6.208 ± 0.003 rs	11.399 ± 0.006 n
JP02	6.785 ± 0.003 h	10.426 ± 0.006 j	14.935 ± 0.009 l	5.698 ± 0.002 jk	10.727 ± 0.006 j
JP03	5.283 ± 0.003 a	8.340 ± 0.005 b	12.391 ± 0.009 e	4.932 ± 0.003 c	8.737 ± 0.007 d
JP04	6.398 ± 0.003 f	9.227 ± 0.003 f	12.460 ± 0.003 e	5.039 ± 0.001 d	9.185 ± 0.002 e
JP05	10.568 ± 0.002 y	14.811 ± 0.003 γ	19.935 ± 0.005 δ	7.681 ± 0.001 η	14.929 ± 0.003 δ
JP06	8.966 ± 0.001 u	13.578 ± 0.002 x	19.356 ± 0.004 γ	6.946 ± 0.001 z	13.997 ± 0.003 z
JP07	7.504 ± 0.001 m	12.269 ± 0.003 r	18.221 ± 0.006 x	6.052 ± 0.001 p	12.746 ± 0.004 t
JP08	10.271 ± 0.003 x	13.945 ± 0.005 z	18.245 ± 0.008 x	7.344 ± 0.003 δ	13.890 ± 0.006 y
JP09	7.187 ± 0.070 j	9.931 ± 0.130 g	13.066 ± 0.167 g	5.718 ± 0.038 kl	9.862 ± 0.120 f
JP10	7.297 ± 0.002 k	10.948 ± 0.003 lm	15.379 ± 0.004 m	5.945 ± 0.002 n	11.150 ± 0.003 m
JP11	6.017 ± 0.005 d	8.651 ± 0.006 d	11.652 ± 0.009 c	4.924 ± 0.004 c	8.623 ± 0.007 c
JP12	8.211 ± 0.004 r	12.410 ± 0.003 s	17.660 ± 0.001 v	6.764 ± 0.001 x	12.790 ± 0.002 t
JP13	5.207 ± 0.021 a	8.012 ± 0.031 a	11.189 ± 0.108 a	3.866 ± 0.011 a	8.013 ± 0.051 a
JP14	8.795 ± 0.004 t	12.749 ± 0.007 t	17.508 ± 0.012 u	6.746 ± 0.002 x	12.922 ± 0.008 u
JP15	6.978 ± 0.004 i	10.518 ± 0.006 k	14.773 ± 0.011 k	5.551 ± 0.003 h	10.691 ± 0.008 ij
MA01	5.855 ± 0.002 c	8.992 ± 0.005 e	12.772 ± 0.010 f	5.083 ± 0.002 e	9.176 ± 0.006 e
ML01	7.974 ± 0.004 p	12.117 ± 0.009 q	17.128 ± 0.015 s	6.210 ± 0.003 rs	12.360 ± 0.010 r
MY01	9.431 ± 0.004 w	13.803 ± 0.007 y	19.183 ± 0.013 β	7.513 ± 0.002 ε	14.113 ± 0.009 α
NG01	7.663 ± 0.005 no	12.449 ± 0.011 s	18.598 ± 0.023 y	6.331 ± 0.004 t	13.037 ± 0.015 v
PE01	9.132 ± 0.252 v	14.378 ± 0.123 α	20.965 ± 0.166 ζ	6.968 ± 0.040 α	14.901 ± 0.016 δ
PE02	9.038 ± 0.001 uv	12.832 ± 0.001 u	17.368 ± 0.002 t	7.002 ± 0.001 β	12.955 ± 0.001 u
PE03	7.392 ± 0.002 kl	11.090 ± 0.003 n	15.682 ± 0.003 n	6.194 ± 0.002 r	11.391 ± 0.003 n
PE04	8.187 ± 0.005 qr	11.730 ± 0.006 p	15.961 ± 0.007 o	6.481 ± 0.003 u	11.857 ± 0.006 q
PE05	6.663 ± 0.010 g	10.426 ± 0.013 j	14.943 ± 0.017 l	5.470 ± 0.004 g	10.643 ± 0.013 i
PE06	5.732 ± 0.002 b	8.491 ± 0.005 c	11.799 ± 0.010 d	4.943 ± 0.003 c	8.606 ± 0.006 c
PH01	8.325 ± 0.006 s	14.328 ± 0.011 α	22.233 ± 0.011 η	6.841 ± 0.002 y	15.296 ± 0.007 ε
PH02	7.930 ± 0.005 p	12.871 ± 0.007 u	19.051 ± 0.008 α	6.594 ± 0.002 w	13.409 ± 0.007 x
TH01	7.754 ± 0.003 o	11.517 ± 0.005 o	16.121 ± 0.007 p	6.313 ± 0.003 t	11.747 ± 0.005 p
TZ01	8.105 ± 0.005 q	13.467 ± 0.008 w	20.448 ± 0.012 ε	6.506 ± 0.004 v	14.211 ± 0.008 β
US01	5.797 ± 0.002 bc	8.460 ± 0.003 c	11.488 ± 0.003 b	4.682 ± 0.002 b	8.417 ± 0.002 b
US02	8.318 ± 0.003 s	12.302 ± 0.004 r	17.192 ± 0.009 s	6.846 ± 0.002 y	12.583 ± 0.006 s
US03	7.479 ± 0.003 lm	12.132 ± 0.008 q	17.856 ± 0.017 w	6.124 ± 0.004 q	12.555 ± 0.011 s
US04	6.576 ± 0.004 g	10.584 ± 0.008 k	15.694 ± 0.014 n	5.707 ± 0.004 jk	11.045 ± 0.009 l
US05	7.362 ± 0.003 k	11.482 ± 0.006 o	16.521 ± 0.008 q	5.929 ± 0.003 mn	11.792 ± 0.006 p
US06	9.025 ± 0.001 u	13.153 ± 0.004 v	18.263 ± 0.010 x	7.169 ± 0.001 γ	13.452 ± 0.006 x
US07	6.203 ± 0.002 e	9.900 ± 0.002 g	14.609 ± 0.002 j	5.556 ± 0.001 h	10.321 ± 0.002 g
Sig.	0.322	0.410	0.671	0.849	0.422

The d(0.2), d(0.5), and d(0.8) are the granule size at which 20%, 50%, and 80% of all the granules by volume are smaller. The D[3,2] and D[4,3] are the surface- and volume-weighted mean diameter, respectively. Sig.: the significance of normal distribution of the 44 samples by Shapiro–Wilk test. Data are means ± standard deviations, $n = 3$. The values with different letters in the same column are significantly different ($p < 0.05$).

2.2. Iodine Absorption and Amylose Content of Starch

Starch contains amylose and amylopectin. Both amylose and amylopectin influence the absorption of starch and iodine [23]. In this research, the iodine absorption spectra of 44 starches were analyzed (data not shown), and the iodine absorption parameters including the value of optical density (OD) at 550 nm (OD550), 620 nm (OD620), and 680 nm (OD680) were measured. The OD680 is usually defined as blue value (BV) of starch, and displays the iodine binding capacity of starch [24]. The ratio of OD620 to OD550

(OD620/550) can reflect the relative proportion of long chains in starch [23]. The OD680 and OD620/550 ranged from 0.259 to 0.382 and from 1.142 to 1.237 among 44 starches, respectively (Table 2), indicating that amylose and amylopectin were different among these starches.

Table 2. Iodine absorption parameters and amylose contents of starches.

Accession ID	OD680	OD620/550	AAC (%)	TAC (%)	ΔAC (%)
AO01	0.307 ± 0.004 ghijk	1.164 ± 0.026 abcdefg	25.6 ± 0.8 ijk	17.4 ± 0.7 efghi	8.2
AR01	0.324 ± 0.006 klmno	1.222 ± 0.023 gh	26.5 ± 0.7 jklm	17.4 ± 0.2 efghi	9.1
CB01	0.281 ± 0.007 bcd	1.192 ± 0.004 abcdefgh	22.2 ± 0.7 cd	16.4 ± 0.1 cdefgh	5.8
CG01	0.329 ± 0.011 no	1.157 ± 0.003 abcd	28.2 ± 0.9 mno	17.7 ± 0.4 fgghi	10.5
CN01	0.300 ± 0.007 efghi	1.155 ± 0.001 abc	24.9 ± 0.6 fghij	17.1 ± 0.2 efghi	7.8
CN02	0.306 ± 0.007 ghijk	1.160 ± 0.012 abcde	25.7 ± 0.8 ijkl	18.2 ± 0.4 hij	7.5
CN03	0.308 ± 0.002 ghijkl	1.208 ± 0.011 cdefgh	21.8 ± 0.2 bcd	14.7 ± 0.3 abc	7.1
CN04	0.295 ± 0.005 defghi	1.186 ± 0.017 abcdefgh	23.6 ± 0.5 defgh	15.7 ± 0.6 abcde	7.9
JP01	0.303 ± 0.004 fghij	1.183 ± 0.004 abcdefgh	24.5 ± 0.6 efghi	17.2 ± 0.4 efghi	7.3
JP02	0.294 ± 0.004 defghi	1.191 ± 0.007 abcdefgh	23.5 ± 0.2 defgh	16.6 ± 0.5 defgh	6.9
JP03	0.291 ± 0.005 cdefgh	1.218 ± 0.019 efgh	23.2 ± 0.7 cdef	17.7 ± 0.3 fgghi	5.5
JP04	0.336 ± 0.003 o	1.185 ± 0.011 abcdefgh	28.3 ± 0.4 mno	17.7 ± 0.3 fgghi	10.6
JP05	0.299 ± 0.007 defghi	1.237 ± 0.028 h	23.4 ± 0.9 cdefgh	17.1 ± 0.9 efghi	6.3
JP06	0.327 ± 0.007 mno	1.158 ± 0.015 abcd	27.9 ± 0.6 mno	16.1 ± 0.3 bcdefg	11.8
JP07	0.337 ± 0.003 o	1.186 ± 0.001 abcdefgh	28.5 ± 0.2 no	17.2 ± 0.5 efghi	11.3
JP08	0.304 ± 0.001 ghij	1.174 ± 0.012 abcdefg	25.0 ± 0.4 fghij	16.4 ± 0.1 cdefgh	8.6
JP09	0.312 ± 0.007 ijklmn	1.200 ± 0.006 abcdefgh	25.5 ± 0.9 ijk	17.1 ± 0.2 efghi	8.4
JP10	0.304 ± 0.009 ghij	1.167 ± 0.016 abcdefg	25.2 ± 1.1 ghij	20.2 ± 0.9 k	5.0
JP11	0.291 ± 0.006 cdefgh	1.181 ± 0.002 abcdefgh	23.4 ± 0.5 cdefgh	17.6 ± 0.4 efghi	5.8
JP12	0.260 ± 0.005 a	1.209 ± 0.015 cdefgh	19.3 ± 0.5 a	15.0 ± 0.5 abcd	4.3
JP13	0.282 ± 0.003 bcde	1.189 ± 0.025 abcdefgh	22.3 ± 0.7 cd	16.7 ± 0.7 defgh	5.6
JP14	0.326 ± 0.002 mno	1.169 ± 0.019 abcdefg	28.3 ± 0.2 nmo	19.7 ± 0.4 jk	8.6
JP15	0.310 ± 0.008 hijklm	1.161 ± 0.015 abcdef	25.8 ± 0.8 ijkl	17.2 ± 0.3 efghi	8.6
MA01	0.319 ± 0.008 jklmno	1.192 ± 0.014 abcdefgh	22.9 ± 0.8 cde	17.4 ± 0.8 efghi	5.5
ML01	0.303 ± 0.003 fghij	1.160 ± 0.014 abcde	25.4 ± 0.5 hijk	17.4 ± 0.0 efghi	8.0
MY01	0.323 ± 0.008 klmno	1.142 ± 0.006 a	27.8 ± 0.4 mno	18.3 ± 0.6 hij	9.5
NG01	0.325 ± 0.005 lmno	1.179 ± 0.014 abcdefgh	27.4 ± 0.6 lmno	17.8 ± 0.6 fgghi	9.6
PE01	0.382 ± 0.013 p	1.146 ± 0.015 ab	29.2 ± 1.3 o	17.7 ± 0.7 fgghi	11.5
PE02	0.284 ± 0.008 bcdef	1.197 ± 0.028 abcdefgh	22.1 ± 0.7 cd	14.5 ± 0.3 ab	7.6
PE03	0.281 ± 0.002 bcd	1.206 ± 0.011 cdefgh	21.7 ± 0.3 bcd	16.1 ± 0.6 bcdefg	5.6
PE04	0.259 ± 0.010 a	1.212 ± 0.021 cdefgh	19.2 ± 0.9 a	15.2 ± 0.1 abcd	4.0
PE05	0.296 ± 0.009 defghi	1.158 ± 0.011 abcd	24.4 ± 0.8 efghi	16.0 ± 0.9 bcdef	8.4
PE06	0.303 ± 0.006 fghij	1.160 ± 0.010 abcde	25.0 ± 0.6 fghij	14.2 ± 0.1 a	10.8
PH01	0.331 ± 0.002 o	1.180 ± 0.010 abcdefgh	27.8 ± 0.2 mno	17.7 ± 0.3 fgghi	10.1
PH02	0.303 ± 0.007 fghij	1.190 ± 0.003 abcdefgh	24.3 ± 0.5 efghi	16.5 ± 0.7 cdefgh	7.8
TH01	0.299 ± 0.003 defghi	1.193 ± 0.038 abcdefgh	24.3 ± 0.2 efghi	18.0 ± 0.2 ghij	6.3
TZ01	0.320 ± 0.007 jklmno	1.162 ± 0.044 abcdef	27.2 ± 0.5 klmn	17.9 ± 0.1 fgghi	9.3
US01	0.298 ± 0.002 defghi	1.177 ± 0.010 abcdefg	24.4 ± 0.2 efghi	18.2 ± 0.4 hij	6.2
US02	0.311 ± 0.003 ijklm	1.205 ± 0.010 bcdefgh	25.3 ± 0.3 ghijk	18.7 ± 0.2 ijk	6.6
US03	0.274 ± 0.008 abc	1.220 ± 0.018 fgh	21.5 ± 1.0 bc	16.2 ± 0.1 bcdefg	5.3
US04	0.270 ± 0.003 ab	1.203 ± 0.018 bcdefgh	20.2 ± 0.3 ab	15.2 ± 0.7 abcd	5.0
US05	0.331 ± 0.007 o	1.178 ± 0.010 abcdefg	27.8 ± 0.9 mno	17.7 ± 0.4 fgghi	10.1
US06	0.294 ± 0.003 defghi	1.215 ± 0.026 defgh	23.4 ± 0.1 cdefg	16.6 ± 0.2 defgh	6.8
US07	0.290 ± 0.006 cdefg	1.193 ± 0.039 abcdefgh	23.4 ± 0.8 cdefg	17.5 ± 0.3 efghi	5.9
Sig.	0.094	0.588	0.306	0.171	0.336

AAC: apparent amylose content; TAC: true amylose content; ΔAC: the difference between AAC and TAC (AAC–TAC); Sig.: the significance of normal distribution of the 44 samples by Shapiro–Wilk test. Data are means ± standard deviations, $n = 3$. The values with different letters in the same column are significantly different ($p < 0.05$).

Amylose content is the important structure parameter, determining the applications of starch [25,26]. The amylose content is usually determined with the iodine colorimetry method according to the OD₆₂₀ of starch–iodine complex. However, the iodine colorimetry usually overestimates the amylose content of starch because of the branch-chains of amylopectin that can bind the iodine. Therefore, the amylose content determined by iodine colorimetry is called the apparent amylose content (AAC) [23]. In this study, the AAC varied from 19.2% to 29.2% (Table 2), and is in the range of sweet potatoes reported by previous references [14,19,27]. The concanavalin A (Con A) precipitate method can accurately determine the amylose content to avoid the overestimation of amylose content. Using this method, starch is completely dissolved into amylose and amylopectin, and separated into two aliquots. The Con A specifically binds and precipitates the amylopectin in an aliquot, and the remaining amylose in the supernatant is hydrolyzed by amylolytic enzymes to glucose, which is measured with glucose oxidase/peroxidase reagent for determining the quality of amylose. The amylose and amylopectin in another aliquot are similarly hydrolyzed to glucose for measuring their quality. The amylose content is the quality percentage of amylose to both amylose and amylopectin. The measured amylose content is not influenced by the purity and moisture of starch, and is usually defined as true amylose content (TAC) [23]. The TAC ranged from 14.2% to 20.2% among 44 sweet potato starches (Table 2). The TAC was significantly lower than AAC in all starches, and the Δ AC (AAC–TAC) was significantly different among different varieties from 4.0% to 11.8%, indicating that varieties with different genotype backgrounds had significantly different amylopectin structure with different iodine binding capacity. The amylose is biosynthesized simply by granule-bound starch synthase I (GBSSI) encoded by the *Waxy* (*Wx*) gene in plant storage tissue, and amylopectin is biosynthesized complexly by soluble starch synthases (SSSs), starch branching enzymes (SBEs), and starch debranching enzymes (DBEs) [28]. There are many *Wx* alleles responsible for amylose synthesis from low to high in different varieties of the same species [29]. The SSSs, SBEs, and DBEs have many isoforms, and their quality and activities determine the amylopectin structure [30]. In this research, sweet potato varieties originate from different countries and areas. Their different genotype backgrounds with different qualities and activities of GBSSI, SSSs, SBEs, and DBEs led to different amylose contents and amylopectin structures among 44 sweet potato varieties.

The hierarchical cluster analysis based on OD₆₈₀, OD_{620/550}, AAC, and TAC was carried out to investigate the differences and similarities between sweet potato varieties (Figure 2). The 44 sweet potato varieties were divided into cluster 1 (C1) and cluster 2 (C2). The C2 contained 16 sweet potato varieties with OD₆₈₀ from 0.259 to 0.319, OD_{620/550} from 1.167 to 1.237, AAC from 19.2% to 25.3%, and TAC from 15.0% to 20.2%. The C1 was further divided into two subgroups of C1A and C1B. The C1A contained eight sweet potato varieties with OD₆₈₀ from 0.303 to 0.382, OD_{620/550} from 1.146 to 1.186, AAC from 25.0% to 29.2%, and TAC from 14.2% to 17.7%, and the C1B contained 20 varieties with OD₆₈₀ from 0.284 to 0.326, OD_{620/550} from 1.142 to 1.222, AAC from 21.8% to 28.3%, and TAC from 14.5% to 19.7% (Figure 2; Table 2). The Δ AC ranged from 4.0% (PE04) to 6.6% (US02) in C2, from 6.8% (US06) to 9.6% (NG01) in C1B, and from 10.1% (PH01) to 11.8% (JP06) in C1A (Table 2), indicating that amylopectin structure plays an important role in influencing starch components and iodine absorption. Though some varieties originated from the same area, their genotypes exhibited significant differences. For example, for 15 varieties (JP01–JP15) originating from Japan, there were three, six, and six varieties in C1A, C1B and C2, respectively.

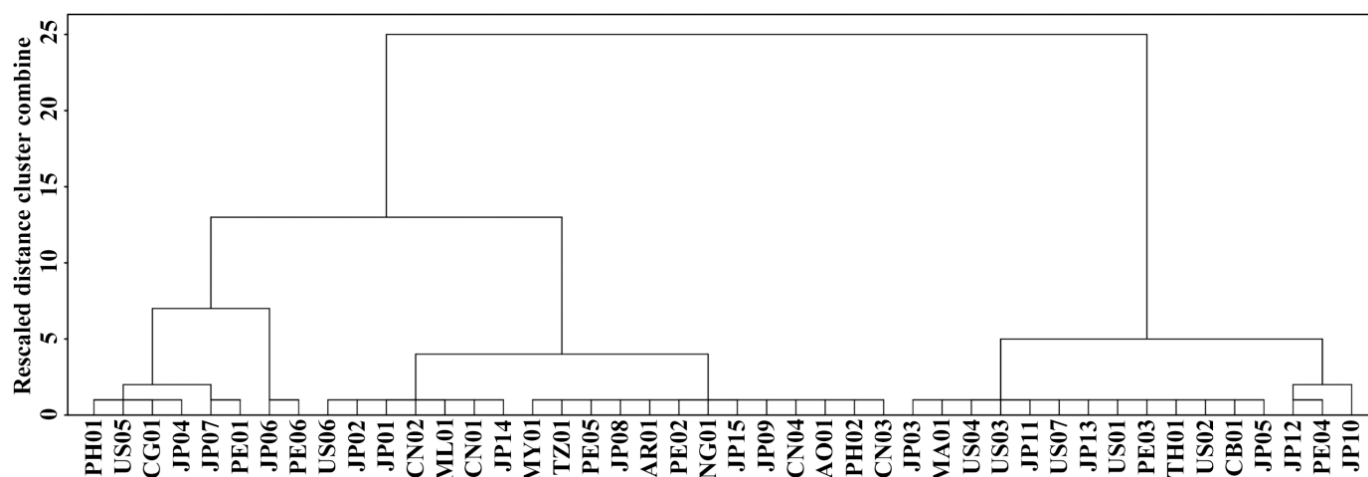


Figure 2. Hierarchical cluster analysis of 44 sweet potato varieties based on OD680, OD620/550, AAC, and TAC in Table 2.

2.3. Crystalline Structure of Starch

The branch-chains of amylopectin can form A- and B-type crystallinity, which can be detected by X-ray diffraction (XRD). The XRD patterns of 44 starches are presented in Figure 3. Starches from plant tissues have A-, B-, and C-type. A- and B-type starch contains only A- and B-type crystallinity, respectively, but C-type starch simultaneously contains both A- and B-type crystallinities. According to the ratio of A- to B-type crystallinities from high to low, C-type starch is usually further classified into C_A -, C_C -, and C_B -type. The C_C -type starch has diffraction peaks at 2θ 5.6° , 15° , 17° , and 23° ; C_A -type starch exhibits significant shoulder peak at 2θ 18° , a characteristic peak of A-type crystallinity; and C_B -type starch has significant shoulder peaks at 2θ 22° and 24° , two characteristic peaks of B-type crystallinity [7,31]. In this study, 44 sweet potato varieties had A-, C_A -, C_C -, and C_B -type starches (Figure 3). The JP14 starch was A-type, the PE06 starch was C_B -type, the AO01, CB01, CN02, JP01, JP06, JP12, JP13, JP15, ML01, PE01, PE04, PH01, PH02, TH01, TZ01, US03, US06, and US07 starches were C_A -type, and the other starches were C_C -type (Figure 3). The A-, C_A -, C_C -, and C_B -type starches have been reported in sweet potato varieties [10,13,14,19], but the B-type starch has not been reported in references. Genkina et al. [16,32] reported that the soil temperature determines the crystallinity of sweet potato starch. The root tuber synthesizes A-type starch in soil temperature above 33°C and B-type starch in soil temperature below 15°C . In fact, the temperature, moisture, and amylopectin branch-chain length all influence the crystal conformation during starch synthesis. The low temperature, wet condition, and amylopectin long branch-chains tend to form B-type crystallinity, and the high temperature, dry condition, and amylopectin short branch-chains tend to form A-type crystallinity [33]. In this study, all varieties grew in the same environment, and underwent the same soil temperature and moisture variation during starch synthesized and accumulated. The expression and activities of starch synthesis related enzymes were different among the 44 sweet potato varieties because their different genotypes responded to the variation in soil temperature differently, leading to different crystalline structures among the 44 sweet potato starches. The RC of starch was measured, and ranged from 15.9% to 27.3% among 44 starches (Figure 3). The RC of starch is affected by amylose, amylopectin, crystallinity, and granule size [7,24,34].

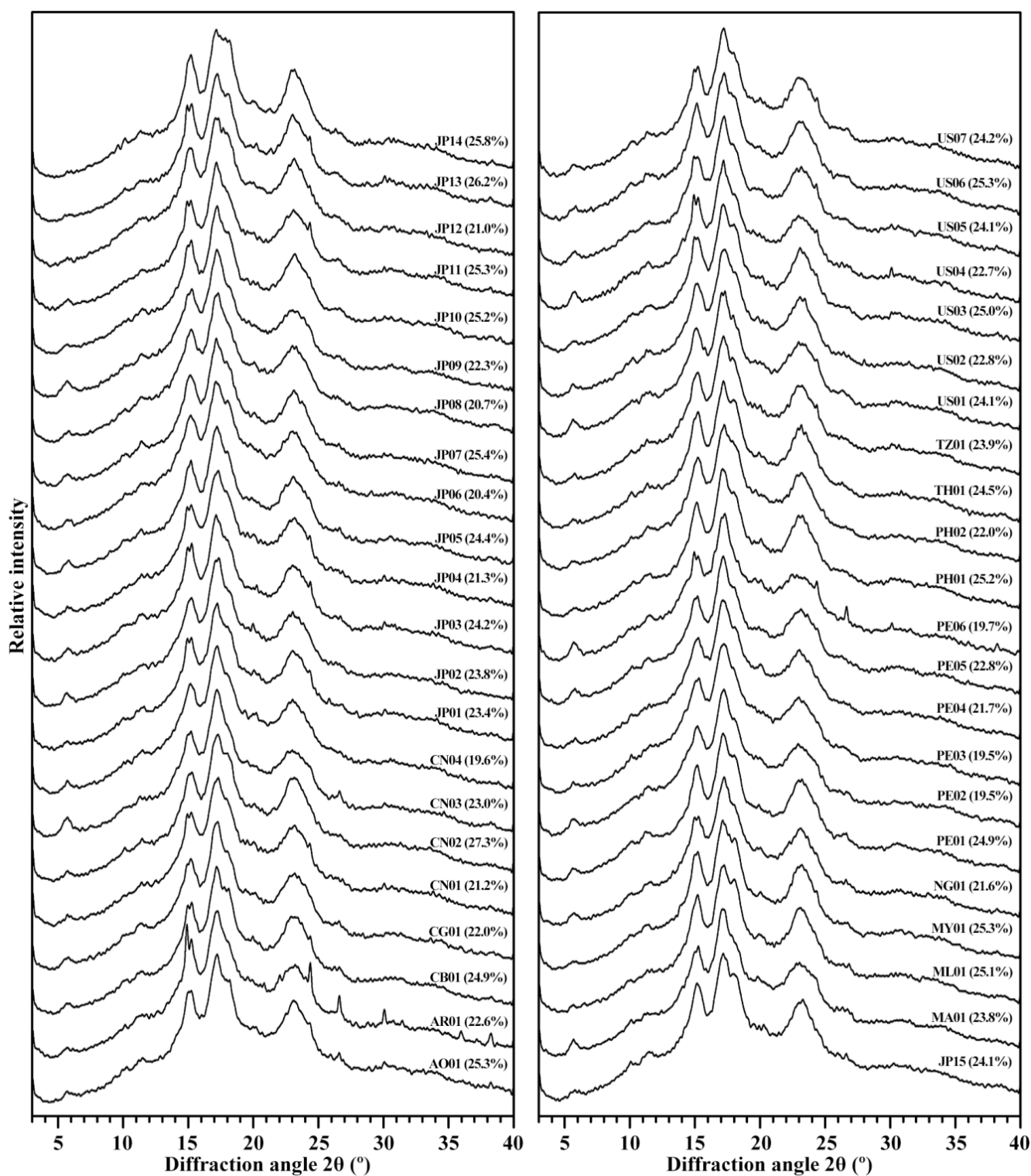


Figure 3. XRD patterns of starches from different sweet potato varieties. The relative crystallinity (RC) is given in the parenthesis after accession ID.

2.4. Thermal Properties of Starch

The thermal properties are mainly functional properties and an important index for evaluating starch applications. The differential scanning calorimetric (DSC) thermograms of the 44 starches are shown in Figure 4. Significantly different thermograms were observed among the 44 sweet potato starches. These thermograms were divided into three types of one-peak thermogram (namely, JP14, JP06, ML01, and MY01), two-peak ther-

mogram (namely, JP04, CN03, US04, and PE05), and three-peak thermogram (namely, JP10, AO01, US01, and TZ01) according to their peak patterns (Figure 4). The gelatinization onset (T_o), peak (T_p), and conclusion temperature (T_c) ranged from 52.2 to 73.8 °C, from 59.7 to 80.0 °C, and from 75.3 to 86.9 °C among the 44 varieties, respectively. The gelatinization temperature range (ΔT) varied from 13.1 to 29.2 °C, and the gelatinization enthalpy (ΔH) ranged from 10.7 to 16.9 J/g (Table 3). The large gelatinization parameter variation among the 44 varieties was mainly due to the significantly different thermal curves. Similar thermal properties have been shown in different sweet potatoes from different references [13,19,35–37]. For example, Osundahunsi et al. [37] reported one-peak thermogram with gelatinization temperature from 67 to 75 °C in sweet potato varieties white-skinned TIS-1499 and red-skinned TIB-2. Kim et al. [13] reported the ΔT from 13.0 to 36.7 °C among eight sweet potato varieties. Lee and Lee [36] reported the ΔT from 24.0 to 28.0 °C among three sweet potato varieties. Duan et al. [35] reported a two-peak DSC curve in sweet potato variety Jishu 25. Genkina et al. [32] fitted the two-peak DSC curve of sweet potato starch into two gelatinization peaks with the low gelatinization temperature peak for B-type crystallinity and the high gelatinization temperature peak for A-type crystallinity. Guo et al. [38] fitted one-, two-, and three-peak DSC curves of different sweet potato starches into three gelatinization peaks, and the low, middle, and high gelatinization temperature peaks are the gelatinization of B-, C-, and A-type starch granules, respectively, meaning that sweet potato root tuber contains A-, B-, and C-type starch. In the present study, the different proportions of A-, B-, and C-type starch in sweet potatoes led to the different patterns of DSC curves among the 44 sweet potato starches.

The hierarchical cluster analysis based on T_p , T_c , ΔT , and ΔH was carried out to investigate the differences and similarities between sweet potato varieties (Figure 5). The JP14 was divided into one cluster (C2), and exhibited significant differences to the other sweet potato varieties in cluster 1 (C1) because JP14 starch had a typical one-peak DSC pattern with the highest gelatinization temperature and the most narrow ΔT among the 44 sweet potato starches. The cluster 1 contained two subclusters of C1A and C1B. The C1A had 21 sweet potato varieties with T_p , T_c , ΔT , and ΔH from 59.7 to 77.1 °C, from 75.3 to 86.7 °C, from 22.0 to 29.2 °C, and from 10.7 to 15.0 J/g, respectively. The C1B had 22 sweet potato varieties with T_p , T_c , ΔT , and ΔH from 66.8 to 77.5 °C, from 78.8 to 85.4 °C, from 18.0 to 23.9 °C, and from 13.2 to 16.9 J/g, respectively. It is noteworthy that some varieties from the same country, such as the JP01–JP15 varieties originating from Japan, were distributed into different groups, indicating that varieties from the same country had significantly different thermal properties.

2.5. Relationships of Starch Properties and Cluster Analysis of Sweet Potato Varieties

The relationships between starch properties were analyzed (Table 4). Among the 44 sweet potato starches, the granule size (D[4,3]) had no significant relationship with amylose content, RC, and thermal properties except the ΔT . The OD680 was significantly positively correlated to AAC, TAC, and ΔH , the OD620/550 was negatively correlated to AAC, TAC, T_p , T_c , and ΔH , and the AAC, TAC, and RC were positively correlated to T_p , T_c , and ΔH . Amylose and amylopectin are important components in starch, especially amylose, its content significantly affects the physicochemical properties and applications of starch [23,25,26]. Although granule size also influences the starch thermal properties [9,34], the thermal properties of starch were mainly affected by amylose content (AAC, TAC), amylopectin structure (OD620/550), and crystal structure (RC) in sweet potato (Table 4).

The hierarchical cluster analysis based on D[4,3], OD680, OD620/550, AAC, TAC, RC, T_p , T_c , ΔT , and ΔH was further carried out to investigate the differences and similarities between sweet potato varieties (Figure 6). The JP14 was divided into cluster 2 (C2), and the other sweet potato varieties were divided into cluster 1 (C1), indicating that JP14 had significantly different starch properties, especially for its thermal properties. The result also agreed with their crystalline structure that only JP14 had A-type starch. In cluster 2,

the 43 sweet potato varieties were divided into different groups, showing that they had different starch properties due to different genotype backgrounds.

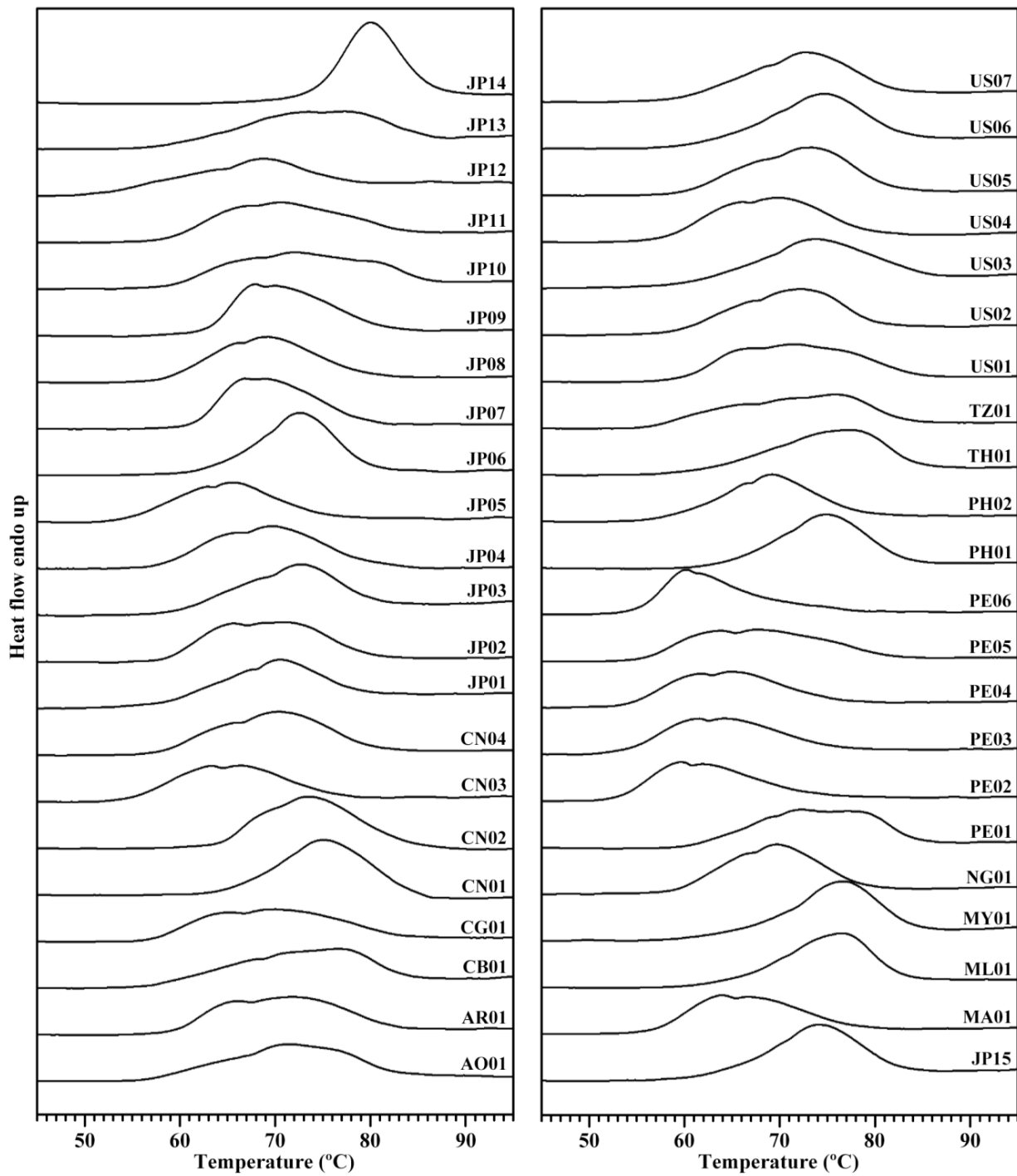


Figure 4. DSC thermograms of starches from different sweet potato varieties.

Table 3. Thermal property parameters of starches.

Accession ID	To (°C)	Tp (°C)	Tc (°C)	ΔT (°C)	ΔH (J/g)
AO01	57.4 ± 0.6 fgh	71.6 ± 0.1 klm	82.7 ± 0.6 jklmn	25.3 ± 1.2 klmnop	13.6 ± 0.1 bcdefghijk
AR01	59.8 ± 0.6 jklm	71.8 ± 0.4 lmn	82.9 ± 0.0 jklmno	23.2 ± 0.6 ghijklm	14.3 ± 0.0 fghijklm
CB01	56.7 ± 0.5 def	76.5 ± 0.4 vw	84.5 ± 0.3 nopqr	27.9 ± 0.2 qr	14.2 ± 0.3 efghijklm
CG01	57.3 ± 0.3 efg	70.5 ± 0.6 ij	84.2 ± 1.0 mnopqr	26.9 ± 0.7 opqr	13.8 ± 0.0 cdefghijkl
CN01	64.2 ± 0.2 qr	75.3 ± 0.3 tu	85.4 ± 0.4 pqrst	21.3 ± 0.2 cdefgh	16.9 ± 0.5 o
CN02	64.0 ± 0.0 pqr	73.6 ± 0.1 pqr	84.8 ± 0.4 opqr	20.8 ± 0.4 cdefg	16.8 ± 0.5 o
CN03	54.4 ± 0.2 bc	65.8 ± 0.7 d	76.6 ± 1.2 ab	22.2 ± 1.0 efghi	12.6 ± 0.3 bcd
CN04	58.0 ± 0.1 fghi	70.2 ± 0.0 ij	80.4 ± 0.1 defgh	22.5 ± 0.1 efghi	14.7 ± 0.0 ijklm
JP01	58.3 ± 0.1 fghij	70.5 ± 0.1 ij	81.5 ± 0.4 efghij	23.3 ± 0.5 ghijklm	13.0 ± 0.2 bcdefg
JP02	58.7 ± 0.0 ghijk	70.6 ± 0.6 ijk	80.0 ± 0.4 defg	21.3 ± 0.4 cdefgh	14.7 ± 0.2 hijklm
JP03	59.6 ± 0.0 ijkl	72.9 ± 0.1 op	82.4 ± 0.8 ijklm	22.8 ± 0.8 fghijk	13.7 ± 0.1 cdefghijkl
JP04	55.6 ± 1.5 cd	69.9 ± 0.1 hij	81.7 ± 1.7 fghijk	26.2 ± 2.2 nopq	15.0 ± 0.6 jklmn
JP05	54.3 ± 0.1 bc	65.7 ± 0.1 d	75.7 ± 1.1 ab	21.4 ± 1.2 cdefgh	12.3 ± 0.0 bc
JP06	62.4 ± 0.2 no	72.6 ± 0.1 mno	80.3 ± 0.3 defgh	18.0 ± 0.5 b	14.9 ± 0.3 jklmn
JP07	61.0 ± 0.4 lmn	66.8 ± 0.1 e	79.7 ± 0.1 de	18.7 ± 0.3 bc	14.7 ± 0.3 hijklm
JP08	58.1 ± 0.0 fghij	69.1 ± 0.1 gh	80.5 ± 0.5 defghi	22.4 ± 0.5 efghi	14.6 ± 0.1 hijklm
JP09	62.6 ± 0.2 nopq	68.0 ± 0.1 f	82.0 ± 0.0 hijkl	19.5 ± 0.2 bcd	15.3 ± 0.2 mn
JP10	59.1 ± 0.1 hijk	72.1 ± 0.1 mno	86.1 ± 0.1 rst	27.0 ± 0.0 pqr	14.6 ± 0.3 hijklm
JP11	58.8 ± 0.1 ghijk	70.8 ± 0.1 jkl	84.2 ± 0.0 mnopqr	25.4 ± 0.1 lmnopq	14.1 ± 0.6 efghijklm
JP12	52.2 ± 0.3 a	68.8 ± 0.1 fg	80.1 ± 0.1 defgh	27.9 ± 0.1 qr	10.7 ± 0.5 a
JP13	57.5 ± 0.0 fgh	77.1 ± 0.2 wx	86.7 ± 0.0 st	29.2 ± 0.0 r	14.2 ± 0.6 fghijklm
JP14	73.8 ± 0.0 s	80.0 ± 0.0 y	86.9 ± 0.1 t	13.1 ± 0.1 a	16.2 ± 0.1 no
JP15	62.5 ± 0.7 nop	74.1 ± 0.0 rs	83.1 ± 0.1 jklmno	20.6 ± 0.8 cdefg	14.3 ± 0.1 fghijklm
MA01	56.8 ± 0.4 def	63.9 ± 0.1 c	78.8 ± 0.4 cd	22.1 ± 0.1 defghi	12.7 ± 0.0 bcde
ML01	64.1 ± 1.1 pqr	76.7 ± 0.3 vwx	83.6 ± 0.6 klmnop	19.5 ± 1.8 bcd	14.1 ± 0.7 efghijklm
MY01	64.4 ± 1.2 r	76.8 ± 0.0 vwx	84.9 ± 0.1 opqrs	20.5 ± 1.1 cdefg	15.0 ± 0.7 jklmn
NG01	59.1 ± 0.0 hijk	69.9 ± 0.1 hij	79.3 ± 0.2 d	20.2 ± 0.2 bcdef	14.0 ± 0.2 defghijklm
PE01	60.3 ± 0.0 klm	72.5 ± 0.4 mno	84.7 ± 0.6 opqr	24.4 ± 0.6 ijklmno	14.7 ± 0.2 hijklm
PE02	53.3 ± 0.3 ab	59.9 ± 0.2 a	75.3 ± 0.1 a	22.0 ± 0.2 defghi	13.0 ± 0.3 bcdefg
PE03	53.9 ± 0.0 b	61.4 ± 0.1 b	76.5 ± 0.8 ab	22.6 ± 0.8 efghij	12.8 ± 0.2 bcde
PE04	54.6 ± 0.5 bc	65.0 ± 0.0 d	77.4 ± 0.6 bc	22.9 ± 0.1 fghijkl	12.3 ± 0.1 b
PE05	55.8 ± 0.1 cde	67.9 ± 0.3 f	81.8 ± 0.3 fghijk	26.1 ± 0.4 nopq	13.3 ± 0.1 bcdefghi
PE06	54.8 ± 0.3 bc	59.7 ± 0.7 a	77.2 ± 0.2 bc	22.4 ± 0.1 efghi	12.9 ± 0.7 bcdef
PH01	63.8 ± 0.2 opqr	75.0 ± 0.1 st	83.6 ± 0.2 klmnop	19.8 ± 0.0 bcde	14.9 ± 0.5 jklmn
PH02	57.8 ± 0.1 fgh	69.6 ± 0.4 ghi	78.8 ± 0.1 cd	21.0 ± 0.0 cdefg	13.2 ± 0.1 bcdefgh
TH01	61.0 ± 0.2 lmn	77.5 ± 0.0 x	84.9 ± 0.1 opqrs	23.9 ± 0.3 hijklmn	15.1 ± 0.5 klmn
TZ01	56.6 ± 0.1 def	76.0 ± 0.0 uv	84.0 ± 0.4 lmnopq	27.4 ± 0.5 pqr	13.5 ± 0.1 bcdefghij
US01	60.2 ± 0.1 klm	71.8 ± 0.4 lmn	85.3 ± 0.6 pqrst	25.1 ± 0.6 jklmnop	14.9 ± 0.1 jklmn
US02	59.0 ± 1.0 ghijk	71.6 ± 0.7 klmn	80.6 ± 0.1 defghi	21.6 ± 1.1 defgh	13.7 ± 0.3 cdefghijk
US03	60.3 ± 0.1 klm	74.0 ± 0.3 qrs	85.8 ± 0.8 qrst	25.5 ± 0.9 mnopq	14.4 ± 0.3 ghijklm
US04	57.9 ± 0.1 fghi	69.9 ± 0.1 hij	79.9 ± 0.1 def	22.0 ± 0.1 defghi	14.9 ± 0.3 jklmn
US05	60.0 ± 0.1 klm	73.1 ± 0.1 opq	81.9 ± 0.3 ghijk	21.9 ± 0.1 defghi	15.2 ± 0.5 lmn
US06	61.4 ± 0.7 mn	74.5 ± 0.4 rst	83.6 ± 0.1 klmnop	22.2 ± 0.8 defghi	14.3 ± 0.9 fghijklm
US07	59.5 ± 0.0 ijkl	72.7 ± 0.4 nop	82.0 ± 0.3 hijkl	22.5 ± 0.3 efghi	14.2 ± 0.5 efghijklm
Sig.	0.009	0.180	0.189	0.128	0.224

To, Tp and Tc: onset, peak, and conclusion temperature of gelatinization, respectively; ΔT and ΔH: gelatinization temperature range and enthalpy, respectively; Sig.: the significance of normal distribution of the 44 samples by Shapiro–Wilk test. Data are means ± standard deviations, $n = 3$. The values with different letters in the same column are significantly different ($p < 0.05$).

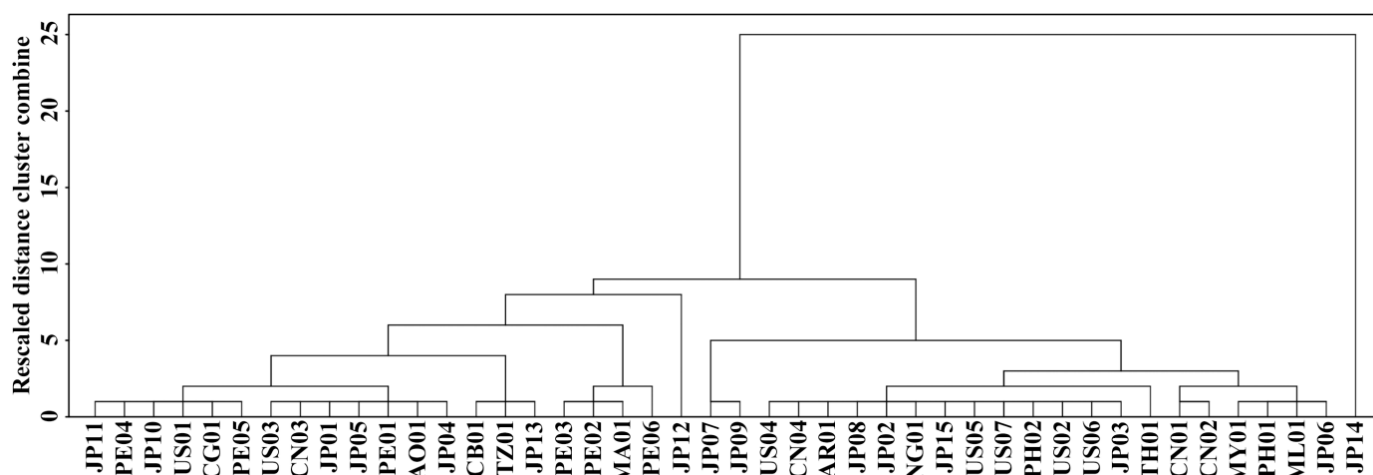


Figure 5. Hierarchical cluster analysis of the 44 sweet potato varieties based on Tp, Tc, ΔT, and ΔH in Table 3.

Table 4. Correlation coefficients between starch property parameters.

	D[4,3]	OD680	OD620/550	AAC	TAC	RC	Tp	Tc
OD680	0.273							
OD620/550	−0.066	−0.501 **						
AAC	0.251	0.908 **	−0.619 **					
TAC	0.006	0.483 **	−0.304 *	0.593 **				
RC	−0.036	0.164	−0.106	0.187	0.583 **			
Tp	0.122	0.183	−0.300 *	0.343 *	0.602 **	0.625 **		
Tc	−0.144	0.201	−0.416 **	0.354 *	0.646 **	0.632 **	0.858 **	
ΔT	−0.327 *	−0.289	0.070	−0.323 *	−0.113	0.018	−0.015	0.205
ΔH	−0.029	0.372 *	−0.423 **	0.522 **	0.498 **	0.338 *	0.590 **	0.623 **

The analysis is based on property parameters with the significance of normal distribution over 0.05. The RC is relative crystallinity, and its significance of normal distribution is 0.067. The other abbreviations and their normal distributions are listed in Tables 1–3. * and ** indicate the significance at the $p < 0.05$ and $p < 0.01$ levels, respectively.

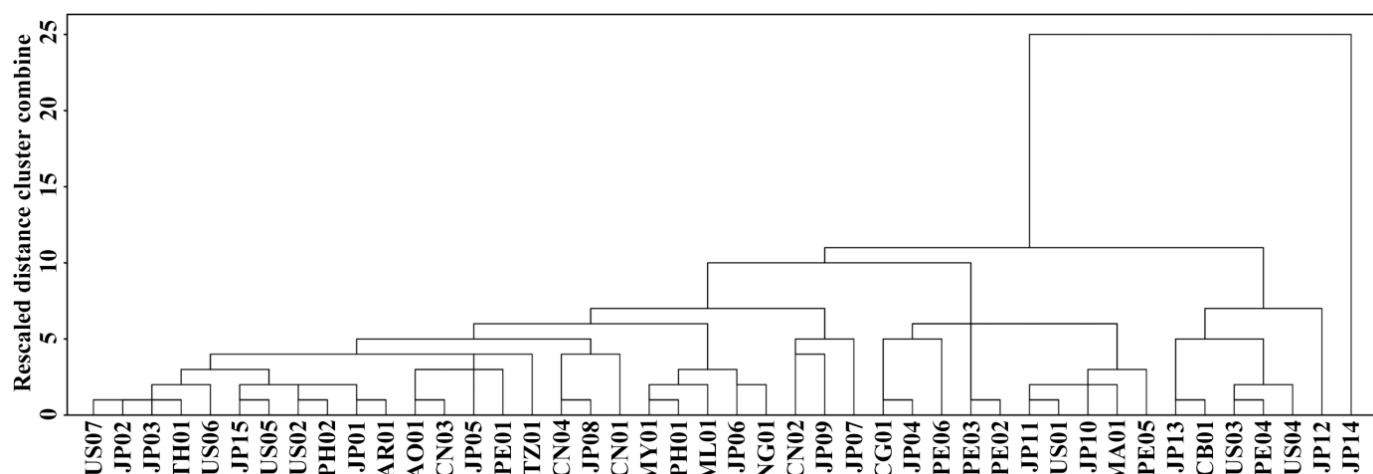


Figure 6. Hierarchical cluster analysis of the 44 sweet potato varieties based on D[4,3], OD680, OD620/550, AAC, TAC, RC, Tp, Tc, ΔT, and ΔH in Table 4.

Though the 44 sweet potato varieties were divided into different clusters according to their starch properties (Figure 6), it is noteworthy that the growing conditions significantly affect starch properties in sweet potato, especially for temperature [16] and fertilizer treatment [21]. Recent study also shows that starch physicochemical properties are affected

significantly by varieties, growing locations, and their interaction in sweet potato [39]. In this study, the sweet potato varieties originating from different countries were planted in the same place and cultivated conditions to avoid the effects of growing environment on starch properties. However, the selected growing conditions are significantly different from growth habits of varieties in their original country. Therefore, the starch properties of sweet potato varieties in the present study might be different from those in their original countries.

3. Materials and Methods

3.1. Plant Materials

The 44 sweet potato varieties were randomly chosen, and their fresh root tubers were provided by Sweetpotato Research Institute, China Agricultural Academy of Sciences. These germplasm resources are all public varieties or landraces, and conserved in National Sweetpotato Genebank in Xuzhou, China. Among the 44 varieties, 15 were from Japan, 7 from United States, 6 from Peru, 4 from China, 2 Philippines, and the others from Angola, Argentina, Cambodia, Congo, Morocco, Mali, Malaysia, Nigeria, Thailand, and Tanzania. Their accession IDs and original areas are listed in Table 5. These sweet potato varieties were planted simultaneously in the farm of Xuzhou Sweetpotato Research Center (32°27' N, 117°29' E), Jiangsu Province, China, on April 28, and harvested on 26 October 2020. The soil in the experimental field was yellow fluvo-aquic soil with a sandy texture. The available K, available P, hydrolysable N, total N, and organic matter in 0–20 cm soil layer before the experiment were 95 mg kg⁻¹, 19.7 mg kg⁻¹, 94.2 mg kg⁻¹, 1.06 g kg⁻¹, and 16.2 g kg⁻¹, respectively, and its pH was 7.54. The fertilizer including 75 kg ha⁻¹ P₂O₅ (calcium superphosphate) and 120 kg ha⁻¹ K₂O (potassium chloride) was applied as base fertilizer in the ridge before planting. The seedlings were planted in 5 rows with 90 cm between rows and 20 cm between hills. The temperature and rainfall of growing location during sweet potato growth stage are presented in Table 6.

3.2. Isolation of Starch

Starches from fresh root tubers were prepared following the method of Guo et al. [2]. Briefly, the root tubers were washed cleanly and cut into some pieces. The sample was homogenized in H₂O with a home blender. The tissue suspension was filtered through four layers of gauze, and the residue was homogenized and filtered again to release more starch. The filtrate was filtered through 100-, 200-, and 300-mesh sieve, successively, and centrifuged (3000 × g, 5 min). The starch precipitate was washed 5 times with H₂O and 3 times with anhydrous ethanol. Finally, the starch was dried at 40 °C for 2 d, and ground into powder through 100-mesh sieve.

3.3. Granule Morphology and Size Analysis of Starch

Isolated starch in 25% glycerol was viewed and photographed with a polarized light microscope (BX53, Olympus, Tokyo, Japan) under normal and polarized light. Starch size was analyzed with a laser size analyzer (Mastersizer 2000, Malvern, Worcestershire, UK) according to the procedures of Guo et al. [2]. The obscuration of starch–water suspension was about 12%, and the sample was stirred at 2000 rpm during analysis.

3.4. Analysis of Starch–Iodine Absorption

Starch was dispersed in dimethyl sulfoxide and stained with iodine solution according to the procedures of Man et al. [24]. Briefly, 10 mg starch in 5 mL dimethyl sulfoxide containing 10% 6.0 M urea was heated at 95 °C for 1 h. The starch suspension was swirled at intervals of 15 min during heating. The dispersed amylose and amylopectin (1 mL) was colorized for 20 min with iodine solution (1 mL of 0.2% I₂ and 2% KI) in 50 mL volumetric flask diluted with H₂O. The sample was scanned from 400 to 900 nm using a spectrophotometer (BioMate 3S, Thermo Scientific, Chino, CA, USA).

Table 5. List of sweet potato accessions used in this study.

Accession ID Used in This Study	Origin Accession ID in China National Sweetpotato Genebank	Accession Name without Origin Accession ID in China National Sweetpotato Genebank	Original Area
AO01		Angola	Angola
AR01	SY00332		Argentina
CB01		Cambodia 1	Cambodia
CG01		Congo 2	Congo
CN01	SY00018		China
CN02	SY00019		China
CN03	SY00192		China
CN04	SY00215		China
JP01	SY00075		Japan
JP02	SY00081		Japan
JP03	SY00083		Japan
JP04	SY00087		Japan
JP05	SY00145		Japan
JP06	SY00147		Japan
JP07	SY00148		Japan
JP08	SY00159		Japan
JP09	SY00369		Japan
JP10		Ayamurasaki	Japan
JP11		Hongyao 2	Japan
JP12		Hongyou	Japan
JP13		Japanese Black	Japan
JP14		Kokei 14	Japan
JP15		Okinawa 100	Japan
MA01	SY00089		Morocco
ML01	SY00091		Mali
MY01	SY00130		Malaysia
NG01	SY00219		Nigeria
PE01	SY00175		Peru
PE02	SY00183		Peru
PE03	SY00190		Peru
PE04	SY00283		Peru
PE05		Peru 1	Peru
PE06		Peru 384	Peru
PH01	SY00114		Philippines
PH02	SY00118		Philippines
TH01		Taizi 1506	Thailand
TZ01		Tanzania	Tanzania
US01	SY00001		United States
US02	SY00003		United States
US03	SY00004		United States
US04	SY00006		United States
US05	SY00014		United States
US06	SY00025		United States
US07	SY00277		United States

Table 6. The climatic data of Xuzhou city in 2020.

Month	Average Low Temperature (°C)	Average High Temperature (°C)	Total Rainfall (mm)
Apr	10 ± 4	21 ± 4	16
May	18 ± 3	27 ± 5	36
Jun	22 ± 2	30 ± 4	340
Jul	22 ± 2	29 ± 3	359
Aug	25 ± 2	32 ± 3	72
Sep	19 ± 2	29 ± 3	2
Oct	11 ± 4	20 ± 2	18

3.5. Measurement of Amylose Content

The apparent amylose content was determined using the absorption value of starch-iodine complex at 620 nm [24]. The true amylose content was measured using concanavalin A precipitation method through an Amylose/Amylopectin Assay Kit (K-AMYL, Megazyme, Bray, Ireland).

3.6. XRD Analysis of Starch

Starch was analyzed with an X-ray diffractometer (XRD) (D8, Bruker, Karlsruhe, Germany). Before analysis, the sample was moisturized for 1 week at 25 °C in a desiccator containing a saturated solution of NaCl with a relative humidity about 75%. The testing setting contained an X-ray beam at 200 mA and 40 kV and scanning range of diffraction angle from 2 θ 3 to 40° with a step size of 0.02°. The relative crystallinity (RC) was evaluated with the percentage of diffraction peak area to total diffraction area over the diffraction angle 2 θ 4 to 30° following the method of Wei et al. [40].

3.7. DSC Analysis of Starch

The 5 mg starch and 15 μ L water were mixed and sealed hermetically in an aluminum pan. After equilibrating for 2 h at room temperature, the sample was heated from 25 to 130 °C at 10 °C/min using a differential scanning calorimeter (DSC 200-F3, Netzsch, Selb, Germany).

3.8. Statistical Analysis

The statistical differences between data from varieties were detected using one-way analysis of variance (ANOVA) by Tukey's test using the SPSS 19.0 Statistical Software Program. The Pearson correlation analysis and hierarchical cluster analysis were also evaluated using SPSS 19.0 Statistical Software Program. Prior to the analysis, the normal distribution of structural property parameters was assessed using the Shapiro–Wilk test with SPSS 16.0. Only structural property parameters with their significances of normal distributions over 0.05 were used to evaluate the Pearson correlation and hierarchical cluster analysis.

4. Conclusions

Starches from 44 sweet potato varieties originating from 15 countries were investigated for their sizes, amylose contents, crystalline structures, and thermal properties. The D[4,3], AAC, TAC, and Δ AC (AAC–TAC) ranged from 8.01 to 15.30 μ m, from 19.2% to 29.2%, from 14.2% to 20.2%, and from 4.0% to 11.8% among the 44 starches, respectively. Starches had A-, C_A-, C_C-, and C_B-type with RC from 19.5% to 27.3%. One-, two-, and three-peak DSC curves were detected, and the T_o, T_p, T_c, and Δ T ranged from 52.2 to 73.8 °C, from 59.7 to 80.0 °C, from 75.3 to 86.9 °C, and from 13.1 to 29.2 °C among the 44 starches, respectively. Based on starch property parameters, the 44 sweet potato varieties were divided into different groups. This research offers references for the utilization of sweet potato germplasm resources.

Author Contributions: C.W. and Q.C. conceived the study and designed the experiments; Y.L., L.Z., L.S. and L.L. performed the experiments; Y.L. and L.Z. wrote the original draft manuscript; and C.W. reviewed and edited the manuscript. All authors discussed the contents of the manuscript and approved the submission. All authors have read and agreed to the published version of the manuscript.

Funding: This study was financially supported by grants from the National Key Research and Development Program of China (2018YFD1000705, 2018YFD1000700), Accurate Identification of Sweetpotato Excellent Germplasm Resources (19211139), and Priority Academic Program Development of Jiangsu Higher Education Institutions.

Institutional Review Board Statement: Not applicable.

Informed Consent Statement: Not applicable.

Data Availability Statement: The data are available upon request from the corresponding author.

Conflicts of Interest: The authors declare no conflict of interest.

Sample Availability: Samples of some starches are available from the corresponding author upon reasonable request.

References

1. FAOSTAT. Available online: <http://www.fao.org/faostat/en/#data> (accessed on 24 October 2021).
2. Guo, K.; Liu, T.; Xu, A.; Zhang, L.; Bian, X.; Wei, C. Structural and functional properties of starches from root tubers of white, yellow, and purple sweet potatoes. *Food Hydrocoll.* **2019**, *89*, 829–836. [CrossRef]
3. Moorthy, S.N.; Naskar, S.K.; Shanavas, S.; Radhika, G.S.; Mukherjee, A. Physicochemical characterization of selected sweet potato cultivars and their starches. *Int. J. Food Prop.* **2010**, *13*, 1280–1289. [CrossRef]
4. Song, H.G.; Choi, I.C.; Lee, J.S.; Chung, M.N.; Yoon, C.S.; Han, J. Comparative study on physicochemical properties of starch films prepared from five sweet potato (*Ipomoea batatas*) cultivars. *Int. J. Biol. Macromol.* **2021**, *189*, 758–767. [CrossRef] [PubMed]
5. Truong, V.D.; Avula, R.Y.; Pecota, K.V.; Yencho, G.C. Sweetpotato production, processing, and nutritional quality. In *Handbook of Vegetables and Vegetable Processing*; Siddiq, M., Uebersax, M.A., Eds.; John Wiley & Sons Ltd.: Hoboken, NJ, USA, 2018; pp. 811–838.
6. Emmambux, M.N.; Taylor, J.R.N. Morphology, physical, chemical, and functional properties of starches from cereals, legumes, and tubers cultivated in Africa: A review. *Starch* **2013**, *65*, 715–729. [CrossRef]
7. He, W.; Wei, C. Progress in C-type starches from different plant sources. *Food Hydrocoll.* **2017**, *73*, 162–175. [CrossRef]
8. Hoover, R. Composition, molecular structure, and physicochemical properties of tuber and root starches: A review. *Carbohydr. Polym.* **2001**, *45*, 253–267. [CrossRef]
9. Lindeboom, N.; Chang, P.R.; Tyler, R.T. Analytical, biochemical and physicochemical aspects of starch granule size, with emphasis on small granule starches: A review. *Starch* **2004**, *56*, 89–99. [CrossRef]
10. Wang, H.; Yang, Q.; Ferdinand, U.; Gong, X.; Qu, Y.; Gao, W.; Ivanistau, A.; Feng, B.; Liu, M. Isolation and characterization of starch from light yellow, orange, and purple sweet potatoes. *Int. J. Biol. Macromol.* **2020**, *160*, 660–668. [CrossRef]
11. Yang, Y.; Shi, D.; Wang, Y.; Zhang, L.; Chen, X.; Yang, X.; Xiong, H.; Bhattarai, G.; Ravelombola, W.; Olaoye, D.; et al. Transcript profiling for regulation of sweet potato skin color in Sushu8 and its mutant Zhengshu20. *Plant Physiol. Biochem.* **2020**, *148*, 1–9. [CrossRef]
12. Collado, L.S.; Mabesa, R.C.; Corke, H. Genetic variation in the physical properties of sweet potato starch. *J. Agric. Food Chem.* **1999**, *47*, 4195–5201. [CrossRef]
13. Kim, J.; Ren, C.; Shin, M. Physicochemical properties of starch isolated from eight different varieties of Korean sweet potatoes. *Starch* **2013**, *65*, 923–930. [CrossRef]
14. Zhu, F.; Xie, Q. Rheological and thermal properties in relation to molecular structure of New Zealand sweetpotato starch. *Food Hydrocoll.* **2018**, *83*, 165–172. [CrossRef]
15. Ahmed, S.; Ru, W.; Han, H.; Cheng, L.; Bian, X.; Li, G.; Jin, L.; Wu, P.; Bao, J. Fine molecular structure and its effects on physicochemical properties of starches in potatoes grown in two locations. *Food Hydrocoll.* **2019**, *97*, 105172. [CrossRef]
16. Genkina, N.K.; Noda, T.; Koltisheva, G.I.; Wasserman, L.A.; Tester, R.F.; Yuryev, V.P. Effects of growth temperature on some structural properties of crystalline lamellae in starches extracted from sweet potatoes (Sunnyred and Ayamurasaki). *Starch* **2003**, *55*, 350–357. [CrossRef]
17. Li, H.; Liu, Y. Effects of variety and growth location on the chain-length distribution of rice starches. *J. Cereal Sci.* **2019**, *85*, 77–83. [CrossRef]
18. Tappiban, P.; Sraphet, S.; Srisawad, N.; Wu, P.; Han, H.; Smith, D.R.; Bao, J.; Triwitayakorn, K. Effects of cassava variety and growth location on starch fine structure and physicochemical properties. *Food Hydrocoll.* **2020**, *108*, 106074. [CrossRef]
19. Waramboi, J.G.; Dennien, S.; Gidley, M.J.; Sopade, P.A. Characterisation of sweetpotato from Papua New Guinea and Australia: Physicochemical, pasting and gelatinisation properties. *Food Chem.* **2011**, *126*, 1759–1770. [CrossRef]
20. Zhang, L.; Zhao, L.; Bian, X.; Guo, K.; Zhou, L.; Wei, C. Characterization and comparative study of starches from seven purple sweet potatoes. *Food Hydrocoll.* **2018**, *80*, 168–176. [CrossRef]
21. Guo, K.; Bian, X.; Jia, Z.; Zhang, L.; Wei, C. Effects of nitrogen level on structural and functional properties of starches from different colored-fleshed root tubers of sweet potato. *Int. J. Biol. Macromol.* **2020**, *164*, 3235–3242. [CrossRef]
22. Jane, J.L.; Kasemsuwan, T.; Leas, S.; Zobel, H.; Robyt, J.F. Anthology of starch granule morphology by scanning electron microscopy. *Starch* **1994**, *46*, 121–129. [CrossRef]
23. Lin, L.; Zhang, Q.; Zhang, L.; Wei, C. Evaluation of the molecular structural parameters of normal rice starch and their relationships with its thermal and digestion properties. *Molecules* **2017**, *22*, 1526. [CrossRef]
24. Man, J.; Lin, L.; Wang, Z.; Wang, Y.; Liu, Q.; Wei, C. Different structures of heterogeneous starch granules from high-amylose rice. *J. Agric. Food Chem.* **2014**, *62*, 11254–11263. [CrossRef]
25. Richardson, P.H.; Jeffcoat, R.; Shi, Y.C. High-amylose starches: From biosynthesis to their use as food ingredients. *MRS Bull.* **2000**, *25*, 20–24. [CrossRef]
26. Zhong, Y.; Zhu, H.; Liang, W.; Li, X.; Liu, L.; Zhang, X.; Yue, H.; Xue, J.; Liu, X.; Guo, D. High-amylose starch as a new ingredient to balance nutrition and texture of food. *J. Cereal Sci.* **2018**, *81*, 8–14. [CrossRef]

27. Zheng, Y.; Wang, Q.; Li, B.; Lin, L.; Tundis, R.; Loizzo, M.R.; Zheng, B.; Xiao, J. Characterization and prebiotic effect of the resistant starch from purple sweet potato. *Molecules* **2016**, *21*, 932. [CrossRef]
28. Crofts, N.; Nakamura, Y.; Fujita, N. Critical and speculative review of the roles of multi-protein complexes in starch biosynthesis in cereals. *Plant Sci.* **2017**, *262*, 1–8. [CrossRef]
29. Huang, L.; Sreenivasulu, N.; Liu, Q. *Waxy* editing: Old meets new. *Trends Plant Sci.* **2020**, *25*, 963–966. [CrossRef]
30. Tian, Z.; Qian, Q.; Liu, Q.; Yan, M.; Liu, X.; Yan, C.; Liu, G.; Gao, Z.; Tang, S.; Zeng, D.; et al. Allelic diversities in rice starch biosynthesis lead to a diverse array of rice eating and cooking qualities. *Proc. Natl. Acad. Sci. USA* **2009**, *106*, 21760–21765. [CrossRef]
31. Cheetham, N.W.H.; Tao, L. Variation in crystalline type with amylose content in maize starch granules: An X-ray powder diffraction study. *Carbohydr. Polym.* **1998**, *36*, 277–284. [CrossRef]
32. Genkina, N.K.; Wasserman, L.A.; Noda, T.; Tester, R.F.; Yuryev, V.P. Effects of annealing on the polymorphic structure of starches from sweet potatoes (Ayamurasaki and Sunnyred cultivars) grown at various soil temperatures. *Carbohydr. Res.* **2004**, *339*, 1093–1098. [CrossRef]
33. Pérez, S.; Baldwin, P.M.; Gallant, D.J. Structural features of starch granules I. In *Starch: Chemistry and Technology*, 3rd ed.; BeMiller, J., Whistler, R., Eds.; Academic Press: San Diego, CA, USA, 2009; pp. 149–192.
34. Dhital, S.; Shrestha, A.K.; Hasjim, J.; Gidley, M.J. Physicochemical and structural properties of maize and potato starches as a function of granule size. *J. Agric. Food Chem.* **2011**, *59*, 10151–10161. [CrossRef] [PubMed]
35. Duan, W.; Zhang, H.; Xie, B.; Wang, B.; Zhang, L. Impacts of nitrogen fertilization rate on the root yield, starch yield and starch physicochemical properties of the sweet potato cultivar Jishu 25. *PLoS ONE* **2019**, *14*, e0221351. [CrossRef] [PubMed]
36. Lee, B.H.; Lee, Y.T. Physicochemical and structural properties of different colored sweet potato starches. *Starch* **2017**, *69*, 1600001. [CrossRef]
37. Osundahunsi, O.F.; Fagbemi, T.N.; Kesselman, E.; Shimoni, E. Comparison of the physicochemical properties and pasting characteristics of flour and starch from red and white sweet potato cultivars. *J. Agric. Food Chem.* **2003**, *51*, 2232–2236. [CrossRef]
38. Guo, K.; Zhang, L.; Bian, X.; Cao, Q.; Wei, C. A-, B- and C-type starch granules coexist in root tuber of sweet potato. *Food Hydrocoll.* **2020**, *98*, 105279. [CrossRef]
39. Shi, L.; Li, Y.; Lin, L.; Bian, X.; Wei, C. Effects of variety and growing location on physicochemical properties of starch from sweet potato root tuber. *Molecules* **2021**, *26*, 7137. [CrossRef]
40. Wei, C.; Qin, F.; Zhou, W.; Yu, H.; Xu, B.; Chen, C.; Zhu, L.; Wang, Y.; Gu, M.; Liu, Q. Granule structure and distribution of allomorphs in C-type high-amylose rice starch granule modified by antisense RNA inhibition of starch branching enzyme. *J. Agric. Food Chem.* **2010**, *58*, 11946–11954. [CrossRef]

Article

Influence of Gamma Irradiation on Different Phytochemical Constituents of Dried Rose Hip (*Rosa canina* L.) Fruits

Manol Ognyanov ^{1,*}, Petko Denev ¹, Desislava Teneva ¹, Yordan Georgiev ¹, Sabina Taneva ², Iskra Totseva ², Mariana Kamenova-Nacheva ³, Yana Nikolova ³ and Svetlana Momchilova ²

- ¹ Laboratory of Biologically Active Substances-Plovdiv, Institute of Organic Chemistry with Centre of Phytochemistry, Bulgarian Academy of Sciences, 139 Ruski Blvd., 4000 Plovdiv, Bulgaria; petkodenev@yahoo.com (P.D.); desislava.teneva@orgchm.bas.bg (D.T.); yordan.georgiev@orgchm.bas.bg (Y.G.)
- ² Laboratory of Lipid Chemistry, Institute of Organic Chemistry with Centre of Phytochemistry, Bulgarian Academy of Sciences, 9 Acad. Georgi Bonchev Str., 1113 Sofia, Bulgaria; sabina.taneva@orgchm.bas.bg (S.T.); iskra.totseva@orgchm.bas.bg (I.T.); svetlana.momchilova@orgchm.bas.bg (S.M.)
- ³ Laboratory of Organic Synthesis and Stereochemistry, Institute of Organic Chemistry with Centre of Phytochemistry, Bulgarian Academy of Sciences, 9 Acad. Georgi Bonchev Str., 1113 Sofia, Bulgaria; mariana.nacheva@orgchm.bas.bg (M.K.-N.); yana.nikolova@orgchm.bas.bg (Y.N.)
- * Correspondence: manol.ognyanov@orgchm.bas.bg; Tel.: +359-32642759

Abstract: Gamma irradiation is efficiently applied to many foods, but nevertheless there is a distinct lack of information about the changes of macro- and micronutrients (e.g., carbohydrates, lipids, organic acids, and phenolics) in dried rose hip (RH) fruits. Therefore, in this study, for the first time, the effect of gamma irradiation (10 and 25 kGy) on RH constituents is investigated. Different analytical techniques (GC-FID, HPLC-UV, HPSEC-RID, IR-FT, and SEM) are employed to examine this effect. The irradiation treatment (10 kGy) increased the glucose content by 30% and released cellobiose from RH fruits, thus revealing cellulose destruction. The extractability of total uronic acids increased from 51% (control) to 70.5% (25 kGy-irradiated), resulting in a higher pectin yield (10.8% < 12.8% < 13.4%) and molecular heterogeneity. Moreover, de-esterification was not a major effect of the irradiation-induced degradation of pectin. The sample exposure to the highest dose did not change the content of total carotenoids, β -carotene, and (un)saturated fatty acids, but it affected the tocopherols levels. Gamma rays had a negligible effect on the phenolic constituents and did not affect ORAC and HORAC antioxidant activity. In conclusion, it can be compromised that the exposition of dried RH is safe and can be successfully applied to decontaminate fruits without affecting their nutritional value and biological activity.

Keywords: gamma irradiation; rose hip; seed oil; polysaccharides; carbohydrates; lipids

Citation: Ognyanov, M.; Denev, P.; Teneva, D.; Georgiev, Y.; Taneva, S.; Totseva, I.; Kamenova-Nacheva, M.; Nikolova, Y.; Momchilova, S. Influence of Gamma Irradiation on Different Phytochemical Constituents of Dried Rose Hip (*Rosa canina* L.) Fruits. *Molecules* **2022**, *27*, 1765. <https://doi.org/10.3390/molecules27061765>

Academic Editor: Mirella Nardini

Received: 9 February 2022

Accepted: 7 March 2022

Published: 8 March 2022

Publisher's Note: MDPI stays neutral with regard to jurisdictional claims in published maps and institutional affiliations.



Copyright: © 2022 by the authors. Licensee MDPI, Basel, Switzerland. This article is an open access article distributed under the terms and conditions of the Creative Commons Attribution (CC BY) license (<https://creativecommons.org/licenses/by/4.0/>).

1. Introduction

The irradiation of foodstuffs with gamma rays was developed as a technology in the second half of the 20th century, and is nowadays among the most widely used approaches for microbial decontamination and the shelf-life extension of foods [1,2]. It is considered a safe, efficient, environmentally friendly, and energy-efficient method, and is particularly important in industrial food decontamination [3]. Preventing microbial spoilage by irradiating dried foods, such as fruits, herbs, spices, and nuts, at doses of 3–10 kGy is an important alternative to fumigation with microbicidal gases, however, doses above 20 kGy have also been used to reduce the microbial population in dry foods [4,5]. Along with the benefits of gamma ray treatment, adverse effects associated with changes in the chemical composition of irradiated foods can be expected. It is known, for example, that irradiation could have a negative effect on the structure of fatty acids in nuts or to affect the anthocyanin and

polyphenol content of fresh fruits, such as pomegranates [6,7]. Due to conflicting results, scientists are still looking for fresh evidence to accept or reject the hypothesis about the positive or negative influence of irradiation on foods. Moreover, due to a great variety of foods with specific chemical compositions, each food must be examined individually.

Rose hip (RH) fruits (*Rosa canina* L.) are mainly used for producing jams, jellies, marmalades, tea, soups, food additives, and functional ingredients [8,9]. Although fresh RH fruits having the highest nutrient quality are particularly suitable for the production of various functional foods and food supplements, they are most often stored, transported, sold, and processed in a dried form. Some fruits' characteristics appeared interesting enough to require a more detailed study of their changes after irradiation. Many studies, for example, provide empirical evidence to prove that RH is a rich source of vitamins, lipids, phenolic antioxidants, macro- and micro-elements, and polysaccharides (PSs) [8–11]. Moreover, because of their well-known beneficial health properties, the RH fruits are also used as the main ingredient in fruit teas [12]. In spite of this, to the best of our knowledge, studies on the effect of gamma irradiation on the changes in the chemical composition of dried RH have not been found.

Therefore, the present study aims to investigate the effects of gamma irradiation on the changes in the levels of different macro- and micronutrient constituents of dried RH fruits.

2. Results

2.1. Influence of Gamma Irradiation on Sugar and Organic Acid Composition

The changes in the content of free sugars in dried RH fruits caused by gamma irradiation are shown in Figure 1. It can be seen that glucose (53%) was the major sugar in non-irradiated fruits. Together with fructose (33%), it occupied more than 80% of the total free sugars, whereas galactose and xylose were very minor constituents. Surprisingly, the glucose content increased substantially by 30% ($p < 0.05$) with increasing the irradiation dosage, while the quantity of the other sugars seemed to be mainly unaffected by irradiation. It is interesting to note that this effect was particularly noticeable at a lower dose (10 kGy), and a further increase in the dose (25 kGy) did not have any considerable influence on the quantity of the glucose. Despite this, the irradiation influenced the pattern of sugar accumulation. One of the most interesting observations was that cellobiose was found in 10 kGy- and 25 kGy-irradiated fruits. The presence of cellobiose combined with an additionally liberated glucose amount presented a clear sign that a higher dose could inflict damage on the cellulose fibers that constituted the primary cell walls of plants. Additionally, the quantity of non-reducing sucrose was found to increase when RH fruits were irradiated (≥ 10 kGy). It was scarcely possible that a part of the starch/cellulose was converted into sucrose and glucose by affecting the carbohydrate-active enzymes.

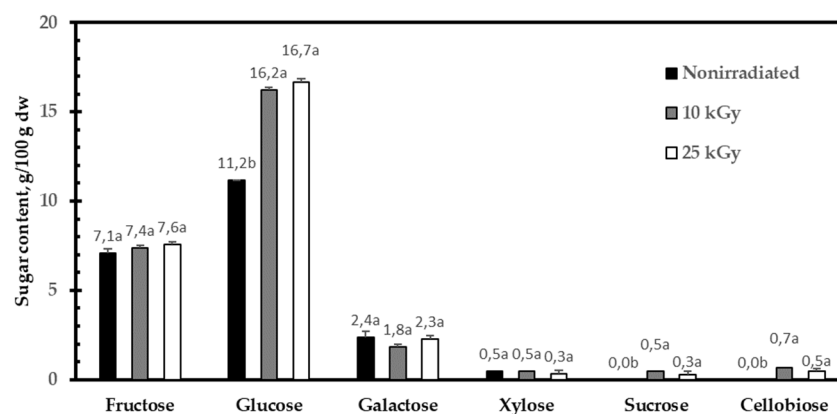


Figure 1. Sugar composition of non-irradiated, 10 kGy-, and 25 kGy-irradiated RH fruits. Different letters denote statistically different values, $p < 0.05$; dw—dry weight.

Further, the effect of gamma irradiation on the organic acid profile was examined (Table 1). It should be mentioned that organic acids are a very important component of foods, which have a part to play in determining the taste of foods. As can be seen, citric acid, a member of the Krebs cycle, was predominantly present (2768 mg/100 g), because it occupied 55% of the total organic acids. Non-irradiated RH fruits also contained quinic acid (1344 mg/100 g) and ascorbic acid (624 mg/100 g) in smaller amounts, but, nevertheless, they accounted for almost 40% of the total organic acids content. From the data in Table 1, it is apparent that the exposition of fruits to gamma radiation has a minor or no effect on quinic, malic, and ascorbic acid content. It is evident that citric, α -ketoglutaric, and succinic acids increase in quantity. The increasing levels of these acids suggested a stimulation of respiration through the citric acid cycle, if we assume the presence of viable cells. However, the latter statement looked highly unlikely because the cell's/tissue's metabolism could be dramatically slowed down by moisture loss during freeze-drying (<10%). Thus, it is not wrong to assume that the cell walls and/or even (non)membrane-bound cell organelles (such as vacuole and mitochondrion) suffered extensive damage by irradiation, thus making small molecules more easily extractable. Further, the level of tartaric acid, a product of the oxidation of sugars, decreased slightly, but it was statistically significant at the highest level of radiation (25 kGy). An important point brought to mind is that organic acids and, above all, tartaric acid, have closely related metabolism to ascorbic acid [13]. It is possible that the level of tartaric acid was reduced in an attempt to compensate for the loss of ascorbic acid whose amount did not change significantly.

Table 1. Organic acid composition of non-irradiated, 10 kGy- and 25 kGy-irradiated RH fruits (mg/100 g dw).

Organic Acid	Non-Irradiated	10 kGy	25 kGy
Quinic acid	1344.7 ± 187.5 ^{ab *}	1568.0 ± 48.4 ^a	1376.8 ± 81.0 ^b
Malic acid	111.8 ± 6.4 ^b	133.0 ± 3.1 ^a	118.7 ± 9.2 ^b
Ascorbic acid	623.5 ± 13.6 ^a	646.0 ± 12.2 ^a	654.1 ± 19.0 ^a
Citric acid	2768.7 ± 196.6 ^b	3299.9 ± 55.8 ^a	3536.7 ± 303.5 ^a
α -Ketoglutaric acid	<50 ^b	75.8 ± 5.1 ^a	71.5 ± 5.2 ^a
Succinic acid	70.8 ± 1.6 ^b	79.9 ± 10.4 ^b	107.6 ± 7.3 ^a
Tartaric acid	49.2 ± 4.9 ^a	50.7 ± 1.2 ^a	34.2 ± 1.8 ^b

* Different letters within each row indicate statistically different values ($p < 0.05$).

2.2. Influence of Gamma Irradiation on the Lipid Composition of Seed Oil

The results of the lipid composition of RH seed oil are presented in Table 2. Our experiment indicated that the yield of oil did not change considerably with irradiation (6.3–6.5%). Further, it can be seen that palmitic acid (16:0; 3.7%) and stearic acid (18:0; 2.2%) were the most abundant saturated fatty acids in the oil of non-irradiated RH fruits. Considering unsaturated fatty acid composition, seed oil was characterized by a high degree of unsaturation. Linoleic acid (18:2; 55%) represented the major polyunsaturated fatty acid constituent, followed by α -linolenic (18:3; 21%) and oleic acid (16:1; 16%). Despite this fact, it seemed that irradiation did not cause any significant changes in the fatty acid composition (Table 2), even though the sample was exposed to the highest dose (25 kGy). Considering the carotenoids, it was evident that neither the 10 kGy nor 25 kGy doses had any negative influence on β -carotene and, in general, on the total carotenoid content. It is worth mentioning that the total carotenoid content did not change significantly not only in seed oil, but also in fruit flesh (about 820 mg/kg) when the irradiation doses increased (Table 2). Our findings were in line with those of an earlier study that demonstrated that a 10 kGy irradiation of RH tea did not cause any change in the carotenoid content [14]. Further, one of the most interesting findings was that there was a noticeable difference in the amounts of α - and γ -tocopherol as a result of irradiation ($p < 0.05$) (Table 2). It is well known that tocopherols (vitamin E) are powerful antioxidants able to scavenge free

radicals. It may be that the tocopherols were reduced because of their active participation in the neutralization of free radicals.

Table 2. Yield and lipid composition of seed oil extracted from non-irradiated, 10 kGy-, and 25 kGy-irradiated RH fruits.

	Non-Irradiated	10 kGy	25 kGy
Yield, w/w%	6.3 ± 0.1 ^{a *}	6.5 ± 0.6 ^a	6.4 ± 0.8 ^a
Saturated fatty acids (rel. %)			
Palmitic acid (16:0)	3.7 ± 0.1 ^a	3.6 ± 0.1 ^a	3.7 ± 0.1 ^a
Stearic acid (18:0)	2.2 ± 0.0 ^a	2.2 ± 0.0 ^a	2.2 ± 0.0 ^a
Arachidic acid (20:0)	0.9 ± 0.1 ^a	0.9 ± 0.1 ^a	0.9 ± 0.1 ^a
Behenic acid (22:0)	0.1 ± 0.0 ^a	0.1 ± 0.0 ^a	0.1 ± 0.0 ^a
Unsaturated fatty acids (rel. %)			
Palmitoleic acid (16:1)	0.2 ± 0.0 ^a	0.2 ± 0.0 ^a	0.2 ± 0.0 ^a
Oleic acid (18:1)	16.1 ± 0.5 ^a	16.5 ± 0.6 ^a	16.4 ± 0.5 ^a
<i>cis</i> -Vaccenic acid (18:1)	0.5 ± 0.0 ^a	0.5 ± 0.0 ^a	0.5 ± 0.0 ^a
Linoleic acid (18:2)	54.8 ± 1.2 ^a	54.4 ± 1.3 ^a	54.6 ± 1.5 ^a
α -Linolenic acid (18:3)	21.1 ± 0.8 ^a	21.3 ± 0.9 ^a	21.0 ± 1.0 ^a
Gondoic acid (20:1)	0.4 ± 0.0 ^a	0.4 ± 0.0 ^a	0.4 ± 0.0 ^a
Total carotenoids (mg/kg)	365 ± 12 (816 ± 30) ^{a **}	336 ± 35 (818 ± 26) ^a	350 ± 10 (825 ± 30) ^a
β -Carotene (mg/kg)	105 ± 7 ^a	110 ± 13 ^a	115 ± 11 ^a
α -Tocopherol (mg/kg)	364 ± 28 ^a	295 ± 5 ^b	272 ± 1 ^c
γ -Tocopherol (mg/kg)	1042 ± 16 ^a	937 ± 17 ^{ab}	914 ± 9 ^b
Acid value (mg KOH/g)	1.3 ± 0.0 ^b	1.3 ± 0.0 ^b	1.7 ± 0.0 ^a
conj. Dienes (A ₂₃₂ , 1%)	2.4 ± 0.1 ^c	3.0 ± 0.1 ^b	4.3 ± 0.8 ^a
conj. Trienes (A ₂₆₈ , 1%)	0.6 ± 0.0 ^b	0.6 ± 0.0 ^b	0.8 ± 0.0 ^a

* in each row, no statistically significant changes are observed for the yield and each fatty acid. For the other components, different letters within each row denote statistically significant differences between the values ($p < 0.05$); ** Values in brackets represent the total carotenoid content of RH fruit flesh.

In addition, important parameters, such as the acid value, amounts of conjugated dienes, and trienes, were determined. These parameters are reliable indicators of the degree of lipid oxidation. The results obtained are also summarized in Table 2. Our findings indicated that the conjugated trienes, and especially dienes, were slightly influenced by a higher dose (25 kGy). The results obtained are broadly in line with the expectations, because unsaturated fatty acids comprised 93% of the total fatty acid content. In general, a higher amount of unsaturated fatty acids suggested a higher instability of oil due to oxidation. Therefore, the determination of the induction period of auto-oxidation of RH oil has a more practical significance when the degree of oxidation stability should be evaluated (Figure 2). It represents the time interval during which the antioxidants present in the sample still effectively inhibit the auto-oxidation processes in the oil, and the rate of formation and accumulation of hydroperoxides still does not increase exponentially. As illustrated in Figure 2, it seems that gamma irradiation (<25 kGy) does not significantly change the oxidative stability of RH seed oil because of the presence of antioxidants.

2.3. Influence of Gamma Irradiation on the Phenolic Constituents and Antioxidant Activity

The content of the total phenolics and in vitro antioxidant activity of non-irradiated, 10 kGy-, and 25 kGy-irradiated RH fruits was investigated. Together with the quantitative data for the phenolic components, they are included in Table 3.

In general, gamma irradiation had a negligible effect on the content of the phenolic compounds and their profile. As it is evident from the results, the total polyphenol content shows a trend towards increase, however without reaching significant differences ($p < 0.05$). The only significant difference was observed in the quercetin content, which increased from 13.9 mg/100 g to 18.9 mg/100 g, and 18.3 mg/100 g for fruits irradiated with 10 kGy and 25 kGy, respectively ($p < 0.05$). On the other hand, the detected amounts of quercetin-3-*O*-glucoside and rutin decreased dose-dependently after irradiation ($p > 0.05$), which explained the increase in quercetin content and could be attributed to the cleavage of

glycosidic bonds from the high-energy electromagnetic radiation [15]. Gamma irradiation showed no effect on the amounts of chlorogenic acid, catechin, and epicatechin in RH fruits. Even though quercetin is a stronger radical scavenger than its glycosides, the antioxidant activity measured by the ORAC and HORAC assays did not change as a result of the treatment.

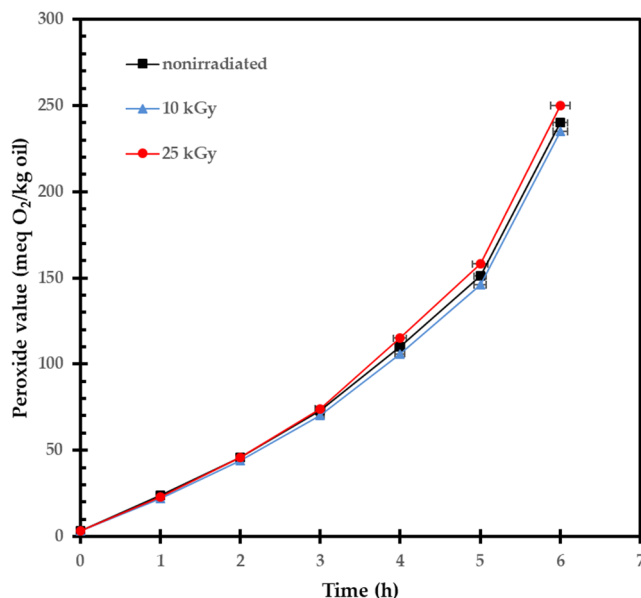


Figure 2. Induction periods of RH seed oils extracted from non-irradiated, 10 kGy-, and 25 kGy-irradiated RH fruits.

Table 3. Phenolic constituents and in vitro antioxidant activity of non-irradiated, 10 kGy-, and 25 kGy-irradiated RH fruits.

		Non-Irradiated	10 kGy	25 kGy
Total phenolics, mg GAE/100 g dw		13,148 ± 775 ^{a *}	13,840 ± 625 ^a	13,677 ± 646 ^a
Phenolic constituents, mg/100 g dw	Chlorogenic acid	139.7 ± 2.9 ^a	129.9 ± 2.7 ^a	128.8 ± 1.9 ^b
	Quercetin	13.9 ± 0.6 ^b	18.9 ± 0.8 ^a	18.3 ± 0.3 ^a
	Quercetin 3-O-β-D-glucopyranoside	68.2 ± 0.6 ^a	67.0 ± 2.6 ^{ab}	63.9 ± 0.5 ^b
	Rutin	355.7 ± 2.8 ^a	350.7 ± 4.9 ^{ab}	347.1 ± 2.7 ^b
	Catechin	645.4 ± 21.7 ^a	633.3 ± 23.1 ^a	661.6 ± 9.2 ^a
	Epicatechin	425.2 ± 5.8 ^a	426.1 ± 15.1 ^a	429.1 ± 1.5 ^a
Antioxidant activity	ORAC (μmol TE/g)	3890 ± 282 ^a	3862 ± 198 ^a	3899 ± 208 ^a
	HORAC (μmol GAE/g)	593 ± 68 ^a	573 ± 55 ^a	599 ± 50 ^a

* Different letters within each row denote the statistically significant differences between values ($p < 0.05$); ORAC—oxygen radical absorbance capacity; TE—Trolox equivalents; HORAC—hydroxyl radical averting capacity; and GAE—gallic acid equivalents.

2.4. Influence of Gamma Irradiation on Polysaccharide Constituents

We were very interested in knowing more about the potential changes in different PSs because they are the most important plant cell wall constituents. The results of different analyses are summarized in Table 4. From the table, it is evident that the yield of alcohol-insoluble solids (AISs) decreases with increasing the radiation dose ($0 > 10 > 25$ kGy). Accordingly, this means having a higher proportion of alcohol-soluble small molecules as a result of irradiation ($0 < 10 < 25$ kGy). These results provide us with the next clear evidence to support our assertion about the damage of plant cell wall constituents during irradiation. These cell wall changes should facilitate the extraction of initially present

or additionally formed (as a result of irradiation) low molecular weight alcohol-soluble compounds (such as sugars and oligomers). It is interesting to mention that the yield of PS also increased significantly when RH fruits were exposed to higher doses of radiation: non-irradiated—10.8%, 10 kGy—12.8%, and 25 kGy—13.4%. These results suggest that some cell wall constituents are adversely affected by irradiation, thus directly contributing to the additional release of PS populations. The latter results are very closely related to the finding of a considerable percentage of uronic acids extracted from the fruits as a result of irradiation (Table 4; control—51% and 25 kGy—71%). It is well known that uronic acids are major constituents of pectic PSs and, together with hemicelluloses, mainly comprise the primary cell walls of plants. Table 4 shows that the 10 kGy- and 25 kGy-irradiation does not exert any changes in the amount of the total uronic acid in the initial RH fruits (9.5–10.5%). At first sight, it can be interpreted to mean a ‘lack of changes in pectin’. The PSs obtained were characterized as typical high-methyl-ester pectins having a uronic acid content in the range between 49 and 53%. Surprisingly, it seemed that the degree of methyl-esterification was not affected by radiation (Table 4; 69–70 mol%), strongly suggesting that de-esterification is not a major effect of the irradiation-induced degradation of pectic PS. However, the degree of acetylation tended to be increased with increasing the irradiation dose. It may be that PS fractions carrying a higher number of acetyl groups were additionally released as a result of irradiation. Further, it could be observed that irradiation exerted a profound influence on cellulose that led to a reduction in its amount (Table 4). This was a key finding, which directly confirmed our above-mentioned statement about cellulose destruction. It could be argued that a minor part of the cellulose skeleton was broken down into cellobiose, low-molecular-weight cello-dextrins, or other oligomers (alcohol soluble), thus causing a reduction in the cellulose level and a rise in the yield of alcohol-soluble solids. Taken together, the above results suggest that a part of the pectin was trapped in the (hemi)cellulose network, and by degrading a part of the cellulose segments, additional pectic PSs were released leading to a rise in the yield of PSs. An interaction between pectin and cellulose was demonstrated in a previous study [16]. In fact, it should not rule out the possibility that the gamma radiation caused a direct degradative action on the pectin, in addition to that of cellulose.

Table 4. Yield and chemical characteristics of alcohol-insoluble solids, initial RH fruits, and polysaccharides (*w/w%*).

	Characteristic Parameter	Non-Irradiated	10 kGy	25 kGy
Alcohol-insoluble solids	Yield	44.1 ± 0.2 ^{a *}	42.5 ± 0.3 ^b	40.6 ± 0.2 ^c
Initial RH fruits	Uronic acids	10.5 ± 0.5 ^a	9.5 ± 0.5 ^a	10.1 ± 0.2 ^a
	% of total uronic acids extracted	51.0	63.4	70.5
	Cellulose	7.0 ± 0.1 ^a	6.0 ± 0.2 ^b	5.7 ± 0.0 ^c
	Crude protein (N×6.25)	1.7	-	-
Polysaccharides	Yield	10.8 ± 0.2 ^c	12.8 ± 0.1 ^b	13.4 ± 0.3 ^a
	Uronic acids	49.5 ± 1.5 ^b	47.5 ± 1.0 ^b	53.1 ± 0.6 ^a
	Degree of methyl-esterification **	69.6 ± 0.5 ^a	70.5 ± 1.0 ^a	70.1 ± 0.7 ^a
	Degree of acetylation ** (Acetyl content)	10.5 ± 0.5 ^b (1.3)	13.0 ± 0.2 ^a (1.5)	13.3 ± 0.3 ^a (1.7)
	Protein	1.7 ± 0.2 ^a	1.6 ± 0.0 ^a	1.7 ± 0.1 ^a

* Different letters in each row denote the statistically significant difference between values ($p < 0.05$); ** moles methanol or acetyl per 100 moles of uronic acids (mol%).

2.4.1. Influence of Gamma Irradiation on Monosaccharide Composition

Table 5 shows the results of the monosaccharide composition analysis of non- and 25 kGy-irradiated PSs fraction. It can be seen that commonly reported pectic monosaccharides constitute the PS fractions. The PS isolated from non-irradiated fruits was composed

mostly of galacturonic acid, glucose, and rhamnose. Other monosaccharides, such as galactose and arabinose, were present in lower amounts. Irradiation did not have a considerable influence on different sugar constituents. It appears that gamma-irradiation contributes only to the reduction in the glucose content, whereas that of fucose is raised, possibly due to changes in the extractability of PSs and plant cell walls.

Table 5. Monosaccharide composition of the polysaccharides isolated from non-irradiated and 25 kGy-irradiated RH fruits (mol%).

Monosaccharide	Non-Irradiated	25 kGy
Neutral sugars		
Rhamnose	7.1 ± 1.0 ^{a *}	8.8 ± 0.8 ^a
Arabinose	9.6 ± 1.0 ^a	11.0 ± 1.2 ^a
Galactose	6.5 ± 0.7 ^a	5.7 ± 1.0 ^a
Glucose	11.2 ± 1.3 ^a	7.5 ± 0.4 ^b
Mannose	0.1 ± 0.0 ^a	0.0 ± 0.0 ^a
Fucose	1.5 ± 0.6 ^b	4.2 ± 1.0 ^a
Uronic acids		
Galacturonic acid	56.5 ± 1.5 ^a	58.8 ± 0.5 ^a
Glucuronic acid	7.4 ± 0.4 ^a	3.9 ± 1.2 ^b

* Different letters in each row denote the statistically significant difference between values ($p < 0.05$).

2.4.2. Influence of Gamma Irradiation on Molecular Weight Distribution

The molecular weight distribution pattern of the isolated PSs fraction is shown in Figure 3A. It can be seen that the PS fraction, isolated from non-irradiated fruits, consists mainly of two high molecular weight populations covering the range between 78.8×10^4 and 21.2×10^4 g/mol (Figure 3A solid line). Moreover, the main peak is accompanied by a pronounced tailing suggesting that heterogeneity exists within the sample. It ranges between 21.2×10^4 and 4.73×10^4 g/mol. What is immediately striking, from a close inspection of Figure 3A, is that irradiation causes the PS molecular weight elution pattern to change visibly. A 10 kGy-irradiation leads to a decrease in the main peak intensity (78.8×10^4 g/mol), suggesting that part of the high molecular weight populations is converted into lower molecular weight compounds (Figure 3A dash line). As a consequence, the increase in the area representing medium and low molecular weight fractions is found (RT > 7.1 min). Interestingly, this negative effect on the PSs became stronger when the sample was exposed to the highest dose (25 kGy), and thus resulted in an even greater increase in the area representing lower molecular weights. More specifically, it is easy to be observed that, if we integrate the chromatograms (Figure 3A), the high molecular weight populations (RT 5.5–7.0 min) occupied a smaller percentage of the total (100%) peak area, hence a smaller percentage of PSs, when the irradiation dose increased: 0–60%, 10 kGy—48%, 25 kGy—40%. Accordingly, the percentage of lower molecular weight populations (RT 7.0–11.6 min) that comprised the PSs jumped: 0–40%, 10 kGy—52%, 25 kGy—60%.

To receive more information about the structural features of PSs, an *endo*-polygalacturonase (*endo*-PG) hydrolysis of the PS fraction was performed. It is a well-known fact that *endo*-PG can cleave α -1,4 glycosidic bonds between two non-esterified galacturonic acid units in the homogalacturonan (HG) region of pectin [17]. Figure 3B illustrates the elution pattern of *endo*-PG-treated samples. It can be observed that the *endo*-PG carried out the conversion of the part of the high molecular weight material into a broad range of lower molecular weight compounds. As a result, the change of the elution profile was observed by comparison with the non-enzyme-treated PS (Figure 3A solid line). This presented a reasonable reason to suppose that the HG region of pectin was adversely affected by gamma irradiation. A surprising finding of this study was that the PSs, isolated from 10 kGy- and 25 kGy-irradiated fruits, were degraded by *endo*-PG more efficiently than those isolated from the non-irradiated control. This led to an additional increase in the

peak area and shift in the retention time reflecting the accumulation of a large number of lower molecular weight compounds (Figure 3B dash and dot line).

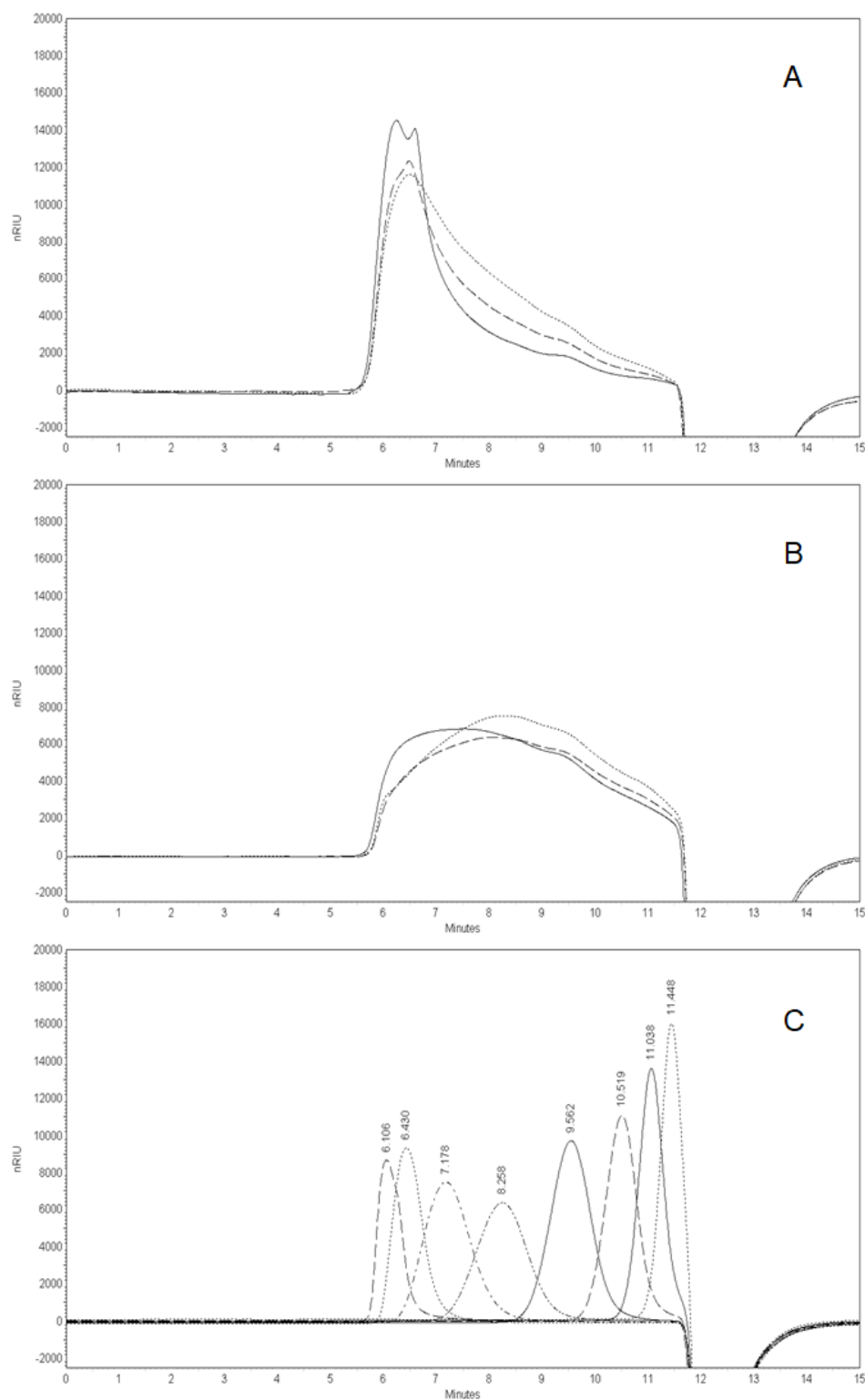


Figure 3. High-performance size-exclusion chromatography (HPSEC) elution pattern of PSs isolated from non-irradiated, 10 kGy-, and 25 kGy-irradiated RH fruits as: (A) initial PSs; (B) *endo*-PG-degraded PSs (solid—non-irradiated; dash—10 kGy; dot—25 kGy); and (C) Pullulan standards ($0.59\text{--}78.8 \times 10^4$ g/mol) were used to estimate the molecular weights.

These results could be expressed in numerical data, if we integrate the chromatograms (Figure 3B). It was precisely calculated that the percentage of the total peak area ascribed to high molecular weight compounds (RT 5.5–7.0 min) decreased by 7%: 0–23%, 10 kGy—18%, 25 kGy—16%. Accordingly, the area percentage of lower molecular weight populations (RT 7.0–11.6 min) increased by 7%: 0–77%, 10 kGy—82%, 25 kGy—84%.

This finding can be interpreted in different ways. On the one hand, it is known that *endo*-PG requires a sequence of 2–3 unesterified galacturonic acid units to cleave them [17]. However, keeping in mind that the irradiation did not cause any appreciable effect on the degree of methyl-esterification (Table 5), we can suppose a difference between the esterification pattern of the PSs. On the other hand, it may be that lower molecular weight HG segments were a better substrate for *endo*-PG action.

2.4.3. Fourier Transformed Infrared (FT-IR) Spectroscopy

The FT-IR spectra of the studied PSs are presented in Figure 4. FT-IR can identify the presence of specific functional groups prevailing in the sample. The typical bands for pectic PSs were found [18]. The broadened band that occurs in the region ranging from 3730 to 3100 cm^{-1} was assigned to the $\nu(\text{OH})$ stretching vibrations of free hydroxyl groups involved in intra- and intermolecular H-bonding. The band at 2940–2960 cm^{-1} was attributed to the $\nu(\text{CH})$ stretching of CH_2 groups. The presence of a well-separated sharp signal that appears at 1745–1735 cm^{-1} was typical for the $\text{C}=\text{O}$ stretching vibration of methyl-esterified carbonyl groups of pectic PSs ($\nu_{(\text{C}=\text{O})\text{COOH}}$). The bands at 1630 and 1438 cm^{-1} , together with that at 1440 cm^{-1} , were due to the asymmetric $\nu_{\text{as}}(\text{O}=\text{CO}-)$ and symmetric $\nu_{\text{s}}(\text{O}=\text{CO}-)$ stretching vibrations of the non- and esterified carboxyl groups, respectively. The signals at 1523–1525 cm^{-1} could originate from the aromatic ring vibrations of residual co-extracted phenolics in PSs because their protein content was low (Table 4). The presence of a band at 1238 cm^{-1} corresponded to $-\text{C}-\text{O}$ stretching of the acetyl residue, which was consistent with a higher value of the degree of acetylation (Table 4). In addition, bands at 1145 cm^{-1} , 1101 cm^{-1} , and 1018 cm^{-1} could be interpreted with the glycosidic bond vibrations involving $\nu(\text{C}-\text{OC})$, $-\nu(\text{CC})(\text{CO})$, and $-\delta(\text{O}=\text{C}-\text{H})$ bending in the pyranose ring. The $\text{C}1-\text{OH}$ vibrations of the monosaccharide ring at 831 cm^{-1} showed the presence of α -anomeric configuration, which is typical for galacturonic acid in pectins.

It was apparent that the characteristic infrared bands neither disappeared from the spectra nor appeared new ones. At first sight, according to these spectra, there was no reason to suppose that gamma irradiation caused a negative effect on the chemical composition of pectic PS. It is possible for the changes to have been minor, as they could not be seen in the spectra. However, an increase in the band intensities suggested some changes in the amorphous state of PSs, as demonstrated for starch.

2.5. Scanning Electron Microscopy (SEM) of the Fruit Material

If the gamma irradiation of the fruits caused severe damage to the components of the plant cell walls and tissues, they would be reflected in a change in the surface morphology of the plant material. Therefore, we examined the surface and internal parts of non-irradiated and 25 kGy-irradiated RH fruit material. Figure 5 shows the generated images of the internal and external parts of the fruits. No characteristic changes in the morphology of the surface (exocarp) of the irradiated sample were observed, despite the fact that a very large part of the surface was carefully inspected (Figure 5A,B). However, the examination of the internal part (mesocarp) of the 25 kGy-irradiated fruits revealed that the inner walls became less thick, and the cavities were enlarged (Figure 5C,D). Nevertheless, a more precise histochemical test must be performed to help confirm the latter statement.

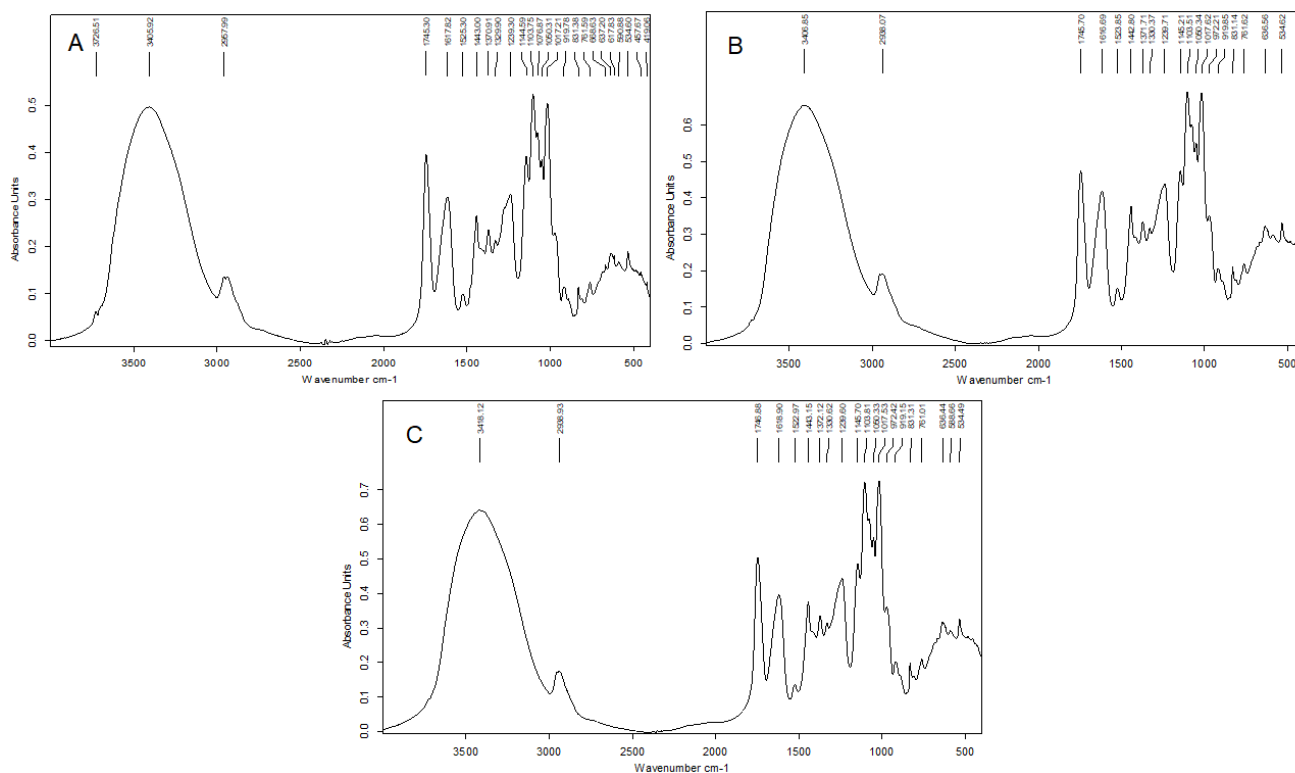


Figure 4. FT-IR spectra of the PSs isolated from non-irradiated (A), 10 kGy- (B), and 25 kGy-irradiated (C) RH fruits.

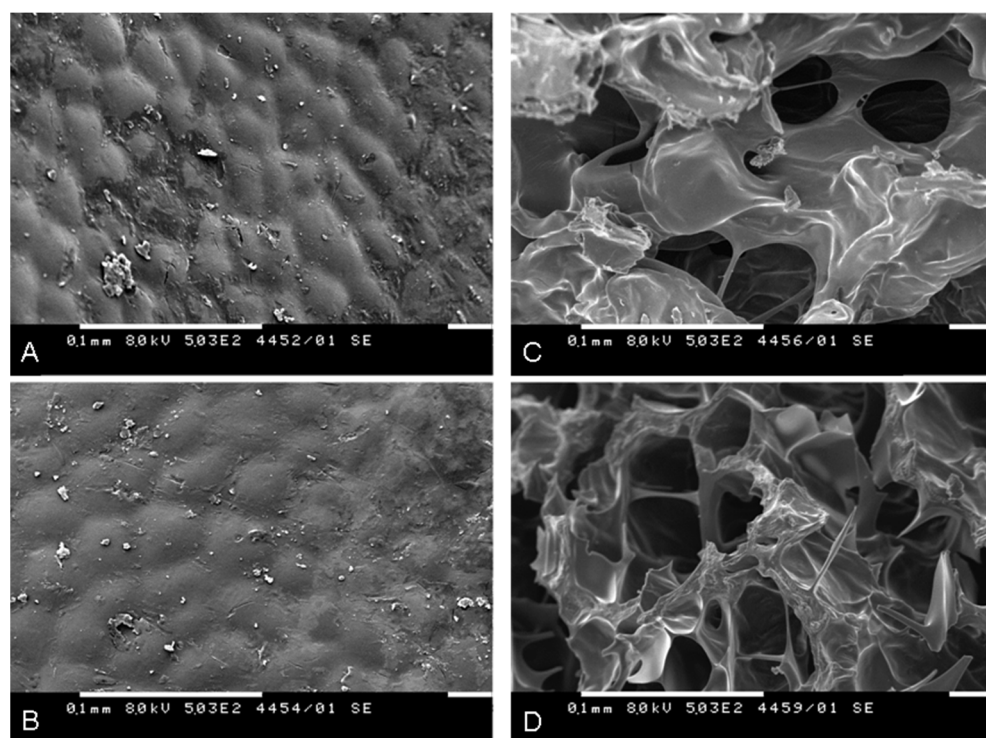


Figure 5. SEM images of the surface of non-irradiated (A) and 25 kGy-irradiated (B) RH fruit, and the internal part of non-irradiated (C) and 25 kGy-irradiated (D) RH fruit (8 kV, 0.1 mm, 500 \times).

3. Discussion

In general, gamma irradiation is a low-cost technology for the sterilization and decontamination of foods. However, together with the positive results, irradiation brings about a negative impact on the nutritional and functional properties of the foods. This effect is strongly determined by the received irradiation dose [3]. The quality of food depends upon the chemical composition (for instance, water, lipids, proteins, and PSs), and thus the changes in the level of constituents have an immediate impact on them. Therefore, in the current study, RH was investigated in detail to determine whether the gamma-irradiation processing contributed to the changes in the phytochemical constituents of the fruits.

3.1. Influence of Gamma Irradiation on Carbohydrate Constituents

Our research findings indicated that the carbohydrate constituents of RH fruits were among the most seriously affected by irradiation. Irradiation contributed to an increase in the reducing sugars content (mainly glucose), which can be ascribed to the structural breakdown of cellulose and, to a lesser extent, starch. A similar effect of gamma radiation on reducing the sugar content was observed in a previous study on the irradiation of dates [19]. According to these authors, irradiation (0.9–1.8 kGy) contributed to a high level of glucose, but it could not bring about a significant change in the fructose content. Moreover, scientists highlighted the fact that the decrease in starch content is paralleled by an increase in the glucose amount [19]. Our results on cellulose and glucose content follow a similar pattern. It is useful to recall that cellulose is a glucose-containing polymer organized into stable microfibrils with crystalline and amorphous regions. Cellulose meshes into a cell wall polymer matrix together with pectin, lignin, and hemicellulose. More importantly, cellulose fibers play a crucial role, mainly in maintaining the strong mechanical resistance of plants [20]. Therefore, it can be safely predicted that irradiation (≥ 10 kGy) leads to a change in the mechanical properties of dried RH fruits. It is interesting to speculate whether the strength of this effect can be increased after the pectic backbone also suffers serious damage as a result of irradiation. Pectin is an amorphous heteropolysaccharide found in the middle lamella, which is composed of the HG, rhamnogalacturonan-I, and rhamnogalacturonan-II regions. HG is the main pectic structural fragment that only consists of an unbranched chain of α -1,4-linked galacturonic acid units. These residues can be methyl-esterified and/or acetyl-esterified. Our results strongly suggest that RH pectin also mostly consists of HG (Table 5; ≈ 50 mol%). For that reason, together with a decrease in the molecular weight before and after *endo*-PG action (Figure 3A,B), we assumed HG to be mainly affected. The depolymerization of HG is a clear sign pointed to contribute to an undesired defect of RH fruits. Further, monosaccharide composition analysis revealed that gamma irradiation contributed only to the reduction in the glucose content, while that of fucose was raised. Glucose, in this regard, is not a typical constituent of pectin. However, this observation could be explained by the decomposition of very closely cross-linked pectin and cellulose complexes. Apart from that, it can be speculated that a higher amount of fucose in 25 kGy-irradiated PS could be due to an increased extractability of fucose-containing rhamnogalacturonan-II segments of pectin.

The degradation of cellulose and pectin by gamma irradiation was investigated in previous studies [21–23]. None of these studies, however, investigated the changes in polymer nature directly in the plant material. In contrast, observations of the effects of radiation were performed on purified dry substances and/or sugar-containing solutions (for pectin). As a sign of degradation, authors mainly used the changes in the viscosities of the solution of the irradiated samples. Concerning cellulose, the authors' findings suggested that crystallinity and the amorphous region were changed due to additional oxidation seen by a decrease in the degree of polymerization and an increase in the absorbance of the carbonyl groups band at 1730–1750 cm^{-1} [21,23]. It should be noted that the alteration in cellulose was observed at dosages (100–2000 kGy) far exceeding ours (10 and 25 kGy). As regards the pectin, an increase in the degree of heterogeneity and a decrease in specific viscosity of 1% citrus pectin solution occurred on irradiation at a high dose level (20.56 kGy) [24]. Other

scientists demonstrated by viscosity measurements and jelly tests that, unlike dried pectin, pectin in solution degraded more rapidly by irradiation (10–40 kGy). Interestingly, the jellies were not affected [25]. Our findings concerning the changes in the molecular weights were in accordance with another study that dealt with apple pectin exposed to 0.5–10 kGy of gamma radiation. On the contrary, the degree of esterification was a sharp contrast to our result [26]. However, our result is in agreement with a previous study on the examination of pectin solution exposed to 0.1–1.0 kGy of radiation, where any changes in methanol content were not confirmed [27]. It can be concluded that the differences that can be observed with the other results lie in the way the plant material is prepared (fresh or dried), the amount of carbohydrate constituents, and last but not least the irradiation doses applied.

3.2. Influence of Gamma Irradiation on Organic Acids

Concerning organic acids, we found evidence to suggest that the exposition of RH fruits to gamma radiation had a negligible effect on the content of quinic, malic, and ascorbic acids. However, most previous studies showed that ascorbic acid was highly susceptible to irradiation. It has been noted that an oxidized dehydroascorbic acid was formed as a direct result of irradiation. For example, the exposition of dried lycium fruit to gamma irradiation (2–14 kGy) had a devastating effect on ascorbic acid at higher doses (14 kGy)—close to the used in the current study [28]. An appreciable loss of ascorbic acid was also found in spice and herb extracts of black pepper, cinnamon (32%), nutmeg (48%), oregano, and sage after being exposed to irradiation (10 kGy) [29]. However, another study indicated that vitamin C content had not been dramatically affected when using a lower dose of radiation (0.15–1 kGy) [30]. The thing to remember is that ascorbic acid is a major water-soluble antioxidant molecule in RH fruits, and therefore the lack of change in its amount was an important finding for the preservation of the quality of treated fruits. Furthermore, it has little information about the changes in the citric and malic acid contents [31]. These authors linked the changes in the citric acid content of fresh potatoes exposed to irradiation (150 Gy) to the storage temperatures and time. A marked increase in citric acid content, for example, was observed at the sixth month of storage, whereas malic acid did not significantly change [31]. It should be noted that great care is needed when interpreting these results, because a large variety of experimental patterns occur.

3.3. Influence of Gamma Irradiation on Lipid Constituents

Our results reveal that irradiation at doses 10 and 25 kGy have no significant effect on the RH seed fat content, fatty acid composition, and carotenoids amount. Although a slight increase in the acid value, conjugated dienes, and trienes, together with a decrease in the tocopherols were detected, the oxidative stability of oil presented by the induction period of autoxidation was not practically changed. The scientific literature on the topic was not full of examples of irradiated RH fruits and seed oil in particular, and thus to be compared with our results. To date, to our knowledge, only one study, which has not specifically dealt with RH fruits, demonstrated that the carotenoid content of RH tea was not influenced by a dose of up to 10 kGy, probably due to the very low moisture content [14]. Our results generally support this view. It all points to the conclusion that not only plant sources, but also irradiation and post-irradiation storage conditions (such as temperature, light, and oxygen) were all important factors in cases of different lipid compositions.

3.4. Influence of Gamma Irradiation on Phenolic Constituents and In Vitro Antioxidant Activity

Our study provided evidence to prove that gamma irradiation did not have a dramatic effect on the content of the phenolic components of dried RH fruit. However, it is a known fact that gamma irradiation can affect the number of antioxidant components in plant foods. It could be attributed either to the increased ability of a plant to produce radioprotective antioxidants, or the increased extractability of phenolic antioxidants from the degraded plant matter [32]. The literature contains some observations on the effect of gamma irradiation on the antioxidant activity and polyphenol content of food matrices, but researchers found

conflicting results. For example, the total polyphenol content and antioxidant activity of pomegranate peel powder and dried apricots increased as a result of irradiation, whereas no changes were observed in navel oranges [33–35]. The effect of gamma rays on foodstuffs depends on many factors, such as the radiation dose, moisture content, and the type and amount of endogenous polyphenols [32]. The enhanced antioxidant activity of irradiated plant material was mainly attributed to the increased enzyme activities or to the increased extractability from degraded plant tissues. On the other hand, gamma irradiation could reduce the antioxidant activity, which can be ascribed to the irradiation-derived degradation components or the formation of free radicals [32]. In our study, despite the degradation of dried RH matter, no significant changes in both the polyphenol content and the antioxidant activity of the treated samples were observed. This can be attributed to the lower moisture content of RH, which drastically limited enzymes' activity, to the absence of the oxidative changes in irradiated fruits, and/or the impossibility of polyphenols taking part in the process of inactivating free radicals. This effect was in agreement with the findings of other authors, who observed that the total polyphenols in linden flowers did not alter during irradiation (<10 kGy) [14].

4. Materials and Methods

4.1. Fruit Material

The RH fruit material (an orange-red color; reached maturity; 47% dry matter) was obtained from a local producer (Smolyan, the Rhodope Mountains, Bulgaria). The material was enclosed in polyethylene bags and stored frozen (−18 °C) before further freeze-drying (<10% moisture content).

4.2. Gamma Irradiation

Before irradiation, the fruit flesh was separated from the seeds mechanically. The samples were irradiated separately at a radionuclide ^{60}Co source with 8200 Ci activity. The gamma rays facility has a mobile irradiation chamber with 4.0 L volume and dimensions: 13.5 cm diameter and 22 cm height. During the irradiation, the chamber rotates on its vertical axis. For the study of the absorbed dose, distribution Alanine dosimeters (Kodak BioMax) were used, measured by ESR spectrometer E-scan Bruker, and calibrated in units of absorbed dose in water. At each point, three dosimeters were placed. The chosen absorbed doses were 10 kGy and 25 kGy. The fruit flesh and seeds (control and irradiated samples) were kept in polyethylene bags at room temperature. The irradiation of samples was performed in the National Center of Radiobiology and Radiation Protection at the Ministry of Health (Sofia, Bulgaria). Irradiated fruits and seeds, together with non-irradiated (control) samples were subjected to analyses immediately after irradiation.

4.3. Chemical Characterization of Non-irradiated and Irradiated Fruits

4.3.1. Preparation of Alcohol-Insoluble Solids

RH fruits (non-, 10 kGy-, and 25 kGy-irradiated) without seeds were used for the preparation of AIS. For that purpose, the initially ground samples were incubated at 50 °C for 1 h with 70% (*v/v*) aqueous ethanol and then the solids were separated by centrifugation ($18.187 \times g$, 10 min, 5 °C). The same procedure was repeated 3 times. Finally, the residue was washed 2 times with acetone at room temperature and vacuum-dried until there was no change in the mass.

4.3.2. Crude Protein Content

The crude protein content was evaluated by the micro-Kjeldahl method. The determination of nitrogen expressed as the ammonia content of the digested sample was performed by the acetylacetone–formaldehyde colorimetric method using ammonium sulfate as a standard [36]. The results were calculated using 6.25 as a conversion factor.

4.3.3. Total Uronic Acid and Cellulose Content

The uronic acid content of the plant material was estimated as described [37]. As a sample for the analysis served AIS-prepared as described above (Section 4.3.1). In brief, the sample was suspended in 72% (*w/w*) H₂SO₄ (1 h, 30 °C), and after dilution with water to 1 M H₂SO₄, hydrolysis was achieved through further incubation for 3 h at 100 °C. An aliquot of hydrolysate was taken for an automated 3-phenylphenol colorimetric analysis using a continuous flow analyzer Skalar San⁺⁺ system (Skalar Analytical BV, Breda, the Netherlands). The analysis was conducted according to the instructions of the manufacturer. Absorption was measured at 530 nm and galacturonic acid (12.5–100.0 µg/mL) was used for a calibration curve construction.

The quantitative estimation of cellulose in control and irradiated plant material was performed according to the gravimetric method of Kürschner and Hanak with a modification [38]. Briefly, a sample (0.5 g) was gently boiled (30 min) with 25 mL of acetic acid-HNO₃ reagent (acetic acid: H₂O:HNO₃ 8:2:1 *v/v/v*) in a round-bottom flask fitted with a reflux condenser. After cooling the insoluble residue was filtered through a sintered glass filter (G3) under vacuum, washed with deionized water to neutral pH, then with ethanol (96% *v/v*), and finally with an excess of petroleum ether. The obtained residue was dried in a laboratory oven at 50 °C to a constant weight. The resulting cellulose was corrected for its ash content.

4.3.4. Total Lipid Content

The total lipid content of the seeds was determined gravimetrically after an exhaustive extraction with *n*-hexane in a Soxhlet extractor (8 h) [39].

4.3.5. Total Carotenoids, β-Carotene, and Tocopherol Content

For the estimation of the total carotenoid content of the fruit flesh, 1 mL methanol, 2 mL chloroform, and 1 mL of 50 mM Tris buffer (pH 7.5, containing 1 M NaCl) were added to 20 mg of the ground sample. The mixture was centrifuged (6000 rpm, 10 min), and after that, the chloroform-containing bottom phase was removed. The upper phase was re-extracted with 2 mL chloroform, and after centrifugation, two chloroform phases were combined, dried under a stream of nitrogen, re-dissolved in a mixture of cyclohexane and dichloromethane (9:1 *v/v*), and the absorbance of the solution was then measured at 445 nm (Cecil Series 8000 UV/VIS spectrophotometer, Cecil Instruments Ltd., Cambridge, UK). A calibration curve constructed with β-carotene was used for the quantification [40].

The quantities of β-carotene and tocopherols were performed by a high-performance liquid chromatography (HPLC) analysis of a hexane solution of oil. The analyses were conducted by Agilent 1100 apparatus equipped with a DAD detector operating at 292, 298, and 450 nm for the monitoring of α-, γ- tocopherols, and β-carotene, respectively, on a Nucleosil 100-5 (250 mm × 4.6 mm, 5 µm) column connected with a pre-column EC 4/3 Nucleosil 100-5 (Macherey-Nagel). The elution of tocopherols was performed with a mobile phase of hexane and tetrahydrofuran (96:4 *v/v*), at a flow rate of 1 mL/min [41], whereas β-carotene was eluted with a mixture of *n*-hexane and 2-propanol (98:2 *v/v*) at 1.0 mL/min. The identification of different analytes was performed by the comparison of retention times with those of individual standards, while the concentration was calculated using calibration curves.

4.3.6. Conjugated Dienes and Trienes Contents

The conjugated dienes and trienes contents of RH seed oils were estimated by measuring the absorbance at 232 nm and 268 nm, respectively, of 1% solution of oil in *iso*-octane (Cecil Series 8000 UV/VIS spectrophotometer) with reference of pure solvent [42].

4.3.7. Acid Value, Peroxide Value, and Induction Period

The acid value of RH seed oils was determined titrimetrically with ethanolic KOH [43]. The peroxide value, expressed as meq O₂/kg oil, was determined according to the modified

iodometric method of Yanishlieva et al. [44]. The induction period was evaluated as follows: oxidation of oil (2 g) was carried out at 100 °C by blowing a stream of air (50 mL/min). The peroxide value was estimated periodically at different intervals during oxidation and the increase in the value was monitored graphically. The induction period was determined by the method of Le Tutour and Guedon [45].

4.3.8. Fatty Acid Composition

The fatty acid composition was determined by gas chromatography (GC) with a flame ionization detector after transesterification of oil to methyl esters with 1% H₂SO₄ in methanol [46]. Prior to the GC analysis, fatty acid methyl esters (FAMES) were purified by thin-layer chromatography on a silica gel plate with a mobile phase composed of hexane-acetone (100:6 *v/v*). GC was conducted on a Shimadzu 17A apparatus coupled to a flame ionization detector using a Simplicity-wax (30 m × 0.32 mm × 0.25 µm, Supelco) column. The separation took place at the following temperature regime: from 170 °C, at 2 °C/min to 260 °C (5 min). The injector and detector temperatures were kept at 260 °C and 280 °C, respectively. Helium was used as a carrier gas at a flow rate of 0.5 mL/min and a split ratio of 1:50. The peak identification was according to retention times compared to that of a standard mixture of FAMES.

4.3.9. HPLC Determination of Free Sugars

About 1 g of the ground sample was extracted with a 3% solution of *meta*-phosphoric acid in water (30 mL) for 1 h at 30 °C shaking on a thermostatic water bath (NÜVE, Turkey). The residue and extract were separated through centrifugation (6000×*g*, 20 min) and an additional filtration through a PTFE filter (0.45 µm). The filtrate was taken for chromatographic analysis. The separation of sugars was performed on a ZORBAX Carbohydrate (5 µm, 4.6 × 150 mm, Agilent, Santa Clara, CA, USA) and a ZORBAX Reliance Cartridge guard column connected to an Agilent 1220 Infinity HPLC system with a 1260 refractive index detector (RID). The elution was performed at a flow rate of 1.0 mL/min at 25 °C with a mobile phase composed of acetonitrile and water (80:20 *v/v*). The concentration of sugars in the sample was deduced using a calibration curve constructed by plotting the peak area against five different concentrations for each sugar. The peak corresponding to different sugars in the sample was confirmed by a comparison of retention time with that of the standards.

4.3.10. HPLC Determination of Organic Acids

HPLC determination of organic acids was performed on an HPLC system (Agilent 1220, Agilent Technology, Santa Clara, CA, USA), with a binary pump and UV-Vis detector (Agilent Technology, USA). Separation was performed on an Agilent TC-C18 column (5 µm, 4.6 mm × 250 mm) at 25 °C. Twenty microliters of the extract, prepared as described in 4.3.9., were injected and eluted (1.0 mL/min) isocratically with a 25 mM solution of K₂HPO₄ in water, whose pH was finely adjusted to 2.4 with H₃PO₄. The UV detector was set at 210 nm. The concentration of each organic acid in the sample was calculated using a calibration curve obtained by using five different concentrations for each acid. The peak corresponding to different acids was confirmed by a comparison of the retention time with that of the standards.

4.3.11. HPLC Determination of Phenolic Components

Before analysis, the finely ground (<500 µm) sample (0.5 g) was mixed with 40 mL of a solvent containing 60% ethanol in 0.5% formic acid, and further constantly stirred at room temperature for 1 h. The mixture was centrifuged (6000×*g*, 20 min) and the supernatant was then used for HPLC analysis, total polyphenols, and *in vitro* antioxidant activity determination. Different phenolic components were determined using an HPLC system (Agilent 1220, Agilent Technology, USA), with a binary pump and UV-Vis detector (Agilent Technology, USA). Separation was performed on an Agilent TC-C18 column

(5 μm , 4.6 mm \times 250 mm) at 25 $^{\circ}\text{C}$ and a wavelength of 280 nm was used. The following mobile phases were used: 0.5% acetic acid (A) and 100% acetonitrile (B) at a flow rate of 0.8 mL/min. The gradient elution started with 14% B, between 6 min and 30 min, linearly increased to 25% B, and then to 50% B at 40 min. The identification of the compounds was confirmed by a comparison of retention times utilizing the standard solutions and standard calibration curves of different phenolics.

4.3.12. Total Polyphenolic Content and In Vitro Antioxidant Activity

The total phenolic content was determined according to the method of Singleton and Rossi with Folin–Ciocalteu’s reagent [47]. Gallic acid (10–200 $\mu\text{g}/\text{mL}$) was employed as a calibration standard. The oxygen radical absorbance capacity (ORAC) and hydroxyl radical averting capacity (HORAC) were measured according to the methodology used by Denev et al. (2010) [48]. Both analyses were carried out on a FLUOstar OPTIMA plate reader (BMG Labtech, Ortenberg, Germany).

4.3.13. Scanning Electron Microscopy

The surface and internal topography and composition of the dried non- and 25 kGy-irradiated RH fruit flesh (non-ground) were examined by a digitalized SEM Philips 515 (accelerating voltage 8 kV, magnification 500 \times , 0.1 mm) equipped with an Everhart–Thornley secondary and Robinson backscattered electron detector (Philips, Amsterdam, the Netherlands). An SC7620 Mini Sputter Coater (Quorum Technologies, Laughton, East Sussex, UK) was used for coating specimens prior to examination with the microscope. The preparation and examination of the specimens were carried out in the Laboratory of Electron Beam Microscopy, Institute of Optical Materials and Technologies “Acad. Jordan Malinowski” (Bulgarian Academy of Sciences, Sofia, Bulgaria).

4.4. Extraction of the Polysaccharide Fraction

The ground sample (dried non-, 10 kGy-, and 25 kGy-irradiated fruit flesh of RH) was extracted with distilled water at 80 $^{\circ}\text{C}$ for 1 h, mixing the plant material and solvent in a ratio of 1 to 25 (*w/v*). After cooling, the solid was separated from the liquid through centrifugation (4428 \times g for 30 min at 20 $^{\circ}\text{C}$) and an additional Büchner funnel filtration (filter paper, KA-4, OP Papírna, s.r.o., Olšany, Czech Republic). To the filtrate, 3.0 volumes of 96% (*v/v*) cold ethanol were added, and after standing overnight at 4 $^{\circ}\text{C}$, the resulting precipitate was collected by centrifugation (20 min, 4 $^{\circ}\text{C}$, 3490 \times g). Then, the precipitate was re-dissolved in distilled water, dialyzed (mwco 12,000–14,000 Da; VISKING[®], SERVA Electrophoresis) for 72 h against distilled water (4 $^{\circ}\text{C}$), and freeze-dried.

4.5. Endo-Polygalacturonase (endo-PG) Hydrolysis of the Polysaccharide Fraction

Initially, PSs (2 mg/mL), isolated as described in 4.4., were dissolved in 50 mM of sodium acetate buffer (pH 5.2) and incubated for 24 h at 40 $^{\circ}\text{C}$ with endo-PG-I-M2 (EC 3.2.1.15; *Aspergillus aculeatus*; 5000 U/mL; 0.16 U/mL [S]) purchased from Megazyme International Ltd. (Bray, Co., Wicklow, Ireland). Finally, the enzyme was inactivated at 95 $^{\circ}\text{C}$ for 5 min, and after cooling the digest was centrifuged at 18,187 \times g, at 5 $^{\circ}\text{C}$ for 10 min. The supernatant obtained was further analyzed for the molecular weight distribution.

4.6. Physico-Chemical Characterization of Polysaccharides

4.6.1. General Analytical Methods

For the estimation of the total uronic acid content of the PSs, appropriately diluted solutions of PSs were directly assayed by the colorimetric method as described above (4.3.3.). For the estimation of the degree of methyl esterification, PSs (1 mg/mL) were saponified (0.5 M NaOH) and after neutralization (1.0 M HCl) the quantity of methanol was evaluated using a combined alcohol oxidase/4-amino-5-hydrazino-1,2,4-triazole-3-thiol (Purpald[®]) method [49]. The analysis was carried out according to the methodology used by Anthon and Barrett [50]. The acetyl content was determined photometrically by the hy-

droxamic acid reaction method of McComb and McCready, using β -D-glucose pentaacetate (24–120 $\mu\text{g}/\text{mL}$) as a standard [51]. The degrees of methylation and acetylation were expressed as moles of methyl esters or acetyl groups per 100 moles of uronic acid, respectively. The protein content was estimated by the dye-binding method of Bradford using Coomassie[®] Brilliant blue G-250 dye (Amresco[®]) and bovine serum albumin as a standard [52].

4.6.2. Monosaccharide Composition Analysis

The monosaccharide composition analysis of non-irradiated and 25 kGy-irradiated PSs was carried out according to the method of Honda et al. as modified by Yang et al. [53,54]. In brief, the PSs were hydrolyzed (4M TFA, 8 h at 110 °C) and then the released monosaccharides were derivatized employing 1-phenyl-3-methyl-5-pyrazolone (PMP) to UV-absorbing products. The resulting PMP derivatives were separated on an Agilent 1220 HPLC system with a UV detector (250 nm). The separation was conducted on an Agilent TC-C18 (4.6 \times 250 mm, 5 μm) column with a mobile phase consisting of 50 mM phosphate buffer ($\text{Na}_2\text{HPO}_4\text{-NaH}_2\text{PO}_4$, pH 6.9) and acetonitrile using a gradient elution [54].

4.6.3. Molecular Weight Distribution Analysis

PSs samples (initial and *endo*-PG-digested) were analyzed using an HPSEC Agilent 1220 Infinity LC system coupled with a 1260 RID detector using an Agilent Bio SEC-3 (300 Å, 4.6 \times 300 mm, 3 μm) column. The elution was performed with a mobile phase of 150 mM NaH_2PO_4 (pH 7.0) employing a flow rate of 0.5 mL/min. Pullulan standards (Shodex 159 standard P-82 kit, Showa Denko, Kawasaki, Japan) with molecular weights in the range of 0.59×10^4 to 78.8×10^4 g/mol were used for the construction of a standard curve by plotting the logarithm of the molecular weight and retention time.

4.7. FT-IR Spectroscopy

The sample (4 mg) was mixed with spectroscopic grade KBr and was then pressed into a pellet. FT-IR spectrum was collected on a Nicolet Avatar 330 (Thermo Electron Corp., Waltham, MA, USA) spectrometer. The spectrum was recorded over a wavenumber range of 4000–400 cm^{-1} at 132 scans with a spectral resolution of 4 cm^{-1} . The analysis and processing of the obtained spectrum were performed using the Spekwin32 software (version 1.71.5).

4.8. Statistical Analysis

Measurements were carried out in triplicate. The results are presented as a mean value of parallel determinations \pm standard deviation and were compared by the Student's *t*-test (MS Excel 2010 software).

5. Conclusions

For the first time, an in-depth study entirely devoted to the examination of the effect of gamma irradiation on phytochemical constituents of dried RH fruits was carried out. What is more, the current study is the first provide valuable insight into the cell wall PS constituents of irradiated RH fruits. To our knowledge, the gathered data for carbohydrate, organic acids, and lipid composition are also reported for the first time in this study. The results of our experiment indicate that the gamma irradiation of dried RH does not significantly change the content of fructose, most organic acids, fatty acids, β -carotene, and total polyphenols. By contrast, cellulose and pectin, which constituted the majority of plant cell walls, were adversely affected proportionately to the irradiation dose ($0 < 10 < 25$ kGy), which was indicated by changes in the yield, sugar content, and molecular weight distribution pattern. Therefore, our findings could be interpreted in various ways. On the one hand, it seems reasonable to suggest that the exposition of dried RH fruits on doses less than or even equal to 25 kGy have a negligible effect on the lower molecular weight constituents (such as some lipids, sugars, pigments, organic acids, and polyphenols).

This means that some nutritional and functional properties of food predetermined by these components would not significantly change. On the other hand, it seems that PSs constituents may be affected by doses even lower than 10 kGy. However, the fruits may change their textural properties when their PS components are changed/decomposed, thus exerting an influence on the way the fruit is further technologically processed. In addition, there is an expectation that pectin would change its jellifying properties. Nevertheless, it could be compromised that the exposition of dried RH up to 10 kGy is safe and can be used to decontaminate fruits, which are very often used as an ingredient in fruit-based teas and functional beverages.

Author Contributions: Conceptualization, S.M., P.D., and M.O.; methodology, M.O.; formal analysis, M.O.; investigation, M.O., D.T., Y.G., S.T., I.T., M.K.-N., and Y.N.; resources, S.M. and P.D.; data curation, M.O., Y.G., P.D., and S.M.; writing—original draft preparation, M.O.; writing—review and editing, P.D., S.M., and Y.G.; visualization, M.O.; supervision, S.M., P.D., and M.O.; project administration, S.M.; funding acquisition, S.M. All authors have read and agreed to the published version of the manuscript.

Funding: This research was funded by the Bulgarian National Science Fund, grant number DN 19/14 from 12 December 2017.

Institutional Review Board Statement: Not applicable.

Informed Consent Statement: Not applicable.

Data Availability Statement: Not applicable.

Acknowledgments: The first author is very grateful to Galina Maleshkova and Daniela Karashanova from the Laboratory of Electron Beam Microscopy at the Institute of Optical Materials and Technologies “Acad. Jordan Malinowski” (Bulgarian Academy of Sciences, Sofia) for conducting the SEM of the samples and the useful discussions. He owes Irina Yanakieva a great debt of gratitude for her valuable technical assistance in this work.

Conflicts of Interest: The authors declare no conflict of interest. The funders had no role in the design of the study; in the collection, analyses, or interpretation of data; in the writing of the manuscript, or in the decision to publish the results.

Sample Availability: Samples of the compounds are available from the authors.

References

- Molins, R.A. Introduction. In *Food Irradiation: Principles and Applications*; Molins, R.A., Ed.; Wiley Interscience: New York, NY, USA, 2001; pp. 1–21.
- Golge, E.; Ova, G. The effects of food irradiation on quality of pine nut kernels. *Radiat. Phys. Chem.* **2008**, *77*, 365–369. [CrossRef]
- Diehl, J.F. *Safety of Irradiated Foods*, 2nd ed.; Marcel Dekker Inc.: New York, NY, USA, 1995; ISBN 0-8247-9344-7.
- Farkas, J. Irradiation as a method for decontaminating food. A review. *Int. J. Food Microbiol.* **1998**, *44*, 189–204. [CrossRef]
- Farkas, J.; Mohácsi-Farkas, C. History and future of food irradiation. *Trends. Food Sci. Technol.* **2011**, *22*, 121–126. [CrossRef]
- Gecgel, U.; Gumus, T.; Tasan, M.; Daglioglu, O.; Arici, M. Determination of fatty acid composition of γ -irradiated hazelnuts, walnuts, almonds, and pistachios. *Rad. Phys. Chem.* **2011**, *80*, 578–581. [CrossRef]
- Shahbaz, H.; Ahn, J.; Akrama, K.; Kim, H.; Park, E.; Kwon, J. Chemical and sensory quality of fresh pomegranate fruits exposed to gamma radiation as quarantine treatment. *Food Chem.* **2014**, *145*, 312–318. [CrossRef] [PubMed]
- Ognyanov, M.; Georgiev, Y.; Denev, P.; Yanakieva, I.; Kratchanova, M. Bioactive compounds and health effects of rose hip fruits. *Nauka Diet.* **2014**, *3–4*, 14–27. (In Bulgarian)
- Patel, S. Rose hip as an underutilized functional food: Evidence based review. *Trends. Food Sci. Technol.* **2017**, *63*, 29–38. [CrossRef]
- Denev, P.; Lojek, A.; Ciz, M.; Kratchanova, M. Antioxidant activity and polyphenol content of Bulgarian fruits. *Bulg. J. Agric. Sci.* **2013**, *19*, 22–27.
- Ognyanov, M.; Remoroza, C.; Schols, H.A.; Georgiev, Y.; Kratchanova, M.; Kratchanov, C. Isolation and structure elucidation of pectic polysaccharide from rose hip fruits (*Rosa canina* L.). *Carbohydr. Polym.* **2016**, *151*, 803–811. [CrossRef]
- Petkova, N.; Ognyanov, M.; Kirchev, M.; Stancheva, S. Bioactive compounds in water extracts prepared from rosehip-containing herbal blends. *J. Food Process. Preserv.* **2021**, *45*, e14645. [CrossRef]
- Burbidge, C.A.; Ford, C.M.; Melino, V.J.; Wong, D.C.J.; Jia, Y.; Jenkins, C.L.D.; Soole, K.L.; Castellarin, S.D.; Darriet, P.; Rienth, M.; et al. Biosynthesis and cellular functions of tartaric acid in grapevines. *Front. Plant Sci.* **2021**, *12*, 643024. [CrossRef] [PubMed]

14. Katušin-Ražem, B.; Matić, S.; Ražem, D.; Mihoković, V. Radiation decontamination of tea herbs. *J. Food Sci.* **1988**, *53*, 1120–1126. [CrossRef]
15. Harrison, K.; Were, L.M. Effect of gamma irradiation on total phenolic content yield and antioxidant capacity of almond skin extracts. *Food Chem.* **2007**, *102*, 932–937. [CrossRef]
16. Broxterman, S.E.; Schols, H.A. Interactions between pectin and cellulose in primary plant cell walls. *Carbohydr. Polym.* **2018**, *192*, 263–272. [CrossRef] [PubMed]
17. Benen, J.A.E.; Kester, H.C.M.; Visser, J. Kinetic characterization of *Aspergillus niger* N400 endopolygalacturonases I, II and C. *Eur. J. Biochem.* **1999**, *259*, 577–585. [CrossRef]
18. Kačuráková, M.; Capek, P.; Sasinková, V.; Wellner, N.; Ebringerová, A. FT-IR study of plant cell wall model compounds: Pectic polysaccharides and hemicelluloses. *Carbohydr. Polym.* **2000**, *43*, 195–203. [CrossRef]
19. Azelmat, K.; ElGarrouj, D.; Mouhib, M.; Sayah, F. Irradiation of ‘Boufeggous’ dates: Effects on chemical composition during storage. *Postharvest Biol. Technol.* **2006**, *39*, 217–222. [CrossRef]
20. Jarvis, M.C. Plant cell walls: Supramolecular assemblies. *Food Hydrocoll.* **2011**, *25*, 257–262. [CrossRef]
21. Takács, E.; Wojnárovits, L.; Borsa, J.; Földváry, C.; Hargittai, P.; Zöld, O. Effect of γ -irradiation on cotton-cellulose. *Radiat. Phys. Chem.* **1999**, *55*, 663–666. [CrossRef]
22. Horio, M.; Imamura, R.; Mizukami, H. Effect of gamma irradiation upon cellulose. *Bull. Inst. Chem. Res. Kyoto Univ.* **1963**, *41*, 17–38.
23. Wang, K.-Q.; Xiong, X.-Y.; Chen, J.-P.; Chen, L.; Liu, Y. Effect of gamma irradiation on microcrystalline structure of *Phragmites* cellulose. *Wood Fiber Sci.* **2011**, *43*, 225–231.
24. Skinner, E.R.; Kertesz, Z.I. The effect of gamma radiation on the structure of pectin. An electrophoretic study. *J. Polym. Sci.* **1960**, *47*, 99–109. [CrossRef]
25. Kertesz, Z.I.; Morgan, B.H.; Tuttle, L.W.; Lavin, M. Effect of ionizing radiations on pectin. *Radiat. Res.* **1956**, *5*, 372–381. [CrossRef] [PubMed]
26. Sjöberg, A.-M. The effects of γ irradiation on the structure of apple pectin. *Food Hydrocoll.* **1987**, *1*, 271–276. [CrossRef]
27. Zegota, H. Some quantitative aspects of hydroxyl radical induced reactions in γ -irradiated aqueous solutions of pectins. *Food Hydrocoll.* **2002**, *16*, 353–361. [CrossRef]
28. Wen, H.-W.; Chung, H.-P.; Chou, F.-I.; Lin, I.-H.; Hsieh, P.-C. Effect of gamma irradiation on microbial decontamination, and chemical and sensory characteristic of lycium fruit. *Radiat. Phys. Chem.* **2006**, *75*, 596–603. [CrossRef]
29. Calucci, L.; Pinzino, C.; Zandomenoghi, M.; Capocchi, A.; Ghiringhelli, S.; Saviozzi, F.; Tozzi, S.; Gallechi, L. Effects of γ -irradiation on the free radical and antioxidant contents in nine aromatic herbs and spices. *J. Agric. Food Chem.* **2003**, *51*, 927–934. [CrossRef]
30. Golding, J.B.; Blades, B.L.; Satyan, S.; Jessup, A.J.; Spohr, L.J.; Harris, A.M.; Banos, C.; Davies, J.B. Low dose gamma irradiation does not affect the quality, proximate or nutritional profile of ‘Brigitta’ blueberry and ‘Maravilla’ raspberry fruit. *Postharvest Biol. Technol.* **2014**, *96*, 49–52. [CrossRef]
31. Lisińska, G.; Aniołowski, K. Organic acids in potato tubers: Part 2—The effect of gamma irradiation on citric and malic acid contents of potato tubers. *Food Chem.* **1991**, *40*, 207–212. [CrossRef]
32. Alothman, M.R.; Bhat, K.A. Effects of radiation processing on phytochemicals and antioxidants in plant produce. *Trends. Food Sci. Technol.* **2009**, *20*, 201–212. [CrossRef]
33. McDonald, H.; Arpaia, M.L.; Caporaso, F.; Obenland, D.; Were, L.; Rakovski, C.; Prakash, A. Effect of gamma irradiation treatment at phytosanitary dose levels on the quality of ‘Lane Late’ navel oranges. *Postharvest Biol. Technol.* **2013**, *86*, 91–99. [CrossRef]
34. Mali, A.; Khedkar, K.; Lele, S. Effect of gamma irradiation on total phenolic content and in vitro antioxidant activity of pomegranate (*Punica granatum* L.) peels. *Food Nutr. Sci.* **2012**, *2*, 428–433.
35. Hussain, P.R.; Chatterjee, S.; Variyar, P.S.; Sharma, A.; Dar, M.A.; Wani, A.M. Bioactive compounds and antioxidant activity of gamma irradiated sun dried apricots (*Prunus armeniaca* L.). *J. Food Compos. Anal.* **2013**, *30*, 59–66. [CrossRef]
36. GB 5009.5—400; Determination of Protein in Foods. National Food Safety Standard of the People’s Republic of China (NFSS). China National Center for Food Safety Risk Assessment: Beijing, China, 2016.
37. Ahmed, A.E.R.; Labavitch, J.M. A simplified method for accurate determination of cell wall uronide content. *J. Food Biochem.* **1978**, *1*, 361–365. [CrossRef]
38. Kürschner, K.; Hanak, A. Zur Bestimmung der sog. Rohfaser. Ein neues Verfahren der Bestimmung der Rohcellulose in Kakao. *Z. Unters. Lebensm.* **1930**, *59*, 484–494. [CrossRef]
39. ISO 659:2009; Oilseeds—Determination of Oil Content (Reference Method). International Organization for Standardization: Geneva, Switzerland, 2009.
40. British Standard Methods of Analysis—B.S.684, Section 2.20:1997; Determination of Carotene in Vegetable Oils. BSI Group: London, UK, 1997.
41. ISO 9936:2012; Animal and Vegetable Fats and Oils—Determination of Tocopherol and Tocotrienol Content by High-Performance Liquid Chromatography. International Organization for Standardization: Geneva, Switzerland, 2012.
42. AOCS Official method Ch 5-91. Specific Extinction of Oils and Fats, Ultraviolet Absorption. In *Official Methods and Recommended Practices of the AOCS*; AOCS Press: Urbana, IL, USA, 1991.

43. AOCS Official method Cd 3d-63. Acid Value of Fats and Oils. In *Official Methods and Recommended Practices of the AOCS*; AOCS Press: Champaign, IL, USA, 1999.
44. Yanishlieva, N.; Popov, A.; Marinova, E. Eine Modifizierte Jodometrische Methode zur Bestimmung der Peroxidzahl in kleinen Lipidproben. *C. R. Acad. Bulg. Sci.* **1978**, *31*, 869.
45. Le Tutour, B.; Guedon, D. Antioxidative activities of *Olea europaea* leaves and related phenolic compounds. *Phytochemistry* **1992**, *31*, 1173–1178. [CrossRef]
46. Christie, W.W. *Lipid Analysis: Isolation, Separation, Identification, and Structural Analysis of Lipids*, 3rd ed.; Oily Press: Bridgwater, UK, 2003; pp. 205–224.
47. Singleton, V.; Rossi, J. Colorimetry of total phenolic with phosphomolibdophosphotungstic acid reagents. *Am. J. Enol. Vitic.* **1965**, *16*, 144–158.
48. Denev, P.; Ciz, M.; Ambrozova, G.; Lojek, A.; Yanakieva, I.; Kratchanova, M. Solid-phase extraction of berries' anthocyanins and evaluation of their antioxidative properties. *Food Chem.* **2010**, *123*, 1055–1061. [CrossRef]
49. Klavons, J.A.; Bennett, R.D. Determination of methanol using alcohol oxidase and its application to methyl ester content of pectins. *J. Agric. Food Chem.* **1986**, *34*, 597–599. [CrossRef]
50. Anthon, G.E.; Barrett, D.M. Combined enzymatic and colorimetric method for determining the uronic acid and methylester content of pectin: Application to tomato products. *Food Chem.* **2008**, *110*, 239–247. [CrossRef] [PubMed]
51. McComb, E.A.; McCready, R.M. Determination of acetyl in pectin and in acetylated carbohydrate polymers. *Anal. Chem.* **1957**, *29*, 819–821. [CrossRef]
52. Bradford, M.M. A rapid and sensitive method for the quantitation of microgram quantities of protein utilizing the principle of protein-dye binding. *Anal. Biochem.* **1976**, *72*, 248–254. [CrossRef]
53. Honda, S.; Akao, E.; Suzuki, S.; Okuda, M.; Kakehi, K.; Nakamura, J. High-performance liquid chromatography of reducing carbohydrates as strongly ultraviolet-absorbing and electrochemically sensitive 1-phenyl-3-methyl-5-pyrazolone derivatives. *Anal. Biochem.* **1989**, *180*, 351–357. [CrossRef]
54. Yang, X.; Zhao, Y.; Wang, Q.; Wang, H.; Mei, Q. Analysis of the monosaccharide components in *Angelica* polysaccharides by high performance liquid chromatography. *Anal. Sci.* **2005**, *21*, 1177–1180. [CrossRef] [PubMed]

Article

L-Lysine-Based Gelators for the Formation of Oleogels in Four Vegetable Oils

Qiannan Li, Jieying Zhang, Guiju Zhang * and Baocai Xu *

School of Light Industry, Beijing Technology and Business University, No. 11 Fucheng Road, Haidian District, Beijing 100048, China; liqiannan0611@163.com (Q.L.); 13716454528@163.com (J.Z.)

* Correspondence: zhangguiju@btbu.edu.cn (G.Z.); xubaoc@btbu.edu.cn (B.X.)

Abstract: Supramolecular oleogel is a soft material with a three-dimensional structure, formed by the self-assembly of low-molecular-weight gelators in oils; it shows broad application prospects in the food industry, environmental protection, medicine, and other fields. Among all the gelators reported, amino-acid-based compounds have been widely used to form organogels and hydrogels because of their biocompatibility, biodegradation, and non-toxicity. In this study, four N^α , N^ϵ -diacyl-L-lysine gelators (i.e., N^α , N^ϵ -dioctanoyl-L-lysine; N^α , N^ϵ -didecanoyl-L-lysine; N^α , N^ϵ -dilauroyl-L-lysine; and N^α , N^ϵ -dimyristoyl-L-lysine) were synthesized and applied to prepare oleogels in four kinds of vegetable oils. Gelation ability is affected not only by the structure of the gelators but also by the composition of the oils. The minimum gel concentration (MGC) increased with the increase in the acyl carbon-chain length of the gelators. The strongest gelation ability was displayed in olive oil for the same gelator. Rheological properties showed that the mechanical strength and thermal stability of the oleogels varied with the carbon-chain length of the gelators and the type of vegetable oil. The microstructure of oleogels is closely related to the carbon-chain length of gelators, regardless of oil type. The highest oil-binding capacity (OBC) was obtained in soybean oil for all four gelators, and N^α , N^ϵ -dimyristoyl-L-lysine showed the best performance for entrapping oils.

Keywords: N^α ; N^ϵ -diacyl-L-lysine; vegetable oil; oleogel; gelator; oil-binding capacity

Citation: Li, Q.; Zhang, J.; Zhang, G.; Xu, B. L-Lysine-Based Gelators for the Formation of Oleogels in Four Vegetable Oils. *Molecules* **2022**, *27*, 1369. <https://doi.org/10.3390/molecules27041369>

Academic Editor: Mirella Nardini

Received: 14 January 2022

Accepted: 16 February 2022

Published: 17 February 2022

Publisher's Note: MDPI stays neutral with regard to jurisdictional claims in published maps and institutional affiliations.



Copyright: © 2022 by the authors. Licensee MDPI, Basel, Switzerland. This article is an open access article distributed under the terms and conditions of the Creative Commons Attribution (CC BY) license (<https://creativecommons.org/licenses/by/4.0/>).

1. Introduction

Gel is a solid-like form of soft matter comprised of a liquid phase as the main component and a low concentration of a molecular gelator [1]. When the mass of the gelator is less than 2000 Da, the corresponding gel is defined as supramolecular gel or low-molecular-weight gel (LMWG) [2–6], which is formed by small molecular gelators through supramolecular interactions, including hydrogen-bonding, van der Waals, π -stacking, coordination, donor-acceptor, and charge-transfer interactions.

Two types of gels are commonly described in the literature: organogels and hydrogels [7]. Recently, ionic liquid gels, i.e., gels obtained in ionic liquids [8–10] and eutectogels, i.e., gels obtained in deep eutectic solvents [11,12] have also been described. Organogels are gels in which the liquid phase is an organic solvent, unlike hydrogels, which are gels with a continuous liquid-aqueous phase. Supramolecular organogels can be used in various everyday applications, including processing petroleum, food, pharmaceuticals, or cosmetics [13–15]. If liquid oils are used as organic solvents, the resulting organogels are called oleogels. In general, the solid lipids possess specific characteristics over liquid oils for food products. Thus far, high-melting lipids containing *trans* fatty acids, and saturated fatty acid moieties have been commonly employed. However, it has recently been claimed that the intake of high levels of *trans* and saturated fats contribute to global epidemics related to metabolic syndrome and cardiovascular disease [16]. The mechanistic resemblance of oleogels to *trans* and saturated fats makes liquid oil gelation an ideal alternative in developing fat-based food products. In practical application, both the mechanical and aesthetic

properties of oleogels are vital for food and other products. Modulating various parameters for ideal mechanical and aesthetic properties has gained significant interest in recent years. Currently, a lot of research has been conducted on oleogels, to discover the relationship between gelator structure, the nature of the oil, and gelation ability [17,18]. However, it is still not well understood, due to the complicated systems. A better understanding of these oleogel systems will help to improve applications in cosmetic products, drug delivery and pharmaceuticals, and provide an alternative for making healthy foods that are free of trans fats and contain minimal saturated fats [19].

Among many small molecular gelators reported, amino-acid-based compounds have received tremendous attention because they are available in large quantities as inexpensive starting materials, and synthetic methods are relatively simple and well-established [20–22]. The demand for better and environmentally friendly gelators makes amino-acid-based amphiphiles very attractive, as these compounds are generally biodegradable and biocompatible. There is at least one amide linkage between the hydrophobic tail and the polar headgroup in the structure of amino-acid-based gelators, providing one of the interactions responsible for their supramolecular assembly, i.e., hydrogen bonding [23,24]. The gelation ability also depends on the hydrophobic interactions (van der Waals force) [25,26]. Seeking a balance between hydrogen bonding and van der Waals forces is very important for gelation.

N^α , N^ϵ -diacyl-L-lysine and its derivatives are called all-powerful gelators [27–29]. Its ester derivatives can form organogels in a wide variety of organic fluids, such as alkanes, alcohols, ketones, esters, cyclic ethers, aromatic solvents, polar solvents, and mineral and vegetable oils. Its carboxylate derivatives can form hydrogels in an aqueous solution. N^α , N^ϵ -diacyl-L-lysine itself has also displayed good organogelation ability. In this study, four N^α , N^ϵ -diacyl-L-lysines (i.e., N^α , N^ϵ -dioctanoyl-L-lysine; N^α , N^ϵ -didecanoyl-L-lysine; N^α , N^ϵ -dilauroyl-L-lysine; and N^α , N^ϵ -dimyristoyl-L-lysine) were synthesized and used as gelators to prepare oleogels in four kinds of vegetable oils. As the hydrogen-bonding and hydrophobic interactions between gelators and vegetable oils are responsible for the gelation behaviors and the properties of formed oleogels, the chemical structures of both N^α , N^ϵ -diacyl-L-lysines (i.e., the carbon-chain length) and oils (i.e., the fatty acid composition) are the key parameters of oleogel systems. The rheological properties, morphology, and oil-binding capacity of formed oleogels were studied, with hopes of providing better insight into the gelation abilities of L-lysine-based gelators with different carbon-chain lengths in different oils.

2. Materials and Methods

2.1. Materials

Octanoyl chloride (99%), decanoyl chloride (98%), lauroyl chloride (98%), myristoyl chloride (98%), and L-lysine (98%) were purchased from Shanghai Macklin Biochemical Co., Ltd. (Shanghai, China). Petroleum ether (bp 60–90 °C), anhydrous ethanol (99.8%), sodium hydroxide ($\geq 98\%$), and hydrochloric acid (37%) were obtained from Beijing InnoChem Science & Technology Co., Ltd. (Beijing, China). Corn germ oil was purchased from Shandong Xiwang Food Co., Ltd. (Tianjin, China). Soybean oil was purchased from COFCO Fulinmen Food Marketing Co., Ltd. (Zouping, China). Olive oil was purchased from Shanghai Jiage Food Co., Ltd. (Shanghai, China). Linseed oil was purchased from Hebei Jiafeng vegetable oil Co., Ltd. (Handan, China). All the reagents were used as received.

2.2. Synthesis and Characterization of N^α , N^ϵ -diacyl-L-lysines

The L-lysine and fatty acid chloride were weighed in a molar ratio of 1:2. L-lysine was added into a four-necked flask, followed by a mixture of anhydrous ethanol and deionized water (2:1, *v/v*). The reaction mixture was cooled in an ice-water bath under stirring. Then fatty acid chloride was added slowly via a dropping funnel. In the meantime, the pH of the reaction solution was adjusted by an aqueous sodium hydroxide solution (10 wt%) and maintained at 9–10. The reaction continued for 3 h after the dropwise addition. At last,

the reaction solution was taken out and allowed to stand at room temperature for 3–4 h. After acidification with dilute hydrochloric acid, the precipitate was filtered and washed with deionized water, then rinsed with petroleum ether three times, giving a white, solid appearance the final product.

Four N^α , N^ϵ -diacyl-L-lysines were characterized by FT-IR, ESI-MS, and ^1H NMR measurements. IR spectra were obtained on a Nicolet iS10 FT-IR Spectrometer (Thermo Fisher Scientific, Madison, WI, USA) using KBr tablets at room temperature. ESI-MS spectra were recorded using an API3200 triple-quadrupole mass spectrometer (AB SCIEX, Redwood, CA, USA). The ^1H NMR spectra were acquired on a DRX-600 NMR spectrometer (Bruker, Ettlingen, German).

2.3. Oleogel Preparation

The oleogel formation of N^α , N^ϵ -diacyl-L-lysines was investigated by the heating–cooling method [30]. The gelator was added to vegetable oil in a sealed vial. Then, the mixture was heated until a transparent solution was obtained, then cooled to room temperature by simply removing it from the heat. The gelation properties were evaluated by inversion of the vial, and the absence of gravitational flow was utilized to determine the successful achievement of gelation. The minimum gel concentration (MGC) for a gelator was determined by weighing up the minimum amount of gelator needed to form a stable gel through the heating–cooling cycle.

2.4. Characterization of Vegetable Oils

Analysis of the fatty acid composition of the oils was carried out using a 7890A/5975C gas chromatography–mass spectrometry system (GC-MS, Agilent, Santa Clara, CA, USA) equipped with a HP-5MS (30 m \times 0.25 mm \times 0.25 μm) capillary column. Helium (99.999%) was the carrier gas, with a flow rate of 1.2 mL/min. The initial temperature of 100 $^\circ\text{C}$ was held for 2 min and increased to 220 $^\circ\text{C}$ at 10 $^\circ\text{C}/\text{min}$. The temperature was held at 220 $^\circ\text{C}$ for 1 min and increased to 230 $^\circ\text{C}$ at 2 $^\circ\text{C}/\text{min}$, then held 2 min. Oils were trans-esterified to fatty acid methyl esters for GC-MS analyses. The injection (1 μL) was performed in the split mode at a split ratio of 1:20. The samples were run by electron ionization, and the source temperature and electron energy were 230 $^\circ\text{C}$ and 70 eV. The auxiliary heater temperature was 200 $^\circ\text{C}$.

2.5. Rheological Behavior Measurements

The rheological analysis of the oleogels was measured by HAAKE MARS III rheometer (Thermo Electron GmbH, Dreieich, Germany). The time dependences of the storage modulus (G') and loss modulus (G'') of oleogels were measured at 25 $^\circ\text{C}$ with a fixed rotational speed of 1 rad/s and a shear strain of 0.25 Pa. The temperature dependence of the storage modulus (G') and loss modulus (G'') for oleogels was determined at a heating temperature from 20 $^\circ\text{C}$ to 145 $^\circ\text{C}$, with a constant rotational speed of 1 rad/s and a shear strain of 0.25 Pa.

2.6. TEM Measurements

The morphology of oleogels was observed using TEM measurements. The samples were prepared according to the literature method of [21]. Firstly, a small amount of oleogel was cast on carbon-coated copper grids (300 mesh), then the sample was vacuum dried at 50 $^\circ\text{C}$, 0.08 MPa for 2 days to evaporate the oils before observation. The microscopic images of oleogels were monitored using an X-MAX JEM-2100 transmission electron microscope (JEOL, Tokyo, Japan), operating at 120 kV.

2.7. Oil-Binding Capacity (OBC) Determination

The oil-binding capacity was measured according to the literature method of [21,31]. This methodology allows us to understand the degree of oil retention in the oleogel structure. First, 2 mL of the melted oleogel (the concentration corresponded to the MGC of each

gelator) was put into a previously weighed (m_1) centrifuge tube and kept at room temperature for 24 h. Then, the tube was weighed (m_2) again. Finally, the tube was centrifuged at 10000 rpm for 15 min at room temperature and turned over to drain the released liquid oil. After drainage, the tubes were weighed (m_3) again. The oil-binding capacity (OBC) values were calculated by the following equations.

$$\text{Released oil (\%)} = \frac{(m_2 - m_1) - (m_3 - m_1)}{m_2 - m_1} \times 100 \quad (1)$$

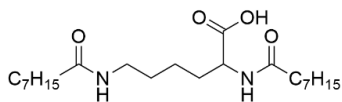
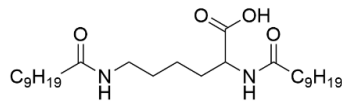
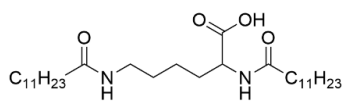
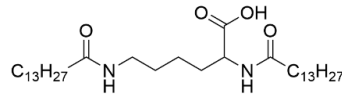
$$\text{OBC (\%)} = 100 - \text{Released oil (\%)} \quad (2)$$

3. Results and Discussion

3.1. Preparation and Characterization of L-Lysine-Based Gelators

Four N^α, N^ϵ -diacyl lysine-based gelators were synthesized using the Schotten–Baumann reaction previously reported in the literature with minor modifications [32,33]. Briefly, fatty acyl chlorides were used as acyl donors, and reacted with L-lysine under alkaline conditions, followed by acidification with HCl aqueous solution. Four fatty acyl chlorides, i.e., octanoyl chloride, decanoyl chloride, lauroyl chloride, and myristoyl chloride, were applied in this paper. Both the α amino group and the ϵ amino group of L-lysine readily reacted with a fatty acyl chloride, forming chemically stable amide bonds. Four N^α, N^ϵ -diacyl L-lysine-based gelators were obtained with a yield of 42%–71% (Table 1). In the case of N^α, N^ϵ -dimyristoyl-L-lysine, the reason for the low yield was perhaps a low solubility of the reactants in the solvent used, due to the longer carbon-chain length.

Table 1. Product list of four N^α, N^ϵ -diacyl lysine-based gelators.

Gelator	Structure	Abbreviation	Yield (%)
N^α, N^ϵ -dioctanoyl-L-lysine		C8-lys-C8	69
N^α, N^ϵ -didecanoyl-L-lysine		C10-lys-C10	71
N^α, N^ϵ -dilauroyl-L-lysine		C12-lys-C12	65
N^α, N^ϵ -dimyristoyl-L-lysine		C14-lys-C14	42

The synthesized four N^α, N^ϵ -diacyl lysines were characterized by FT-IR, ESI-MS, and ^1H NMR. The results are presented below.

N^α, N^ϵ -dioctanoyl-L-lysine (C8-lys-C8). IR (ν_{max} , cm^{-1}): 3326.75 (N-H), 1724.29 (C=O), 1639.58 (C=O, amide band I), 1536.28 (δ N-H, amide band II). ESI-MS: $m/z = 396.8$, which was assigned as $[\text{M} - \text{H}]^-$, while M is molar weight of N^α -octanoyl- N^ϵ -octanoyl-L-lysine. ^1H NMR (DMSO- d_6 , 600 MHz) δ ppm: 0.85 (t, $J = 6.6$ Hz, 6H, 2CH_3), 1.23 (m, 18H, 9CH_2), 1.35 (m, 2H, CH_2), 1.47 (m, 2H, CH_2), 1.54 (m, 2H, CH_2), 1.66 (m, 2H, CH_2), 2.02 (t, $J = 7.8$ Hz, 2H, CH_2), 2.10 (t, $J = 6.0$ Hz, 2H, CH_2), 2.99 (m, 2H, CH_2), 4.12 (m, 1H, CH), 7.72 (t, $J = 4.8$ Hz, 1H, NH), 7.97 (d, $J = 7.8$ Hz, 1H, NH), 12.41 (s, 1H, COOH).

N^α, N^ϵ -didecanoyl-L-lysine (C10-lys-C10). IR (ν_{max} , cm^{-1}): 3326.75 (N-H), 1724.29 (C=O), 1639.58 (C=O, amide band I), 1536.28 (δ N-H, amide band II). ESI-MS: $m/z = 396.8$, which was assigned as $[\text{M} - \text{H}]^-$, while M is molar weight of N^α -octanoyl- N^ϵ -octanoyl-L-

lysine. $^1\text{H NMR}$ ($\text{DMSO-}d_6$, 600 MHz) δppm : 0.85 (t, $J = 6.6$ Hz, 6H, 2CH_3), 1.23 (m, 26H, 13CH_2), 1.35 (m, 2H, CH_2), 1.46 (m, 2H, CH_2), 1.54 (m, 2H, CH_2), 1.66 (m, 2H, CH_2), 2.01 (t, $J = 7.2$ Hz, 2H, CH_2), 2.10 (t, $J = 7.2$ Hz, 2H, CH_2), 2.99 (m, 2H, CH_2), 4.12 (m, 1H, CH), 7.72 (t, $J = 5.4$ Hz, 1H, NH), 7.97 (d, $J = 7.8$ Hz, 1H, NH), 12.44 (s, 1H, COOH).

$\text{N}^\alpha, \text{N}^\epsilon$ -dilauroyl-L-lysine (C12-lys-C12). IR (ν_{max} , cm^{-1}): 3326.75 (N-H), 1724.29 (C=O), 1639.58 (C=O, amide band I), 1536.28 ($\delta\text{N-H}$, amide band II). ESI-MS: $m/z = 396.8$, which was assigned as $[\text{M} - \text{H}]^-$, while M is molar weight of N^α -lauroyl- N^ϵ -lauroyl-L-lysine. $^1\text{H NMR}$ ($\text{DMSO-}d_6$, 600 MHz) δppm : 0.85(t, $J = 7.2$ Hz, 6H, 2CH_3), 1.23 (m, 34H, 17CH_2), 1.35 (m, 2H, CH_2), 1.46 (m, 2H, CH_2), 1.54 (m, 2H, CH_2), 1.65 (m, 2H, CH_2), 2.01 (t, $J = 7.2$ Hz, 2H, CH_2), 2.10 (t, $J = 6.0$ Hz, 2H, CH_2), 2.99 (m, 2H, CH_2), 4.12 (m, 1H, CH), 7.71 (t, $J = 5.4$ Hz, 1H, NH), 7.96 (d, $J = 7.8$ Hz, 1H, NH), 12.41 (s, 1H, COOH).

$\text{N}^\alpha, \text{N}^\epsilon$ -dimyristoyl-L-lysine (C14-lys-C14). IR (ν_{max} , cm^{-1}): 3326.75 (N-H), 1724.29 (C=O), 1639.58 (C=O, amide band I), 1536.28 ($\delta\text{N-H}$, amide band II). ESI-MS: $m/z = 396.8$, which was assigned as $[\text{M} - \text{H}]^-$, while M is molar weight of N^α -myristoyl- N^ϵ -myristoyl-L-lysine. $^1\text{H NMR}$ ($\text{DMSO-}d_6$, 600 MHz) δppm : 0.85 (t, $J = 6.6$ Hz, 6H, 2CH_3), 1.23 (m, 42H, 21CH_2), 1.35 (m, 2H, CH_2), 1.46 (m, 2H, CH_2), 1.54 (m, 2H, CH_2), 1.66 (m, 2H, CH_2), 2.01 (t, $J = 7.2$ Hz, 2H, CH_2), 2.09 (t, $J = 6.6$ Hz, 2H, CH_2), 2.99 (m, 2H, CH_2), 4.12 (m, 1H, CH), 7.71 (t, $J = 4.8$ Hz, 1H, NH), 7.97 (d, $J = 7.8$ Hz, 1H, NH), 12.45 (s, 1H, COOH).

3.2. Preparation of Oleogels

The four $\text{N}^\alpha, \text{N}^\epsilon$ -diacyl-L-lysines with different carbon chains can form oleogels in four vegetable oils, i.e., linseed oil, soybean oil gel, corn germ oil, and olive oil, and the gel pictures are shown in Figure 1. All the oleogels did not flow after the vial was inverted, which means $\text{N}^\alpha, \text{N}^\epsilon$ -diacyl-L-lysines can be used as effective gelators for vegetable oil structuring. As in Figure 1, gels formed in soybean oil and corn germ oil were white or translucent, while light yellow or yellow gels were obtained in linseed oil and olive oil. A similar phenomenon was reported in the literature [21], which may be related to the color of vegetable oils.

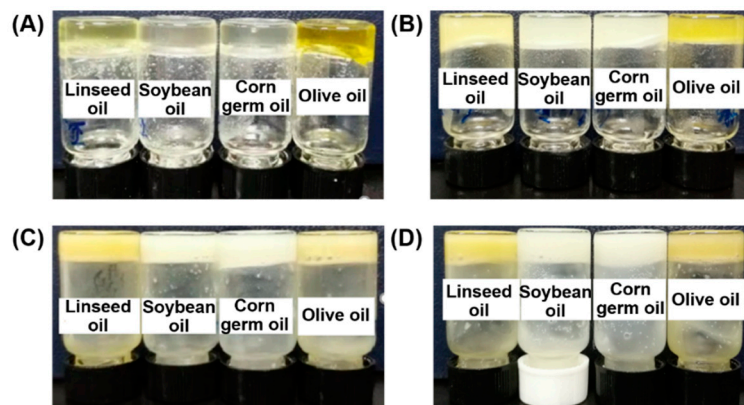


Figure 1. Oleogels formed by lysine-based gelators in linseed oil, soybean oil gel, corn germ oil and olive oil: (A) C8-lys-C8, (B) C10-lys-C10, (C) C12-lys-C12, (D) C14-lys-C14.

The MGC values of all the above-mentioned oleogel samples are listed in Table 2. As can be seen from the data, the gelation ability of gelators is closely related to their chemical structure, i.e., the acyl carbon-chain length. In the same vegetable oil, MGC increased with the increase in the acyl carbon-chain length of the gelators. Stable gel can be formed by 1.08 wt% of C8-lys-C8 in olive oil, while the MGC of C14-lys-C14 in linseed oil was even higher than 10 wt%. On the one hand, this may be due to two long carbon chains in the gelator molecules. The greater steric hindrance of longer chains is not conducive to the formation of gels. On the other hand, the reason linseed oil showed the higher MGC may be due to the composition of the fatty acids. This oil is mainly composed of linolenic acid (Table 3).

Table 2. Gelation ability of four gelators in vegetable oils.

Vegetable Oils	MGC (wt%)			
	C8-lys-C8	C10-lys-C10	C12-lys-C12	C14-lys-C14
Olive oil	1.08	1.28	4.28	7.79
Corn germ oil	1.18	1.93	4.37	8.63
Soybean oil	1.36	2.14	4.42	8.84
Linseed oil	1.67	2.27	4.55	10.57

Table 3. Fatty acid composition of four vegetable oils (%; mean values \pm SD, $n = 3$).

Vegetable Oils	SFA ¹	Oleic Acid	Linoleic Acid	Linolenic Acid
Olive oil	18.66 \pm 0.11	74.55 \pm 0.06	6.07 \pm 0.02	0.72 \pm 0.10
Corn germ oil	17.01 \pm 0.14	30.26 \pm 0.03	51.70 \pm 0.07	1.03 \pm 0.21
Soybean oil	18.82 \pm 0.21	26.83 \pm 0.18	47.40 \pm 0.08	6.95 \pm 0.23
Linseed oil	14.04 \pm 0.08	22.15 \pm 0.30	14.90 \pm 0.19	48.91 \pm 0.03

¹ SFA, saturated fatty acids, which mainly contained palmitic acid and stearic acid.

The gelation ability of the gelators was also affected by the type of vegetable oil. For the same gelator, the MGC increased in the order of olive oil, corn germ oil, soybean oil, and linseed oil, indicating the strongest gelation ability in olive oil. This was caused by the different compositions of the four vegetable oils. It can be seen from Table 3 that the fatty acids of the four vegetable oils are mainly composed of saturated fatty acids and unsaturated fatty acids, of which unsaturated fatty acids account for the largest proportion [21]. Unsaturated fatty acids include oleic acid, linoleic acid, and linolenic acid, which contain one double bond, two double bonds, and three double bonds, respectively. Combined with MGC values in Table 2, there is a certain positive correlation between the gelling ability and the percentage of oleic acid. However, the composition of vegetable oils was really complicated. The differences in the degree of unsaturation and carbon-chain length, as well as different proportions, affected the intermolecular hydrogen bonding and hydrophobic interaction between the vegetable oils and gelators, leading to different gelation abilities of the gelators in different vegetable oils.

3.3. Rheological Properties

The viscoelastic characteristics of the oleogels formed by N ^{α} , N ^{ϵ} -diacyl-L-lysines (at the MGC mass fraction) were investigated by rheological measurements. The results of storage modulus (G') and loss modulus (G'') are presented in Figure 2. In each case, the storage modulus (G') is larger than the loss modulus (G''), and the storage modulus G' is mainly independent on time, thus indicating the formation of stable oleogels.

When C8-lys-C8 was used as a gelator, a slightly higher G' value of linseed oil gel and soybean oil gel, compared with corn germ oil gel and olive oil gel, indicates the higher mechanical strength due to the different composition of four vegetable oils. When C10-lys-C10 was used as a gelator, an obviously higher G' value of linseed oil gel was observed among the four oleogels. Then comes corn germ oil gel, followed by soybean oil gel. Olive oil gel presented the lowest G' value, indicating the weakest gel strength. As for C12-lys-C12, the G' values of soybean oil gel and linseed oil gel were much higher than the other two oleogels, even ten times that of oleogel formed in corn germ oil. Similarly, when C14-lys-C14 acted as a gelator, soybean oil gel possessed the strongest mechanical strength due to the highest G' value. However, the G' value of linseed oil gel was as low as that of corn germ oil gel.

The mechanical strength of oleogels did not show apparent regularity with the vibration of the carbon-chain length of gelators and the type of vegetable oils. This is likely because of the complicated composition of the vegetable oils. Moreover, the amount of gelator in each gel sample was different, as there was a different MGC for each gelator.

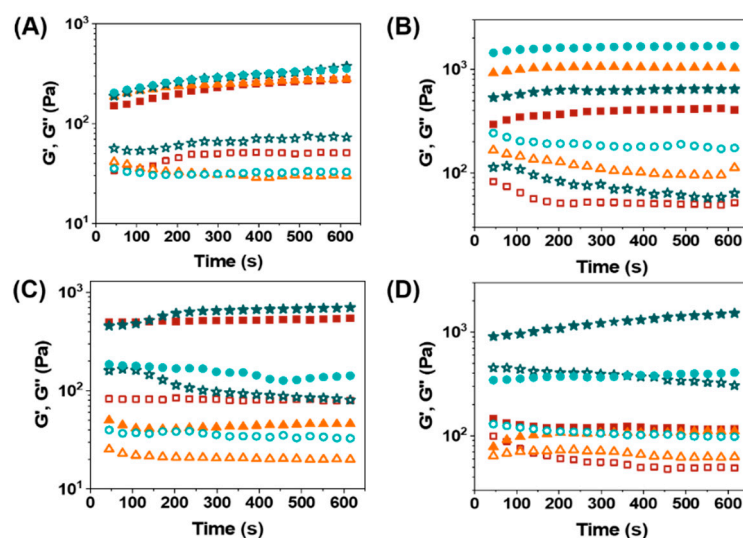


Figure 2. Variation of storage modulus (G') and loss modulus (G'') for oleogels formed by L-lysine-based gelators: (A) C8-lys-C8, (B) C10-lys-C10, (C) C12-lys-C12, and (D) C14-lys-C14 at 25 °C. Solid squares—Olive oil gel (G'); Open squares—Olive oil gel (G''); Solid triangles—Corn germ oil gel (G'); Open triangles—Corn germ oil gel (G''); Solid stars—Soybean oil gel (G'); Open stars—Soybean oil gel (G''); Solid circles—Linseed oil gel (G'); Open circles—Linseed oil gel (G'').

The thermal stability of the oleogels was then evaluated. The mechanical properties of the oleogels as a function of temperature are presented in Figure 3. The rheological measurements indicated that the gels formed in vegetable oils at an MGC of C8-lys-C8 were stable up to 100 °C; above this temperature, the supramolecular interactions responsible for the formation of the gel weaken, and the sample melts to a viscous liquid. Similarly, the gels formed in corn germ oil and linseed oil at an MGC of C10-lys-C10 presented high thermal stability, keeping the gel-like consistency with mainly stable G' and G'' values until about 130 °C and 100 °C. However, the gels formed in olive oil and soybean oil at an MGC of C10-lys-C10 displayed poor thermal stability, with slowly declining G' values from about 30 °C, which then drastically decreased after 100 °C. As for C12-lys-C12 and C14-lys-C14, all the gels formed in vegetable oils were much more unstable, with a rapid decrease in G' and G'' values with the increase in temperature.

For each gel, the values of G' and G'' gradually decreased when the temperature increased. G' was higher than G'' at the beginning, indicating that its gel state with solid behavior dominates. With the temperature continuing to rise, G'' surpassed G' , with the gel liquid behavior dominating. The intersection of the G' and G'' curve can be defined as a phase transition point. The temperature at this point was summarized in Table 4. The phase transition temperatures of oleogels formed by C8-lys-C8 are all higher than 100 °C, while those of C12-lys-C12 and C14-lys-C14 gels were in the range of 40–75 °C, showing that the thermal stability of oleogels are mainly related to the carbon-chain length of gelators.

Table 4. The phase transition temperature of oleogels formed by L-lysine-based gelators.

Vegetable Oils	Phase Transition Temperature (°C)			
	C8-lys-C8	C10-lys-C10	C12-lys-C12	C14-lys-C14
Olive oil	101.1	62.3	48.4	51.5
Corn germ oil	102.5	130.9	51.5	41.1
Soybean oil	102.5	84.2	60.8	57.0
Linseed oil	112.9	104.4	44.9	71.4

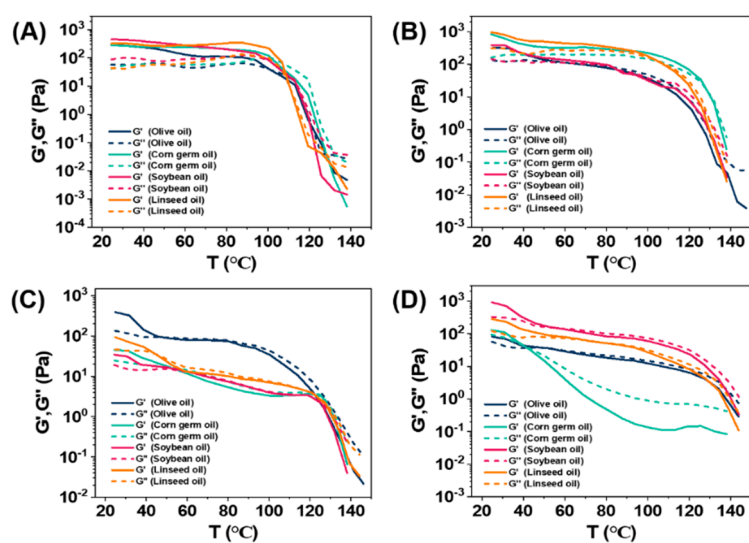


Figure 3. Dependence of the storage modulus (G') and loss modulus (G'') with the temperature for a gelator mass fraction of corresponding MGC in four vegetable oils: (A) C8-lys-C8, (B) C10-lys-C10, (C) C12-lys-C12, and (D) C14-lys-C14.

3.4. Morphology of Oleogels

In order to observe the network structure of oleogels produced with different gelators and vegetable oils, TEM was utilized, and the images are shown in Figures 4 and 5. Long fibers were observed in the olive oil gel network when C8-lys-C8 was used as gelator at MGC (Figure 4A), while shorter fibers were displayed in olive oil gel with C10-lys-C10 at MGC (Figure 4B). However, olive oil gels formed by C12-lys-C12 and C14-lys-C14 yielded needle-like crystals (Figure 4C,D), which are a desirable feature for gel formation, as such crystals entrap a larger amount of liquid oil [16,34,35]. The needle-shaped crystals were about 2–3 μm long in the olive oil gel formed by C12-lys-C12, and about 1–2 μm long in the olive oil gel formed by C14-lys-C14.

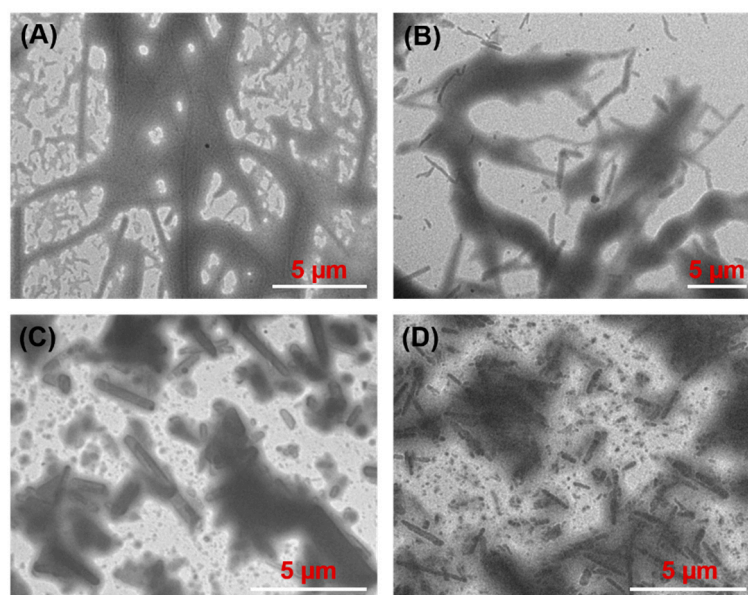


Figure 4. TEM images of oleogels prepared by lysine-based gelators in olive oil: C8-lys-C8 (A), C10-lys-C10 (B), C12-lys-C12 (C), and C14-lys-C14 (D).

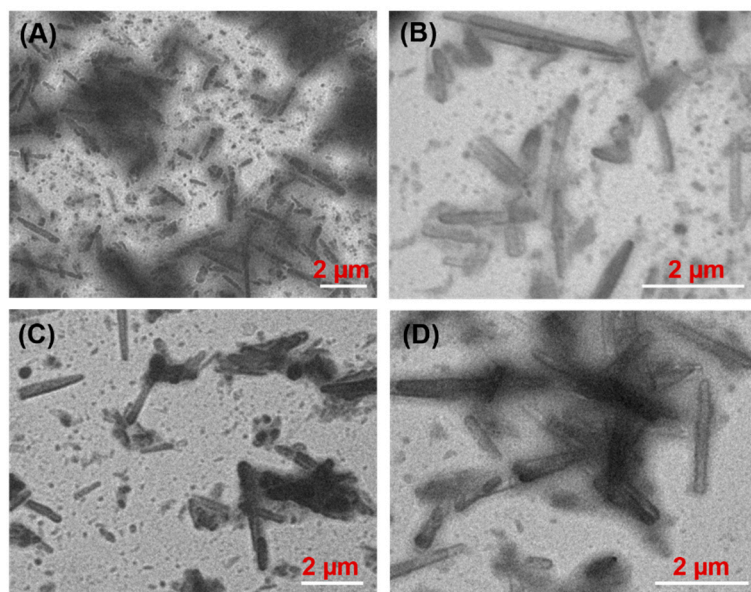


Figure 5. TEM images of oleogels prepared by C14-lys-C14 in olive oil (A), corn germ oil (B), soybean oil (C), and linseed oil (D).

Figure 5 presents the TEM images of the crystal network of oleogels formed by C14-lys-C14 in four vegetable oils, which show that all oleogel crystals were needle-like, regardless of oil type. For the four tested samples, the dimensions of the needle-like crystals were apparently unaffected by the oil type.

3.5. OBC of Oleogels

The OBC evaluation relates the strength of oleogels with the ability to retain the oil in the oleogel structure, showing the capacity of the oleogel structure to entrap oil. The OBC results of different vegetable oil gels are shown in Figure 6. We can see from Figure 6 that, at MGC concentration, the OBC of the oleogels is related to both the gelator and the vegetable oil type. When C8-lys-C8 was used as a gelator, the soybean oil gel showed the best capacity for entrapping oil, while the corn germ oil gel showed a weak oil-binding capacity. When C10-lys-C10 was used as a gelator, the linseed oil gel showed the weakest oil-entrapping capacity. As for C12-lys-C12, the order of oil-entrapping capacity in different vegetable oils was consistent with C8-lys-C8. While for C14-lys-C14, the order was consistent with C10-lys-C10. In general, C14-lys-C14 as a gelator performed the best in entrapping oils. This might be due to the sufficient amount of gelator in vegetable oils, because of the highest MGC for C14-lys-C14. Contrasting the rheological properties of gels in Figure 2, there is a positive correlation between the OBC values and the strength of the gels formed by C8-lys-C8, C12-lys-C12 and C14-lys-C14, but no such correlation was found for C10-lys-C10 gels.

Similarly, the OBC increased with increased gelator concentration within a certain range, and the ability to retain oil was enhanced [21]. For all four gelators, the highest OBC was obtained in soybean oil, followed by olive oil. This is likely owing to the different compositions of vegetable oils, which in turn, affects the interaction between gelators and vegetable oil molecules, resulting in the difference in OBC.

The oil-binding capacity of an oleogel is perhaps its most important measure of functionality since it will dictate which applications may benefit from oil gelation. For example, oleogels have been considered as fat replacements for meat products. An oleogel with a low oil-entrapping capacity would easily exude oil into the surrounding food matrix upon chewing, altering the textural and sensory properties of the product in an undesirable manner [36].

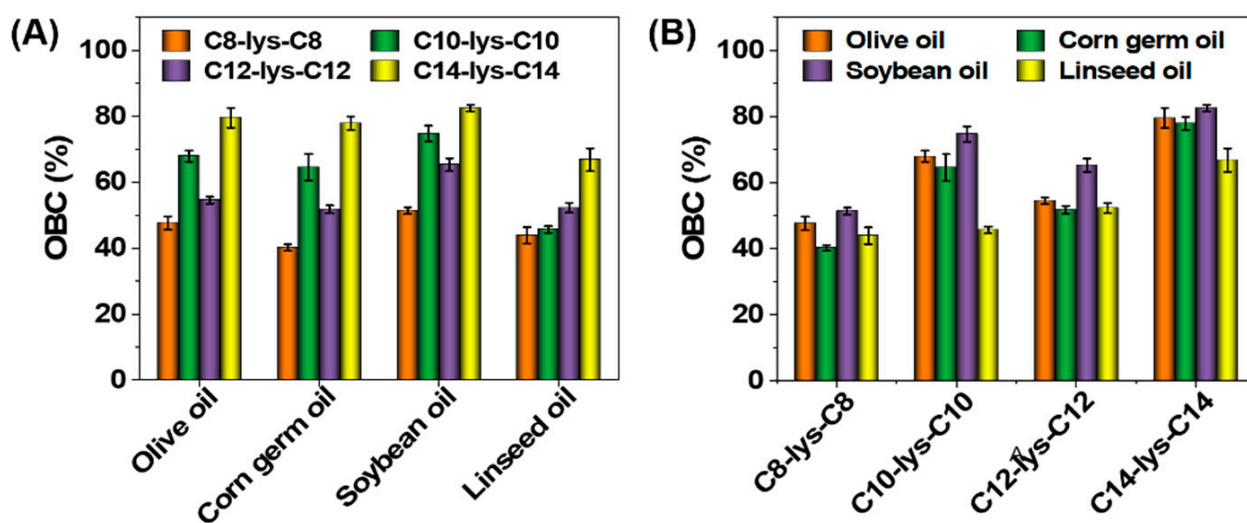


Figure 6. OBC of oleogels formed by four L-lysine-based gelators in different vegetable oils: (A) Comparison of different gelators, (B) Comparison of different oils.

4. Conclusions

Four N^α, N^ϵ -diacyl-L-lysines (i.e., N^α, N^ϵ -dioctanoyl-L-lysine; N^α, N^ϵ -didecanoyl-L-lysine; N^α, N^ϵ -dilauroyl-L-lysine; and N^α, N^ϵ -dimyristoyl-L-lysine) were synthesized through the Schotten–Baumann reaction. The four compounds can be applied as organogelators for preparing oleogels in olive oil, corn germ oil, soybean oil, and linseed oil. The gelation ability is not only related to the structure of the gelator, but is also affected by the composition of the oil. The MGC increased with the increase in the acyl carbon-chain length of the gelators. For each gelator, the strongest gelation ability was displayed in olive oil. The rheological properties, morphology, and oil-binding capacity of the formed oleogels were also affected by both gelators and oil types, because the hydrophobicity and H-bonding provided by the alkyl chain and amide group are probably responsible for the gelation of N^α, N^ϵ -diacyl-L-lysines in vegetable oils.

Author Contributions: Q.L. was responsible for analyzing the data and for writing and preparation of the original draft; J.Z. was responsible for data curation. G.Z. was responsible for reviewing and editing the writing; B.X. was responsible for supervision. All authors have read and agreed to the published version of the manuscript.

Funding: This research was funded by the National Key R&D Program of China, grant number 2017YFB0308701, and the National Natural Science Foundation of China, grant numbers 21676003, 21902004, and 22008002.

Institutional Review Board Statement: Not applicable.

Informed Consent Statement: Not applicable.

Data Availability Statement: Not applicable.

Acknowledgments: All the authors gratefully acknowledge the National Key R&D Program of China (2017YFB0308701), and the National Natural Science Foundation of China (21676003, 21902004, and 22008002).

Conflicts of Interest: The authors declare no conflict of interest.

Sample Availability: Samples of the compounds prepared in the paper are available from the authors.

References

- Du, X.; Zhou, J.; Shi, J.; Xu, B. Supramolecular hydrogelators and hydrogels: From soft matter to molecular biomaterials. *Chem. Rev.* **2015**, *115*, 13165–13307. [CrossRef] [PubMed]
- Draper, E.R.; Adams, D.J. Low-Molecular-Weight gels: The state of the art. *Chem* **2017**, *3*, 390–410. [CrossRef]

3. Raeburn, J.; Zamith Cardoso, A.; Adams, D.J. The importance of the self-assembly process to control mechanical properties of low molecular weight hydrogels. *Chem. Soc. Rev.* **2013**, *42*, 5143–5156. [CrossRef]
4. Heeres, A.; van der Pol, C.; Stuart, M.; Friggeri, A.; Feringa, B.L.; van Esch, J. Orthogonal Self-Assembly of low molecular weight hydrogelators and surfactants. *J. Am. Chem. Soc.* **2003**, *125*, 14252–14253. [CrossRef] [PubMed]
5. Bonifazi, E.L.; Edelsztejn, V.C.; Menéndez, G.O.; Samaniego López, C.; Spagnuolo, C.C.; Di Chenna, P.H. Versatile Supramolecular Organogel with Outstanding Stability toward Aqueous Interfaces. *ACS Appl. Mater. Interfaces* **2014**, *6*, 8933–8936. [CrossRef]
6. Sangeetha, N.M.; Maitra, U. Supramolecular gels: Functions and uses. *Chem. Soc. Rev.* **2005**, *34*, 821–836. [CrossRef]
7. Mayr, J.; Saldías, C.; Díaz Díaz, D. Release of small bioactive molecules from physical gels. *Chem. Soc. Rev.* **2018**, *47*, 1484–1515. [CrossRef]
8. Rizzo, C.; Andrews, J.L.; Steed, J.W.; D’Anna, F. Carbohydrate-supramolecular gels: Adsorbents for chromium(VI) removal from wastewater. *J. Colloid Interfaces Sci.* **2019**, *548*, 184–196. [CrossRef]
9. Marr, P.C.; Marr, A.C. Ionic liquid gel materials: Applications in green and sustainable chemistry. *Green Chem.* **2016**, *18*, 105–128. [CrossRef]
10. D’Anna, F.; Rizzo, C.; Vitale, P.; Lazzara, G.; Noto, R. Dicationic organic salts: Gelators for ionic liquids. *Soft Matter* **2014**, *10*, 9281–9292. [CrossRef]
11. Wang, J.; Zhang, S.; Ma, Z.; Yan, L. Deep eutectic solvents eutectogels: Progress and challenges. *Green Chem. Eng.* **2021**, *2*, 359–367. [CrossRef]
12. Marullo, S.; Meli, A.; Giannici, F.; Anna, F.D. Supramolecular eutecto gels: Fully natural soft materials. *ACS Sustain. Chem. Eng.* **2018**, *6*, 12598–12602. [CrossRef]
13. Terech, P.; Weiss, R.G. Low molecular mass gelators of organic liquids and the properties of their gels. *Chem. Rev.* **1997**, *97*, 3133–3160. [CrossRef] [PubMed]
14. Hu, B.; Wang, W.; Wang, Y.; Yang, Y.; Xu, L.; Li, S. Degradation of glutamate-based organogels for biodegradable implants: In vitro study and in vivo observation. *Mater. Sci. Eng. C* **2018**, *82*, 80–90. [CrossRef]
15. Hu, B.; Yan, H.; Sun, Y.; Chen, X.; Sun, Y.; Li, S.; Jing, Y.; Li, H. Organogels based on amino acid derivatives and their optimization for drug release using response surface methodology. *Artif. Cells Nanomed. Biotechnol.* **2020**, *48*, 266–275. [CrossRef]
16. Dassanayake, L.S.K.; Kodali, D.R.; Ueno, S. Formation of oleogels based on edible lipid materials. *Curr. Opin. Colloid Interface Sci.* **2011**, *16*, 432–439. [CrossRef]
17. Patel, A.R. Edible “oleocolloids”: The final frontier in food innovation? *J. Agric. Food Chem.* **2017**, *65*, 3432–3433. [CrossRef]
18. Weiss, R.G. The past, present, and future of molecular gels. What is the status of the field, and where is it going? *J. Am. Chem. Soc.* **2014**, *136*, 7519–7530. [CrossRef]
19. Callau, M.; Sow-Kébé, K.; Nicolas-Morgantini, L.; Fameau, A. Effect of the ratio between behenyl alcohol and behenic acid on the oleogel properties. *J. Colloid Interfaces Sci.* **2020**, *560*, 874–884. [CrossRef]
20. Feng, G.; Chen, H.; Cai, J.; Wen, J.; Liu, X. L-Phenylalanine based Low-Molecular-Weight efficient organogelators and their selective gelation of oil from Oil/Water mixtures. *Soft Mater.* **2014**, *12*, 403–410. [CrossRef]
21. Luo, C.; Yang, B.; Zhou, Y.; Yang, J.; Han, F.; Baocai, X. Gelation properties and application based on amino acids gelators with four kinds of edible oils. *Colloid. Surf. A* **2020**, *585*, 124184. [CrossRef]
22. Pal, A.; Dey, J. L-Cysteine-Derived ambidextrous gelators of aromatic solvents and Ethanol/Water mixtures. *Langmuir* **2013**, *29*, 2120–2127. [CrossRef] [PubMed]
23. Ghosh, S.; Dey, J. Binding of fatty acid amide amphiphiles to bovine serum albumin: Role of amide hydrogen bonding. *J. Phys. Chem. B* **2015**, *119*, 7804–7815. [CrossRef] [PubMed]
24. Ghosh, A.; Dey, J. Effect of hydrogen bonding on the physicochemical properties and bilayer Self-Assembly formation of N-(2-Hydroxydodecyl)-l-alanine in aqueous solution. *Langmuir* **2008**, *24*, 6018–6026. [CrossRef]
25. Hai-Kuan, Y.; Hong, Z.; Pei-Ran, Y.; Chao-Hai, H. How do molecular structures affect gelation properties of supramolecular gels? Insights from low-molecular-weight gelators with different aromatic cores and alkyl chain lengths. *Colloid. Surf. A* **2017**, *535*, 242–250.
26. Suzuki, M.; Nakajima, Y.; Yumoto, M.; Kimura, M.; Shirai, H.; Hanabusa, K. Effects of Hydrogen Bonding and van der Waals Interactions on Organogelation Using Designed Low-Molecular-Weight Gelators and Gel Formation at Room Temperature. *Langmuir* **2003**, *19*, 8622–8624. [CrossRef]
27. Suzuki, M.; Hanabusa, K. l-Lysine-based low-molecular-weight gelators. *Chem. Soc. Rev.* **2009**, *38*, 967–975. [CrossRef]
28. Masahiro, S.; Tomoko, A.; Kenji, H. Low-molecular-weight gelators based on N^α-acetyl-N^ε-dodecyl-L-lysine and their amphiphilic gelation properties. *J. Colloid Interfaces Sci.* **2009**, *341*, 69–74.
29. Suzuki, M.; Yumoto, M.; Shirai, H.; Hanabusa, K. Supramolecular gels formed by amphiphilic low-molecular-weight gelators of N alpha, N epsilon-diacyl-L-lysine derivatives. *Chemistry* **2008**, *14*, 2133–2144. [CrossRef]
30. Ni, C.; Qi, K.; Jianhong, X.; Na, D.; Li, Y. Supramolecular gels: Using an amide-functionalized imidazolium-based surfactant. *J. Colloid Interfaces Sci.* **2018**, *511*, 215–221.
31. Fayaz, G.; Goli, S.A.H.; Kadivar, M. A novel propolis Wax-Based organogel: Effect of oil type on its formation, crystal structure and thermal properties. *J. Am. Oil Chem. Soc.* **2017**, *94*, 47–55. [CrossRef]
32. Sreenu, M.; Nayak, R.R.; Prasad, R.B.N.; Sreedhar, B. Synthesis, surface and micellar properties of sodium N-oleoyl amino acids. *Colloid. Surf. A* **2014**, *449*, 74–81. [CrossRef]

33. Deepnath, B.; Debmalya, G.; Joykrishna, D. A comparison of the self-assembly behaviour of sodium *N*-lauroyl sarcosinate and sodium *N*-lauroyl glycinate surfactants in aqueous and aqueo-organic media. *J. Colloid Interfaces Sci.* **2018**, *529*, 314–324.
34. Dassanayake, L.S.K.; Kodali, D.R.; Ueno, S.; Sato, K. Crystallization kinetics of organogels prepared by rice bran wax and vegetable oils. *J. Oleo Sci.* **2012**, *61*, 1–9. [CrossRef]
35. Doan, C.D.; Van de Walle, D.; Dewettinck, K.; Patel, A.R. Evaluating the Oil-Gelling properties of natural waxes in rice bran oil: Rheological, thermal, and microstructural study. *J. Am. Oil Chem. Soc.* **2015**, *92*, 801–811. [CrossRef]
36. Blake, A.I.; Marangoni, A.G. The use of cooling rate to engineer the microstructure and oil binding capacity of wax crystal networks. *Food Biophys.* **2015**, *10*, 456–465. [CrossRef]

Article

Neuraminidase Inhibitor of *Garcinia atroviridis* L. Fruits and Leaves Using Partial Purification and Molecular Characterization

Muchtaridi Muchtaridi ^{1,2,*}, Rina Fajri Nuwarda ², Emmy Hainida Khairul Ikram ³,
Aisyah Saad Abdul Rahim ⁴, Amirah Mohd Gazzali ⁵ and Habibah A. Wahab ⁵

¹ Functional Nano Powder University Center of Excellence (FiNder U CoE), Universitas Padjadjaran, Jl. Bandung-Sumedang KM 21, Jatinangor 45363, Indonesia

² Department of Pharmaceutical Analysis and Medicinal Chemistry, Faculty of Pharmacy, Universitas Padjadjaran, Jl. Bandung-Sumedang KM 21, Jatinangor 45363, Indonesia; rina.nuwarda@unpad.ac.id

³ Faculty of Health Sciences, Universiti Teknologi MARA, Bandar Puncak Alam 42300, Malaysia; emmy4546@uitm.edu.my

⁴ Faculty of Pharmacy, Universiti Teknologi MARA, Bandar Puncak Alam 42300, Malaysia; aisyahsaad@uitm.edu.my

⁵ School of Pharmaceutical Sciences, Universiti Sains Malaysia, Minden 11800, Malaysia; amirahmg@usm.my (A.M.G.); habibahw@usm.my (H.A.W.)

* Correspondence: muchtaridi@unpad.ac.id; Tel.: +62-22-8784288888 (ext. 3210)

Abstract: Neuraminidase (NA) is an enzyme that prevents virions from aggregating within the host cell and promotes cell-to-cell spread by cleaving glycosidic linkages to sialic acid. The best-known neuraminidase is the viral neuraminidase, which present in the influenza virus. Thus, the development of anti-influenza drugs that inhibit NA has emerged as an important and intriguing approach in the treatment of influenza. *Garcinia atroviridis* L. (GA) dried fruits (GAF) are used commercially as seasoning and in beverages. The main objective of this study was to identify a new potential neuraminidase inhibitor from GA. A bioassay-guided fractionation method was applied to obtain the bioactive compounds leading to the identification of garcinia acid and naringenin. In an enzyme inhibition study, garcinia acid demonstrated the highest activity when compared to naringenin. Garcinia acid had the highest activity, with an IC₅₀ of 17.34–17.53 µg/mL or 91.22–92.21 µM against *Clostridium perfringens*-NA, and 56.71–57.85 µg/mL or 298.32–304.31 µM against H1N1-NA. Based on molecular docking results, garcinia acid interacted with the triad arginine residues (Arg118, Arg292, and Arg371) of the viral neuraminidase, implying that this compound has the potential to act as a NA enzyme inhibitor.

Keywords: neuraminidase; *Garcinia atroviridis*; influenza virus

Citation: Muchtaridi, M.; Nuwarda, R.F.; Ikram, E.H.K.; Abdul Rahim, A.S.; Gazzali, A.M.; Wahab, H.A. Neuraminidase Inhibitor of *Garcinia atroviridis* L. Fruits and Leaves Using Partial Purification and Molecular Characterization. *Molecules* **2022**, *27*, 949. <https://doi.org/10.3390/molecules27030949>

Academic Editor: Mirella Nardini

Received: 18 November 2021

Accepted: 2 December 2021

Published: 30 January 2022

Publisher's Note: MDPI stays neutral with regard to jurisdictional claims in published maps and institutional affiliations.



Copyright: © 2022 by the authors. Licensee MDPI, Basel, Switzerland. This article is an open access article distributed under the terms and conditions of the Creative Commons Attribution (CC BY) license (<https://creativecommons.org/licenses/by/4.0/>).

1. Introduction

Influenza continues to be a significant public health concern since it causes annual epidemics, and has the potential to spark a global pandemic. Globally, annual seasonal influenza epidemics are predicted to result in approximately 3 to 5 million cases of severe illness, and 290,000 to 650,000 respiratory-related deaths [1]. Among the four genera of influenza viruses (influenza types A, B, C, and D), type A is the most pathogenic group of viruses capable of causing severe respiratory illnesses or death [2]. The 2009 swine flu H1N1 and the highly pathogenic avian flu H5N1 are among influenza A viruses that have posed significant health risks in many parts of the world. The World Health Organization determined swine flu (H1N1) to be a pandemic. There were 94,512 confirmed cases in 123 countries, including 112 cases in Malaysia [3].

In Indonesia, 200 cases of bird flu (H5N1) have been reported since 2003, with 168 deaths (case fatality rate: 84%) [4].

The influenza virus (IV) contains two major transmembrane glycoproteins: hemagglutinin (HA), and neuraminidase (NA), whose antigenic and genetic diversity are used to

determine IV subtypes. HA and NA can recognize the same host cell molecule, which is the sialic acid (SA) and play complementary roles during the replication cycle. A well-balanced action of HA and NA is crucial for establishing a productive infection [5].

The HA is responsible for the virus's initial attachment on the surface of cell receptor that is linked with terminal sialic acid. Furthermore, HA aids in the virus's internalization into the host cell via endocytosis, delivering the nucleoprotein into the cytoplasm. NA functions as a biological scissor, cleaving sialic acid residues from HA and cell surface glycans and facilitating virus movement during entry, and from the surface glycoprotein of newly synthesized virions, allowing the virus to be released from the host and spread to other cells [2].

As well as viruses, NA is also found in bacteria, protozoa, some invertebrates, and mammals [6,7]. Although they differ in binding affinity or substrate preference, they share several conserved domains and structural similarities [6]. NA plays a vital role in influenza virus replication and the presence of the conserved active site residues between species allows effective inhibition by the host immune defense and delay of virus progeny release from the infected cells. This will reduce the virus population and allow time for the host cell's immunity to eliminate the virus [8]. NA hydrolyzes α -2,3-sialic acid from sugar (galactose) and is also involved in α -2,6-sialic acid-galactosyl hydrolysis, but this is less efficient, especially if the aglycon is weak (sialic acid) [9]. As a result, the inhibition of NA has become the potential target in the design of anti-influenza drugs.

Oseltamivir (OTV) and zanamivir (ZANA) are two extensively used clinically effective anti-influenza drugs which were developed using the structure-based drug design (SBDD) approach. Both drugs are well-known to be effective in treating influenza in humans, but they do have resistance issues. Consequently, the discovery of new active compounds that are potent against NA but are not susceptible to resistance has become an important goal in the drug discovery of anti-influenza drugs, which is also the goal for this project.

Most NA inhibitors were developed through synthetic chemistry, as exemplified by oseltamivir [10], zanamivir [11], and peramivir [12]; however, natural products-derived bioactive compounds remain a viable option. The combination of the two approaches may also be possible. For example, shikimic acid, the starting compound in the synthesis of oseltamivir, is not economically feasible to be obtained via chemical synthesis, but can be efficiently isolated from Chinese star anise [13]. Indeed, natural products have been shown to contribute significantly in the development of potential drug candidates [14].

In peninsular Malaysia and Sumatra, Indonesia, *Garcinia atroviridis* (GA) dried fruits (GAF) are used commercially as seasoning and in beverages. The dried fruits, when sliced, are highly acidic. Its biological activities were previously reported, including antitumor, antioxidant, and antimicrobial activity [15]. The root part has also been shown to have anticancer and anti-inflammatory properties. On the east coast of Malaysia, and Sumatra, Indonesia, the leaves of GA (GAL) are eaten as a salad or vegetable. The leaves are wrapped around fish to prevent spoilage in steamed fish. In Sumatra, GAL is used to treat stomach pains caused by pregnancy [16]. A decoction of the leaves and roots of GA is used empirically to treat ear-aches [17].

Flavonoids are phytochemicals with a variety of phenolic structures. They are present in many plants, fruits, vegetables, and leaves, with potential applications in medicinal chemistry [18]. Flavonoids possess anti-inflammatory, anticancer, antioxidant [18], and antiviral properties [19,20]. These natural products are well known for their beneficial effects on health, and numerous efforts are being made to isolate the compounds [21]. As reviewed by Badshah et al., some flavonoids exhibit stronger antiviral activity than commercially available drugs in the treatment of viral infections. Flavonoid's phytochemicals suppress and act on viruses in a variety of ways. They can prevent viruses from attaching to and entering cells, interfering with several stages of viral DNA replication, protein translation, and polyprotein processing. Additionally, they can prevent viruses from being released and continue to infect other cells [20]. The current study aims to investigate the inhibitory activity of isolated compounds from *G. atroviridis* L. against

C. perfringens-NA and H1N1-NA. A bioassay-guided study was employed to isolate potential NA-inhibitors from GA. Bacterial NA from *Clostridium perfringens* were used as a starting point for bio-guided screening, followed by testing against NA from H1N1 virus.

2. Materials and Methods

2.1. Materials

2.1.1. Plant Materials

GA dried fruits and leaves were collected in Beruas, Perak. *G. atroviridis* leaves and fruits were oven-dried (40 °C). The specimens were identified in the Department of Biology's Laboratory of Plant Taxonomy Herbarium, Faculty of Mathematics and Natural Sciences, University of Padjadjaran (Bandung, Indonesia). Maceration with methanol (MeOH, 3 × 3 L, every 24 h) was used to extract dried fruit slices (1.1 kg), and the solvent was evaporated under reduced pressure to yield a concentrated MeOH extract (135.6 g). The MeOH extract (130 g) was partitioned with H₂O/MeOH (7:3) (300 mL) and extracted with *n*-hexane (1:1), followed by ethyl acetate (EtOAc, 3 × 300 mL), yielding 15.3 g *n*-hexane extract and 20.0 g EtOAc extract. *G. atroviridis* dried leaves (GAL, 220.78 g) were macerated with MeOH (3 × 1 L) to produce green gum (47.4 g). It was partitioned with H₂O/MeOH (4:1) (250 mL) and extracted with *n*-hexane (1:1), followed by EtOAc (3 × 250 mL). Under reduced pressure, *n*-hexane and EtOAc were removed, yielding a greenish gum weighing 8.5 g and 23.2 g as *n*-hexane extract and EtOAc extract, respectively.

2.1.2. Chemicals Assay

NA from bacteria *C. perfringens*, 2'-2-(4-Methylumbelliferyl)- α -D-N-acetylneuraminic acid sodium salt hydrate (MUNANA), and 2-(*N*-morpholino) ethanesulfonic acid (MES) were obtained from Sigma (New York, NY, USA). NA from H1N1 virus was obtained from SinoBio (Shanghai, China).

2.1.3. NA Enzymes Preparation

The bacterial NA stock 100U (*C. perfringens*) (Sigma, N2876, New York, NY, USA) and 600 μ L of NA from H1N1 strain A/CALIFORNIA/04/2009 (SinoBio, Shanghai, China) were suspended separately in 1 mL of MES buffer. The NA stock concentration was 200 mU/mL (*C. perfringens*) and 1200 pmoles/mL (H1N1). The NA solutions were stored at -20 °C unless used immediately. The optimization of NA was performed according to a previously reported study [22]. MUNANA (50 μ M), *C. perfringens*-NA (50 mU/mL), and H1N1-NA (45 mU/mL) were determined to be the best concentrations.

2.2. Methods

2.2.1. Column Chromatography

Column chromatography was performed using silica gel 60 (Merck, Kenilworth, NJ, USA, 230–400 mesh) and Cosmosil[®] 75C-18PREP reverse phase columns (150–230 mesh) (Nacalai Tasque Inc., Kyoto, Japan). Thin Layer Chromatography (TLC) was performed using pre-coated silica gel 60 F254 and RP-18 reversed phase C18 (Merck, layer thickness 0.25 mm). The components were detected under UV 254 and 366 nm or sprayed with 1% vanillin in concentrated H₂SO₄, followed by heating (40 °C). On a glass plate, preparative layer chromatography (PLC) was carried out using pre-coated silica gel 60 F254 (Merck, 20 × 20 cm, layer thickness 0.25, 0.5, or 1.0 mm).

2.2.2. General Experiments and Spectroscopy

The ¹H and ¹³C NMR spectra were recorded at 500 MHz using a BRUKER AVANCE III spectrometer (Rheinstetten, Germany), and the values were reported in parts per million (ppm). Depending on the solubility of the compounds, samples (isolated compounds) were dissolved in deuterated organic solvents. Semi-polar compounds were dissolved in deuterated chloroform (CDCl₃), whereas polar compounds were dissolved in 99% D₂O. The mass spectra were obtained using an Agilent 1100 Series LC-MSD-Trap-VL

spectrometer (Agilent Technologies, Avondale, AZ, USA) using electrospray ionization as the ion source type. FTIR and UV spectra were recorded using IR-Prestige-21 (Shimadzu, Kyoto, Japan) spectrometer, and a UV-Vis spectrophotometer (specord-200, Analytical Jena, Germany), respectively. An electrothermal melting point apparatus was used STUART-SMP10 (Cole Parmer, Staffordshire, UK) to obtain melting points. The rotation index was determined using ADP 120 Bellingham (Bellingham & Stanley, Kent, UK).

2.2.3. Isolation of Compounds from GAF

Since EtOAc extract was the most active against *C. perfringens*-NA and H1N1-NA, it was fractionated to isolate the active compounds. The fractionation of EtOAc extract was performed column chromatography vacuum with gradient system n-Hexane:EtOAc stepwise 10%, (10:0 to 0:10). It yielded five fractions (GF1: 0.9 g, GF2: 0.9 g, GF3: 0.9 g, GF4: 1.6 g, and GF5: 0.9 g). In terms of fractions with activity, only GF3 and GF4 were isolated further to yield GF31 and GF41, respectively. EtOAc was used to purify the GF3 precipitate to obtain GF31 (567.5 mg). GF41 was obtained by precipitating GF4 and washing it with hexane-EtOAc (7:3) to produce a white powder (1.1102 g). The hexane-EtOAc filtrate was evaporated to obtain a solid amorphous yellow GAF1 (254.0 mg). TLC (RP-C18) was used to monitor GF31, GF41, and GF42 using BuOH-CH₃COOH-H₂O, 4:1:5 as the mobile phase.

2.2.4. Spectral Data of Garcinia Acid (GM6 or D2)

GF31, GF41, and GF42 all had the same R_f (0.45) and were consequently classified as GAF1. It was obtained in the form of a brownish amorphous solid with a melting point of 176–178 °C (178 °C, [23]). Garcinia acid was characterized as follows: $[\alpha]_D^{25} = +100^\circ$ (c = 1, H₂O); UV(MeOH), λ_{\max} at 273 nm. IR-max cm⁻¹: 3435 (br, OH), 1801, 1762 (C=O). 1120, 1087 (CO-O). ESI-MS m/z 378.99 [2M-H]⁺ and ESI (pos)-MS m/z 191.1 [M+H]⁺ (calcd for C₆H₈O₈, 190.11). ¹H NMR (500 MHz, MeOD) δ ppm 2.72 (d, J = 17.50 Hz, H-4a), 3.26 (d, J = 17.5 Hz, H-4b), 4.31 (s, 3-OH), 4.92 (1H, H-2). ¹³C NMR (500 MHz, MeOD) δ ppm 41.06 (s, C-4) 80.78 (C-3) 86.23 (C-2) 170.16 (C-5) 172.77 (C-1') 175.86 (C-2'). These results were consistent with the previously published garcinia acid data [24].

2.2.5. Extraction and Isolation of Compounds from GAL

The EtOAc extract (6.3 g) was then subjected to vacuum silica gel column chromatography (1 × 30 cm), and successively eluted with n-hexane-EtOAc stepwise 10%, EtOAc-MeOH (7:3), and MeOH to yield 28 fractions (60 mL each) labelled as GALF1 (1–2), GALF2 (3–18), GALF3 (19–22), and GALFF4 (23–28). These fractions were monitored by TLC silica gel 60 F254 using n-hexane-EtOAc (3:2) as the mobile phase. GALF2 was further subjected to column chromatography with the solvent n-hexane-EtOAc (3:2), yielding a green precipitate. This precipitate was washed with n-hexane (8.9 mg) to obtain naringenin (GAL1). Acetone was used to dissolve the GALF3 precipitate, which was then crystallized by EtOAc to produce the amorphous GAL2 (22.6 mg). GAL2 had the same R_f as garcinia acid.

2.2.6. Spectral Data of Naringenin (GAL1)

GAL1 was white amorphous, with a melting point of 250–253 °C (250–252 °C, [25]). GAF1 was characterized as follows: $[\alpha]_D^{25} = -100^\circ$ (c = 1, MeOH); UV[(MeOH), λ_{\max}] at 326 and 289. IR-max cm⁻¹: 3257, 3404 (br, OH), 1609 (C=O), 2969, 2925 (C=C). ESI-MS m/z: 273 [M+H]⁺ (calcd for C₁₅H₁₂O₅, 272.25). ¹H NMR (500 MHz, DMSO-*d*₆) δ ppm 2.69 (dd, J = 17.10, 3.07 Hz, 1H, H-3eq), 3.27 (dd, J = 17.18, 12.77 Hz, 1H, H-3ax), 5.44 (dd, J = 12.77, 2.84 Hz, 1H, H-2), 5.89 (s, 1H, H-6), 6.80 (d, J = 9, 1H, H-3', H-5'), 7.31 (d, J = 9, 1H, H-2', H-6'), 8.31 (s, 7-OH), 9.6 (s-5-OH), 12.15 (s, 4'H). ¹³C NMR (500 MHz, DMSO-*d*₆) δ ppm 41.93 (C-3), 78.39 (C-2), 94.94 (C-8), 95.75 (C-6), 101.73 (C-10), 115.12 (C-3', C-5'), 128.29 (C-2', C-6'), 128.82 (C-1'), 157.68 (C-4'), 162.91 (C-9), 163.44 (C-5), 166.62

(C-7), 196.34 (C-4). These findings were consistent with the previously published narigenin data [26,27].

2.2.7. MUNANA Assays

The MUNANA assay was used to evaluate compounds, extracts, and fractions. MUNANA is a fluorescence-based assay that measures the fluorogenic product 4-methylumbelliferone released by the enzymatic activity of influenza virus NA from the substrate 2'-(4-methylumbelliferyl)-D-N-acetylneuraminic acid (MUNANA). MUNANA is a reliable method for assessing the inhibitory effects of NA drugs. MUNANA compares uninhibited NA activity of a virus or bacteria to enzymatic activity after incubation with a range of NI drug concentrations, allowing the determination of IC₅₀ value as the drug concentration required to reduce NA activity by 50% [28]. Using a micropipette, 25 L of MES buffer was first added to rows A-G and columns 2–12. 50 µL of 1000 µg/mL NA inhibitors were added to the first empty column A-C for one NI and D-F for the second NI. Following that, 25 µL NA was added to each well (row A-G and column 1–12), while 50 µL MES buffer was added to wells in row H (column 1–2) for blank readings. The mixtures were incubated for 30 min in a 37 °C incubator with the plate covered with aluminum foil.

Following incubation, 50 µL of MUNANA substrate was added to each well, whereas 50 µL of NA and MUNANA were added to row H as a positive control (column 3–4). The mixtures were then incubated for an additional hour at 37 °C. After incubation, the reaction was stopped by adding 100 µL of stop solution to each well. Finally, the plate was read using UV excitation on a microplate reader (Turner Biosystem, Sunnyvale, USA).

2.2.8. Data Analysis of Assay

The results were processed using GraphPad Prism v. 5 by fitting experimental data to the logistic graph, which involved percent inhibition over a range of concentrations. The inhibition constant (IC₅₀) was determined by plotting the graph at 50% inhibition using nonlinear regression analysis with the GraphPad Prism software (San Diego, CA, USA). On a semi-log plot, the results were plotted as percent inhibition activity versus inhibitor concentration (nM). The inhibitor concentration was expressed as 0.48 to 250 µg/mL, as the concentration of the inhibitor in the final assay volume.

2.2.9. Molecular Docking

The methods of molecular docking simulation were performed from our previous study [29]. The NA protein of subtype N1 in complex with zanamivir (PDB code: 3B7E) was used as the target. This PDB (3B7E) is NA crystal structures with resolution 1.45 Å from protein virus isolated that recombinant NA from the 1918 influenza virus [30]. Molecular docking simulations were performed with AutoDock 4.2 [31].

3. Results

3.1. Bioassay-Guided Isolation of Active Compounds from GA

3.1.1. Isolation of Compounds from GAF (*G. atroviridis* Fruits)

The MeOH extract was evaluated against *C. perfringens*-NA, which resulted in an IC₅₀ value of 9.43 g/mL as shown in Figure 1. *n*-Hexane extracts were found to be less active against *C. perfringens*-NA, whereas EtOAc extracts were observed to be the most active against both *C. perfringens*-NA and H1N1-NA. Since EtOAc is the most active, it was further fractionated. The fractionation of EtOAc extract resulted in five fractions (GF1: 0.9112 g, GF2: 0.9395 g, GF3: 0.8918 g, GF4: 1.6145 g, and GF5: 0.9011 g).

The assay results revealed that GF2, GF3, and GF4 were active in inhibiting *C. perfringens*-NA. In contrast, as shown in Figure 2, GF2 was ineffective in inhibiting H1N1-NA.

GF3 precipitate was purified using EtOAc to obtain GF31 (567.5 mg). GF41 was obtained by precipitating GF4 and washing it with hexane-EtOAc, yielding a white powder (1.1102 g) and amorphous yellow solid? GF42 (254.0 mg). GF31, GF41, and GF42 showed the same 1D-NMR data (proton and carbon), thus the compounds were labelled GAF1.

The crude GAF1 was purified by washing with EtOAc and drying in a desiccator to yield clusters of brownish needle-shaped lactone crystals.

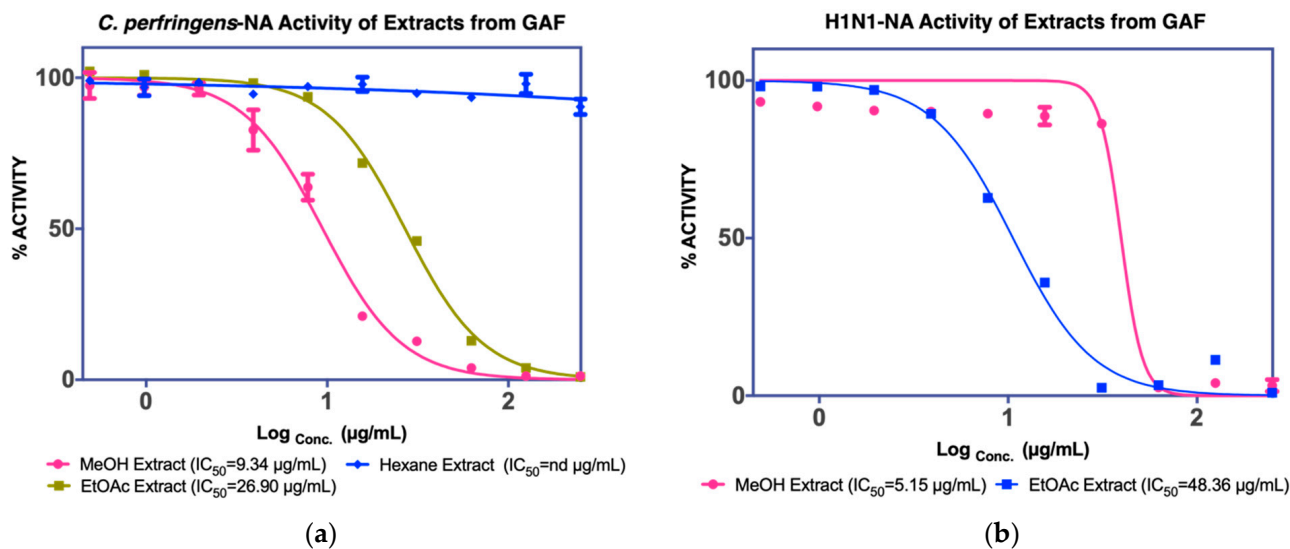


Figure 1. NA inhibition activity of GAF extracts against (a) *C. perfringens*-NA, (b) H1N1-NA.

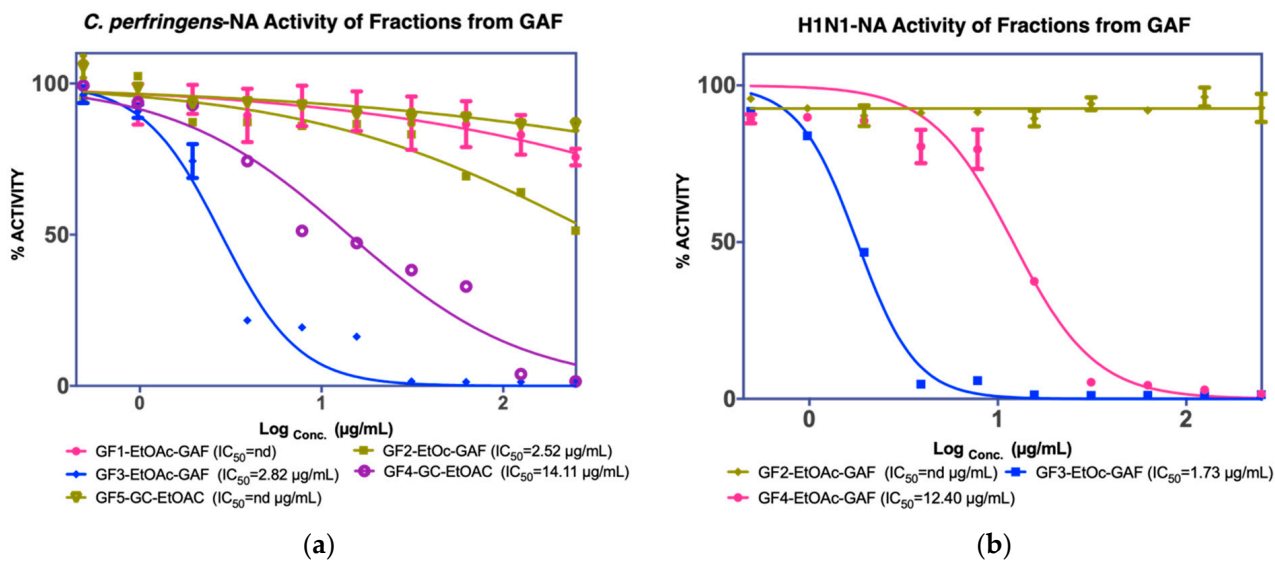


Figure 2. NA inhibition activity of GAF EtOAc fractions against (a) *C. perfringens*-NA, (b) H1N1-NA.

As illustrated in Figure 3, GAF1 was active against *C. perfringens*-NA and H1N1-NA. The IC_{50} values for *C. perfringens*-NA and H1N1-NA were 17.53 µg/mL or 92.21 µM and 57.85 µg/mL or 304.31 µM, respectively.

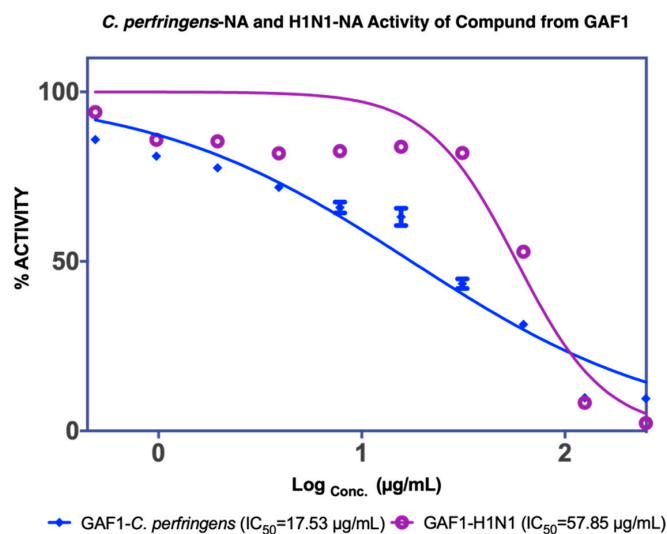


Figure 3. NA inhibition activity of GAF1 isolated compound from EtOAc fractions against *C. perfringens*-NA (blue) and H1N1-NA (purple).

3.1.2. Isolation of Compounds from GAL (*G. atroviridis* Leaves)

The MUNANA assay was performed to evaluate both extracts to confirm their activity against *C. perfringens*-NA and H1N1-NA, as shown in Figure 4a. The MeOH extract of GAL demonstrated significant inhibition of *C. perfringens*-NA with an IC₅₀ value of 36.17 g/mL and the EtOAc extract exhibited inhibitory activity against both NA (38.39 g/mL), and thus was isolated further to yield four fractions (GALF1, GALF2, GALF3, and GALF4).

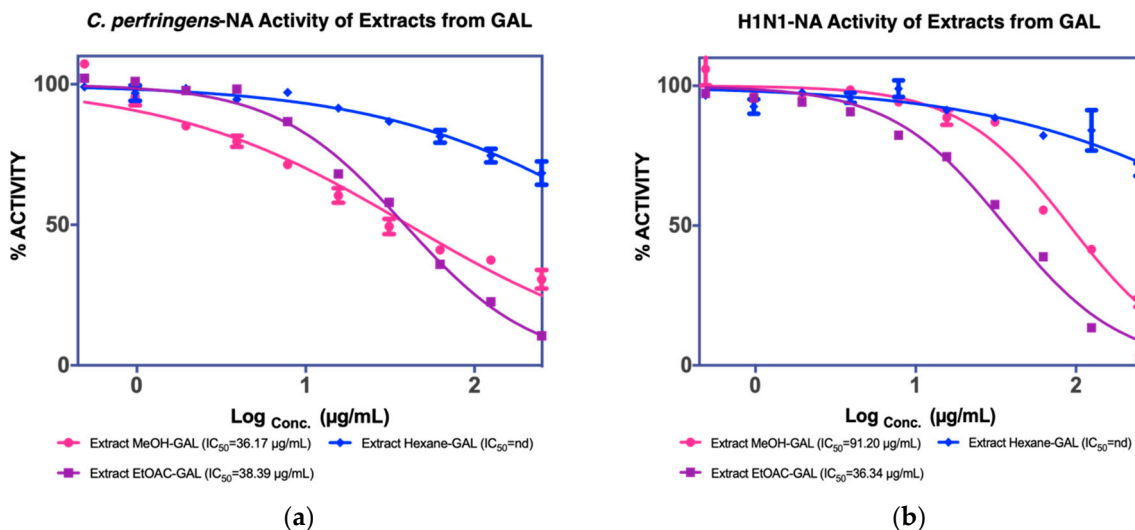


Figure 4. NA inhibition activity of GAL extract against (a) *C. perfringens*-NA, (b) H1N1-NA.

From the four fractions obtained, fractions GALF2 and (1.7772 g) and GALF3 (2.0258 g) showed good NA inhibition on both *C. perfringens* and H1N1, and GALF2 was further isolated to yield GAL1 (8.9 mg) and GAL2 (22.6 mg) (Figure 5). GAL2 has the same R_f as GAF1 (0.45, BuOH-CH₃COOH-H₂O 4:1:5) and showed inhibition against H1N1-NA with a maximum inhibitory concentration of 63.7% or an IC₅₀ of 56.71 µg/mL, as shown in Figure 6b.

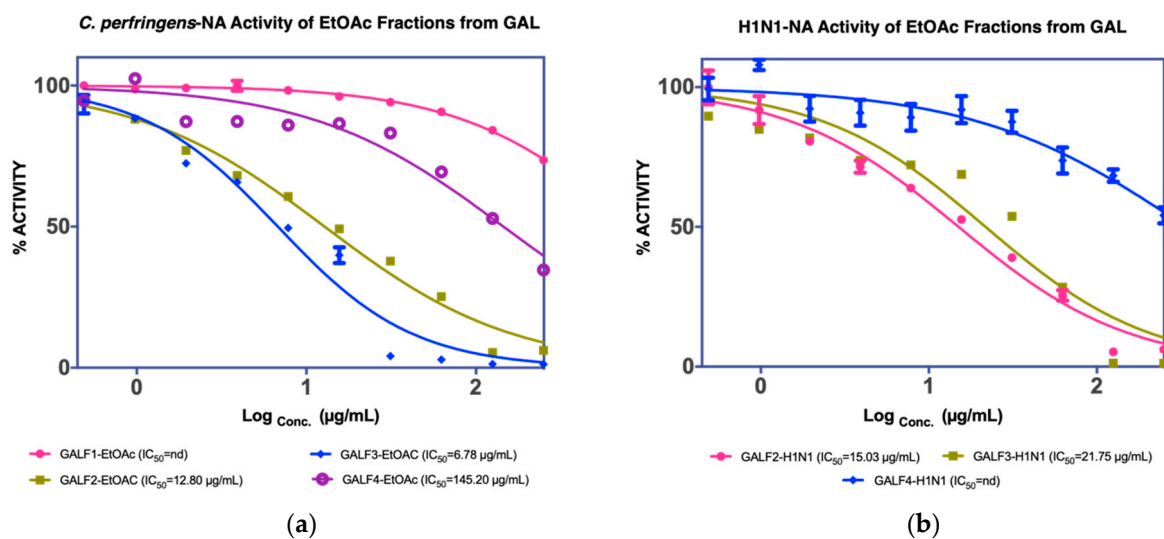


Figure 5. NA inhibition activity of GAL EtOAc fractions against (a) *C. perfringens*-NA, (b) H1N1-NA.

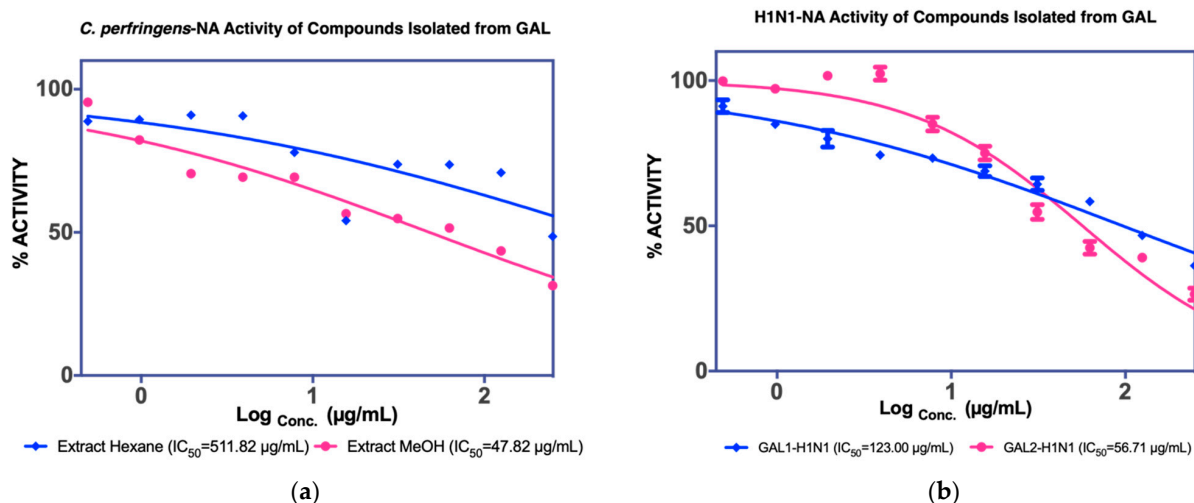


Figure 6. NA inhibition activity of GAL1 and GAL2 isolated compound from EtOAc fractions against (a) *C. perfringens*-NA, (b) H1N1-NA.

3.2. Structure Characterisation

3.2.1. Structure of GAF1 Compound

GAF1 crystallized into brownish crystals, as shown in Figure 7.



Figure 7. Crystal form of GAF1 compound.

The IR spectra at wavenumber 3376 cm^{-1} revealed a broad absorption band identified as the carboxylic acid hydroxyl group. Additionally, it was associated with the presence of a carbonyl group at 1734 cm^{-1} , while C-O-C ether was detected with a broad signal at 1232 cm^{-1} . However, this structure lacked a conjugated system of alkenes or an aromatic group, as evidenced by the absence of a weak stretching vibration at $2800\text{--}2900\text{ cm}^{-1}$.

The ^{13}C -NMR analysis revealed the presence of six carbons at δ 41.06 (C-4), 80.78 (C-2), 86.23 (C-3), 170.16 (C-1), 172.77 (C-6), and 175.86 (C-1) (C-5). 2D-HSQC findings showed that the chemical shift ^{13}C -NMR at δ 41.06 ppm was correlated with the ^1H -NMR at δ 2.72 and 3.26 ppm, whereas the chemical shift ^{13}C -NMR at δ 83.26 ppm was associated with δ 4.31 ppm (3-OH).

The chemical shift at 175.86 ppm in the 2D-HMBC spectrum, as shown in Table S1 and Figure 8, was identified as a carbonyl carbon, which correlated with three-bond correlations with H-4a, H-4b, and H-2 protons. The chemical shift at δ 170.16 ppm was identified as lactone carbonyl of C-5 by correlation (HMBC) between H-2 proton (δ 4.92, s) and H-4a (δ 2.72) and H-4b (δ 3.26). The C-2' carbonyl of carboxylic acid group was predicted to have a chemical shift at δ 175.86 ppm. The other carbonyl at δ 172.77 ppm was assigned to the other carbonyl of carboxylic acid group (C-1'), which was confirmed by its correlation with H-2 protons (4.92). (s, 1H). The positive-ESI mass spectrum's molecular ion peak at m/z 191 $[\text{M} + \text{H}]^+$ indicated that this compound had the molecular formula $\text{C}_6\text{H}_6\text{O}_7$. Compared to previous studies [24,32,33], GAF1 had the same structure as (2*S*,3*S*)-tetrahydro-3-hydroxy-5-oxofuran-2,3-dicarboxylic acid or garcinia acid, as illustrated in Figure 8.

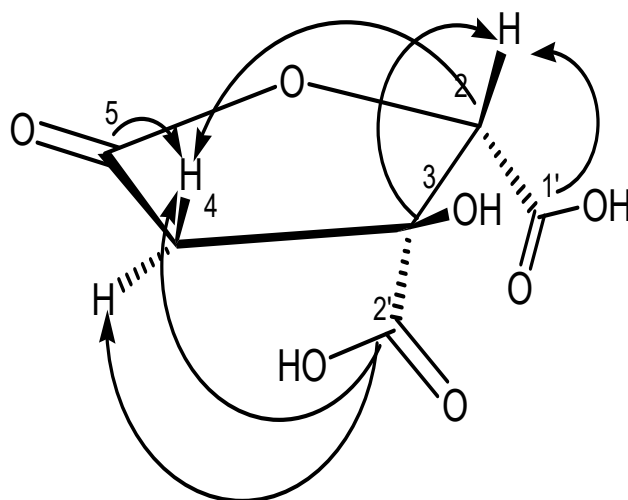


Figure 8. ^1H - ^{13}C long-range correlations in the 2D HMBC spectrum of GAF1.

The NMR data of GAL2 also showed similar spectra as GAF1, and is interpreted as garcinia acid. This was also in accordance with the data reported by Polavarapu et al. [33]. This means garcinia acid can be obtained from the fruits and leaves of *G. atroviridis*.

3.2.2. Structure of GAL1 Compounds

Absorption bands were detected in the IR spectra at 3404 cm^{-1} (-OH); 2967 cm^{-1} (sp² C-H stretching); 1609 cm^{-1} (>C=O); and 1460 cm^{-1} (C=C stretching aromatic). The UV spectra indicated the presence of phenolic derivatives at 225, 289, and 326 nm [34].

Two signals at δ 2.69 (3-H α , d, $J = 17.0$) and 3.27 ppm (3-H β , dd, $J = 17.0$) were attributed to C-3. The pattern of 1,2,3-tetrasubstituted ring A was generated by proton at 5.89 (H-6, $J = 2.95$) and 5.64 (H-8, $J = 2.95$). The doublet peak signals at 7.31 ($J = 9.0$) and 6.80 ($J = 9.0$) in ring B were assigned to H-2' or H-6' and H-3' or H-5', respectively. The ^1H -NMR spectrum data were not observed by the ^1H -NMR signals, despite the presence of the phenolic group indicated by the UV and IR spectrum.

The presence of fifteen carbons was confirmed by the ^{13}C NMR spectrum. DEPT90 demonstrated seven methylene carbons at 78.39 (C-2), 94.93 (C-8), 95.75 (C-6), 115.12 (x2) (C-3' and C-5'), and 128.29 (x2) (C-2' and C-6'), while DEPT135 revealed one methylene carbon at 41.93. (C-3). Six quaternary carbons were found at 128.82 (C-1'), 157.68 (C-4'), 162.90 (C-9), 101.73 (C-10), 168.48 (C-5), and 170.88 (C-5) (C-7). The presence of carbonyl (C-4) was indicated by the signal at 197.2. There were correlation signals in 2D-HMBC between C-2 at δc 78.39 and δH 7.31 (H-2') and 3.27 (H-3a) and 2.69 (H-3b); C-4 at δc 196.34 and δH 3.27 (H-3a) and 2.69 (H-3b); C-6 (95.75) and δH 5.64 (H-8); C-9 (162.90) and H-2' (7.31); C-4' (157.68) with 7.31 (H-2') and 6.80 (C-3'); C-5' (115.12) with 6.80 (C-3') and 7.31 (C-2'); C-6' (128.29) with 5.44 (H-2) and 7.31 (C-2'). The molecular ion peak of ESI-MS at m/z 273.2 ($\text{M}+\text{H}^+$) indicated that the structure corresponded to the molecular formula $\text{C}_{15}\text{H}_{12}\text{O}_5$.

As shown in Figure 9, the spectroscopic data were consistent with the literature [26,27] for naringenin or 2S-5,7,4'-trihydroxyflavanone, and the NMR data are listed in Table S2.

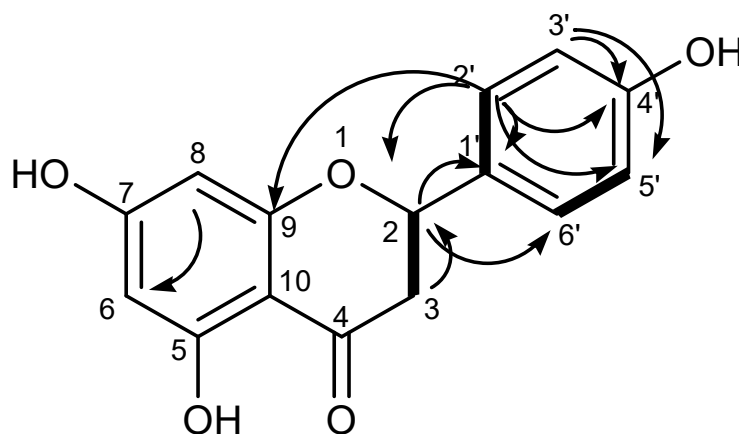


Figure 9. ^1H - ^{13}C long-range correlations in the 2D HMBC spectrum of compound GAL1.

3.3. Binding Interaction of Isolated Compound from *G. atroviridis*

The result of bioassay-guided isolation of GA is presented in Table 1. Molecular docking simulation was conducted on GAF1 and GAL1 against NA. As shown in Figure 10, GAF1 and GAL1 interacted well with the active site of NA.

The two carboxylic acid moieties present in the garcinia acid structure may play an important role in its activity against NA. As shown in Figure 10a, the carboxylic acid group at C-2 docked close to the arginine triad with strong hydrogen bonds (2–3 Å) and interacted with Tyr406 at a distance of 2.7–2.8 Å. However, no hydrophobic interaction was observed as it moved away from the hydrophobic residues (Ile222, Arg224, Ser246, and Glu276).

Naringenin interacted with the arginine triad via hydrogen bonding (with Arg118 and Arg371) and cation- π interactions (with Arg292), as illustrated in Figure 10b. Arg224 also formed a cation- π interaction with naringenin's ring C, but it docked away from the hydrophobic residues Ile222, Glu276, and Ser246, resulting in a less favorable interaction with the NA binding site.

Table 1. Highlight of NA inhibition activity isolation of *G. atroviridis* (fruits and leaves).

	Fractions-1	Fractions-2	Compounds
	Hexane fraction		
		F1 Not active	-
Fruits	MeOH extract IC ₅₀ <i>C. perfringens</i> -NA 9.4 µg/mL IC ₅₀ NA-H1N1 5.15 µg/mL	EtOAc fraction IC ₅₀ <i>C. perfringens</i> -NA 26.9 µg/mL IC ₅₀ NA-H1N1 48.36 µg/mL	F2 2.82 µg/mL ^a nd ^c
			F3 2.82 µg/mL ^a 1.73 µg/mL ^b
			F4 2.52 µg/mL ^a 12.4 µg/mL ^b
	Hexane fraction		
		F1 nd ^c	-
Leaves	MeOH extract IC ₅₀ <i>C. perfringens</i> -NA 36.17 µg/mL IC ₅₀ NA-H1N1 36.34 µg/mL	EtOAc fraction IC ₅₀ <i>C. perfringens</i> -NA 38.39 µg/mL IC ₅₀ NA-H1N1 48.36 µg/mL	F2 12.80 µg/mL ^a 15.03 µg/mL ^b
			F3 6.78 µg/mL ^a 15.03 µg/mL ^b
			F4 145.20 µg/mL ^a nd ^c

^a NA inhibition activity against *C. perfringens*-NA; ^b NA inhibition activity against H1N1-NA; ^c nd: not detected.

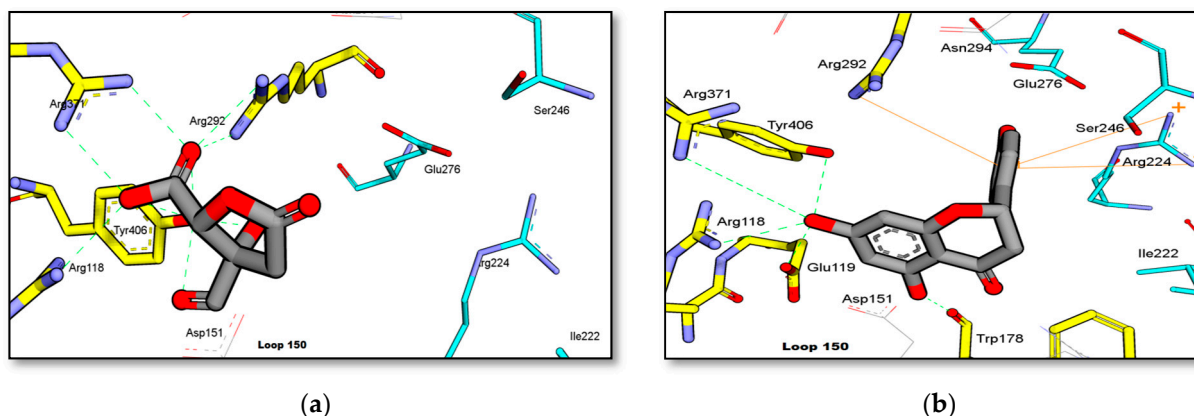


Figure 10. Binding interaction of (a) GAF1 (garcinia acid) and (b) GAL1 (naringenin) against H1N1-NA (PDB code: 3B7E). (Blue carbon: hydrophobic residue).

4. Discussion

The two compounds isolated from *G. atroviridis* were found to be active against NA. GAF1 and GAL2 have been identified as garcinia acid, while GAL1 has been identified as naringenin. Garcinia acid was found to be more active than naringenin, with IC₅₀ values of between 17.34–17.53 µg/mL against *C. perfringens*-NA and 56.71–57.85 µg/mL

against H1N1-NA. Garcinia acid and its derivatives have been shown to have biological activities including antifungal [35] and anti-atherosclerosis [36], besides being used as an active ingredient to aid in weight loss [37] or anti-obesity [38] via appetite suppression and inhibition of fat production. They form most of the content in GA's fruits, and are also known to be present in the root. In addition to garcinia acid, atroviridone, naringenin, and 3,8''-bi-naringenin were also previously reported to be isolated from the root, while atroviridin was isolated from the stem bark [39]. Garcinia acid obtained from the fruits (GAF1) and leaves (GAL2) of *G. atroviridis* has previously been isolated from *Garcinia cambogia*, *Hibiscus cannabinus* [23], *Garcinia indica*, and *Garcinia atroviridis* [40]. Although other pharmacological activities of garcinia acid have been described in the literature, its activity against NA or as anti influenza has never been reported.

Naringenin, on the other hand, is a flavanone derivative with a skeleton similar to xanthone. Citrus and grapefruit are the most common sources of this compound [41]. It was also discovered in the bark of *G. atroviridis*. Naringenin has been shown to have potent antioxidant [42], anti-inflammatory [43,44], antiandrogenic [45], estrogenic [46], monoamine oxidase (MAO)-inhibitor, [41] anticancer-antitumor [47], and anti-dyslipidaemia [44,46] properties. In this study, naringenin was found to have weak activity against NA, with IC₅₀ values of 107 µg/mL or 393.38 µM for *C. perfringens*-NA and 123 µg/mL or 452.20 µM for H1N1-NA. This is consistent with Liu et al. (2008) [48] who reported that this compound has a weak NA inhibitory activity with an IC₅₀ value greater than 100 µM. However, the authors did not explore the binding interaction in detail. This will be explained further below.

Based on the molecular docking results, the binding free energy of garcinia acid (−8.31 kcal/mol) and naringenin (−8.51 kcal/mol) against NA-H1N1 (3BE7) did not differ much. Both garcinia acid and naringenin interacted with important amino acids via hydrogen bonding, as can be seen in their interaction with the triad arginine residues. These triad arginine residues interacted with the carboxylate of the sialic acid substrate from the virus [49], providing a structural basis in the development of potent inhibitors. However, there was no hydrophobic interactions between garcinia acid and the lipophilic pocket of NA that consisted of several amino acids including Glu276, Ala246, Arg224, and Ile222 [50]. Naringenin has a strong hydrophobic interaction due to the formation of a *pi-pi* cation interaction between its aromatic ring and the hydrophobic residue of NA (orange line) as shown in Figure 10b. This interaction is believed to confer the inhibitory activity of these two compounds against NA [51]. NA inhibition activity of garcinia acid was contributed favourably by the carboxylic acid groups. However, the absence of hydrophobic interaction may be the reason for its weak activity. On the other hand, the lack of carboxylic acid moiety in naringenin can be considered as a significant drawback, thus seem to contribute towards the reduction of the activity reduces the activity of naringenin against NA. This is because of the important interaction that the carboxylic acid moiety contributed in the interaction of a ligand with Arg371, which is considered as the most important residue among the arginine triads that interact with the carboxylic acid moieties of NA inhibitors [52].

5. Conclusions

Bioassay-guided fractionation yielded garcinia acid and naringenin from *G. atroviridis* L. fruit and leaves, respectively. Both have inhibitory activity against the NA enzymes. Garcinia acid has a good inhibitory activity against *C. perfringens*-NA, with an IC₅₀ of 17.34–17.53 µg/mL, and 56.71–57.85 µg/mL against H1N1-NA. Garcinia acid was found to form a strong ionic interaction with triad arginine based on molecular docking study. The findings in this study provides insight into the ability of *G. atroviridis* to inhibit neuraminidase of influenza virus.

Supplementary Materials: The following are available online, Figure S1: Spectroscopy data of GAF1, Figure S2: Spectroscopy data of GAL1, Table S1: NMR data of Garcinia Acid and Table S2: NMR data of Naringenin.

Author Contributions: Conceptualization M.M. and H.A.W.; methodology, M.M. and A.S.A.R.; software, M.M.; validation, M.M., R.F.N. and E.H.K.I.; formal analysis, M.M. and R.F.N.; investigation, M.M. and A.M.G.; resources, M.M. and H.A.W.; data curation, M.M., R.F.N. and A.M.G.; writing—original draft preparation, M.M., A.M.G., E.H.K.I. and A.S.A.R.; writing—review and editing, M.M., H.A.W., E.H.K.I., A.M.G. and R.F.N.; visualization, R.F.N.; supervision A.S.A.R. and H.A.W.; project administration, M.M.; funding acquisition M.M. and H.A.W. All authors have read and agreed to the published version of the manuscript.

Funding: This research was funded by a Malaysian Ministry of Science, Technology, and Innovation grant through the Nutraceuticals R&D Initiative (09-05-IFN-MEB 004) and Academic Leadership Grants of Universitas Padjadjaran (1959/UN6.3.1/PT.00/2021).

Institutional Review Board Statement: Not applicable.

Informed Consent Statement: Not applicable.

Data Availability Statement: Not available.

Conflicts of Interest: The authors declare no conflict of interest.

Sample Availability: Samples of the garcinia acid and naringenin compounds are available from the authors.

References

- Iuliano, A.D.; Roguski, K.M.; Chang, H.H.; Muscatello, D.J.; Palekar, R.; Tempia, S.; Cohen, C.; Gran, J.M.; Schanzer, D.; Cowling, B.J.; et al. Estimates of global seasonal influenza-associated respiratory mortality: A modelling study. *Lancet* **2018**, *391*, 1285–1300. [CrossRef]
- Nuwarda, R.F.; Alharbi, A.A.; Kayser, V. An Overview of Influenza Viruses and Vaccines. *Vaccines* **2021**, *9*, 1032. [CrossRef]
- Lee, C.K. Influenza A/H1N1 Pandemic: The Scare of 2009. *Malays. J. Med. Sci.* **2009**, *16*, 1–4.
- Wignjadiputro, I.; Widaningrum, C.; Setiawaty, V.; Widuri Wulandari, E.; Sihombing, S.; Prasetyo, W.A.; Azhar, M.; iL Rim, K.; Pang Junxiong, V.; Waworuntu, W.; et al. Whole-of-society approach for influenza pandemic epicenter Containment exercise in Indonesia. *J. Infect. Public Health* **2020**, *13*, 994–997. [CrossRef]
- Gaymard, A.; Le Briand, N.; Frobert, E.; Lina, B.; Escuret, V. Functional balance between neuraminidase and haemagglutinin in influenza viruses. *Clin. Microbiol. Infect.* **2016**, *22*, 975–983. [CrossRef]
- Schwerdtfeger, S.M.; Melzig, M.F. Sialidases in biological systems. *Pharmazie* **2010**, *65*, 551–561.
- Sander-Wewer, M.; Schauer, R.; Corfield, A.P. Substrate specificity of viral, bacterial and mammalian sialidases with regard to different N,O-acetylated sialic acids and GM1. *Adv. Exp. Med. Biol.* **1982**, *152*, 215–222. [PubMed]
- Garman, E.; Laver, G. Controlling influenza by inhibiting the virus's neuraminidase. *Curr. Drug Targets* **2004**, *5*, 119–136. [CrossRef]
- Barnard, K.N.; Alford-Lawrence, B.K.; Buchholz, D.W.; Wasik, B.R.; LaClair, J.R.; Yu, H.; Honce, R.; Ruhl, S.; Pajic, P.; Daugherty, E.K.; et al. Modified Sialic Acids on Mucus and Erythrocytes Inhibit Influenza A Virus Hemagglutinin and Neuraminidase Functions. *J. Virol.* **2020**, *94*, e01567-19. [CrossRef] [PubMed]
- Kim, C.U.; Lew, W.; Williams, M.A.; Liu, H.; Zhang, L.; Swaminathan, S.; Bischofberger, N.; Chen, M.S.; Mendel, D.B.; Tai, C.Y.; et al. Influenza neuraminidase inhibitors possessing a novel hydrophobic interaction in the enzyme active site: Design, synthesis, and structural analysis of carbocyclic sialic acid analogues with potent anti-influenza activity. *J. Am. Chem. Soc.* **1997**, *119*, 681–690. [CrossRef] [PubMed]
- von Itzstein, M.; Wu, W.Y.; Kok, G.B.; Pegg, M.S.; Dyason, J.C.; Jin, B.; Van Phan, T.; Smythe, M.L.; White, H.F.; Oliver, S.W.; et al. Rational design of potent sialidase-based inhibitors of influenza virus replication. *Nature* **1993**, *363*, 418–423. [CrossRef] [PubMed]
- Mancuso, C.E.; Gabay, M.P.; Steinke, L.M.; Vanosdol, S.J. Peramivir: An intravenous neuraminidase inhibitor for the treatment of 2009 H1N1 influenza. *Ann. Pharm.* **2010**, *44*, 1240–1249. [CrossRef] [PubMed]
- Anderson, K.A. Method of Isolating Shikimic Acid from a Plant. U.S. Patent 8,203,020, 19 June 2012.
- Newman, D.J.; Cragg, G.M.; Snader, K.M. Natural products as sources of new drugs over the period 1981-2002. *J. Nat. Prod.* **2003**, *66*, 1022–1037. [CrossRef] [PubMed]
- Mackeen, M.M.; Mooi, L.Y.; Amran, M.; Mat, N.; Lajis, N.H.; Ali, A.M. Noncytotoxic and Antitumour-Promoting Activities of Garcinia Acid Esters from *Garcinia atroviridis* Griff. ex T. Anders (Guttiferae). *Evid. Based Complementary Altern. Med.* **2012**, *2012*, 829814. [CrossRef] [PubMed]
- Grosvenor, P.W.; Gothard, P.K.; McWilliam, N.C.; Supriono, A.; Gray, D.O. Medicinal plants from Riau province, Sumatra, Indonesia. Part 1: Uses. *J. Ethnopharmacol.* **1995**, *45*, 75–95. [CrossRef]

17. Burkill, I.H.; William, B.; Foxworthy, F.W.; Scrivenor, J.B.; Watson, J.G. *Dictionary of the Economic Products of the Malay Peninsula*, 2nd ed.; Crown Agent: Kuala Lumpur, Malaysia, 1966; p. 255.
18. Ullah, A.; Munir, S.; Badshah, S.L.; Khan, N.; Ghani, L.; Poulson, B.G.; Emwas, A.H.; Jaremko, M. Important Flavonoids and Their Role as a Therapeutic Agent. *Molecules* **2020**, *25*, 5243. [CrossRef] [PubMed]
19. Adamczak, A.; Ożarowski, M.; Karpiński, T.M. Antibacterial Activity of Some Flavonoids and Organic Acids Widely Distributed in Plants. *J. Clin. Med.* **2019**, *9*, 109. [CrossRef] [PubMed]
20. Badshah, S.L.; Faisal, S.; Muhammad, A.; Poulson, B.G.; Emwas, A.H.; Jaremko, M. Antiviral activities of flavonoids. *Biomed. Pharmacother.* **2021**, *140*, 111596. [CrossRef]
21. Atanasov, A.G.; Zotchev, S.B.; Dirsch, V.M.; Orhan, I.E.; Banach, M.; Rollinger, J.M.; Barreca, D.; Weckwerth, W.; Bauer, R.; Bayer, E.A.; et al. Natural products in drug discovery: Advances and opportunities. *Nat. Rev. Drug Discov.* **2021**, *20*, 200–216. [CrossRef]
22. Ikram, N. *Discovery of New Neuraminidase Inhibitors from Plant Natural Compounds: Virtual Screening and Bioassays Studies*; USM: Penang, Malaysia, 2012.
23. Lewis, Y.S.; Neelakantan, S. (–)-Hydroxycitric acid—The principal acid in the fruits of *Garcinia cambogia* desr. *Phytochemistry* **1965**, *4*, 619–625. [CrossRef]
24. Hida, H.; Yamada, T.; Yamada, Y. Production of hydroxycitric acid by microorganisms. *Biosci. Biotechnol. Biochem.* **2005**, *69*, 1555–1561. [CrossRef]
25. Andrade, C.A.d.; Carvalho, J.L.d.S.; Cunico, M.M.; Lordello, A.L.L.; Higaskino, C.E.K.; Almeida, S.C.d.C.; Dias, J.d.F.G.; Kerber, V.A.; Miguel, M.D.; Miguel, O.G. Antioxidant and antibacterial activity of extracts, fractions and isolated substances from the flowers of *Acacia podalyriifolia* A. Cunn. ex G. Don. *Braz. J. Pharm. Sci.* **2010**, *46*, 715–722. [CrossRef]
26. Ibrahim, A.R. Sulfation of naringenin by *Cunninghamella elegans*. *Phytochemistry* **2000**, *53*, 209–212. [CrossRef]
27. Du, Q.; Jerz, G.; Winterhalter, P. Preparation of Three Flavonoids from the Bark of *Salix alba* by High-Speed Countercurrent Chromatographic Separation. *J. Liq. Chromatogr. Relat. Technol.* **2005**, *27*, 3257–3264. [CrossRef]
28. Hurt, A. Fluorometric Neuraminidase Inhibition Assay. Available online: http://www.nisn.org/documents/A.Hurt_Protocol_for_NA_fluorescence.pdf (accessed on 3 March 2015).
29. Muchtaridi, M.; Sugijanto, M.; Mohd Gazzali, A.; Wahab, H.A. Anti-Neuraminidase Bioactives from Manggis Hutan (*Garcinia celebica* L.) Leaves: Partial Purification and Molecular Characterization. *Molecules* **2020**, *25*, 821. [CrossRef]
30. Xu, X.; Zhu, X.; Dwek, R.A.; Stevens, J.; Wilson, I.A. Structural characterization of the 1918 influenza virus H1N1 neuraminidase. *J. Virol.* **2008**, *82*, 10493–10501. [CrossRef] [PubMed]
31. Lindstrom, W.; Morris, G.M.; Weber, L.; Huey, R. Using AutoDock for Virtual Screening. Available online: http://autodock.scripps.edu/faqs-help/tutorial/using-autodock-for-virtual-screening/UsingAutoDockforVirtualScreening_v7.pdf (accessed on 14 February 2003).
32. Ibnusaud, I.; Thomas, P.T.; Rani, R.N.; Sasi, P.V.; Beena, T.; Hisham, A. Chiral γ -butyrolactones related to optically active 2-hydroxycitric acids. *Tetrahedron* **2002**, *58*, 4887–4892. [CrossRef]
33. Polavarapu, P.L.; Scalmani, G.; Hawkins, E.K.; Rizzo, C.; Jeirath, N.; Ibnusaud, I.; Habel, D.; Nair, D.S.; Haleema, S. Importance of solvation in understanding the chiroptical spectra of natural products in solution phase: *Garcinia* acid dimethyl ester. *J. Nat. Prod.* **2011**, *74*, 321–328. [CrossRef]
34. Mabry, T.; Markham, K.; Thomas, M. *The Systematic Identification of Flavonoids*; Springer: Berlin-Heidelberg, Germany; New York, NY, USA, 1970; Volume 1, pp. 84–234.
35. Mackeen, M.M.; Ali, A.M.; Lajis, N.H.; Kawazu, K.; Kikuzaki, H.; Nakatani, N. Antifungal *Garcinia* acid esters from the fruits of *Garcinia atroviridis*. *Z. Für Nat. C J. Biosci.* **2002**, *57*, 291–295. [CrossRef]
36. Amran, A.A.; Zaiton, Z.; Faizah, O.; Morat, P. Effects of *Garcinia atroviridis* on serum profiles and atherosclerotic lesions in the aorta of guinea pigs fed a high cholesterol diet. *Singap. Med. J.* **2009**, *50*, 295–299.
37. Onakpoya, I.; Hung, S.K.; Perry, R.; Wider, B.; Ernst, E. The Use of *Garcinia* Extract (Hydroxycitric Acid) as a Weight loss Supplement: A Systematic Review and Meta-Analysis of Randomised Clinical Trials. *J. Obes.* **2011**, *2011*, 509038. [CrossRef]
38. Heymsfield, S.B.; Allison, D.B.; Vasselli, J.R.; Pietrobello, A.; Greenfield, D.; Nunez, C. *Garcinia cambogia* (hydroxycitric acid) as a potential antiobesity agent: A randomized controlled trial. *J. Am. Med. Assoc.* **1998**, *280*, 1596–1600. [CrossRef] [PubMed]
39. Kosin, J.; Ruangrunsi, N.; Ito, C.; Furukawa, H. A xanthone from *Garcinia atroviridis*. *Phytochemistry* **1998**, *47*, 1167–1168. [CrossRef]
40. Venkateswara Rao, G.; Karunakara, A.C.; Santhosh Babu, R.R.; Ranjit, D.; Chandrasekara Reddy, G. Hydroxycitric acid lactone and its salts: Preparation and appetite suppression studies. *Food Chem.* **2010**, *120*, 235–239. [CrossRef]
41. Collins, D.; Kopic, S.; Geibel, J.P.; Hogan, A.M.; Medani, M.; Baird, A.W.; Winter, D.C. The flavonone naringenin inhibits chloride secretion in isolated colonic epithelia. *Eur. J. Pharmacol.* **2011**, *668*, 271–277. [CrossRef]
42. Cavia-Saiz, M.; Busto, M.D.; Pilar-Izquierdo, M.C.; Ortega, N.; Perez-Mateos, M.; Muniz, P. Antioxidant properties, radical scavenging activity and biomolecule protection capacity of flavonoid naringenin and its glycoside naringin: A comparative study. *J. Sci. Food Agric.* **2010**, *90*, 1238–1244. [CrossRef]
43. Bodet, C.; La, V.D.; Epifano, F.; Grenier, D. Naringenin has anti-inflammatory properties in macrophage and ex vivo human whole-blood models. *J. Periodontal Res.* **2008**, *43*, 400–407. [CrossRef]
44. Salehi, B.; Fokou, P.V.T.; Sharifi-Rad, M.; Zucca, P.; Pezzani, R.; Martins, N.; Sharifi-Rad, J. The Therapeutic Potential of Naringenin: A Review of Clinical Trials. *Pharmaceuticals* **2019**, *12*, 11. [CrossRef] [PubMed]

45. Zierau, O.; Morrissey, C.; Watson, R.W.; Schwab, P.; Kolba, S.; Metz, P.; Vollmer, G. Antiandrogenic activity of the phytoestrogens naringenin, 6-(1,1-dimethylallyl)naringenin and 8-prenylnaringenin. *Planta Med.* **2003**, *69*, 856–858. [CrossRef]
46. Zierau, O.; Gester, S.; Schwab, P.; Metz, P.; Kolba, S.; Wulf, M.; Vollmer, G. Estrogenic activity of the phytoestrogens naringenin, 6-(1,1-dimethylallyl)naringenin and 8-prenylnaringenin. *Planta Med.* **2002**, *68*, 449–451. [CrossRef]
47. Sabarinathan, D.; Mahalakshmi, P.; Vanisree, A.J. Naringenin promote apoptosis in cerebrally implanted C6 glioma cells. *Mol. Cell. Biochem.* **2010**, *345*, 215–222. [CrossRef] [PubMed]
48. Liu, A.L.; Wang, H.D.; Lee, S.M.; Wang, Y.T.; Du, G.H. Structure-activity relationship of flavonoids as influenza virus neuraminidase inhibitors and their in vitro anti-viral activities. *Bioorg. Med. Chem.* **2008**, *16*, 7141–7147. [CrossRef] [PubMed]
49. McAuley, J.L.; Gilbertson, B.P.; Trifkovic, S.; Brown, L.E.; McKimm-Breschkin, J.L. Influenza Virus Neuraminidase Structure and Functions. *Front. Microbiol.* **2019**, *10*, 39. [CrossRef] [PubMed]
50. Kim, C.U.; Lew, W.; Williams, M.A.; Wu, H.; Zhang, L.; Chen, X.; Escarpe, P.A.; Mendel, D.B.; Laver, W.G.; Stevens, R.C. Structure-activity relationship studies of novel carbocyclic influenza neuraminidase inhibitors. *J. Med. Chem.* **1998**, *41*, 2451–2460. [CrossRef] [PubMed]
51. Kim, C.U.; Chen, X.; Mendel, D.B. Neuraminidase inhibitors as anti-influenza virus agents. *Antivir. Chem. Chemother.* **1999**, *10*, 141–154. [CrossRef] [PubMed]
52. Yen, H.-L.; Hoffmann, E.; Taylor, G.; Scholtissek, C.; Monto, A.S.; Webster, R.G.; Govorkova, E.A. Importance of neuraminidase active-site residues to the neuraminidase inhibitor resistance of influenza viruses. *J. Virol.* **2006**, *80*, 8787–8795. [CrossRef]

Article

Preservative Effect on Canned Mackerel (*Scomber colias*) Lipids by Addition of Octopus (*Octopus vulgaris*) Cooking Liquor in the Packaging Medium

José M. Malga ¹, Marcos Trigo ¹, Beatriz Martínez ² and Santiago P. Aubourg ^{1,*}

¹ Department of Food Technology, Marine Research Institute (CSIC), c/Eduardo Cabello, 6, 36208 Vigo, Spain; jmalga@alumnos.uvigo.es (J.M.M.); mtrigo@iim.csic.es (M.T.)

² Department of Food Technologies, CIFP Coroso, Avda. da Coruña, 174, 15960 Ribeira, Spain; bmartinezr@edu.xunta.gal

* Correspondence: saubourg@iim.csic.es

Abstract: The preservative properties of waste liquor obtained from octopus (*Octopus vulgaris*) cooking were investigated. Three different concentrations (high, medium, and low) of octopus cooking liquor (OCL) were included, respectively, in the aqueous packaging medium employed for mackerel (*Scomber colias*) canning. As a result, the canning process led to an increase ($p < 0.05$) of lipid content, lipid oxidation (development of fluorescent compounds and thiobarbituric acid reactive substances, TBARS), lipid hydrolysis (formation of free fatty acids, FFA) and $\omega 3/\omega 6$ ratio in fish muscle. In all canned samples, primary (peroxides) and secondary (TBARS) levels of lipid oxidation were low. Remarkably, the presence in the packaging medium of the high and medium OCL concentrations led to lower ($p < 0.05$) lipid oxidation development (fluorescent compound and TBARS detection, respectively). Furthermore, an increasing OCL presence led to an average decrease of peroxide and FFA content and to an average increase of the polyene index (PI). All OCL-packaged muscle showed lower average values of saturated fatty acids and $\omega 3/\omega 6$ ratio and higher average values of PI and monounsaturated fatty acid presence. This study provides a first approach to novel and beneficial use of the present marine waste to inhibit lipid damage of commercial canned fish.

Keywords: *octopus vulgaris*; cooking liquor; *scomber colias*; canning; packaging medium; lipid hydrolysis; lipid oxidation; polyene index; $\omega 3/\omega 6$ ratio

Citation: Malga, J.M.; Trigo, M.; Martínez, B.; Aubourg, S.P. Preservative Effect on Canned Mackerel (*Scomber colias*) Lipids by Addition of Octopus (*Octopus vulgaris*) Cooking Liquor in the Packaging Medium. *Molecules* **2022**, *27*, 739. <https://doi.org/10.3390/molecules27030739>

Academic Editor: Mirella Nardini

Received: 22 December 2021

Accepted: 21 January 2022

Published: 24 January 2022

Publisher's Note: MDPI stays neutral with regard to jurisdictional claims in published maps and institutional affiliations.



Copyright: © 2022 by the authors. Licensee MDPI, Basel, Switzerland. This article is an open access article distributed under the terms and conditions of the Creative Commons Attribution (CC BY) license (<https://creativecommons.org/licenses/by/4.0/>).

1. Introduction

As a result of processing, the fishing, aquaculture, and foodstuff industries generate a wide range of byproducts and wastes [1,2]. Among such undervalued products, wastewaters generated by seafood processing have been recognised as rich in healthy and nutritional constituents but constitute one of the most important environmental problems of coastline areas [3,4]. Commonly, these byproducts are dumped into the sea without previous treatment of depuration, thus causing serious environmental pollution [3,5]. To prevent water pollution, achieve complete utilisation of available nutrients (mainly proteins, $\omega 3$ polyunsaturated fatty acids, and valuable flavour and aroma compounds), and offer a commercial gain for the food industry, an effective recycle and utilisation of wastewater byproducts is of critical importance [5,6].

On the basis of the great commercial importance of tuna species canning, the greatest efforts for employing wastewaters from seafood processing have been addressed for tuna cooking juices [7]. Thus, Ahn and Kim [8] showed that taurine, glutamic acid, phenylalanine, and alanine were the major amino acids resulting from neutrase hydrolysis of tuna skipjack (*Katsuwonus pelamis*) cooking juice. Later on, Jao and Ko [9] proved the DPPH (2,2'-diphenyl-1-picrylhydrazyl) radical scavenging capacity of the hydrolysate tuna (*Thunnus*

tonggol) cooking juice by isolation and identification of the resulting peptides from proteolytic digestion. Remarkably, tuna cooking juices without previous enzymatic treatment were satisfactorily employed for producing dried tuna flavour powder [10] and proved to be rich in nutrients and antioxidant properties (DPPH and ABTS, 3-ethylbenzothiazoline-6-sulphonic acid, assays) [11].

Octopus species constitute popular seafood that are typically commercialised fresh, frozen, or dried salted, both at the artisan and industrial scales [12,13]. In addition to highly nutritional and medicinal value products, octopus processing has shown to generate a lot of byproducts including high functional value, thus indicating a promising potential for the integrated exploitation and utilisation of bioactive substances [14,15]. Among octopus processing wastes, cooking liquor or juice has acquired the interest of technologists and the fish trade, although previous research cannot be considered as abundant as in the case of tuna cooking liquor. Thus, Oh et al. [16] showed remarkable antihypertensive and antioxidant (Rancimat assay) effects for this kind of octopus waste material. Furthermore, Kim et al. [17] proved that a 70% ethanol extract from the cooking drip of Giant Pacific octopus (*Enteroctopus dofleini*) included a marked polyphenol compound content as well as manifested a radical scavenging activity (DPPH and FRAP, ferric reducing antioxidant power, assays) and an inhibitory activity against tyrosine and angiotensin I-converting enzyme. An antioxidant capacity (DPPH assay) was also detected by Choi et al. [18] in cooking drip from the same octopus species, with this effect increasing if a previous gamma-irradiation was applied. With an industrial and microbiological focus, Vázquez and Murado [19] showed that enzymatic hydrolysis of wastewater from industrial processing of octopus (*Octopus vulgaris*) could be a good source of peptones for lactic acid bacteria production.

In the current study, the preservative properties of waste liquor obtained from octopus (*Octopus vulgaris*) cooking were investigated. Three different volumes of such liquor (10, 15, and 50 mL) were included, respectively, in the packaging medium employed for Atlantic mackerel (*Scomber colias*) canning (C-10, C-15, and C-50 packaging conditions, respectively) and compared to control canned fish (C-CT packaging condition). The effect of OCL packaging on lipid hydrolysis and oxidation, fatty acid (FA) profile (saturated FA, STFA; monounsaturated FA, MUFA; polyunsaturated FA, PUFA), and FA ratios (polyene index, PI; $\omega 3/\omega 6$ ratio) in canned mackerel was determined.

2. Results and Discussion

2.1. Moisture and Lipid Content

Values obtained in raw samples for moisture ($690.4 \pm 19.1 \text{ g}\cdot\text{kg}^{-1}$ muscle) and lipid ($80.7 \pm 2.10 \text{ g}\cdot\text{kg}^{-1}$ muscle) constituents (Table 1) are in agreement with those values found for fatty fish species [20]. Canning process led to a decrease ($p < 0.05$) in moisture content, with values in the $596\text{--}611 \text{ g}\cdot\text{kg}^{-1}$ range. This level of decrease can be explained on the basis of denaturation and decrease of water-holding capacity of fish proteins as a result of the thermal treatment, thus leading to water loss from the muscle into the packaging medium [21,22]. Contrarily, lipid content in canned mackerel muscle showed a marked ($p < 0.05$) increase that can be explained as a result of the loss of water and hydrophilic constituents from the muscle into the packaging medium [23].

Table 1. Moisture and lipid content ($\text{g}\cdot\text{kg}^{-1}$ muscle) * in initial and canned mackerel packaged under different conditions including octopus cooking liquor (OCL) **.

Constituent	Initial Fish	Canned Fish			
		C-CT	C-10	C-25	C-50
Moisture	690.4 ^b (19.1)	596.6 ^a (17.1)	601.0 ^a (20.9)	610.6 ^a (24.3)	598.5 ^a (30.8)
Lipids	80.7 ^a (21.0)	153.5 ^b (9.5)	148.4 ^b (20.5)	132.6 ^b (12.6)	156.2 ^b (34.5)

* Average values of four replicates ($n = 4$); standard deviations are indicated in brackets. Average values accompanied by different lowercase letters (^{a,b}) denote significant differences ($p < 0.05$) as a result of packaging condition. ** Packaging conditions: C-CT (control packaging), C-10 (low-concentrated OCL packaging), C-25 (medium-concentrated OCL packaging), and C-50 (high-concentrated OCL packaging).

Concerning the effect of the OCL in the covering system, comparison of control canned fish with canned samples including the OCL packaging did not provide significant differences ($p > 0.05$) for moisture and lipid contents; additionally, a definite trend on the presence of both constituents was not detected ($p > 0.05$) by increasing or decreasing the OCL concentration tested. The fact that no differences of moisture value were detected can be explained on the basis that the canned fish muscle was imbibed in an aqueous packaging medium; therefore, a strong interchange of water between both phases included in the can would be expected to occur [23,24]. Concerning possible lipid content differences, relevant fish-to-fish differences have been reported for the lipid content of fish muscle as a result of several internal and external factors [20,25]; consequently, the OCL presence and concentration in the packaging medium would not be likely to produce content differences in this muscle constituent.

Previous research concerning the effect on moisture and lipid content in canned fish muscle as a result of including preservative compounds in the covering medium can be considered very scarce. According to the present study, no effect on lipid content in canned Chub mackerel (*S. colias*) was observed by including alga (*Fucus spiralis* or *Ulva lactuca*) extracts in the filling medium [23].

2.2. Determination of Lipid Hydrolysis

This damage pathway was analysed by the free FA (FFA) assessment. A very low value was detected in starting raw fish (Figure 1), thus showing a good quality of the starting material employed in the current study. Canning led to a great ($p < 0.05$) increase of FFA content in all kinds of canned fish (28.0–31.6 $\text{g}\cdot\text{kg}^{-1}$ muscle range) (Figure 1). This result was in agreement with previous research related to fish canning [26,27]. A lower average FFA content was detected in canned samples including OCL in the packaging medium when compared to their counterpart samples corresponding to the canned control; remarkably, decreasing average values were obtained by increasing the OCL presence in the covering medium.

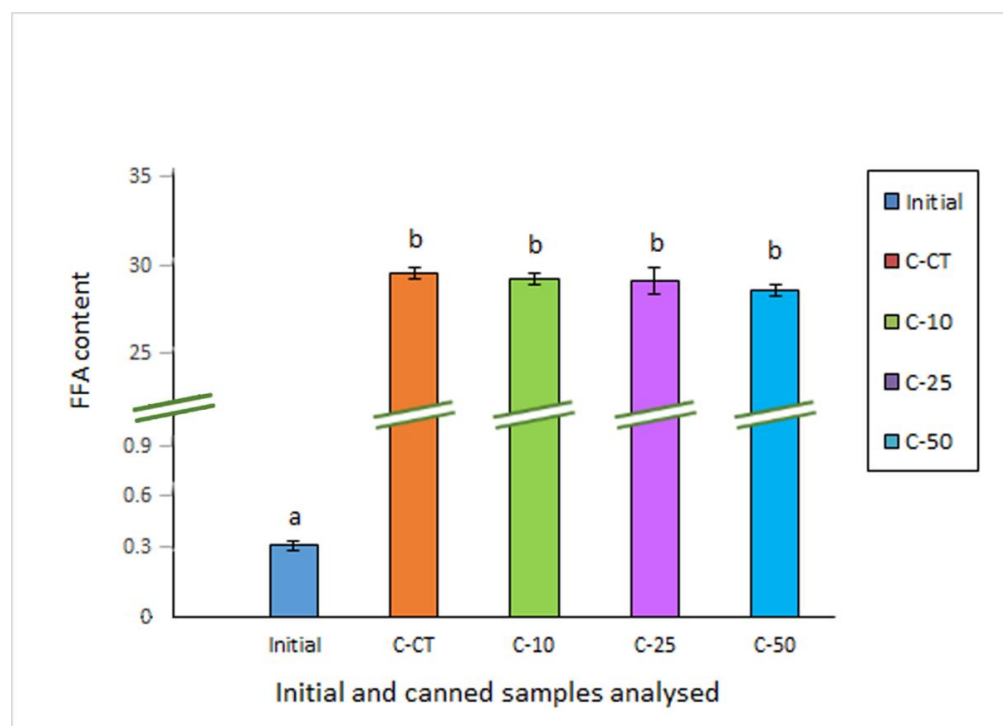


Figure 1. Determination of free fatty acid (FFA) content ($\text{g}\cdot\text{kg}^{-1}$ muscle) * in initial and canned mackerel packaged under different conditions including octopus cooking liquor (OCL) **. * Average values of four replicates ($n = 4$); standard deviations are indicated by bars. Average values accompanied by different lowercase letters (a,b) denote significant differences ($p < 0.05$) as a result of packaging condition. ** Packaging conditions as described in Table 1.

It is generally accepted that accumulation of FFA resulting from lipid hydrolysis in fish muscle has no nutritional significance. Nevertheless, this damage pathway has been recognised as an important event during fish processing leading to deteriorative changes of muscle texture, acceleration of lipid oxidation compounds formation, and off-odour and off-taste development [28,29]. In the current research, FFA content can be considered as the result of several factors. First, the sterilisation process can lead to hydrolysis of lipid classes such as triacylglycerides (TG) and phospholipids (PL) [24]. On the other hand, FFA are known to be rapidly oxidised by heating according to the fact that they provide a greater accessibility to oxygen and other oxidants in general when compared to TG and PL [30]. Finally, preservative compounds (i.e., antioxidant molecules) present in the OCL-packaging medium may protect FFA from oxidation and subsequent breakdown during the heating process. According to the marked differences found between raw and all canned samples, a strong hydrolytic effect of heating on TG and PL was produced in the present study. Furthermore, none of the OCL concentrations tested led to significant differences ($p > 0.05$) when compared to the control packaging. However, the fact that a lower average FFA content was detected in canned fish by increasing the presence of OCL indicates that some inhibitory effect on FFA formation has been produced, this effect being more notorious in fish corresponding to the C-50 packaging condition.

Previous research provides contradictory results when addressing the effect of packaging conditions on lipid hydrolysis development during the canning process. Thus, Medina et al. [31] showed that the extent and mechanism of lipolysis were not influenced by the packaging medium used (brine and soybean oil) when considering canned albacore (*Thunnus alalunga*). However, hydrolytic rancidity showed that FFA content in canned silver carp (*Hypophthalmichthys molitrix*) including olive oil or sunflower oil as covering medium was lower than in the case of employing brine or soybean oil [32]. Furthermore, the use of sunflower oil increased the protective effect of processed tuna (*Thunnus albacares*) against

lipid hydrolysis (FFA assessment) when compared to coconut and groundnut oils [33]. Remarkably, higher average FFA values were obtained in canned Atlantic mackerel (*Scomber scombrus*) by including *Bifurcaria bifurcata* extracts in the packaging medium [25]. Similarly, the presence of *F. spiralis* or *U. lactuca* extracts in the covering medium led to a higher average FFA value in canned Chub mackerel (*S. colias*) [23]. However, if a previous nine-day chilling storage was applied to canned Chub mackerel (*S. colias*), the presence of *F. spiralis* extracts in the packaging medium led to lower average FFA values in canned muscle [34].

2.3. Determination of Lipid Oxidation

Canning and thermal treatments in general have been proven to enhance lipid oxidation development during seafood processing [21,24]. This effect has been explained on the basis of the catalytic behaviour of thermal treatment on lipid oxidation development in marine lipids, such lipids being especially rich in PUFA. In order to provide an accurate analysis of the lipid oxidation evolution in the current study, determination of this damage pathway was carried out by assessing the formation of oxidation compounds at different levels, i.e., primary (peroxide value, PV), secondary (thiobarbituric acid reactive substances, TBARS), and tertiary (fluorescence ratio, FR).

Levels of primary oxidation compounds can be considered very low in raw and canned samples [35–37], with values in the 0.24–0.48 meq. active oxygen·kg⁻¹ lipids range (Table 2). Notably, higher average values were detected in canned fish corresponding to OCL-packaging conditions when compared to canned control and initial fish. Thus, canned fish muscle including any of the OCL packaging conditions showed higher ($p < 0.05$) peroxide levels than the raw fish; among OCL-treated fish, the lowest average value was obtained in the C-50 batch.

Table 2. Determination of lipid oxidation * in initial and canned mackerel packaged under different conditions including octopus cooking liquor (OCL) **.

Quality Index	Initial Fish	Canned Fish			
		C-CT	C-10	C-25	C-50
Peroxide value (meq. active oxygen·kg ⁻¹ lipids)	0.24 ^a (0.04)	0.29 ^{ab} (0.08)	0.48 ^b (0.17)	0.35 ^b (0.03)	0.31 ^b (0.09)
Thiobarbituric acid index (mg malondialdehyde·kg ⁻¹ muscle)	0.21 ^a (0.07)	0.43 ^b (0.10)	0.42 ^{ab} (0.13)	0.26 ^a (0.03)	0.29 ^{ab} (0.11)
Fluorescence ratio	3.53 ^a (0.47)	4.80 ^b (0.34)	4.18 ^{ab} (0.92)	3.87 ^{ab} (0.80)	3.72 ^a (0.66)

* Average values of four replicates ($n = 4$); standard deviations are indicated in brackets. Average values accompanied by different lowercase letters (^{a, b}) denote significant differences ($p < 0.05$) as a result of packaging condition. ** Packaging conditions as described in Table 1.

As for peroxides, thiobarbituric acid index (TBA-i) levels observed in raw and canned samples can be considered low [33,35] and were in the 0.21–0.43 mg malondialdehyde·kg⁻¹ muscle range. Additionally, TBARS formation during processing reflected a slight average value increase in all kinds of canned samples (Table 2). This increase was found to be higher ($p < 0.05$) in canned control samples, while canned samples including any of the OCL-packaging media did not provide significant differences ($p > 0.05$) with starting values. Remarkably, canned samples corresponding to C-25 condition showed lower values ($p < 0.05$) than their counterpart control samples.

Concerning tertiary lipid oxidation compounds, canning led to a general increase of fluorescent compound formation (FR increase), the highest average value being obtained for the control canned fish (Table 2). Notably, canned fish corresponding to the C-50 condition

showed a significantly lower ($p < 0.05$) value than control canned fish and did not provide significant differences ($p > 0.05$) when compared to the starting raw fish. Consequently, an inhibitory effect on the formation of this kind of lipid oxidation molecules was detected in the C-50 packaging batch.

In the present study, heat treatment had two opposite effects on the different kinds of lipid oxidation compounds [38,39]. Thermal treatment oxidised and facilitated the formation of primary, secondary, and tertiary oxidation compounds. On the other hand, heat treatment itself may cause degradation of such molecules, especially those produced in the first stages (namely, peroxides) of the development of this damage pathway. At advanced stages of lipid oxidation, both peroxide and carbonyl compounds (i.e., TBARS) are susceptible to react with nucleophilic-type molecules present in the fish muscle and lead to fluorescent compound formation [24,40]. Concerning the effect of OCL presence in the packaging medium, a slight preservative effect on peroxide breakdown could be concluded in fish corresponding to all OCL-canning conditions. Related to secondary and tertiary oxidation compounds, a marked formation was detected in canned samples (comparison between raw and canned control samples), so that formation of such molecules can be considered more important than their breakdown. Notably, an inhibitory effect ($p < 0.05$) of OCL packaging could be concluded on TBARS and fluorescent compound formation in C-25 and C-50 batches, respectively.

An antioxidant behaviour of liquors obtained from octopus species cooking has already been mentioned in previous literature concerning in vitro assays. Thus, Oh et al. [16] studied the components of octopus cooking drips and proved an antioxidant behaviour according to the Rancimat assay. Similarly, cooking drip from Giant Pacific octopus (*E. dofleini*) showed an antioxidant capacity (DPPH assay) that could be increased by previous gamma-irradiation [18]. Kim et al. [17] studied the 70% ethanol extract from the same octopus species; notably, the radical scavenging activity (FRAP and DPPH assays) and the content on proteins and polyphenol compounds was enhanced by increasing the previous gamma-irradiation dose. Related to cooking juice of tuna species, Li et al. [11] demonstrated an antioxidant behaviour according to the DPPH and ABTS assays. Furthermore, Jao and Ko [9] isolated and identified seven antioxidant peptides from tuna (*T. tonggol*) cooking juice by reversed phase HPLC; peptide sequences comprised four to eight amino acid residues, including valine, serine, proline, histidine, alanine, asparagine, lysine, glutamic acid, glycine, or tyrosine. Interestingly, low-molecular-weight peptides have been reported as having antioxidant properties (i.e., free radical scavengers and reducing agents) [41,42].

Previous research has addressed the effect on lipid oxidation by including other sources of antioxidant compounds in the packaging medium during fish canning. Thus, packaging employing extra-virgin olive oil showed a marked inhibition of lipid oxidation progress in canned tuna (*T. alalunga*) when compared to a covering medium consisting of a brine solution [43]; this effect was attributed to the high presence of polyphenol compounds in extra-virgin olive oil. A lower development of lipid oxidation (i.e., fluorescent compound formation) was observed by Naseri and Rezaei [44] in sunflower oil-canned sprat (*Clupeonella cultriventris*) when compared to its counterpart packaged in brine solution. Furthermore, the employment of olive oil as filling medium led to a lower TBARS formation in canned silver carp (*H. molitrix*) than in the case of including sunflower oil, soybean oil, or brine as packaging medium [31]. Similarly, the use of sunflower oil increased the protective effect of canned tuna (*T. albacares*) against lipid oxidation (TBARS assessment) when compared to packaging with coconut and groundnut oils [32]. The use of packaging media including antioxidant compounds obtained from algae species has also proved the inhibition of lipid oxidation progress in canned fish. This result was obtained in canned Atlantic mackerel (*S. scombrus*) by employing *B. bifurcata* extracts [33] and in Chub mackerel (*S. colias*) by addition of *F. spiralis* or *U. lactuca* extracts [23].

2.4. FA Analysis

Initial mackerel presented the following FA average composition ($\text{g}\cdot\text{kg}^{-1}$ lipids): 30.5 (C14:0), 4.5 (C15:0), 133.0 (C16:0), 37.8 (C16:1 ω 7), 7.3 (C17:0), 39.0 (C18:0), 162.3 (C18:1 ω 9), 35.8 (C18:1 ω 7), 8.5 (C18:2 ω 6), 20.9 (C20:1 ω 9), 2.7 (C20:2 ω 6), 7.3 (C20:4 ω 6), 3.5 (C22:1 ω 9), 62.2 (C20:5 ω 3), 2.9 (C22:4 ω 6), 5.1 (C24:1 ω 9), 13.4 (C22:5 ω 3), and 124.8 (C22:6 ω 3). FA analysis was carried out on all canned samples (data not shown). In order to better focus on possible quality changes, discussion of FA results is addressed to FA groups (STFA, MUFA, and PUFA) and FA ratios (PI and ω 3/ ω 6).

Concerning the STFA group, comparison between initial and control canned samples showed a slight increase of the average value as a result of the canning process (Table 3); remarkably, lower average values were detected in all canned samples including OCL in the packaging medium. However, differences were only found significant ($p < 0.05$) by comparing the initial samples and canned fish corresponding to C-25 and C-50 packaging conditions.

Table 3. Values * obtained for fatty acid (FA) groups ($\text{g}\cdot 100 \text{g}^{-1}$ total FA) and total ω 3/total ω 6 ratio in initial and canned mackerel packaged under different conditions including octopus cooking liquor (OCL) **.

FA Group or Ratio	Initial Fish	Canned Fish			
		C-CT	C-10	C-25	C-50
Total saturated FA	33.79 ^b (0.34)	34.41 ^{ab} (2.81)	32.16 ^{ab} (1.49)	33.18 ^a (0.18)	32.51 ^a (1.24)
Total monounsaturated FA	35.35 ^b (2.82)	30.51 ^{ab} (6.44)	34.79 ^{ab} (0.95)	31.29 ^a (0.95)	32.36 ^{ab} (4.16)
Total polyunsaturated FA	30.36 ^a (3.04)	35.07 ^{ab} (3.79)	33.05 ^{ab} (2.35)	35.52 ^b (1.13)	35.12 ^{ab} (4.87)
ω 3/ ω 6 ratio	9.04 ^a (1.10)	10.83 ^b (0.46)	9.09 ^{ab} (1.86)	9.53 ^{ab} (0.67)	9.86 ^{ab} (1.63)

* Average values of four replicates ($n = 4$); standard deviations are indicated in brackets. Average values accompanied by different lowercase letters (^a,^b) denote significant differences ($p < 0.05$) as a result of packaging condition. ** Packaging conditions as described in Table 1.

The MUFA average content in fish muscle showed a general decrease after the canning process (Table 3); however, the presence of OCL in the packaging medium led to higher average values than in the control canned fish. Differences were found significant ($p < 0.05$) in the case of the C-25 batch, with such samples showing a lower ($p < 0.05$) MUFA presence than in the initial raw fish.

An important increase in PUFA presence was detected in all canned samples when compared with the initial fish (Table 3); this effect was found to be significant ($p < 0.05$) in the case of C-25 canned fish. Notably, canned fish corresponding to C-25 and C-50 batches provided higher average values than fish corresponding to the control canned batch. A PUFA retention was also detected in canned salmon (*Salmo salar*) when including seaweed (*U. lactuca*, *Durvillaea antarctica*, and *Pyropia columbina*) extracts as part of the covering liquid [37]; additionally, a higher retention of astaxanthine was detected in canned salmon by the presence of algae extracts.

The assessment of the PI, measured as a FA content ratio, has recently attracted a great attention as a way of measuring the possible increase or decrease of the PUFA content during fish canning or fish processing in general and being directly related to the nutritional value [38,39]. In the current study, a general increase of the average PI score was obtained after the canning process (Figure 2). This increase was found to be higher when increasing the presence of OCL in the packaging medium; remarkably, the highest average value was

obtained in fish corresponding to the C-50 batch. Therefore, some preservative effect on PUFA compounds could be inferred from the presence of OCL in the covering medium.

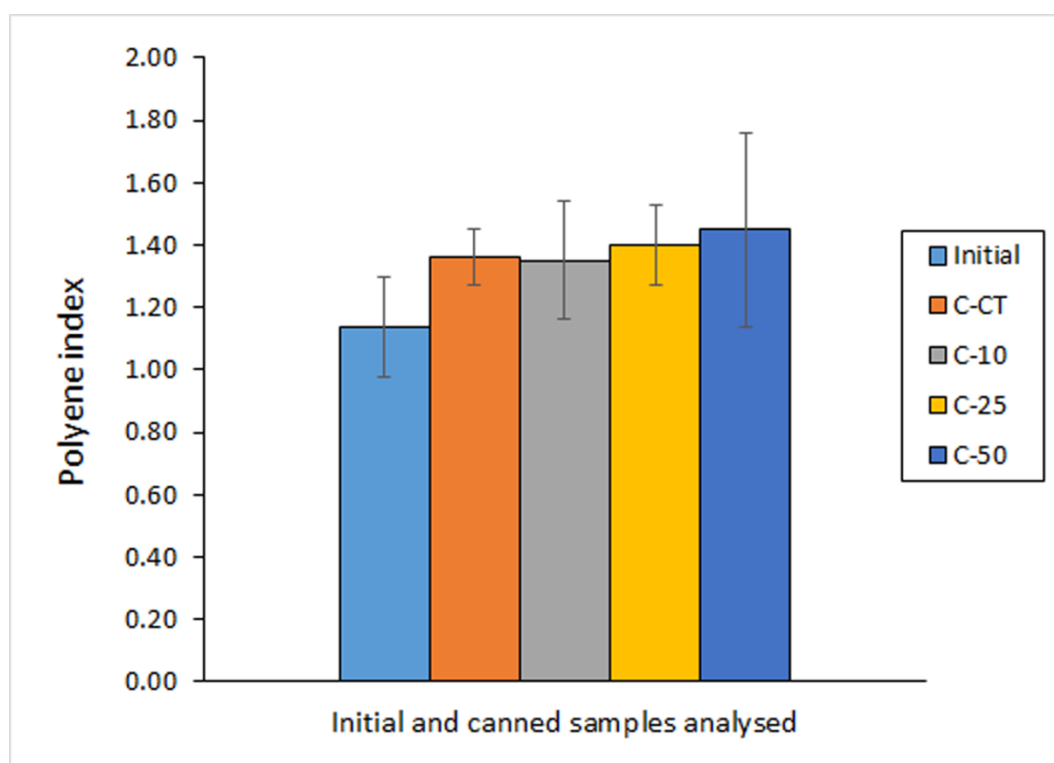


Figure 2. Determination of the polyene index * in initial and canned mackerel packaged under different conditions including octopus cooking liquor (OCL) **. * Average values of four replicates ($n = 4$); standard deviations are indicated by bars. ** Packaging conditions as described in Table 1.

Previous research related to the addition of antioxidant compounds in the packaging medium has already shown a preservative effect on the PI. Thus, Ortiz et al. [37] showed a significant PI retention in canned Atlantic salmon (*S. salar*) muscle when packaged in a water medium including an ulte (basal part of alga *D. antarctica*) extract; however, no differences were obtained in such study when other algae (cochayuyo, frond of *D. antarctica*; *U. lactuca*; *p. columbina*) extracts were included in the water-packaging systems. Similarly, higher PI scores were observed in Atlantic mackerel (*S. scombrus*) by addition of *B. bifurcata* extracts [25] and in Chub mackerel (*S. colias*) by addition of *F. spiralis* or *U. lactuca* extracts [23]. Contrarily, no effect on the PI of a three-year canned sprat (*C. cultriventris*) was observed with brine as packaging medium instead of sunflower oil [44].

Concerning PUFA series (namely, $\omega 3$ and $\omega 6$), great attention has recently been accorded to the $\omega 3/\omega 6$ ratio in seafood and food in general [45]. In order to prevent inflammatory, cardiovascular, and neurological disorders, the World Health Organisation (WHO) currently recommends that this ratio should be higher than 0.1 in the human diet [46]. Additionally, the European Nutritional Society reported that a human diet with a $\omega 3/\omega 6$ ratio of 1/5 or higher would have health benefits [47].

In the current study, $\omega 3/\omega 6$ ratio of raw and canned samples was included in a straight range (i.e., 9.0–10.8) (Table 3). Notably, the canning process led to a significant ($p < 0.05$) increase (comparison between initial and control canned samples); however, the presence of OCL in the packaging medium led to lower average values than in control canned fish, although significant differences were not attained ($p > 0.05$). Among OCL-treated fish, the highest average values were observed in mackerel corresponding to C-50 batch. Nevertheless, values in all cases can be considered as highly nutritional, according to the abovementioned health requirements for this FA ratio.

3. Materials and Methods

3.1. Sample Preparation

Commercial OCL was provided by Frigoríficos Rosa de los Vientos S. L. (Marín, Pontevedra, Spain) in vacuum-sealed bottles protected from light. Liquor was stored under refrigerated conditions (4 °C) before use.

Sample (40 fish) of Atlantic Chub mackerel (*S. colias*) (length range: 29–35 cm; weight range: 240–300 g) were obtained at Vigo harbour (North-Western Spain) in May 2021 and transported (10 min) on ice to the laboratory. As the initial fish batch (starting raw mackerel; raw control), eight fish were selected and divided into four groups (two fish per group). Sample were beheaded, eviscerated, filleted, and analysed for moisture and lipid content, lipid damage, and FA composition according to the methods described later. Within each group, the white muscle was analysed independently ($n = 4$).

The remaining samples (32 fish) were stored at -40 °C for 48 h and then kept frozen (-18 °C) for a 6-month period. At that time, fish were thawed overnight (4 °C), beheaded, eviscerated, and filleted. Then, 45-g portions of mackerel fillets were placed in small flat rectangular cans (105 × 60 × 25 mm; 150 mL). As packaging media, 10, 25, and 50 mL of OCL were added to the cans, followed by the addition of distilled water (85, 70, and 45 mL, respectively) to be filled. As a result, low-concentrated (C-10 batch), medium-concentrated (C-25 batch), and high-concentrated (C-50 batch) packaging conditions were prepared, respectively. Additionally, canned control samples were prepared by introducing in the can 45 g of fish fillet and filling it with distilled water (95 mL; C-CT batch). The various OCL concentrations used in this study were based on several preliminary tests. Thus, a 50-mL volume addition corresponded to the highest concentration without modifying the sensory descriptors of canned mackerel (i.e., flesh colour, odour, or flavour). In order to analyse the effect of the OCL content, two lower volumes (namely, 10 and 25 mL, C-10 and C-25 batches, respectively) were also checked in this study.

Each can was prepared with a single-fish fillet. For each packaging condition, eight different cans were prepared that were pooled into four groups (two cans per group), each group being analysed independently ($n = 4$). All cans were vacuum sealed in a horizontal steam retort (115 °C, 45 min; $F_0 = 7$ min) (CIFP Coroso, Ribeira, A Coruña, Spain). Once the heating time was completed, steam was cut off and air was used to flush away the remaining steam. The cans were cooled at reduced pressure. After a 3-month storage at room temperature (20 °C), the cans were opened, and the liquid part was carefully drained off gravimetrically and filtered through a filter paper. Then, the mackerel white muscle was separated, wrapped in filter paper, and used for analysis.

All solvents and chemical reagents used were of reagent grade (Merck, Darmstadt, Germany).

3.2. Determination of Moisture and Lipid Content

Moisture content was determined as the weight difference in homogenised fish white muscle (1–2 g) before and after 4 h at 105 °C [48]. Results were calculated as $\text{g}\cdot\text{kg}^{-1}$ muscle.

Lipids were obtained by extraction of the mackerel white muscle by applying the Bligh and Dyer [49] method, which employs a chloroform-methanol (1:1) mixture. Quantification was carried out according to Herbes and Allen [50]. Lipid content was calculated as $\text{g}\cdot\text{kg}^{-1}$ mackerel muscle.

3.3. Assessment of Lipid Damage

FFA content was determined on the lipid extract of the fish muscle by the Lowry and Tinsley [51] method, which is based on complex formation with cupric acetate-pyridine followed by spectrophotometric (715 nm) assessment (Beckman Coulter DU 640 spectrophotometer, Beckman Coulter Inc., Brea, CA, USA). Results were calculated as $\text{g FFA}\cdot\text{kg}^{-1}$ muscle.

PV was determined spectrophotometrically (520 nm) on the lipid extract by peroxide reduction with ferric thiocyanate [52]. Results were calculated as meq. active oxygen $\cdot\text{kg}^{-1}$ lipids.

TBA-i was determined according to Vyncke [53]. Content of TBARS was spectrophotometrically measured at 532 nm and calculated from a standard curve using 1,1,3,3-tetraethoxy-propane (TEP). Results were calculated as mg malondialdehyde·kg⁻¹ muscle.

The formation of fluorescent compounds (Fluorimeter LS 45; Perkin Elmer España; Tres Cantos, Madrid, Spain) was determined in the lipid extract of the fish muscle as described previously [39]. The relative fluorescence (RF) was calculated as follows: $RF = F/F_{st}$, where F is the fluorescence measured at each excitation/emission wavelength pair and F_{st} is the fluorescence intensity of a quinine sulphate solution (1 µg·mL⁻¹ in 0.05 M H₂SO₄) at the corresponding wavelength pair. Results were calculated as the FR, which was calculated as the ratio between the two RF values: $FR = RF_{393/463\text{ nm}}/RF_{327/415\text{ nm}}$.

Lipid extracts were converted into FA methyl esters (FAME) by using acetyl chloride in methanol and then analysed using a Perkin-Elmer 8700 gas chromatograph (Madrid, Spain) equipped with a fused silica capillary column SP-2330 (0.25 mm i.d. × 30 m, 0.20 µm film, Supelco Inc., Bellefonte, PA, USA) [12]. Peaks corresponding to FAME were identified by comparing their retention times with those of standard mixtures (Qualmix Fish, Larodan, Malmo, Sweden; FAME mix, Supelco, Inc.). Peak areas were automatically integrated; C19:0 FA was used as the internal standard for quantitative purposes.

Content of each FA was calculated as g·100 g⁻¹ total FA. Such values were employed in order to obtain the content on FA groups (STFA, MUFA, and PUFA) (g·100 g⁻¹ total FA) and the ω3/ω6 ratio. Additionally, the PI was calculated as the following FA content ratio: $(C20:5\omega3 + C22:6\omega3)/C16:0$.

3.4. Statistical Analysis

Chemical values were subjected to the ANOVA method to explore differences obtained from the effect of canning and packaging conditions. As expressed above, four replicates ($n = 4$) were considered in the study. The least-squares difference (LSD) method was used to perform the comparison of means. Analyses were carried out using the PASW Statistics 18 software for Windows (SPSS Inc., Chicago, IL, USA); differences were considered significant for a confidence interval at the 95% level ($p < 0.05$).

4. Conclusions

The preservative properties of waste liquor obtained from common octopus cooking were investigated. OCL was included in the aqueous packaging medium employed for mackerel canning. As a result, the canning process led to an increase of lipid content, lipid oxidation (development of fluorescent compounds), and hydrolysis (FFA content increase) and ω3/ω6 ratio in fish muscle. In all canned samples, primary (peroxides) and secondary (TBARS) levels of lipid oxidation were low (0.29–0.48 meq. active oxygen·kg⁻¹ lipids and 0.26–0.43 mg malondialdehyde·kg⁻¹ muscle, respectively). Remarkably, the presence in the packaging medium of OCL led to lower ($p < 0.05$) TBARS (0.26 mg malondialdehyde·kg⁻¹ muscle) and fluorescent compound (3.72) formation in canned fish corresponding to C-25 and C-50 batches, respectively. Furthermore, an increasing OCL presence led to an average decrease of peroxide and FFA content and to an average increase of the PI. All OCL-packaged muscle showed lower average values of STFA and ω3/ω6 ratio and higher average values of PI and MUFA presence. Among OCL-treated fish, the C-50 batch showed the lowest average peroxide (0.31 meq. active oxygen·kg⁻¹ lipids) and FFA (27.98 g·kg⁻¹ muscle) values and the highest PI scores (1.45). Globally, this concentration is considered the most accurate for quality enhancement in the present investigation.

The current study constitutes a novel and beneficial strategy to enhance the quality of commercial canned fish, thus enabling environmental sustainability and circular economy. OCL was satisfactorily employed for quality enhancement of a canned product. It is considered that the development of optimised conditions of this cooking-liquor packaging system may open the way to its application in all kinds of canned fish species, including high-value fatty fish such as tuna, bonito, or salmon. Further research envisaged to analyse

molecules present in OCL and involved in the mechanism of lipid preservation ought to be addressed.

Author Contributions: Conceptualisation, B.M. and S.P.A.; methodology, J.M.M., M.T. and B.M.; data curation, M.T. and J.M.M.; writing—original draft preparation, J.M.M. and S.P.A.; writing—review and editing, S.P.A. All authors have read and agreed to the published version of the manuscript.

Funding: This research was funded by the SPANISH MINISTRY OF RESEARCH AND INNOVATION, grant number RTI2018-095659-B-I00 (2019–2022).

Institutional Review Board Statement: Not applicable.

Informed Consent Statement: Not applicable.

Data Availability Statement: The data presented in this study are available on request from the corresponding author.

Acknowledgments: Frigoríficos Rosa de los Vientos S. L. (Marín, Pontevedra, Spain) is greatly acknowledged for kindly providing the octopus cooking liquor.

Conflicts of Interest: The authors declare no conflict of interest.

Sample Availability: Samples of the compounds are not available from the authors.

References

- Blanco, M.; Sotelo, C.G.; Chapela, M.J.; Pérez-Martín, R.I. Towards sustainable and efficient use of fishery resources: Present and future trends. *Trends Food Sci. Technol.* **2007**, *18*, 29–36. [CrossRef]
- Venugopal, V. Marine product for health care. In *Marine Product for Health Care*; Venugopal, V., Ed.; CRC Press: Boca Raton, FL, USA, 2009; pp. 185–214.
- Gharsallah, N.; Khannous, L.; Souissi, N.; Nasri, M. Biological treatment of saline wastewaters from marine-products processing factories by a fixed-bed reactor. *J. Chem. Technol. Biotechnol.* **2002**, *77*, 865–870. [CrossRef]
- Uttamangkabovorn, M.; Prasertsan, P.; Kittikun, A.H. Water conservation in canned tuna plant in Thailand. *J. Clean. Prod.* **2005**, *13*, 547–555. [CrossRef]
- Arvanitoyannis, I.S.; Kassaveti, A. Fish industry waste: Treatments, environmental impacts, current and potential uses. *Int. J. Food Sci. Technol.* **2008**, *43*, 726–745. [CrossRef]
- Rustad, T.; Storro, I.; Slizyte, R. Possibilities for the utilisation of marine by-products. *Int. J. Food Sci. Technol.* **2011**, *46*, 2001–2014. [CrossRef]
- Achour, M.; Khelifi, O.; Bouazizi, I.; Hamdi, M. Design of an integrated bioprocess for the treatment of tuna processing liquid effluents. *Process Biochem.* **2000**, *35*, 1013–1017. [CrossRef]
- Ahn, C.B.; Kim, H.R. Processing of the extract powder using skipjack cooking juice and its taste compounds. *Korean J. Food Sci. Technol.* **1996**, *28*, 696–701.
- Jao, C.L.; Ko, W.C. 1,1-Diphenyl-2-picrylhydrazyl (DPPH) radical scavenging by protein hydrolyzates from tuna cooking juice. *Fish. Sci.* **2002**, *68*, 430–435. [CrossRef]
- Kanpairo, K.; Usawakesmanee, W.; Sirivongpaisal, P.; Siripongvutikorn, S. The compositions and properties of spray dried tuna flavor powder produced from tuna precooking juice. *Int. Food Res. J.* **2012**, *19*, 893–899.
- Li, K.X.; Ding, H.P.; Zhou, X.J.; Zhang, J.; Zhang, H.Q.; Liu, L.P. Antioxidant and deodorizing treatment of tuna steamed juice and development of its flavor salad. *Sci. Technol. Food Ind.* **2020**, *41*, 153–160.
- Sieiro, M.P.; Aubourg, S.P.; Rocha, F. Seasonal study of the lipid composition in different tissues of the common octopus (*Octopus vulgaris*). *Eur. J. Lipid Sci. Technol.* **2006**, *108*, 479–487. [CrossRef]
- Barbosa, A.; Vaz-Pires, P. Quality index method (QIM): Development of a sensorial scheme for common octopus (*Octopus vulgaris*). *Food Cont.* **2004**, *15*, 161–168. [CrossRef]
- Lee, S.Y.; Hur, S.J. Antihypertensive peptides from animal products, marine organisms, and plants. *Food Chem.* **2017**, *228*, 506–517. [CrossRef] [PubMed]
- Lin, Y.; Tang, X.; Xua, L.; Wanga, S. Antibacterial properties and possible action mechanism of chelating peptides-zinc nanocomposite against *Escherichia coli*. *Food Cont.* **2019**, *106*, 106675. [CrossRef]
- Oh, H.S.; Kang, K.T.; Kim, H.S.; Lee, J.H.; Jee, S.J.; Ha, J.H.; Kim, J.J.; Heu, M.S. Food Component characteristics of seafood cooking drips. *J. Korean Soc. Food Sci. Nutr.* **2007**, *36*, 595–602. [CrossRef]
- Kim, Y.J.; Kim, H.J.; Choi, J.I.; Kim, J.H.; Chun, B.S.; Ahn, D.H.; Kwon, J.H.; Kim, Y.J.; Byun, M.W.; Lee, J.W. Effect of electron beam irradiation on the physiological activities of cooking drips from Enteropneust *dofleini*. *J. Korean Soc. Food Sci. Nutr.* **2008**, *37*, 1190–1195. [CrossRef]

18. Choi, J.I.; Kim, Y.J.; Sung, N.Y.; Kim, J.H.; Ahn, D.H.; Chun, B.S.; Cho, K.Y.; Byun, M.W.; Lee, J.W. Investigation on the increase of antioxidant activity of cooking drip from *Enteroctopus dofleini* by irradiation. *J. Korean Soc. Food Sci. Nutr.* **2009**, *38*, 121–124. [CrossRef]
19. Vázquez, J.A.; Murado, M.A. Enzymatic hydrolysates from food wastewater as a source of peptones for lactic acid bacteria productions. *Enz. Microb. Technol.* **2008**, *43*, 66–72. [CrossRef]
20. Piclet, G. Le poisson aliment. Composition-Intérêt nutritionnel. *Cah. Nutr. Diét.* **1987**, *22*, 317–335.
21. Horner, W. Canning fish and fish products. In *Fish Processing Technology*, 2nd ed.; Hall, G., Ed.; Blackie Academic and Professional, Chapman and Hall: London, UK, 1997; pp. 119–159.
22. Lukoshkina, M.; Odoeva, G. Kinetics of chemical reactions for prediction of quality of canned fish during storage. *App. Biochem. Microb.* **2003**, *39*, 321–327. [CrossRef]
23. Barbosa, R.G.; Trigo, M.; Campos, C.A.; Aubourg, S.P. Preservative effect of algae extracts on lipid composition and rancidity development in brine-canned Atlantic chub mackerel (*Scomber colias*). *Eur. J. Lipid Sci. Technol.* **2019**, *121*, 1900129. [CrossRef]
24. Aubourg, S.P. Review: Loss of quality during the manufacture of canned fish products. *Food Sci. Technol. Int.* **2001**, *7*, 199–215. [CrossRef]
25. Barbosa, R.G.; Trigo, M.; Prego, R.; Fett, R.; Aubourg, S.P. The chemical composition of different edible locations (central and edge muscles) of flat fish (*Lepidorhombus whiffiagonis*). *Int. J. Food Sci. Technol.* **2018**, *53*, 271–281. [CrossRef]
26. Aubourg, S.P.; Gallardo, J.M.; Medina, I. Changes in lipids during different sterilising conditions in canning albacore (*Thunnus alalunga*) in oil. *Int. J. Food Sci. Technol.* **1997**, *32*, 427–431. [CrossRef]
27. Rodríguez, A.; Carriles, N.; Aubourg, S.P. Effect of chill storage under different icing conditions on sensory and physical properties of canned farmed salmon (*Oncorhynchus kisutch*). *Int. J. Food Sci. Technol.* **2010**, *45*, 295–304. [CrossRef]
28. Refsgaard, H.; Brockhoff, P.; Jensen, B. Free polyunsaturated fatty acids cause taste deterioration of salmon during frozen storage. *J. Agric. Food Chem.* **2000**, *48*, 3280–3285. [CrossRef] [PubMed]
29. Aubourg, S.P. Fluorescence study of the prooxidant activity of free fatty acids on marine lipids. *J. Sci. Food Agric.* **2001**, *81*, 385–390. [CrossRef]
30. Labuza, T. Kinetics of lipid oxidation in foods. *CRC Crit. Rev. Food Technol.* **1971**, *2*, 355–405. [CrossRef]
31. Medina, I.; Sacchi, R.; Aubourg, S.P. A ¹³C-NMR study of lipid alterations during fish canning: Effect of filling medium. *J. Sci. Food Agric.* **1995**, *69*, 445–450. [CrossRef]
32. Naseri, M.; Rezaei, M.; Moieni, S.; Hosseini, H.; Eskandari, S. Effects of different filling media on the oxidation and lipid quality of canned silver carp (*Hypophthalmichthys molitrix*). *Int. J. Food Sci. Technol.* **2011**, *46*, 1149–1156. [CrossRef]
33. Mohan, C.O.; Remya, S.; Murthy, L.N.; Ravishankar, C.N.; Kumar, K.A. Effect of filling medium on cooking time and quality of canned yellowfin tuna (*Thunnus albacares*). *Food Cont.* **2015**, *50*, 320–327. [CrossRef]
34. Aubourg, S.P.; Trigo, M.; Martínez, B.; Rodríguez, A. Effect of prior chilling period and alga-extract packaging on the quality of a canned underutilised fish species. *Foods* **2020**, *9*, 1333. [CrossRef] [PubMed]
35. Selmi, S.; Monser, L.; Sadok, S. The influence of local canning process and storage on pelagic fish from Tunisia: Fatty acids profile and quality indicators. *J. Food Proc. Preserv.* **2008**, *32*, 443–457. [CrossRef]
36. Uriarte-Montoya, M.H.; Villalba-Villalba, A.G.; Pacheco-Aguilar, R.; Ramírez-Suárez, J.C.; Lugo-Sánchez, M.E.; García-Sánchez, G.; Carvallo-Ruiz, M.G. Changes in quality parameters of Monterey sardine (*Sardinops sagax caerulea*) muscle during the canning process. *Food Chem.* **2010**, *122*, 482–487. [CrossRef]
37. Ortiz, J.A.; Vivanco, J.P.; Aubourg, S.P. Lipid and sensory quality of canned Atlantic salmon (*Salmo salar*): Effect of the use of different seaweed extracts as covering liquids. *Eur. J. Lipid Sci. Technol.* **2014**, *116*, 596–605. [CrossRef]
38. Aubourg, S.P.; Medina, I. Quality differences assessment in canned sardine (*Sardina pilchardus*) by fluorescence detection. *J. Agric. Food Chem.* **1997**, *45*, 3617–3621. [CrossRef]
39. Losada, V.; Rodríguez, A.; Ortiz, J.; Aubourg, S.P. Quality enhancement of canned sardine (*Sardina pilchardus*) by a preliminary chilling treatment. *Eur. J. Lipid Sci. Technol.* **2006**, *108*, 598–605. [CrossRef]
40. Wu, H.C.; Shiau, C.Y.; Chen, H.M.; Chiou, T.K. Antioxidant activities of carnosine, anserine, some free amino acids and their combination. *J. Food Drug Anal.* **2003**, *11*, 148–153. [CrossRef]
41. Pokorný, J. Browning from lipid-protein interactions. *Prog. Food Nutr. Sci.* **1981**, *5*, 421–428.
42. Cheong, H.S. Antioxidant effect of histidine containing low molecular weight peptide isolated from skipjack boiled extract. *Korean J. Food Cook. Sci.* **2007**, *23*, 221–226.
43. Medina, I.; Sacchi, R.; Giudicianni, I.; Aubourg, S.P. Oxidation in fish lipids during thermal stress as studied by ¹³C-NMR spectroscopy. *J. Amer. Oil Chem. Soc.* **1998**, *75*, 147–154. [CrossRef]
44. Naseri, M.; Rezaei, M. Lipid changes during long-term storage of canned sprat. *J. Aquat. Food Prod. Technol.* **2012**, *21*, 48–58. [CrossRef]
45. Uauy, R.; Valenzuela, A. Marine oils: The health benefits of n-3 fatty acids. *Nutrition* **2000**, *16*, 680–684. [CrossRef]
46. Kumari, P.; Kumar, M.; Reddy, C.R.; Jha, B. Algal lipids, fatty acids and sterols. In *Functional Ingredients from Algae for Foods and Nutraceuticals*; Domínguez, H., Ed.; Woodhead Publishing: Cambridge, UK, 2013; pp. 87–134.
47. Simopoulos, A.P. The importance of the ratio of omega-6/omega-3 essential fatty acids. *Biomed. Pharmacother.* **2002**, *56*, 365–379. [CrossRef]

48. AOAC. *Official Methods for Analysis of the Association of Analytical Chemistry*, 15th ed.; Association of Official Chemists, Inc.: Arlington, VA, USA, 1990; pp. 931–937.
49. Bligh, E.; Dyer, W. A rapid method of total extraction and purification. *Can. J. Biochem. Physiol.* **1959**, *37*, 911–917. [CrossRef] [PubMed]
50. Herbes, S.E.; Allen, C.P. Lipid quantification of freshwater invertebrates: Method modification for microquantitation. *Can. J. Fish. Aquat. Sci.* **1983**, *40*, 1315–1317. [CrossRef]
51. Lowry, R.; Tinsley, I. Rapid colorimetric determination of free fatty acids. *J. Am. Oil Chem. Soc.* **1976**, *53*, 470–472. [CrossRef] [PubMed]
52. Chapman, R.; McKay, J. The estimation of peroxides in fats and oils by the ferric thiocyanate method. *J. Am. Oil Chem. Soc.* **1949**, *26*, 360–363. [CrossRef]
53. Vyncke, W. Direct determination of the thiobarbituric acid value in trichloroacetic acid extracts of fish as a measure of oxidative rancidity. *Fette Seifen Anstrichm.* **1970**, *72*, 1084–1087. [CrossRef]

Article

Efficacy of Probiotic Compounds in Relieving Constipation and Their Colonization in Gut Microbiota

Yuan He ^{1,2}, Leilei Zhu ¹, Jialun Chen ³, Xin Tang ³, Mingluo Pan ¹, Weiwei Yuan ^{1,2} and Hongchao Wang ^{1,2,*} 

¹ State Key Laboratory of Food Science and Technology, Jiangnan University, Wuxi 214122, China; 6200113031@stu.jiangnan.edu.cn (Y.H.); 7190112086@stu.jiangnan.edu.cn (L.Z.); 6190111135@stu.jiangnan.edu.cn (M.P.); 6180111089@stu.jiangnan.edu.cn (W.Y.)

² School of Food Science and Technology, Jiangnan University, Wuxi 214122, China

³ Sirio Pharma Co., Ltd., Shantou 515000, China; dane.chen@siriopharma.com (J.C.); xin.tang@siriopharma.com (X.T.)

* Correspondence: hcwang@jiangnan.edu.cn; Tel.: +86-510-85912155

Abstract: A number of studies have confirmed the relationship between constipation and gut microbiota. Additionally, many human and animal experiments have identified probiotics as effectors for the relief of constipation symptoms. In this study, probiotic compounds, including *Lactobacillus acidophilus* LA11-Onlly, *Lactocaseibacillus rhamnosus* LR22, *Limosilactobacillus reuteri* LE16, *Lactiplantibacillus plantarum* LP-Onlly, and *Bifidobacterium animalis* subsp. *lactis* BI516, were administered to mice with loperamide-induced constipation, and the impacts of these strains on constipation-related indicators and gut microbiota were evaluated. The effects of probiotic compounds on constipation relief were associated with various aspects, including gastrointestinal transit rate, number and weight of stools, serum and intestinal gastrointestinal regulatory hormones, and serum cytokines. Some of the probiotic compounds, including *Limosilactobacillus reuteri*, *Lactiplantibacillus plantarum*, and *Lactocaseibacillus rhamnosus*, were found to colonize the intestinal tract. Furthermore, higher dosages promoted the colonization of specific strains. This study yields a new perspective for the clinical use of probiotics to improve constipation symptoms by combining strains with different mechanisms for the alleviation of constipation.

Keywords: constipation; probiotic compounds; gastrointestinal transit rate; gut microbiota; colonize

Citation: He, Y.; Zhu, L.; Chen, J.; Tang, X.; Pan, M.; Yuan, W.; Wang, H. Efficacy of Probiotic Compounds in Relieving Constipation and Their Colonization in Gut Microbiota. *Molecules* **2022**, *27*, 666. <https://doi.org/10.3390/molecules27030666>

Academic Editor: Mirella Nardini

Received: 20 December 2021

Accepted: 11 January 2022

Published: 20 January 2022

Publisher's Note: MDPI stays neutral with regard to jurisdictional claims in published maps and institutional affiliations.



Copyright: © 2022 by the authors. Licensee MDPI, Basel, Switzerland. This article is an open access article distributed under the terms and conditions of the Creative Commons Attribution (CC BY) license (<https://creativecommons.org/licenses/by/4.0/>).

1. Introduction

Constipation is a common, burdensome functional bowel disorder in which symptoms of difficult, infrequent, or incomplete defecation predominate [1]. It has a negative effect on quality of life [2]. Approximately 12–30% of people worldwide suffer from constipation [3]. Constipation not only increases the financial burdens of patients, but also increases the social burden of the healthcare system [4]. Some studies have shown that the probability of constipation symptom onset increases beyond the age of 65, and is twice as high in women as in men [5,6]. Despite the range of treatments available, including laxatives and fiber supplements, approximately half of patients are dissatisfied with current management strategies, with the main complaint being limited efficacy [7,8]. Hence, there is an unmet need for alternative treatments for the management of constipation-related symptoms.

The gut is home to trillions of microbes, the composition of which correlates with many disease states. The gut microbiota serves as an endocrine organ, facilitating the production and regulation of various neurotransmitters and hormones. While recent studies have started to unravel the effects of this vast microbial community and its complex metabolic repertoire on intestinal physiology, its true potential remains underexplored [9]. Accumulated evidence shows that some probiotic strains ameliorate functional constipation (FC) via the modulation of specific gastrointestinal peptide pathways [10,11]. In the past decade, research has focused on their effectiveness for treating constipation, possibly mediated

through regulation of gut dysmotility by impacting the gut microbiota, with the subsequent release of metabolites such as tryptamine [12] and short-chain fatty acids (SCFAs) during fermentation, which are known to interact with the intestinal barrier, intestinal immune system, and nervous system. Thus, new trends in constipation management have considered probiotic administration as a possible strategy.

Most research has studied the relieving effect of a single strain of probiotics on mice with constipation, and we studied combinations of a variety of probiotics (*Lactobacillus acidophilus* LA11-Only, *Lacticaseibacillus rhamnosus* LR22, *Limosilactobacillus reuteri* LE16, *Lactiplantibacillus plantarum* LP-Only, *Bifidobacterium animalis* subsp. *lactis* BI516) that can relieve constipation. The aim of this study was to investigate the roles of probiotic compounds in relieving constipation and colonizing the intestine. For this, the effects of probiotic compounds on gastrointestinal (GI) transit rate, serum and intestinal gastrointestinal regulatory hormones, and serum cytokines were assessed in mice with constipation. The effects of probiotic compounds on regulating the gut microbiome and their ability to colonize the intestinal tract were assessed. Overall, this study aids our understanding of the relationship between probiotic compounds and constipation, providing insights into a new intervention strategy for constipation.

2. Materials and Methods

2.1. Preparation of Probiotic Suspensions

Lactobacillus (*L. acidophilus*, *L. rhamnosus*, *L. reuteri*, *L. plantarum*) culture conditions were 37 °C for 16 h. The conditions of *Bifidobacterium* (*Bifidobacterium animalis* subsp. *lactis*) were anaerobic culturing at 37 °C for 30 h. The two-generation activated strains were placed in 1 L of fresh culture medium; the inoculum amount was 2%. These cultures were placed in the incubator with the corresponding conditions. The obtained bacterial liquid was centrifuged at 6000 × g for 15 min. After the bacteria were washed twice with saline solution, they were resuspended with a sucrose solution (as a protective solution) and stored at −80 °C for later use. We measured the concentration of the bacterial solution before use. The probiotic compounds were prepared by Sirio Pharma. They contained only compounds of the five strains above.

We mixed the probiotic compounds and saline solution in proportion to make a probiotic suspension for subsequent gavage into mice. We ensured that the concentration of each probiotic reached 2.5×10^9 CFU/mL for the low-dose group, and 2.5×10^{10} CFU/mL for the high-dose group.

2.2. Animals and Experimental Design

Six-week-old, male, SPF-grade BALB/c mice were obtained from Shanghai Slack Company. The animal experimental protocol was approved by the Ethics Committee of Jiangnan University (JN.No20190930b0600120) and implemented in accordance with existing EU guidelines (2010/63/EU). The breeding environment was maintained at a temperature of 23 ± 2 °C and relative humidity of $50 \pm 10\%$, with a 12/12 h light/dark cycle. Fifty mice were randomly divided into a normal group, model group, positive group (*Lactobacillus rhamnosus* GG 0.1 g/kg BW bacterial suspension), low-dose group (0.1 g/kg BW bacterial suspension), and high-dose group (1.0 g/kg BW bacterial suspension)—ten mice per group. All animal experiments were performed in strict accordance with the regulations of the Animal Management and Use Committee of Jiangnan University (SYXK 2012-0002). The mice were gavaged daily after 7 days of adaptation to the environment. During days 8–14, mice in the normal and model groups were intragastrically administered 0.2 mL of saline solution, while the other groups were given 0.2 mL of bacterial suspension daily. All mice except for those in the normal were gavaged with loperamide hydrochloride daily (10 mg/kg BW) during days 15–21, while the mice in the normal group were orally administered saline solution daily. Low and high-dose groups were gavaged bacterial suspension continuously; the loperamide hydrochloride treatment was performed 1 h before bacterial suspension gavage daily on days 15–21 (Figure 1). The mice were anesthetized

with isoflurane inhalation before pricking an eyeball for collecting blood. Carbon dioxide euthanasia and cervical dislocation were performed after blood collecting.

Thirty mice were randomly divided into a control group (BK), low-dose group (CD) (0.1 g/kg BW bacterial suspension), and high-dose group (CG) (1.0 g/kg BW bacterial suspension)—ten mice per group. During days 8–37, mice were given 0.2 mL of bacterial suspension daily in the CD and CG groups, and the mice in BK were orally administered saline solution (vehicle) daily. Mouse feces were collected in sterile tubes, snap-frozen on day 38, day 45, and day 52, and stored at -80°C for high-throughput sequencing (Figure 1). The experimental conditions were consistent with those described above. After 52 days of treatment, the mice were sacrificed via carbon dioxide euthanasia and cervical dislocation.

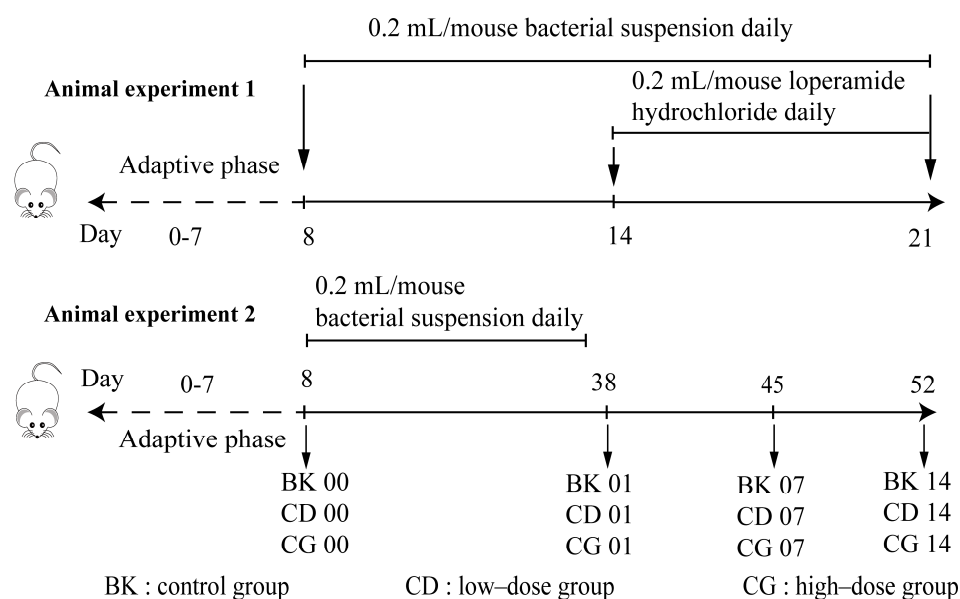


Figure 1. Animal experimental groups. Normal group, BK; low-dose group, CD; high-dose group, CG; the first gavage, 00; the last gavage, 01; one week after stopping gavage, 07; two weeks after stopping gavage, 14.

2.3. Determination of the Time Taken for First Black Stool

On day 21, the fifty mice were intragastrically administered activated carbon mixed with probiotic suspensions (or saline solution). The mice were then placed into clean, dry cages, and the time when each mouse expelled its first black stool, along with the number and weight of black stools discharged within six hours, were recorded.

2.4. Determination of the Gastrointestinal Transit Rate

On day 21, the mice were starved overnight (water was provided). At 8:30 a.m. on day 22, 0.2 mL distilled water was given to mice in the normal group, while all other mice were given 0.2 mL of loperamide hydrochloride solution (10 mg/kg BW). After 30 min, activated carbon was intragastrically administered to all mice. After another 30 min, the mice were sacrificed with carbon dioxide euthanasia and cervical dislocation. The entire small intestine from the pylorus to the caecum was removed, and the total length of the small intestine was measured. The distance to the front edge of the activated carbon was also measured. For each mouse, the GI transit rate was calculated as the percentage of prosthetic advancement of the activated carbon relative to the total length of the small intestine.

2.5. Determination of Peptide and Serotonin Factor Concentrations

Mice that had starved for 12 h were intraperitoneally injected with a sodium pentobarbital solution (0.5 mL/10 g BW) and subsequently sacrificed. Serum samples were obtained from animal experiment 1's blood samples by centrifugation ($3000\times g$, 15 min) in which the concentrations of motilin (MTL), substance P (SP), endothelin (ET-1), somatostatin (SS), vasoactive intestinal peptide (VIP), gastrin (GAS), and cytokines (IL-2, IL-4, IL-6, IL-10, IL-12, IL-17) were measured using commercial ELISA kits (Nanjing SenBeiJia Biological Technology Co., Ltd., Nanjing, China) according to the manufacturer's instructions. The colon tissue was washed with pre-cooled phosphate buffered saline (PBS), the surrounding adipose tissue was removed, and the colon was cut and weighed. The tissue was disrupted using a tissue disrupter in a corresponding volume of PBS (weight to volume ratio of 1:9), and finally centrifuged at $5500\times g$ for 10 min. The supernatant was taken to detect the concentrations of gastrointestinal regulatory peptides.

2.6. DNA Extraction from Fecal Samples and High-Throughput Sequencing of the Gut Microbiota

Fecal samples were collected in appropriate sterile tubes to explore changes in the gut microbiome. Each fecal sample was frozen immediately at $-80\text{ }^{\circ}\text{C}$ to prevent distortion of the bacterial community profile. Each fecal sample (200 mg) was subjected to DNA extraction using the FastDNA Spin Kit for Feces (MP Biomedicals, Solon, OH, USA). The V3–V4 region was amplified using polymerase chain reaction (PCR), and the PCR primers were forward primer 5'-CCTAYGGGRBGCASCAG-3' and reverse primer 5'-GGACTACNNGGTATCTAAT-3' (Supplementary Table S1). After PCR, an agarose gel was cut for purification using the DNA Gel/PCR Purification Miniprep Kit (BW-DC3511, Beiwo Meditech Co., Ltd., Hangzhou, China) according to the manufacturer's instructions. The DNA was further targeted for amplification in order to quantify the species of *Lactobacillus* and *Bifidobacterium* in feces: *Bifidobacterium*-specific primers (Bif-GroelF (5'-TCCGATTACGAYCGYGAGAAGCT-3') and Bif-GroelR (5'-CSGCYTCCGTSBTCAGGAACAG3')) and *Lactobacillus*-specific primers (Lac-GroelF (5'-GCYGGTGCWAACCCNGTTGG-3') and Lac-GroelR (5'-AANGTNCCVCGVATCTTGTT-3')) were used to amplify specific fragments of the Groel genes of *Bifidobacterium* and *Lactobacillus*, respectively. A specific adapter was used for subsequent sequencing on the MiSeq PE300 platform (Illumina, Santiago, CA, USA).

2.7. Gut Microbiome Analysis

Paired-end sequencing reads were merged using QIIME2. The reads were demultiplexed and quality filtered using Quantitative Insights into Microbial Ecology software (QIIME2) [13]. To get good operational taxonomic unit sequences (OTUs), low-quality reads should be discarded because they often cause spurious OTUs. The OTUs were chosen to ensure 97% identity. The latest Silva 16s rRNA v132 database and the Groel gene sequence database cpnDB were used to produce the most precise species composition results. Taxonomy assignment of V3–V4 was performed within QIIME2. Taxonomy assignments of *Lactobacillus* and *Bifidobacterium* proceeded as in the previous article [14,15]. To avoid bias due to different sequencing depths, the OTU tables were rarefied to 10,000 sequences per sample for computing alpha-diversity metrics (Pielou evenness, Faith_pd, Observed-otus and Shannon) within QIIME2. Beta-diversity was calculated with the Bray–Curtis by the method of non-metric multidimensional scaling (NMDS) and principal component analysis (PCoA) [16]. We analyzed the differences between the groups of bacteria through the method of linear discriminant analysis effect size (LEfSe) [17]. To construct the percentage accumulation map of the microbiota, we first removed genera with relative abundances of less than 0.01%.

2.8. Evaluation of Strain Colonization Characteristics

The feces were collected before the test: one day after the last gavage, one week after the last gavage, and two weeks after the last gavage for the CD, CG, and BK groups. A known number of artificially synthesized spike plasmids were added to the sample. Then we performed bioinformatic analysis after sequencing for absolute quantitative analysis. That way, we detected the absolute abundances of bacteria in feces collected at different time points.

2.9. Statistical Analysis

The statistical analyses were processed with GraphPad Prism 8 (La Jolla, CA, USA) and IBM SPSS Statistics 20 (SPSS Inc., Chicago, IL, USA). All data are expressed as mean \pm standard error of the mean. Significant differences between groups were analyzed using one-way analysis of variance (ANOVA); $p < 0.05$ was considered statistically significant (confidence interval $> 95\%$). Gut microbiota diversity and phylum taxon abundance were compared using the Wilcoxon rank-sum test in R statistical software package 4.1.0 (<https://www.r-project.org/>, accessed on 1 December 2021). The statistical analyses of the Gut microbiota were processed with R statistical software package 4.1.0.

3. Results

3.1. Probiotic Compounds Significantly Regulate Intestinal Health in Mice with Constipation

The GI transit rate reflects the dynamics of the small intestine and may thus reflect the effects of probiotic compounds on intestinal motility. A higher GI transit rate indicates a shorter residence of chyme in the small intestine and greater small intestinal motility. Loperamide challenge led to a low GI transit rate in the model group, indicating that the constipation model was successfully established. After the intragastric administration of probiotic compounds, mice with constipation in low and high-dose groups exhibited significantly improved GI transit rates ($p < 0.05$) (Figure 2A). This observation suggests that treatment with probiotic compounds can effectively improve intestinal motility and accelerate the movement and exit of chyme via the small intestine. There was no significant difference in GI transit rate between the low and high-dose group.

The time till the first black stool defecation represents motility throughout the intestine. Specifically, a shorter time till the first black stool defecation indicates more rapid whole intestinal tract motility and a stronger intestinal transport capacity. After 7 days of loperamide challenge, the time till first black stool defecation was significantly longer in the model group than that in the normal group ($p < 0.05$) (Figure 2B). Mice that received intragastric administrations of either low or high doses of probiotic compounds exhibited significantly shorter times to the first black stool defecation compared to the model group ($p < 0.05$). This result indicates that probiotic compounds can significantly improve the intestinal transit rate in constipation model mice by improving intestinal function and intestinal motility, thereby reducing the time till the first black stool defecation. However, there was no significant difference between the low and high-dose groups in reducing the time until the first black stool defecation. At the same time, the numbers and weights of black stools in the low and high-dose groups were significantly increased compared with the model group ($p < 0.05$), but there were no significant differences between the low and high-dose groups (Figure 2C,D).

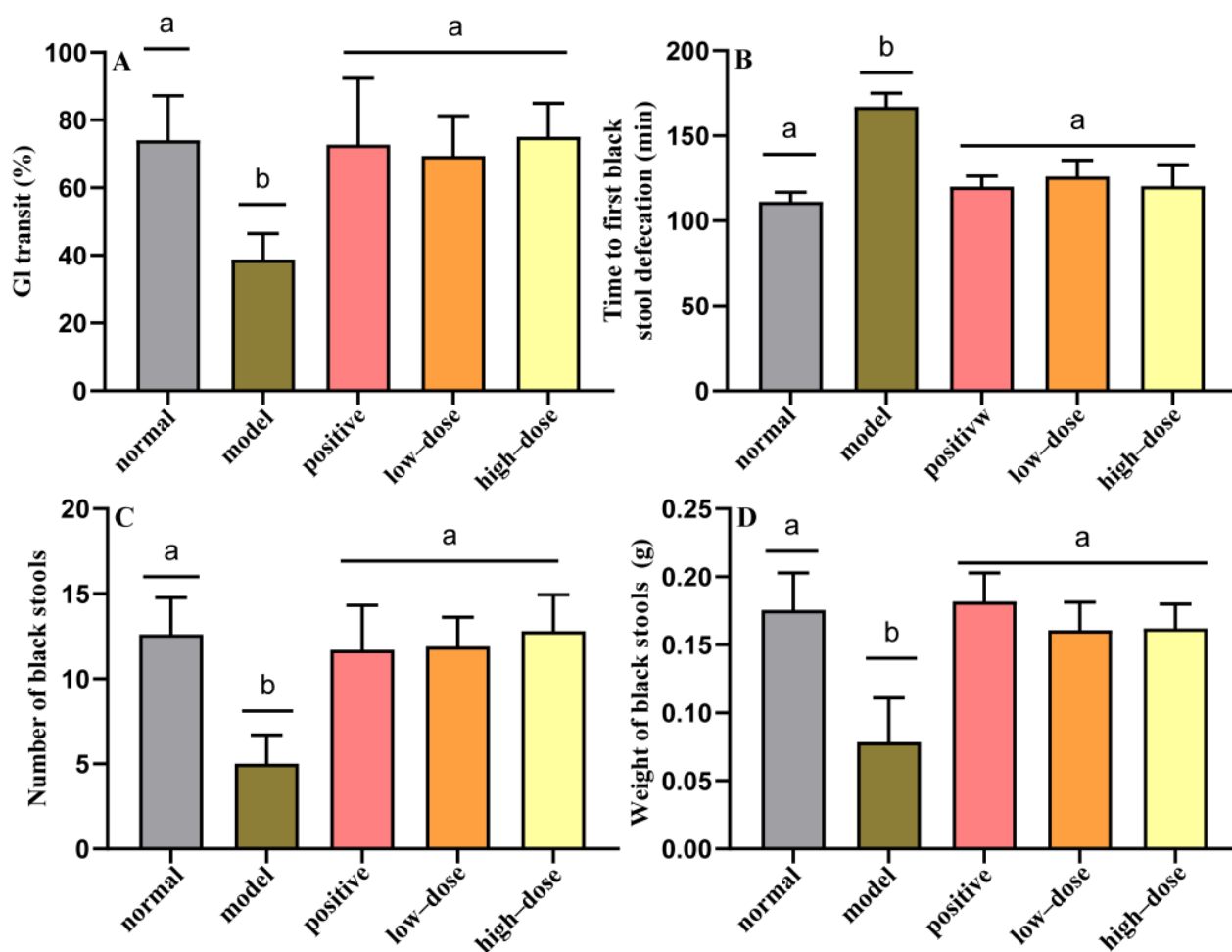


Figure 2. Effects of probiotic compounds on defecation in a mouse model of constipation. (A) Gastrointestinal transit rates. (B) Times to first black stool defecation. (C) Number of black stools. (D) Weight of black stools. Data are means with SEM. a–d: Different letters indicate significant differences ($p < 0.05$), and the same letters or no letters indicate no significant difference. Same as below.

3.2. Effects of Probiotic Compounds on Serum Levels of Gastrointestinal Regulatory Hormones in Mice with Constipation

To investigate the effects of probiotic compounds on adhesion properties and tolerance of gastric and small intestine juices, the serum levels of gastrointestinal peptide neurotransmitter MTL, GAS, SP, ET-1, SS, and VIP were evaluated in the serum samples of mice with constipation. After the loperamide challenge, the serum concentrations of SP, MTL, and GAS were significantly reduced in model mice compared to the normal group ($p < 0.05$) (Figure 3A–C); and the concentrations of VIP, SS, and ET-1 were significantly increased in model mice relative to the control group ($p < 0.05$) (Figure 3D–F), suggesting that loperamide-induced constipation may also be associated with abnormalities in serum SP, MTL, GAS, VIP, SS, and ET-1 concentrations. The concentrations of all regulatory hormones showed a recovery trend in the sera of mice treated with probiotic compounds (Figure 3). We found that the serum concentrations of MTL, VIP, and SS could be restored to their normal levels in all groups by the administration of either high or low doses of probiotic compounds. The high-dose administrations of probiotic compounds were able to restore the serum concentrations of SP and GAS to normal. Compared to the low dose, the high doses of probiotic compounds were better able to restore the concentrations of SP and GAS in mice with constipation. These probiotic strains may increase GI transit in mice

with constipation by regulating the secretion of gastrointestinal regulatory hormones in a dose-dependent manner.

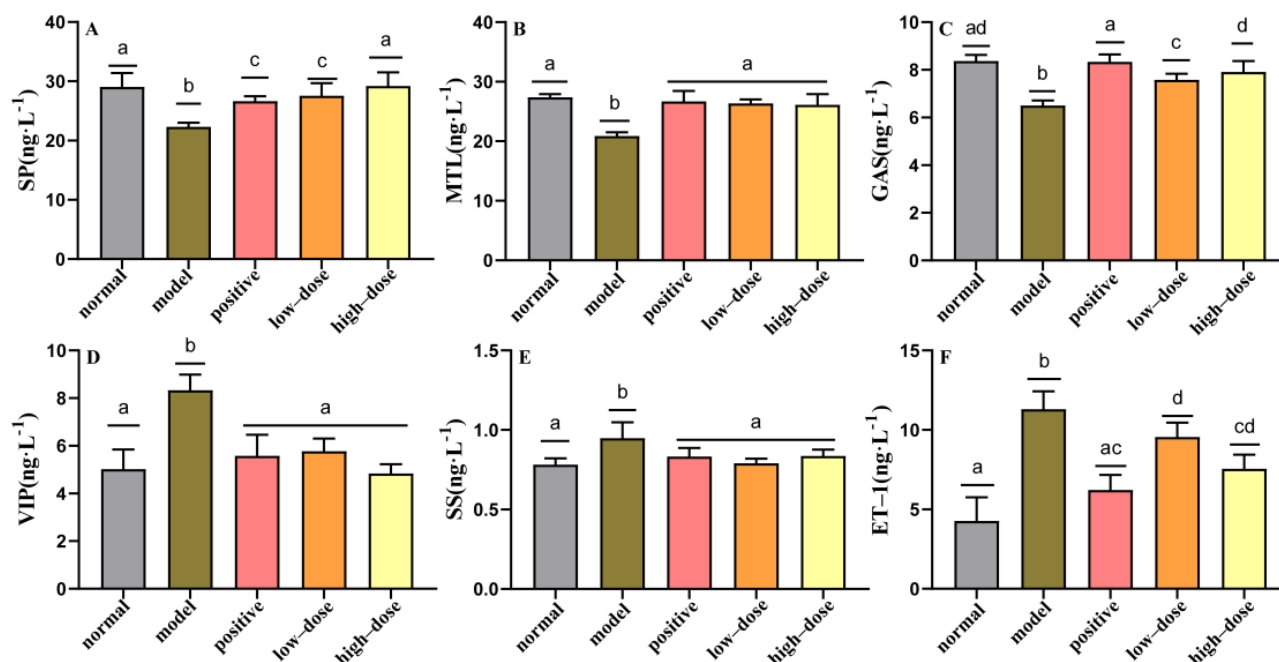


Figure 3. Effects of probiotic compounds on gastrointestinal peptides in the sera of constipated mice. (A) Substance P (SP); (B) motilin (MTL); (C) gastrin (GAS); (D) vasoactive intestinal peptide (VIP); (E) somatostatin (SS); (F) endothelin (ET-1). Data are means with SEM. a–d: Different letters indicate significant differences ($p < 0.05$), and the same letters or no letters indicate no significant difference.

3.3. Effects of Probiotic Compounds on Intestinal Gastrointestinal Regulatory Hormones in Mice with Constipation

The loperamide challenge led to significant decreases in the levels of SP, MTL, and GAS in the colons of model mice relative to the normal group ($p < 0.05$) (Figure 4A–C). Additionally, the intestinal concentrations of VIP, SS, and ET-1 in model mice were significantly increased after the loperamide challenge ($p < 0.05$) (Figure 4D–F), suggesting that loperamide-induced constipation may also be associated with abnormalities in intestinal SP, MTL, GAS, VIP, SS, and ET-1 concentrations. Once again, the concentrations of all regulatory hormones showed a recovery trend in the sera of mice treated with probiotic compounds (Figure 4). The intestinal concentrations of MTL and VIP could be restored to their normal levels by the administration of either high or low doses of probiotic compounds. Taken together, these results indicate that probiotic compounds could restore the deficient levels of SP and MTL, and reduce the elevated levels of VIP, SS, and ET-1, thereby regulating gastrointestinal regulatory hormones and relieving constipation.

3.4. Effects of Probiotic Compounds on Serum Cytokines in Mice with Constipation

We found that treatments with probiotic compounds had no negative impacts on host health and did not destroy the cytokine levels in the host (Supplementary Figures S1 and S2).

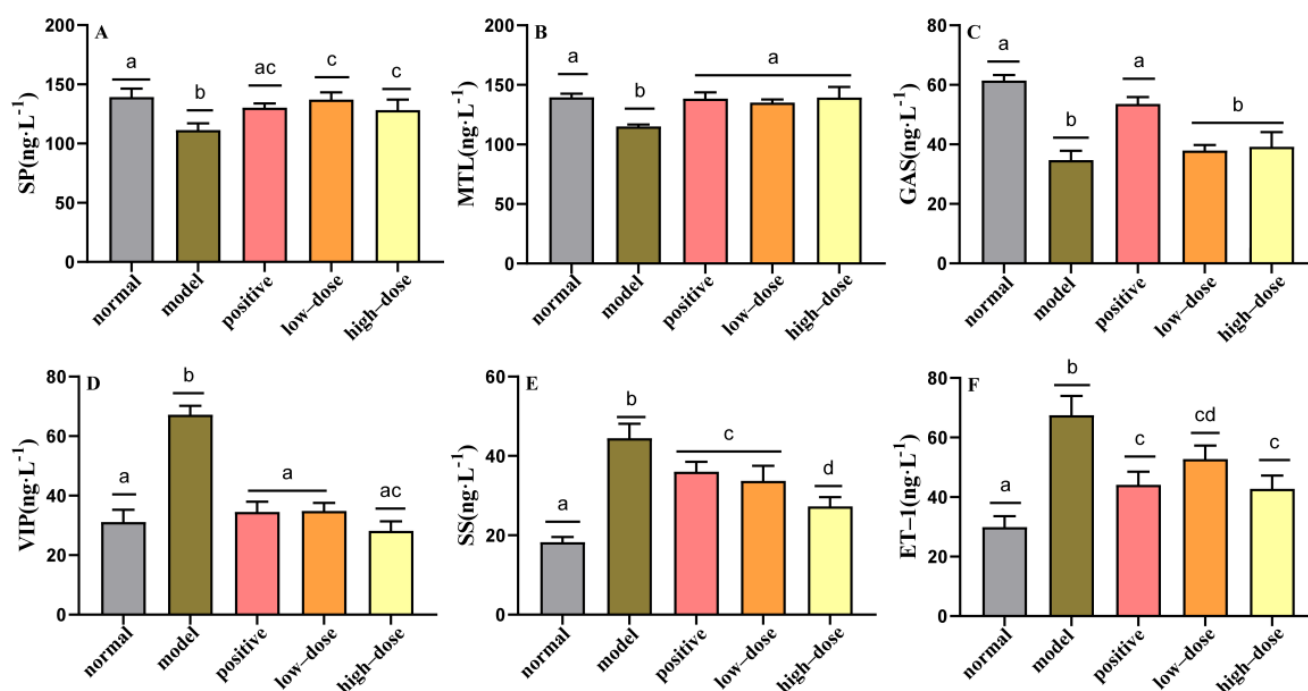


Figure 4. Effect of probiotic compounds on gastrointestinal peptides in intestinal tissues of constipated mice. (A) Substance P (SP). (B) Motilin (MTL). (C) Gastrin (GAS). (D) Vasoactive intestinal peptide (VIP). (E) Somatostatin (SS). (F) Endothelin (ET-1). Data are means with SEM. a–d: Different letters indicate significant differences ($p < 0.05$), and the same letters or no letters indicate no significant difference.

3.5. Effects of Probiotic Compounds on the Gut Microbiome

The components of α diversity (Pielou evenness, Faith index, Observed_otus, and Shannon index) were calculated to illustrate the effects of different concentrations of probiotic compounds on the gut microbiota. These indices allowed us to assess the changes in species richness and evenness, along with the overall diversity of the gut microbiota, at different intervention times. After the first gavage, the last gavage, one week after stopping gavage, and two weeks after stopping gavage, the Pielou index and Shannon index of the intestinal microbiota in the BK group remained stable, and the Faith and Observed_otus did not change significantly. However, the Pielou, Faith index, Observed_otus, and Shannon index changed in the groups fed probiotic compounds (Figure 5). In addition, different doses of probiotic compounds affected the species richness of the intestinal microbiota of mice. After stopping gavage for two weeks, the Pielou_e and Shannon index in the CD group were lower than those after the first gavage ($p < 0.05$). The Faith_pd index changed significantly between one and two weeks after stopping gavage ($p < 0.05$), but there was no significant difference between these points in the CG group (Figure 5D). The above results indicate that probiotic compounds affected the abundance and homogeneity of gut microbiota relative to the BK group, and different concentrations of probiotic compounds had different effects on the mice's microbiota over time after the end of the intervention. This may indicate that high-dose probiotic compounds maintain the diversity of intestinal microbiota and better maintain the stability of intestinal health. Thus, we conclude that probiotic compounds can colonize the intestines of mice, and different concentrations of probiotic compounds have different effects on colonization.

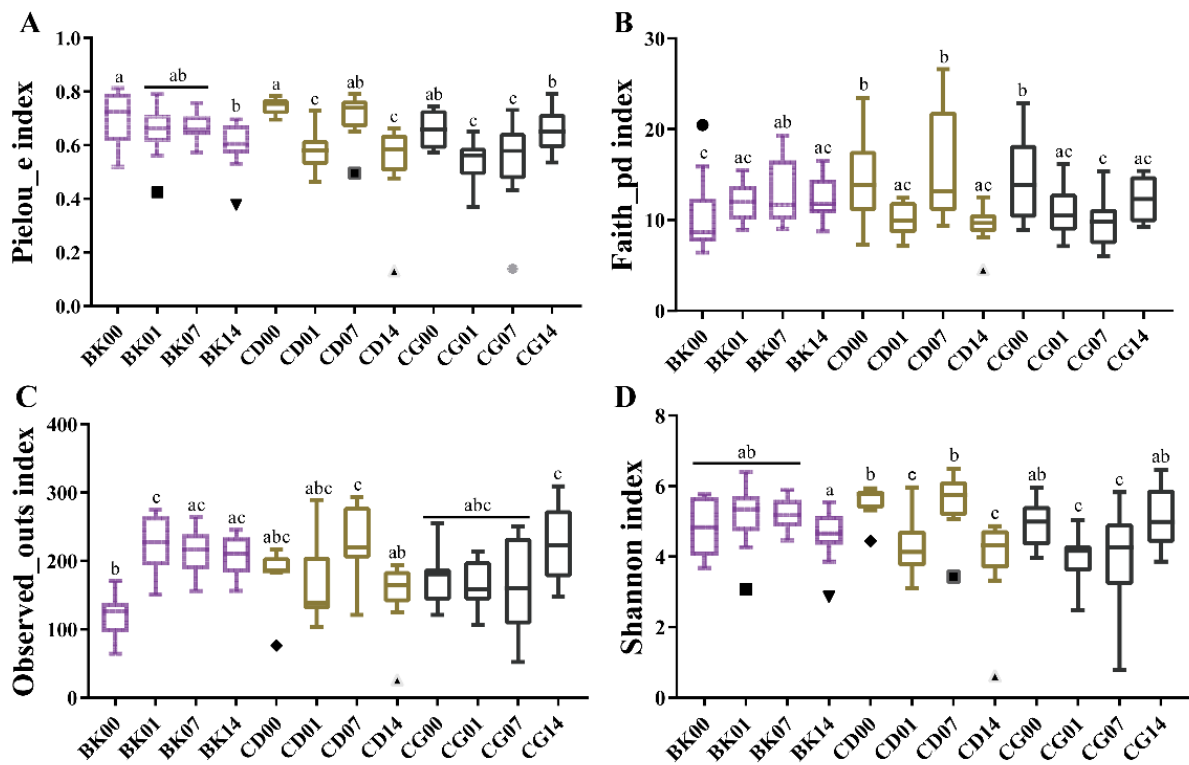


Figure 5. Treatment with probiotic compounds alters the diversity and structure of the gut microbiota. (A) α -Diversity index: Pielou_e. (B) α -Diversity index: Faith_pd. (C) α -Diversity index: Observed_otus. (D) α -Diversity index: Shannon. Normal group, BK; low-dose group, CD; high-dose group, CG; the first gavage, 00; the last gavage, 01; one week after stopping gavage, 07; two weeks after stopping gavage, 14. Statistical significance between groups is indicated by a–c, and different letters indicate that there was a significant difference between groups ($p < 0.05$, ANOVA, Tukey test).

Based on three different β -diversity distances (Bray–Curtis), the composition of gut microbiota was analyzed after the first gavage, the last gavage, one week after stopping gavage, and two weeks after stopping gavage with different concentrations of probiotic compounds. NMDS based on the Bray–Curtis index was used to analyze the beta diversity of gut microbiota in the four groups. The β -diversity showed that there was no significant change in the gut microbiota between the group fed probiotic compounds and the control group at the first gavage (Supplementary Figure S3), but the β -diversity of gut microbiota changed significantly over time ($p < 0.05$) (Figure 6A–C). Such findings indicate that the probiotic compounds affected the overall structure of the gut microbiota. After stopping gavage for two weeks, the gut microbiota in both the CD and CG groups still demonstrated a significant change ($p < 0.05$). PCoA analysis showed that the compositions of gut microbiota in the CD and CG groups changed significantly after the last gavage and two weeks after stopping gavage compared with the first gavage (Figure 6B,C). One week after stopping gavage and two weeks after stopping gavage, the microbiota in the CD and CG groups were different from that of the BK ($p < 0.05$) (Figure 6E,F).

The above results tell us that although the gut microbiota of each group did not change significantly at the beginning of the intervention, probiotic compounds were able to influence the gut microbiota, and that the effects persisted even when the interventions were stopped. This effect varied with time after the end of the intervention period. In addition, these results are consistent with the aforementioned results of the effects on intestinal microbiota diversity, further indicating that probiotic compounds were able to colonize the intestines of mice and that different concentrations of probiotic compounds had different effects on colonization.

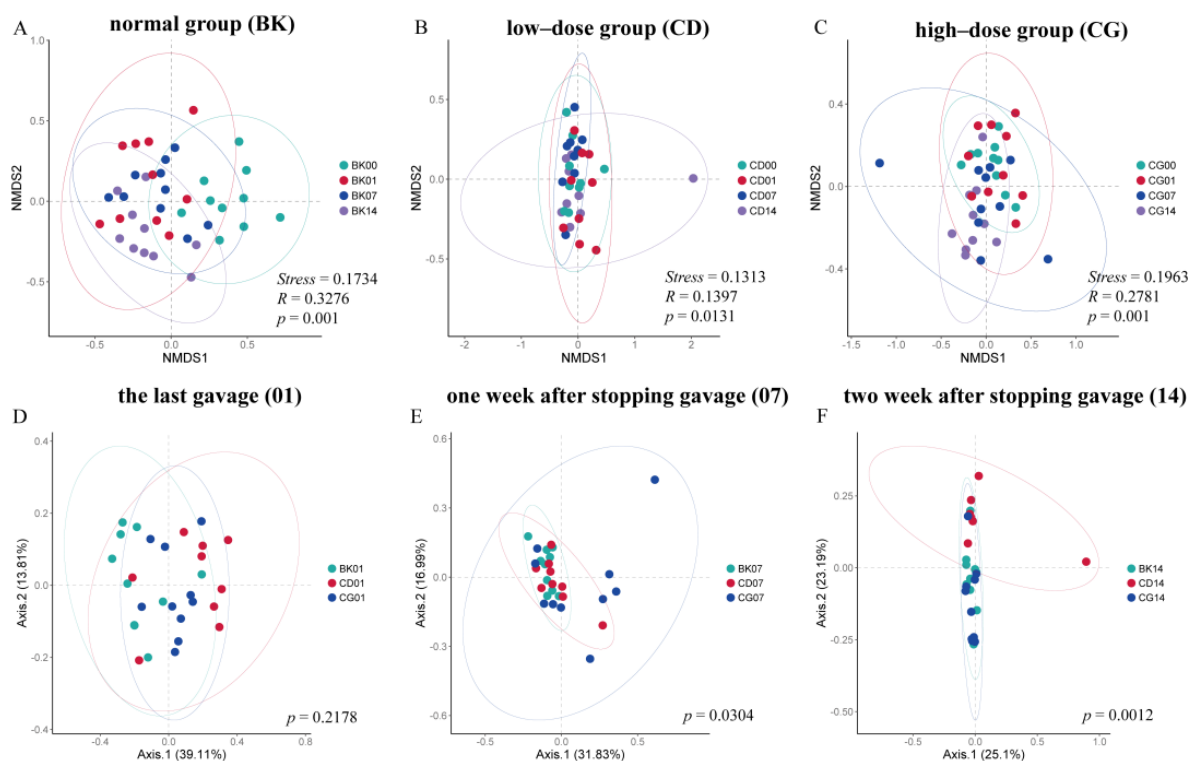


Figure 6. The effects of probiotic compounds on the overall structure of mouse gut microbiome. β -Diversity of gut microbiota at different time in (A) BK group, (B) CD group, (C) CG group. Principal component analysis based on Bray–Curtis distance matrices showed differences in the β -diversity of the gut microbiome among all groups at (D) the last gavage, (E) one week after stopping gavage, and (F) two weeks after stopping gavage. Normal group, BK; low-dose group, CD; high-dose group, CG; the first gavage, 00; the last gavage, 01; one week after stopping gavage, 07; two weeks after stopping gavage, 14.

At the phylum level, the gavage of probiotic compounds led to a decrease in the relative abundance of Bacteroides and an increase in that of Firmicutes (Figure 7A). A percentage accumulation map of the microbiota with the relative abundances of the top thirty at the genus level was created to reveal the gut microbial alterations. The abundances of *Lactobacillus* were high in the CD and CG groups, and *Akkermansia* was enriched in both CD14 and CG00 groups (Figure 7B). At the genus level, the relative abundance of *Lactobacillus* in the CD and CG groups increased with the gavage series, but slightly decreased with time after the end of the gavage period (Figure 7C). The relative abundance of *Bifidobacterium* decreased after the feeding of probiotic compounds, and did not change significantly after gavage stopped (Figure 7D). We further explored which *Lactobacillus* species changed after gavage, and found that *Ligilactobacillus murinus*, *Limosilactobacillus reuteri*, *Lactobacillus johnsonii*, and *Lacticaseibacillus rhamnosus* were enriched in CD and CG groups (Figure 7E). Lefse analysis was used to analyze the differences in gut microbiota of mice that were fed probiotic compounds at different times. In the CD group, the abundances of *Rikenellaceae* and *Lachnospiraceae* in fecal microbiota increased before gavage; the genes *Alistipes* increased significantly at the last gavage; the genera *Lactobacillus*, *Negativibacillus*, *Lachnospiraceae*, *FCS020.group*, *Blautia*, *Ruminococcaceae UCG_009*, and *Ruminiclostridium 9* increased significantly after one week of stopping gavage; and *Akkermansia* saw a significant increase two weeks after stopping gavage (Figure 7F). In contrast, in the CG group, the genera that significantly increased two weeks after stopping gavage included *Ruminiclostridium*, *Mucispirillum*, *Ruminiclostridium 9*, *Oscillibacter*, *Angelakisella*, *Bilophila*, *Ruminiclostridium 5*, *Tyzzereella*, *Ruminococcaceae UCG_004*, *Ruminococcaceae UCG_005*, *Ruminococcaceae UCG_003*, and *Peptococcus* (Figure 7G). The above results demonstrate that the gut microbiota of the mice were significantly altered at the genus level after interventions with probiotic compounds.

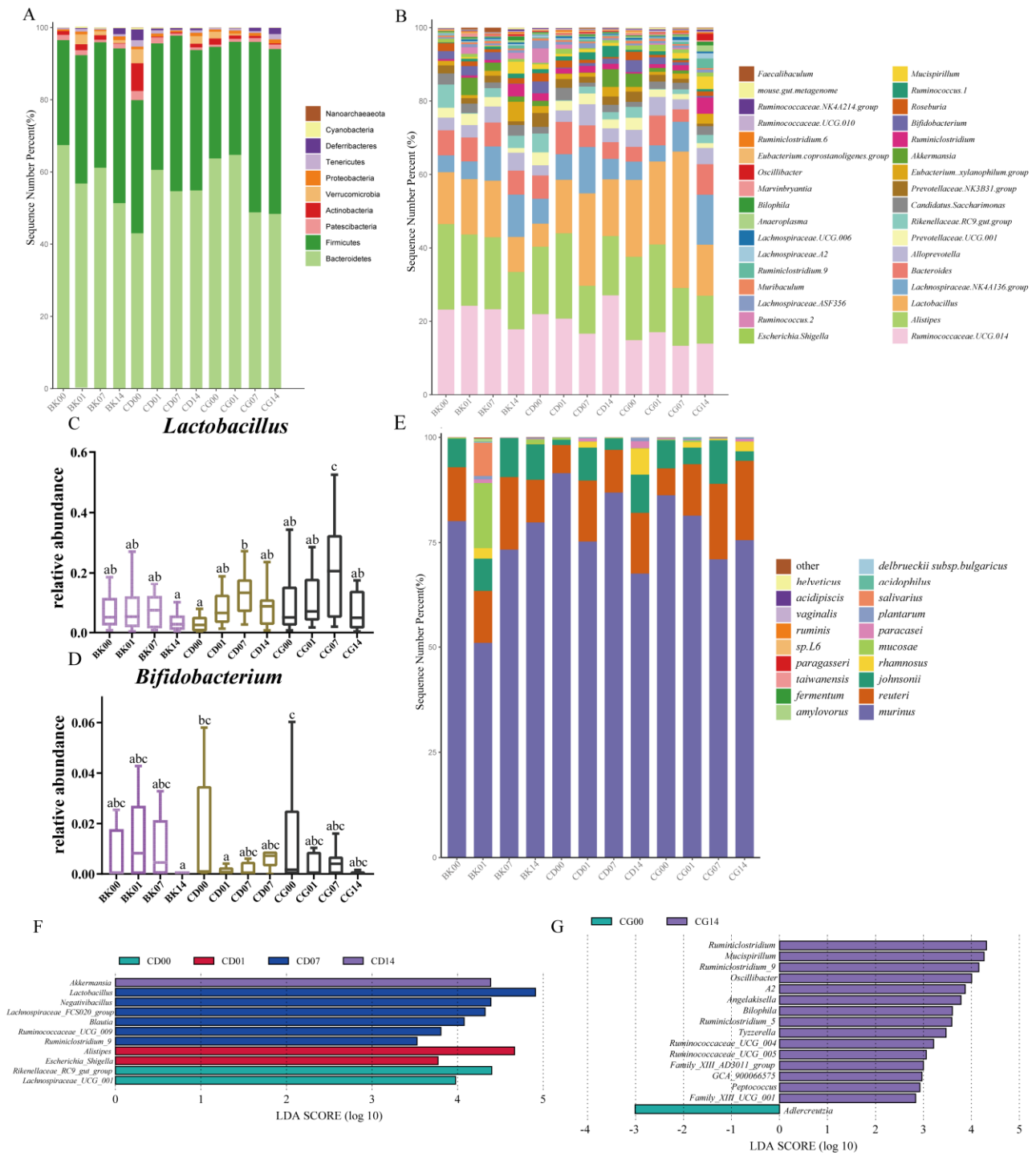


Figure 7. The effects of probiotic compounds on the composition of gut microbiota. (A) Microbial distribution at the phylum level. (B) Microbial distribution at the genus levels. (C,D) Relative abundances of the genera *Lactobacillus* and *Bifidobacterium*. Statistical significance between groups is indicated by a–c: different letters indicate that there is a difference between groups ($p < 0.05$, ANOVA, Tukey test). (E) Treatment with different concentrations of probiotic compounds altered the gut microbiota at the *Lactobacillus* species level. (F) Effects of low-dose probiotic compounds on the gut microbiota of mice at different times. (G) Effects of high-dose probiotic compounds on the gut microbiota of mice at different times. Normal group, BK; low-dose group, CD; high-dose group, CG; the first gavage, 00; the last gavage, 01; one week after stopping gavage, 07; two weeks after stopping gavage, 14.

Different concentrations of probiotic compounds affected the intestinal microbiome diversity, and continued to regulate the gut microbiota after the intervention was stopped, indicating that this product may colonize the intestinal tracts of mice. Therefore, we performed absolute quantitative sequencing of *Lactobacillus* and *Bifidobacterium* to further determine the amounts of compound probiotic colonization in the mice's intestines.

3.6. Colonization of Probiotic Compounds in Gut Microbiota

At the first gavage, the gut microbiota in the BK, CD, and CG groups mainly contained *L. rhamnosus*, *L. reuteri*, and *L. johnsonii* (Figure 7E). The relative abundance of *L. acidophilus* in the mouse intestine increased after the last gavage with probiotic compounds ($p < 0.05$). The colonization effect of the CG group was higher than that of the CD group; however, its relative abundance gradually returned to the state before gavage as time progressed, which indicates that the *L. acidophilus* in probiotic compounds could not colonize the mouse intestine for a long time. The relative abundance of *L. acidophilus* in the intestines of mice in the CD and CG groups reached its peak during the last gavage (Figure 8A). Our findings highlight that different concentrations of probiotic compounds have different effects on *L. acidophilus* colonization in the mouse intestine. After calculating its absolute content, it was found that *L. acidophilus* increased only during the last gavage in the CG group ($p < 0.05$), and that there were no major fluctuations in any other group during other periods (Figure 9A). This would suggest that the probiotic compounds cannot promote long-term colonization of *L. acidophilus* in the intestine.

The relative contents of *L. rhamnosus* and *L. plantarum* in the intestinal tract of the BK group were almost zero. After the last gavage of probiotic compounds, the relative abundances of these two types of *Lactobacillus* increased slightly (Figure 8B,D). Two weeks after stopping gavage, the relative abundances of *L. plantarum* in both CD and CG groups increased ($p < 0.05$); the increase in CD was larger than in CG ($p > 0.05$) (Figure 8D). Plus, the relative abundance of *L. rhamnosus* in CG increased. This indicates that *L. plantarum* and *L. rhamnosus* can be colonized very well in the mouse intestine under the beneficial effects of probiotic compounds, and that the colonization of *L. rhamnosus* was better at high concentrations, whereas the colonization of *L. plantarum* was better at low concentrations. The absolute content calculation results also showed that *L. plantarum* and *L. rhamnosus* had no major fluctuations after the first gavage, end of gavage, or one week after stopping gavage; but when the time reached two weeks after gavage, the absolute contents of *L. plantarum* and *L. rhamnosus* increased much more in mice fed probiotic compounds compared to the BK group (Figure 9C,D). This demonstrated that *L. plantarum* and *L. rhamnosus* indeed did colonize in the intestine, and for *L. rhamnosus* the effect of a high concentration was much greater than that of a low concentration. The colonization of *L. plantarum* was better at low concentrations.

Regardless of the relative or absolute level of *L. reuteri*, the abundance of *L. reuteri* increased compared the first gavage (Figures 8C and 9B). The effects of probiotic compounds on the *L. reuteri* colonization could be evaluated. The relative abundance of *L. reuteri* was increased gradually in CG groups, and the absolute contents increased in CD and CG groups, but decreased two weeks after stopping gavage compared to one weeks after stopping gavage. Such findings indicate that the probiotic compounds affected the structure of the gut microbiota, and *L. reuteri* could only colonize the intestines for a short time.

In addition to the changes in the relative abundances of *L. acidophilus*, *L. plantarum*, *L. reuteri*, and *L. rhamnosus*, the relative abundances of other microorganisms in the mouse intestine also changed after gavaging with different concentrations of probiotic compounds (Figure 8). The relative amounts of *L. fermentum* increased two weeks after stopping gavage in mice fed probiotic compounds. The relative abundance of *Lactobacillus johnsonii* increased two weeks after stopping gavage in CD group, and decreased two weeks after stopping gavage in the CG group. Importantly, such findings indicate that high doses of probiotics promoted the growth of *L. fermentum*, whereas low doses promoted that of *L. johnsonii* (Figure 8E,F). Through absolute quantification of *Bifidobacterium animalis* subsp. *Lactis*,

it was found that the BK group had a high content of *B. lactis*, and the CD group had a high content of *B. lactis*, initially. After one month of intragastric administration, the content of *B. lactis* decreased, and the content of *B. lactis* gradually increased and remained steady, indicating that the *B. lactis* in the intestines have the ability to self-regulate. The *B. lactis* did not increase after gavage with high-dose probiotics compounds, and its content gradually decreased after the gavage, which indicated that the ability of *B. lactis* to colonize the intestinal tract in the high-dose group was not as good as in the low-dose group (Supplementary Figure S3).

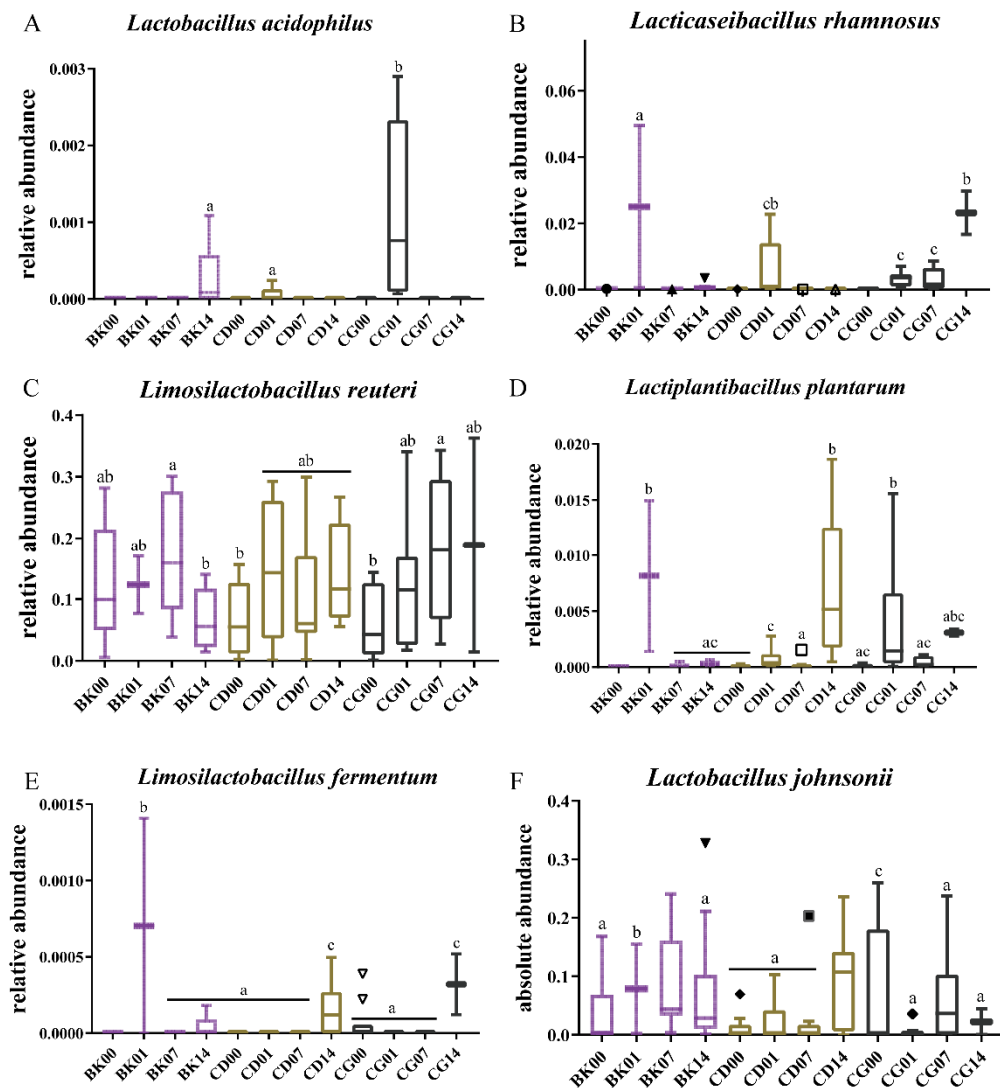


Figure 8. Effects of different probiotic compound combinations on the gut microbiota at the *Lactobacillus* species level. (A–F) Relative abundances of the genera *Lactobacillus acidophilus*, *Lacticaseibacillus rhamnosus*, *Limosilactobacillus reuteri*, *Lactiplantibacillus plantarum*, *Limosilactobacillus fermentum*, and *Lactobacillus johnsonii*. Normal group, BK; low-dose group, CD; high-dose group, CG; the first gavage, 00; the last gavage, 01; one week after stopping gavage, 07; two weeks after stopping gavage, 14. Statistical significance between groups is indicated by a–c: different letters indicate that there is a difference between groups ($p < 0.05$, ANOVA, Tukey test).

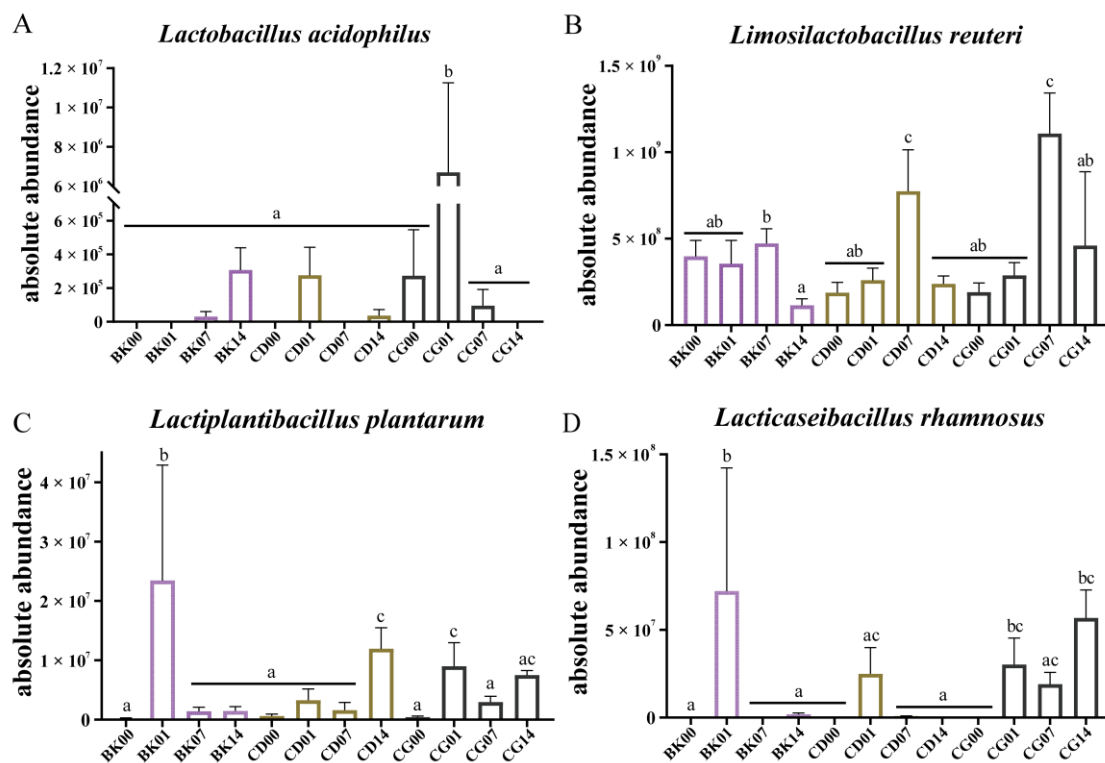


Figure 9. Absolute abundances of the *Lactobacillus* species with respect to the effects of probiotic compounds. Probiotic compounds included (A) *Lactobacillus acidophilus*; (B) *Limosilactobacillus reuteri*; (C) *Lactiplantibacillus plantarum*; (D) *Lacticaseibacillus rhamnosus*. Normal group, BK; low-dose group, CD; high-dose group, CG; the first gavage, 00; the last gavage, 01; one week after stopping gavage, 07; two weeks after stopping gavage, 14. Statistical significance between groups is indicated by a–c: different letters indicate that there is a difference between groups ($p < 0.05$, ANOVA, Tukey test).

4. Discussion

Constipation is a common and highly prevalent condition worldwide [18,19]. It is conventionally treated with laxatives and other drugs that cannot be used long-term because of their side effects [20]. Therefore, there is an urgent need for a safe and long-term treatment for constipation. To that end, the use of probiotics has been recommended by some scholars based on evidence from animal and clinical studies [8,21,22]. Despite the popularity of probiotics as a dietary approach for the treatment of constipation, their specific mechanism of action remains unknown [23]. In this study, the effects of probiotic compounds on the symptoms of constipation in mice and their mechanisms of colonization in gut microbiota were investigated. The probiotic compounds can promote bowel movement, improve bowel movement frequency, increase the number and weight of stools, and effectively alleviate constipation. We found that the symptoms of constipation and gut microbiome composition were both significantly changed as a result of interventions with probiotic compounds. Thus, our results provide valuable insights into the interactions among probiotics, the microbiome, and constipation.

Recent clinical studies have found that probiotics can be a useful tool for the treatment of constipation and can yield significant results [24–26], such as improvements in gastrointestinal regulatory peptides, neurotransmitters, neurotrophic factors, and the gut microbiota. We found that probiotic compounds could improve the GI transit rate significantly in low and high-dose groups by improving intestinal function and intestinal motility, thereby reducing the time till the first black stool defecation. Treatment with probiotic compounds can effectively improve intestinal motility and accelerate the movement and exit of chyme via the small intestine. The GI transit rate reflects the dynamics of the small intestine and may thus reflect the effect of probiotic compounds on intestinal motility. We

found no significant difference between the low and high-dose groups in improving either the intestinal transit rate or small intestinal motility. The gastrointestinal hormones play important physiological roles in the regulation of the motor activity of the gastrointestinal tract. In our study, we found that probiotic compounds can enhance the abnormalities of SP, MTL, and GAS, and reduce the abnormalities of VIP, SS, and ET-1, thereby regulating gastrointestinal regulatory hormones and relieving constipation.

Intake of probiotics can regulate the fecal microbiota, increase the levels of organic acids to promote intestinal peristalsis, shorten the colon operation time, and lessen symptoms of constipation. Studies have also found that the abundances of *Bifidobacterium* and *Lactobacillus* in the feces of adults with constipation are significantly reduced [27,28]. After supplementing with specific probiotics, constipation can be improved by promoting intestinal peristalsis and defecation frequency under the action of the gut microbiome [29–31], mainly by increasing the relative abundance of *Ruminococcaceae* [32]. In a population experiment using the probiotics of *Streptococcus thermophilus* and *L. plantarum*, it was found that the abundances of *Lactobacillus* and *Bifidobacterium* in the intestines increased after the intervention, thereby shortening the transit time of feces in the intestine and increasing the frequency and volume of bowel movements [33]. In addition, prebiotic chitosan oligosaccharides can significantly increase intestinal motility, inhibit intestinal barrier damage and the inflammatory response, and improve the water–electrolyte balance in constipation model mice, thereby increasing the frequency of defecation and the dry-wet weight ratio of feces in mice [34]. They further explored why chitosan oligosaccharides can relieve constipation, and found that it improves the gut microbiome imbalance of constipated mice at the levels of phyla, family, and genus. They accomplish this by reducing the ratio of Firmicutes to Bacteroides [35]; increasing the abundances of *Bacteroides*, *Lactobacillus*, and *Faecalibaculus*; and decreasing the populations of *Bilophila*, *Lachnospiraceae*, and *Ruminococcaceae* in constipated mice, thereby regulating the metabolism of bile acid and tryptophan [34,36]. Tryptamine produced by the metabolism of tryptophan by gut bacteria can activate G-protein-coupled receptors (5-HT₄ receptors) on colonic epithelial cells, thereby increasing colonic secretion, promoting gastrointestinal transport, and bringing inspiration for the treatment of constipation [12]. In our experiment, it was also found that *Lactobacillus* abundance increased after intervention with low and high doses of probiotic compounds; *Ruminococcaceae* abundance increased after intervention with low and high doses of probiotic compounds; and *Akkermansia* were enriched two weeks after stopping gavage in the low-dose group (Figure 6F). A double-blind, randomized, cross-over intervention study analyzed the effect of inulin consumption on stool frequency in healthy adults with mild constipation. They found inulin did not significantly change the metabolome and had a mild effect on the composition of the gut microbiota. It specifically increased the *Anaerostipes* and *Bifidobacterium* abundances, and reduced the relative abundance of *Bilophila* [37]. However, in our experiment, *Bilophila* had a significant role two weeks after stopping gavage in the CG group (Figure 7G). This difference could be due to differences in the intestinal microbiota of humans and mice. In addition, probiotics can be regarded as safe and natural agents for the alleviation of functional constipation in adults, and there are some probiotic products that can relieve constipation. The strains used included *Streptococcus salivarius* subsp. *thermophilus*, *Enterococcus faecium*, *L. rhamnosus* GG, *L. acidophilus*, *L. plantarum*, *Lactocaseibacillus paracasei*, *L. bulgaricus*, and *Bifidobacterium* (*breve* and *animalis* subsp. *lactis*) [38,39], and the weekly stool volumes of probiotic-treated subjects increased significantly. The probiotic compounds we used to gavage the mice also contained *L. acidophilus*, *L. rhamnosus*, *L. reuteri*, *L. plantarum*, and *Bifidobacterium animalis* subsp. *lactis*. More importantly, the probiotic compounds were found to modulate intestinal bacterial communities—the main gut microbiota in the CD and CG group became *L. rhamnosus*, *L. reuteri*, and *L. johnsonii*. Even two weeks after stopping the gavage, we found that *L. plantarum* and *L. rhamnosus* could still colonize the intestinal tract, and that a higher dose of probiotic could promote the colonization of specific strains. In addition, studies have reported that *L. plantarum* and *L. reuteri* can metabolize tryptophan and produce metabolites

that help relieve constipation [40]. The above results show that different concentrations of probiotic compounds promote *Lactobacillus* colonize the intestines of mice, and that the colonization after high-dosage probiotic treatments was generally better than after low-dose treatments. From the perspective of the relative abundances of specific species, the colonization extents of different *Lactobacillus* species in the mouse intestine were also different. The colonization extents of *L. plantarum* and *L. rhamnosus* were generally better than those of *L. acidophilus* and *L. reuteri*. In addition, different concentrations of probiotic compounds impacted the species composition of *Lactobacillus* in the gut microbiota of the mice.

5. Conclusions

The probiotic compounds alleviated the symptoms of constipation, improved the rate of intestinal motility, and increased the amount of stool. At the same time, the *Lactobacillus* and *Bifidobacterium* in the intestinal tract were changed to regulate the gut microbiota. More importantly, after the intervention was over, the abundances of probiotic compounds could still be detected, which meant that they could be colonized in the intestinal tract and played a role in regulating the gut microbiota and alleviating constipation. The effect of regulating the microbiota of the five strains combined might be better than that of a single probiotic. We found that probiotic compounds are beneficial for the clinical treatment of constipation.

Supplementary Materials: Figure S1: Effect of probiotic compounds on serum cytokines in a mouse model of constipation, (A) IL-2. (B) IL-4. (C) IL-6. (D) IL-10. (E) IL-12. (F) IL-17. (G) TNF- α . (H) TNF- γ . Figure S2: Effect of probiotic compounds on serum indexes in a mouse model of constipation. (A) Occludin. (B) D-lactic acid. (C) sIgA. Figure S3: Principal component analysis based on Bray–Curtis distance matrices showed difference in the β -diversity of the gut microbiome at the first gavage and absolute abundance of the *Bifidobacterium animalis* subsp. *lactis*. Table S1: Bacterias 16S rRNA V3-V4 50 μ L PCR reaction system.

Author Contributions: Conceptualization, H.W.; methodology, L.Z. and Y.H.; software, W.Y., M.P. and L.Z.; validation, Y.H., H.W. and J.C.; formal analysis, W.Y., L.Z. and M.P.; investigation, Y.H. and J.C.; resources, J.C. and X.T.; data curation, W.Y., M.P. and L.Z.; writing—original draft preparation, Y.H. and H.W.; writing—review and editing, Y.H., H.W. and X.T.; visualization, Y.H., M.P. and L.Z.; supervision, H.W. and X.T.; project administration, H.W.; funding acquisition, H.W. All authors have read and agreed to the published version of the manuscript.

Funding: This work was supported by the National Natural Science Foundation of China (No. 3140038).

Institutional Review Board Statement: The animal study protocol was approved by the Ethics Committee of Jiangnan University (JN.No20190930b0600120).

Data Availability Statement: All data generated or used during the study appear in the submitted article. The raw sequencing data have been deposited in the NCBI SRA repository, bioproject accession number is PRJNA793720.

Acknowledgments: The probiotic powder contains *Lactobacillus acidophilus* LA11-Only, *Lactis-eibacillus rhamnosus* LR22, *Limosilactobacillus reuteri* LE16, *Lactiplantibacillus plantarum* LP-Only, and *Bifidobacterium animalis* subsp. *lactis* BI516, is provided by Sirio Pharma Co., Ltd. (Guangdong, China).

Conflicts of Interest: The authors declare no conflict of interest.

Sample Availability: Not available.

References

1. Dimidi, E.; Zdanaviciene, A.; Christodoulides, S.; Taheri, S.; Louis, P.; Duncan, P.I.; Emami, N.; Crabbe, R.; De Castro, C.A.; McLean, P.; et al. Randomised clinical trial: *Bifidobacterium lactis* NCC2818 probiotic vs placebo, and impact on gut transit time, symptoms, and gut microbiology in chronic constipation. *Aliment. Pharmacol. Ther.* **2019**, *49*, 251–264. [CrossRef] [PubMed]
2. Rao, S.S.C.; Rattanakovit, K.; Patcharatrakul, T. Diagnosis and management of chronic constipation in adults. *Nat. Rev. Gastroenterol. Hepatol.* **2016**, *13*, 295–305. [CrossRef]

3. Choopani, R.; Ghourchian, A.; Hajimehdipoor, H.; Kamalinejad, M.; Ghourchian, F. Effect of *Descurainia sophia* (L.) Webb ex Prantl on Adult Functional Constipation: A Prospective Pilot Study. *J. Evid. Based Integr. Med.* **2017**, *22*, 646–651. [CrossRef] [PubMed]
4. Sharma, A.; Rao, S. Constipation: Pathophysiology and Current Therapeutic Approaches. *Handb. Exp. Pharmacol.* **2017**, *239*, 59–74. [CrossRef]
5. Johanson, J.F.; Kralstein, J. Chronic constipation: A survey of the patient perspective. *Aliment. Pharmacol. Ther.* **2007**, *25*, 599–608. [CrossRef] [PubMed]
6. Koliiani-Pace, J.; Lacy, B.E. Update on the Management of Chronic Constipation. *Curr. Treat. Options Gastroenterol.* **2017**, *15*, 126–134. [CrossRef]
7. Wen, Y.; Li, J.; Long, Q.; Yue, C.C.; He, B.; Tang, X.G. The efficacy and safety of probiotics for patients with constipation-predominant irritable bowel syndrome: A systematic review and meta-analysis based on seventeen randomized controlled trials. *Int. J. Surg.* **2020**, *79*, 111–119. [CrossRef] [PubMed]
8. Kamiński, M.; Skonieczna-Żydecka, K.; Loniewski, I.; Koulaouzidis, A.; Marlicz, W. Are probiotics useful in the treatment of chronic idiopathic constipation in adults? A review of existing systematic reviews, meta-analyses, and recommendations. *Prz. Gastroenterol.* **2020**, *15*, 103–118. [CrossRef]
9. Dimidi, E.; Scott, S.M.; Whelan, K. Probiotics and constipation: Mechanisms of action, evidence for effectiveness and utilisation by patients and healthcare professionals. *Proc. Nutr. Soc.* **2020**, *79*, 147–157. [CrossRef]
10. Riezzo, G.; Chimienti, G.; Orlando, A.; D’Attoma, B.; Clemente, C.; Russo, F. Effects of long-term administration of *Lactobacillus reuteri* DSM-17938 on circulating levels of 5-HT and BDNF in adults with functional constipation. *Benef. Microbes* **2019**, *10*, 137–147. [CrossRef]
11. Miller, L.E.; Ouwehand, A.C.; Ibarra, A. Effects of probiotic-containing products on stool frequency and intestinal transit in constipated adults: Systematic review and meta-analysis of randomized controlled trials. *Ann. Gastroenterol.* **2017**, *30*, 629–639. [CrossRef]
12. Bhattarai, Y.; Williams, B.B.; Battaglioli, E.J.; Whitaker, W.R.; Till, L.; Grover, M.; Linden, D.R.; Akiba, Y.; Kandimalla, K.K.; Zachos, N.C.; et al. Gut Microbiota-Produced Tryptamine Activates an Epithelial G-Protein-Coupled Receptor to Increase Colonic Secretion. *Cell Host Microbe* **2018**, *23*, 775. [CrossRef]
13. Bolyen, E.; Rideout, J.R.; Dillon, M.R.; Bokulich, N.A.; Abnet, C.C.; Al-Ghalith, G.A.; Alexander, H.; Alm, E.J.; Arumugam, M.; Asnicar, F.; et al. Reproducible, interactive, scalable, and extensible microbiome data science using QIIME 2. *Nat. Biotechnol.* **2019**, *37*, 852–857. [CrossRef]
14. Hu, L.J.; Lu, W.W.; Wang, L.L.; Pan, M.L.; Zhang, H.; Zhao, J.X.; Chen, W. Assessment of *Bifidobacterium* Species Using *groEL* Gene on the Basis of Illumina MiSeq High-Throughput Sequencing. *Genes* **2017**, *8*, 15. [CrossRef] [PubMed]
15. Xie, M.Q.; Pan, M.L.; Jiang, Y.; Liu, X.M.; Lu, W.W.; Zhao, J.X.; Zhang, H.; Chen, W. *groEL* Gene-Based Phylogenetic Analysis of *Lactobacillus* Species by High-Throughput Sequencing. *Genes* **2019**, *10*, 12. [CrossRef]
16. Rivas, M.N.; Burton, O.T.; Wise, P.; Zhang, Y.Q.; Hobson, S.A.; Lloret, M.G.; Chehoud, C.; Kuczynski, J.; DeSantis, T.; Warrington, J.; et al. A microbiota signature associated with experimental food allergy promotes allergic sensitization and anaphylaxis. *J. Allergy Clin. Immunol.* **2013**, *131*, 201–212. [CrossRef] [PubMed]
17. Segata, N.; Izard, J.; Waldron, L.; Gevers, D.; Miropolsky, L.; Garrett, W.S.; Huttenhower, C. Metagenomic biomarker discovery and explanation. *Genome Biol.* **2011**, *12*, 18. [CrossRef]
18. Vriesman, M.H.; Koppen, I.J.N.; Camilleri, M.; Di Lorenzo, C.; Benninga, M.A. Management of functional constipation in children and adults. *Nat. Rev. Gastroenterol. Hepatol.* **2020**, *17*, 21–39. [CrossRef] [PubMed]
19. Sbahi, H.; Cash, B.D. Chronic Constipation: A Review of Current Literature. *Curr. Gastroenterol. Rep.* **2015**, *17*, 47. [CrossRef]
20. Korterink, J.J.; Rutten, J.; Venmans, L.; Benninga, M.A.; Tabbers, M.M. Pharmacologic Treatment in Pediatric Functional Abdominal Pain Disorders: A Systematic Review. *J. Pediatr.* **2015**, *166*, 424. [CrossRef]
21. Wang, L.L.; Hu, L.J.; Xu, Q.; Jiang, T.; Fang, S.G.; Wang, G.; Zhao, J.X.; Zhang, H.; Chen, W. *Bifidobacteria* exert species-specific effects on constipation in BALB/c mice. *Food Funct.* **2017**, *8*, 3587–3600. [CrossRef]
22. Tan, A.H.; Lim, S.Y.; Chong, K.K.; Hor, J.W.; Lim, J.L.; Low, S.C.; Chong, C.W.; Mahadeva, S.; Lang, A.E. Probiotics for Constipation in Parkinson Disease: A Randomized Placebo-Controlled Study. *Neurology* **2021**, *96*, e772–e782. [CrossRef]
23. Wang, G.; Yang, S.; Sun, S.; Si, Q.; Wang, L.; Zhang, Q.; Wu, G.; Zhao, J.; Zhang, H.; Chen, W. *Lactobacillus rhamnosus* Strains Relieve Loperamide-Induced Constipation via Different Pathways Independent of Short-Chain Fatty Acids. *Front. Cell. Infect. Microbiol.* **2020**, *10*, 423. [CrossRef]
24. Yoon, J.Y.; Cha, J.M.; Oh, J.K.; Tan, P.L.; Kim, S.H.; Kwak, M.S.; Jeon, J.W.; Shin, H.P. Probiotics Ameliorate Stool Consistency in Patients with Chronic Constipation: A Randomized, Double-Blind, Placebo-Controlled Study. *Dig. Dis. Sci.* **2018**, *63*, 2754–2764. [CrossRef]
25. Ibarra, A.; Latreille-Barbier, M.; Donazzolo, Y.; Pelletier, X.; Ouwehand, A.C. Effects of 28-day *Bifidobacterium animalis* subsp. *lactis* HN019 supplementation on colonic transit time and gastrointestinal symptoms in adults with functional constipation: A double-blind, randomized, placebo-controlled, and dose-ranging trial. *Gut Microbes* **2018**, *9*, 236–251. [CrossRef] [PubMed]
26. Barichella, M.; Pacchetti, C.; Bolliri, C.; Cassani, E.; Iorio, L.; Pusani, C.; Pinelli, G.; Privitera, G.; Cesari, I.; Faierman, S.A.; et al. Probiotics and prebiotic fiber for constipation associated with Parkinson disease: An RCT. *Neurology* **2016**, *87*, 1274–1280. [CrossRef] [PubMed]

27. Shin, A.; Preidis, G.A.; Shulman, R.; Kashyap, P.C. The Gut Microbiome in Adult and Pediatric Functional Gastrointestinal Disorders. *Clin. Gastroenterol. Hepatol.* **2019**, *17*, 256–274. [CrossRef] [PubMed]
28. Zhu, L.X.; Liu, W.S.; Alkhoury, R.; Baker, R.D.; Bard, J.E.; Quigley, E.M.; Baker, S.S. Structural changes in the gut microbiome of constipated patients. *Physiol. Genom.* **2014**, *46*, 679–686. [CrossRef]
29. Husebye, E.; Hellstrom, P.M.; Sundler, F.; Chen, J.; Midtvedt, T. Influence of microbial species on small intestinal myoelectric activity and transit in germ-free rats. *Am. J. Physiol. Gastroint. Liver Physiol.* **2001**, *280*, G368–G380. [CrossRef]
30. Ishizuka, A.; Tomizuka, K.; Aoki, R.; Nishijima, T.; Saito, Y.; Inoue, R.; Ushida, K.; Mawatari, T.; Ikeda, T. Effects of administration of *Bifidobacterium animalis* subsp. *lactis* GCL2505 on defecation frequency and bifidobacterial microbiota composition in humans. *J. Biosci. Bioeng.* **2012**, *113*, 587–591. [CrossRef] [PubMed]
31. Escribano, J.; Ferrer, N.; Gispert-Llaurado, M.; Luque, V.; Rubio-Torrents, C.; Zaragoza-Jordana, M.; Polanco, I.; Codoner, F.M.; Chenoll, E.; Morera, M.; et al. *Bifidobacterium longum* subsp. *infantis* CECT7210-supplemented formula reduces diarrhea in healthy infants: A randomized controlled trial. *Pediatr. Res.* **2018**, *83*, 1120–1128. [CrossRef]
32. Martoni, C.J.; Evans, M.; Chow, C.E.T.; Chan, L.S.; Leyer, G. Impact of a probiotic product on bowel habits and microbial profile in participants with functional constipation: A randomized controlled trial. *J. Dig. Dis.* **2019**, *20*, 435–446. [CrossRef] [PubMed]
33. Eor, J.Y.; Tan, P.L.; Lim, S.M.; Choi, D.H.; Yoon, S.M.; Yang, S.Y.; Kim, S.H. Laxative effect of probiotic chocolate on loperamide-induced constipation in rats. *Food Res. Int.* **2019**, *116*, 1173–1182. [CrossRef]
34. Zhang, X.Y.; Yang, H.B.; Zheng, J.P.; Jiang, N.; Sun, G.J.; Bao, X.K.; Lin, A.Z.; Liu, H.T. Chitosan oligosaccharides attenuate loperamide-induced constipation through regulation of gut microbiota in mice. *Carbohydr. Polym.* **2021**, *253*, 13. [CrossRef] [PubMed]
35. Kashyap, P.C.; Marcobal, A.; Ursell, L.K.; Larauche, M.; Duboc, H.; Earle, K.A.; Sonnenburg, E.D.; Ferreyra, J.A.; Higginbottom, S.K.; Million, M.; et al. Complex Interactions Among Diet, Gastrointestinal Transit, and Gut Microbiota in Humanized Mice. *Gastroenterology* **2013**, *144*, 967–977. [CrossRef] [PubMed]
36. Alemi, F.; Poole, D.P.; Chiu, J.; Schoonjans, K.; Cattaruzza, F.; Grider, J.R.; Bunnett, N.W.; Corvera, C.U. The Receptor TGR5 Mediates the Prokinetic Actions of Intestinal Bile Acids and Is Required for Normal Defecation in Mice. *Gastroenterology* **2013**, *144*, 145–154. [CrossRef]
37. Vandeputte, D.; Falony, G.; Vieira-Silva, S.; Wang, J.; Sailer, M.; Theis, S.; Verbeke, K.; Raes, J. Prebiotic inulin-type fructans induce specific changes in the human gut microbiota. *Gut* **2017**, *66*, 1968–1974. [CrossRef]
38. Zhang, C.C.; Jiang, J.C.; Tian, F.W.; Zhao, J.X.; Zhang, H.; Zhai, Q.X.; Chen, W. Meta-analysis of randomized controlled trials of the effects of probiotics on functional constipation in adults. *Clin. Nutr.* **2020**, *39*, 2960–2969. [CrossRef]
39. Liu, A.L.T.; Chen, S.; Jena, P.K.; Sheng, L.L.; Hu, Y.; Wan, Y.J.Y. Probiotics Improve Gastrointestinal Function and Life Quality in Pregnancy. *Nutrients* **2021**, *13*, 9. [CrossRef] [PubMed]
40. Wang, G.; Huang, S.; Wang, Y.M.; Cai, S.; Yu, H.T.; Liu, H.B.; Zeng, X.F.; Zhang, G.L.; Qiao, S.Y. Bridging intestinal immunity and gut microbiota by metabolites. *Cell. Mol. Life Sci.* **2019**, *76*, 3917–3937. [CrossRef]

Article

Chemical Composition and Thermogravimetric Behaviors of Glanded and Glandless Cottonseed Kernels

Zhongqi He ^{1,*} , Sunghyun Nam ¹ , Hailin Zhang ²  and Ocen Modesto Olanya ³ 

¹ United States Department of Agriculture-Agricultural Research Service, Southern Regional Research Center, 1100 Robert E Lee Blvd., New Orleans, LA 70124, USA; sunghyun.nam@usda.gov

² Department of Plant and Soil Sciences, Oklahoma State University, Stillwater, OK 74078, USA; hailin.zhang@okstate.edu

³ United States Department of Agriculture-Agricultural Research Service, Eastern Regional Research Center, Wyndmoor, PA 19038, USA; modesto.olanya@usda.gov

* Correspondence: zhongqi.he@usda.gov

Abstract: Common “glanded” (Gd) cottonseeds contain the toxic compound gossypol that restricts human consumption of the derived products. The “glandless” (Gl) cottonseeds of a new cotton variety, in contrast, show a trace gossypol content, indicating the great potential of cottonseed for agro-food applications. This work comparatively evaluated the chemical composition and thermogravimetric behaviors of the two types of cottonseed kernels. In contrast to the high gossypol content (3.75 g kg⁻¹) observed in Gd kernels, the gossypol level detected in Gl kernels was only 0.06 g kg⁻¹, meeting the FDA’s criteria as human food. While the gossypol gland dots in Gd kernels were visually observed, scanning electron microscopy was not able to distinguish the microstructural difference between ground Gd and Gl samples. Chemical analysis and Fourier transform infrared (FTIR) spectroscopy showed that Gl kernels and Gd kernels had similar chemical components and mineral contents, but the former was slightly higher in protein, starch, and phosphorus contents. Thermogravimetric (TG) processes of both kernels and their residues after hexane and ethanol extraction were based on three stages of drying, de-volatilization, and char formation. TG-FTIR analysis revealed apparent spectral differences between Gd and Gl samples, as well as between raw and extracted cottonseed kernel samples, indicating that some components in Gd kernels were more susceptible to thermal decomposition than Gl kernels. The TG and TG-FTIR observations suggested that the Gl kernels could be heat treated (e.g., frying and roasting) at an optimal temperature of 140–150 °C for food applications. On the other hand, optimal pyrolysis temperatures would be much higher (350–500 °C) for Gd cottonseed and its defatted residues for non-food bio-oil and biochar production. The findings from this research enhance the potential utilization of Gd and Gl cottonseed kernels for food applications.

Keywords: cottonseed; fourier transform infrared spectroscopy; glandless; scanning electron microscopy; thermogravimetric analysis

Citation: He, Z.; Nam, S.; Zhang, H.; Olanya, O.M. Chemical Composition and Thermogravimetric Behaviors of Glanded and Glandless Cottonseed Kernels. *Molecules* **2022**, *27*, 316. <https://doi.org/10.3390/molecules27010316>

Academic Editor: Mirella Nardini

Received: 3 December 2021

Accepted: 2 January 2022

Published: 5 January 2022

Publisher’s Note: MDPI stays neutral with regard to jurisdictional claims in published maps and institutional affiliations.



Copyright: © 2022 by the authors. Licensee MDPI, Basel, Switzerland. This article is an open access article distributed under the terms and conditions of the Creative Commons Attribution (CC BY) license (<https://creativecommons.org/licenses/by/4.0/>).

1. Introduction

Cottonseed is a major product of cotton (*Gossypium* spp.) crops after fiber harvest [1,2]. The current global cottonseed production is estimated at 42×10^6 Mg annually [3]. Currently, cotton fiber accounts for 85–90% of the value of the crop while cottonseed accounts for the rest, a small share even though there are 150 kg of cottonseed produced for every 100 kg fiber ginned [4]. Cottonseeds can be utilized directly or further processed into five products, i.e., linter (8%), hulls (27%), crude oil (16%), meal (protein and carbohydrate, 45%), and waste (4%) [4,5]. Refined cottonseed oil is edible, and has been used in the food industry as a cooking oil or an ingredient in salad dressing, shortening, and mayonnaise, so it contributes currently to the major income of cottonseed processing [4,6]. However, the nutrient-rich whole cottonseed and its non-oil products cannot be used

directly for human and other monogastric animal consumption, due to the presence of the toxic compound gossypol [$C_{30}H_{30}O_8$, 1,1,6,6,7,7-hexahydroxy-5,5-diisopropyl-3,3-dimethyl-(2,2-binaphthalene)-8,8-dicarbaldehyde, or 2,2'-bis-(formyl-1,6,7-trihydroxy-5-isopropyl-3-methylnaphthalene)] stored mainly in the pigment glands [7,8]. Gossypol not only can lead to liver damage and even fibrosis itself, but also can combine easily with the ϵ -amino group of lysine of protein fractions, resulting in a decrease of lysine activity, which makes lysine become the first limiting amino acid in nutrition [9,10]. Thus, research efforts have been made to produce a new type of cottonseed in which gossypol is present only in trace amounts so that the cottonseed and its value added products can be used for animal feeds and human foods [11–13]. To distinguish the two types of cottonseeds, the new type is called “glandless” (Gl) while the traditional type is called “glanded” (Gd) cottonseed (Figure 1). While there is plenty of research on characterization and utilization of Gd products [2,14,15], research on Gl samples is quite limited. Generally, Gl protein-based adhesives have shown similar bonding performance as their Gd counterparts [16]. Both Gd and Gl kernels contained some bioactive ingredients and antioxidant activities [17–19]. However, peptide profiling indicated that there might be some differences in the distribution patterns of the storage proteins in Gd and Gl preparations, although more quantitative studies are needed [9,20]. Compared to soy protein, Gl protein isolate showed lower water-holding and oil-holding capacity but had similar gelation properties, elevated foaming capacity at high pH values, and greater emulsion stability [21]. With a trace content of toxic gossypol, Gl cottonseed is especially promising if processed for food applications, such as roasted nut-like products and cottonseed butter although no viable processing details have been reported [22,23]. Reyes-Jáquez et al. [24,25] formulated and evaluated Gl-meal/corn flour snacks by extrusion cooking. Shrimp feed with Gl cottonseed meal as a protein source was made by extrusion and its structural, rheological and calorimetric properties evaluated, showing the Gl meal-based shrimp feed is a reasonable option to decrease feeding costs [26,27]. Specifically, Gl cottonseed protein could replace up to 75% fishmeal protein in the diet of southern flounder without compromising its growth potential [28]. In other words, Gl cottonseed could be an inexpensive protein source for the commercial culture of southern flounder and other finfish species.

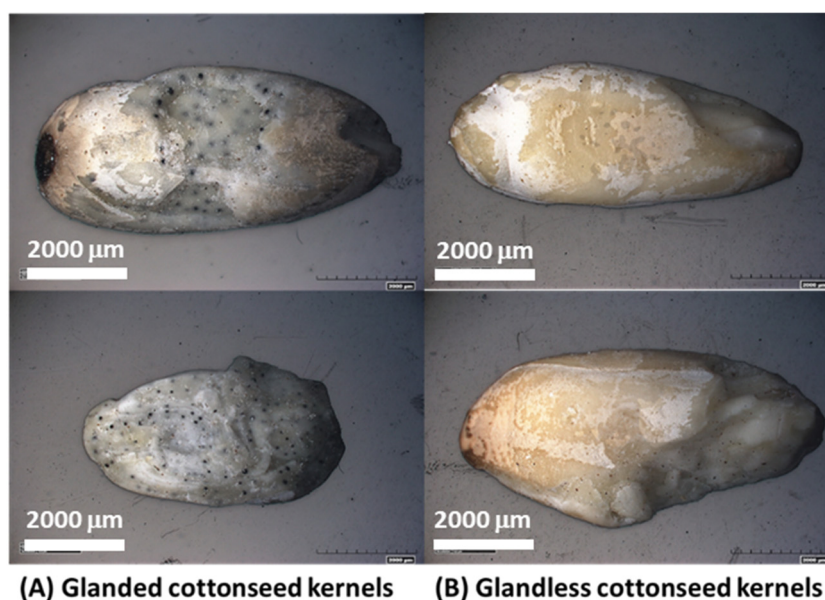


Figure 1. Images of glanded (A) and glandless (B) cottonseed kernels. The small black dots appearing on the kernel surfaces of sample (A) are the gossypol glands.

Fourier transform infrared (FTIR) spectroscopy is one of the non-destructive instrumental techniques widely used in applied cotton fiber, cottonseed, and other cotton biomass

research [29–32]. Cottonseed-derived oil [33,34], protein [35,36] and carbohydrate products [31,37] have shown different FTIR features. Specifically, FTIR intensities of 1665 to 1680 cm^{-1} , 1646 to 1660 cm^{-1} , 1638 to 1645 cm^{-1} , and 1615 to 1637 cm^{-1} have been used to evaluate cottonseed protein's secondary structures (β -turns, α -helices, random coils, and β -sheets) [38–40]. Sun et al. [41] used FTIR to detect the chemical and conformational changes between transgenic cottonseeds and their non-transgenic counterparts. While not much difference was observed in original FTIR spectra between these samples, spectral treatments by Fourier self-deconvolution (FSD) and peak-smoothing in the regions between 2000 and 1000 cm^{-1} showed that the differences in band patterns observed between transgenic cottonseeds and their counterparts depended on the varieties used.

A thermogravimetric analyzer (TG) is another advanced instrument used to analyze the mass changes of a sample with increasing temperatures and time [42]. Heat treatments such as roasting and frying are frequently employed in the food processing of seeds and nuts to improve their sensory quality, digestibility, and microbiological safety [43–45]. Thus, TG analysis has been applied to detect the mass loss of various volatile compounds as well as appropriate roasting temperatures for heat treatments [44,46,47]. The coupling of TG with FTIR (i.e., TG-FTIR) has provided a unique capability to obtain the transient mass loss and evaluation of the volatile functional groups of a sample, which could not be obtained by the TG and FTIR individually [42,48]. In previous research, this technology revealed the presence of phenols, esters, alcohols, and aldehydes as the volatile compounds in hazel sterculia (*Sterculia foetida* L.) seeds [49]. Examination of defatted safflower seeds by TG-FTIR analysis found that CO_2 , $\text{C}_6\text{H}_5\text{OH}$, and C=C-containing compounds were the main pyrolysis gas products of defatted safflower seeds [50]. TG-FTIR observations have shown that the devolatilization sensitivity to heating rate followed the order of hemicellulose > starch > oil > cellulose \approx protein > lignin [51]. In a characterization of five herb essential oils, the TG of the essential oils and the TG-FTIR analyses of the evolved gases showed that the essential oils' thermal behavior was due to the volatilization of the major components in these herbs without thermal degradation [52].

Similarly, data on the thermal behavior and stability will be useful for safe and proper handling of cottonseed during product formulations. To the best of our knowledge, there are only limited TG-FTIR studies of cottonseed with the purpose of pyrolysis applications so far [53–55]. Thus, in this research work, chemical analysis, FTIR, and TG-FTIR were applied to evaluate the thermochemical properties of Gd and Gl cottonseed kernels. Knowledge and data obtained from the thermal behavior and stability are useful for a safe and proper handling of cottonseed during product formulation for food and non-food applications. Therefore, the primary objective of this research was to determine the thermal properties and stability of Gd and Gl using TG-FTIR analysis.

2. Results and Discussion

2.1. Chemical Composition of Gd and Gl Kernels

Selected chemical components of Gd and Gl cottonseed kernels are listed in Table 1. These data are generally in the range described in the literature [56–59]. The unique features in the presence or absence of gossypol are clearly demonstrated by the difference in gossypol content between the two types of cottonseeds. These data indicated that Gl kernels, but not the Gd kernels, meet FDA's criteria as human food products with free gossypol < 450 ppm [2,23]. Otherwise, the chemical components of Gd and Gl were quite similar. In both types of kernels, oil and protein accounted for about 40% of the total biomass. The carbohydrates, moisture, and mineral ash constituted the remaining biomass. Even though a significant ($p < 0.05$) difference was observed, the starch content was low in both Gd and Gl samples, consistent with the data in the literature [22,60]. While cottonseed could be a source of human food and animal feed for low-starch diets [22], external addition of starch may promote the processing and dietary properties of cottonseed products [24,26]. Statistically significant ($p \leq 0.05$) differences were also observed in the contents of protein and total phosphorus between Gd and Gl kernels. The similar significant impact seems

reasonable as phosphorus in cottonseeds is generally present in the phytate form [61] and positively correlated with cottonseed protein content [62]. While the composition of major components of the Gd and Gl cottonseeds are available in the literature [22,23], Table 1 also compared the mineral contents between the two types of cottonseeds. Twelve of the thirteen minerals (except for Al) are essential elements. Aluminum is a non-essential element whose presence is of concern to both human and ecosystem health [56,63]. The general similarity of the mineral levels between the two cottonseeds implied that the decrease of gossypol in Gl cottonseed did not dramatically alter the mineral composition of cottonseeds. Therefore, the quality of mineral nutrients of the cottonseeds was not impacted by the reduction of the toxicity of high gossypol content.

Table 1. Selected chemical components of Gd and Gl cottonseed kernels. Data are reported on a dry weight basis with average (A) and standard deviation (SD, n = 3). ADF, acid detergent fiber. ADL, acid detergent lignin.

(A) Major component (g kg ⁻¹)							
	Moisture	Gossypol *** ¹	Oil	Protein **	ADF	ADL	Starch **
Gd	67.9 ± 0.5	3.75 ± 0.02	387 ± 18	397 ± 8	100 ± 18	52.3 ± 10.1	12.2 ± 1.0
Gl	68.3 ± 0.2	0.06 ± 0.00	350 ± 14	421 ± 6	109 ± 23	67.8 ± 15.6	16.6 ± 0.4
(B) Macro element and ash (g kg ⁻¹)							
	P *	Ca	K	Mg	Na	S	Ash
Gd	9.8 ± 0.8	2.0 ± 0.3	12.0 ± 0.7	5.4 ± 0.4	0.6 ± 0.0	4.5 ± 0.3	46.7 ± 0.8
Gl	11.5 ± 0.6	2.3 ± 0.2	12.8 ± 0.5	6.1 ± 0.3	0.6 ± 0.0	4.9 ± 0.2	47.9 ± 0.7
(C) Trace element (mg kg ⁻¹)							
	Fe	Zn	Cu	Mn	B	Ni	Al
Gd	104 ± 43	70.5 ± 8.2	18.1 ± 1.1	12.9 ± 1.2	13.8 ± 1.1	1.9 ± 0.3	91.6 ± 61.2
Gl	111 ± 3	74.3 ± 2.5	19.0 ± 1.2	13.3 ± 0.7	14.2 ± 0.5	2.1 ± 0.1	109.8 ± 8.4

¹ Symbols *, **, and *** indicate the values between Gd and Gl samples significantly differed at $p \leq 0.05$, 0.01 and 0.001, respectively.

2.2. Microstructure of Gd and Gl Cottonseed Kernels

Figure 2 shows the SEM images of the Gd and Gl kernel particles and their extraction residues at two different scales. The SEM images of both Gd-k and Gl-k appear to have no apparent differences. The images at the larger scale (1 mm) showed that the powder particles of both kernels seemed to form sticky aggregates. The images at the smaller scale (10 µm) revealed that the morphology of these kernel powders had stacked granules of irregular spherical shapes. By careful comparison of the images of Gd-k2 and Gl-k2, it can be seen that the granule surfaces of the latter are smoother than the former. These micrographs indicate that the presence of gossypol did not result in any difference in micromorphology of the two types of cottonseed powders. On the other hand, some differences in the microstructures were observed in the kernel residues after hexane and 80% ethanol extraction. In a comparison to Gd-k1 and Gl-k1, the images of the Gd-r1 and Gl-r1 appeared to be more separated and with large chunks disrupting the outer layer of the fibers, similar to the microstructures of those defatted cottonseed and soy meal products [64,65]. Thus, we attributed this micromorphological difference to the oil component. Another observation was that almost all granules in the Gl-k2 image were round and smoothy, but there were only a few such round-shaped granules in the microstructural matrix in the Gd-r2 image (Figure 2). More data from future research are needed to confirm if the microstructural difference was due to the effects of a broken gossypol gland wall matrix which is not hexane extractable [66].

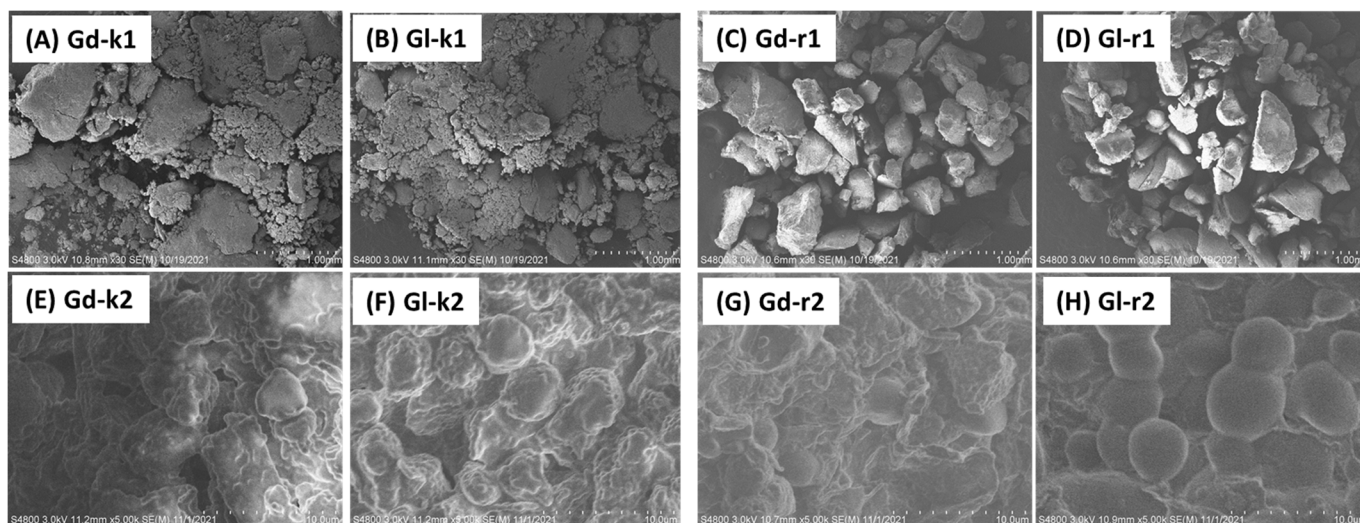


Figure 2. SEM images of Gd and Gl kernels (Gd-k and Gl-k) and their residues (Gd-r and Gl-r) after sequential 100% hexane and 80% ethanol (in water) extractions. Bar distances are 1.00 mm and 10 μ m, respectively, for series 1 (upper row panel (A–D)) and 2 (lower row panel (E–H)) images.

2.3. ATR FTIR Spectra of Gd and Gl Kernels and Their Extraction Residues

The ATR FTIR spectra of the four samples are shown in Figure 3. As per the previous band assignments of cotton biomass sample research [31,32,38,44,67], the typically broad and strong band around 3288 cm^{-1} was due to the O-H or N-H stretching modes of carbohydrates, adsorbed water, and proteins. The twin or triple bands at 2927 and 2854 cm^{-1} were assigned to hydrophobic CH_2 asymmetrical and symmetrical stretching vibrations from the oil portion in cottonseed. The band at 1745 cm^{-1} was contributed by the C=O stretching modes of carbonyl groups. The bands at 1632 , 1539 , and 1235 cm^{-1} were attributed to amide I (C=O stretching), II (CN stretching, NH bending), and III (CN stretching, NH bending) bands of proteins, respectively. The bands at 1070 – 995 cm^{-1} were assigned mainly to carbohydrates with a possible minor contribution of phosphate in cottonseeds. Similar to the chemical composition, the spectral features of Gd and Gl samples were similar with some differences only in band strength. Therefore, gossypol did not make any remarkable visual differences in the FTIR spectral features of Gd and Gl samples. This is only due to the low gossypol content (0.375%), and also due to the fact that the FTIR spectrum of gossypol possesses no unique spectral features, rather than the general band characteristics of aromatic rings, aldehydes, and phenolic hydroxyl groups [68]. A complicated mathematical model is needed to reveal the gossypol-related difference between Gd and Gl samples, such as a partial squares method based on all the band data from 3700 – 2400 cm^{-1} and from 1900 – 750 cm^{-1} for determination of gossypol in cottonseed oil samples [68].

After sequential 100% hexane and 80% ethanol extraction, the spectra of the residues (Gd-r and Gl-r) (Figure 3) of the two kernels showed relatively weaker peaks around the 2927 and 2854 cm^{-1} region, compared to the unextracted kernel samples (Gd-k and Gl-k), apparently due to the removal of the oil components [32,69]. This observation was further confirmed by the ATR FTIR spectra of the hexane extracts (Gd-n and Gl-n) (Figure 4), which are typical for seed oil samples with strong bands at 2927 and 2854 cm^{-1} regions as well as at 1745 cm^{-1} [32,70]. Compared to the Gd-k and Gl-k samples, Gd-n and Gl-n showed a more apparent minor peak at 3009 cm^{-1} . This peak was associated with the stretching vibration of CH cis-olefinic groups [45]. In comparison to their untreated kernel samples, no other apparent changes in FTIR features of the extraction residues (Gd-r and Gl-r) were observed, leading to their features being similar to those of defatted cottonseed meal products [71].

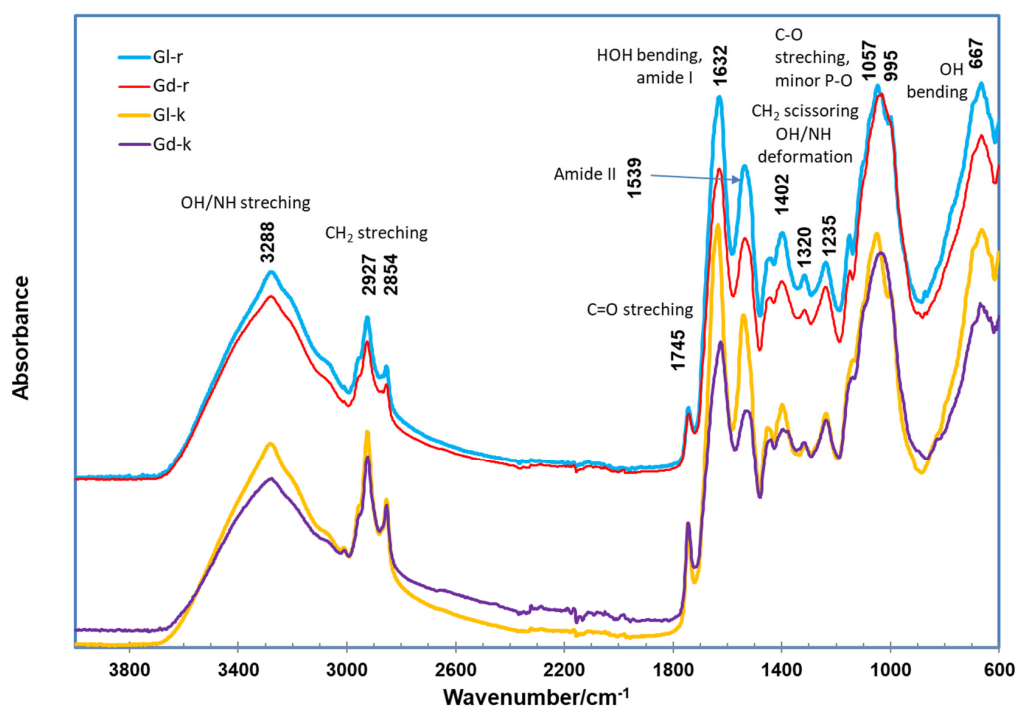


Figure 3. ATR FTIR spectra of Gd and Gl kernels (Gd-k and Gl-k) and their residues after 100% hexane and 80% ethanol (in water) extraction (Gd-r and Gl-r).

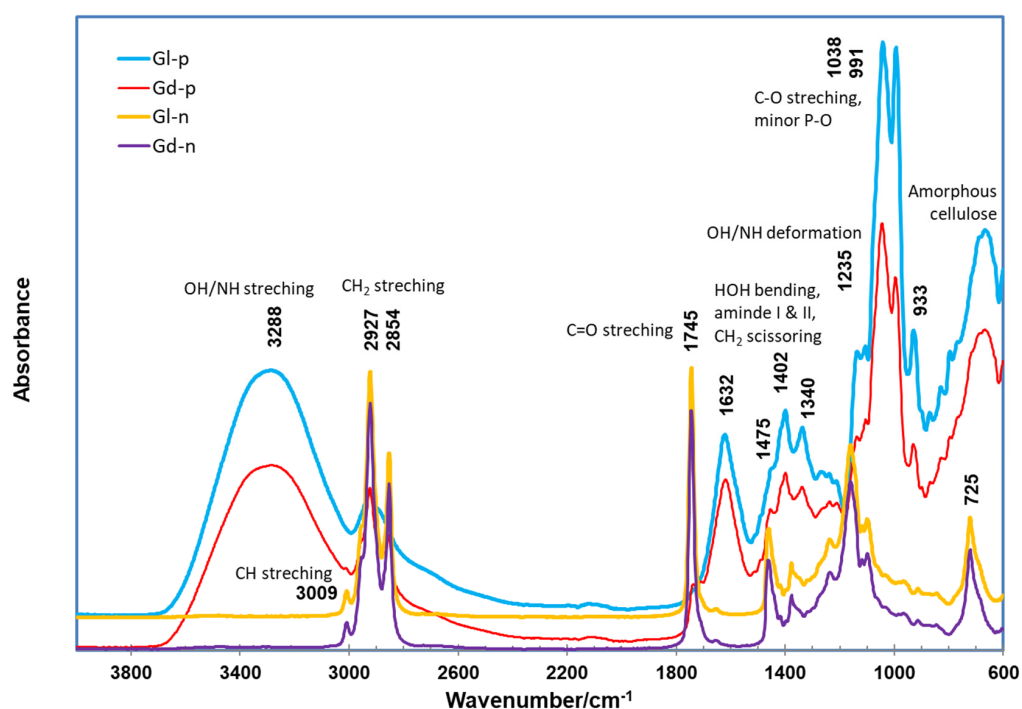


Figure 4. ATR FTIR spectra of the extracts of Gd and Gl kernels by nonpolar 100% hexane (Gd-n and Gl-n) and polar 80% ethanol (Gd-p and Gl-p).

As there were only minor spectral differences between the two cottonseed samples, we further examined the spectral features of the hexane and methanol extracts of Gd and Gl samples to enhance the understanding of the chemical composition of the specific extractable nonpolar and polar ingredients in cottonseeds. The spectra of the ethanol extracts (Gd-p and Gl-p) were totally different from the features of nonpolar extracts

Gd-n and Gl-n, and were characterized by the highest bands of carbohydrates at the 1038–991 cm^{-1} region (Figure 4). While no FTIR information on the ethanol extracts of cottonseed kernels is available in the literature, HPLC-MS analysis revealed the ethanol extracts of Gd and Gl cottonseed with 27 peaks and mass values equivalent to possible flavonols or derivatives and 16 peaks possible matched to apiosyl, rhamnosyl, and glucosyl-derivative mass [17]. Ultrahigh resolution mass spectrometry may be needed to identify definitely these compounds in the ethanol extracts of Gd and Gl kernels [72].

2.4. Thermogravimetric Observations

The TG plots of the Gd and Gl samples are shown in Figure 5, respectively. The general features of these TG and DTG plots were the typical three-stage (drying, de-volatilization, and char formation) weight loss of the testing samples over the heating temperature range from 50–700 °C. Analysis of the first derivative curves of the TG measurement (DTG) of the kernel samples showed more clearly that the second stage of decomposition processed with three substeps had maximum temperature peaks of around 215 (shoulder), 315 (shoulder), and 380 °C (major peak) (Figure 5). This thermal behavior of cottonseed kernels was more complex than the relative sample DTG curves of cottonseed oil [73], protein [36], and fiber [30]. Furthermore, the DTG curves of the extraction residues (Gd-r and Gl-r) showed different decomposition characteristics with the unnoticeable first shoulder (215 °C), a major peak at 380 °C, and switching the peak at 380 °C to a shoulder. Thus, in addition to the attributed common decomposition of hemicellulose, cellulose, and lignin assigned for cottonseed and other natural products [48,53,55], the differences of DTG maximal temperature peak shape between the kernels (Gd-k and Gl-k) and extraction residues (Gd-r and Gl-r) indicated that the oil component should be a major contribution of the decomposition around 380 °C. Those ethanol extractable compounds volatilized or decomposed around 215 °C. Protein components were decomposed in a wide range of temperatures from 215 to 380 °C [36,74].

The thermal gravimetric observations of the Gd and Gl samples were similar, but not exactly like those of cottonseed samples in the literature [53–55]. The differences were due to the fact that dehulled kernels were used in the study while whole cottonseeds were used in the three studies reported previously. Similar to the thermal behavior of hazel seeds [49], the first stage of drying of our cottonseed kernels at 90 °C was the loss of moisture. Calculating from the weight loss from 50 °C to 144 °C as the onset of decomposition, the evaporation (drying) of moisture contents of Gd-k was about 5.9% weight loss (Table 2). In the second stage of devolatilization, the rapid decomposition of the sample occurred between 150 and 472 °C representing about 70.4% (i.e., $80.3\%(\text{WL}_e) - 5.9\%(\text{WL}_o)$) weight loss due to devolatilization, breaking of chemical bonds, and destruction of the parent molecular skeletons. In the last stage above 472 °C (degradation), decomposition of char (19.7%) occurred with the formation of secondary pyrolytic vapors, but some char or ash remained (<16.1%). While the Gl-k sample demonstrated similar thermogravimetric properties, the values of four of the seven parameters measured (Table 2) were significantly different ($p \leq 0.05$) from the corresponding values of the Gd-k sample. Compared to Gd-k, Gl-k kernels started the devolatilization stage at a higher temperature (147 °C), but the ending temperature (469 °C) was lower. Despite this, there was more weight loss of Gl-k (82.2%) than Gd-k (80.3)%. In contrast, the T_o values differed only significantly between the residual Gd-r and Gl-r samples. Therefore, the thermogravimetric properties of the two extraction residues were more similar to each other than the Gd and Gl kernels themselves. This observation implied that the extractable components in Gl kernels were less thermally stable. However, we did not establish a correlation of the thermogravimetric difference with any of these components between Gd and Gl-samples.

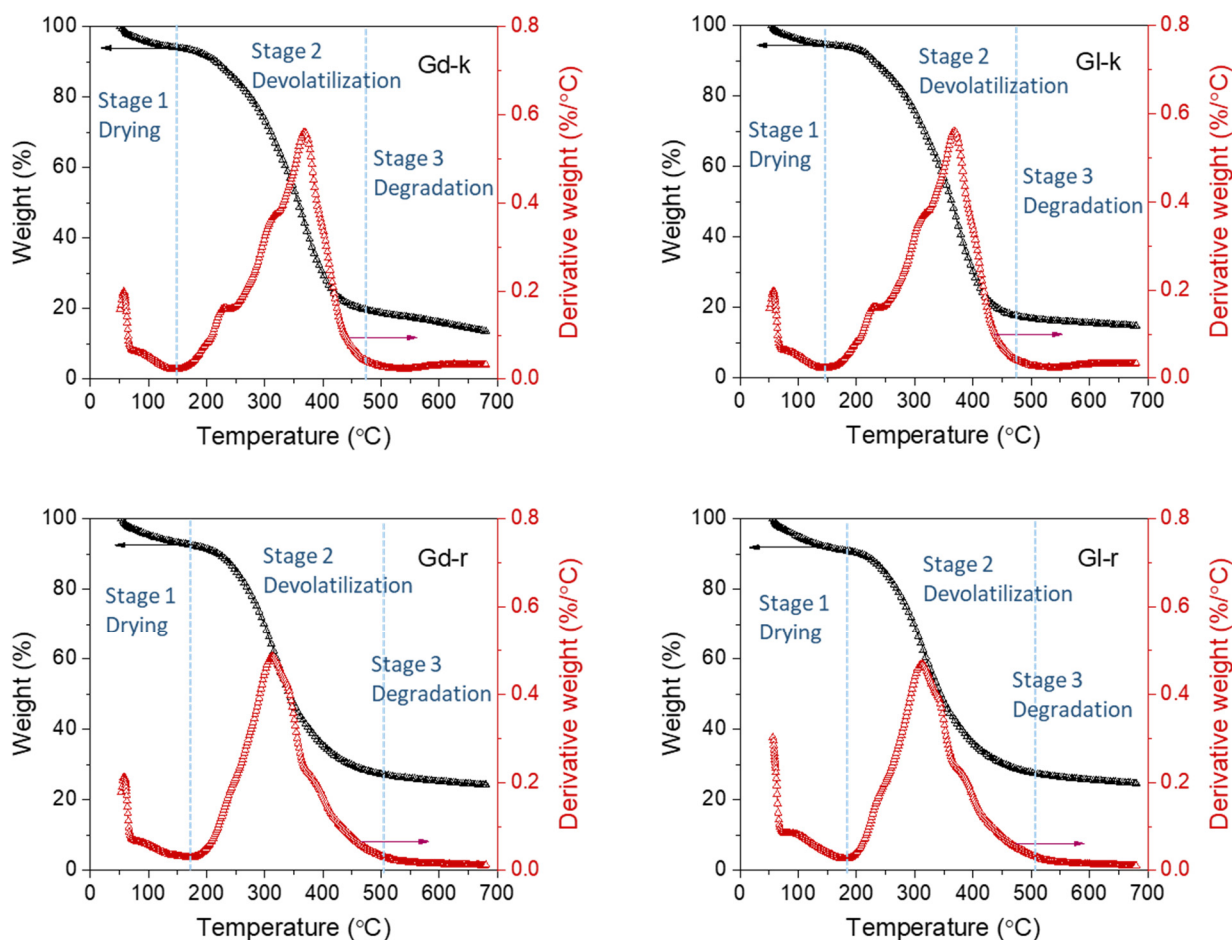


Figure 5. Thermograms of Gd and GI kernels (Gd-k and GI-k) and their residues after hexane and 80% ethanol extraction (Gd-r and GI-r). Left y axis: TG plots. Right y axis: DTG plots.

Table 2. Thermogravimetric and differential thermogravimetric data for Gd and GI cottonseed kernels. *T*: temperature; *WL*: weight loss; *o*: onset decomposition; *m*: maximum decomposition rate; *e*: end decomposition. Data are presented as the average of triplicate measurements with standard deviation in parentheses. Symbol *, and ns at the data in row GI-k and GI-r indicate the values of the GI samples significantly and not significantly different ($p = 0.05$), respectively, from their corresponding Gd-k and Gd-r samples.

	T_o (°C)	WL_o (%)	T_m (°C)	WL_m (%)	T_e (°C)	WL_e (%)	Char (%) ¹
Gd-k	143.5 (1.2)	5.9 (0.7)	368.4 (0.8)	55.9 (0.5)	471.7 (1.2)	80.3 (0.7)	16.1 (1.5)
GI-k	147.1 * (1.3)	5.5 ns (0.9)	368.4 ns (0.7)	52.9 * (0.7)	468.7 * (1.5)	82.2 * (1.1)	15.6 ns (1.1)
Gd-r	177.9 (1.2)	7.6 (1.0)	313.2 (0.9)	36.8 (1.1)	504.9 (1.2)	72.9 (1.2)	25.3 (1.2)
GI-r	183.6 * (1.0)	9.1 ns (0.8)	314.5 ns (0.9)	37.4 ns (1.0)	504.9 ns (1.0)	72.4 ns (0.9)	25.7 ns (1.3)

¹, char yield measured at 600 °C.

High-quality cottonseed and its derived products/byproducts have been developed as animal feeds and human foods [23,26,75–78]. These low quality or non-edible cottonseed, oil, and other byproducts may be used for raw materials of bio-fuels and biochars [54,55,79–81]. These applications are frequently involved with various heat pre-treatments (such as low-

temperature roasting/frying and mid- or high-temperature pyrolysis). While there are no clear-cut point of temperature settings for each heat treatment, thermogravimetric observations would be helpful in understanding the chemico-physical changes of the cottonseed under a given heating temperature range. Specifically, the temperature of the devolatilization stage would be a critical reference for product optimization (such as flavors of roasting and yield of bio-oil/bio-gas) as vaporization of the volatile components of the biomass occur. Thus, we applied TG-FTIR to elucidate more information on transient mass loss and evaporation of the volatile functional groups of the two cottonseed samples during the stage (Section 2.5).

2.5. TG-FTIR Observations

The three-dimensional TG-FTIR spectra with the coordinates of absorbance, wave number, and temperature of the four samples are shown in Figure 6. This method of TG analysis coupled with IR spectroscopy detected the real-time gaseous products that evolved during the pyrolysis process [48]. The intensive FTIR signals of the evolved gases were detected within a temperature range of 150 and 500 °C which is consistent with TGA measurements (Figure 5). The presence of H₂O was demonstrated by O–H stretching vibrations between 4000–3400 cm⁻¹ and the sharp band at 1514 cm⁻¹ [48]. The broad band in the range of 3000–2700 cm⁻¹ represented hydrocarbon gases, mainly CH₄, and the remarkable peak and a small band between 2400 to 2000 cm⁻¹ represented the C = O stretching vibrations of CO₂ and CO [49,53]. The presence of aldehydes, ketones, and acids was indicated by the band at 1776 cm⁻¹. The broad bands between 1460–1365 cm⁻¹ and 1200–1000 cm⁻¹ were attributed to the presence of C–H alkanes, esters, and alcohols. In addition, the band between 1200 to 1000 cm⁻¹ further confirmed the presence of alcohol in these gaseous products [48,49].

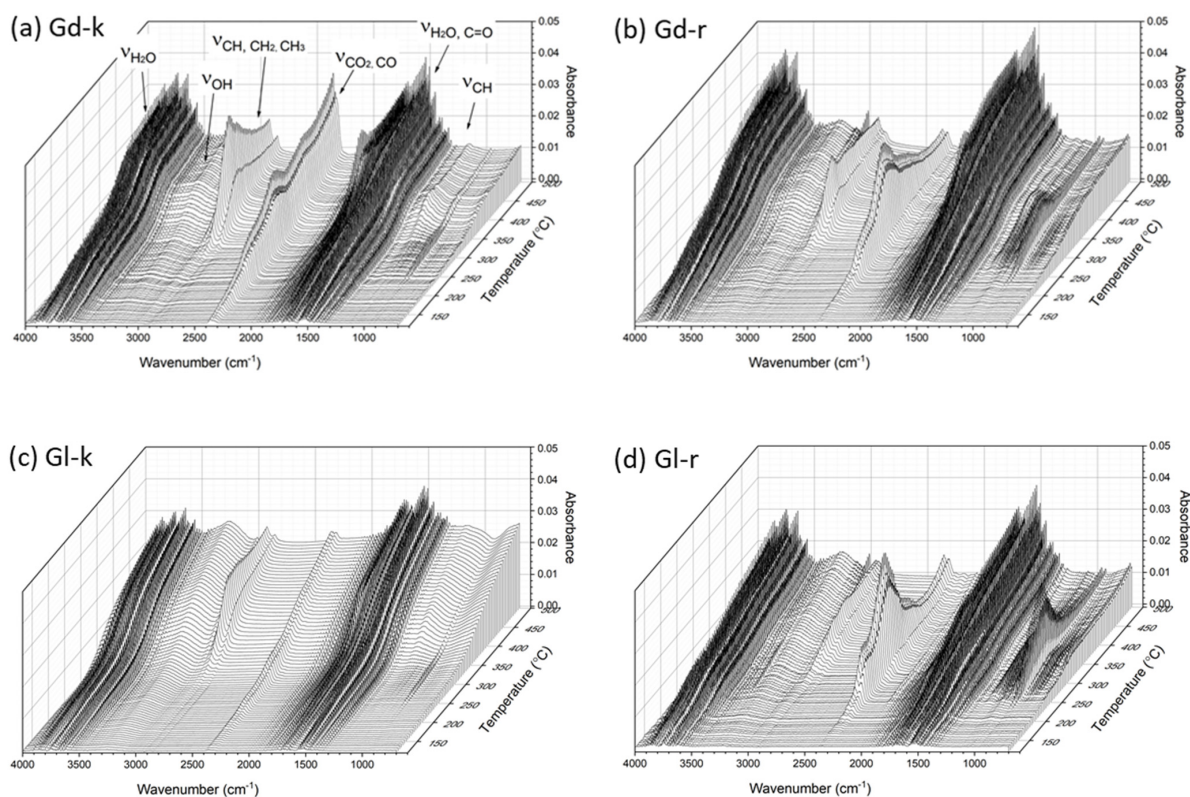


Figure 6. TG-FTIR spectra of Gd and Gl kernels (Gd-k and Gl-k) and their residues after 100% hexane and 80% ethanol extraction (Gd-r and Gl-r).

The main differences between the TG-FTIR spectra of the Gd-k and Gl samples were the presence of much stronger peaks in three regions of 3000–2700 cm⁻¹ (CH₄), 2400–2300 cm⁻¹

(CO₂, CO) and the minor bands around 1000 cm⁻¹ (alcohol) with the Gd-k sample. This observation implied that the biomass components in Gd kernels decomposed faster than those in Gl kernels. However, the spectra of the residues after hexane and ethanol extractions of the glanded and glandless cottonseed samples were more similar to each other. Indeed, the FTIR bands in the three above regions were somewhat stronger in Gl-r sample than Gd-r samples. As the two-step extractions mainly removed the major oil components and minor flavonols or similar compounds alike [17], it seemed that the oil component made the difference in TG-FTIR spectra of Gd and Gl samples. As free gossypol is lipophilic [68], we hypothesize that it was gossypol dissolved in oil that promoted the faster devolatilization in the glanded cottonseed kernel sample GD-k although the hypothesis should be further examined with more experimental data. The TG-FTIR spectra also showed that the CO₂ and CO bands (2400–2300 cm⁻¹) reached the highest point around 315 °C, but the CH₄ peak (3000–2700 cm⁻¹) was at its highest point later at approximately 375 °C. The latter CH₄ peak was also weaker in the oil-extracted residual samples (Gd-r and Gl-r) than their corresponding original kernel samples (GD-k and Gl-k), indicating that CH₄ detected in the TG-FTIR spectra was mainly from the oil component of cottonseed. In contrast to that, these CO₂ and CO products that appeared at early stages should be mainly from carbohydrates (cellulose, hemicellulose, starch) [48,51]. Compared to the kernel samples, the relatively stronger multiple bands from 1500 to 700 cm⁻¹ in Gd-r and Gl-r) indicated easier decomposition of protein components after oil removal [51]. This observation was supported by N-enriched compounds of the defatted cottonseed meal bio-oil which were the condensed gaseous products of pyrolysis [54,80]. In other words, it was difficult to pyrolyze the biomass rich in oil and lignin but easy to pyrolyze the biomass rich in cellulose, starch, hemicellulose, and protein [51].

Similar to other seeds or nuts for food applications [45,47,82–85], roasting is a necessary heating process for enhanced use of cottonseed kernels as nutrient food products [23]. While roasting temperatures were reported in the range of 100 to 160 °C for various plant-based butters [86], the negligible CO₂ and CO bands (2400–2300 cm⁻¹) in TG-FTIR spectra of Gd-k and Gl-k below 215 °C of the first shoulder in DTG curves (Figure 5) suggested that the cottonseed kernels could be roasted in the temperature range without significant occurrence of decomposition (carbonization). On the other hand, the optimal roasting temperature would be lower than or around 140–150 °C in the first stage of drying or dehydration (Figure 5) to reduce evaporation of some volatile flavor compounds [43]. The TG-FTIR spectra also confirmed that 350 to 500 °C were optimal pyrolysis temperatures of cottonseed kernels and their defatted residues (i. e., defatted meal or cake) for bio-oil and biochar production [55,80,87] with some flexibility of higher temperatures (e.g., 600–700 °C) [53,54].

3. Materials and Methods

3.1. Cottonseed Source and Treatment

The Gl cottonseed of the NuMex series was provided by Cotton, Inc. (Cary, NC, USA) [9,88]. These seeds were dehulled mechanically by cracking with a 20.32 cm plate mill, and then separated with a vibration shaker. The kernel products were further cleaned by passing the material through a laboratory aspirator to remove the non-kernel material. The presence of contamination of Gd cottonseeds in the Gl products due to cross fertilization by windblown or insect-carried pollen of Gd varieties was noticeable [23]. These Gd kernels were hand-picked or removed and used as the comparative Gd sample in this study. Both Gl and Gd kernels were then ground for 3 min in a stainless-steel jar of Waring Commercial Blender (Model WF2211214, Torrington, CT, USA). The experimental procedure, methodologies, and sample labelling are shown in Figure 7 and described in the sub-sections below.

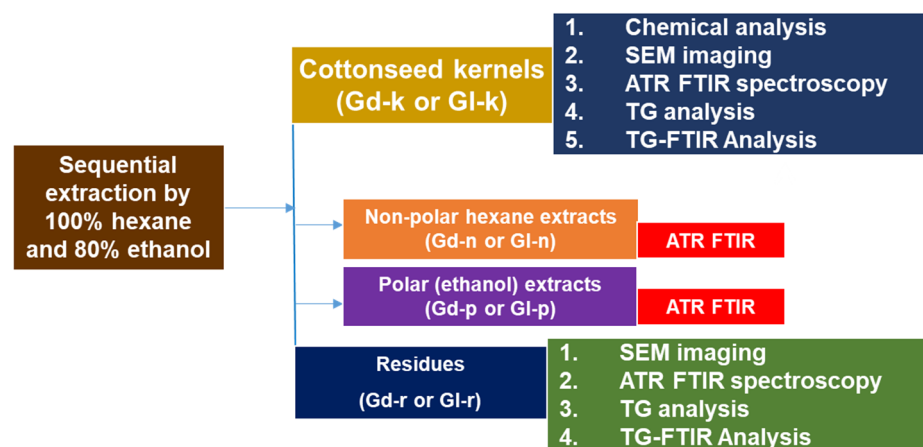


Figure 7. Flow chart of the sample processing, experimentation, and analysis performed in this work. Gd series, glanded cottonseed samples; GI series, glandless cottonseed samples.

3.2. Non-Polar and Polar Solvent Extraction

Cottonseed kernels were subjected to sequential extraction by 100% reagent grade hexane [89,90] and 80% reagent grade ethanol in water [17,83]. Grounded Gd and GI kernels (5.00 g each) were placed in 50 mL centrifuge tubes with 15 mL of hexane and extracted overnight (18 h) at room temperature (26 °C) under rotary shaking (60 rpm). Those tubes were then centrifuged for 30 min at 5 °C and 2500× *g*. After centrifugation, the supernatant in each tube was carefully removed and the pellets (residual parts) were extracted one more time following the same procedure mentioned above. The residual parts were subsequently washed twice with hexane (5 mL each). The supernatants and washing solutions of each tube were pooled and placed in a venting hood to evaporate hexane out at room temperature. The non-evaporated part was the nonpolar oil fraction of the cottonseed kernels. The dried residual pellets were further extracted twice by 80% ethanol (15 mL each) following the same procedure as in the hexane extraction. Both the ethanol supernatants (polar extracts) and the extracted residues were dried in a vacuum oven at 40 °C to constant weights.

3.3. Microstructural Imaging Analysis

For scanning electron microscopy (SEM), a thin layer of sample particles (grounded cottonseed kernel or the extraction residues) was gently attached to an 8 mm × 12 mm double-side sticky carbon tape on an aluminum stud. The butter sample was coated with 3 nm thickness of carbon using a Cressington 208HR Sputter Coater (Watford, England, UK). The cottonseed kernel samples were observed and imaged with a Hitachi S-4800 Field Emission Scanning Electron Microscope (Hitachi, Japan), operating at 3 kV [30]. Microscopic images were done on multiple samples with different scales and the representative images were reported.

3.4. Chemical Analysis

All chemical analysis and data were reported on a dry weight basis. Moisture content was determined as the loss in weight upon drying a sample in a forced draft oven at 105 °C for 5 h [91]. Both (+) and (−) isomers of gossypol were detected by a modified procedure of AOCS Recommended Practice Ba 8a-99, using about 100 mg sample for each analysis [92,93]. Briefly, 100 mg of ground sample was weighed into a 12 mL screw-cap test tube. A complexing reagent (2 mL) consisting of 2/10/88 (*v/v/v*) R-(−)-2-amino-1-propanol, glacial acetic acid, and dimethylformamide was added. The tube was then heated at 95 to 100 °C for 30 min to convert gossypol's aldehyde groups into Schiff's bases with the chiral amine. The formed gossypol complexes were detected on-line at 254 nm after they were separated on a Hewlett-Packard Series 1100 HPLC system equipped with a photodiode array detector (Palo Alto, CA, USA). Total gossypol content was computed as the sum of

these isomers. Starch content was measured per Sigma–Aldrich starch assay kit (SA20, Sigma–Aldrich, St. Louis, MO, USA). Crude protein content in the samples was calculated by multiplying the total N by a factor of 6.25 [57]. Oil content was estimated per the yield of hexane extraction [90]. Acid detergent fiber (ADF) and acid detergent lignin (ADL) were determined using the filter bag methods with an Ankom Fiber Analyzer (Ankom Technology, Macedon, NY, USA). The kernel samples were first pre-extracted by acetone before the fiber analysis to remove the inherent oil [94].

The elemental composition of the samples was analyzed following acid digestion. Briefly, 0.50 g of grounded sample was mixed in 10.0 mL of concentrated HNO₃ for 1 h in a HotBlock™ 200 digestion system (Environmental Express, Charleston, SC, USA). The sample was then heated to 115 °C for 2.25 h. The concentrations of 13 elements (i.e., Al, B, Ca, Cu, Fe, K, Mg, Mn, Na, Ni, P, S, and Zn) in these digests were determined by a Spectro CirOs ICP spectrometer (Mahwah, NJ, USA) [57]. The concentrations of total N in each sample were determined using a LECO Truspec dry combustion Carbon/Nitrogen Analyzer (LECO, St. Joseph, MI, USA). Ash content was determined by measuring the residual mass of a sample (1.0 g) after heating in a muffle furnace at 550 °C for 4 h [95]. Samples were replicated (3×) and chemical analyses were repeated.

3.5. Instrumental Analysis

ATR FTIR spectra were measured using a Vertex 70v FTIR spectrometer (Bruker Daltonics, Billerica, MA, USA) equipped with a MIRacle ATR accessory (Pike Technologies, Fitchburg, WI, USA) that incorporated a diamond crystal plate as the reflector. The ground solid samples or oily-like extracts were placed on the ATR crystal surface and secured with a metal clamp to ensure a reproducible pressure which was applied to the samples to achieve intimate contact with the ATR crystal. The spectra were collected over the range of 4000–600 cm^{−1} at 4 cm^{−1} resolution and with 16 scans. All spectra were normalized and presented in absorbance [80].

Thermogravimetric analysis was carried out using a TGA Q500 thermal gravimetric analyzer (TA Instruments, New Castle, DE, USA) under a nitrogen atmosphere. The nitrogen flow into the furnace was maintained at a rate of 90 mL/min. About 8 mg of the sample placed in a platinum pan was heated to 700 °C with a heating rate of 10 °C/min. The evolved gas during the thermal decomposition of the sample was analyzed using TG-FTIR. A TG analyzer was equipped with a gas purge through which pyrolysis vapors were conveyed to a TG-FTIR interface inside the infrared spectrometer. A series of FTIR spectra were collected from 100 °C to 500 °C with 16 scans at a 4 cm^{−1} resolution from replicated samples. Two spectra were obtained every minute [48].

3.6. Statistical Analysis

Data are presented in the format of average ± standard deviations. Average values, if significantly different ($p \leq 0.05$), are indicated by the relevant symbols in Tables 1 and 2.

4. Conclusions

This work showed a comparative investigation of the chemical and thermal properties of glanded and glandless cottonseed kernels. While the whole glanded kernels were full of visible dark gossypol gland dots, scanning electron microscopy was not able to show the microstructural difference between grounded Gd and Gl kernel particles. With only 1.6% of the typical gossypol content of glanded kernels, the tested glandless kernels had slightly, yet statistically significant higher ($p \leq 0.05$) contents of protein, starch and phosphorus as compared to the glanded sample. Chemical analysis and FTIR spectroscopy showed similar composition in C functional groups and minerals in the two types of cottonseeds. TG analysis showed a typical three-stage process (drying, de-volatilization, and char formation) of weight loss of the tested kernel samples when subjected to temperatures of 50–700 °C. TG-FTIR spectroscopy revealed apparent differences in thermogravimetric properties between the two kernel samples, as well as between the raw and extracted

kernel samples as some components in glanded kernels were more prone to thermal decomposition than glandless kernels.

With very low gossypol content, G1 cottonseed and its derived products could be developed as value added animal feeds and human foods, and part of the low quality (or non-edible grade) G1 cottonseed as well as the high-gossypol Gd cottonseed products can be used as feedstock for bio-energy and biochars. These applications all need certain heat treatments (such as low-temperature roasting/frying, and mid- or high-temperature pyrolysis). While there is no clear cut point of temperature settings for heat processing, thermogravimetric observations would be helpful in understanding the chemico-physical changes of the cottonseed under a given heating temperature range. Such increased knowledge derived from this work would help in optimizing the heating processes (e.g., roasting and frying) of cottonseed kernels for enhanced food applications and pyrolysis strategies of unconsumable cottonseed or defatted meals for bio-oil and biochar production.

Author Contributions: Project conceptualization, Z.H.; methodology and investigation, Z.H., S.N., H.Z. and O.M.O.; writing—original draft preparation, Z.H.; writing—review and editing, Z.H., S.N., H.Z. and O.M.O. All authors have read and agreed to the published version of the manuscript.

Funding: This research received no external funding.

Institutional Review Board Statement: Not applicable.

Informed Consent Statement: Not applicable.

Data Availability Statement: The data presented in this study are available upon request from the corresponding author.

Acknowledgments: The authors thank Mike Dowd (USDA-ARS SRRC) and Jibao He (Tulane University) for their help on gossypol and SEM data collection. This research was supported in part by the U.S. Department of Agriculture, Agricultural Research Service. Mention of trade names or commercial products is solely for the purpose of providing specific information and does not imply recommendation or endorsement by USDA. USDA is an equal opportunity provider and employer.

Conflicts of Interest: The authors declare no conflict of interest.

Sample Availability: Samples of the cottonseed kernels with limited quantity are available from the authors.

References

1. Rojo-Gutiérrez, E.; Buenrostro-Figueroa, J.; López-Martínez, L.; Sepúlveda, D.; Baeza-Jiménez, R. Biotechnological potential of cottonseed, a by-product of cotton production. In *Valorisation of Agro-Industrial Residues—Volume II: Non-Biological Approaches*, Zainul Akmar Zakaria; Aguilar, C.N., Kusumaningtyas, R.D., Binod, P., Eds.; Springer: Amsterdam, The Netherlands, 2020; pp. 63–82.
2. Kumar, M.; Tomar, M.; Punia, S.; Grasso, S.; Arrutia, F.; Choudhary, J.; Singh, S.; Verma, P.; Mahapatra, A.; Patil, S. Cottonseed: A sustainable contributor to global protein requirements. *Trends Food Sci. Technol.* **2021**, *111*, 100–113. [CrossRef]
3. Statista. Global Cottonseed Production from 2013/2014 to 2020/2021. Available online: <https://www.Statista.Com/statistics/259489/worldwide-production-of-cottonseed/> (accessed on 1 January 2022).
4. NCPA. National Cottonseed Products Association—The Products. Available online: <https://www.Cottonseed.Com/products/> (accessed on 1 January 2022).
5. He, Z.; Cheng, H.N. Preparation and utilization of water washed cottonseed meal as wood adhesives. In *Bio-Based Wood Adhesives: Preparation, Characterization, and Testing*; He, Z., Ed.; CRC Press: Boca Raton, FL, USA, 2017; pp. 156–178.
6. Dowd, M.K. Seed. In *Cotton: Agronomy Monograph*, 2nd ed.; Fang, D.D., Percy, R.G., Eds.; ASA, CSSA, and SSSA: Madison, WI, USA, 2015; Volume 57, pp. 745–781.
7. Risco, C.; Chase, C. Gossypol. In *Handbook of Plant and Fungal Toxicants*; D’Mello, J.P.F., Ed.; CRC Press: Boca Raton, FL, USA, 1997; pp. 87–98.
8. He, Z.; Waldrip, H.M.; Wang, Y. Application of capillary electrophoresis in agricultural and soil chemistry research. In *Capillary Electrophoresis: Fundamentals, Techniques and Applications*; He, Z., Ed.; Nova Science Publishers: New York, NY, USA, 2012; pp. 131–151.
9. He, Z.; Mattison, C.P.; Zhang, D.; Grimm, C.C. Vicilin and legumin storage proteins are abundant in water and alkali soluble protein fractions of glandless cottonseed. *Sci. Rep.* **2021**, *11*, 9209. [CrossRef]

10. Xie, S.; Zhou, Q.; Zhang, X.; Zhu, T.; Guo, C.; Yang, Z.; Luo, J.; Yuan, Y.; Hu, X.; Jiao, L. Effect of dietary replacement of fish meal with low-gossypol cottonseed protein concentrate on growth performance and expressions of genes related to protein metabolism for swimming crab (*Portunus trituberculatus*). *Aquaculture* **2022**, *549*, 737820. [CrossRef]
11. Zhao, T.; Li, C.; Li, C.; Zhang, F.; Mei, L.; Chindudzi, E.; Chen, J.; Zhu, S. Genome-wide analysis of genetic variations between dominant and recessive nils of glanded and glandless cottons. *Sci. Rep.* **2019**, *9*, 9226. [CrossRef] [PubMed]
12. Rathore, K.S.; Pandeya, D.; Campbell, L.M.; Wedegaertner, T.C.; Puckhaber, L.; Stipanovic, R.D.; Thenell, J.S.; Hague, S.; Hake, K. Ultra-low gossypol cottonseed: Selective gene silencing opens up a vast resource of plant-based protein to improve human nutrition. *Critic. Revi. Plant Sci.* **2020**, *39*, 1–29. [CrossRef]
13. Bellaloui, N.; Saha, S.; Tonos, J.; Scheffler, J.; Jenkins, J.; McCarty, J.; Stelly, D.M. Effect of chromosome substitution from alien tetraploid cotton species in upland cotton on (+) and (–) gossypol enantiomer levels in cottonseed. *J. Cotton Sci.* **2021**, *25*, 7–20.
14. Cheng, H.N.; He, Z.; Ford, C.; Wyckoff, W.; Wu, Q. A review of cottonseed protein chemistry and non-food applications. *Sustain. Chem.* **2020**, *1*, 256–274. [CrossRef]
15. He, Z.; Zhang, D.; Cheng, H.N. Modeling and thermodynamic analysis of the water sorption isotherms of cottonseed products. *Foundations* **2021**, *1*, 32–44. [CrossRef]
16. He, Z.; Cheng, H.N.; Chapital, D.C.; Dowd, M.K. Sequential fractionation of cottonseed meal to improve its wood adhesive properties. *J. Am. Oil Chem. Soc.* **2014**, *91*, 151–158. [CrossRef]
17. Cao, H.; Sethumadhavan, K.; Bland, J.M. Isolation of cottonseed extracts that affect human cancer cell growth. *Sci. Rep.* **2018**, *8*, 1–12. [CrossRef] [PubMed]
18. Cao, H.; Sethumadhavan, K.; Wu, X.; Zeng, X. Cottonseed-derived gossypol and ethanol extracts differentially regulate cell viability and vegf gene expression in mouse macrophages. *Sci. Rep.* **2021**, *11*, 15700. [CrossRef] [PubMed]
19. He, Z.; Zhang, D.; Olanya, O.M. Antioxidant activities of the water-soluble fractions of glandless and glanded cottonseed protein. *Food Chem.* **2020**, *325*, 126907. [CrossRef] [PubMed]
20. He, Z.; Zhang, D.; Cao, H. Protein profiling of water and alkali soluble cottonseed protein isolates. *Sci. Rep.* **2018**, *8*, 9306. [CrossRef] [PubMed]
21. Delgado, E.; Valverde-Quiroz, L.; Lopez, D.; Cooke, P.; Valles-Rosales, D.; Flores, N. Characterization of soluble glandless cottonseed meal proteins based on electrophoresis, functional properties, and microscopic structure. *J. Food Sci.* **2019**, *84*, 2820–2830. [CrossRef] [PubMed]
22. Spadaro, J.J.; Gardner, H.K. Food uses for cottonseed protein. *J. Am. Oil Chem. Soc.* **1979**, *56*, 422–424. [CrossRef]
23. Lusas, E.; Jividen, G. Glandless cottonseed: A review of the first 25 years of processing and utilization research. *J. Am. Oil Chem. Soc.* **1987**, *64*, 839–854. [CrossRef]
24. Reyes-Jáquez, D.; Casillas, F.; Flores, N.; Andrade-González, I.; Solís-Soto, A.; Medrano-Roldán, H.; Carrete, F.; Delgado, E. The effect of glandless cottonseed meal content and process parameters on the functional properties of snacks during extrusion cooking. *Food Nutr. Sci.* **2012**, *3*, 1716–1725. [CrossRef]
25. Reyes-Jáquez, D.; Casillas, F.; Flores, N.; Cooke, P.; Licon, E.D.; Soto, A.S.; González, I.A.; Carreón, F.O.C.; Roldán, H.M. Effect of glandless cottonseed meal content on the microstructure of extruded corn-based snacks. *Adv. Food Sci.* **2014**, *36*, 125–130.
26. Delgado, E.; Valles-Rosales, D.; Pámanes-Carrasco, G.; Cooke, P.; Flores, N. Structural, rheological and calorimetric properties of an extruded shrimp feed using glandless cottonseed meal as a protein source. *J. Aquac. Res. Develop.* **2021**, *12*, 637.
27. Delgado, E.; Valles-Rosales, D.J.; Flores, N.C.; Reyes-Jáquez, D. Evaluation of fish oil content and cottonseed meal with ultralow gossypol content on the functional properties of an extruded shrimp feed. *Aquac. Rep.* **2021**, *19*, 100588. [CrossRef]
28. Alam, M.S.; Watanabe, W.O.; Carroll, P.M.; Gabel, J.E.; Corum, M.A.; Seaton, P.; Wedegaertner, T.C.; Rathore, K.S.; Dowd, M.K. Evaluation of genetically-improved (glandless) and genetically-modified low-gossypol cottonseed meal as alternative protein sources in the diet of juvenile southern flounder *paralichthys lethostigma* reared in a recirculating aquaculture system. *Aquaculture* **2018**, *489*, 36–45. [CrossRef]
29. Abidi, N.; Manike, M. X-ray diffraction and ftir investigations of cellulose deposition during cotton fiber development. *Text. Res. J.* **2018**, *88*, 719–730. [CrossRef]
30. He, Z.; Nam, S.; Fang, D.D.; Cheng, H.N.; He, J. Surface and thermal characterization of cotton fibers of phenotypes differing in fiber length. *Polymers* **2021**, *13*, 994. [CrossRef]
31. Liu, Y.; He, Z.; Shankle, M.; Tewolde, H. Compositional features of cotton plant biomass fractions characterized by attenuated total reflection fourier transform infrared spectroscopy. *Ind. Crop. Prod.* **2016**, *79*, 283–286. [CrossRef]
32. He, Z.; Liu, Y. Fourier transform infrared spectroscopic analysis in applied cotton fiber and cottonseed research: A review. *J. Cotton Sci.* **2021**, *25*, 167–183.
33. Kaur, A.; Singh, B.; Kaur, A.; Singh, N. Chemical, thermal, rheological and ftir studies of vegetable oils and their effect on eggless muffin characteristics. *J. Food Process. Preser.* **2019**, *43*, e13978. [CrossRef]
34. Mahesar, S.A.; Shah, S.N.; Mahesar, A.W.; Kandhro, A.A.; Khaskheli, A.R.; Menghwar, P.; Sherazi, S.T.H. A chemometric approach for the quantification of free fatty acids in cottonseed oil by fourier transform infrared spectroscopy. *Inter. J. Food Propert.* **2017**, *20*, 1913–1920. [CrossRef]
35. Cheng, H.N.; Kilgore, K.; Ford, C.; Fortier, C.; Dowd, M.K.; He, Z. Cottonseed protein-based wood adhesive reinforced with nanocellulose. *J. Adhes. Sci. Technol.* **2019**, *33*, 1357–1368. [CrossRef]

36. Liu, M.; Wang, Y.; Wu, Y.; He, Z.; Wan, H. “Greener” adhesives composed of urea-formaldehyde resin and cottonseed meal for wood-based composites. *J. Clean. Prod.* **2018**, *187*, 361–371. [CrossRef]
37. Liu, Y.; He, Z.; Uchimiya, M. Comparison of biochar formation from various agricultural by-products using ftir spectroscopy. *Modern Appl. Sci.* **2015**, *9*, 246–253. [CrossRef]
38. He, Z.; Cao, H.; Cheng, H.N.; Zou, H.; Hunt, J.F. Effects of vigorous blending on yield and quality of protein isolates extracted from cottonseed and soy flours. *Mod. Appl. Sci.* **2013**, *7*, 79–88. [CrossRef]
39. Li, N.; Prodyawong, S.; He, Z.; Sun, X.S.; Wang, D. Effect of drying methods on the physicochemical properties and adhesion performance of water-washed cottonseed meal. *Ind. Crop. Prod.* **2017**, *109*, 281–287. [CrossRef]
40. Silwal, D.K.; Phambu, N.; Pokharel, B.; Aziz, A.N. Identification of hydrated and dehydrated lipids and protein secondary structures in seeds of cotton (*Gossypium hirsutum*) line. *Pure App. Biol.* **2017**, *6*, 965–975.
41. Sun, C.; Wu, X.; Wang, L.; Wang, Y.; Zhang, Y.; Chen, L.; Wu, Z. Comparison of chemical composition of different transgenic insect-resistant cotton seeds using fourier transform infrared spectroscopy (ftir). *Afric. J. Agric. Res.* **2012**, *7*, 2918–2925.
42. Ong, H.C.; Chen, W.-H.; Singh, Y.; Gan, Y.Y.; Chen, C.-Y.; Show, P.L. A state-of-the-art review on thermochemical conversion of biomass for biofuel production: A tg-ftir approach. *Energy Conver. Manag.* **2020**, *209*, 112634. [CrossRef]
43. Fischer, M.; Wohlfahrt, S.; Varga, J.; Matuschek, G.; Saraji-Bozorgzad, M.R.; Walte, A.; Denner, T.; Zimmermann, R. Evolution of volatile flavor compounds during roasting of nut seeds by thermogravimetry coupled to fast-cycling optical heating gas chromatography-mass spectrometry with electron and photoionization. *Food Anal. Met.* **2017**, *10*, 49–62. [CrossRef]
44. Valdés García, A.; Beltrán, A.; Karabagias, I.; Badeka, A.; Kontominas, M.G.; Garrigós, M.C. Monitoring the oxidative stability and volatiles in blanched, roasted and fried almonds under normal and accelerated storage conditions by dsc, thermogravimetric analysis and atr-ftir. *Eur. J. Lipid Sci. Technol.* **2015**, *117*, 1199–1213. [CrossRef]
45. Valdés García, A.; Beltrán Sanahuja, A.; Karabagias, I.K.; Badeka, A.; Kontominas, M.G.; Garrigós, M.C. Effect of frying and roasting processes on the oxidative stability of sunflower seeds (*Helianthus annuus*) under normal and accelerated storage conditions. *Foods* **2021**, *10*, 944. [CrossRef] [PubMed]
46. Raza, H.; Zaaboul, F.; Shoaib, M.; Ashraf, W.; Hussain, A.; Zhang, L. Physicochemical and structural characterization of microwave-roasted chickpea. *J. Glob. Inno. Agri. Soci. Sci* **2019**, *7*, 23–28. [CrossRef]
47. Rojas, S.M.; Chejne, F.; Ciro, H.; Montoya, J. Roasting impact on the chemical and physical structure of criollo cocoa variety (*Theobroma cacao* L.). *J. Food Proc. Engineer.* **2020**, *43*, e13400. [CrossRef]
48. Nam, S.; Condon, B.D.; Liu, Y.; He, Q. Natural resistance of raw cotton fiber to heat evidenced by the suppressed depolymerization of cellulose. *Polymer Degrad. Stabili.* **2017**, *138*, 133–141. [CrossRef]
49. Volli, V.; Gollakota, A.R.K.; Shu, C.-M. Thermal behavior of hazel sterculia seeds: A tg-ftir study. *J. Innov. Technol.* **2021**, *3*, 1–6.
50. Tahir, M.H.; Mahmood, M.A.; Çakman, G.; Ceylan, S. Pyrolysis of oil extracted safflower seeds: Product evaluation, kinetic and thermodynamic studies. *Bioresour. Technol.* **2020**, *314*, 123699. [CrossRef]
51. Zong, P.; Jiang, Y.; Tian, Y.; Li, J.; Yuan, M.; Ji, Y.; Chen, M.; Li, D.; Qiao, Y. Pyrolysis behavior and product distributions of biomass six group components: Starch, cellulose, hemicellulose, lignin, protein and oil. *Energy Conver. Manag.* **2020**, *216*, 112777. [CrossRef]
52. González-Rivera, J.; Duce, C.; Falconieri, D.; Ferrari, C.; Ghezzi, L.; Piras, A.; Tine, M.R. Coaxial microwave assisted hydrodistillation of essential oils from five different herbs (lavender, rosemary, sage, fennel seeds and clove buds): Chemical composition and thermal analysis. *Innov. Food Sci. Emerg. Technol.* **2016**, *33*, 308–318. [CrossRef]
53. Apaydin-Varol, E.; Uzun, B.B.; Onal, E.; Putun, A.E. Synthetic fuel production from cottonseed: Fast pyrolysis and a tga/ft-ir/ms study. *J. Anal. Appl. Pyrol.* **2014**, *105*, 83–90. [CrossRef]
54. Seal, S.; Panda, A.K.; Kumar, S.; Singh, R. Production and characterization of bio oil from cotton seed. *Environ. Progress Sustain. Energy* **2015**, *34*, 542–547. [CrossRef]
55. Primaz, C.T.; Ribes-Greus, A.; Jacques, R.A. Valorization of cotton residues for production of bio-oil and engineered biochar. *Energy* **2021**, *235*, 121363. [CrossRef]
56. He, Z.; Shankle, M.; Zhang, H.; Way, T.R.; Tewolde, H.; Uchimiya, M. Mineral composition of cottonseed is affected by fertilization management practices. *Agron. J.* **2013**, *105*, 341–350. [CrossRef]
57. He, Z.; Zhang, H.; Olk, D.C.; Shankle, M.; Way, T.R.; Tewolde, H. Protein and fiber profiles of cottonseed from upland cotton with different fertilizations. *Mod. Appl. Sci.* **2014**, *8*, 97–105. [CrossRef]
58. Bellaloui, N.; Turley, R.B.; Stetina, S.R. Cottonseed protein, oil, and minerals in cotton (*Gossypium hirsutum* L.) lines differing in curly leaf morphology. *Plants* **2021**, *10*, 525. [CrossRef]
59. Bolek, Y.; Tekerek, H.; Hayat, K.; Bardak, A. Screening of cotton genotypes for protein content, oil and fatty acid composition. *J. Agri. Sci.* **2016**, *8*, 107–121. [CrossRef]
60. Hu, W.; Dai, Z.; Yang, J.; Snider, J.L.; Wang, S.; Meng, Y.; Wang, Y.; Chen, B.; Zhao, W.; Zhou, Z. Cultivar sensitivity of cotton seed yield to potassium availability is associated with differences in carbohydrate metabolism in the developing embryo. *Field Crop. Res.* **2017**, *214*, 301–309. [CrossRef]
61. Han, Y.W. Removal of phytic acid from soybean and cottonseed meals. *J. Agric. Food Chem.* **1988**, *36*, 1181–1183. [CrossRef]
62. He, Z.; Zhang, H.; Fang, D.D.; Zeng, L.; Jenkins, J.N.; McCarty, J.C. Effects of inter-species chromosome substitution on cottonseed mineral and protein nutrition profiles. *Agron. J.* **2020**, *112*, 3963–3974. [CrossRef]
63. Fageria, N.K.; Baligar, C.; Clark, R.B. Micronutrients in crop production. *Adv. Agron.* **2002**, *77*, 185–268.

64. He, Z.; Cheng, H.N.; Olanya, O.M.; Uknalis, J.; Zhang, X.; Koplitz, B.D.; He, J. Surface characterization of cottonseed meal products by sem, sem-eds, xrd and xps analysis. *J. Mater. Sci. Res.* **2018**, *7*, 28–40. [CrossRef]
65. Peng, Y.; Kyriakopoulou, K.; Ndiaye, M.; Bianeis, M.; Keppler, J.; van der Goot, A. Characteristics of soy protein prepared using an aqueous ethanol washing process. *Foods* **2021**, *10*, 2222. [CrossRef]
66. Yatsu, L.; Jacks, T.J.; Kircher, H.W.; Godshall, M.A. Chemical and microscopic studies of the matrix substance in pigment glands of cotton (*Gossypium hirsutum* L.) seeds. *J. Am. Oil Chem. Soc.* **1986**, *63*, 534–537. [CrossRef]
67. Shah, S.; Mahesar, S.A.; Abro, K.A.; Sherazi, S.T.H.; Nizamani, S.M. Ftir characterization and physicochemical evaluation of cottonseed oil. *Pak. J. Anal. Environ. Chem.* **2017**, *18*, 46–53. [CrossRef]
68. Abdelrahman, S.A.; Yassin, A.A.; Mirghani, M.E.S.; Bashir, N.H. Determination of gossypol in hamid and bt (seeni 1) cottonseed oil using fourier transform infrared spectroscopy. *Borneo J. Pharmacy* **2020**, *3*, 227–234. [CrossRef]
69. Riaz, T.; Iqbal, M.W.; Mahmood, S.; Yasmin, I.; Leghari, A.A.; Rehman, A.; Mushtaq, A.; Ali, K.; Azam, M.; Bilal, M. Cottonseed oil: A review of extraction techniques, physicochemical, functional, and nutritional properties. *Crit. Rev. Food Sci. Nutrit.* **2021**. [CrossRef]
70. Arslan, F.N.; Akin, G.; Elmas, Ş.N.K.; Yilmaz, I.; Janssen, H.-G.; Kenar, A. Rapid detection of authenticity and adulteration of cold pressed black cumin seed oil: A comparative study of atr-ftir spectroscopy and synchronous fluorescence with multivariate data analysis. *Food Control* **2019**, *98*, 323–332. [CrossRef]
71. He, Z.; Chapital, D.C.; Cheng, H.N.; Dowd, M.K. Comparison of adhesive properties of water- and phosphate buffer-washed cottonseed meals with cottonseed protein isolate on maple and poplar veneers. *Int. J. Adhes. Adhes.* **2014**, *50*, 102–106. [CrossRef]
72. He, Z.; Sleighter, R.L.; Hatcher, P.G.; Liu, S.; Wu, F.; Zou, H.; Olanya, O.M. Molecular level comparison of water extractives of maple and oak with negative and positive ion esi ft-icr mass spectrometry. *J. Mass Spectrom.* **2019**, *54*, 655–666. [CrossRef]
73. Ling, T.-R.; Chang, J.-S.; Chiou, Y.-J.; Chern, J.-M.; Chou, T.-C. Characterization of high acid value waste cottonseed oil by temperature programmed pyrolysis in a batch reactor. *J. Anal. Appl. Pyrol.* **2016**, *120*, 222–230. [CrossRef]
74. Villalpando, A.; Easson, M.; Cheng, H.; Condon, B. Use of cottonseed protein as a strength additive for nonwoven cotton. *Textile Res. J.* **2019**, *89*, 1725–1733. [CrossRef]
75. Swiatkiewicz, S.; Arczewska-Wlosek, A.; Jozefia, D. The use of cottonseed meal as a protein source for poultry: An updated review. *World Poultry Sci. J.* **2016**, *72*, 473–484. [CrossRef]
76. Kumar, M. Paruthi paal, a nutrient-rich healthy drink from cottonseed: An indian delicacy. *J. Ethnic Foods* **2019**, *6*, 32. [CrossRef]
77. Kumar, M.; Potkule, J.; Patil, S.; Mageshwaran, V.; Radha; Satankar, V.; Berwal, M.K.; Mahapatra, A.; Saxena, S.; Ashtaputre, N.; et al. Evaluation of detoxified cottonseed protein isolate for application as food supplement. *Toxin Rev.* **2021**, 1–8. [CrossRef]
78. Kumar, M.; Potkule, J.; Patil, S.; Saxena, S.; Patil, P.G.; Mageshwaran, V.; Punia, S.; Varghese, E.; Mahapatra, A.; Ashtaputre, N.; et al. Extraction of ultra-low gossypol protein from cottonseed: Characterization based on antioxidant activity, structural morphology and functional group analysis. *LWT* **2021**, *140*, 110692. [CrossRef]
79. Venkatesan, H.; Sivamani, S. Cotton seed biodiesel as alternative fuel: Production and its characterization analysis using spectroscopic studies. *Inter. J. Renew. Energy Res.* **2017**, *7*, 1333–1339.
80. He, Z.; Guo, M.; Sleighter, R.L.; Zhang, H.; Fortier, C.A.; Hatcher, P.G. Characterization of defatted cottonseed meal-derived pyrolysis bio-oil by ultrahigh resolution electrospray ionization fourier transform ion cyclotron resonance mass spectrometry. *J. Anal. Appl. Pyrol.* **2018**, *136*, 96–106. [CrossRef]
81. He, Z.; Uchimiya, S.M.; Guo, M. Production and characterization of biochar from agricultural by-products: Overview and use of cotton biomass residues. In *Agricultural and Environmental Applications of Biochar: Advances and Barriers*; Guo, M., He, Z., Uchimiya, S.M., Eds.; Soil Science Society of America, Inc.: Madison, WI, USA, 2016; pp. 63–86.
82. de Freitas Floriano, R.; Gräbin, K.; Rossi, R.C.; Ferreira, C.D.; Ziegler, V. Impact of roasting conditions on the quality and acceptance of the peanut paste. *J. Texture Stud.* **2020**, *51*, 841–848. [CrossRef] [PubMed]
83. Marzocchi, S.; Pasini, F.; Verardo, V.; Ciemniowska-Żytkeiwicz, H.; Caboni, M.F.; Romani, S. Effects of different roasting conditions on physical-chemical properties of polish hazelnuts (*Corylus avellana* L. Var. Kataloński). *LWT* **2017**, *77*, 440–448. [CrossRef]
84. Ciemniowska-Żytkeiwicz, H.; Bryś, J.; Sujka, K.; Koczoń, P. Assessment of the hazelnuts roasting process by pressure differential scanning calorimetry and mid-ft-ir spectroscopy. *Food Anal. Methods* **2015**, *8*, 2465–2473. [CrossRef]
85. Siegmund, B.; Murkovic, M. Changes in chemical composition of pumpkin seeds during the roasting process for production of pumpkin seed oil (part 2: Volatile compounds). *Food Chem.* **2004**, *84*, 367–374. [CrossRef]
86. Gorrepati, K.; Balasubramanian, S.; Chandra, P. Plant based butters. *J. Food Sci. Technol.* **2015**, *52*, 3965–3976. [CrossRef] [PubMed]
87. He, Z.; Guo, M.; Fortier, C.; Cao, X.; Schmidt-Rohr, K. Fourier transform infrared and solid state ¹³c nuclear magnetic resonance spectroscopic characterization of defatted cottonseed meal-based biochars. *Mod. Appl. Sci.* **2021**, *15*, 108–121. [CrossRef]
88. Zhang, J.; Wedegaertner, T.; Idowu, O.J.; Flynn, R.; Hughs, S.E.; Jones, D.C. Registration of ‘numex cot 15 gls’ glandless cotton. *J. Plant Registr.* **2016**, *10*, 223–227. [CrossRef]
89. Chen, N.; Huang, J.; Li, K. Investigation of a formaldehyde-free cottonseed flour-based adhesive for interior plywood. *BioResour.* **2020**, *15*, 5546–5557. [CrossRef]
90. Pettigrew, W.T.; Dowd, M.K. Nitrogen fertility and irrigation effects on cottonseed composition. *J. Cotton Sci.* **2014**, *18*, 410–419.
91. McCall, E.R.; Jurgens, J.F. Chemical composition of cotton. *Text. Res. J.* **1951**, *21*, 19–21. [CrossRef]
92. He, Z.; Zhang, H.; Olk, D.C. Chemical composition of defatted cottonseed and soy meal products. *PLoS ONE* **2015**, *10*, e0129933. [CrossRef] [PubMed]

93. Pettigrew, W.T.; Dowd, M.K. Varying planting dates or irrigation regimes alters cottonseed composition. *Crop Sci.* **2011**, *51*, 2155–2164. [CrossRef]
94. Novotny, L.; Fahey, G.; Layton, B.; Walter, M. Critical factors in determining fiber in feeds and forages. *AAFCO's Lab. Methods Serv. Comm.* **2017**, *1*, 1–14.
95. He, Z.; Klasson, K.T.; Wang, D.; Li, N.; Zhang, H.; Zhang, D.; Wedegaertner, T.C. Pilot-scale production of washed cottonseed meal and co-products. *Mod. Appl. Sci.* **2016**, *10*, 25–33. [CrossRef]

Article

Structural Changes of β -Casein Induced by Temperature and pH Analysed by Nuclear Magnetic Resonance, Fourier-Transform Infrared Spectroscopy, and Chemometrics

Tatjana Markoska ¹, Davor Daniloski ^{1,2}, Todor Vasiljevic ¹ and Thom Huppertz ^{1,3,4,*}

¹ Advanced Food Systems Research Unit, Institute for Sustainable Industries & Liveable Cities, College of Health and Biomedicine, Victoria University, Melbourne, VIC 8001, Australia; tatijana.markoska@live.vu.edu.au (T.M.); davor.daniloski@live.vu.edu.au (D.D.); todor.vasiljevic@vu.edu.au (T.V.)

² Teagasc Food Research Centre, Food Chemistry and Technology Department, Moorepark, Fermoy, P61 C996 Cork, Ireland

³ FrieslandCampina, 3818 LE Amersfoort, The Netherlands

⁴ Food Quality and Design Group, Wageningen University & Research, 6808 WG Wageningen, The Netherlands

* Correspondence: thom.huppertz@wur.nl

Abstract: This study investigated structural changes in β -casein as a function of temperature (4 and 20 °C) and pH (5.9 and 7.0). For this purpose, nuclear magnetic resonance (NMR) and Fourier-transform infrared (FTIR) spectroscopy were used, in conjunction with chemometric analysis. Both temperature and pH had strongly affected the secondary structure of β -casein, with most affected regions involving random coils and α -helical structures. The α -helical structures showed great pH sensitivity by decreasing at 20 °C and diminishing completely at 4 °C when pH was increased from 5.9 to 7.0. The decrease in α -helix was likely related to the greater presence of random coils at pH 7.0, which was not observed at pH 5.9 at either temperature. The changes in secondary structure components were linked to decreased hydrophobic interactions at lower temperature and increasing pH. The most prominent change of the α -helix took place when the pH was adjusted to 7.0 and the temperature set at 4 °C, which confirms the disruption of the hydrogen bonds and weakening of hydrophobic interactions in the system. The findings can assist in establishing the structural behaviour of the β -casein under conditions that apply as important for solubility and production of β -casein.

Keywords: FTIR; NMR; β -casein; secondary structure; temperature; pH

Citation: Markoska, T.; Daniloski, D.; Vasiljevic, T.; Huppertz, T. Structural Changes of β -Casein Induced by Temperature and pH Analysed by Nuclear Magnetic Resonance, Fourier-Transform Infrared Spectroscopy, and Chemometrics. *Molecules* **2021**, *26*, 7650. <https://doi.org/10.3390/molecules26247650>

Academic Editor: Mirella Nardini

Received: 4 December 2021

Accepted: 15 December 2021

Published: 17 December 2021

Publisher's Note: MDPI stays neutral with regard to jurisdictional claims in published maps and institutional affiliations.



Copyright: © 2021 by the authors. Licensee MDPI, Basel, Switzerland. This article is an open access article distributed under the terms and conditions of the Creative Commons Attribution (CC BY) license (<https://creativecommons.org/licenses/by/4.0/>).

1. Introduction

Caseins represent the major protein constituents of the bovine milk (80%), comprised of four major phosphoproteins, α_{S1} -, α_{S2} -, β -, and κ -casein at concentration of 12–15, 3–4, 9–11 and 2–4 g/L, respectively [1]. In the dairy industry, the structural organisation of caseins can have a great effect on the functional properties of milk and the quality of the final product due to various interactions (hydrophobic, electrostatic, van der Waals forces, or covalent bonds) yielding to different properties. As the most amphiphilic, bovine β -casein represents 35% of the caseins in the bovine milk with 209 amino acids in the polypeptide chain and average molecular weight of 24 kDa [2]. Due to the presence of many relatively hydrophobic parts in the β -casein molecule with great number of Pro residues, the molecule can adopt flexible conformations. These conformations are characterised by large range of inter or intra molecular interactions, fewer secondary and tertiary structures, while containing more random coil organisations [3].

There have been multiple studies analysing the secondary structure of β -casein. The summarised findings included the presence of 7–25% α -helical structures, 15–33% β -sheets,

20–30% turns, and 20–25% polyproline II structures [2,4–6]. The predicted α -helical structures are likely in the N-terminal part of the β -casein, f(1–40), due to the presence of phosphoserine residues that carry the net charge of the molecule [7]. The apolar residues present in the C-terminal part of β -casein, f(136–209), are responsible for the appearance of β -sheet structures due to higher hydrophobicity in this region [7,8].

Temperature is an important factor in regards to the β -casein release from the casein micelle. In a cold environment, due to weakening of hydrophobic attraction, selective solubilisation of β -casein takes place, leading to increased solubility of β -casein during cold storage [9]. At low temperature, β -casein appears as monomer with structural transitions due to cold denaturation. The dissociation of β -casein from the casein micelle was previously observed to be the greatest at pH 5 and a temperature below 4 °C [10]. Moreover, the net negative charge at high pH increases as a result of deprotonation of carboxyl groups and loss of the positive charge of amino acids including His. The increase in electrostatic repulsion takes place as a result of the negative charge of the phosphoserine residues [11]. The transition that takes place on the β -casein molecule based on pH and temperature adjustment can have a significant effect on the secondary structure of the molecule. The impact of both pH and temperature on β -casein and overall milk protein structure play an important role in protein stability during processing of milk and milk products and their storage. The pH of dairy products may vary from <4 for some fermented dairy to >7 for some dairy ingredients and infant formula products, whereas storage occurs both at ~4 °C for pasteurised products and at room temperature for sterilised products.

Even though several studies already confirmed the presence of some structural elements in the β -casein molecule, it would be valuable to know how this particular casein adapts its secondary structural elements in different environments [4,12,13]. Thus, the aim of the present research was to identify the structural components of β -casein using Fourier-transform infrared spectroscopy (FTIR) and nuclear magnetic resonance (NMR). FTIR spectroscopy provides information of the structural changes in proteins by absorption of the stretching/bending vibrations in different regions [14]. Consequently, NMR provides detailed information of the protons in the molecule, which evaluates the primary position of the atoms in the molecule [15]. Both methods are nondestructive with minimal sample preparation and can provide information under any condition. The current work involved structural analysis of β -casein at two pH values (pH 5.9 and pH 7.0) and two temperatures (4 and 20 °C) in order to establish the structural transitions of β -casein. The selected temperature was used to observe the structural transition of β -casein in most used storage conditions for milk proteins. The pH 7.0 was used to observe how β -casein structure changes in pH environment close to native pH in milk and pH 5.9 were used as the native pH of synthesised β -casein and also were important for curd stability during milk coagulation.

2. Results and Discussion

In the current study, FTIR and NMR were used to examine the structural changes in β -casein resulting from changes in pH and temperature. In the Amide I region of the FTIR spectra, six structural features were distinguished and analysed (Table 1).

From the peak area calculations of the second derivative spectra, the most significant differences ($p \leq 0.05$) as a result of changes in pH and temperature were observed in random coil, α -helix, and β -turn structures. At pH 7.0, the percentage of random coil structure was ~15% higher at 4 °C than at 20 °C, whereas random coil structures were not detected at pH 5.9 at either temperature. The assigned random coil structures have previously been shown to include short polyproline II (PPII) helix/chains [16]. Bovine β -casein contains 35 Pro residues, evenly distributed along the 209 amino acid polypeptide chain, which favours the formation of PPII structures [4]. The lack of detected random coil structures at pH 5.9 indicates that there was no substantial unfolding of the secondary structure of the protein at this pH [17]. The absence of random coils in β -casein at pH 5.9 appeared to correlate with a greater amount of α -helical structures, at both 4 and 20 °C. At

20 °C, the α -helix content at pH 7.0 was half of that observed at pH 5.9, whereas α -helical structures were not detected at pH 7.0 at 4 °C. The β -turn structures were affected by temperature, but not by pH; at both pH 5.9 and 7.0, fewer β -turns were observed at 20 than at 4 °C. Farrell et al. [4] stated that with the temperature increase the conversion from β -turns and β -sheet to PPII conformations might occur. Hence, in line with these previous findings in combination with the present data of random and turn conformations (Table 1), there is a reasonable possibility of transformation of these structures into PPII helices, whose content was found to be between 20 and 25% within the β -casein molecule [5,6]. The formation of β -turns in caseins is promoted by the Pro residues by cross-linking with neighbouring residues via van der Waals interactions acting as a β -turn inducer [8].

Table 1. Total percentage areas of different secondary structures in Amide I in β -CN in FTIR including side chain, β -sheet, random coil, α -helix β -turn, and aggregated β -sheets. The selected band frequency for each structural component is presented in cm^{-1} . The peak area percentage is presented for temperature of 4 and 20 °C and pH of 5.9 and 7.0.

Band Assessment	Band Frequency (cm^{-1})	Peak Area (%)			
		Temperature 4 °C		Temperature 20 °C	
		pH 5.9	pH 7.0	pH 5.9	pH 7.0
Side chain	1608–1610	3.99 \pm 0.53 ^a	5.40 \pm 0.09 ^a	3.92 \pm 0.34 ^a	4.33 \pm 0.60 ^a
β -sheet	1620–1630	26.04 \pm 3.55 ^a	23.07 \pm 4.24 ^a	26.70 \pm 4.03 ^a	23.72 \pm 2.47 ^a
Random coil	1640–1645	n/d	46.53 \pm 5.81 ^b	n/d	31.07 \pm 8.71 ^a
α -helix	1646–1652	42.98 \pm 3.41 ^b	n/d	45.24 \pm 3.76 ^b	21.77 \pm 2.59 ^a
β -turn	1677–1679	22.25 \pm 1.87 ^c	20.04 \pm 1.35 ^{bc}	17.00 \pm 2.29 ^{ab}	13.34 \pm 4.66 ^a
Aggregated β -sheet	1689–1690	4.75 \pm 1.61 ^a	4.96 \pm 0.97 ^a	7.15 \pm 1.36 ^a	5.78 \pm 2.02 ^a

^{a,b,c} Mean values within a row that do not share a common superscript letter are significantly different ($p \leq 0.05$); n/d = not detected.

The observed differences in the peak area (Table 1) were further confirmed by PCA results (Figure 1).

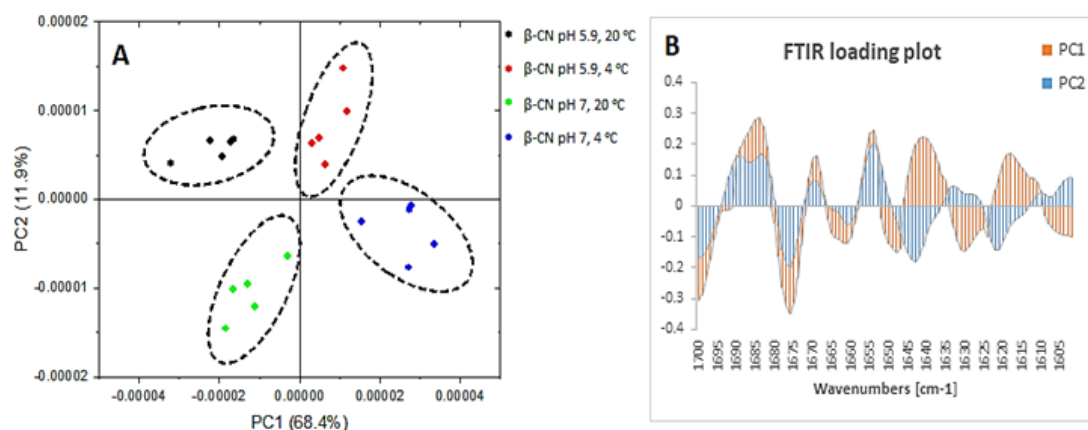


Figure 1. Principal components score plot (A) and loading plot (B) of β -casein of the FTIR spectra in region 1700–1600 cm^{-1} where β -casein at pH 5.9 and temperature of 20 °C (black), β -casein at pH 5.9 and temperature of 4 °C (red), β -casein at pH 7.0 and temperature of 20 °C (green) and β -casein at pH 7.0 and temperature of 4 °C (blue) are in (A) and PC1 (orange) and PC2 (blue) are in (B).

In addition, PC1 confirmed 68.4% difference between the samples at 4 and 20 °C, while PC2 confirmed 11.9% difference between samples at pH 5.9 and pH 7.0 (Figure 1A). The loading score in Figure 1A visually separated the groupings of samples that differed in temperature along the PC1. The PC1 also distinguished the differences in the structural components between these samples, which are confirmed in the loading plot in Figure 1B.

The PC1 identified high loading for a peak at 1650 cm^{-1} (α -helix) for samples at $20\text{ }^{\circ}\text{C}$, confirming a greater presence of this secondary structure at this temperature. On the other hand, the observed high loading for peak at 1640 cm^{-1} for samples at $4\text{ }^{\circ}\text{C}$ confirmed the high level of random structures. PC1 also depicted slight changes in β -sheets by greater presence of intramolecular β -sheets (1630 cm^{-1}) for samples at $20\text{ }^{\circ}\text{C}$ and greater intermolecular β -sheets (1620 cm^{-1}) for samples at $4\text{ }^{\circ}\text{C}$. Similarly, PC2 differentiated the structural features occurring between samples with different pH values which were also present with different loadings in the loading plot in Figure 1B. In the PC2 loading plot (Figure 1B), great loadings were observed for a peak at 1653 cm^{-1} (α -helix) for samples at pH 5.9 and at 1643 cm^{-1} (random coils) for samples at pH 7.0. Regarding the β -sheet structures, greater loading for a peak at 1630 cm^{-1} (intramolecular β -sheets) was observed for samples at pH 5.9 and at pH 7.0 greater loading shifted to indicate intermolecular β -sheets (peak 1623 cm^{-1}). Thus, PC1 and PC2 successfully confirmed the previously observed changes for α -helix and random structures and additionally confirmed differences in inter- and intramolecular β -sheets.

The ^1H -NMR chemical shifts in proteins are sensitive to local structural rearrangements. Moreover, the conformational differences can be a result of multiple contributions including torsion angles coming from backbone and side chains, hydrogen bonding, electric fields, rings vibrations, and steric repulsions [18]. In the current work, we observed the variations in chemical shift distribution in four regions including methyl $-\text{CH}_3-$ ($0\text{--}1.5\text{ ppm}$), aliphatic $-\text{CH}_2-$ ($1.5\text{--}3.5\text{ ppm}$), H^α amide region ($3.5\text{--}5\text{ ppm}$), and aromatic/ H^N -amino region ($5.5\text{--}10\text{ ppm}$). From the overlaid spectra in Figure 2A, a downfield shift of the proton chemical shifts can be seen at $4\text{ }^{\circ}\text{C}$ compared to at $20\text{ }^{\circ}\text{C}$. In addition, the deshielding was observed in all the regions, except in the amino or backbone region (Figure 2A). Thus, in the amino region the peaks appeared in a broad pattern which overlaid in identical chemical shift positions (Figure 2A).

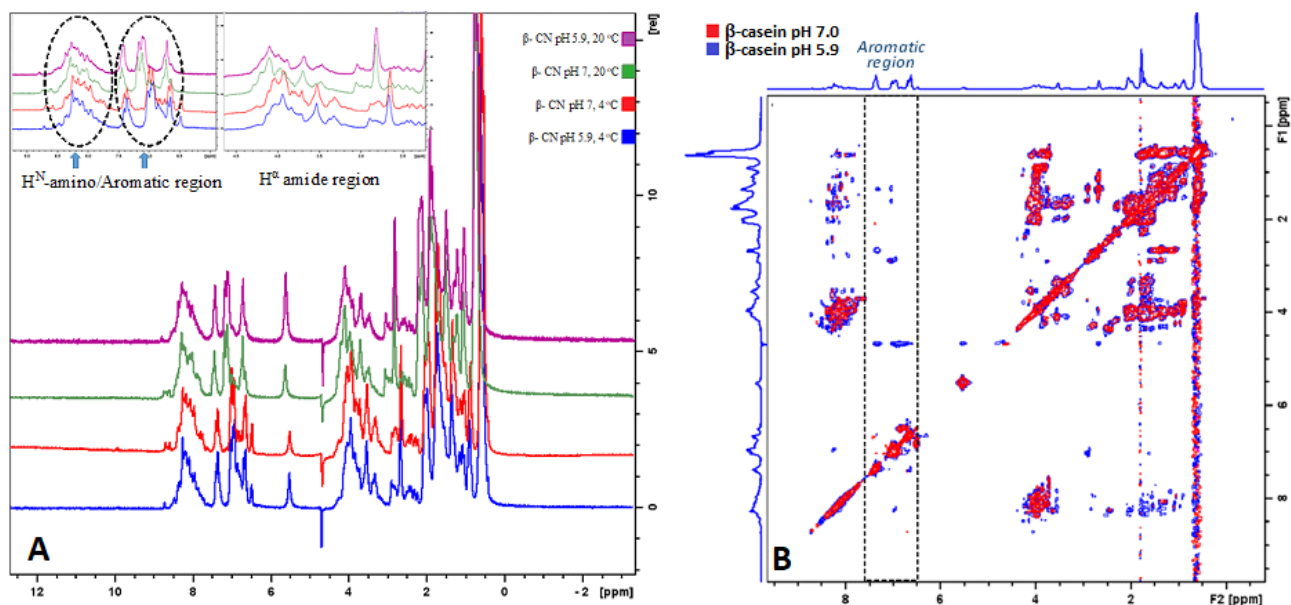


Figure 2. (A) Overlaid ^1H NMR spectra of β -casein at pH 5.9 and temperature of $20\text{ }^{\circ}\text{C}$ (purple), β -casein at pH 5.9 and temperature of $4\text{ }^{\circ}\text{C}$ (blue), β -casein at pH 7.0 and temperature of $20\text{ }^{\circ}\text{C}$ (green) and β -casein at pH 7.0 and temperature of $4\text{ }^{\circ}\text{C}$ (red). (B) Overlaid TOCSY NMR spectra of β -casein at pH 7.0 (red) and β -casein at pH 5.9 (blue).

The deshielding in the other regions resulted by lowering of temperature to $4\text{ }^{\circ}\text{C}$ was observed to be $0.2\text{--}0.3\text{ ppm}$. The sensitivity of the ^1H chemical shift can be promoted by multiple factors, including the protein sensitivity to conformations, hydrogen bonding, ring vibrations, or electric fields [19]. In addition, the upfield and downfield shielding of the ^1H chemical shift can result from changes in the different components in the secondary

structure [18,20]. In this study, an opposite effect by 0.3 ppm downfield shift for the amide region was observed, which can relate to a lower presence of α -helical structures at low temperature. In addition, from the integrated amide region we observed a significant decrease (≤ 0.05) in the peak intensities by $\sim 3\%$ at $4\text{ }^\circ\text{C}$ compared to at $20\text{ }^\circ\text{C}$ (Table 2). This further confirms previously discussed FTIR results (Figure 1 and Table 1) regarding the absence or decline in α -helical structures at low temperature.

Table 2. Total percentage areas peaks in different regions for β -casein in NMR including methyl, aliphatic, amide and amino region. The difference in the percentage is presented for β -casein at temperature of 4 and $20\text{ }^\circ\text{C}$ and pH of 5.9 and 7.0.

Temperature	4 °C		20 °C	
	pH 5.9	pH 7.0	pH 5.9	pH 7.0
Region/Integral	β -Casein			
Methyl	19.48 \pm 0.16 ^a	17.63 \pm 0.27 ^b	16.78 \pm 0.13 ^{bc}	16.22 \pm 0.17 ^c
Aliphatic	16.22 \pm 0.16 ^{ab}	17.73 \pm 0.75 ^a	14.91 \pm 1.64 ^b	13.90 \pm 0.35 ^{bc}
Amide	42.29 \pm 0.04 ^b	42.82 \pm 0.21 ^b	46.69 \pm 0.14 ^a	46.32 \pm 0.17 ^a
Amino	22.01 \pm 0.34 ^b	21.83 \pm 0.82 ^b	22.62 \pm 0.41 ^{ab}	23.47 \pm 0.89 ^a

^{a,b,c} Mean values within a row that do not share a common superscript letter are significantly different ($p \leq 0.05$).

From the other regions of the NMR spectrum a greater amount of methyl groups at low temperature was observed, which was more present at pH 5.9 (Figure 2A). The peak observed in this region (0–0.8 ppm) likely appeared from the side chains (CH_3) groups from Ile, Val, and Leu in β -casein [21]. The lower peak intensity for methyl groups at room temperature can be due losses of signal from the methyl side chains of Ile, Val, and Leu. An increase in pH from 5.9 to 7.0 led to slightly lower peaks for the methyl side chains (Table 2). The amide region of the β -casein presented slightly greater intensity at $20\text{ }^\circ\text{C}$ compared to that at $4\text{ }^\circ\text{C}$ at both pH values (Table 2).

The change in pH from 5.9 to 7.0 lead to lower detection of the cross peaks in the aromatic region of the TOCSY spectra (Figure 2B). This spectral pattern was not affected by the temperature, i.e., at both 4 and $20\text{ }^\circ\text{C}$ the TOCSY spectra of β -casein showed the same pattern in regard to the pH. In the aromatic region of the TOCSY spectra the cross peaks present the interactions of the proton rings with the neighbouring protons of the amino acids [15]. It was previously suggested that charge-induced disruption of the cohesive interactions in the hydrophobic regions of the caseins occur as a result of pH-induced charge modifications on side groups of amino acids, including Tyr, Lys, His, and Arg [22]. In the pH range currently studied, His would be the most susceptible to (de)protonation as a result of pH change. The side groups of these amino acids are detected in the aromatic region of the TOCSY spectra and the cross peaks in this region denote their connection with the neighbouring protons. It is known that increase in pH leads to greater intermolecular repulsion of caseins [11]. The addition of alkali to the β -casein solution can lead to disruption of existing hydrophobic connections, which was observed by reduction of the proton–proton cross association in the TOCSY spectra.

The observed structural differences resulted from changes in temperature and pH were also evaluated by PCA analysis (Figure 3).

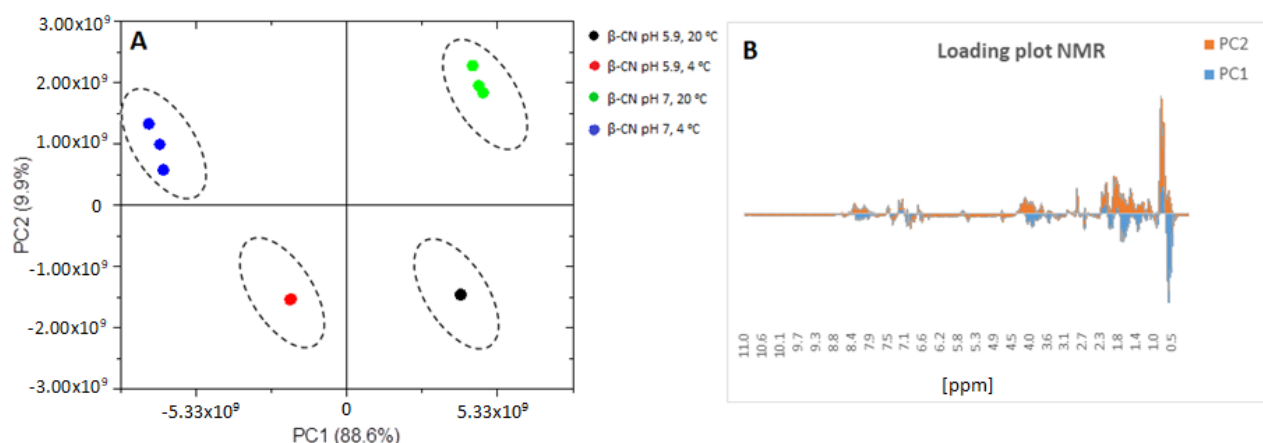


Figure 3. Principal components score plot (A) and loading plot (B) of β -casein of the NMR spectra in where β -casein at pH 5.9 and temperature of 20 °C (black), β -casein at pH 5.9 and temperature of 4 °C (red), β -casein at pH 7.0 and temperature of 20 °C (green) and β -casein at pH 7.0 and temperature of 4 °C (blue) are in (A) and PC1 (blue) and PC2 (orange) are in (B).

In the PCA loading score (Figure 3A), PC1 separated the results based on the temperature with 88.6% variance. On the other hand, PC2 separated the β -casein based on pH effect with 9.9% variance. PC1 has shown greater loading for a peak at 0.5 ppm for samples at low temperature and PC2 indicated that this peak was mainly present for samples at pH 7.0. Moreover, PC2 showed that peak loadings in aliphatic (1.5–3.5 ppm) and amide regions (3.5–5.0 ppm) were more prominent for samples at pH 7.0, whereas at pH 5.9 greater loading was observed for the aromatic region (6.5–8.0 ppm). Furthermore, both PC1 and PC2 confirmed that in the aliphatic and aromatic regions the peak loading was more intense for samples at pH 7.0 and temperature of 4 °C, which can confirm the structural changes observed by FTIR occurring as a result of a cold environment and pH.

3. Material and Methods

3.1. Sample Preparation

Bovine β -casein was purchased from Sigma-Aldrich (Sigma-Aldrich, St. Louis, MO, USA) with >98% purity. The preparation process was performed by dispersion of 10 mg β -casein in 1 mL of a mixture of H₂O:D₂O (90%:10%, Sigma-Aldrich, St. Louis, MO, USA) for both FTIR and NMR analyses. The pH of β -casein in H₂O/D₂O solution was measured using a pH meter (Metrohm AG, Herisau, Switzerland) equipped with a combined pH electrode with temperature sensor and fixed cable. The original pH of the protein solution was 5.9. The pH was further adjusted to 7.0 using 0.25 M NaOH. The pH adjustment was carried out under continuous stirring of the solution and pH was additionally controlled before the structural measurements. Both β -casein solutions with pH 5.9 and pH 7.0 were analysed for structural features at 4 and 20 °C. The temperature for the FTIR analysis was monitored with temperature probe, however for the NMR analysis the temperature control was automated by the instrument.

3.2. Fourier Transform Infrared Spectroscopy

The secondary structure of β -casein as a function of pH and temperature was analysed using a FTIR spectrometer (Frontier, PerkinElmer, Boston, MA, USA) in the range of 4000 to 600 cm⁻¹ with a resolution of 4 cm⁻¹ and 16 scans for each spectrum. Before the start of the measurement for every sample, the background spectra were scanned using a blank diamond attenuated total reflectance (ATR) cell. At the start of the analysis the solvent spectrum (90% H₂O/10% D₂O) was recorded and used for subtraction from the sample spectra to eliminate the intense solvent signal. The spectra of five subsamples of each sample were taken by refilling the ATR cell. For the secondary structure analysis, the amide I region (1700–1600 cm⁻¹) was analysed for C=O stretching after

applying Savitzky–Golay smoothing and 2nd derivative. The FTIR spectra and mean centering were analysed using Spectragryph software (version 1.2.7, Oberstdorf, Germany). The baseline of five repetitions for each sample was subtracted and the area of the peak was analysed by Origin software (Origin Pro 2021, v. 95E, OriginLab Corporation, Northampton, MA, USA). To estimate the area of each component representing secondary structures, a technique previously described elsewhere [23] was utilised. Briefly, each spectrum from five repetitions was treated by interpolation baseline mode and adjacent-averaging smoothing, then each peak in the 2nd derivative spectra was selected and integrated by high percentage. In the amide I region several peaks were analysed, including side chain ($1608\text{--}1610\text{ cm}^{-1}$), β -sheets ($1620\text{--}1630\text{ cm}^{-1}$), random coil ($1640\text{--}1645\text{ cm}^{-1}$), α -helix ($1646\text{--}1652\text{ cm}^{-1}$), β -turns ($1677\text{--}1679\text{ cm}^{-1}$) and aggregated β -sheets ($1689\text{--}1690\text{ cm}^{-1}$) [24].

3.3. Nuclear Magnetic Resonance

The NMR analysis was performed on a Bruker Avance spectrometer (Bruker BioSpin GmbH, Rheinstetten, Germany) operating at a 600 MHz transmitter frequency using 5 mm TXI probe with z-gradient. Proton NMR ($^1\text{H-NMR}$) spectra were acquired using 16 scans and spectral width of 9615 Hz in three replications. The two-dimensional methods used in this study were total correlation spectroscopy (TOCSY) and nuclear Overhauser effect spectroscopy (NOESY). The 2D spectra were recorded using 8 scans and spectral width of 8196 Hz for TOCSY and 5882 Hz for NOESY spectra. The water suppression for spectra was performed using excitation sculpting with gradients with acquisition mode of States-TPPI (time-proportional phase incrementation). All spectral data were processed using TopSpin (version 4.0.6) software (Bruker BioSpin). The phase correction was performed manually by either 0th or 1st order correction for pk or the baseline and the noise correction was adjusted using qfil mode to 0.1 ppm filter width and symmetrical noise correction for the homonuclear spectra. The NMR spectra were analysed using three NMR regions, i.e., amino/aromatic (H^{N}), amide (H^{α}), and aliphatic. From the aliphatic region, the methyl peak (CH_3) was analysed separately due to its high loading. All the peaks observed in these regions were manually integrated in TopSpin (version 4.0.6) software (Bruker BioSpin).

3.4. Statistical Analysis and Spectral Data

To assess the experimental results, Minitab version 20 software was used to analyse the data (Minitab Inc., State College, PA, USA). Hence, a two-way ANOVA and Tukey's test were performed with β -casein as fixed factor to evaluate if there was a difference between means ($p \leq 0.05$). Unless otherwise specified, all measurements were taken in triplicate. In addition, principal component analysis (PCA) was used for both FTIR and NMR results to identify the changes in the secondary structure in β -casein samples based on the temperature and pH effect. PCA gives information by generating principal components (PCs) as a coordinated axis with a least possible loss of information. The groupings of the different samples were depicted in score plots and the loading plots were used for the wavenumbers responsible for peaks classification. The multivariate analysis was carried out at a 95% confidence level.

4. Conclusions

The combination of FTIR and NMR was very efficient in characterisation of structural differences in the β -casein molecule as affected by temperature and pH. Moreover, both methods confirmed similar structural transitions of the β -casein molecule in regard to the applied conditions, indicating greater structural changes taking place as a result of the temperature. A temperature of $4\text{ }^\circ\text{C}$ is critical for β -casein molecules due to lowering of hydrophobicity that results in unfolding and opening up of the native conformers and liberalisation of the monomers from the casein micelle. The restructuring of the β -casein was confirmed by FTIR results implying formation of more random coils at $4\text{ }^\circ\text{C}$ at the expense of the α -helical structure. Moreover, this was intensified by changing the pH

to 7.0. Hence, the side chains of amino acids known as α -helix inducers showed lower detection due to loss of hydrogen bonding resulting in reduction of the α -helix in the β -casein polypeptide chain. The observed structural changes promoted by the temperature change were more intense at high pH, however at pH 5.9 the structural reorganisation was minor. The current findings confirmed that both pH and temperature have a great effect on structure of a β -casein molecule. Moreover, the results can assist in understanding the behavior of β -casein during β -casein production, solubility, processing of milk and milk products, and storage. In addition, FTIR and NMR have proven to successfully detect structural transition in β -casein. The combination of these methods can be further expanded to other proteins and assist in understanding protein behavior during food processing.

Author Contributions: T.M. conceived the study and research question; designed and wrote the original draft, conceptualised, reviewed, and edited the manuscript. D.D. gave critical feedback and analysis, and reviewed and edited the manuscript. T.H. and T.V. provided critical feedback and analysis, secured funding, reviewed and edited the manuscript, and supervised the study. All authors have read and agreed to the published version of the manuscript.

Funding: The first author is funded by a Victoria University Research Training Stipend Scholarship (Grant number—INT010).

Institutional Review Board Statement: Not applicable.

Informed Consent Statement: Not applicable.

Data Availability Statement: Data are contained within the article.

Conflicts of Interest: The authors declare that they have no known competing financial interest or personal relationships that could have appeared to influence the work reported in this paper.

Sample Availability: Samples of the compounds are not available from the authors.

References

- Huppertz, T. Chemistry of the caseins. In *Advanced Dairy Chemistry*; Springer: Boston, MA, USA, 2013; pp. 135–160. [CrossRef]
- Huppertz, T.; Fox, P.; Kelly, A. The caseins: Structure, stability, and functionality. In *Proteins in Food Processing*, 2nd ed.; Yada, R.Y., Ed.; Woodhead Publishing: Sawston, UK, 2018; pp. 49–92. [CrossRef]
- Zhou, Z.; Zhu, M.; Zhang, G.; Hu, X.; Pan, J. Novel insights into the interaction mechanism of 5-hydroxymethyl-2-furaldehyde with β -casein and its effects on the structure and function of β -casein. *LWT* **2021**, *152*, 112360. [CrossRef]
- Farrell, H.; Qi, P.; Wickham, E.; Unruh, J. Secondary structural studies of bovine caseins: Structure and temperature dependence of β -casein phosphopeptide (1-25) as analyzed by circular dichroism, FTIR spectroscopy, and analytical ultracentrifugation. *J. Protein. Chem.* **2002**, *21*, 307–321. [CrossRef]
- Qi, P.X.; Wickham, E.D.; Farrell, H.M. Thermal and Alkaline Denaturation of Bovine β -Casein. *Protein. J.* **2004**, *23*, 389–402. [CrossRef] [PubMed]
- Qi, P.X.; Wickham, E.D.; Piotrowski, E.G.; Fagerquist, C.K.; Farrell, H.M. Implication of C-terminal deletion on the structure and stability of bovine β -casein. *Protein. J.* **2005**, *24*, 431–444. [CrossRef] [PubMed]
- Creamer, L.; Richardson, T.; Parry, D. Secondary structure of bovine α s1- and β -casein in solution. *Arch. Biochem. Biophys.* **1981**, *211*, 689–696. [CrossRef]
- Kumosinski, T.; Brown, E.; Farrell, H., Jr. Three-dimensional molecular modeling of bovine caseins: An energy-minimized β -casein structure. *J. Dairy Sci.* **1993**, *76*, 931–945. [CrossRef]
- Huppertz, T.; Hennebel, J.-B.; Considine, T.; Kelly, A.L.; Fox, P.F. A method for the large-scale isolation of β -casein. *Food Chem.* **2006**, *99*, 45–50. [CrossRef]
- Post, A.; Arnold, B.; Weiss, J.; Hinrichs, J. Effect of temperature and pH on the solubility of caseins: Environmental influences on the dissociation of α S- and β -casein. *J. Dairy Sci.* **2012**, *95*, 1603–1616. [CrossRef]
- Horne, D.S. Casein interactions: Casting light on the black boxes, the structure in dairy products. *Int. Dairy J.* **1998**, *8*, 171–177. [CrossRef]
- Condict, L.; Kaur, J.; Hung, A.; Ashton, J.; Kasapis, S. Combined spectroscopic, molecular docking and quantum mechanics study of β -casein and ferulic acid interactions following UHT-like treatment. *Food Hydrocoll.* **2019**, *89*, 351–359. [CrossRef]
- Farrell Jr, H.; Wickham, E.; Unruh, J.; Qi, P.; Hoagland, P. Secondary structural studies of bovine caseins: Temperature dependence of β -casein structure as analyzed by circular dichroism and FTIR spectroscopy and correlation with micellization. *Food Hydrocoll.* **2001**, *15*, 341–354. [CrossRef]
- Gallagher, W. FTIR analysis of protein structure. *Biochemistry* **1997**, *392*, 662–666.

15. Markoska, T.; Vasiljevic, T.; Huppertz, T. Unravelling Conformational Aspects of Milk Protein Structure—Contributions from Nuclear Magnetic Resonance Studies. *Foods* **2020**, *9*, 1128. [CrossRef] [PubMed]
16. Dukor, R.K.; Keiderling, T.A. Reassessment of the random coil conformation: Vibrational CD study of proline oligopeptides and related polypeptides. *Biopolymers* **1991**, *31*, 1747–1761. [CrossRef]
17. Nishinari, K.; Zhang, H.; Ikeda, S. Hydrocolloid gels of polysaccharides and proteins. *Curr. Opin. Colloid. Interface. Sci.* **2000**, *5*, 195–201. [CrossRef]
18. Shen, Y.; Bax, A. Protein backbone chemical shifts predicted from searching a database for torsion angle and sequence homology. *J. Biomol. NMR* **2007**, *38*, 289–302. [CrossRef]
19. Mulder, F.A.; Filatov, M. NMR chemical shift data and ab initio shielding calculations: Emerging tools for protein structure determination. *Chem. Soc. Rev.* **2010**, *39*, 578–590. [CrossRef]
20. Wang, Y.; Jardetzky, O. Investigation of the neighboring residue effects on protein chemical shifts. *J. Am. Chem. Soc.* **2002**, *124*, 14075–14084. [CrossRef]
21. De Angelis Curtis, S.; Curini, R.; Delfini, M.; Brosio, E.; D’Ascenzo, F.; Bocca, B. Amino acid profile in the ripening of Grana Padano cheese: A NMR study. *Food Chem.* **2000**, *71*, 495–502. [CrossRef]
22. Vaia, B.; Smiddy, M.A.; Kelly, A.L.; Huppertz, T. Solvent-mediated disruption of bovine casein micelles at alkaline pH. *J. Agric. Food. Chem.* **2006**, *54*, 8288–8293. [CrossRef]
23. Daniloski, D.; McCarthy, N.A.; Markoska, T.; Auld, M.J.; Vasiljevic, T. Conformational and physicochemical characteristics of bovine skim milk obtained from cows with different genetic variants of β -casein. *Food Hydrocoll.* **2022**, *124*, 107186. [CrossRef]
24. Markoska, T.; Huppertz, T.; Grewal, M.K.; Vasiljevic, T. FTIR analysis of physicochemical changes in raw skim milk upon concentration. *LWT* **2019**, *102*, 64–70. [CrossRef]

Article

Effects of Variety and Growing Location on Physicochemical Properties of Starch from Sweet Potato Root Tuber

Laiquan Shi ^{1,2,†}, Yibo Li ^{1,2,†}, Lingshang Lin ^{1,2}, Xiaofeng Bian ³ and Cunxu Wei ^{1,2,*} 

¹ Key Laboratory of Crop Genetics and Physiology of Jiangsu Province/Jiangsu Key Laboratory of Crop Genomics and Molecular Breeding, Yangzhou University, Yangzhou 225009, China; MZ120201523@yzu.edu.cn (L.S.); DX120180133@yzu.edu.cn (Y.L.); 007520@yzu.edu.cn (L.L.)

² Co-Innovation Center for Modern Production Technology of Grain Crops of Jiangsu Province/Joint International Research Laboratory of Agriculture & Agri-Product Safety of the Ministry of Education, Yangzhou University, Yangzhou 225009, China

³ Institute of Food Crops, Jiangsu Academy of Agricultural Sciences, Nanjing 210014, China; bianxiaofeng2@163.com

* Correspondence: cxwei@yzu.edu.cn

† L.S. and Y.L. contributed equally to this work.

Abstract: Three sweet potato varieties with purple-, yellow-, and white-fleshed root tubers were planted in four growing locations. Starches were isolated from their root tubers, their physicochemical properties (size, iodine absorption, amylose content, crystalline structure, ordered degree, lamellar thickness, swelling power, water solubility, and pasting, thermal and digestion properties) were determined to investigate the effects of variety and growing location on starch properties in sweet potato. The results showed that granule size (D[4,3]) ranged from 12.1 to 18.2 μm , the iodine absorption parameters varied from 0.260 to 0.361 for OD620, from 0.243 to 0.326 for OD680 and from 1.128 to 1.252 for OD620/550, and amylose content varied from 16.4% to 21.2% among starches from three varieties and four growing locations. Starches exhibited C-type X-ray diffraction patterns, and had ordered degrees from 0.634 to 0.726 and lamellar thicknesses from 9.72 to 10.21 nm. Starches had significantly different swelling powers, water solubilities, pasting viscosities, and thermal properties. Native starches had rapidly digestible starch (RDS) from 2.2% to 10.9% and resistant starch (RS) from 58.2% to 89.1%, and gelatinized starches had RDS from 70.5% to 81.4% and RS from 10.8% to 23.3%. Two-way ANOVA analysis showed that starch physicochemical properties were affected significantly by variety, growing location, and their interaction in sweet potato.

Citation: Shi, L.; Li, Y.; Lin, L.; Bian, X.; Wei, C. Effects of Variety and Growing Location on Physicochemical Properties of Starch from Sweet Potato Root Tuber. *Molecules* **2021**, *26*, 7137. <https://doi.org/10.3390/molecules26237137>

Academic Editor: Mirella Nardini

Received: 3 November 2021

Accepted: 23 November 2021

Published: 25 November 2021

Publisher's Note: MDPI stays neutral with regard to jurisdictional claims in published maps and institutional affiliations.



Copyright: © 2021 by the authors. Licensee MDPI, Basel, Switzerland. This article is an open access article distributed under the terms and conditions of the Creative Commons Attribution (CC BY) license (<https://creativecommons.org/licenses/by/4.0/>).

Keywords: sweet potato; variety; growing location; starch; physicochemical properties

1. Introduction

Sweet potato (*Ipomoea batatas*), an essential root tuber starchy crop, is widely cultivated in over 100 countries. There are over 90 million tonnes in annual production [1]. The root tuber contains about 50–80% starch in dry basis (d.b.) [2,3]. Sweet potato starch is widely used to make conventional noodle, vermicelli, thickening agent, and syrup in processed foods, and can also produce film, ethanol, citric acid, lactic acid, and other chemicals in non-food industries [4,5]. The physicochemical properties of starch determine its utilizations in food and nonfood industries [3]. Therefore, the research of sweet potato starch has been getting great attentions.

Due to artificial selection, natural hybrids, and mutations, there are hundreds of varieties or lines of sweet potato [4]. Their root tubers have different flesh colors [2,6]. Starches from different varieties have been investigated for their physicochemical properties and utilizations in sweet potato [2,3,7–9]. Though starch content in root tuber exhibits significant differences among different colored varieties, starch properties are not affected by the color of root tuber [2,8].

Effects of plant growing condition on starch properties have been reported in sweet potato [10–13]. Crystalline structure of starch significantly changes when sweet potato is planted in soils with different temperatures. A-type starch forms and accumulates in root tuber grown in soil with high temperature, and B-type crystallinity gradually does in root tuber with the decrease of soil temperature [11]. Recently, Duan et al. [10] planted one sweet potato variety in soils with different treatments of nitrogen fertilizer, and found that nitrogen treatment can change starch physicochemical properties. However, Noda et al. [13] found that starch properties do not significantly change in four sweet potato varieties grown in different levels of fertilizer. Guo et al. [12] planted three white, three yellow, and three purple fleshed varieties in soils with three treatments of nitrogen fertilizer, and found that nitrogen treatments have different effects on starch properties among different varieties, indicating that different genotypes have different responses to nitrogen fertilizer treatment.

In recent years, the effects of genotype and growing environment on starch characteristics have been studied in rice [14,15], wheat [16], potato [17,18], and cassava [19]. The effects exhibit some differences among different references or crops. For examples, Li and Liu [14] reported that components and chain-length distribution of rice starch are affected significantly by variety, growing location, and their interaction, but Sar et al. [15] found that the structures of amylose and amylopectin are affected only by varieties but have no significant relationship with growing location and the interaction of variety and growing location. Pelpolage et al. [18] reported that thermal properties and pasting peak, breakdown and final viscosities of potato starch are significantly affected by variety, growing location, and their interaction, but Ahmed et al. [17] found that gelatinization conclusion temperature, gelatinization enthalpy, and pasting final viscosity of potato starch are not affected by growing location. In addition, Nhan and Copeland [16] reported that thermal and pasting properties of wheat starch are affected significantly by variety and growing location. For cassava starch, some physicochemical properties are affected significantly by variety, or growing location, or both variety and growing location, or the interaction of variety and growing location [19]. Sweet potato is extensively grown in the tropical and subtropical areas [6]. However, the effects of growing location on starch characteristics are unclear in sweet potato, restricting the utilization of sweet potato variety in different regions.

Therefore, the objective of this work was to study the effect of sweet potato variety and growing location on the changes of starch properties. To achieve this objective, three sweet potato varieties with purple-, yellow-, and white-fleshed root tubers planted in four different growing locations were collected and analyzed their physicochemical properties (size, iodine absorption, amylose content, crystalline structure, ordered degree, lamellar thickness, swelling power, water solubility, and pasting, thermal and digestion properties).

2. Results and Discussion

2.1. Effects of Variety and Growing Location on Starch Size

Starches from three varieties in four growing locations followed similar size distribution patterns (Figure 1). Though there were two granule populations about from 0.8 to 3 μm and from 6 to 40 μm , the small-sized granules had very low weight percentage. Similar phenomenon has been reported in previous papers [2,9]. In the present research, the volume-weighted mean diameter ($D[4,3]$) was used to reflect the granule size (Table 1). Among four growing locations, granule size varied from 13.33 μm (YZ) to 18.22 μm (RG), from 13.53 μm (YZ) to 15.39 μm (RG), and from 12.11 μm (YZ) to 14.19 μm (RG) for Ningzishu 1, Sushu 16, and Sushu 28, respectively. Three sweet potato varieties all exhibited the largest starch size in growing location of RG and the smallest starch size in growing location of YZ. Two-way ANOVA analysis showed that starch size was significantly affected by variety, growing location, and their interaction ($p < 0.001$) (Table 1). Abegunde et al. [20] found that starch size is affected by plant physiology except variety and growing condition in sweet potato. Similar conclusion is also given in potato [18]. Guo et al. [2] reported that starches have significantly different granule sizes among different colored sweet potato

varieties grown in the same environment, and the starch size is determined mainly by genotype but has no relationship with fleshed color.

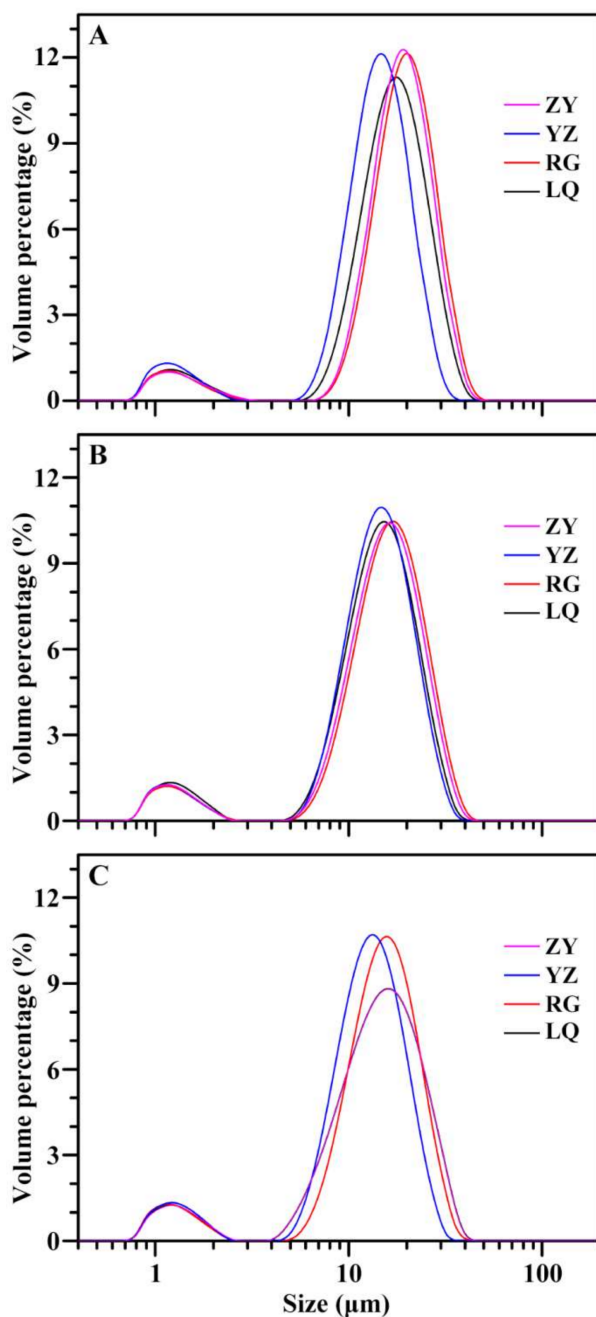


Figure 1. Granule size distributions of starches from root tubers of Ningzishu 1 (A), Sushu 16 (B), and Sushu 28 (C) in growing locations of Linquan (LQ), Rugao (RG), Yangzhou (YZ), and Zunyi (ZY).

2.2. Effects of Variety and Growing Location on Starch–Iodine Absorption Parameters

The starch–iodine absorption spectrum is presented in Figure 2, and spectrum parameters including OD620, OD680, OD620/550 and the maximum absorption wavelength (λ_{max}) are presented in Table 1. The OD620 indicates the iodine-binding of amylose and amylopectin long branch-chains, and the OD680 (also called blue value) reflects the iodine-binding capacity of starch [21]. The OD620 of starch–iodine complex ranged from 0.275 (YZ) to 0.361 (ZY), from 0.322 (YZ) to 0.353 (ZY), and from 0.260 (YZ) to 0.347 (ZY) for Ningzishu 1, Sushu 16, and Sushu 28, respectively. The OD680 ranged from 0.257

(YZ) to 0.321 (ZY), from 0.294 (YZ) to 0.326 (ZY), and from 0.243 (YZ) to 0.316 (ZY) for Ningzishu 1, Sushu 16, and Sushu 28, respectively, indicating that sweet potato grown in YZ and ZY had the lowest and the highest starch–iodine binding ability, respectively. The OD620/550, absorption ratio of OD620 and OD550, is an index reflecting the relative proportion of long molecule chains in starch [21]. The OD620/550 varied from 1.128 (ZY) to 1.232 (YZ), from 1.193 (RG) to 1.235 (ZY), and from 1.175 (LQ) to 1.252 (YZ) for Ningzishu 1, Sushu 16, and Sushu 28, respectively. The λ_{\max} among four growing locations varied from 606.1 nm (RG) to 625.6 nm (YZ), from 609.2 nm (YZ) to 613.9 nm (LQ), and from 606.4 nm (ZY) to 629.0 nm (YZ) for Ningzishu 1, Sushu 16, and Sushu 28, respectively. Two-way ANOVA analysis showed that starch–iodine absorption parameters of OD620, OD680, OD620/550 and λ_{\max} were significantly affected by variety, growing location, and their interaction ($p < 0.001$) (Table 1). Both amylose/amylopectin ratio and amylopectin structure determine the starch–iodine absorption parameters [22]. Starch is synthesized by some starch synthesis-related enzymes. The expression regulation of these enzymes is influenced by genotype and growing condition of plant, especially for environment temperature [23–25].

Table 1. Effects of variety and growing location on granule size, iodine absorption parameters, and amylose content of starch from sweet potato root tuber.

Variety	Location	D[4,3] (μm)	Iodine Absorption Parameters				AC (%)
			OD620	OD680	OD620/550	λ_{\max} (nm)	
Ningzishu 1	LQ	16.06 \pm 0.01iB	0.332 \pm 0.010bcB	0.297 \pm 0.005bB	1.145 \pm 0.017abA	606.5 \pm 0.5aA	16.4 \pm 0.9aA
	RG	18.22 \pm 0.02kD	0.339 \pm 0.010bcdB	0.302 \pm 0.006bcB	1.156 \pm 0.033abcA	606.1 \pm 0.2aA	16.6 \pm 0.3aA
	YZ	13.33 \pm 0.01bA	0.275 \pm 0.002aA	0.257 \pm 0.005aA	1.232 \pm 0.021efB	625.6 \pm 2.4dB	16.7 \pm 0.3aA
	ZY	17.50 \pm 0.02jC	0.361 \pm 0.005eC	0.321 \pm 0.004deC	1.128 \pm 0.021aA	606.4 \pm 0.4aA	17.7 \pm 0.4abA
Sushu 16	LQ	13.79 \pm 0.01dB	0.339 \pm 0.002bcdB	0.308 \pm 0.004bcdAB	1.196 \pm 0.006cdeA	613.9 \pm 2.6cB	18.4 \pm 0.1bcA
	RG	15.39 \pm 0.01hD	0.339 \pm 0.010bcdB	0.308 \pm 0.011bcdAB	1.193 \pm 0.021bcdeA	609.3 \pm 0.8abA	19.5 \pm 0.5cdeA
	YZ	13.53 \pm 0.02cA	0.322 \pm 0.005bA	0.294 \pm 0.007bA	1.208 \pm 0.006defA	609.2 \pm 2.0abA	19.0 \pm 0.4bcdA
	ZY	14.75 \pm 0.03gC	0.353 \pm 0.003deB	0.326 \pm 0.007eB	1.235 \pm 0.006efB	610.7 \pm 0.4bcAB	21.2 \pm 0.2fB
Sushu 28	LQ	14.14 \pm 0.01eB	0.334 \pm 0.010bcdB	0.302 \pm 0.010bcB	1.175 \pm 0.015abcdA	611.1 \pm 0.6bcB	19.8 \pm 0.6cdefAB
	RG	14.19 \pm 0.01fC	0.333 \pm 0.007bcB	0.298 \pm 0.006bB	1.178 \pm 0.010bcdA	606.8 \pm 1.2aA	21.1 \pm 0.3efB
	YZ	12.11 \pm 0.01aA	0.260 \pm 0.006aA	0.243 \pm 0.004aA	1.252 \pm 0.026fB	629.0 \pm 2.4eC	18.3 \pm 0.6bcA
	ZY	14.13 \pm 0.02eB	0.347 \pm 0.003cdeB	0.316 \pm 0.003cdeC	1.191 \pm 0.016bcdeA	606.4 \pm 0.4aA	20.3 \pm 0.3defB
F-value	Variety (2)	94054.64 ***	25.00 ***	29.17 ***	18.10 ***	10.95 ***	109.55 ***
	Location (3)	63443.40 ***	161.64 ***	120.35 ***	19.68 ***	180.67 ***	19.14 ***
	Variety \times Location (6)	9144.67 ***	15.41 ***	9.15 ***	7.02 ***	61.03 ***	5.93 **

D[4,3]: volume-weighted mean diameter; OD620 and OD680: absorption value of starch–iodine complex at 620 and 680 nm, respectively; OD620/550: ratio of absorption value of starch–iodine complex at 620 and 550 nm; λ_{\max} : maximum absorption wavelength of starch–iodine complex; AC: amylose content. Data are means \pm standard deviations, $n = 3$. Values with different lowercase letters in the same column are significantly different ($p < 0.05$), and values with different capital letters in the same column and the same variety are significantly different ($p < 0.05$). The number in the parentheses is the freedom degree, and ** and *** indicates statistically significant effect at 0.01 and 0.001 level, respectively.

2.3. Effects of Variety and Growing Location on Amylose Content of Starch

The AC determines starch physicochemical properties, and can be measured with iodine colorimetry and concanavalin A precipitation [21]. The iodine colorimetry is often used to evaluate the apparent amylose content due to that iodine can bind amylopectin long branch-chains to overestimate AC. The concanavalin A can specifically bind with amylopectin and form precipitation. The ratio of amylose to both amylose and amylopectin measured by concanavalin A precipitation is usually called true amylose content due to being not influenced by starch purity and amylopectin long branch-chains [21]. In this study, the AC was measured using concanavalin A precipitation method (Table 1). The AC ranged from 16.4% (LQ) to 17.7% (ZY), from 18.4% (LQ) to 21.2% (ZY), and from 18.3% (YZ) to 21.1% (RG) for Ningzishu 1, Sushu 16, and Sushu 28, respectively. Two-way ANOVA analysis showed that AC was significantly affected by variety, growing location, and their interaction (Table 1). Some researchers reported that both genotype and environment contribute significantly to the variability in AC in wheat [26] and rice [14]. Amylose is synthesized by granule-bound starch synthase I (GBSSI) encoded by *Waxy* (*Wx*) in plant

storage tissue. Many *Wx* alleles have been reported in cereal crops. They are responsible for significantly different expressions and activities of GBSSI, leading to starches with different ACs among different varieties [27]. Therefore, it is easy to understand that amylose is determined by genotype. Some references reported that AC has no significant effect from the growing location, and is influenced only by genotype in potato [18], cassava [19], and rice [15]. However, more references reported that *Wx* expression and GBSSI activity are influenced by environment temperature. The low temperature increases amylose synthesis, and high temperature decreases amylose synthesis [23,24]. In the present study, four growing locations had different temperatures during sweet potato starch development (Figure 3). Therefore, AC is affected by variety, growing location, and their interaction in sweet potato.

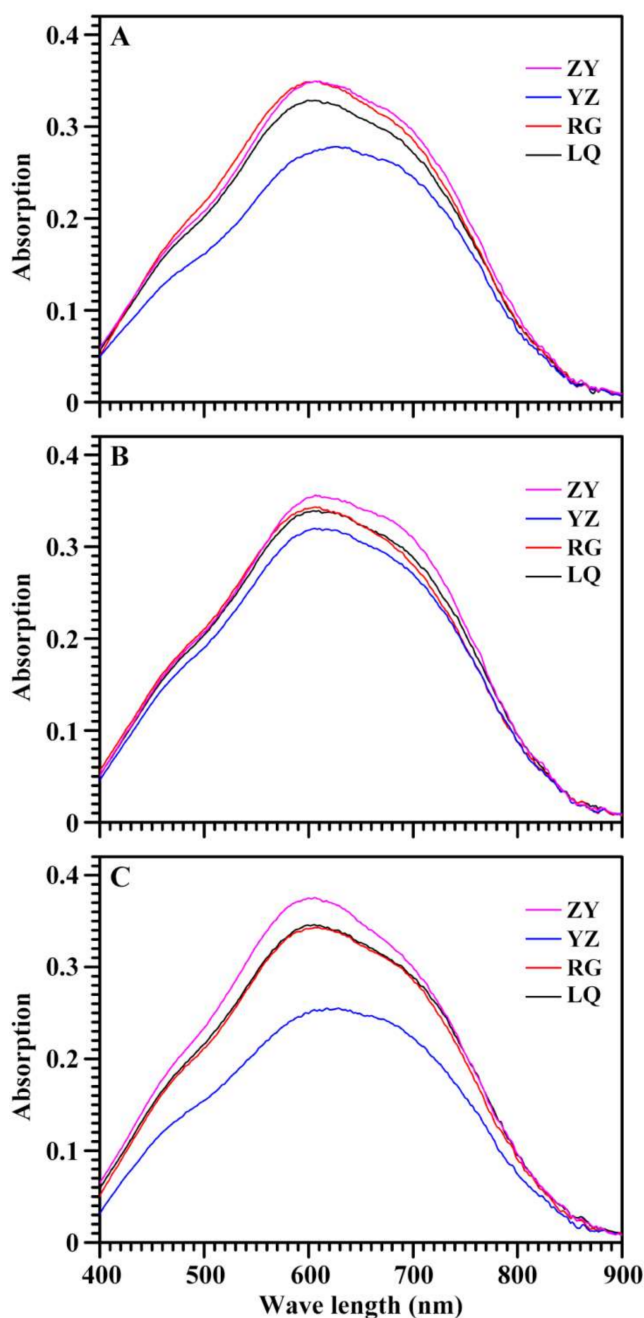


Figure 2. Iodine absorption spectra of starches from root tubers of Ningzishu 1 (A), Sushu 16 (B), and Sushu 28 (C) in growing locations of Linquan (LQ), Rugao (RG), Yangzhou (YZ), and Zunyi (ZY).

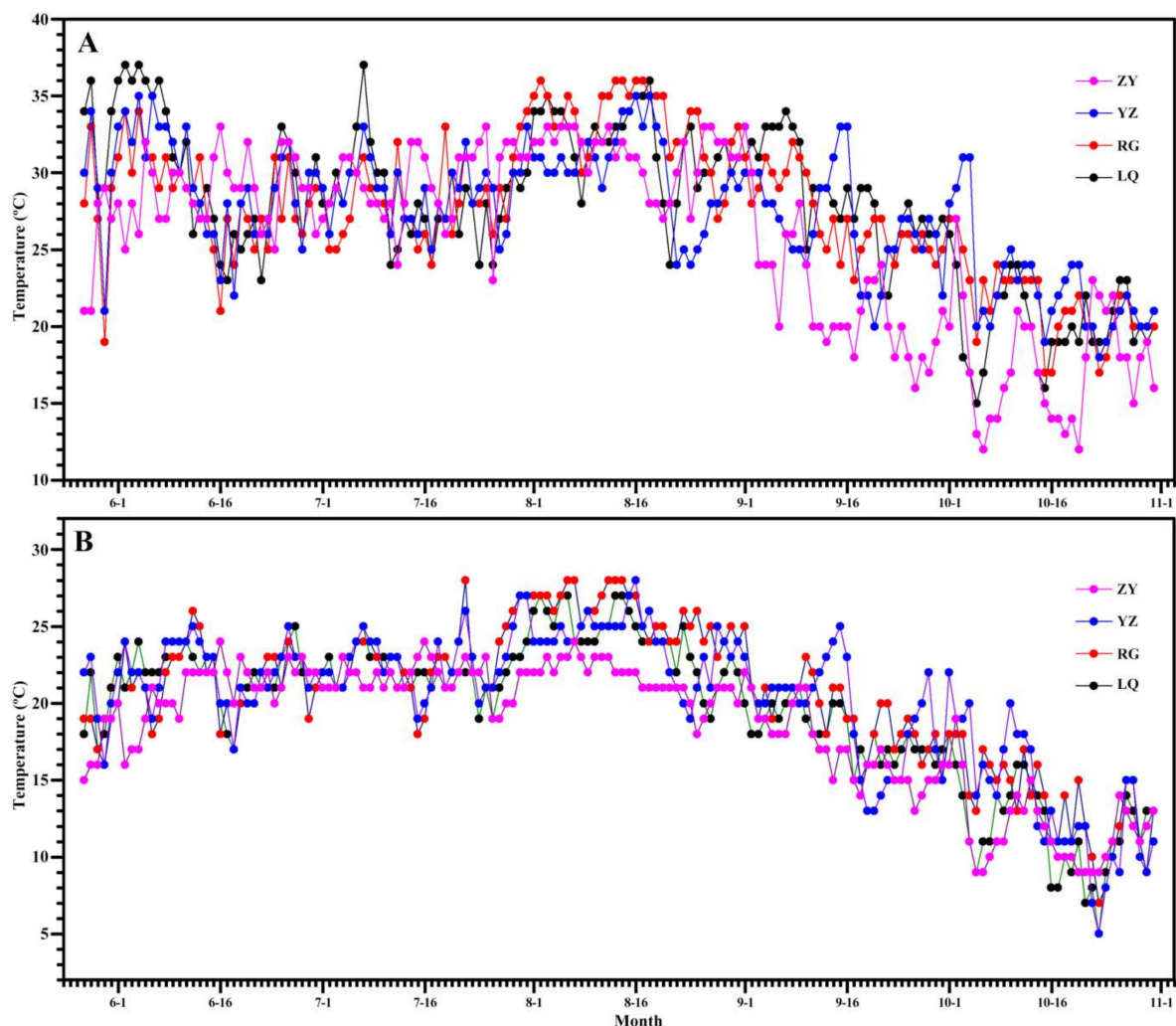


Figure 3. High temperature (A) and low temperature (B) of every day during growth stage of sweet potato in growing locations of Linquan (LQ), Rugao (RG), Yangzhou (YZ), and Zunyi (ZY).

2.4. Effects of Variety and Growing Location on Crystalline Structure of Starch

The XRD patterns of starches from three sweet potato varieties and four growing locations are shown in Figure 4. Amylopectin in plants can form A- and B-type crystallinities. Native starches from botany sources are usually divided into A-, B-, and C-type according to their crystallinity types [28]. A- and B-type starch contains only A- and B-type crystallinity, respectively, but C-type starch contains both A- and B-type crystallinities. According to the proportion of A- and B-type crystallinity from high to low, C-type starch is usually divided into C_A -, C_C -, and C_B -type [28]. Though XRD patterns of starches from Ningzishu 1, Sushu 16, and Sushu 28 grown in LQ, RG, YZ, and ZY all exhibited C-type, the intensity of shoulder peak at 2θ 18° , a characteristic peak of A-type crystallinity, was significantly different, exhibiting a different proportion of A- and B-type crystallinity in starch (Figure 4). A-, C_A -, C_C -, and C_B -type starches have been found in some sweet potato varieties [9,29,30]. Genkina et al. [11] found that A-type starch forms and accumulates in sweet potato root tuber grown in soil of high temperature (over 33°C), and C_C -type starch exists in root tuber grown in soil of low temperature about 15°C . Guo et al. [31] found that A-, B-, and C-type starch granules can simultaneously exist in root tuber of sweet potato. Therefore, variety and environment temperature affect starch crystalline structure of sweet potato. However, RC of starch was found to have no significant relationship with sweet potato variety and growing location ($p > 0.05$) (Table 2).

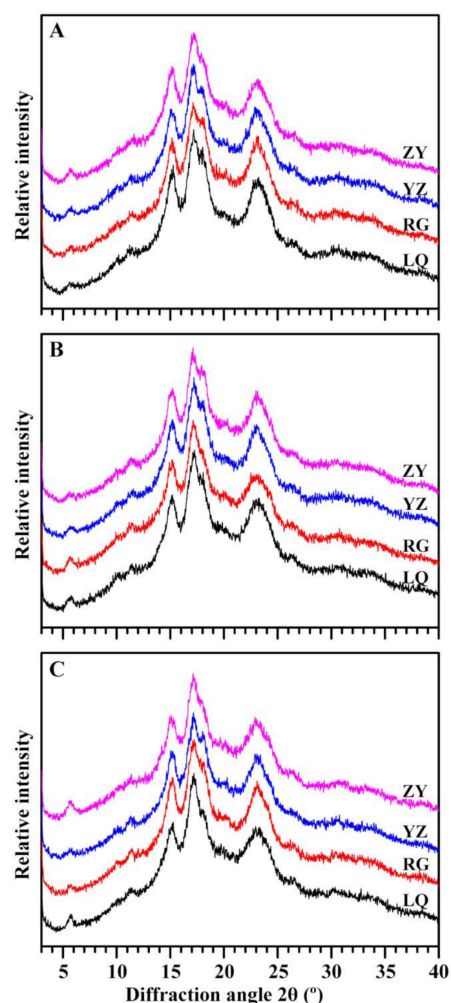


Figure 4. XRD spectra of starches from root tubers of Ningzishu 1 (A), Sushu 16 (B), and Sushu 28 (C) in growing locations of Linquan (LQ), Rugao (RG), Yangzhou (YZ), and Zunyi (ZY).

Table 2. Effects of variety and growing location on relative crystallinity, ordered structure, and lamellar structure parameters of starch from sweet potato root tuber.

Variety	Location	RC (%)	IR Ratio		Lamellar Parameters	
			1045/1022 (cm ⁻¹)	1022/995 (cm ⁻¹)	PI (a.u.)	D (nm)
Ningzishu 1	LQ	26.2 ± 0.9aA	0.650 ± 0.002abA	0.974 ± 0.005efC	382.3 ± 2.0cdB	9.72 ± 0.00aA
	RG	25.0 ± 1.3aA	0.699 ± 0.013deB	0.983 ± 0.015fC	418.6 ± 0.6dC	9.80 ± 0.01abcBC
	YZ	25.3 ± 0.7aA	0.709 ± 0.006deB	0.896 ± 0.003aA	357.1 ± 3.0bcA	9.78 ± 0.00abcB
	ZY	24.5 ± 0.5aA	0.676 ± 0.012bcdAB	0.934 ± 0.005bcdB	384.8 ± 4.6cdB	9.82 ± 0.02abcC
Sushu 16	LQ	24.9 ± 1.9aA	0.634 ± 0.001aA	1.103 ± 0.009gB	331.2 ± 1.5bC	9.86 ± 0.03bcA
	RG	22.8 ± 1.7aA	0.659 ± 0.004abcA	0.954 ± 0.010deA	257.7 ± 7.3aA	10.15 ± 0.02eC
	YZ	24.3 ± 0.1aA	0.702 ± 0.012deB	0.945 ± 0.002cdA	289.2 ± 0.8aB	10.21 ± 0.01eC
	ZY	24.9 ± 0.3aA	0.697 ± 0.014deB	0.922 ± 0.014bcA	332.4 ± 4.7bC	10.02 ± 0.01dB
Sushu 28	LQ	23.7 ± 0.4aA	0.678 ± 0.007bcdA	0.977 ± 0.005efC	275.5 ± 8.3aA	9.87 ± 0.08bcA
	RG	26.2 ± 0.8aA	0.695 ± 0.012cdeA	0.925 ± 0.002bcB	417.8 ± 7.2dB	9.76 ± 0.01abA
	YZ	24.7 ± 0.8aA	0.726 ± 0.019eA	0.931 ± 0.003bcdB	332.0 ± 35.1bA	9.88 ± 0.00cA
	ZY	23.4 ± 1.3aA	0.703 ± 0.012deA	0.911 ± 0.003abA	283.2 ± 1.6aA	9.89 ± 0.07cA
F-value	Variety (2)	2.15	13.42 **	73.34 ***	119.16 ***	163.16 ***
	Location (3)	0.46	30.45 ***	197.87 ***	15.42 ***	18.20 ***
	Variety × Location (6)	2.69	3.33 *	52.74 ***	43.11 ***	18.96 ***

RC: relative crystallinity; 1045/1022: ratio of peak intensity at 1045 and 1022 cm⁻¹; 1022/995: ratio of peak intensity at 1022 and 995 cm⁻¹; PI: lamellar peak intensity; D: lamellar thickness. Data are means ± standard deviations, *n* = 3. Values with different lowercase letters in the same column are significantly different (*p* < 0.05), and values with different capital letters in the same column and the same variety are significantly different (*p* < 0.05). The number in the parentheses is the degree of freedom, and *, ** and *** indicates statistically significant effect at the 0.05, 0.01 and 0.001 level, respectively.

2.5. Effects of Variety and Growing Location on Ordered Structure of Starch

The deconvolution FTIR spectra of starches from different varieties and growing locations are shown in Figure 5. The absorption bands at 1045 and 1022 cm^{-1} are associated with crystalline and amorphous regions in starch, respectively [32]. The intensity ratio of band at 1045 to 1022 cm^{-1} ($1045/1022 \text{ cm}^{-1}$) is often used as an index reflecting the ordered degree, and that at 1022 to 995 cm^{-1} ($1022/995 \text{ cm}^{-1}$) indicates the proportion of amorphous to ordered carbohydrate structure in starch [33]. The $1045/1022 \text{ cm}^{-1}$ ranged from 0.650 (LQ) to 0.709 (YZ), from 0.634 (LQ) to 0.702 (YZ), and from 0.678 (LQ) to 0.726 (YZ) for Ningzishu 1, Sushu 16, and Sushu 28, respectively. The $1022/995 \text{ cm}^{-1}$ varied from 0.896 (YZ) to 0.983 (RG), from 0.922 (ZY) to 1.103 (LQ), and from 0.911 (ZY) to 0.977 (LQ) for Ningzishu 1, Sushu 16, and Sushu 28, respectively. Two-way ANOVA analysis showed that ordered structure of sweet potato starch was significantly affected by variety, growing location, and their interaction (Table 2).

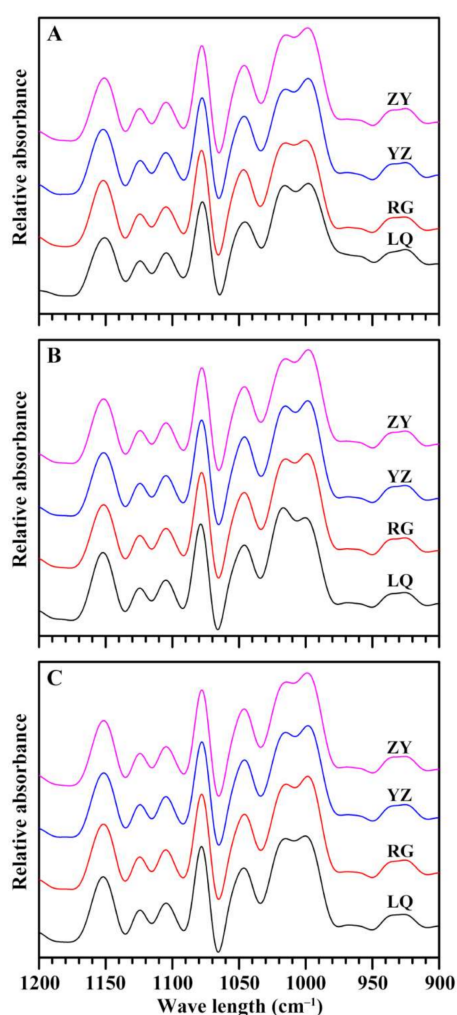


Figure 5. FTIR spectra of starches from root tubers of Ningzishu 1 (A), Sushu 16 (B), and Sushu 28 (C) in growing locations of Linquan (LQ), Rugao (RG), Yangzhou (YZ) and Zunyi (ZY).

2.6. Effects of Variety and Growing Location on Lamellar Structure of Starch

The SAXS spectra of starches from different sweet potato varieties grown in different locations are presented in Figure 6. Their intensities at 0.2 \AA^{-1} were normalized, resulting in comparable peak intensities among different samples [34]. The peak intensity of SAXS profile is determined by the ordered structure in semicrystalline regions, and lamellar distance reflects the thickness of repeated crystalline and amorphous lamellae [35]. The lamellar structure is formed by amylopectin branch-chains [36]. The peak intensity ranged

from 357.1 (YZ) to 418.6 (RG), from 257.7 (RG) to 332.4 (ZY), and from 275.5 (LQ) to 417.8 (RG) for Ningzishu 1, Sushu 16, and Sushu 28, respectively. The lamellar thickness ranged from 9.72 nm (LQ) to 9.82 nm (ZY), from 9.86 nm (LQ) to 10.21 nm (YZ), and from 9.76 nm (RG) to 9.89 nm (ZY) for Ningzishu 1, Sushu 16, and Sushu 28, respectively. Two-way ANOVA analysis exhibited that lamellar peak intensity and thickness of sweet potato starch were significantly affected by variety, growing location, and their interaction (Table 2).

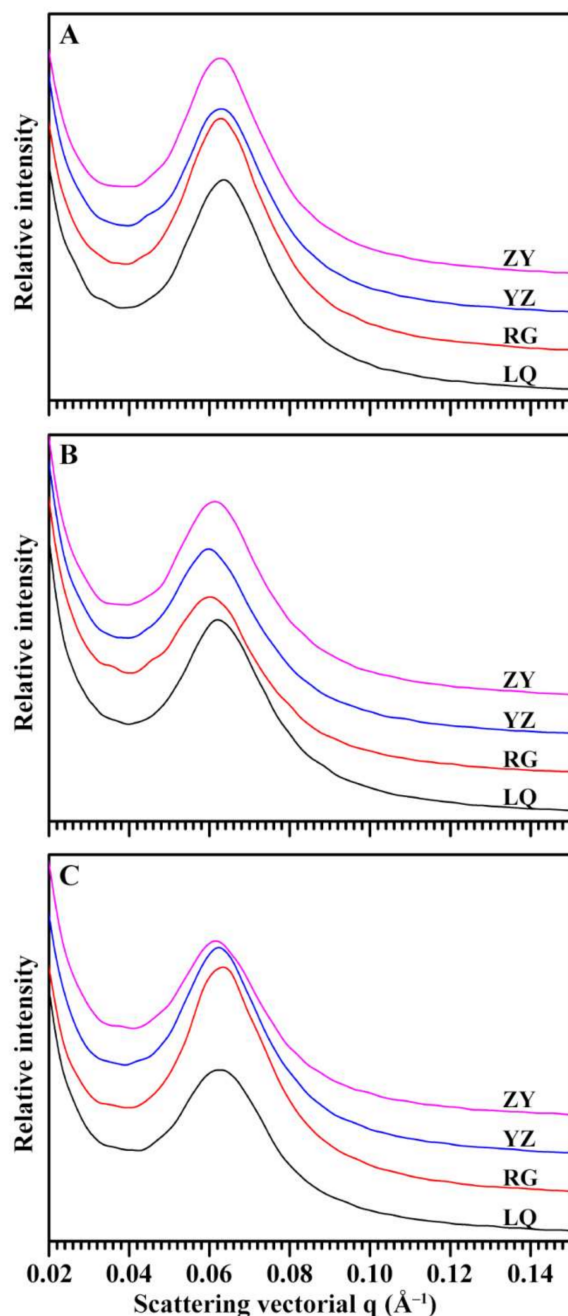


Figure 6. SAXS profiles of starches from root tubers of Ningzishu 1 (A), Sushu 16 (B), and Sushu 28 (C) in growing locations of Linquan (LQ), Rugao (RG), Yangzhou (YZ) and Zunyi (ZY).

2.7. Effects of Variety and Growing Location on Pasting Properties of Starch

RVA can heat and cool an aqueous suspension of starch under constant shear and simultaneously measures the viscosity, producing a RVA curve of viscosity change as a function of temperature and time [37]. RVA curve is usually converted into RVA parameters including pasting temperature (P_{Temp}), peak time (P_{Time}), and peak (PV), hot (HV), break-

down (BV), final (FV), and setback viscosity (SV). These parameters are used as pasting properties of starch, which reflect eating, cooking, and processing qualities of starch and are also important parameters to design starch blend products as well as new products based on starch [19,37]. RVA curves of sweet potato starches from different varieties grown in different locations are shown in Figure 7. PV refers to the maximum viscosity during heating of starch paste, reflecting the capability of binding water and the granular swelling of starch [37]. PV ranged from 4171 mPa s (RG) to 4635 mPa s (LQ), from 4102 mPa s (YZ) to 4656 mPa s (LQ), and from 3918 mPa s (RG) to 4929 mPa s (LQ) for Ningzishu 1, Sushu 16, and Sushu 28, respectively (Table 3). The swollen granules disrupt during heating, leading to the decrease of viscosity. The HV is the lowest viscosity of heating starch paste, and is affected by granule swelling, amylose leaching, and amylose–lipid complex [38]. HV ranged from 2171 mPa s (ZY) to 2788 mPa s (YZ), from 2113 mPa s (YZ) to 2363 mPa s (LQ), and from 2274 mPa s (ZY) to 2846 mPa s (YZ) for Ningzishu 1, Sushu 16, and Sushu 28, respectively (Table 3). BV is the different value between PV and HV, reflecting paste resistance to heat and shear [20]. BV ranged from 1504 mPa s (YZ) to 2102 mPa s (ZY), from 1839 mPa s (RG) to 2293 mPa s (LQ), and from 1479 mPa s (RG) to 2591 mPa s (LQ) for Ningzishu 1, Sushu 16, and Sushu 28, respectively (Table 3). FV is the viscosity of starch paste after cooling, and indicates the stability to cooled starch paste or gel [2]. FV ranged from 2802 mPa s (ZY) to 3471 mPa s (YZ), from 2769 mPa s (YZ) to 2947 mPa s (ZY), and from 2920 mPa s (ZY) to 3579 mPa s (YZ) for Ningzishu 1, Sushu 16, and Sushu 28, respectively (Table 3). SB is the different viscosity between FV and HV, reflecting the tendency of starch pastes to retrograde [20]. SV ranged from 541 mPa s (LQ) to 682 mPa s (YZ), from 562 mPa s (LQ) to 769 mPa s (ZY), and from 587 mPa s (RG) to 733 mPa s (YZ) for Ningzishu 1, Sushu 16, and Sushu 28, respectively. P_{Temp} reflects the energy cost required during cooking, and ranged from 73.08 °C (YZ) to 78.98 °C (ZY), from 71.68 °C (LQ) to 76.05 °C (ZY), and from 70.07 °C (YZ) to 76.88 °C (RG) for Ningzishu 1, Sushu 16, and Sushu 28, respectively (Table 3). P_{Time} is the time of PV, and can reflect starch swelling with high swelling starch having low P_{Time} [20]. P_{Time} ranged from 4.40 min (LQ) to 4.62 min (YZ), from 4.22 min (ZY) to 4.60 min (RG), and from 4.07 min (ZY) to 4.51 (RG) for Ningzishu 1, Sushu 16, and Sushu 28, respectively. Two-way ANOVA analysis showed that the RVA parameters were significantly affected by variety, growing location, and their interaction (Table 3). Similar phenomenon exists in potato starch [18]. However, Ahmed et al. [17] reported that no significant effects of environment are observed on HV, FV, SV and P_{Temp} of potato starch. Nhan and Copeland [16] reported that PV, HV, and FV of wheat starch are affected by genotype, growing location, and their interaction, but BV, SV, and P_{Temp} are not affected by genotype. Tappiban et al. [19] reported that BV of cassava starch is affected by genotype, environment, and their interaction; PV is affected by genotype and environment; P_{Temp} and P_{Time} are affected by genotype; HV, FV, and SV are not affected by genotype, environment, and their interaction.

2.8. Effects of Variety and Growing Location on Swelling Power and Water Solubility of Starch

Swelling powers and water solubilities of sweet potato starches at 95 °C are presented in Table 4. Swelling power ranged from 29.9 g/g (RG) to 30.9 g/g (LQ), from 29.1 g/g (ZY) to 32.6 g/g (LQ), and from 26.7 g/g (YZ) to 29.8 g/g (ZY) for Ningzishu 1, Sushu 16, and Sushu 28, respectively. Water solubility ranged from 12.5% (RG) to 14.4% (ZY), from 14.2% (YZ) to 17.9% (ZY), and from 12.8% (YZ) to 15.3% (ZY) for Ningzishu 1, Sushu 16, and Sushu 28, respectively. The results are comparable with previous reports that swelling powers range from 24.5 to 32.7 g/g and water solubilities range from 12.1% to 24.1% among starches from 44 sweet potato varieties [39]. Two-way ANOVA analysis indicated that swelling power and water solubility of sweet potato starch were significantly affected by variety, growing location, and their interaction (Table 4). Pelpolage et al. [18] reported that swelling power of potato starch is not influenced by growing location, and water solubility is not affected by variety.

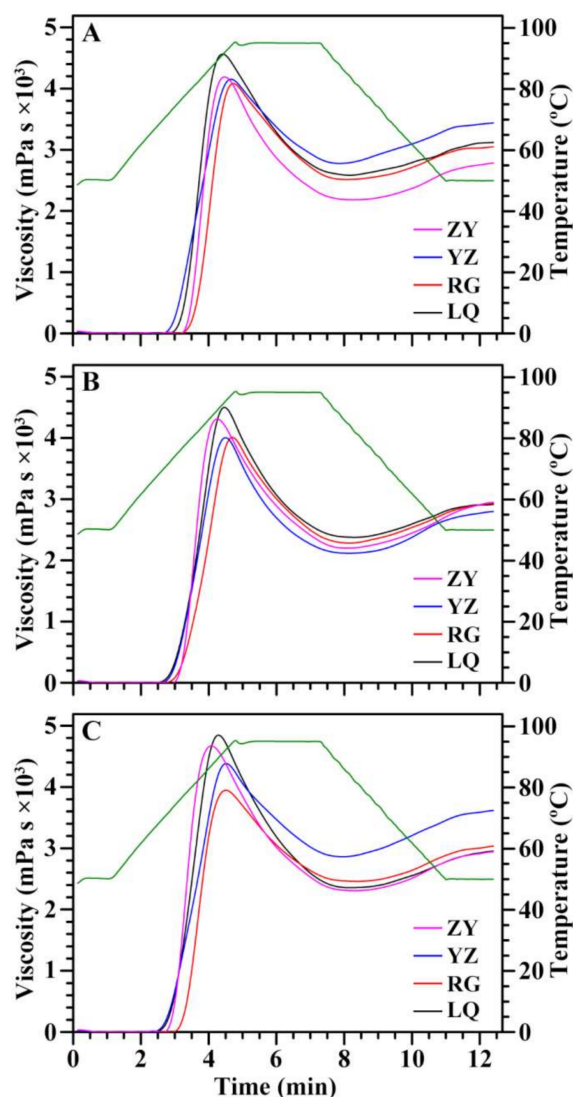


Figure 7. RVA profiles of starches from root tubers of Ningzishu 1 (A), Sushu 16 (B), and Sushu 28 (C) in growing locations of Linqan (LQ), Rugao (RG), Yangzhou (YZ), and Zunyi (ZY).

Table 3. Effects of variety and growing location on pasting properties of starch from sweet potato root tuber.

Variety	Location	PV (mPa s)	HV (mPa s)	BV (mPa s)	FV (mPa s)	SV (mPa s)	P _{Temp} (°C)	P _{Time} (min)
Ningzishu 1	LQ	4635 ± 29 gC	2546 ± 27eC	2090 ± 29eC	3087 ± 51cB	541 ± 25aA	75.47 ± 0.45eB	4.40 ± 0.07cA
	RG	4171 ± 20bcdA	2478 ± 27dB	1693 ± 45bB	3034 ± 17cB	556 ± 11abA	78.73 ± 0.46gC	4.60 ± 0.07dB
	YZ	4293 ± 65defB	2788 ± 26fD	1504 ± 43aA	3471 ± 42dC	682 ± 16deC	73.08 ± 0.51cA	4.62 ± 0.04dB
	ZY	4273 ± 26cdeB	2171 ± 16aA	2102 ± 10eC	2802 ± 21aA	631 ± 24bcdB	78.98 ± 0.08gC	4.42 ± 0.08cA
Sushu 16	LQ	4656 ± 63gC	2363 ± 42cB	2293 ± 45fD	2925 ± 12bB	562 ± 49abA	71.68 ± 0.03bA	4.42 ± 0.04cB
	RG	4145 ± 34bcA	2306 ± 28bcB	1839 ± 28cA	2938 ± 13bB	633 ± 20bcdAB	74.18 ± 0.03dC	4.60 ± 0.01dC
	YZ	4102 ± 25bA	2113 ± 29aA	1989 ± 7dB	2769 ± 26aA	656 ± 33cdB	72.47 ± 0.03bcB	4.47 ± 0.01cB
	ZY	4383 ± 42efB	2178 ± 16aA	2205 ± 39fC	2947 ± 36bB	769 ± 43fC	76.05 ± 0.48efD	4.22 ± 0.04bA
Sushu 28	LQ	4929 ± 52hD	2338 ± 39bcA	2591 ± 14hC	2942 ± 55bA	604 ± 16abcdA	70.55 ± 0.48aA	4.20 ± 0.07bB
	RG	3918 ± 89aA	2439 ± 26dB	1479 ± 64aA	3026 ± 21cB	587 ± 45abcA	76.88 ± 0.45fC	4.51 ± 0.04cdC
	YZ	4415 ± 79fB	2846 ± 36fC	1569 ± 44aA	3579 ± 35eC	733 ± 32efB	70.07 ± 0.06aA	4.44 ± 0.04cC
	ZY	4739 ± 40gC	2274 ± 22bA	2465 ± 43gB	2920 ± 25bA	645 ± 6 cd A	72.80 ± 0.52cB	4.07 ± 0.07aA
F-value	Variety (2)	42.75 ***	289.82 ***	125.27 ***	173.57 ***	10.11 **	384.62 ***	49.45 ***
	Location (3)	268.63 ***	254.21 ***	787.49 ***	233.50 ***	38.92 ***	377.46 ***	81.60 ***
	Variety × Location (6)	34.44 ***	131.76 ***	98.02 ***	142.61 ***	7.75 ***	50.46 ***	6.17 **

PV: peak viscosity; HV: heat viscosity; BV: breakdown viscosity (PV–HV); FV: final viscosity; SV: setback viscosity (FV–HV); P_{Temp}: pasting temperature; P_{Time}: peak time. Data are means ± standard deviations, *n* = 3. Values with different lowercase letters in the same column are significantly different (*p* < 0.05), and values with different capital letters in the same column and the same variety are significantly different (*p* < 0.05). The number in the parentheses is the degree of freedom, and ** and *** indicates statistically significant effect at the 0.01 and 0.001 level, respectively.

Table 4. Effects of variety and growing location on swelling power, water solubility, and thermal property parameters of starch from sweet potato root tuber.

Varieties	Locations	SP (g/g)	WS (%)	Thermal Property Parameters				
				To (°C)	Tp (°C)	Tc (°C)	ΔT (°C)	ΔH (J/g)
Ningzishu 1	LQ	30.9 ± 0.2cA	12.7 ± 0.5aA	59.9 ± 0.1gB	73.3 ± 0.1fB	80.8 ± 0.1cA	20.9 ± 0.2bA	14.3 ± 0.1cB
	RG	29.9 ± 0.9bcA	12.5 ± 0.6aA	62.9 ± 0.1hC	77.2 ± 0.3gD	84.0 ± 0.5fC	21.1 ± 0.3bA	14.2 ± 0.1cB
	YZ	30.1 ± 0.7bcA	12.9 ± 0.5aA	57.6 ± 0.1fA	69.5 ± 0.6deA	82.1 ± 0.4deB	24.5 ± 0.4cdC	13.2 ± 0.6abcA
	ZY	30.2 ± 0.6bcA	14.4 ± 0.7bcB	60.1 ± 0.1gB	76.2 ± 0.2gC	83.3 ± 0.3efC	23.1 ± 0.2cB	14.1 ± 0.5cB
Sushu 16	LQ	32.6 ± 0.6dB	15.4 ± 0.1cA	54.8 ± 0.2cA	61.2 ± 0.2aA	80.9 ± 0.4cA	26.1 ± 0.3eB	13.2 ± 0.6abcA
	RG	29.9 ± 0.6bcA	15.2 ± 0.8cA	57.7 ± 0.5fC	70.0 ± 0.9eC	83.0 ± 0.3efB	25.3 ± 0.6deB	12.2 ± 0.6abA
	YZ	29.8 ± 0.5bcA	14.2 ± 0.5bcA	55.7 ± 0.4dB	68.7 ± 0.4dB	82.3 ± 0.7deB	26.6 ± 0.9eB	12.7 ± 0.4abcA
	ZY	29.1 ± 0.4bA	17.9 ± 0.6dB	62.8 ± 0.2hD	73.0 ± 0.4fB	80.7 ± 0.5cA	17.9 ± 0.6aA	13.3 ± 0.7bcA
Sushu 28	LQ	28.9 ± 0.2bB	13.5 ± 0.1abA	53.1 ± 0.1bB	66.4 ± 0.5cB	77.4 ± 0.4aA	24.3 ± 0.4cdB	12.8 ± 0.7abcA
	RG	29.4 ± 0.5aA	14.6 ± 0.1bcB	57.9 ± 0.2fD	73.5 ± 0.3fD	81.5 ± 0.3cdC	23.6 ± 0.4cB	13.3 ± 0.7bcA
	YZ	26.7 ± 0.4aA	12.8 ± 0.4aA	51.1 ± 0.3aA	64.1 ± 0.4bA	79.2 ± 0.9bB	28.1 ± 1.1fC	11.7 ± 0.7aA
	ZY	29.8 ± 0.5bcB	15.3 ± 0.6cB	56.5 ± 0.4cC	69.1 ± 0.2deC	77.3 ± 0.2aA	20.9 ± 0.2bA	12.9 ± 0.6abcA
F-value	Variety (2)	62.68 ***	75.16 ***	1467.13 ***	796.78 ***	205.24 ***	41.10 ***	18.39 ***
	Location (3)	23.27 ***	41.71 ***	911.93 ***	644.24 ***	73.36 ***	173.62 ***	5.29 **
	Variety × Location (6)	11.76 ***	4.42 **	195.71 ***	157.12 ***	11.25 ***	62.30 ***	2.78 *

SP: swelling power; WS: water solubility; To: gelatinization onset temperature; Tp: gelatinization peak temperature; Tc: gelatinization conclusion temperature; ΔT: gelatinization temperature range (Tc–To); ΔH: gelatinization enthalpy. Data are means ± standard deviations, $n = 3$. Values with different lowercase letters in the same column are significantly different ($p < 0.05$), and values with different capital letters in the same column and the same variety are significantly different ($p < 0.05$). The number in the parentheses is the degree of freedom, and *, **, and *** indicates statistically significant effect at the 0.05, 0.01, and 0.001 level, respectively.

2.9. Effects of Variety and Growing Location on Thermal Properties of Starch

Thermal properties provide important reference parameters for evaluating cooking and processing quality of starch. Significant differences in thermograms were detected among different sweet potato varieties and growing locations (Figure 8). Some starches such as starch from Ningzishu 1 grown in ZY exhibited single-peak DSC curve with wide gelatinization temperature range, some starches such as starch from Sushu 28 grown in LQ exhibited two-peak DSC curve, and some starches such as starch from Sushu 16 grown in RG showed three-peak DSC curve (Figure 8). Similar single-, two-, and three-peak DSC curves are detected in sweet potato starches from different varieties [2,9,11]. This complex gelatinization curve is due to that C-type starches have different proportions of A-type crystallinity with high gelatinization temperature and B-type crystallinity with low gelatinization temperature [40,41]. Guo et al. [2] systematically studied thermal properties of sweet potato starch. The single-, two-, and three-peak DSC curves with wide gelatinization temperature range of sweet potato starches can all be fitted into three gelatinization peaks corresponding to the gelatinization of B-, C-, and A-type starch according to gelatinization temperature from low to high. The sweet potato C-type starch consists of heterogeneous granules of A-, B-, and C-type starch. Their different proportions result in single-, two-, and three-peak gelatinization curves in sweet potato starches from different varieties [31]. The different DSC curves of starches from different sweet potato varieties and growing locations indicated that thermal properties of starch were influenced by varieties, growing locations, and their interaction. The gelatinization temperature and enthalpy are presented in Table 4. The gelatinization onset temperature varied from 57.6 °C (YZ) to 62.9 °C (RG), from 54.8 °C (LQ) to 62.8 °C (ZY), and from 51.1 °C (YZ) to 57.9 °C (RG) for Ningzishu 1, Sushu 16, and Sushu 28, respectively. The gelatinization peak temperature varied from 69.5 °C (YZ) to 77.2 °C (RG), from 61.2 °C (LQ) to 73.0 °C (ZY), and from 64.1 °C (YZ) to 73.5 °C (RG) for Ningzishu 1, Sushu 16, and Sushu 28, respectively. The gelatinization conclusion temperature varied from 80.8 °C (LQ) to 84.0 °C (RG), from 80.7 °C (ZY) to 83.0 °C (RG), and from 77.3 °C (ZY) to 81.5 °C (RG) for Ningzishu 1, Sushu 16, and Sushu 28, respectively. The gelatinization temperature range varied from 20.9 °C (LQ) to 24.5 °C (YZ), from 17.9 °C (ZY) to 26.6 °C (YZ), and from 20.9 °C (ZY) to 28.1 °C (YZ) for Ningzishu 1, Sushu 16, and Sushu 28, respectively. The gelatinization enthalpy is

the energy requirement for disruption of crystallinity, and ranged from 13.2 J/g (YZ) to 14.3 J/g (LQ), from 12.2 J/g (RG) to 13.3 J/g (ZY), and from 11.7 J/g (YZ) to 13.3 J/g (RG) for Ningzishu 1, Sushu 16, and Sushu 28, respectively. Two-way ANOVA analysis showed that gelatinization temperature and enthalpy of sweet potato were significantly affected by variety, growing location, and their interaction (Table 4). The gelatinization properties of starch are affected by variety, growing location, and their interaction in potato [18] and wheat [16], but only gelatinization onset and peak temperature of starch are affected by varieties in cassava [19].

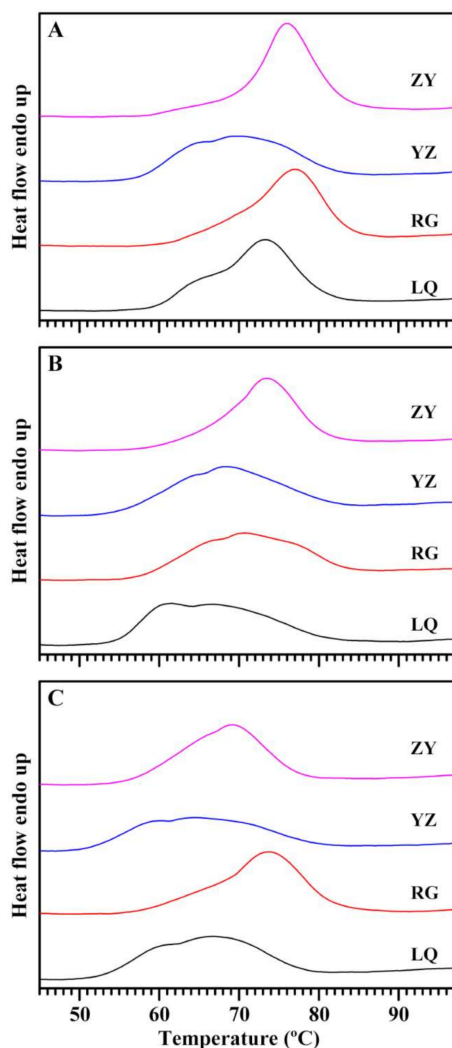


Figure 8. DSC thermograms of starches from root tubers of Ningzishu 1 (A), Sushu 16 (B), and Sushu 28 (C) in growing locations of Linqan (LQ), Rugao (RG), Yangzhou (YZ), and Zunyi (ZY).

2.10. Effects of Variety and Growing Location on Digestion Properties of Starch

The enzyme hydrolysis of starch can provide important references in estimating starch utilizations in food and nonfood industries. The RDS, SDS, and RS are presented in Table 5. For native starch, Ningzishu 1, Sushu 16, and Sushu 28 had significantly different digestibilities. Three sweet potato varieties exhibited the highest and lowest RDS in growing location of YZ and ZY, respectively, and the highest and lowest RS in ZY and YZ, respectively (Table 5). Abegunde et al. [20] measured the digestion of native starches from 11 sweet potato varieties planted in different places, and found that starches from different cultivars exhibit significantly different digestibilities due to that environmental temperature and soil affect starch development. Guo et al. [2] reported that native starches from nine sweet potato varieties grown in the same location exhibit

significantly different digestion properties. In fact, enzyme hydrolysis of native starch is affected by morphology, size, component, amylopectin structure, crystallinity, hydrolysis condition, and type of hydrolyzing enzyme [2,20]. In the present research, two-way ANOVA analysis showed that the digestibility of native starch was significantly influenced by sweet potato variety, growing location, and their interaction (Table 5). For gelatinized starch, the digestion of starch is mainly affected by amylose/amylopectin structure and content [21]. The gelatinized starch had RDS from 70.5% to 81.4%, SDS from 2.1% to 11.0%, and RS from 10.8% to 23.3% among three sweet potato varieties grown in four locations. Two-way ANOVA analysis also showed that the digestibility of gelatinized starch was significantly influenced by sweet potato variety, growing location, and their interaction (Table 5). Tappiban et al. [19] measured the RS of starches from five cassava cultivars grown in two locations, and found that RS of cassava starch is not affected by genotype, environment, and their interaction.

Table 5. Effects of variety and growing location on digestion properties of native and gelatinized starches.

Varieties	Locations	Native Starch			Gelatinized Starch		
		RDS (%)	SDS (%)	RS (%)	RDS (%)	SDS (%)	RS (%)
Ningzishu 1	LQ	3.2 ± 0.1cC	10.3 ± 0.3aB	86.5 ± 0.4gB	70.5 ± 1.1aA	6.2 ± 0.5bcAB	23.3 ± 1.5eB
	RG	2.7 ± 0.1bB	9.2 ± 0.2aA	88.1 ± 0.3ghC	72.9 ± 0.9abcAB	7.9 ± 0.2cdB	19.2 ± 1.1cdA
	YZ	5.1 ± 0.1fD	16.6 ± 0.6cC	78.3 ± 0.7deA	75.0 ± 1.6bcdB	7.7 ± 0.5cdB	17.3 ± 1.4cA
	ZY	2.2 ± 0.1aA	8.8 ± 0.3aA	89.1 ± 0.4hC	74.4 ± 1.8bcdB	5.5 ± 1.6bA	20.1 ± 0.2dA
Sushu 16	LQ	5.0 ± 0.1fC	18.3 ± 0.4dB	76.6 ± 0.5dB	78.4 ± 0.6efB	10.2 ± 0.3efAB	11.5 ± 0.8abA
	RG	4.1 ± 0.1dB	16.3 ± 0.6bcA	79.6 ± 0.7efC	76.0 ± 1.3cdeB	10.7 ± 0.7fB	13.3 ± 0.6bB
	YZ	7.9 ± 0.3hD	29.6 ± 0.9eC	62.5 ± 1.1bA	77.1 ± 0.7deB	11.0 ± 0.4fB	11.8 ± 0.4abA
	ZY	3.3 ± 0.2cA	16.6 ± 0.2cA	80.0 ± 0.4efC	72.6 ± 2.0abA	8.2 ± 1.8cdA	19.2 ± 0.3cdC
Sushu 28	LQ	6.5 ± 0.2gB	19.0 ± 0.6dB	74.5 ± 0.9cB	80.7 ± 0.6fB	8.5 ± 0.3deC	10.8 ± 0.8aA
	RG	4.6 ± 0.0eA	15.1 ± 0.0bcA	80.3 ± 0.1efC	78.3 ± 1.5efA	2.1 ± 0.8aA	19.6 ± 1.1dB
	YZ	10.9 ± 0.3iC	30.9 ± 1.4eC	58.2 ± 1.6aA	81.1 ± 0.3fB	7.9 ± 0.3cdC	11.0 ± 0.5aA
	ZY	4.6 ± 0.1eA	14.7 ± 0.8bA	80.6 ± 0.9fC	81.4 ± 0.2fB	6.7 ± 0.3bcdB	12.0 ± 0.4abA
F-value	Variety (2)	361.59 ***	1267.42 ***	745.02 ***	109.19 ***	75.68 ***	220.52 ***
	Location (3)	125.27 ***	1425.86 ***	727.37 ***	4.77 **	14.92 ***	42.25 ***
	Variety × Location (6)	9.16 ***	88.32 ***	29.75 ***	10.29 ***	19.44 ***	54.79 ***

RDS: rapidly digestible starch degraded within 20 min; SDS: slowly digestible starch degraded between 20 min and 2 h; RS; resistant starch undegraded within 2 h. Data are means ± standard deviations, $n = 3$. Values with different lowercase letters in the same column are significantly different ($p < 0.05$), and values with different capital letters in the same column and the same variety are significantly different ($p < 0.05$). The number in the parentheses is the degree of freedom, and ** and *** indicates statistically significant effect at the 0.01 and 0.001 level, respectively.

3. Materials and Methods

3.1. Plant Materials

Three sweet potato varieties of purple-fleshed Ningzishu 1, yellow-fleshed Sushu 16, and white-fleshed Sushu 28 were planted on 27 May and harvested on 31 October 2020. For each variety in one experimental plot, 100 seedlings were planted in five rows with 90 cm between rows and 20 cm between hills and one seedling per hill under routine agronomic practices in four growing locations of Linqun (LQ) [latitude 32°58'32" N, longitude 115°14'05" E, altitude 38 m], Rugao (RG) [latitude 32°21'38" N, longitude 120°26'36" E, altitude 6 m], Yangzhou (YZ) [latitude 32°23'43" N, longitude 119°25'46" E, altitude 8 m], and Zunyi (ZY) [latitude 27°32'05" N, longitude 107°10'20" E, altitude 893 m]. All varieties in every growing location were planted repeatedly in three experimental plots. The soil in each growing location was given the same nitrogen treatment of 15 kg/ha applied in the ridge before planting. The fertilizers included urea, superphosphate, and potassium sulfate. Temperature variation of growing location during sweet potato growth stage is presented in Figure 3.

3.2. Isolation of Starch from Root Tuber of Sweet Potato

Starch was isolated from fresh root tuber of sweet potato using water homogenization, sieving, and treatment of 0.2% NaOH and anhydrous ethanol following the processes of Guo et al. [2] exactly.

3.3. Analysis of Size Distribution of Starch

Starch and water slurry was analyzed with a laser particle size analyzer (Mastersizer 2000, Malvern, Worcestershire, UK) following the processes of Guo et al. [2]. The testing condition included the opacity between 10% and 11% and the mixing at 2000 rpm. The granule size was expressed with volume-weighted mean diameter (D[4,3]).

3.4. Analysis of Absorption Spectrum Parameters of Starch–Iodine Complex

Starch was dissolved in dimethyl sulfoxide containing 10% 6.0 M urea (UDMSO) and stained with iodine solution following the processes of Man et al. [22] exactly. The sample was analyzed with a spectrophotometer (BioMate 3S, Thermo Scientific, Chino, CA, USA). The parameters including the absorption value at 550, 620, and 680 nm and the maximum absorption wavelength were obtained from the spectrum.

3.5. Determination of Amylose Content

The amylose content (AC) was measured using concanavalin A (Con A) precipitation method with an amylose/amylopectin assay kit (K-AMYL, Megazyme, Bray, Ireland) following its assay procedures. For measuring principle, starch is first dispersed completely into amylose and amylopectin, and separated into two aliquots. The Con A specifically precipitates the amylopectin in an aliquot, and the remaining amylose in the supernatant is quantified. The dispersed amylose and amylopectin in another aliquot are also quantified. The AC is the ratio of amylose to both amylose and amylopectin.

3.6. X-ray Diffraction (XRD) Analysis

Starch was analyzed using an XRD spectrometer (D8, Bruker, Karlsruhe, Germany) following the method of Guo et al. [2] exactly. The testing condition included X-ray beam at 40 kV and 40 mA and scanning angle from 3° to 40° 2 θ with 0.02° step size. The relative crystalline (RC) was the area percentage of crystalline peaks and total diffraction peak between 4° to 30° 2 θ [42].

3.7. Fourier Transform Infrared (FTIR) Analysis

Starch was analyzed using a FTIR spectrometer (7000, Varian, Santa Clara, CA, USA) following the method of Guo et al. [2] exactly. The testing condition included 64 scans with 4 cm⁻¹ resolution from 4000 to 800 cm⁻¹. The spectrum was deconvoluted using Lorentzian line shape with 19 cm⁻¹ half-width and 1.9 resolution enhancement factor after baseline correction from 1200 to 900 cm⁻¹.

3.8. Small Angle X-ray Scattering (SAXS) Analysis

Starch was analyzed using a SAXS system (NanoStar, Bruker, Karlsruhe, Germany) following the method of Cai et al. [43] except that the peak intensity and position were measured with PeakFit V4.12 software. The testing condition included X-ray source with copper rotating anode (0.1 mm filament) at 50 kV and 30 W, cross coupled Göbel mirrors, and 1.5418 Å Cu K α radiation wavelength.

3.9. Rapid Visco Analyzer (RVA) Analysis

Starch was analyzed using a RVA (3D, Newport Scientific, Warriewood, Australia) following the method of Guo et al. [2] exactly. The testing condition included starch (2.5 g) and water (25 mL) slurry, 160 rpm rotating speed, and programmed temperature–time profile with 50 °C for 1 min, from 50 to 95 °C for 3.75 min, 95 °C for 2.5 min, from 95 to 50 °C for 3.75 min, and 50 °C for 1.4 min.

3.10. Determination of Swelling Power and Water Solubility

The swelling power and water solubility of starch at 95 °C were measured following the method of Guo et al. [2] exactly. The soluble carbohydrates measured with anthrone-H₂SO₄ method were used to evaluate the water solubility (percentage of soluble carbohydrates to total starch), and the swelling power was the ratio of precipitated starch to total starch with subtraction of soluble carbohydrates.

3.11. Differential Scanning Calorimetry (DSC) Analysis

Starch was analyzed using a DSC (200-F3, Netzsch, Selb, Germany) following the method of Guo et al. [2] exactly. The testing condition included starch (5 mg) and water (15 µL) sealed in aluminum pan, heating range from 30 to 130 °C, and heating rate at 10 °C/min.

3.12. Analysis of Digestion Properties of Starch

The digestibilities of native and gelatinized starches were evaluated using both porcine pancreatic α -amylase (Sigma, A3176, St. Louis, MO, USA) and *Aspergillus niger* amyloglucosidase (Megazyme, E-AMGDF) following the method of Guo et al. [2] exactly. The released glucose was measured with a glucose assay kit (K-GLUC, Megazyme, Bray, Ireland) to convert the degraded starch quantity. The total starch was measured using a total starch assay kit (K-TSTA, Megazyme, Bray, Ireland). The rapidly digestible starch (RDS) and slowly digestible starch (SDS) are the percentage of degraded starch within 20 min and between 20 min and 2 h to the total starch, respectively, and the resistant starch (RS) is the difference between total starch and both RDS and SDS.

3.13. Data Analysis

The data difference among different starches with Tukey's test and the effects of variety, growing location, and their interaction on starch properties with two-way ANOVA test were analyzed with SPSS 19.0.

4. Conclusions

Three sweet potato varieties grown in four locations were used to investigate the effects of variety and growing location on starch physicochemical properties in sweet potato. The granule size, iodine absorption parameters and AC of starch were influenced significantly by variety, growing location, and their interaction. C-type starches in root tubers had different proportions of A- and B-type crystallinities in different varieties and growing locations. The ordered degree and lamellar thickness of starch were affected by variety and growing location of sweet potato. The pasting properties, swelling power, water solubility, thermal properties, and digestibility exhibited significant differences among different varieties and growing location. Therefore, in consideration of the applications of starch, it is very important to choose an appropriate variety for planting sweet potato in a specific growing location.

Author Contributions: C.W. conceived the study and designed the experiments; L.S., Y.L., L.L. and X.B. performed the experiments; and C.W. and L.S. wrote the manuscript. All authors discussed the contents of the manuscript and approved the submission. All authors have read and agreed to the published version of the manuscript.

Funding: This study was financially supported by grants from the National Natural Science Foundation of China (31570324), Talent Project of Yangzhou University, and Priority Academic Program Development of Jiangsu Higher Education Institutions.

Institutional Review Board Statement: Not applicable.

Informed Consent Statement: Not applicable.

Data Availability Statement: The data are available upon request from the corresponding author.

Conflicts of Interest: The authors declare no conflict of interest.

Sample Availability: Samples of starches are available from the corresponding author upon reasonable request.

References

1. FAOSTAT. Available online: <http://www.fao.org/faostat/en/#data> (accessed on 24 October 2021).
2. Guo, K.; Liu, T.; Xu, A.; Zhang, L.; Bian, X.; Wei, C. Structural and functional properties of starches from root tubers of white, yellow, and purple sweet potatoes. *Food Hydrocoll.* **2019**, *89*, 829–836. [CrossRef]
3. Zhu, F.; Wang, S. Physicochemical properties, molecular structure, and uses of sweetpotato starch. *Trends Food Sci. Technol.* **2014**, *36*, 68–78. [CrossRef]
4. Song, H.G.; Choi, I.C.; Lee, J.S.; Chung, M.N.; Yoon, C.S.; Han, J. Comparative study on physicochemical properties of starch films prepared from five sweet potato (*Ipomoea batatas*) cultivars. *Int. J. Biol. Macromol.* **2021**, *189*, 758–767. [CrossRef]
5. Truong, V.D.; Avula, R.Y.; Pecota, K.V.; Yencho, G.C. Sweetpotato production, processing, and nutritional quality. In *Handbook of Vegetables and Vegetable Processing*; Siddiq, M., Uebersax, M.A., Eds.; John Wiley & Sons Ltd.: Hoboken, NJ, USA, 2018; pp. 811–838.
6. Alam, M.K. A comprehensive review of sweet potato (*Ipomoea batatas* [L.] Lam): Revisiting the associated health benefits. *Trends Food Sci. Technol.* **2021**, *115*, 512–529. [CrossRef]
7. Kim, H.J.; Woo, K.S.; Lee, H.U.; Nam, S.S.; Lee, B.W.; Kim, M.Y.; Lee, Y.Y.; Lee, J.Y.; Kim, M.H.; Lee, B. Physicochemical characteristics of starch in sweet potato cultivars grown in Korea. *Prev. Nutr. Food Sci.* **2020**, *25*, 212–218. [CrossRef] [PubMed]
8. Wang, H.; Yang, Q.; Ferdinand, U.; Gong, X.; Qu, Y.; Gao, W.; Ivanistau, A.; Feng, B.; Liu, M. Isolation and characterization of starch from light yellow, orange, and purple sweet potatoes. *Int. J. Biol. Macromol.* **2020**, *160*, 660–668. [CrossRef] [PubMed]
9. Zhang, L.; Zhao, L.; Bian, X.; Guo, K.; Zhou, L.; Wei, C. Characterization and comparative study of starches from seven purple sweet potatoes. *Food Hydrocoll.* **2018**, *80*, 168–176. [CrossRef]
10. Duan, W.; Zhang, H.; Xie, B.; Wang, B.; Zhang, L. Impacts of nitrogen fertilization rate on the root yield, starch yield and starch physicochemical properties of the sweet potato cultivar Jishu 25. *PLoS ONE* **2019**, *14*, e0221351. [CrossRef]
11. Genkina, N.K.; Noda, T.; Koltisheva, G.I.; Wasserman, L.A.; Tester, R.F.; Yuryev, V.P. Effects of growth temperature on some structural properties of crystalline lamellae in starches extracted from sweet potatoes (Sunnyred and Ayamurasaki). *Starch* **2003**, *55*, 350–357. [CrossRef]
12. Guo, K.; Bian, X.; Jia, Z.; Zhang, L.; Wei, C. Effects of nitrogen level on structural and functional properties of starches from different colored-fleshed root tubers of sweet potato. *Int. J. Biol. Macromol.* **2020**, *164*, 3235–3242. [CrossRef]
13. Noda, T.; Takahata, Y.; Sato, T.; Ikoma, H.; Mochida, H. Physicochemical properties of starches from purple and orange fleshed sweet potato roots at two levels of fertilizer. *Starch* **1996**, *48*, 395–399. [CrossRef]
14. Li, H.; Liu, Y. Effects of variety and growth location on the chain-length distribution of rice starches. *J. Cereal Sci.* **2019**, *85*, 77–83. [CrossRef]
15. Sar, S.; Tizzotti, M.J.; Hasjim, J.; Gilbert, R.G. Effects of rice variety and growth location in Cambodia on grain composition and starch structure. *Rice Sci.* **2014**, *21*, 47–58. [CrossRef]
16. Nhan, M.T.; Copeland, L. Effect of variety and growing environment on pasting and thermal properties of wheat starch. *Starch* **2016**, *68*, 436–445. [CrossRef]
17. Ahmed, S.; Ru, W.; Han, H.; Cheng, L.; Bian, X.; Li, G.; Jin, L.; Wu, P.; Bao, J. Fine molecular structure and its effects on physicochemical properties of starches in potatoes grown in two locations. *Food Hydrocoll.* **2019**, *97*, 105172. [CrossRef]
18. Pelpolage, S.; Nakata, K.; Shinbayashi, Y.; Murayama, D.; Tani, M.; Yamauchi, H.; Koaze, H. Comparison of pasting and thermal properties of starches isolated from four processing type potato varieties cultivated in two locations in Hokkaido. *Food Sci. Technol. Res.* **2016**, *22*, 687–693. [CrossRef]
19. Tappiban, P.; Sraphet, S.; Srisawad, N.; Wu, P.; Han, H.; Smith, D.R.; Bao, J.; Triwitayakorn, K. Effects of cassava variety and growth location on starch fine structure and physicochemical properties. *Food Hydrocoll.* **2020**, *108*, 106074. [CrossRef]
20. Abegunde, O.K.; Mu, T.H.; Chen, J.W.; Deng, F.M. Physicochemical characterization of sweet potato starches popularly used in Chinese starch industry. *Food Hydrocoll.* **2013**, *33*, 169–177. [CrossRef]
21. Lin, L.; Zhang, Q.; Zhang, L.; Wei, C. Evaluation of the molecular structural parameters of normal rice starch and their relationships with its thermal and digestion properties. *Molecules* **2017**, *22*, 1526. [CrossRef]
22. Man, J.; Lin, L.; Wang, Z.; Wang, Y.; Liu, Q.; Wei, C. Different structures of heterogeneous starch granules from high-amylose rice. *J. Agric. Food Chem.* **2014**, *62*, 11254–11263. [CrossRef]
23. Ahmed, N.; Maekawa, M.; Tetlow, I.J. Effects of low temperature on grain filling, amylose content, and activity of starch biosynthesis enzymes in endosperm of basmati rice. *Aust. J. Agric. Res.* **2008**, *59*, 599–604. [CrossRef]
24. Ahmed, N.; Tetlow, I.J.; Nawaz, S.; Iqbal, A.; Mubin, M.; ul Rehman, M.S.N.; Butt, A.; Lightfoot, D.A.; Maekawa, M. Effect of high temperature on grain filling period, yield, amylose content and activity of starch biosynthesis enzymes in endosperm of basmati rice. *J. Sci. Food Agric.* **2015**, *95*, 2237–2243. [CrossRef] [PubMed]
25. Lu, H.F.; Hu, Y.Y.; Wang, C.Y.; Liu, W.X.; Ma, G.; Han, Q.X.; Ma, D.Y. Effects of high temperature and drought stress on the expression of gene encoding enzymes and the activity of key enzymes involved in starch biosynthesis in wheat grains. *Front. Plant. Sci.* **2019**, *10*, 1414. [CrossRef] [PubMed]

26. Nhan, M.T.; Copeland, L. Effects of growing environment on properties of starch from five Australian wheat varieties. *Cereal Chem.* **2014**, *91*, 587–594. [CrossRef]
27. Huang, L.; Sreenivasulu, N.; Liu, Q. Waxy editing: Old meets new. *Trends Plant. Sci.* **2020**, *25*, 963–966. [CrossRef] [PubMed]
28. He, W.; Wei, C. Progress in C-type starches from different plant sources. *Food Hydrocoll.* **2017**, *73*, 162–175. [CrossRef]
29. Kim, J.; Ren, C.; Shin, M. Physicochemical properties of starch isolated from eight different varieties of Korean sweet potatoes. *Starch* **2013**, *65*, 923–930. [CrossRef]
30. Lee, B.H.; Lee, Y.T. Physicochemical and structural properties of different colored sweet potato starches. *Starch* **2017**, *69*, 1600001. [CrossRef]
31. Guo, K.; Zhang, L.; Bian, X.; Cao, Q.; Wei, C. A-, B- and C-type starch granules coexist in root tuber of sweet potato. *Food Hydrocoll.* **2020**, *98*, 105279. [CrossRef]
32. Warren, F.J.; Gidley, M.J.; Flanagan, B.M. Infrared spectroscopy as a tool to characterize starch ordered structure: A joint FTIR-ATR, NMR, XRD and DSC study. *Carbohydr. Polym.* **2016**, *139*, 35–42. [CrossRef]
33. Sevenou, O.; Hill, S.E.; Farhat, I.A.; Mitchell, J.R. Organisation of the external region of the starch granule as determined by infrared spectroscopy. *Int. J. Biol. Macromol.* **2002**, *31*, 79–85. [CrossRef]
34. Sanderson, J.S.; Daniels, R.D.; Donald, A.M.; Blennow, A.; Engelsen, S.B. Exploratory SAXS and HPAEC-PAD studies of starches from diverse plant genotypes. *Carbohydr. Polym.* **2006**, *64*, 433–443. [CrossRef]
35. Blazek, J.; Gilbert, E.P. Application of small-angle X-ray and neutron scattering techniques to the characterisation of starch structure: A review. *Carbohydr. Polym.* **2011**, *85*, 281–293. [CrossRef]
36. Witt, T.; Douth, J.; Gilbert, E.P.; Gilbert, R.G. Relations between molecular, crystalline and lamellar structures of amylopectin. *Biomacromolecules* **2012**, *13*, 4273–4282. [CrossRef]
37. Shar, T.; Sheng, Z.H.; Ali, U.; Fiaz, S.; Wei, X.J.; Xie, L.H.; Jiao, C.A.; Ali, F.; Shao, G.N.; Hu, S.K.; et al. Mapping quantitative trait loci associated with starch paste viscosity attributes by using double haploid populations of rice (*Oryza sativa* L.). *J. Integr. Agric.* **2020**, *19*, 1691–1703. [CrossRef]
38. Singh, N.; Kuar, L.; Sandhu, K.S.; Kuar, J.; Nishinari, K. Relationships between physicochemical, morphological, thermal, rheological properties of rice starches. *Food Hydrocoll.* **2006**, *20*, 532–542. [CrossRef]
39. Collado, L.S.; Mabesa, R.C.; Corke, H. Genetic variation in the physical properties of sweet potato starch. *J. Agric. Food Chem.* **1999**, *47*, 4195–4201. [CrossRef] [PubMed]
40. Bogracheva, T.Y.; Morris, V.J.; Ring, S.G.; Hedley, C.L. The granular structure of C-type pea starch and its role in gelatinization. *Biopolym. Orig. Res. Biomol.* **1998**, *45*, 323–332. [CrossRef]
41. Fan, X.; Zhao, L.; Zhang, L.; Xu, B.; Wei, C. A new allomorph distribution of C-type starch from root tuber of *Apios fortunei*. *Food Hydrocoll.* **2017**, *66*, 334–342. [CrossRef]
42. Wei, C.; Qin, F.; Zhou, W.; Chen, Y.; Xu, B.; Wang, Y.; Gu, M.; Liu, Q. Formation of semi-compound C-type starch granule in high-amylose rice developed by antisense RNA inhibition of starch-branching enzyme. *J. Agric. Food Chem.* **2010**, *58*, 11097–11104. [CrossRef]
43. Cai, C.; Cai, J.; Man, J.; Yang, Y.; Wang, Z.; Wei, C. Allomorph distribution and granule structure of lotus rhizome C-type starch during gelatinization. *Food Chem.* **2014**, *142*, 408–415. [CrossRef] [PubMed]

MDPI
St. Alban-Anlage 66
4052 Basel
Switzerland
Tel. +41 61 683 77 34
Fax +41 61 302 89 18
www.mdpi.com

Molecules Editorial Office
E-mail: molecules@mdpi.com
www.mdpi.com/journal/molecules



MDPI
St. Alban-Anlage 66
4052 Basel
Switzerland
Tel: +41 61 683 77 34
www.mdpi.com



ISBN 978-3-0365-6332-9